1-9-2018

Synthesis and Evaluation of Itraconazole Analogues for the Treatment of Medulloblastoma

Jennifer Pace
University of Connecticut - Storrs, jenrpace@gmail.com

Synthesis and Evaluation of Itraconazole Analogues for the Treatment of Medulloblastoma

Jennifer R. Pace, PhD

University of Connecticut, 2018

Recently, two separate high-throughput screens (HTS) identified itraconazole (ITZ), a well-known antifungal agent, as both an inhibitor of the hedgehog (Hh) pathway and angiogenesis (IC_{50} = 690 nM and 160 nM, respectively). Dysregulation of both the Hh pathway and angiogenesis are implemented in the growth and metastasis of various types of cancer. Aberrant Hh signaling may lead to cell proliferation and tumor growth most notably associated with basal cell carcinoma (BCC) and medulloblastoma (MB). Currently, there are a few Hh pathway inhibitors that are FDA approved for the treatment of BCC. However, there has been an emergence of resistance towards these compounds highlighting the need for novel Hh pathway inhibitors. The ITZ scaffold has not been thoroughly explored in terms of Hh pathway inhibition. As a result, four generations of ITZ analogues were designed, synthesized, and evaluated for Hh pathway inhibitory activity. Structure-activity relationship (SAR) studies indicated that the triazole moiety is not necessary for potent Hh pathway inhibition and removal of this functionality also abolishes coordination with CYP3A4. While the stereochemistry of the *sec*-butyl side chain region was not important, stereochemistry at the 4-position of the dioxolane ring proved to be crucial. In terms of the triazolone/side-chain region of the scaffold, truncation of the side-chain region to the free triazolone and truncation of the triazolone to smaller moieties ($–NO_2$ and $–NH_2$) maintain potency. Amide functionality in replacement of the triazolone/side-chain region is tolerated with preference to polar

substituents at the *meta*- position of the phenyl ring. Early evidence suggests that cyclic functionality is not necessary within the triazolone region indicating that acyclic functionalities could be explored for Hh pathway inhibitory activity. A subset of ITZ analogues was evaluated in two additional assays to explore angiogenesis inhibitory activity. Results indicated that the triazole region of ITZ seems to be important for angiogenesis inhibition. Overall, a total of 60 analogues were designed, synthesized, and evaluated to thoroughly explore the ITZ scaffold in terms of these novel biological activities. In addition to these medicinal chemistry efforts, a preliminary ITZ liposome formulation was designed and evaluated in vitro for Hh pathway inhibition.

Synthesis and Evaluation of Itraconazole Analogues for the Treatment of Medulloblastoma

Jennifer R. Pace

B.A., Saint Anselm College, 2013

A Dissertation

Submitted in Partial Fulfillment of the

Requirements for the Degree of

Doctor of Philosophy

at the

University of Connecticut

2018

APPROVAL PAGE

Doctor of Philosophy Dissertation

Synthesis and Evaluation of Itraconazole Analogues for the Treatment of Medulloblastoma

Presented by
Jennifer R. Pace, B.A.

Major Advisor

_____

M. Kyle Hadden, PhD

Associate Advisor

_____

Diane J. Burgess, PhD

Associate Advisor

_____

Marcy J. Balunas, PhD

University of Connecticut
2018

DEDICATION

To my late grandmother, Evelyn Turner
"Nana Turner"

ACKNOWLEDGEMENTS

I would like to first thank my major advisor and mentor, Dr. Kyle Hadden. Thank you for all of your guidance and patience as I navigated myself through graduate school. You provided a nurturing environment that allowed me to grow immensely as an independent well-rounded scientist. I am grateful for you giving me the opportunity to explore different avenues of science and encouraging me to learn as much as possible during my time at UConn. Thank you to all of those who have served as my committee members including Dr. Diane Burgess, Dr. Marcy Balunas, Dr. Dennis Wright, Dr. Amy Anderson as well as Dr. Andrew Wiemer and Dr. Jose Manautou. You have all been extremely helpful and supportive throughout the past few years. I appreciate the time that you all have sacrificed to help better my scientific career. Thank you to the American Chemical Society (ACS) Division of Medicinal Chemistry for providing financial support for a portion of my time at UConn.

Thank you to all of my collaborators who contributed majorly towards this research project: Dr. Ervine Epstein provided a murine basal cell carcinoma cell line (ASZ-001), which was used throughout my time at UConn; Dr. Robert Wechsler-Reya at Sanford Burnham Prebys Medical Discovery Institute assisted in testing compounds in a primary medulloblastoma cell line (MERP); Dr. James Kim at the University of Texas Southwestern Medical Center aided in testing compounds against Smoothened mutant cells. Dr. Diane Burgess and Rajan Jog, both at UConn, helped with liposome formulation and subsequent assays-- thank you for your patience as I learned and performed experiments outside of my field of expertise.

Thank you to our MS and NMR facilities, specifically the facility managers Dr. Yu-Jun Fu and Dr. Vitaliy Gorbatyuk. Thank you to all the administrative staff for helping with everything behind the scenes, especially Leslie LeBel and Laura Burnett. Thank you to shipping and receiving—Kathy Koji—for always being up for a good conversation or joke. Thanks to Hadden Lab technicians, Vibhavari Sail and Zuleyha Ozen, who have been kind enough to share their immense knowledge within the field of biology.

Working long hours and dealing with the emotional aspect of graduate school could not have been accomplished without the support of the "Hadden Lab Family": Dr. Kelly Teske, Dr. Jiachen Wen, Dr. R.C. Dash, Dr. Divya Chennamadhavuni, Chad Maschinot, Angela Zaino, Kaitlyn McCarthy, Shana Morel, and Kimberly Caroti. Thank you for providing endless scientific conversation and assistance. Laughter and music is always abundant in the Hadden Lab and I do not think I would have survived graduate school without either of these elements. Thank you to past Hadden Lab members, who were instrumental in my success: Dr. Albert DeBerardinis and Dr. Upasana Banerjee. Your advice, guidance, and mentorship were crucial throughout my first three years at UConn and I cannot thank you enough. Thank you to past undergraduate and pre-professional students who have worked closely on this project: Dan Raccuia, Kelly Chan, and Raymond Tran. It was a pleasure working with you all and learning together. To all the friends that I have met along the way at UConn—thank you for all of the memories in Storrs. I have enjoyed our Taco Tuesdays, trips to the Dairy Bar, and impromptu visits to Ted's.

Last, I would like to thank my family and friends outside of the UConn community. My professors and advisors at Saint Anselm College were influential in my

scientific career. Dr. Nicole Eyet helped me find my love for chemistry and Dr. Lisa Bonner introduced me to the field of medicinal chemistry. I have remained close with my friends from Saint Anselm and appreciate all of the support they have provided as I went off on a limb and continued my education. Finally, I am very close with my family and they have been extremely encouraging throughout this process. I would not be where I am today without the support of my grandparents, aunts, uncles, and cousins. My older brothers, Chris and Nick, have always led a challenging path to follow. I have always admired them and strived to be like them in every way possible. I hope I have made them proud by following in their footsteps and pursuing a career in science. Thank you to my sister-in-laws, Jenna and Amanda, for their constant support and love. Thank you to my little niece and nephew, Abigail and Salvatore, for providing endless cuddles and cuteness. Finally, I need to thank my parents as I would not be where I am today without their guidance, support, and love. They have made endless sacrifices so that my brothers and I could have everything. They have instilled in us the importance of education and hard work, which has resulted in all three of their children pursuing PhD degrees in chemistry. I hope we have made you proud, Mom and Dad!

TABLE OF CONTENTS

LIST OF FIGURES

Chapter I

Chapter II

Chapter III

Chapter IV

Chapter V

LIST OF SCHEMES

Chapter I

Chapter II

Chapter III

LIST OF TABLES

Chapter I

Chapter II

Chapter III

Chapter IV

CHAPTER I: Repurposing Itraconazole as an Anticancer Chemotherapeutic

1. Introduction

1.1 Drug Repurposing

Drug development is a long and expensive process; on average it takes about 13-15 years and $2-3 billion for a drug to become clinically approved.[1] To bypass this route, it is becoming increasingly popular to explore FDA-approved or clinical stage compounds for novel biological activities. Applying an existing therapeutic towards a novel biological indication can be described as drug repurposing or drug repositioning.[1] FDA-approved compounds have already been deemed safe in phase I clinical trials and as a result, many of these drugs can immediately enter phase II clinical trials for new disease indications. It has been estimated to cost $300 million and take 6.5 years to repurpose a clinically approved drug for a novel ailment (Figure 1).[2] Drug repurposing may also help improve Eroom's Law which can be described as the efficiency of research and development of new drugs in the United States; on average, this number is said to be cut in half every nine years. [1,2]

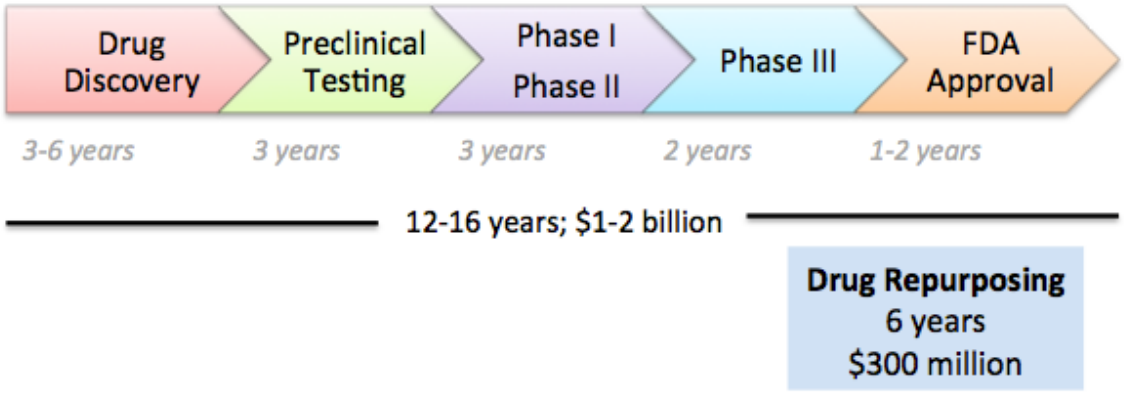

Figure 1. Drug Discovery Pipeline[2]

Although there are clear benefits from drug repurposing, most successes to date have been serendipitous (Figure 2).[1] Some of these successes include repurposing sildenafil, a phosphodiesterase inhibitor designed for angina, which is now marketed as Viagra to treat erectile dysfunction.[1,3] The antibiotic erythromycin has been repurposed for impaired gastric motility. Finally, even drugs with detrimental side effects have been successfully repurposed for novel indications. Thalidomide, originally an antiemetic, is now approved for the treatment of multiple myeloma.[3] Side effects such as teratogenicity may be acceptable for treatment of a life-threatening disease but are not ideal for treatment of a chronic disease such as nausea.[3] It is important to consider the risk versus reward aspect when repurposing a drug.[1,2] Drug repurposing is especially advantageous during disease epidemics when there is not enough time for a novel therapeutic to go through the drug development pipeline.[4] For example, the global outbreaks of both the Ebola and Zika viruses affected a large population of our world and there is still an immediate need for better treatment and/or prevention. High throughput screening efforts of FDA-approved and clinical stage drugs have been performed for both of these disease indications.[5,6]

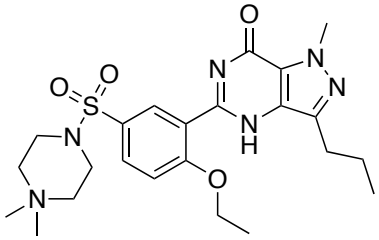

Sildenafil

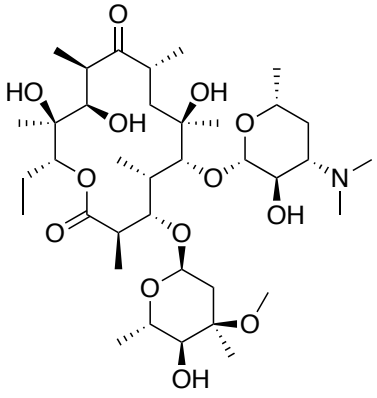

Erythromycin

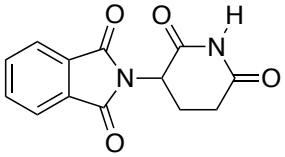

Thalidomide

Figure 2. Structures of Representative Repurposed Drugs

In addition to the plethora of benefits, there are also a few downfalls to this drug repurposing strategy. First, if the dose or mode of administration is significantly different from the original indication, the compound will have to be entered into phase I safety clinical trials.[1–3] As drug repurposing is based upon improving time and cost efficiency, this raises a huge argument. In addition, it is difficult to obtain the rights to explore novel compounds for new indications.[1–3] Generally, pharmaceutical companies are going to explore potential secondary indications before other pharmaceutical competitors or academia can obtain them.[1] Overall, drug repurposing is a promising form of drug development but there are still challenges associated with bypassing clinical stages and maintaining time/cost efficacy.[1,3]

Modern drug discovery focuses on the development of a drug candidate that has high selectivity and potency for one target. "Promiscuous drugs" or "dirty drugs", which have multiple biological activities and target sites, tend to have a negative reputation due to their presumed increase in side effects.[7] However, this idea of one drug having multiple activities, known as polypharmacology, is gaining a renewed appreciation.[7] When a single-target drug is being used, cells may acquire resistance or decrease their dependence on that specific target. For instance, in diseases such as cancer, there is generally a high rate of genetic mutations, which may lead to certain populations of cancer cells that are drug resistant; this ultimately results in treatment failure.[7] Drugs that are able to treat a variety of different diseases may be beneficial in drug development as well as drug repurposing. It is also advantageous to develop one drug that has multiple different biological activities as opposed to using combination therapy.[7] The use of drug cocktails complicates and inconveniences patients, increases the

prevalence of acute and delayed toxicities, and results in unpredictable pharmacokinetic properties. It is more appealing and cost efficient to develop single-molecule drugs with multiple activities rather than administering multiple drug combinations within a single cocktail.[7]

1.2 Itraconazole

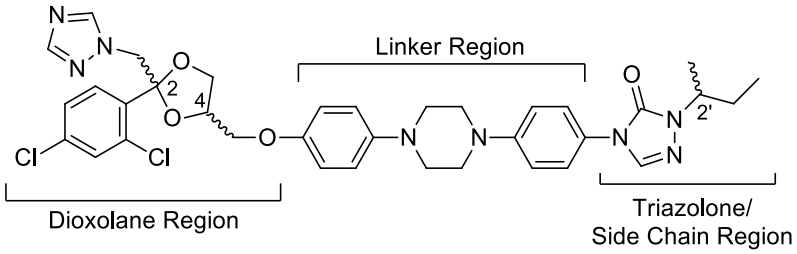

Figure 3. Structures and Regions of Itraconazole

Itraconazole (ITZ) is a clinically efficacious antifungal agent that was FDA approved in 1992 (Figure 3).[8] Recently, two separate high-throughput screens have determined that ITZ inhibits both the hedgehog (Hh) pathway and angiogenesis.[9,10] Both of these screens were performed at Johns Hopkins University School of Medicine and consisted of ~2,400 FDA-approved and post-phase I drugs.[9,10] Preclinical in vitro assays have concluded that ITZ has anticancer activity and may serve as a potential chemotherapeutic. There have been a variety of pilot studies to determine the anticancer effects of ITZ in humans.[11] Clinical trials range from phase 0 to phase 2 and include patients suffering from leukemia, prostate cancer, non-small cell lung cancer (NSCLC), basal cell carcinoma (BCC), ovarian clear cell carcinoma, breast cancer, pancreatic cancer, and T-cell lymphoma (Table 1).[11,12]

Table 1. Itraconazole Clinical Trials

Clinical Trial	Clinical Status	Cancer Type	Reference
NCT01787331	Phase II	Prostate	[11, 12]
NCT02357836	Phase 0	NSCLC	[11, 12]
NCT02120677	Phase 0	BCC	[11, 12]
NCT02354261	Phase II	BCCNS	[11, 12]
NCT02366884	Phase II	All cancer types	[11,12]

ITZ is a member of the well-known azole antifungal class. It is considered to be a small molecule despite its large size (MW = 705.64 g/mol). ITZ is a lipophilic drug with a LogP of 5.66 and as a result, has poor solubility in H_2O (1 ng/mL).[13] ITZ has three stereocenters and has the potential to exist as eight distinct stereoisomers. However, ITZ is clinically administered as a mixture of 1:1:1:1 *cis*-racemates as this orientation predominantly forms during synthesis.[14] ITZ has a complex scaffold highlighted by its triazole moiety and phenyl-piperazine-phenyl linker region. As an antifungal agent, ITZ is generally well tolerated and causes minimal side effects.[15] ITZ has been well studied in terms of its antifungal activity as well as its novel anticancer and antiviral activities.[16]

Table 2. Properties of Itraconazole [13]

Property	Value
Molecular Weight	705.64 g/mol
H-bond Donor	0
H-bond Acceptor	9
Rotatable Bond Count	11
pKa	3.7
LogP	5.66
Melting Point	166.2°C
Solubility in H_2O pH = 7	1 ng/mL

1.2.1 Antifungal Activity of ITZ

The first report of an azole exhibiting antifungal activity was in 1944 with benzimidazole.[8] In 1958, the first topical azole antifungal, chlormidazole, sparked an interest which lead to more topical azole antifungal agents: clotrimazole, miconazole, and econazole. In 1981, ketaconazole was FDA-approved for systemic fungal infections.[8] Ketaconazole remained the standard for treatment and the only orally bioavailable agent for the next decade. However, due to poor toxicity and recurring fungal infections, a second generation of azole derivatives were discovered which included terconazole, fluconazole, and eventually itraconazole.[8] Throughout the 1990s, resistance to azole antifungals was uncommon. [8,17] However, this acquired resistance has become more prevalent as fluconazole is used in immunosuppressed and critically ill patients. Janssen Pharmaceuticals developed itraconazole and it became FDA approved in the United States in 1992.[8,17] ITZ was developed to combat fluconazole-acquired resistance. It is less toxic and can be used to treat a broad range of fungal infections including *Candida, Aspergillus, Cryptococcus neoformans, Coccidioides immitis, Histoplasma capsulatum, Blastomyces dermatitidis, Paracoccidioides brasiliensis, Sporothrix schenekii,* and some phaeohyphomycetes.[8,17] ITZ began to be utilized as the standard form of treatment for non-meningeal, non-life threatening cases of histoplasmosis, blastomycosis, and paracoccidioidomycosis. Despite ITZ's advantageous activity in aspergillosis and sporotrichosis, fluconazole has a more favorable pharmacological and toxicity profile.[8,17]

ITZ is more lipid-soluble than fluconazole and this poses issues with drug formulation and absorption.[8] Originally formulated into a capsule, ITZ was not very

effective due to low blood concentrations (< 500 ng/mL). In 1997, an oral solution was FDA-approved and utilized the excipient hydroxypropyl-β-cyclodextrin to aide in solubility.[8] Eventually, an intravenous formulation was approved and this allowed for a more flexible use of ITZ; steady-state plasma concentrations could be obtained in 2-3 days as opposed to 1-2 weeks with ITZ capsules. This was crucial for patients that had advanced HIV or were in intensive care.[8]

ITZ exhibits its antifungal activity by inhibiting the enzyme cytochrome P450 14-α-demethylase (14LDM). This enzyme represents an intermediate step in the conversion of lanosterol to ergosterol (Scheme 1).[8] Ergosterol is required for cell wall synthesis and disruption of this biosynthesis results in cell death. It is essential for aerobic growth of most fungi. It is important to point out that ergosterol is the major product of sterol biosynthesis in fungi, whereas mammalian systems synthesize cholesterol as the major membrane lipid.[13,18,19]

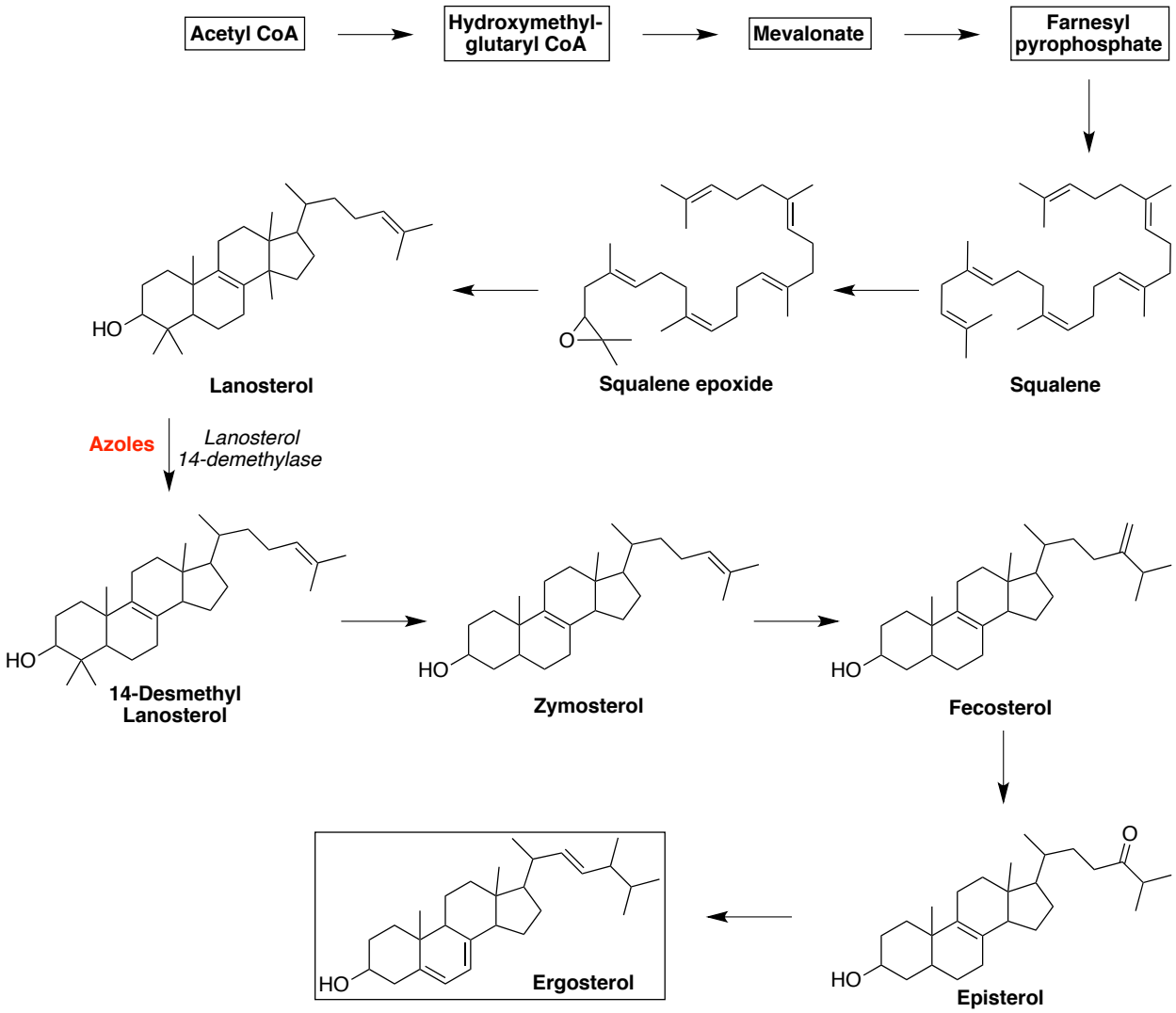

Scheme 1. Biosynthetic Pathway to Ergosterol [19,20]

Cytochrome P450 contains an iron protoporphyrin moiety, which is located at the active site.[14,18] Azole antifungals bind to the iron atom via a nitrogen atom in the imidazole/triazole ring. The remainder of the azole molecule binds to the apoprotein in a manner dependent on the individual azole's structure.[14,18] The exact confirmation of the active site differs between fungal species and amongst the many mammalian P450 mono-oxygenases.[14,18] For ITZ specifically, the N4 of the triazole ring moiety interacts

with the heme group of 14LDM, preventing coordination of the molecular oxygen required to initiate oxidation (Figure 4).[14]

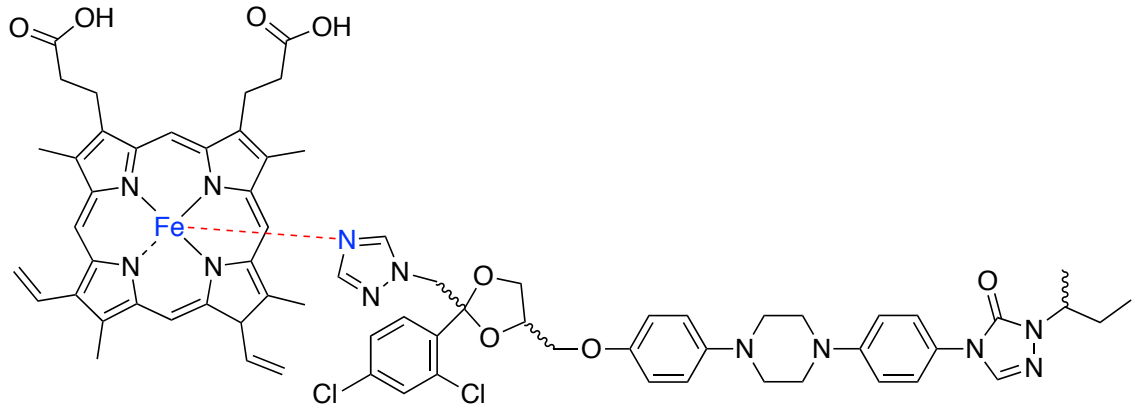

Figure 4. Mechanism of Action: Antifungal Activity

While ITZ is FDA-approved and has been studied for many years, it still contains a few properties that are not considered to be "drug-like". While important for its antifungal activity, the triazole moiety of ITZ is able to coordinate with CYP3A4, which leads to drug-drug reactions and adverse side effects.[21] If ITZ is going to be repurposed for a disease such as cancer, there should be minimal side effects/drug-drug interactions as cancer patients are often on a multi-drug treatment regimen to both treat the cancer and maintain comfort. Second, ITZ is a rather large compound with a molecular weight over the typical threshold of small molecule therapeutic agents (< 500 g/mol). Lastly, ITZ is poorly soluble with a solubility of 1 ng/mL in H_2O at pH 7.[22,23,24] If ITZ is going to be utilized as an anticancer chemotherapeutic agent, it must be evaluated and deemed safe in cancer patients.

1.2.2 Repurposing Screen Results

A library of ~2,400 FDA-approved and post-phase I drugs was screened for Hh pathway inhibition.[9] This screen utilized a reporter cell line Shh-light which contains a

stably integrated Gli-luciferase reporter that responds to stimulation by ShhN, the active form of sonic hedgehog (SHH) signaling protein. This screen yielded a few hits including microtubule inhibitors (vinca alkaloids), which are cytotoxic and were not further explored.[9] In addition, ITZ inhibited the Hh pathway (IC_{50} = ~690 nM) and as a result, a few more azole antifungals were evaluated for this novel biological activity. Results concluded that the azole antifungals as a class did not inhibit the Hh pathway (Table 3).[9]

A library of 2,604 FDA-approved and phase II compounds were screened in an endothelial cell proliferation assay to explore potential angiogenesis inhibitors.[10] This assay was performed in a 96 well plate with human umbilical vein endothelial cells (HUVECs) with a final drug concentration of 10 μM. Cells were incubated for 36h and proliferation was measured with [^{3}H]-thymidine for the final 8h of incubation.[10] Preliminary screen results identified 210 drugs with at least 50% inhibition at 10 μM. Some hits were excluded due to cytotoxicity and some were excluded due to being topical agents.[10] ITZ inhibited VEGF-induced proliferation (IC_{50} = 0.16 μM) and as a result, a few more azole antifungals were explored for this novel biological activity. Results concluded that the azole antifungals as a class did not inhibit angiogenesis (Table 3).[10]

Table 3. Results from High Throughput Screens[9,10]

Azole	IC_{50} Hh Pathway	IC_{50} Angiogenesis
Itraconazole	0.69 μM	0.16 μM
Ketoconazole	9.2 μM	10.4 μM
Miconazole	12.0 μM	2.47 μM
Fluconazole	> 100 μM	> 100 μM

2. Hedgehog (Hh) Pathway

The Hh pathway is an embryonic developmental cell-signaling cascade that plays a role in cell differentiation, tissue growth, and tissue patterning (Figure 5).[25] While the pathway is generally quiescent in healthy adults, it is required for the homeostasis of stem cell populations in the skin and the central nervous system (CNS). Aberrant regulation of the Hh pathway leads to constitutive activation which results in abnormal cell proliferation and tumor growth most notably associated with basal cell carcinoma (BCC) and medulloblastoma (MB).[25]

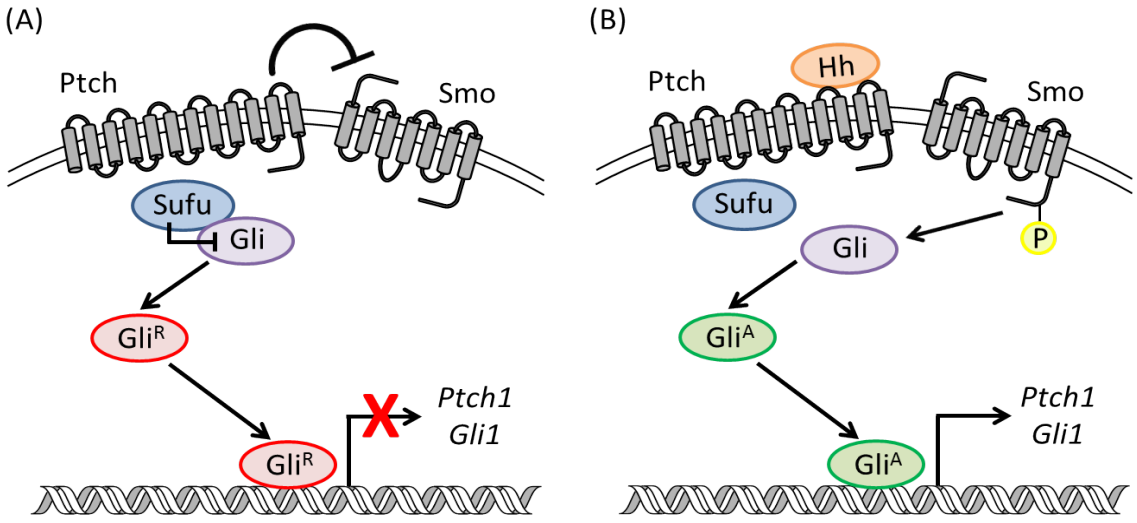

Figure 5. (A) Inactive and (B) active form of the Hh pathway[25]
Reused with permission from John Wiley and Sons

The Hh pathway is regulated by the 12-transmembrane (TM) cell surface receptor, Patched (Ptch) and the 7-TM G-protein coupled receptor (GPCR)-like protein, Smoothened (Smo). In the absence of Hh ligand, Ptch suppresses Smo through a complicated mechanism that is not well understood (Figure 5A). In this state, a heteroprotein complex is formed between Suppressor of Fused (Sufu) and the glioma

(Gli)-associated oncogene family of zinc-finger transcription factors.[26–28] This complex remains in the cytosol where Sufu serves as a negative regulator of Gli by promoting a series of phosphorylation events (PKA, GSK-, and CK1) leading to the proteosomal cleavage of Gli to the N-terminal truncated form (Gli^R). Sufu confiscates the unprocessed cytosolic Gli and only the inactive transcriptional repressors Hh target genes are able to travel to the nucleus.[26–28]

In the presence of Hh ligand (Sonic Hh [SHh], Indian Hh [IHh], and Desert Hh [DHh], Ptch removes its suppression on Smo (Figure 5B). Smo is then able to migrate to the primary cilium where it inhibits the phosphorylation of the Gli-Sufu complex.[26–28] This allows for the formation of full length Gli^A proteins that travel to the nucleus and induce the transcription of Hh target genes. Typical Hh target genes include: PTCH, GLI1, Cyclin D, Cyclin E, Wnt, N-Myc, VEGF, BCL2, SNAIL, ELK1, MSX2, osteopontin, BMI1, and NANOG.[26–28]

2.1 The Hedgehog Pathway and Cancer

Aberrant Hh pathway activity may lead to unwanted cell proliferation and tumor growth most commonly seen in basal cell carcinoma (BCC) and medulloblastoma (MB). Hh pathway dysregulation arises from mutations in Ptch, Smo, or Sufu. For instance, in sporadic BCC cases, mutations include *Ptch1* (~75%), *Smo* (10%), and *Sufu* (~5%).[26,29,30] Cancers resulting from Hh pathway dysregulation have been categorized by either being Hh ligand independent or Hh ligand dependent (Type I and Type II cancer, respectively). Ligand independent aberrant Hh activity can be attributed to loss-of-function mutations in Ptch or Sufu and/or gain-of-function mutations in Smo.[26,27] Ptch mutations include deletions, insertions, or nonsense mutations, which result in loss of

function. Ptch loss of function results in aberrant up-regulation of the Hh pathway, as Smo is no longer repressed even in the "off-state". Loss of function Ptch mutations are commonly seen in Gorlin Syndrome, which predisposes a patient to cancers such as BCC, MB, and rhabdomyosarcoma.[26,27] Smo mutations result in gain of function; Active Smo would result in up-regulation of the Hh pathway as it can continuously generate active forms of Gli leading to increased transcription of Hh target genes. Smo gain of function mutations are typically associated with sporadic BCC and other skin abnormalities.[26,27]

Cancers can also result from aberrant Hh pathway activity that arises from abnormalities regarding Hh ligand. Constitutive pathway activation results from a continuous receiving of Hh ligand.[26,27] This phenomenon can be divided into three different models: autocrine-juxtacrine model, paracrine model, and reverse paracrine model. The autocrine-juxtacrine model involves Hh ligand being secreted and absorbed by the same or adjacent tumor cells; this leads to tumor growth.[26,27] The paracrine model involves Hh ligand being secreted from tumor cells and interacting with normal cells; this leads to angiogenesis and metastasis. Lastly, the reverse-paracrine model involves Hh ligand being excreted from normal cells and interacting with cancer cells.[26,27]

2.1.1 Basal Cell Carcinoma

Basal cell carcinoma (BCC) is the most common form of skin cancer affecting 4 million US residents annually.[31] This cancer arises from the basal layer of the epidermis and usually develops on skin that is exposed to the sun. This skin cancer grows slowly and rarely spreads to other parts of the body. If left untreated, BCC can grow wide and

deep resulting in destroyed skin, tissue and bone.[31] Treatment options for BCC depend on the tumor's size and location as well as the patient's age and general health. All treatment options are effective and include surgery (curettage + electrodessication, excision, and Mohs surgery), radiation therapy, cryotherapy, and chemotherapy (vismodegib and sonidegib). With early diagnosis and treatment, recurrence-free cure rates are between 85-95%.[31,32]

2.1.2 Medulloblastoma

Medulloblastoma (MB) is a cancerous tumor also known as cerebellar primitive neuroectodermal tumor (PNET) that originates in the posterior fossa, the lower rear region of the brain (Figure 6). These tumors rapidly grow in the cerebellum, a part of the brain that is important for balance, posture, and complex motor functions.[33,34] MB tumors have the potential to spread to other regions of the brain or to the spinal cord. It accounts for less than 2% of all primary brain tumors and 20% of childhood brain tumors.[33,34] About 400 children are diagnosed with MB in the United States each year. It is the most common malignant brain tumor in children 4 and under and is the second most common malignant brain tumor in children between the ages of 5-14 years of age.[33,34] It is slightly more common in males over females. About 70% of all MBs are diagnosed in children under 10 and the median age of diagnosis is 7 years old. MB is not common in adults and very few children under 1 receive a diagnosis.[33,34]

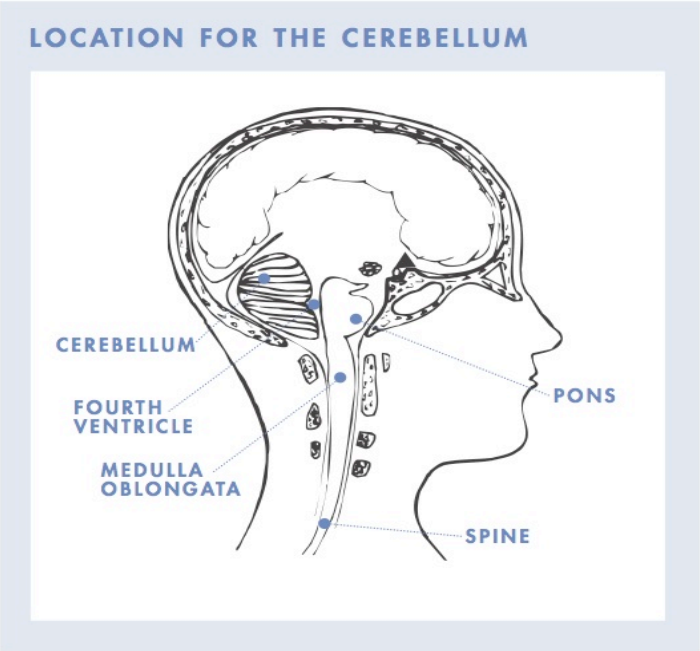

Figure 6. Location of MB Tumors in Brain [33]

Types of MB

MB is considered to be an "embryonal" cancer arising from immature cells. Embryonal tumors are typically pink/purple-gray masses. MB tumors are not all the same and vary histologically. While this is not necessarily important for prognosis, it is important to note that MB should not be considered a single disease but rather a group of different diseases.[33,34] Classic MB tumors contain tissue that is densely packed and have small round cells with large dark nuclei. Desmoplastic nodular medulloblastoma contains scattered densely packed tumor cells mixed with looser-packed cells. MB with extensive nodularity is similar to desmoplastic nodular MB but has more pronounced nodularity. Large-cell MB consists of tumor cells with large round nuclei.[33,34] Anaplastic MB contains tumor cells with increased proliferation and abnormally shaped nuclei. It is

important to make note that sometimes these histological variants co-exist (Figure 7).[33,34]

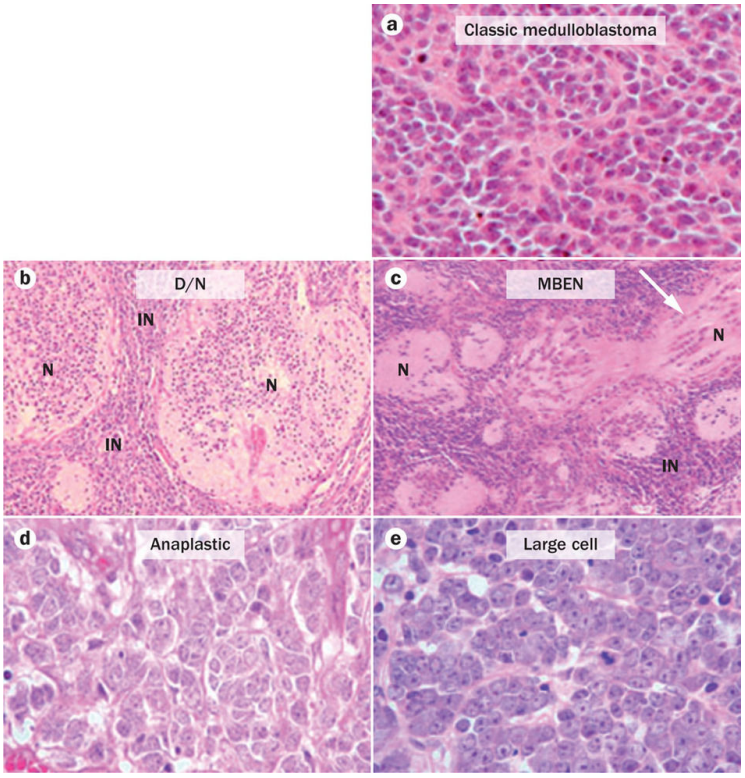

Figure 7. Histological MB Types[35]
Reused with permission from Nature Publishing Group

Genetic subtypes of MB will eventually be important as oncologists predict this will declare route of treatment. MB treatment may become more targeted based on what genetic abnormality is resulting in tumor growth.[33,34] There are currently four different subtypes of MB: WNT, SHH, Group 3, and Group 4. Each subgroup targets a different age of children/adults and may have a different prognosis and survival rate (Figure 8).[33,34] WNT and SHH subtypes are named specifically for the cellular pathway that affects the tumor; Group 3 and Group 4 are more broadly labeled as a distinct pathway has not been found to cause tumor growth to date.[33,34]

The first group of MB is termed WNT. About 10-15% of patients suffer from this subgroup of MB. The average age of diagnosis is 10 years of age and it is the only subgroup that is more common in girls than boys.[33,34] Tumors typically are located in the fourth ventricle of the posterior fossa. Tumors have been found to accumulate a protein, β-catenin, in the nucleus; this results in the activation of the WNT pathway.[33,34] The WNT pathway is a cell-signaling cascade that has been found to play a role in tumor growth. Patients with this subtype of MB have an excellent outcome.[34,33]

The second type of MB is named SHH and affects about 25% of MB patients. It is more prominent in children under 5 years of age and over 16 years of age. This subtype is typically caused by aberrant Hh pathway activity.[33,34] Tumors are generally located in the body of the cerebellum and the tumor can grow on the sides of the organ. Survival rate for this subtype depends on the metastatic rate at time of diagnosis, histology type of tumor, and age of patient at diagnosis.[33,34]

An increased copy of the growth gene MYC generally categorizes group 3 MB. Like SHH, it affects 25% of MB cases. It primarily affects children between the ages of 1-10 years of age and is almost never seen in adults.[33,34] There is often metastasis at the time of diagnosis and the tumor is generally located in the fourth ventricle like WNT subtype MB. The histology type is most commonly large cell/anaplastic.[33,34] Group 3 subtypes have the worst survival rate among all of the MBs; this survival rate depends on the metastatic state at time of diagnosis and the age of patient at diagnosis.[33,34]

Group 4 is the most common subtype of MB accounting for 35-40% of cases. It occurs in all ages but is most prevalent during mid-childhood. Tumors are located in the fourth ventricle similarly to Group 3 and WNT subtypes.[33,34] The hallmark of this

subtype is abnormalities in chromosome 17. If the cancer does not spread, 5-year survival rates with standard therapy are 80% however, with metastasis this drops to 60%.[33,34]

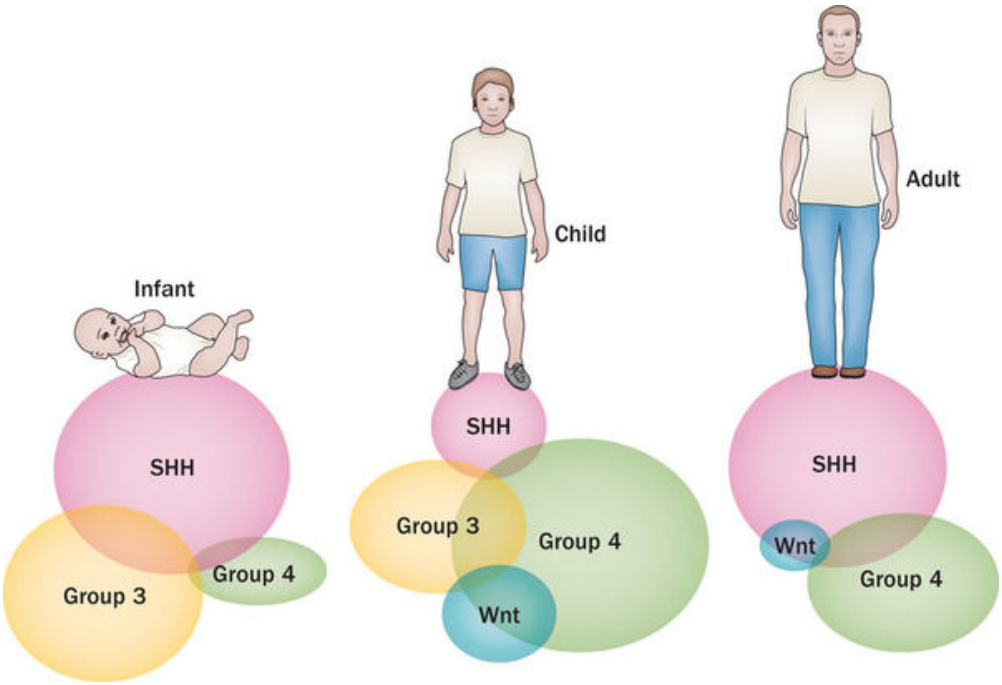

Figure 8. MB Subgroup Prevalence[35]
Reused with permission from Nature Publishing Group

Current Treatment of MB

Current treatment for MB consists of surgery followed by high-dose chemotherapy and radiation. Treatment plans are individualized based on the risk of tumor occurrence.[33,34] This risk is based on the amount of metastasis and the amount of tumor remaining post-surgery. For instance, in pediatric MB, "high" risk patients are less than 3 years of age, have a tumor volume of 1.5 cm^2 post-surgery, and have metastasis.[34,33]

Surgically removing the tumor is an important part of treating MB. The obvious goal is to remove the entirety of the tumor, but sometimes this is not possible as a result

of where the tumor has grown.[33,34] In a third of MB patients, the tumor grows into the brain stem; attempted removal of this tumor type would result in neurological damage. The goals of this initial surgery are to remove as much of the tumor as possible without causing neurological damage, to obtain a tissue sample for diagnosis, and to relieve cerebrospinal fluid buildup caused by tumor growth and swelling.[33,34] Glucocorticosteroids (decadron, dexamethasone) are used before and during surgery to reduce swelling in the tumor. Technological advances have aided in this step of treating MB. MRI scanning and computer-aided navigation tools help with mapping the tumor removal before surgery.[33,34] High powered microscopes, ultrasounds, and gentle suction devices are necessary for tumor removal. MRI scanning is either performed right after surgery or days after surgery to determine how much tumor was resected.[33,34]

After surgery, MB is treated with radiation therapy. Even after removal of the tumor, cancer cells remain in the surrounding brain tissue. If not killed with radiation, these cells can spread and lead to cancer regrowth.[33,34] Radiation to the brain/spinal cord can damage a developing brain and this is important to consider, as MB patients are typically children. Therefore, this form of therapy is not used in children under the age of 3 and caution is used in patients between the ages of 3-7 as they are at the highest risk of neurocognitive defects as a result of radiation.[33,34] On average, radiation therapy is given 5 days a week for 6 weeks. Extra radiation is given to the site where the tumor was removed due to increased risk of tumor growth.[33,34]

Chemotherapy is described as the use of powerful chemicals to kill cancer cells after surgery and radiation therapy. These drugs halt tumor regrowth and the spread of cancer metastatically.[33,34] MB patients fare better with radiation but some children that

are too young to get radiation rely on chemotherapy alone. Chemotherapy generally consists of a cocktail of drugs that target cell death at different cycles of cell growth. The drugs that are mainly used for MB are vincristine, cisplatin, carboplatin, cyclophosphamide, and lomustine (Figure 9).[33,34] These drugs are administered in cycles with each cycle differing between 3-4 weeks; this allowed the body to recover after being administered these harsh chemicals. The cycle length and amount of cycles depends on the severity of the cancer and the age of the patient.[33,34]

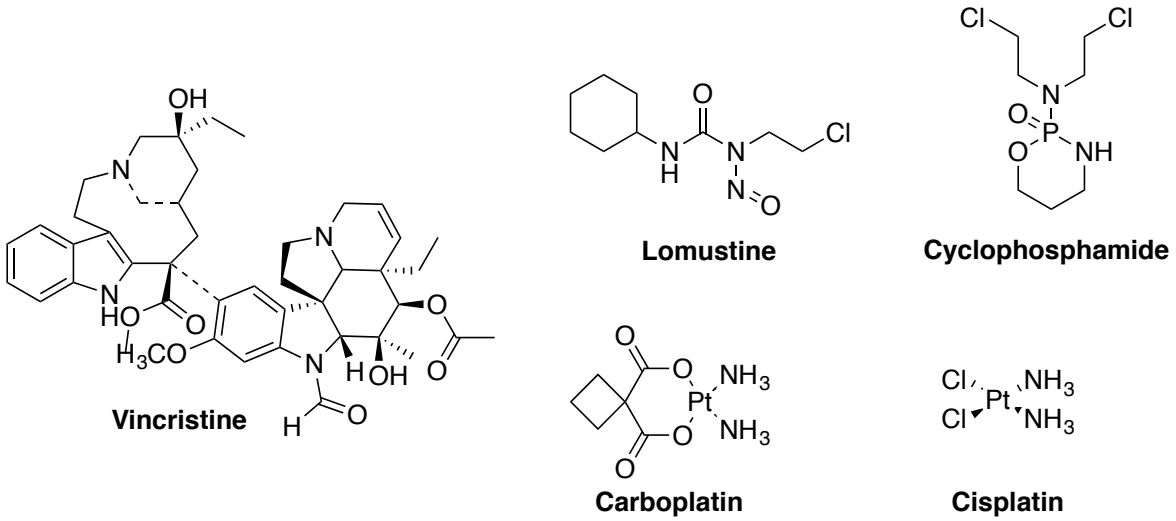

Figure 9. Structures of Common Chemotherapeutic Agents

Side Effects

Unfortunately, side effects are evident due to this harsh treatment regimen combining major surgery, radiation, and chemotherapy. In terms of surgery, about 25% of children experience loss/delay of speech 6-24 hours after waking up; this is referred to as "posterior fossa mutism syndrome."[33,34] A small percentage of children have abnormal speech and unsteadiness years after surgery. Radiation short-term side effects include: fatigue, loss of appetite, nausea, sore throat, difficulty swallowing, and hair loss.[33,34] Long-term side effects include: lower intellectual ability, attention deficit,

and memory loss. Younger children are more prone to these long-term side effects as their brains are still developing. Radiation can also affect the hypothalamus and pituitary gland, which regulate hormones for bodily function and growth.[33,34] This can lead to issues with obesity and hypothyroidism. Generally, children can be treated with growth hormone replacement therapy. Radiation can also cause short stature and scoliosis as the spinal cord is very close to the site of tumor growth. In terms of chemotherapy, short-term side effects are very similar to those of radiation: hair loss, nausea, vomiting, fatigue, and weakness.[33,34] Long-term side effects include early onset lung, heart, and kidney disease as well as the development of secondary cancers such as leukemia. Hearing loss is a direct side effect of the chemotherapeutic agent cisplatin; as this drug is crucial towards MB treatment, additional drugs are currently in development for administration with cisplatin to limit hearing loss.[33,34]

2.2 Established Smo Antagonists

Smo became a popular drug target after the discovery of the first Smo inhibitor, cyclopamine, a naturally occurring alkaloid. While cyclopamine exhibited poor pharmacokinetic properties, it was utilized in the exploration of Hh pathway function and subsequent tumor growth.[36] To date, Smo has been identified as the most druggable target for the development of small molecule Hh pathway inhibitors; each of the Hh pathway inhibitors that have advanced into clinical trials is a direct Smo antagonist (Figure 10).[28] Curis and Genentech co-developed the first small molecule Smo antagonist to enter clinical trials and ultimately gain FDA approval for the treatment of advanced basal cell carcinoma, vismodegib (GDC-0449/Erivedge™). Erismodegib/Sonidegib (NVP-LDE225) was originally identified and developed at the

Novartis Institute for Biomedical Research and has recently been FDA-approved for locally advanced basal cell carcinoma.[11,37] A medicinal chemistry program at Pfizer resulted in the identification and development of PF-04449913 as a potent Smo antagonist that exhibits favorable pharmacological and pharmacokinetic (PK) properties in vitro and in vivo.[38] PF-04449913 is currently being evaluated in multiple Phase I and Phase II studies for the treatment of both acute myeloid leukemia and myelodysplastic syndrome.[11] Exelixis and Bristol-Myers Squibb collaborated to develop XL-139/BMS-833923, which has been studied in Phase I and II trials as both a single agent and in combination regimens (Dasatinib, carboplatin, cisplatin, etoposide, and more) for the treatment of a variety of human cancers including chromic myeloid leukemia and extensive small cell lung cancer.[11,39] Eli Lilly has also advanced a small molecule Smo antagonist, LY2940680 (Taladegib) into Phase I and II trials for pediatric medulloblastoma, rhabdomyosarcoma, and small cell lung cancer; it is also in phase II clinical trials in combination with paclitaxel, carboplatin, and radiation.[11,40] Due to the well-established nature of these compounds as Hh pathway inhibitors, each of them has been extensively reviewed elsewhere and their path to clinical candidacy will not be detailed further.[41,26,27,42,43]

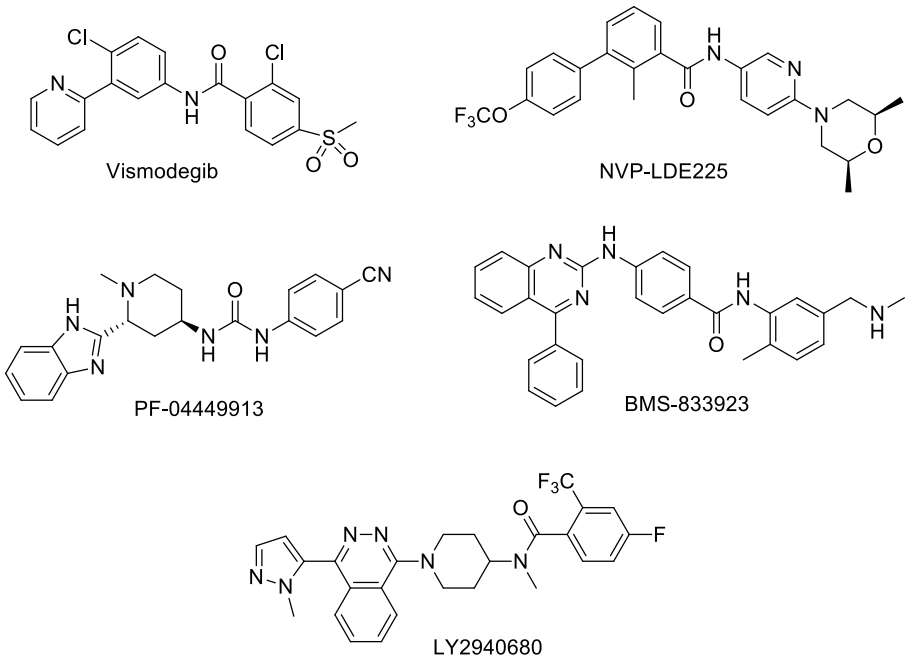

Figure 10. Structures of Established Smo Antagonists

Table 4. Clinically Relevant Synthetic Smo Inhibitors.[26]

Compound	IC_{50} Wild-Type Smo	IC_{50} D473H Smo	Development Status	References
GDC-0449	3-22 nM**	Loss of activity	Clinically approved	[11, 44]
NVP-LDE225	2.5 nM	Loss of activity	Clinically approved	[11,37,45]
PF-04449913	5 nM	ND	Clinical (Phase II)	[11, 38]
BMS-833923	21 nM	ND	Clinical (Phase II)	[11, 46]
LY294068	2.4 nM	Active*	Clinical (Phase II)	[11, 47]

ND: Not determined/reported
*****Specific IC_{50} values were not provided
**Dependent on cellular assay

A major challenge for the continued advancement of small molecule Hh pathway inhibitors towards clinical efficacy is the development of multiple mechanisms of resistance to these Smo antagonists.[48] An unsuccessful clinical trial for vismodegib in an MB patient resulted in the discovery of a clinically relevant Smo mutant (D473H)

(Table 4). This point mutation in Smo rendered the patient insensitive to further treatment with vismodegib.[49,50,51] Additional point mutations in Smo have been identified (H231R, W281C,Q477E, V386A, V321M, I408V, C469Y, T241M) to confer resistance in patients receiving vismodegib for the treatment of advanced BCC.[52,53,54] Half of the vismodegib-treated patients that experienced a relapse in BCC were found to have a Smo mutation. Similar Smo mutations that result in constitutive pathway activation were identified in a preclinical Hh-dependent MB murine model upon treatment with sonidegib.[55] Other mechanisms of Smo antagonist resistance include direct activation of Gli downstream, induced expression of p-glycoprotein, and chromosomal amplification of *GLI2* and *SUFU.*[53,54,55,56,57,48] These results highlight a therapeutic need to determine small molecule Hh pathway inhibitors that maintain potent inhibitory activity in the presence of wild-type Smo and mutant forms of Smo.

While many universities and industrial laboratories are searching for Smo-wild type and Smo-mutant antagonists, there are many other drug targets within the Hh pathway that are less popular in the drug discovery community. The focus on targeting Smo has offered some information regarding limitations.[58] First, Smo inhibitors are characterized by their structural moieties. If one compound succumbs to resistance, the whole class of compounds may result in resistance. Second, there is evidence emerging that the downstream components in the Hh pathway may be compensating for upstream inhibition. There are many oncogenic-cell signaling pathways that interact with the Hh pathway: TGF- β, RAS/RAF/MEK/EK, and PI3K/AKT/Mtor.[58] Gli transcription factors are regulated by other pathways such as TGF-β.[58] Therefore, if vismodegib is inhibiting Smo, Gli transcription activity can still take place if another

pathway is simultaneously producing Gli transcription factors. This crosstalk between Hh pathway and other oncogenic signaling pathways exemplifies an additional need for the exploration of downstream Hh inhibitors.[58]

2.3 Recently Disclosed Smo Antagonists

The emergence of resistance towards vismodegib influenced Novartis to identify a series of pyridazines as second-generation Hh inhibitors that remain potent in the presence of Smo mutant D473H. The most active compound identified through this process, NVP-LEQ506, inhibits Hh signaling in vitro against both wild-type and mutant Smo (IC_{50} values = 1 and 96 nM, respectively) (Figure 9).[59] NVP-LEQ506 reduced Gli mRNA expression and promoted tumor regression in a murine Hh-dependent MB allograft following oral administration (10-40 mg/kg, q.d. dosing).[59] Preclinical in vivo PK studies for NVP-LEQ506 resulted in a good bioavailability profile, low clearance, and the ability to cross the blood-brain barrier.[59]

The Scripps Research Institute, Novartis, and Harvard University collaborated on efforts to identify Hh inhibitors that maintain activity in the presence of wild-type and mutant forms of Smo.[60] Both ALLO-1 and ALLO-2 were discovered via a high-throughput screen of ~50,000 compounds from Maybridge and ChemDiv libraries (Figure 11). Both ALLO-1 and ALLO-2 inhibit Hh signaling in Smo agonist (Hh-Ag1.5) stimulated TM3-Gli-Luc cells, a stable clone of mouse TM3 cells expressing the Gli-luc reporter construct (IC_{50}= 50 nM and 6 nM, respectively).[60] This Hh inhibition was further confirmed in a secondary Gli-luciferase reporter assay utilizing TM3-Gli-Luc cells stimulated with recombinant ligand ShhN (ALLO-1 IC_{50}= 320 nM and ALLO-2 IC_{50}= 39 nM) as well as in a mouse Gli1 expression assay that utilized both human HEPM and

NIH3T3 cells (ALLO-1 IC_{50}= 805 nM and ALLO-2 IC_{50}= 40 nM.)[60] Both compounds inhibited cell proliferation in ShhN stimulated mouse cerebella granule neuron progenitors (CGNPs) (ALLO-1 IC_{50}= 410 nM and ALLO-2 IC_{50}= 22 nM) and *Ptch1*$^{+/-}$*p53*$^{-/-}$ mouse medulloblastoma cells (IC_{50}= 0.47 μM and 0.12 μM, respectively).[60] Due to structural similarity to several kinase inhibitors, ALLO-2 was screened for inhibitory activity against a panel of kinases. ALLO-2 did not show inhibitory activity in the presence of these kinases indicating its specificity for the Hh pathway. A multitude of in vitro assays were utilized to try and determine a mechanism of action for both ALLO-1 and ALLO-2.[60] Neither compound inhibited the Hh pathway following treatment with Sufu-specific siRNA confirming that ALLO-1 and ALLO-2 act upstream within the Hh signaling cascade. Both compounds successfully competed with BODIPY-cyclopamine for binding to murine Smo over-expressed in CHO-K1 cells, indicating that they form direct binding interactions with Smo (ALLO-1, IC_{50} = 140 nM and ALLO-2, IC_{50} = 2.8 nM).[60] Interestingly, while ALLO-2 demonstrated competitive characteristics with [^{3}H]cyclopamine at concentrations comparable to its displacement of BODIPY-Cyc in reporter assays, ALLO-1 did not compete with [^{3}H]cyclopamine. These results suggest that the binding site of ALLO-1 might reside in a pocket adjacent to the Cyc binding site where the BODIPY interacts with Smo.[60] Finally, both ALLO-1 (IC_{50} = 1 μM) and ALLO-2 (IC_{50} = 83 nM) were capable of inhibiting the murine homolog of Smo D473H (D477G) overexpressed in the TM3-Gli-Luc cell line with only a slight reduction in potency compared to wild-type Smo.[60]

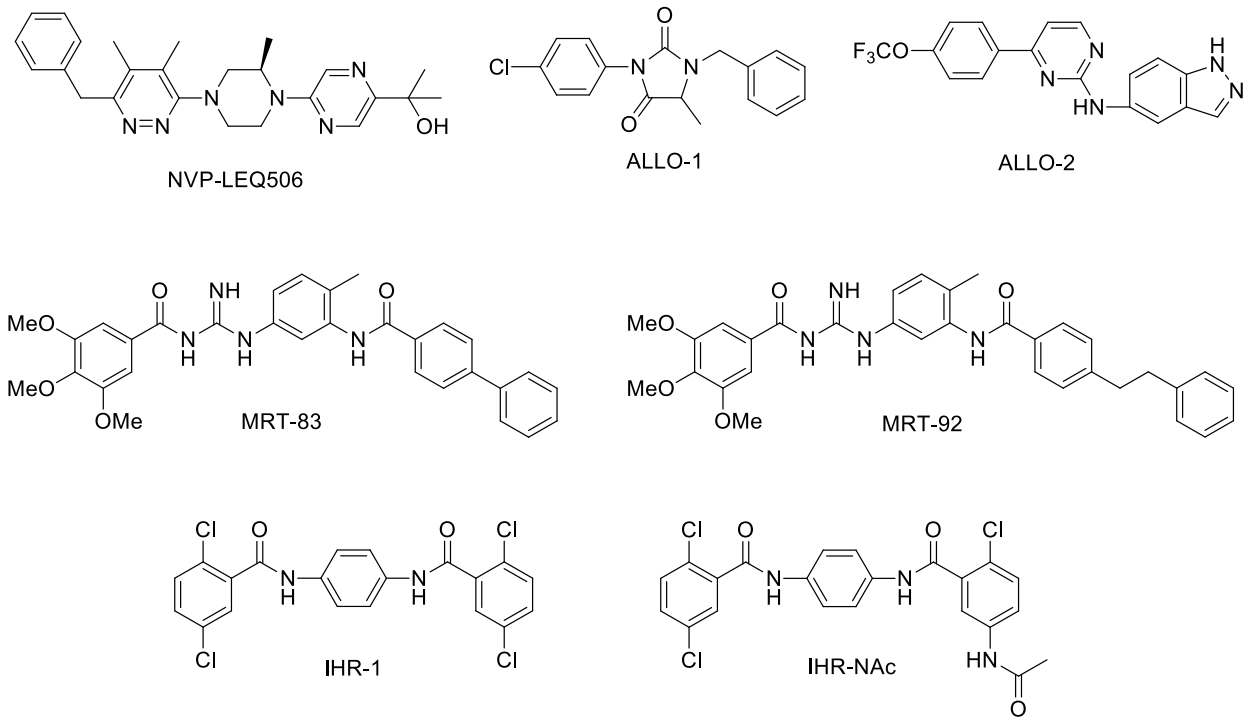

Figure 11. Smo Antagonists

Utilizing a cell based screen, researchers at the University of Texas Southwestern Medical Center identified a series of small molecule Hh pathway inhibitors.[61] Several compounds were identified as potent inhibitors of the Hh signaling pathway (IHR-1 – IHR-7) with IC_{50} values ranging from 7.6 – 200 nM [62] (Figure 11). In a competition assay with BODIPY-Cyc utilizing Smo over-expressed Cos-7 cells, all IHR compounds demonstrated binding to Smo. The most potent of these compounds, IHR-1 (IC_{50} = 8.9 nM) further demonstrated the ability to prevent translocation of Smo to the primary cilia and also exhibited down-regulation of endogenous expression of Gli mRNA in *PTCH1*$^{-/-}$ cells.[61] Interestingly, IHR-1 was significantly less active in the presence of SAG, a small molecule Smo agonist (IC_{50} > 10 μM). Follow-up studies demonstrated that IHR-1 is cell impermeable and is unable to compete with SAG for Smo binding when the receptor is within the cell. An acetylated version of IHR-1, IHR-NAc,

demonstrated enhanced cell permeability and was significantly more active against Hh signaling when the pathway is upregulated with SAG (IC_{50} = 19 nM).[61] These results strongly suggest that Smo antagonists may not be exhibiting maximum results due to potential cell impermeability and subsequent inability to reach all cellular Smo populations.[61]

Researchers at the Centre National de la Recherche Scientifique utilized a combined molecular modeling and virtual screening approach to design, synthesize, and evaluate multiple generations of Smo antagonists consisting of acylureas, acylthioureas, and acylguanidines.[63,64] After comprehensive medicinal chemistry of these molecular scaffolds, acylguanidine MRT-83 was identified as a potent Hh pathway inhibitor (IC_{50} value = 15 nM), with the ability to displace BODIPY-Cyc from Smo (IC_{50} = 5 nM).[64] Molecular docking studies of MRT-83 with several conformations of murine Smo suggested that MRT-83 bound to a cleft-opened conformation of Smo and that further extension of the biaryl moiety would provide enhanced interactions between the scaffold and binding pocket.[65] Based on these computational results, a series of elongated MRT-83 derivatives were synthesized and evaluated for Hh pathway activity. The most potent of these analogues, MRT-92, is a potent inhibiter of Hh signaling (IC_{50} = 6 nM) (Figure 11), prevents Smo accumulation in the primary cilia, and displaces BODIPY-Cyc from human Smo in vitro. Binding studies with a tritiated analogue of MRT-92 demonstrated that the compound binds comparably to both wild type and mutant (D473H) Smo (K_i values for both forms of Smo = 0.7 nM).[65] There have been extensive binding studies between several Smo antagonists (including MRT-92) and various Smo mutants, which account for its ability to retain binding affinity to Smo

D473H and potentially provide a new binding mechanism to be considered for the development of Smo antagonists.[65]

2.4 Novel Smo Antagonist Scaffolds

Combining structural features of ALLO-2, LDE-225, and BMS-833923 lead to a novel series of Smo antagonists consisting of the *N*-(2-pyrimidinylamino)benzamide scaffolds. Researchers at Jiangsu Simcere Pharmaceutical designed this series by incorporating a 4-(trifluoromethoxy)phenyl moiety of LDE-225 and ALLO-2 (A), a pyrimidinylamino moiety of ALLO-2 (B) and a biaryl amide functionality of BMS-833923 (C and D) into a single scaffold (Figure 12). An initial screen of these novel hybrid compounds identified compound **1** as a potent Hh pathway inhibitor (IC_{50} values = 1.3 nM) (Figure 12).[66]

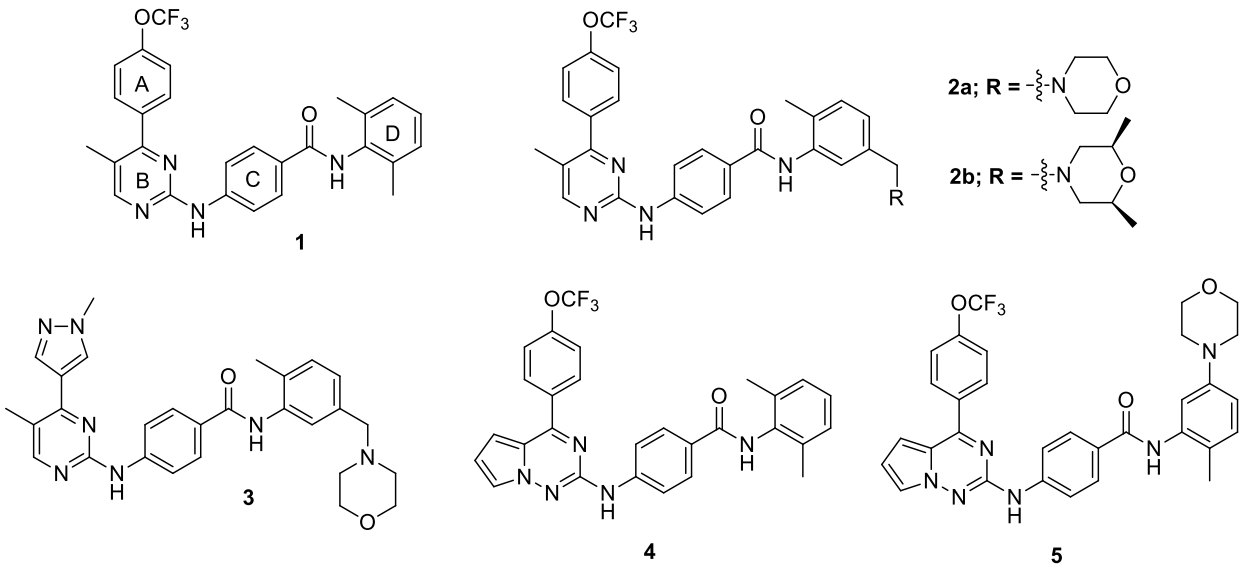

Figure 12. Synthetic Smo Antagonists

This novel scaffold was further explored in order to determine the optimal functionality for potent Hh pathway inhibition. Each region of the scaffold (A-D) was modified to generate a series of *N*-(2-pyrimidinylamino)benzamide analogues that were

evaluated for their ability to inhibit Hh signaling in a luciferase assay utilizing NIH3T3 cells stably transfected with Gli-reporter construct.[66] Structure-activity relationship (SAR) results for region A suggested that a single electron-withdrawing substituent (-OCF_3, -CN, -F) in either the *ortho*- or *para*- position of a phenyl ring was important for optimal Hh inhibition. The incorporation of various heteroaryl functionalities was also well tolerated in this region. SAR results for region B determined that small hydrophobic groups at either position 5 or 6 of the pyrimidinyl moiety retain potent activity.[67] It is important to note that removal of the N-1 of the pyrimidinyl ring was detrimental to Hh inhibition. SAR studies for the benzamide phenyl ring, region D, demonstrated that a wide range of functionalities was tolerated in this portion of the scaffold; however, a basic amine was required to improve the PK properties of the overall scaffold.[67] From this series, analogues **2a** and **2b** demonstrated potent inhibition of Hh signaling (IC_{50} values = 0.53 and 0.73 nM, respectively) (Figure 12); however, both compounds demonstrated unfavorable PK parameters, presumably due to elevated lipophilicity values (**2a**, *A*log*P* = 7.07 and **2b**, *A*log*P* = 7.37).[67] Further structural modifications were made in an attempt to decrease lipophilicity and to improve the overall drug-like properties of the scaffold ultimately resulted in compound **3**, which demonstrated potent inhibition of Hh signaling (IC_{50} = 1.3 nM) and more favorable PK parameters (*A*log*P* = 3.6) (Figure 12).[67] Preliminary in vivo PK studies for compounds **2a**, **2b**, and **3** identified analogue **3** as having enhanced oral bioavailability.

Researchers at Jiangsu also performed parallel optimization of the *N*-(2-pyrimidinylamino)benzamide scaffold by replacing the pyrimidine ring (B) with a pyrrolo[2,1-f][1,2,4]triazine moiety.[68] This substitution proved promising as the initial

compound in this series (compound **4**) demonstrated potent Hh inhibitory activity with an IC_{50} value of 1.6 nM. A typical SAR approach was undertaken and a series of pyrrolo[2,1-f][1,2,4]triazine benzamide analogues was designed, synthesized, and evaluated.[68] These compounds proved promising in terms of in vitro analysis (IC_{50} values = 0.62-12.3 nM) and several of the most potent compounds were further analyzed in vivo to determine preliminary PK properties. Compound **5** contained the initial *para*-trifluoromethoxy aryl ring and a *meta*-morpholine moiety on ring D, had an IC_{50} value = 0.83 nM, demonstrated good serum concentration (C_{max} = 4185 ng/mL), oral exposure (AUC = 1935 h ng/mL), and half-life ($T_{1/2}$ = 8.34 h) (Figure 12).[68]

Jiangsu further developed a third series of Hh inhibitors developed at Jiangsu that replace the pyridine ring functionality of vismodegib with an amide- or urea-linked phenyl ring.[69] The addition of this spacer was hypothesized to enhance hydrogen-bonding interactions with Smo. The initial compound in this series demonstrated modest inhibition of Hh signaling (IC_{50} = 300 nM) and thus further analogues were designed, synthesized, and evaluated.[69] The most active compounds identified, **6a** (IC_{50} = 100 nM) and **6b** (IC_{50} = 40 nM) were also capable of displacing BODIPY-Cyc from human Smo over-expressed in HEK-293T cells (Figure 13). Compound **6b** exhibited enhanced water solubility and was further evaluated in a variety of in vitro and in vivo model systems. Most importantly, compound **6b** significantly decreased fluorescence associated with Gli-dependent RFP in a transgenic zebra fish model of Hh signaling.[69]

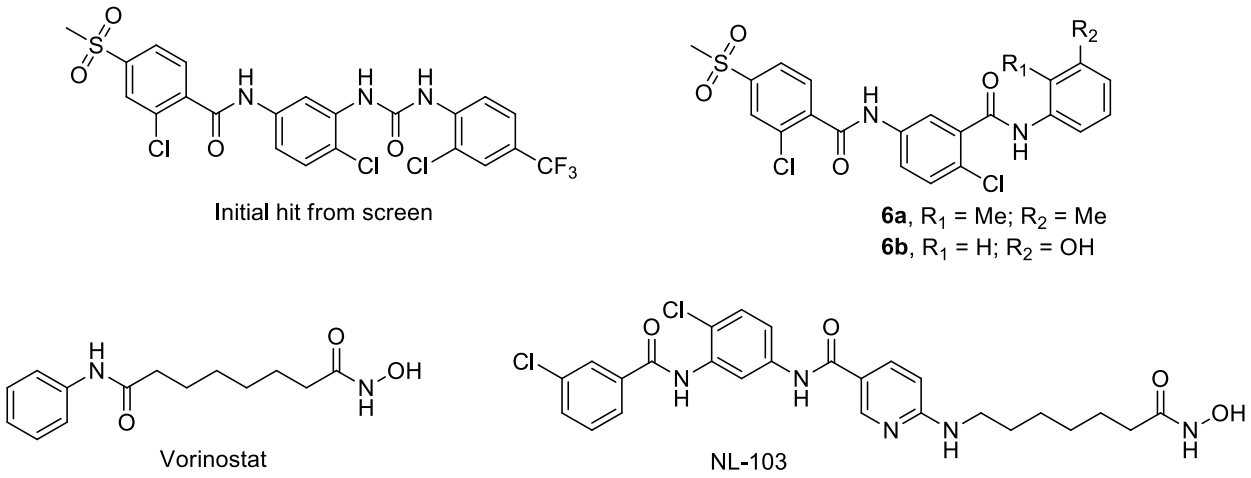

Figure 13. Additional Synthetic Smo Antagonists

A group of researchers at the Chinese Academy of Sciences designed and synthesized a chimeric compound, NL-103, which contains the structural components of both vismodegib and the FDA-approved histone deacetylase enzyme (HDAC) inhibitor, vorinostat (Figure 13).[70,71] This followed strong evidence that HDAC inhibitors exhibited anti-Hh pathway activity. NL-103 potently inhibited Hh signaling in a Gli-reporter cell line (IC_{50} = 19.7 nM) and was capable of displacing BODIPY-Cyc from human Smo overexpressed in HEK293T cells (K_D = 79.6 nM).[71] NL-103 also inhibited HADC1-3 at levels comparable to the FDA-approved vorinostat. Further in vitro evaluation was performed to distinguish vismodegib and vorinostat mediated Hh pathway inhibition. Utilizing Hh-dependent cells, NL-103 was tested for its ability to regulate Gli1, Gli2, and Gli3 mRNA levels.[71] At higher concentrations (1-10 μM) both NL-103 and vorinostat stimulated Gli1 but reduced Gli2 mRNA expression. By contrast, vismodegib demonstrated significant down-regulation of Gli1 at all concentrations evaluated but had minimal effects on Gli2 mRNA expression.[71] These results suggest

that while NL-103 does bind Smo, this binding is non-selective; this scaffold retains significant cellular effects traditionally associated with vorinostat.[71]

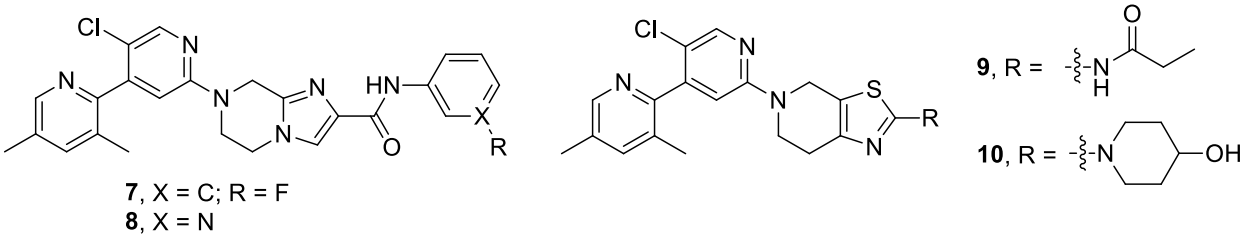

Figure 14. Vismodegib-based Smo Antagonists

Researchers at Soochow University utilized a scaffold hopping approach to design and optimize a series of Smo antagonists based on the combination of known Smo antagonist scaffolds.[72,73,74] Previous reports suggested that the amide bonds of both vismodegib and NVL-LDE225 were not crucial for binding to Smo but where important for linking the aryl regions of these two molecules.[73,74,75,76] It was hypothesized that replacing the amide bond of vismodegib with an alkyl or heteroalkyl ring would reduce planarity and rotatable bonds, resulting in increased solubility, absorption, and metabolic stability.[72] This approach led to the development of two related series of compounds based on either a tetrahydroimidazo[1,2-a]pyrazine or tetrohydrothiazolo[5,4-c]pyridine scaffold.[72,73] An extensive medicinal chemistry effort yielded a variety of substituents on the imidazopyridine moiety: alkyl esters, aryl esters, and amides. Phenyl amides that incorporated an electron withdrawing moiety at the *meta*- or *para*- position demonstrated the most potency.[72] Short alkyl substituents, both straight chain and ring structures, were less active. The most active analogues in this series, **7** and **8**, inhibited pathway signaling (IC_{50} = 87 and 200 nM, respectively) (Figure 14). For the closely related thiazolopyridine scaffold, the most potent compounds

evaluated either contained an ethyl side chain **9** (IC_{50} = 80 nM) or substituted piperidine **10** (IC_{50} = 58 nM) as the substituent (Figure 14).[73] Both of these compounds displaced BODIPY-Cyc from full length human Smo over-expressed in U2OS cells. Preliminary in vivo studies for both **9** and **10** demonstrated promising PK properties similar to those exhibited by vismodegib.[72,73] A comprehensive table of clinically relevant and novel Smo inhibitors is described below (Table 5).

Table 5. Key Synthetic Hh Pathway Inhibitors that Function via Smo.

Compound	IC_{50} Wild-Type Smo	IC_{50} D473H Smo	Reference
NVP-LEQ506	1.0 nM	96.0 nM	[59]
ALLO-1	410 nM	1 μM	[60]
ALLO-2	41 nM	83 nM	[60]
IHR-1	0.01 μM	ND	[77]
IHR-NAc	0.0031 μM	ND	[77]
MRT-92	0.7 ± 0.1 nM	0.7 ± 0.2 nM	[65]
1	1.3 nM	ND	[66]
2a	0.53 nM	ND	[67]
2b	0.73 nM	ND	[67]
3	1.3 nM	ND	[67]
4	1.6 nM	ND	[68]
5	0.83 nM	ND	[68]
6a	100 nM	ND	[69]
6b	40 nM	ND	[69]
NL-103	19.7 nM	Active*	[71]
7	87 nM	ND	[73]
8	200 nM	ND	[73]
9	80 nM	ND	[73]
10	58 nM	ND	[73]

ND: Not determined/reported
*Specific IC_{50} values were not provided
**Dependent on cellular assay

2.5 ITZ and Hedgehog Signaling

The hedgehog (Hh) pathway is an embryonic cell-signaling pathway that is responsible for cell differentiation and tissue growth. There are two main regulating proteins of this pathway: Patched (Ptch) and Smoothened (Smo). As ITZ has been determined to inhibit the Hh pathway, there have been various explorations into how ITZ mediates this anticancer activity. ITZ exhibited similar in vitro results as cyclopamine and cyclopamine mimics including inhibition of Hh signaling in $Ptch^{-/-}$ cells, in cells treated with oxysterols, and in cells over expressing Smo. Because of this, ITZ was originally hypothesized to bind to Smo.[9] However, ITZ failed to compete with BODIPY-

cyclopamine indicating that ITZ does not bind to Smo at the same position as cyclopamine.[9] Additional experiments have been performed in the presence of Smo agonists (SAG) and antagonists (MRT-92); ITZ acts as a non-competitive inhibitor of SAG and is able to inhibit MRT-92 binding to Smo.[65] This evidence suggests that ITZ may be binding to Smo in a distinct manner than other Smo inhibitors. However, the binding mode and way in which ITZ is exhibiting Hh pathway inhibition has not been determined.

In addition to inhibiting the Hh pathway via Smo, ITZ was also found to inhibit the Hh pathway in the presence of vismodegib-resistant mutant Smo^{D477G}.[9,78] Since ITZ acts in a distinct manner from cyclopamine and cyclopamine mimics, it was predicted that ITZ may retain activity in the presence of mutant forms of Smo. In ShhN stimulated $Smo^{-/-}$ mouse embryonic fibroblasts (MEFs) transfected with Smo^{WT} or Smo^{D477G}, ITZ exhibited inhibitory activity (IC_{50}= 270-690 nM and 500 nM, respectively).[9,78] In the presence of Smo^{WT} or Smo^{D477G} expressing MB tumors, ITZ retained similar inhibitory activity (Smo^{WT} IC_{50}= 55 nM and Smo^{D477G} IC_{50}= 62 nM). ITZ was also determined to remain active in the presence of a variety of other Smo mutants (E522K, G457S, S391N, D388N, N223D, L225R).[78] This ability to inhibit the Hh pathway in the presence of wild type Smo and mutant Smo makes ITZ a unique Hh pathway antagonist. As a clinically approved drug, ITZ has a well-known safety profile and has been studied for many years. Taken together, ITZ serves as a promising anticancer chemotherapeutic agent.

3. Angiogenesis

Angiogenesis is described as the formation of new blood vessels. Blood vessels, which are constructed of endothelial cells (ECs), are essential for the distribution of oxygen and nutrients throughout the body. These blood vessels play a major role in embryonic organ growth and development.[79,80] Adult blood vessels are necessary for wound healing, the menstrual cycle, and in the placenta during pregnancy.[81,80] The dysregulation of angiogenesis is a hallmark in a variety of different diseases including cancer, psoriasis, arthritis, and blindness.[79] Angiogenesis is one of the few biological functions that impact the well-being of many people across the world as its presence results in a multitude of ailments; about 500 million people would benefit from therapeutics that modulate angiogenesis.[80] The process of angiogenesis remains complex and involves a large number of cytokines and associated receptors. The step-wise process of forming new blood vessels is thought to consist of multiple signaling pathways including the vascular endothelial growth factor (VEGF) pathway, the mTOR pathway, and the Notch pathway. In healthy adults, a balance between pro-angiogenic and anti-angiogenic molecules tightly regulates angiogenesis.[82,83] Any extreme shift in this equilibrium will lead to uncontrolled angiogenesis, which includes both vascular insufficiency and vascular overgrowth. Various stimuli affect this “angiogenic switch” and include metabolic stress, mechanical stress, immune/inflammatory response, and genetic mutations. In response to these stimuli, the cell releases pro-angiogenic factors and initiates the angiogenic switch.[82,83]

3.1 Pathways Involved in Angiogenesis

The vascular endothelial growth factor (VEGF) receptor family is the most studied in terms of angiogenesis and is responsible for regulating new blood vessel growth. VEGF aids in proliferation and survival of ECs and enhancing vascular permeability. This family includes VEGF A, B, C, D, E, and placental growth factor 1 and 2 (PIGF-1 and PIGF-2). VEGF molecules signal through tyrosine kinase receptors, vascular endothelial growth factor receptors (VEGFR1-3).[84–86] Out of the three isoforms, VEGFR2 is responsible for effects that are directly related to angiogenesis. VEGF is produced by cancer cells and results in tumor metastasis seen in a number of different types of cancers. In cancer, VEGF is induced by a number of pathophysiological factors such as hypoxia, low oxygen tension. After release of VEGF, it can trigger more cellular pathways such as JAK-STAT, Erk/MAPK, and PI3K/Akt, which are involved in DNA synthesis/cell growth and cell survival.[62,84,85,86]

Platelet derived growth factor (PDGF) is an essential protein for blood vessel maturation. It plays a role in the development and differentiation of blood vessel walls. PDGF interacts with VEGF and it is believed that these pathways converge and exhibit activity such as the stabilization and formation of new blood vessels.[84–86] It is also hypothesized that PDGF is activated to overcome resistance acquired from VEGF inhibition. There are four isoforms of PDGF (A-D) and two isoforms of receptor PDGFR (a-b). Ultimately, activation of the PDGF pathway leads to downstream signaling of the PI3K/Atk pathway and subsequent interactions with MAPK molecules, Src proteins, phospholipase C-gamma, Ras protein, STAT proteins, and guanine-5'-triphosphate (GTPase)-activating protein.[62,84,86,85]

The fibroblast growth factor (FGF) pathway has been extensively studied as an embryogenesis pathway. There are 23 isoforms of FGF protein and 5 receptor isoforms. FGF receptors contain an extracellular immunoglobulin (Ig)-like domain and an intracellular tyrosine kinase domain. Ligand binding to receptor causes a dimerization of receptors and an intracellular signaling cascade.[85–87] This signaling cascade involves downstream proteins involved in the MAPK and PI3K/Akt cascades. FGF may also exhibit its angiogenesis activity alongside VEGF; there may also be some crosstalk with the Notch Pathway, which plays a role in cell patterning and differentiation. The Notch Pathway has also been found to play a significant role in angiogenesis regarding endothelial cell differentiation.[62,87,86,85]

Angiopoietin (Ang) exists as two isoforms (Ang-1 and Ang-2) and both may interact with Tie2 receptor to enhance new vessel production.[85,86] Ang-1 acts via the Akt/survivin pathway to help stabilize new blood vessels. Ang-2 acts alone or in combination with other pro-angiogenic factors such as VEGF to establish and enhance vasculature.[85,86] Downstream signaling of the Ang/Tie2 receptor includes the PI3K/Akt pathway, Protein Kinase B, MAPK/Erk molecules, and Ras pathway molecules. Blocking the interaction between Ang/Tie2 leads to decreased sprouting and reduction in number of tumor vessels highlighting this pathways role in angiogenesis.[62,85,86]

3.2 Angiogenesis and Cancer

Angiogenesis was first observed in malignant cancerous tumors over 100 years ago. It was later proposed that tumor growth and metastasis are dependent on the formation of new blood vessels.[88] Additional evidence demonstrated that cells in precancerous tissue develop angiogenic properties on their way to becoming

cancerous.[89] The hypothesis was thus made that inhibition of angiogenesis would arrest tumor growth; the search began for the development of anti-angiogenic agents to be utilized as chemotherapeutic agents.[82] There are a wide variety of pro-angiogenic molecules including the well-known vascular endothelial growth factor (VEGF) and basic fibroblast factor (bFGF). The primary drivers of tumor angiogenesis are hypoxic cells.[82,84,87] Hypoxia results from the distance between the tumor cells and the oxygen source. This stimulus causes the cells to secrete pro-angiogenic factors, such as VEGF, which bind to endothelial cells (ECs). Activation of ECs leads to blood vessel formation. These newly formed blood vessels attach to the tumor mass and invade the local tumor environment leading to tumor growth, metastatic spread, and the pathogenesis of cancer (Figure 15). [84,82,87,62]

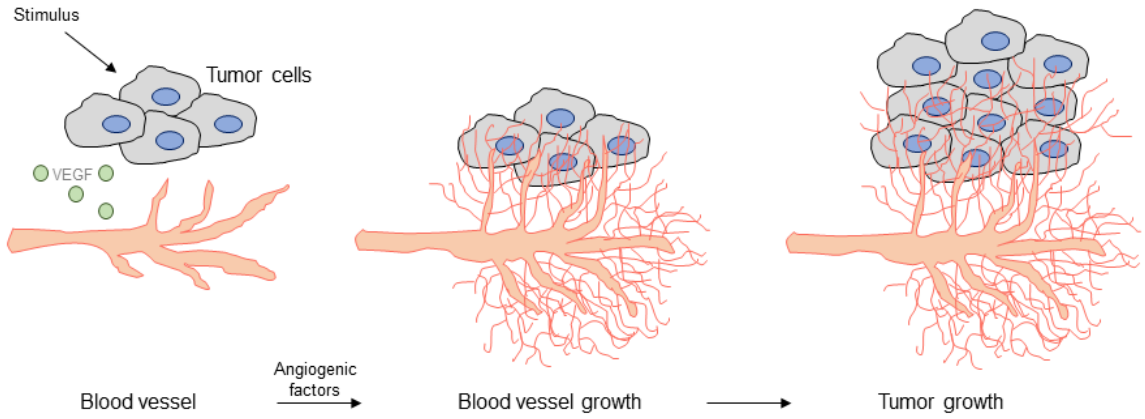

Figure 15. Tumor Angiogenesis

3.3 Established Angiogenesis Inhibitors

This link between angiogenesis and tumor growth provided another therapeutic route towards treating cancer. A number of synthesized and naturally occurring compounds have been explored for angiogenesis inhibition. These angiogenesis

inhibitors would be used to indirectly arrest tumor growth by inhibiting the growth of blood vessels and depriving tumor cells of oxygen and nutrients. Due to the complexity of angiogenesis, there are a variety of drug targets for inhibiting this biological function. As a result, there are a few different classes of angiogenesis antagonists such as compounds that target angiogenic growth factors and compounds that target endothelial cell (EC) migration/proliferation. A few angiogenesis inhibitors have been approved by the FDA including bevacizumab (Avastin), sorafenib (Nexavar), sunitinib (Sutent), pazopanib (Votrient), and everolimus (Afinitor) (Figure 16). Most of these approved agents are dual-action inhibitors targeting VEGFR/PDGFR and/or various pathways such as RAF/MEK/ERK and mTOR.[90–94] Bevacizumab is a monoclonal antibody (anti-VEGF) and serves as the only angiogenesis inhibitor that is not a small molecule.[93] While there has been a modestly positive outcome from angiogenesis antagonists in clinical trials, there has been no long-term survival benefits documented.[83] In most cases, it has been determined that the combination of antiangiogenic agents and chemotherapeutic agents is more effective than either therapy alone. In addition, while most chemotherapeutic agents are toxic and confer resistance, antiangiogenic agents have only shown mild side effects and there are not reported incidents of resistance. This combination of conventional methods and angiogenesis inhibitors provides a novel and safe approach for future cancer treatment.[83,95]

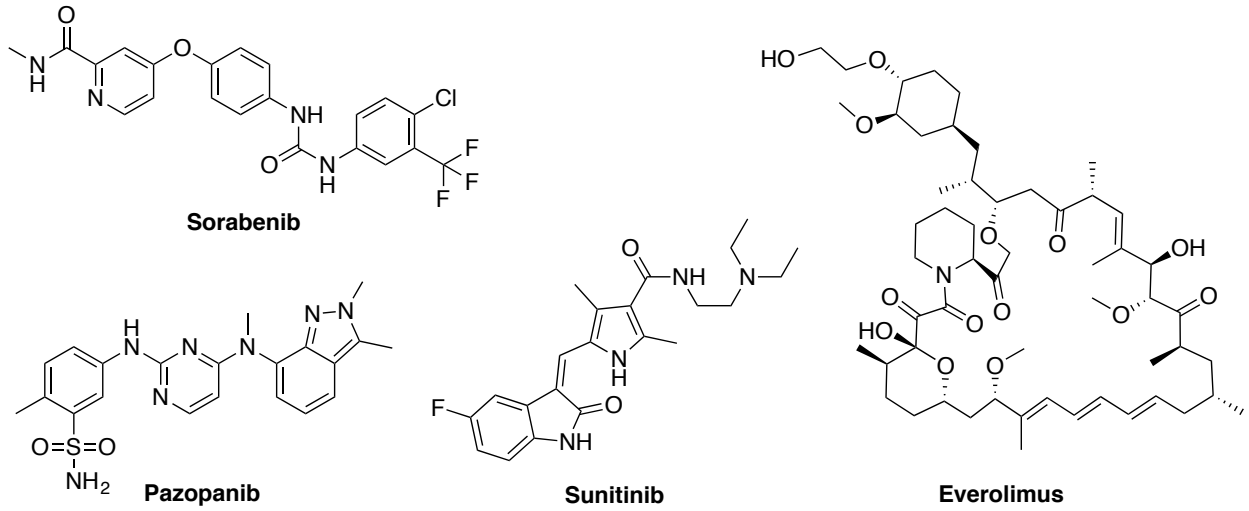

Figure 16. Small Molecule Angiogenesis Inhibitors

3.4 Combination Therapies

As previously mentioned, angiogenesis inhibitors are not productive enough on their own to be administered as monotherapy; in addition, resistance is rapidly acquired, as there are many cellular pathways involved with angiogenesis.[83,84] It is anticipated that the most productive way to utilize angiogenesis inhibitors is in combination with other chemotherapeutic agents. Preclinical and clinical evidence suggest dual treatment with an angiogenesis inhibitor and cytotoxic agents/radiation therapy result in an additive antitumor effect.[83,84] There are several preclinical and clinical trials exploring angiogenesis inhibitors with EGFr/Her2 inhibitors (cetuximab, erlotinib, trastuzumab); PDGFR/bcr-abl inhibitors (imatinib); proteosome inhibitors (bortezomib); and inhibitors of integrins (alphavbeta3 and alpha5beta1).[83,84] While combination therapy seems possible, there are still debates on if this is a practical approach. Paradoxically, an angiogenesis inhibitor may deteriorate blood vessels and blood flow, which would decrease the efficacy of chemotherapy and drug delivery to the tumor site.[83,84]

3.5 ITZ and Angiogenesis

Because angiogenesis is implicated in a variety of ailments, a therapeutic agent that targeted angiogenesis would be beneficial to many people.[10] Johns Hopkins University screened 2,604 FDA approved drugs for antiangiogenic activity utilizing human umbilical vein endothelial cell (HUVEC) proliferation assays. From these screens, ITZ was found to be a potent and selective inhibitor of VEFG-induced proliferation in HUVEC cells (IC_{50}= 0.16 μM).[10] Other azole antifungals were also screened for antiangiogenic activity. All other azole antifungals were less potent than ITZ including ketoconazole and terconazole (IC_{50}= 10.4 μM and 7.1 μM, respectively).[10,96]

Clinically, ITZ is used as a 1:1:1:1 mixture of four diastereomers.[14] Johns Hopkins further explored the antiangiogenic activity of all eight stereoisomers of ITZ. Stereochemistry minimally effected antiangiogenic activity.[97] The most prominent effect was seen within the dioxolane region, where the *cis*-diastereomers were more potent than the *trans*-diastereomers. The stereochemistry of the *sec*-butyl group was found to have little influence on the endothelial cell inhibitory activity.[97] While the ITZ antiangiogenic mechanism is still being unraveled, Johns Hopkins University determined that ITZ inhibits cholesterol trafficking, the mTOR pathway, and VEGFR signaling in HUVECs.[98,96] It has also been determined that ITZ inhibits the mTOR pathway and the ERK1/2 pathway in HMEC-1 cells, a primary cell line with a limited life span and variable characteristics due to multi-donor origins.[99]

The antiangiogenic activity of ITZ can be attributed to its inhibition of the mechanistic Target of Rapamycin (mTOR) signaling pathway via the disruption of

cholesterol trafficking between the plasma membrane and late endosomes/lysosomes.[98] This activity is due to ITZ's ability to inhibit both Niemann-Pick Type C (NPC1) and voltage-dependent anion channel 1 (VDAC1) which inhibit the mTOR pathway through distinct mechanisms.[100,101] NPC1 inhibition prevents the release of cholesterol from the lysosome to the rest of the cell. VDAC1 is a critical regulator of mitochondrial metabolism and its inhibition leads to a drop in cellular energy levels; VDAC1 is shown to be a novel target for modulation of the mTOR pathway (Figure 17).[100,101] This anticancer activity can also be attributed to its ability to inhibit vascular endothelial growth factor receptor 2 (VEGFR2).[96] Because of this, ITZ is currently in several clinical trials that represent a broad range of cancers: breast, prostate, and non-small cell lung.[11]

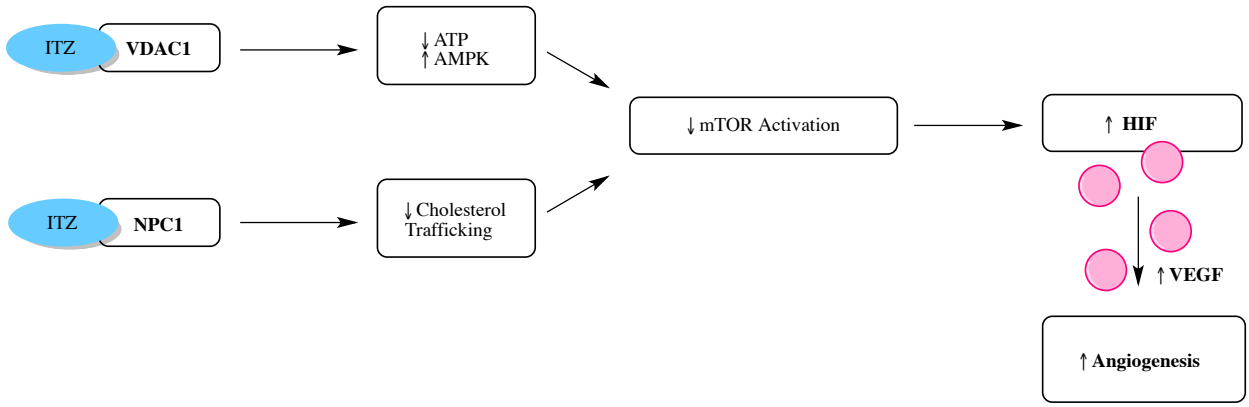

Figure 17. ITZ Proposed Mechanism of Action: Antiangiogenesis Activity[101]

4. Conclusions

Exploring FDA-approved or clinical stage compounds for novel biological activities is becoming a popular way to expedite the long and expensive drug development process.[2] There are many benefits to this approach such as decreased time and expense, however, there are also disadvantages associated with this form of

drug discovery. Recently, two separate screening efforts found ITZ, a clinically efficacious antifungal agent, to inhibit both the Hh pathway and angiogenesis.[9,10] While the Hh pathway has been studied for many years, the emergence of resistance highlights the therapeutic need for novel Hh pathway inhibitors.[50] ITZ is of therapeutic promise due to its unique ability to inhibit the Hh pathway in the presence of both wild type Smo and mutant Smo.[78] In addition, ITZ has been found to contain other biological activities, such as angiogenesis inhibition, that may aid in its anticancer properties. These biological activities all seem to act in distinct manners from one another. It is possible that these activities may yield synergistic effects in anticancer treatment supporting the many clinical trials that ITZ is currently being studied.

The overall goal of this research project is to utilize the scaffold of the FDA-approved antifungal agent, ITZ, for the treatment of SHH subtype MB. To date, ITZ has not been thoroughly explored in terms of its novel anticancer properties. More specifically, ITZ has not been studied as a potential anti-MB chemotherapeutic agent. In terms of its anti-Hh activity, only one SAR study has been reported which focuses on extending the side-chain region of the scaffold. As there is currently not an FDA-approved targeted treatment for MB, it is necessary to explore Hh inhibitors as an alternative option for therapy. The ITZ analogues presented herein will be focused on improving the general “drug-like” properties of this approved compound while also maintaining potent Hh pathway activity. These analogues may be modified to have the optimal properties necessary to penetrate the blood brain barrier (BBB) and treat pediatric MB. If optimal drug-like properties cannot be attained after considerable

structure-activity relationship (SAR) studies, drug formulation will be utilized to assist the most potent in vitro ITZ analogues to cross the BBB and reach the brain.

CHAPTER II: Structure-Activity Relationship Studies of Itraconazole Analogue Generations I and II

1. Introduction

Recently, two separate high-throughput screens of FDA-approved compounds identified itraconazole (ITZ), a well-known antifungal agent, to be an inhibitor of both the Hh pathway and angiogenesis (IC_{50} = 690 nM and 160 nM, respectively).[9,10] The potential to repurpose FDA-approved and clinical stage compounds with novel biological activities is an increasingly popular drug development strategy.[2] While ITZ is now in various clinical trials for its anti-cancer potential, it contains some drug properties that would not make it an ideal chemotherapeutic agent.[12,11] ITZ contains a triazole group, which is capable of coordinating with CYP3A4; this interaction leads to drug-drug interactions and adverse side effects.[102] As cancer patients are often on a multi-drug regimen to both treat the cancer and manage the symptoms, these drug-drug interactions would be probable in the presence of ITZ.

To date, the ITZ scaffold has been minimally explored in terms of its novel anti-cancer properties. The ability for ITZ to inhibit angiogenesis, specifically through vascular-endothelial growth factor receptor 2 (VEGFR2), NPC1, and VDAC1 have been previously reported.[96,101] However, thorough structure-activity relationship (SAR) studies have not been performed in regards to ITZ and its novel biological activities. In terms of anti-Hh activity, the only structural component explored has been the side-chain region.[103] Thus, a series of ITZ analogues have been designed, synthesized, and evaluated to probe the ITZ scaffold for its anti-Hh and anti-angiogenic activities.

2. Design, Synthesis, and Evaluation of Generation I Analogues

2.1 Analogue Design

As previously mentioned, ITZ is a rather large compound that has a complex chemical structure, which is amendable to various modifications. This first generation series of ITZ analogues designed, synthesized, and evaluated consists of conservative modifications to either the dioxolane region or the triazolone/side-chain region (Figure 1). The overall goal of this initial series of analogues is to determine if all the structural functionality of ITZ is necessary for its anticancer properties. This first generation of analogues will provide preliminary data that suggests the favorable and unfavorable structural components of ITZ-mediated Hh inhibition and angiogenesis inhibition.

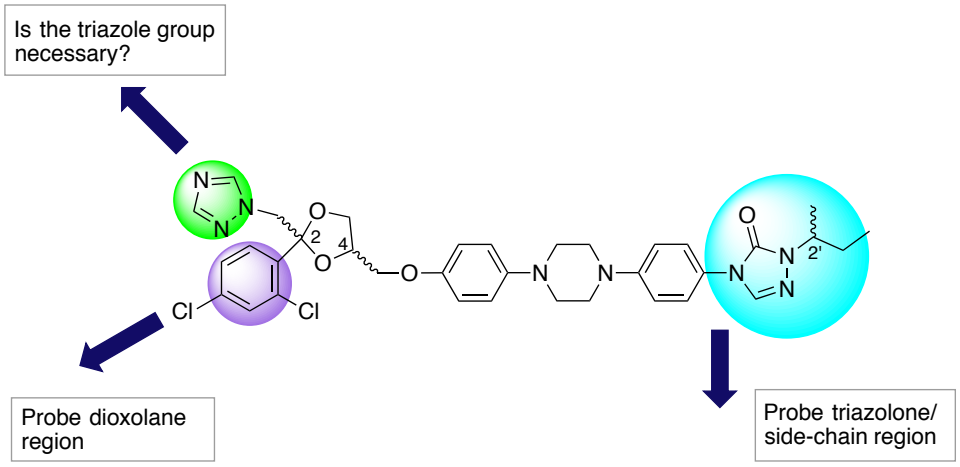

Figure 1. Design of Generation I Analogues

2.2 Synthetic Routes

2.2.1 Synthesis towards Linker Region

All of the first-generation ITZ analogues contain a central phenyl-piperazine-phenyl linker region. This moiety is initially constructed by coupling commercially available *N*-(4-methoxyphenyl)-piperazine (**11**) and 1-chloro-4-nitrobenzene (**12**). The

nitro functionality (**13**) can then be reduced to the aniline (**14**) in the presence of hydrazine monohydrate and 10% palladium on charcoal. The aniline then undergoes a series of two well-characterized transformations to the carbamate (**15**) and hydrazine carboxamide (**16**) intermediates before ultimately forming the triazolone ring (**17**) (Scheme 1).[97] The methoxy- substituent in the commercially available starting material serves as a protecting group throughout this synthetic route; while other protecting groups have been used during this synthesis, such as methoxymethyl- (MOM-), we found that the methoxy- group proved more efficient in generating the triazolone intermediate.[103]

Scheme 1. Synthesis towards Linker Region

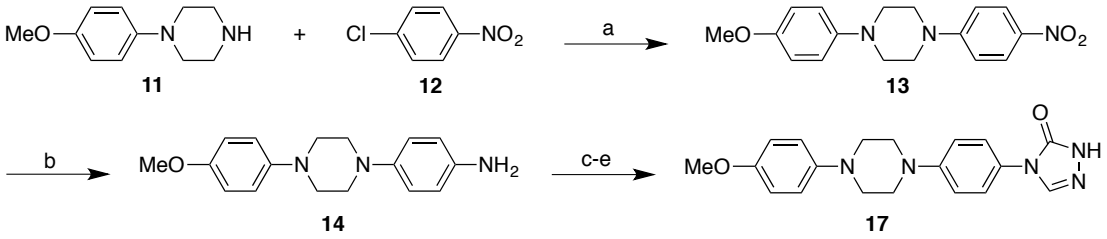

Reagents and conditions: (a) K_2CO_3, reflux, 12 h, 82%; (b) Pd/C, $NH_2NH_2 \cdot H_2O$ (10 eq), reflux, 3.5 h, 71%; (c) Pyr (17 eq), ClCOOPh (1.1 eq), 3 h, 90%; (d) $NH_2NH_2 \cdot H_2O$ (5.5 eq), reflux, 3 h, quant; (e) formamidine acetate (4.5 eq), acetic acid, reflux, 3 h, 91%.

The triazolone intermediate was alkylated (**24-27**) with either commercially available brominated alkyl chains (**22**,**23**) or alkyl brosylates (**20,21**) that were prepared from corresponding commercially available and stereochemically defined alcohols (**18,19**) (Scheme 2).[97] The methoxy- group in the triazolone/side-chain intermediate was removed with 48% hydrobromic acid in toluene to afford various phenols (**28-31**).[104] It is important to note that alkylation of the triazolone inverts the stereochemistry of the side

chain region, for example, (*R*)-brosylates generate (*S*)-intermediates. The stereochemistry of the triazolone/side-chain regions was monitored throughout these reactions. As enantiomers have similar physical properties such as melting points, densities, boiling points, and refractive indexes, a polarimeter was used to aid in determining the optical activity and corresponding orientation of the stereochemically-defined intermediates. If a substance is not optically active, the polarimeter output will read [α] = 0°. However, if a compound is optically active, the plane of light will either be rotated clockwise or counter clockwise and the observer will read a (+) or (–) value. It is important to note that a (+) or (–) value is not indicative of a particular isomer.[105] These polarized values were used in combination with crystal structures to determine the (*R*) or (*S*) configurations of these stereochemically-defined intermediates.

Scheme 2. Synthesis towards Phenol

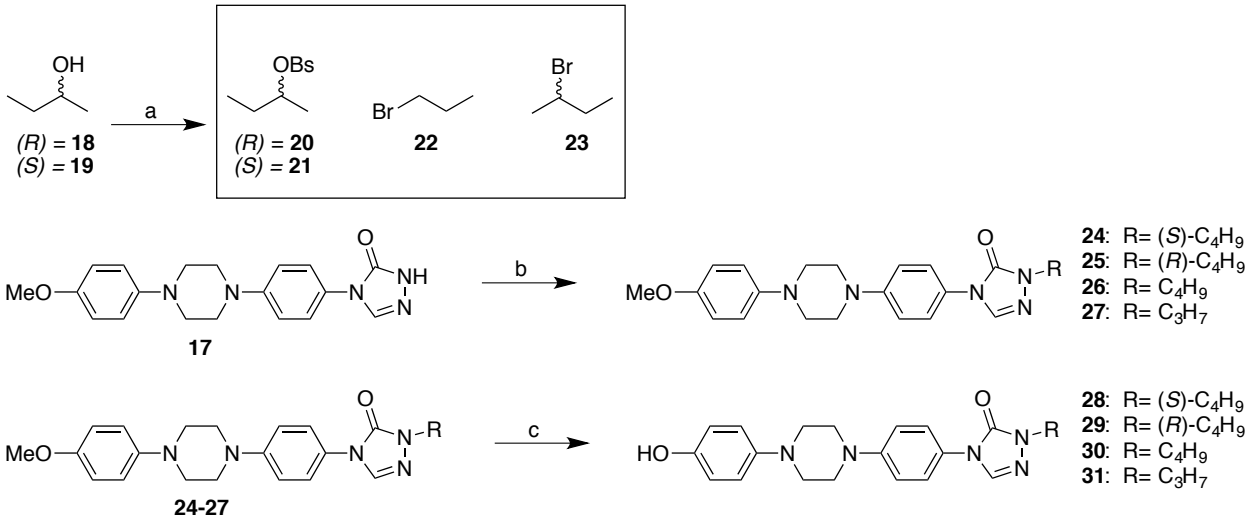

Reagents and conditions: (a) Et_3N, BsCl (1.3 eq), RT, 3 h; 30-50%; (b) Cs_2CO_3, brosyl/bromo alkyl chain, RT, 12 h, 45-88% (c) 48% HBr, toluene, reflux, 12 h, 55-80%.

2.2.2 Synthesis towards Dioxolane Regions

Dioxolane regions containing the triazole moiety could not be formed under standard ketalization conditions due to the basicity of the triazole ring. For these intermediates, the triazole moiety was added to various halogenated ketones. In parallel, tosylated glycerol was formed through standard tosylation of commercially available dioxolane and subsequent acid mediated hydrolysis (Scheme 3).[106] Finally triazole-containing dioxolanes were prepared through a ketalization reaction utilizing tosylated glycerol, ketone intermediates, and triflic acid.[107] Other attempts were made to add the triazole group directly to the dioxolane after the ring closing reaction, as this would be helpful in developing subsequent triazole-mimic analogues; however, this proved unsuccessful. The *des*-triazole dioxolanes were synthesized utilizing standard ketalization conditions that make use of the Dean-Stark apparatus.[108] Tosylated glycerol was used to ketalize 2,4-dichloroacetophenone and yield *des*-triazole dioxolane.[97]

Scheme 3. Synthesis towards Dioxolane Region

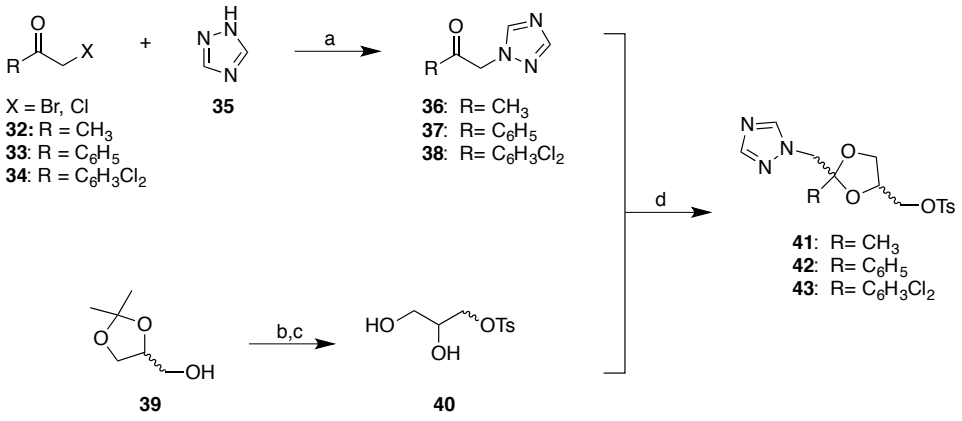

Reagents and conditions: (a) $NaHCO_3$, toluene, reflux, 3h, 25-65%; (b) Pyr, TsCl, 0°C- RT, 12 h, 71%; (c) MeOH, 0.5N HCl, reflux, 5 h, 89%; (d) Triflic acid (3-4 eq), toluene, RT, 60 h 10-70%.

2.2.3 Synthesis towards Generation I Final Analogues

Tosylated dioxolane regions were coupled with the linker/triazolone/side-chain region phenols in anhydrous dimethyl sulfoxide (DMSO) with cesium carbonate (Cs_2CO_3) to yield final analogues (Scheme 4A).[97] Truncated ITZ analogues were synthesized via a reversed synthetic route. Unprotected linker region (**44**) was prepared in the same manner as methoxy-protected linker region.[103] This intermediate was then coupled with the tosylated dioxolane region under standard coupling conditions to yield nitro intermediate (**54**). This intermediate was then reduced to the aniline with palladium on charcoal in the presence of hydrazine monohydrate to yield aniline intermediate (**55**) (Scheme 4B).[103]

Scheme 4. Synthesis towards Final Generation I Analogues

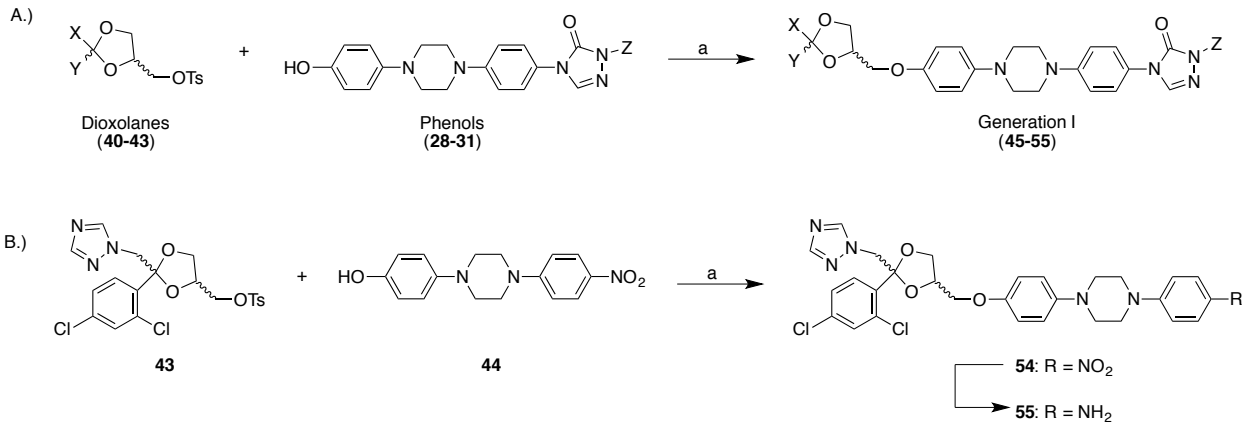

Reagents and conditions: (a) Cs_2CO_3 (10 eq), DMSO, 90ºC, 12 h, 45-88%; (b) Pd/C, $NH_2NH_2 \cdot H_2O$ (10 eq), reflux, 3.5 h, 60-70%. The functional groups represented by X, Y, and Z above can be found in Schemes 2 and 3.

2.3. Biological Evaluation

Table 1. First Generation Series of ITZ Analogues

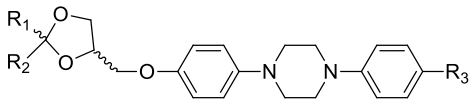

Compound	R_1	R_2	R_3
45, ITZ	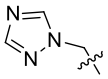	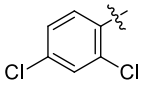	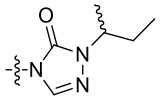
46	-CH_3	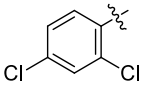	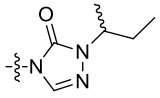
47	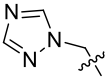		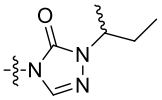
48	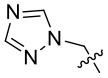	-CH_3	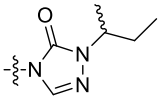
49	-CH_3	-CH_3	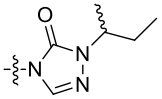
50	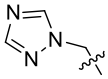	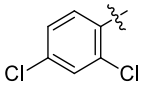	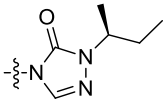
51	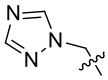	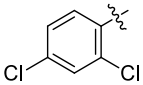	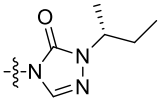
52	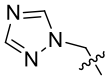	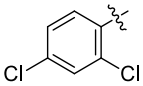	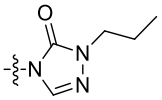
53	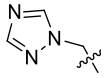	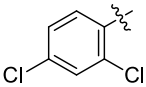	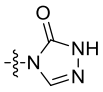
54	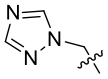	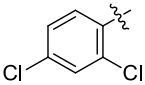	-NO_2
55	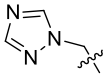	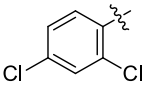	-NH_2

The first generation of ITZ analogues (Table 1) was evaluated for Hh pathway inhibitory activity by monitoring endogenous Gli1 mRNA levels in C3H10T1/2 (C3H)

cells, an Hh-dependent mouse embryonic fibroblast (MEF), at a single concentration (1μM). This is a well-studied in vitro model system for evaluating small molecule inhibition of Hh signaling. Addition of exogenous Hh agonist (recombinant Hh ligand or small molecule) results in a characteristic increase in Gli1 mRNA expression.[109] Combined treatment with Hh agonist and a pathway inhibitor reduces Gli1 expression. ITZ analogues that reduced Gli1 mRNA expression below 20% at 1μM were subsequently evaluated for their ability to reduce Gli1 mRNA expression levels in a concentration dependent fashion in both the C3H cell line and an Hh-dependent murine basal cell carcinoma cell line (ASZ-001).[110,111] Finally, with the help of our collaborators at Sanford Burnham Prebys Medical Discovery Institute, several generation I analogues were also tested for their antiproliferative activity in primary Hh-dependent medulloblastoma cells isolated from conditional Patched knockout Math1-Cre-ER; $Ptc^{fl/fl}$ (MERP) mice.[112,113,114] Only a small subset of analogues was evaluated due to the difficult nature of culturing primary MERP cells.

As ITZ was found to also inhibit angiogenesis, generation I analogues were screened for their ability to inhibit VEGF-induced proliferation of human umbilical vein endothelial cells (HUVECs). Angiogenesis is dependent on endothelial cell proliferation and the inhibition of HUVEC proliferation is commonly utilized as an early stage in vitro model of antiangiogenic activity.[97,103]

Table 2. In Vitro Activity of First Generation ITZ Analogues

Compound	% Gli Expression (1 μM) [b]	IC_{50} (μM) [a] C3H10T1/2 [b]	IC_{50} (μM) [a] ASZ [c]	GI_{50} (μM) [a, d] HUVEC	GI_{50} (μM) [a] MERP MB [c]
ITZ		0.07 ± 0.02	0.14 ± 0.02	0.40 ± 0.03	0.44 ± 0.08
45	1.7 ± 0.3	0.06 ± 0.003	0.17 ± 0.01	0.49 ± 0.09	0.6 ± 0.1
46	17.8 ± 0.5	0.14 ± 0.04	0.17 ± 0.04	23.8 ± 6.7	ND
47	13.1 ± 1.2	0.42 ± 0.2	0.45 ± 0.06	8.3 ± 0.7	ND
48	61.4 ± 3.5	ND	ND	18.4 ± 4.5	ND
49	71.4 ± 5.5	ND	ND	>100	ND
50	6.9 ± 3.1	0.16 ± 0.04	0.14 ± 0.01	2.5 ± 0.3	ND
51	3.0 ± 0.9	0.14 ± 0.04	0.16 ± 0.02	1.7 ± 0.4	ND
52	58.5 ± 6.4	ND	ND	4.7 ± 0.3	ND
53	1.1 ± 0.2	0.043 ± 0.02	0.12 ± 0.03	5.8 ± 0.8	ND
54	1.5 ± 0.05	0.13 ± 0.03	0.09 ± 0.03	8.4 ± 0.7	ND
55	6.1 ± 1.6	0.16 ± 0.06	0.12 ± 0.05	42.7 ± 4.4	0.9 ± 0.7
30	45.7 ± 3.0	ND	ND	>100	ND

[a]IC_{50} and GI_{50} values represent the Mean ± SEM of at least two separate experiments performed in triplicate. [b]All analogues evaluated following 24 hr incubation. [c]All analogues evaluated following 48 hr incubation. [d]All analogues were evaluated following 72 hr incubation.

Evaluation of the first generation of ITZ analogues (Table 2) yielded structural features that appear necessary for Hh pathway inhibition. First, the stereochemistry at the 2' position of the *sec*-butyl side-chain region does not appear to be important (**50** and **51** are equipotent in the MEF and ASZ cell lines). Truncation to a propyl side-chain (**52**) significantly reduces the overall activity of the scaffold. Interestingly, removal of the side-chain region to the free triazolone (**53**) and further truncation of the triazolone region to nitro or aniline substituents (**54** and **55**) maintained Hh pathway inhibition; all three of these analogues maintained potent IC_{50} values in the MEF and ASZ cell lines in relation to ITZ. In terms of the modifications made to the dioxolane region, removal of the chlorine atoms of the phenyl ring (**47**) had minimal effects while truncation of the phenyl ring all together (**48**) resulted in significant loss of Hh pathway inhibition. Removal of the triazole moiety (**46**) maintained potent Hh pathway inhibition. Not

surprisingly, removal of both the triazole and the phenyl functionality (**49**) or complete truncation to the phenol (**30**) significantly reduced Hh pathway inhibitory activity. Our synthesized ITZ (**45**) demonstrated comparable activity to commercially available ITZ in both the MEF and ASZ cell lines. Overall, these analogues were equipotent in their ability to down regulate Gli1 mRNA expression in both cell lines evaluated. ITZ, **45**, and **55** were tested for their ability to inhibit proliferation of Hh-dependent murine MB cells and all three of these compounds had slightly reduced activity (Table 2).[115]

First generation analogues were also evaluated for their ability to inhibit VEGF-induced anti-proliferation in HUVECs, a preliminary assay used to measure angiogenesis inhibitory potential (Table 2). Commercially available ITZ and synthesized ITZ (**45**) demonstrated comparable antiproliferative activity (GI_{50} values = 0.40 and 0.49 μM, respectively). Other ITZ analogues were significantly less active compared to ITZ. Several analogues were moderately active (GI_{50} = 1.7 – 8.4 μM); however, there was no clear SAR pattern in terms of angiogenesis. Finally, ITZ and *des*-triazole ITZ (**46**) were evaluated for their ability to inhibit CYP3A4 (IC_{50} values = 50.4 nM and >10 μM, respectively). Removal of the triazole moiety results in potent Hh inhibition and abolishes CYP3A4 inhibition making compound (**46**) the lead analogue from this first generation of ITZ analogues (Figure 2).[115]

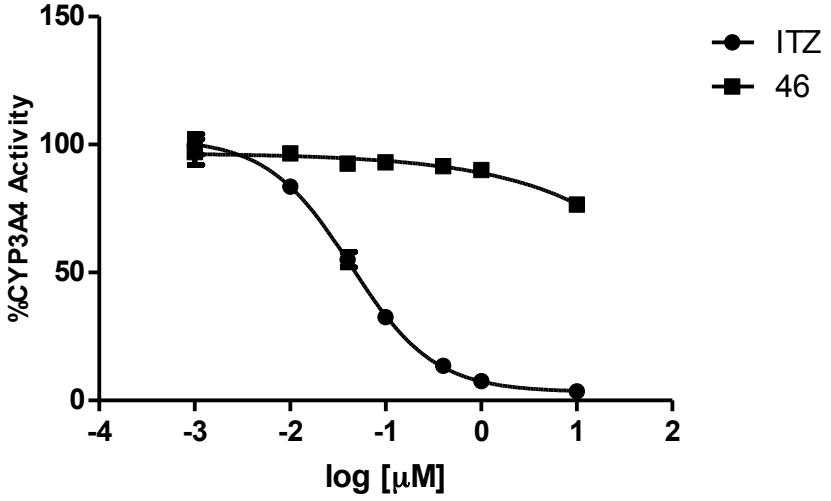

Figure 2. CYP3A4 Inhibition
Calculated IC_{50} values (μM) for inhibition of CYP3A4 activity by the two compounds are as follows: ITZ (0.051 ± 0.01 μM) and *des*-triazole ITZ (>10 μM).

3. Design, Synthesis, and Evaluation of Generation II Analogues

3.1 Analogue Design

Formation of the *cis*-conformation around the dioxolane ring predominates during its synthesis and pharmaceutical preparations of ITZ are typically administered as a 1:1:1:1 mixture of *cis*-diastereomers.[115] For efficiency, the first generation of ITZ analogues was evaluated as mixtures of stereochemical isomers. To probe more fully the absolute structural requirements of this scaffold for its novel biological activities, a second generation of analogues was designed, synthesized, and evaluated (Figure 3). This second generation contains the stereochemically-defined isomers of lead compound, *des*-triazole ITZ (**46**). This generation of compounds will highlight if there is an optimal stereochemical orientation for either Hh pathway inhibition or angiogenesis inhibition.[115]

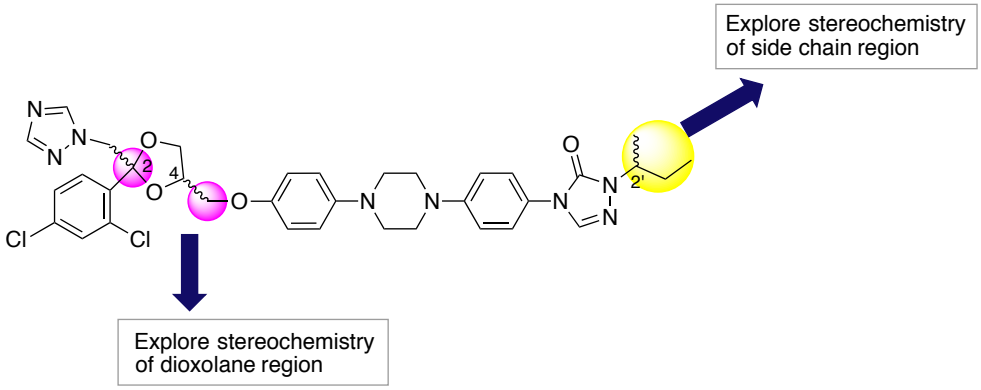

Figure 3. Design of Generation II Analogues

It is important to note the difference in nomenclature of the stereochemistry surrounding the dioxolane region differs between ITZ and *des*-triazole ITZ. In terms of ITZ, the triazole moiety receives the priority within the dioxolane region; therefore, the *cis*- orientation is in reference to the triazole and ether linkage. By contrast, removal of the triazole group shifts the priority to the phenyl ring and a *cis*-*des*-triazole analogue has the opposite absolute configuration between the phenyl ring and the ether linkage as ITZ (Figure 4).[115]

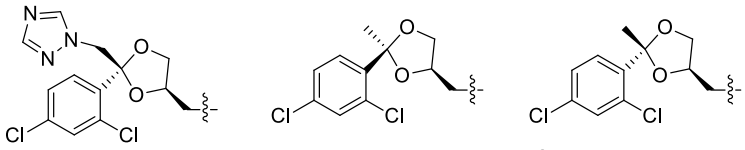

Figure 4. (A) Representative *cis*-ITZ isomer, (B) *cis*- and (C) *trans*-*des*-triazole analogues

3.2 Synthetic Routes

3.2.1 Synthesis towards Stereochemically-Defined Dioxolane Regions

The stereochemically-defined *des*-triazole dioxolane regions were synthesized under standard ketalization reaction conditions utilizing a Dean-Stark apparatus.[108] Stereochemically-defined tosylated glycerols were prepared via the method described

previously only beginning with stereochemically-defined commercially available dioxolane (Scheme 5).[106] Formation of the dioxolane ring predominately forms the *trans*- isomer and these isomers were best separated via preparative thin layer chromatography (TLC).

Scheme 5. Synthesis towards Stereochemically Defined Dioxolanes

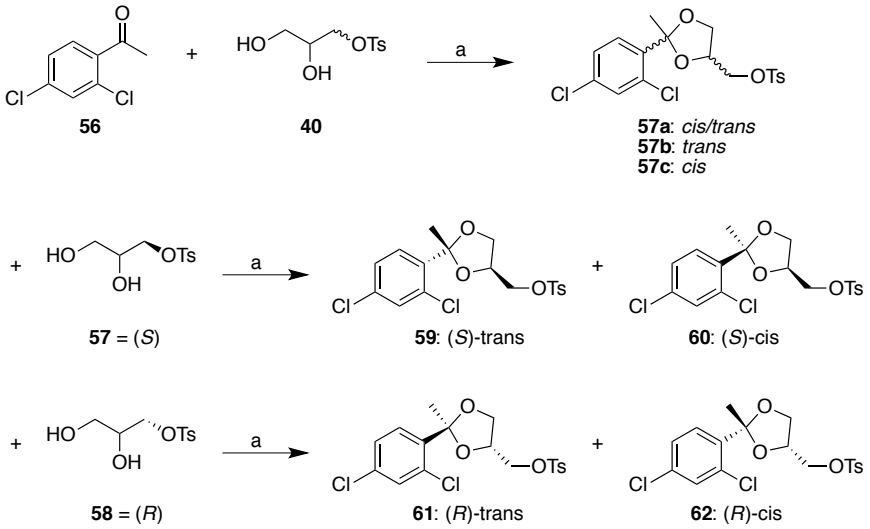

Reagents and conditions: (a) p-TsOH (cat.), toluene, reflux (Dean Stark), 48h, 70-90%.

3.2.2 Synthesis towards Final Stereochemically Defined Analogues

As previously described, tosylated dioxolane regions were coupled with the linker/triazolone/side-chain region phenols in anhydrous dimethyl sulfoxide with cesium carbonate to yield final analogues (Scheme 6).[97]

Scheme 6. Synthesis towards Final Generation II Analogues

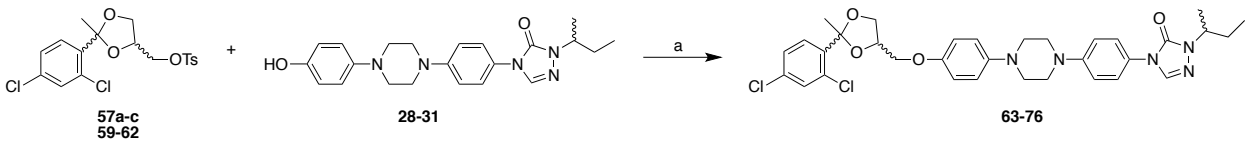

Reagents and conditions: (a) Cs_2CO_3 (10 eq), DMSO, 90ºC, 12h, 45-88%

3.3 Biological Evaluation

Table 3. Second Generation ITZ Analogues

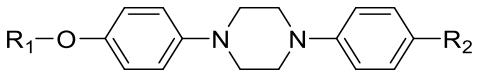

Compound	R_1	R_2	Final Stereochemistry
63	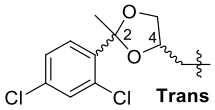	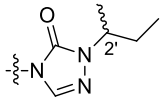	*Trans*-2,4
64	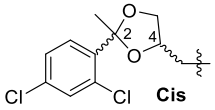	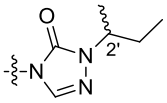	*Cis*-2,4
65	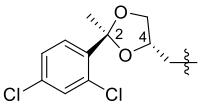	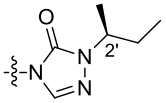	*Trans*-2S,4S,2'S
66	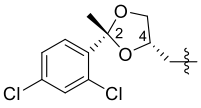	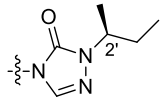	*Cis*-2R,4S,2'S
67	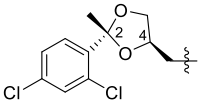	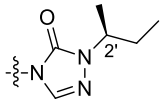	*Trans*-2R,4R,2'S
68	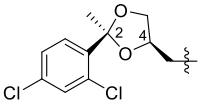	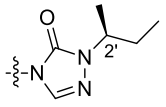	*Cis*-2S,4R,2'S
69	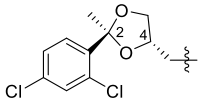	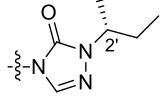	*Trans*-2S,4S,2'R
70	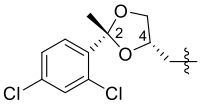	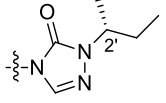	*Cis*-2R,4S,2'R
71	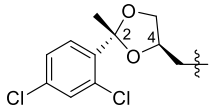	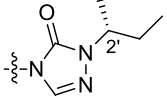	*Trans*-2R,4R,2'R
72	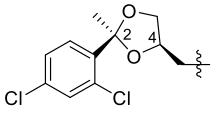	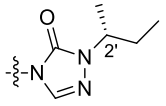	*Cis*-2S,4R,2'R
73	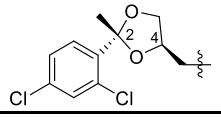	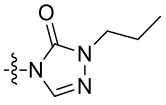	*Trans*-2R,4R

74	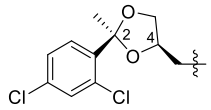	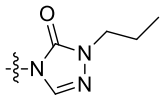	*Cis*-2S,4R
75	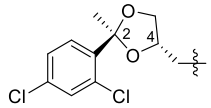	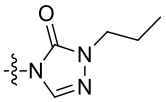	*Trans*-2S,4S
76	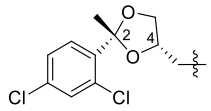	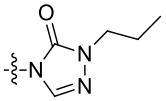	*Cis*-2R,4S

Evaluation of our stereochemically defined analogues (Table 3) for their ability to inhibit Hh signaling in the C3H10T1/2 and ASZ cell lines provided both interesting and confounding results. The majority of compounds evaluated were more active in the ASZ cells, with numerous analogues exhibiting 100- to 1000-fold improvement in activity when compared to C3H cells. Several compounds that were "inactive" in the C3H cells (IC_{50} >10 μM) exhibited potent down-regulation of Gli (IC_{50} – 0.2-0.5 μM) in the ASZ cell line. In addition, several other compounds with modest inhibitory effects in the MEF cell line (**64**, **68**, **72**) exhibited low nanomolar IC_{50} values in the ASZ cells (Table 4).[115]

Table 4. In Vitro Activity of Second Generation ITZ Analogues

Compound	IC_{50} (μM) [a] C3H10T1/2 [b]	ASZ [c]	GI_{50} (μM) [a, d] HUVEC	GI_{50} (μM) [a] MERP MB [c]
63	0.091 ± 0.02	0.077 ± 0.01	3.32 ± 0.55	2.0 ± 1.3
64	0.85 ± 0.1	0.071 ± 0.02	3.69 ± 1.1	2.9 ± 1.9
65	1.1 ± 0.17	2.5 ± 0.7	7.7 ± 4.4	ND
66	>10	0.55 ± 0.07	78.3 ± 17.3	ND
67	0.47 ± 0.001	0.38 ± 0.07	18.3 ± 11.8	ND
68	1.85 ± 0.09	0.15 ± 0.038	2.5 ± 0.7	0.39 ± 0.2
69	0.54 ± 0.24	0.13 ± 0.04	12.1 ± 4.7	ND
70	6.6 ± 0.3	2.8 ± 0.9	65.0 ± 11.5	ND
71	0.19 ± 0.04	0.022 ± 0.01	53.2 ± 25.2	0.6 ± 0.2
72	2.4 ± 0.6	0.024 ± 0.02	12.8 ± 2.9	1.0 ± 0.5
73	4.1 ± 1.5	1.3 ± 0.65	26.5 ± 3.5	ND
74	>10	1.4 ± 0.5	49.9 ± 15.9	ND
75	>10	0.2 ± 0.08	84.1 ± 33.5	22.4 ± 12
76	>10	0.54 ± 0.06	24.9 ± 2.2	ND
PSZ	0.14 ± 0.02	0.54 ± 0.05	1.6 ± 0.02	1.5 ± 0.3

[a]IC_{50} and GI_{50} values represent the Mean ± SEM of at least two separate experiments performed in triplicate. [b]All analogues evaluated following 24 hr incubation. [c]All analogues evaluated following 48 hr incubation. [d]All analogues were evaluated following 72 hr incubation.

Despite the conflicting results between cell lines, several interesting SAR developments with respect to optimal configuration were identified for the second generation of ITZ analogues (Table 4). These results reiterated that the orientation of the *sec*-butyl side-chain substitution is not significant but the methyl group must be present. Truncation to the propyl side-chain region abolishes Hh pathway activity. Compounds containing the propyl side-chain region were significantly less active than *sec*-butyl analogues containing the same dioxolane ring orientation. Generation II analogues with the *trans*-orientation around the dioxolane ring were generally more potent than the *cis*-orientation throughout all cell lines evaluated. Finally, compounds

containing the 4*R* configuration were generally more active than the 4*S* configuration; *des*-triazole analogues with the 2*R*,4*R* configuration demonstrated the most comparable activity between the two cell lines.[115]

After evaluation of Hh pathway inhibitory activity in both the C3H10T1/2 and ASZ cells, select compounds were further evaluated in primary MB (MERP) cells (Table 5).[112,113,114] Analogues selected for the antiproliferative assay were chosen either because they exhibited potency in both cell lines (ASZ and MEF) or because they were significantly less active in the MEFs in comparison to the ASZs. Testing the antiproliferative effects of these analogues in the Hh-dependent primary culture provided additional in vitro data for the most active *trans*-oriented compounds and also aided in determining discrepancies in the Hh pathway inhibitory activity across the two preliminary cell lines. The mixtures containing *trans*- and *cis*- (**63** and **64**) stereoisomers were less active than the single stereochemically defined analogues. The most active analogue in this assay was analogue **68** (GI_{50} = 0.39 μM) which has the *cis*-2*R*,4*R* configuration around the dioxolane moiety. Further, the reduced antiproliferative activity exhibited for analogue **75** further highlights the importance of the methyl group on the side chain region of Hh pathway inhibition. Based on these antiproliferative results, several generation II analogues (**68**, **71**, and **72**) were evaluated for their ability to down regulate endogenous Gli1 mRNA expression in the MERP primary cell line.[112–114] Each of these analogues, along with parent compound ITZ, demonstrated potent down-regulation of Gli1 mRNA expression in this assay. In addition, the anti-Hh activity of these analogues in the MERP MB cells more closely correlated with the data obtained in the ASZ cells. This suggests that the immortalized

BCC cell line may be a more appropriate early stage in vitro cellular model for Hh inhibition. Specifically, this model should be utilized in testing compounds that contain the ITZ scaffold.[115]

Table 5. Down-Regulation of Gli1 mRNA in MERP MB cells

Compound	IC_{50} (μM) [a, b]
ITZ	0.39 ± 0.06
68	0.26 ± 0.12
71	0.19 ± 0.07
72	0.29 ± 0.08

[a]IC_{50} values represent the Mean ± SEM of at least two separate experiments performed in triplicate. [b]All analogues evaluated following 48 hr incubation.

Following the discovery of ITZ and its novel biological activities, the entire class of azole antifungals was screened for Hh-inhibitory activity.[9] The only other compound to exhibit comparable activity to ITZ was posaconazole (PSZ), which interestingly has a very similar chemical structure; ITZ and PSZ share the same phenyl-piperazine-phenyl linker and differ in their dioxolane and furan rings, halogenated substituents, and side-chain regions (Figure 5). PSZ and the most active generation II analogue (**71**) share a similar orientation in terms of their dioxolane/furan rings. Therefore, PSZ was evaluated for its ability to inhibit Gli1 expression in the C3H, ASZ, and MERP cell lines (Table 4). Due to its moderate activity in MERP cells, it was concluded that the dioxolane and hydrophobic side-chain region of ITZ may be more advantageous than the furan and hydroxylated side-chain region of PSZ.[115]

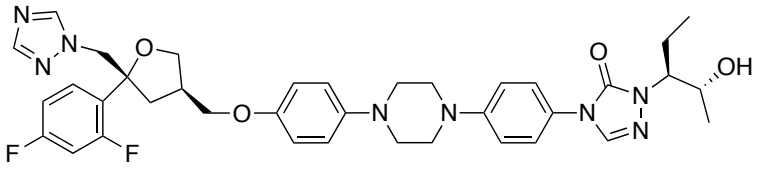

Figure 5. Structure of Posaconazole

In terms of angiogenesis inhibition, results obtained from the HUVEC antiproliferation assay did not yield a clear SAR pattern that distinguished one stereoisomer to be more potent (Table 4). The stereo-defined analogue that had the most potent activity against HUVEC proliferation was **68** (IC_{50} = 2.5 ± 0.7 μM), which contains the (*R*)-*cis*-dioxolane region and the (*S*)-*sec*-butyl side chain region. When only the stereochemistry of the *sec*-butyl moiety is inverted (**72**), activity is weakened (IC_{50} = 12.8 ± 2.9 μM). Overall, compounds containing the (*S*)-*sec*-butyl side chain region were more potent than compounds containing the (*R*)-*sec*-butyl side chain region; compounds containing the (*R*)-dioxolane region were more potent than the (*S*)-dioxolane, specifically, the (*R*)-trans dioxolane region carried the most potent activity. These results differ from the SAR results for Hh pathway inhibition in that the stereochemistry of the *sec*-butyl side chain did not play a crucial role in achieving potent activity. In terms of HUVEC antiproliferation, there is not one dioxolane region that can be determined as the most potent across the second generation of ITZ analogues.[115]

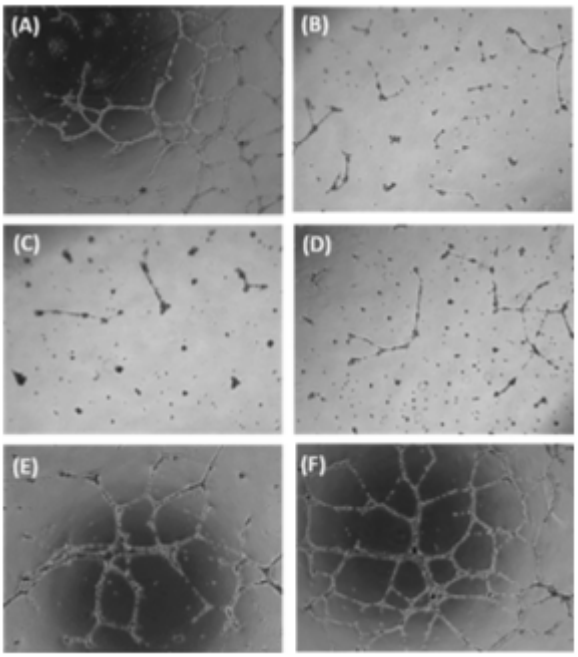

Figure 6. Representative fields from tube formation assay
Treated cells were grown on Matrigel ® for 16h. Phase contrast images were taken from multiple locations in each well (~8 images/well) on an inverted microscope: (A) DMSO treatment served as a negative control; (B) Suramin treatment served as a positive control; (C) ITZ treatment at 10 μM; (D) *des*-triazole ITZ treatment at 10 μM; (E) **69** treatment at 10 μM; (F) **72** treatment at 10 μM.

Due to this lack of clear SAR, a several of the generation II analogues were evaluated in a Matrigel® tube formation assay to further explore antiangiogenic properties of the ITZ scaffold (Figure 6). Normally, HUVECs plated and grown on matrigel migrate toward each other, align, and form tubes that resemble in vivo capillary beds. This type of assay is a more accurate model of angiogenesis as it takes into account several aspects of proper vessel formation: adhesion, migration, and tube formation.[116] Compounds evaluated in this assay were chosen based on their overall structure and activity in antiproliferation assays in an attempt to provide the most relevant preliminary data in terms of generation II analogues and angiogenesis inhibition. Inhibition of tube formation can be measured via two different parameters:

tube length and tube junctions. Based on these parameters, inhibition of tube formation for both ITZ and *des*-triazole ITZ were comparable at 10 μM. At lower concentrations, there was a decrease in activity seen in *des*-triazole ITZ (Figure 7). This highlights the importance of the triazole moiety in terms of ITZ-mediated angiogenesis inhibition. Interestingly, the stereochemically defined analogues presented a decrease in activity even at high concentrations such as 10 μM (Figure 7). Overall, there was minimal correlation between the HUVEC antiproliferation assay and the HUVEC tube formation assay. For example the stereochemically-defined analogues were more potent than the *des*-triazole ITZ mixture in terms of inhibiting HUVEC proliferation, however showed opposite activity against HUVEC tube formation. Taken together, these data suggest that the triazole group of ITZ is important for the antiangiogenic activity of the scaffold and future SAR studies into this region should be undertaken.[115]

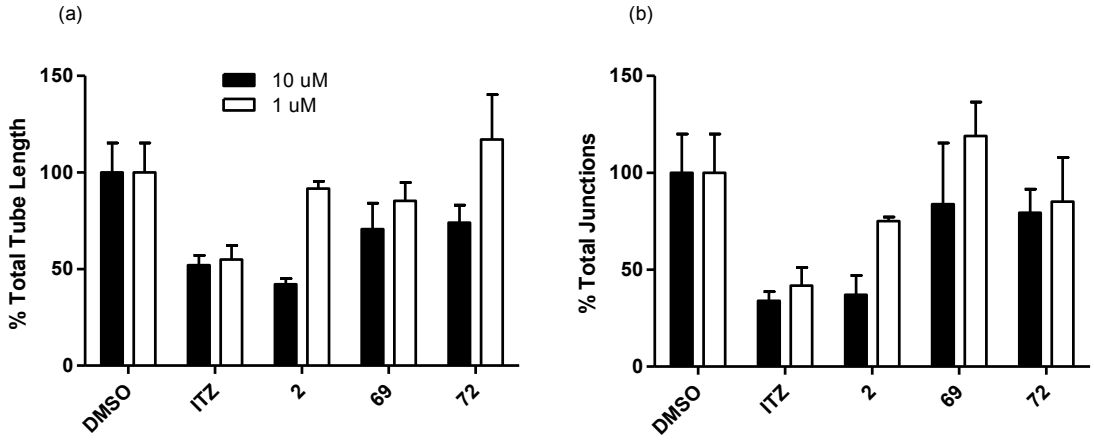

Figure 7. Comparison of (A) total tube length and (B) total tube junctions
Phase contrast images were taken from multiple locations in each well (~ 8 images/well) on an inverted microscope and tube formation parameters (total tube length and total tube junctions) were quantified using ImageJ (NIH) software. DMSO (negative control) was set to 100% tube formation for analysis purposes. Suramin (10 μM) was used as the positive control for each experiment and its ability to inhibit total tube length (51.9 ± 7.8%) and tube junctions (57.6 ± 6.1%) was consistent.

In addition to exploring ITZ and its analogues for these novel biological activities, a few of these compounds were evaluated in pharmacokinetic (PK) assays. These PK data helped determine if the structural changes made were advantageous to improving the overall drug-like properties of the ITZ scaffold (Table 6). None of these compounds are substrates for BBB efflux proteins p-glycoprotein (P-gp) or breast cancer resistant protein (BCRP). The *trans*-dioxolane improves solubility in comparison to the *cis*-dioxolane analogue (Solubility = 1.56 and 0.8 μM, respectively). Interestingly, the *cis*-dioxolane analogue has a more optimal IC_{50} value against CYP3A4. Compounds ITZ, **71**, and **72** were also screened for their ability to passively permeate membranes in a parallel artificial membrane permeability assay (PAMPA). The *des*-triazole ITZ analogues have poor permeability in comparison to parent compound ITZ.

Table 6. Pharmacokinetic Data for Generation II Analogues

Compound	Solubility (μM)	BCRP	P-gp	PAMPA	CYP3A4 IC_{50} (μM)
ITZ	0.8	No	No	Moderate	0.4
71	1.56	No	No	Poor	1.02
72	0.8	No	No	Poor	>20

4. Conclusion

Analogue generations I and II provided interesting information regarding the ITZ scaffold and its novel anticancer activities. First, the triazole moiety can be removed and still maintain Hh pathway inhibition. This is important as removal of this triazole region decreases the overall size of the scaffold and abolishes coordination with CYP3A4. Second, while the stereochemistry of the side-chain region does not play a significant role in Hh pathway inhibition, the stereochemistry of the dioxolane region proved to be important.[115] SAR studies indicated that the most potent stereochemical

orientation was the 2*R*,4*R*-*trans*-dioxolane region. In terms of angiogenesis inhibitory activity, no clear SAR pattern was determined even after a tube formation assay on Matrigel®. While the triazole region is less important for Hh inhibitory activity, this moiety seems to be necessary for angiogenesis inhibition, as ITZ remained the most potent compound in both the HUVEC proliferation assay and the tube formation assay.[115] As future analogues will not contain the triazole region, angiogenesis will no longer be explored. ITZ is a large compound and there are still regions and structural functionality to explore in terms of these novel biological activities. The SAR studies of ITZ analogue generations I and II remain important for the design, synthesis, and evaluation of future *des*-triazole ITZ analogues.

Thank you to Dr. Albert DeBerardinis for his assistance with the synthesis, purification, and preliminary evaluation of the des-triazole ITZ analogues.

4.1 Experimental

Purity Analysis of Final Analogues: It is important to note that generation I final ITZ analogues were synthesized and evaluated as stereoisomeric mixtures. This initial series was not separated into individual isomers and the ratio between *cis*/*trans* was not determined after the dioxolane reaction. The mixtures of these final analogues are reflected in the ^{1}H and ^{13}C NMR characterization data described below and the spectra provided in Appendix A. Purity analysis for all final analogues was determined via one of the following methods.

Method A: ITZ analogues were dissolved in HPLC-grade MeCN and injected (20μL of a 1mM solution) into an Agilent Manual FL-Injection Valve (600 bar) on an Agilent 1100/1200 Series HPLC equipped with an Agilent Eclipse Plus C18 (4.6 x 100mm) column and Agilent 1100 Series Photodiode Array Detector. The mobile phase consisted of 60% MeCN/40% H_2O for analogues containing the triazole moiety and 70% MeCN/30% H_2O for *des*-triazole ITZ analogues. All analogues were run at a flow rate of 1.0 mL/min for 20 min and purity was assessed at 254 nm.

Method B: ITZ analogues were dissolved in HPLC-grade MeCN and injected (20μL of a 1mM solution) into an Agilent HPLC system coupled to an Agilent ESI single quadrupole mass spectrometer equipped with a Kinetix C18 (150 x 4.6 mm) column and an Agilent G1315 diode array detector. The mobile phase consisted of 70% MeCN/30% H_2O for *des*-triazole ITZ analogues. All analogues were run at a flow rate of 0.7 mL/min for 30 min and purity was assessed at 254 nm.

Previously Characterized Intermediates: Common ITZ linker region, dioxolane region, side chain, and coupled intermediates were prepared primarily as described previously for the ITZ scaffold with the minor modifications described in Appendix A.

4-(4-(4-(4-((2-((1H-1,2,4-triazol-1-yl)methyl)-2-(2,4-dichlorophenyl)-1,3-dioxolan-4-yl)methoxy)phenyl)piperazin-1-yl)phenyl)-2-(sec-butyl)-2,4-dihydro-3H-1,2,4-triazol-3-one (46) . To a solution of **30** (50 mg, 0.127 mol) in DMSO (2 mL) was added dioxolane tosylate **43** (67 mg, 0.139 mmol) followed by Cs_2CO_3 (0.41 mg, 1.27 mmol). The mixture was warmed to 80 °C and stirred for 16 h. The mixture was cooled to RT and water was added slowly (6 mL) with vigorous stirring to form a precipitate. The precipitate was filtered, washed with water, and determined to be the product with only

DMOS as an impurity. The precipitate was dissolve in EtOAc (60 mL) and washed with water (50 mL). The aqueous layer was washed with EtOAc (1 X 50 mL) and the combined organic layers were dried (Na_2SO_4), filtered, and concentrated. The crude residue was purified by column chromatography (SiO_2, 0-80% acetone in hexanes) and sonicated in pentanes to produce **46** as a white solid (62 mg, 69%). ^{1}H NMR (500 MHz, $CDCl_3$) δ 8.20 (d, *J* = 8.2 Hz, 1H), 7.91 (d, *J* = 10.6 Hz, 1H), 7.64 – 7.55 (m, 2H), 7.50 – 7.39 (m, 3H), 7.06 – 6.99 (m, 2H), 6.94 (d, *J* = 9.1 Hz, 1H), 6.88 (d, *J* = 8.9 Hz, 1H), 6.84 – 6.77 (m, 1H), 6.69 – 6.61 (m, 1H), 4.88 – 4.70 (m, 2H), 4.40 – 4.19 (m, 2H), 3.96 – 3.87 (m, 1H), 3.85 – 3.76 (m, 2H), 3.54 – 3.44 (m, 1H), 3.36 (m, 4H), 3.23 (m, 4H), 1.87 (m, 1H), 1.72 (m, 1H), 1.39 (dd, *J* = 6.7, 1.4 Hz, 3H), 0.91 (m, 3H). ^{13}C NMR (126 MHz, $CDCl_3$) δ 152.52, 152.43, 151.94, 151.49, 151.31, 150.45, 145.94, 145.89, 144.81, 144.60, 135.98, 135.70, 134.97, 133.97, 133.81, 133.04, 132.89, 131.35, 131.06, 129.52, 129.42, 127.15, 126.98, 125.87, 123.46, 118.37, 118.27, 116.58, 115.19, 115.08, 74.62, 67.57, 67.37, 54.30, 53.53, 52.58, 50.49, 49.15, 28.35, 19.17, 10.70. DART-HRMS: *m/z* calcd. for $C_{35}H_{38}Cl_2N_8O_4$ $[MH]^+$, 705.2471; Found: 705.2474. IR (solid) *v*max: 3125, 2966, 2832, 1698, 1585, 1551, 1510, 1450, 1379, 1228, 1184, 1139, 1042, 976, 944, 824, 736. Purity: 98.0% (Method A).

1-(*sec*-butyl)-4-(4-(4-(4-((2-(2,4-dichlorophenyl)-2-methyl-1,3-dioxolan-4-yl)methoxy)phenyl)piperazin-1-yl)phenyl)-1H-1,2,4-triazol-5(4H)-one (47). To a solution of **30** (64 mg, 0.163 mmol) in DMSO (10 mL) was added sodium hydride (1.14 mmol). The mixture was warmed to 50° C and stirred for 2 h. To this solution was added **57a** (62 mg, 0.148 mmol in DMSO, 5 mL). The solution was warmed to 90° C and stirred for 12 h. The mixture was cooled to RT and H_2O (30 mL) was added slowly with

vigorous stirring. The mixture was washed with EtOAc (3 X 100 mL), and the organic layers were combined, dried (Na_2SO_4), filtered, and concentrated. The crude residue was purified by column chromatography (SiO_2, 0-5% MeOH in DCM) to afford **47** as a reddish-brown solid in modest yield (34%). A portion of **47** was dissolved in chloroform and slow evaporation provided off-white crystals that were utilized for the biological assays. ^{1}H NMR (500 MHz, $CDCl_3$) δ 7.66 – 7.59 (m, 2H), 7.46 – 7.36 (m, 3H), 7.21 (m, 1H), 7.06 – 7.00 (m, 2H), 7.01 – 6.71 (m, 4H), 4.37 – 4.25 (m, 2H), 4.12 (m, 1H), 4.01 (m, 1H), 3.96 (m, 1H), 3.79 (m, 1H), 3.36 (d, *J* = 6.2 Hz, 4H), 3.31 – 3.17 (m, 4H), 1.89 – 1.82 (m, 1H), 1.82 (s, 3H), 1.78 (s, 1H), 1.72 (m, 1H), 1.39 (d, *J* = 6.7 Hz, 3H), 0.90 (t, *J* = 7.4 Hz, 3H). ^{13}C NMR (126 MHz, $CDCl_3$) δ 152.0, 150.5, 138.1, 134.5, 133.8, 132.8, 131.1, 128.8, 128.5, 126.7, 126.6, 125.9, 123.5, 118.4, 116.6, 115.5, 109.0, 73.9, 69.2, 66.9, 52.7, 50.6, 49.2, 28.4, 25.8, 25.7, 19.2, 10.7. DART-HRMS: *m/z* calcd. for $C_{33}H_{38}Cl_2N_5O_4$ $[MH]^+$, 638.2301; Found: 638.2298. IR (solid) *v*max 2960, 2922, 2874, 2850, 1696, 1552, 1509, 1462, 1449, 1376, 1226, 1192, 1149, 1076, 1034, 870, 734. Purity: 98.0% (Method A).

4-(4-(4-(4-((2-((1*H*-1,2,4-triazol-1-yl)methyl)-2-phenyl-1,3-dioxolan-4-yl)methoxy)phenyl)piperazin-1-yl)phenyl)-1-(*sec*-butyl)-1*H*-1,2,4-triazol-5(4*H*)-one (48). ITZ analogue **48** was prepared using the general method described above for analogue **46** utilizing the requisite linker/side chain and dioxolane intermediates (23 mg, 47%). ^{1}H NMR (500 MHz, $CDCl_3$) δ 8.20 (s, 1H), 7.91 (s, 1H), 7.61 (s, 1H), 7.57 – 7.51 (m, 2H), 7.46 – 7.34 (m, 5H), 7.06 – 7.00 (m, 2H), 6.96 – 6.90 (m, 2H), 6.82 – 6.76 (m, 2H), 4.54 (d, *J* = 1.6 Hz, 2H), 4.39 – 4.25 (m, 2H), 3.90 (dd, *J* = 8.4, 6.7 Hz, 1H), 3.77 (m, 2H), 3.44 (m, 1H), 3.39 – 3.33 (m, 4H), 3.26 – 3.16 (m, 4H), 1.93 – 1.80 (m, 1H),

1.78 – 1.65 (m, 1H), 1.39 (d, *J* = 6.8 Hz, 3H), 0.90 (t, *J* = 7.4 Hz, 3H). ^{13}C NMR (126 MHz, $CDCl_3$) δ 152.45, 151.61, 145.20, 139.21, 134.33, 129.63, 129.08, 126.23, 123.97, 118.89, 117.09, 115.69, 74.96, 68.39, 67.73, 56.33, 53.09, 51.03, 49.65, 28.86, 19.67, 11.21. DART-HRMS: *m/z* calcd. for $C_{35}H_{40}N_8O_4$ $[MH]^+$, 637.3251; Found: 637.3271. IR (solid) *v*max 3122, 3058, 2961, 2825, 1693, 1602, 1551, 1508, 1448, 1388, 1327, 1296, 1226, 1180, 1135, 1939, 944, 823, 736, 701, 676. Purity: 97.1% (Method A).

4-(4-(4-(4-((2-((1H-1,2,4-triazol-1-yl)methyl)-2-methyl-1,3-dioxolan-4-yl)methoxy)phenyl)piperazin-1-yl)phenyl)-2-(sec-butyl)-2,4-dihydro-3H-1,2,4-triazol-3-one (**49**). ITZ analogue **49** was prepared using the general method described above for analogue **46** utilizing the requisite linker/side chain and dioxolane intermediates. (45%) ^{1}H NMR (500 MHz, $CDCl_3$) δ 8.30 – 8.10 (m, 1H), 7.94 (s, 1H), 7.62 (s, 1H), 7.43 (d, *J* = 8.5 Hz, 2H), 7.03 (d, *J* = 8.9 Hz, 2H), 6.97 – 6.87 (m, 2H), 6.84 (t, *J* = 9.9 Hz, 2H), 4.49 (t, *J* = 5.8 Hz, 1H), 4.39 (s, 1H), 4.36 – 4.24 (m, 2H), 4.15 (m, 1H), 4.03 – 3.84 (m, 1H), 3.79 (m, 1H), 3.69 – 3.59 (m, 1H), 3.42 – 3.33 (m, 4H), 3.24 (t, *J* = 5.0 Hz, 4H), 1.92 – 1.81 (m, 1H), 1.72 (m, 1H), 1.44 (s, 1H), 1.43 – 1.36 (m, 5H), 0.90 (t, *J* = 7.4 Hz, 3H).^{13}C NMR (126 MHz, $CDCl_3$) δ 152.7, 152.0, 151.4, 150.5, 145.9, 144.6, 133.9, 125.9, 123.5, 118.5, 118.4, 116.6, 115.3, 115.2, 108.0, 75.4, 74.8, 68.5, 67.7, 67.5, 67.1, 55.7, 55.6, 52.6, 50.6, 49.2, 28.4, 23.5, 22.5, 19.2, 10.7. IR (solid) *v*max 3121, 3053, 2930, 2850, 2809, 1702, 1683, 1548, 1510, 1471, 1452, 1336, 1251, 1134, 1106, 1068, 1050, 940, 883, 735. DART-HRMS: *m/z* calcd. for $C_{30}H_{39}N_8O_4$ $[MH]^+$, 575.3094; Found: 575.3090. IR (solid) *v*max: 2967, 2934, 2878, 2837, 1701,

1554, 1510, 1450, 1382, 1225, 1181, 1136, 1042, 1017, 942, 826, 784. Purity: 95.1% (Method A).

1-(*sec*-butyl)-4-(4-(4-(4-((2,2-dimethyl-1,3-dioxolan-4-yl)methoxy)phenyl)piperazin-1-yl)phenyl)-1*H*-1,2,4-triazol-5(4*H*)-one (50). ITZ analogue **50** was prepared using the general method described above for analogue **47** utilizing the requisite linker/side chain and dioxolane intermediates. The crude residue was purified via column chromatography (SiO_2, 0-5% MeOH in DCM) to afford **50** in modest yield (14 mg, 21%) ^{1}H NMR (500 MHz, $CDCl_3$) δ 7.61 (d, *J* = 7.2 Hz, 1H), 7.43 (d, *J* = 8.4 Hz, 2H), 7.03 (d, *J* = 8.5 Hz, 2H), 6.94 (s, 1H), 6.89 (d, *J* = 8.4 Hz, 2H), 4.46 (m, 1H), 4.29 (m, 1H), 4.16 (t, *J* = 7.4 Hz, 1H), 4.04 (m, 1H), 3.90 (m, 2H), 3.37 (s, 2H), 3.24 (s, 2H), 1.86 (m, 1H), 1.71 (m, 1H), 1.46 (s, 3H), 1.39 (d, *J* = 7.8 Hz, 6H), 0.91 (t, *J* = 7.4 Hz, 3H). ^{13}C NMR (126 MHz, $CDCl_3$) δ 152.44, 134.28, 124.08, 123.96, 118.93, 117.14, 115.81, 110.13, 74.49, 69.77, 67.32, 53.11, 51.11, 49.62, 33.08, 28.86, 27.22, 25.79, 19.66, 11.20. DART-HRMS: *m/z* calcd. for $C_{28}H_{37}N_5O_4$ $[MH]^+$, 508.2924; Found: 508.2909. IR (solid) *v*max: 3126, 3060, 2967, 2926, 2878, 2828, 2212, 1681, 1584, 1556, 1510, 1452, 1380, 1226, 1149, 1037, 941, 819, 736. Purity: 97.5% (Method B).

4-(4-(4-(4-((2-((1H-1,2,4-triazol-1-yl)methyl)-2-(2,4-dichlorophenyl)-1,3-dioxolan-4-yl)methoxy)phenyl)piperazin-1-yl)phenyl)-2-((*S*)-*sec*-butyl)-2,4-dihydro-3H-1,2,4-triazol-3-one (51). ITZ analogue **51** was prepared using the general method described above for analogue **46** utilizing the requisite linker/side chain and dioxolane intermediates (55%). ^{1}H NMR (500 MHz, $CDCl_3$) δ 8.20 (s, 1H), 7.89 (s, 1H), 7.61 (s, 1H), 7.57 (d, *J* = 8.3Hz, 1H), 7.47 (d, *J* = 2.1Hz, 1H), 7.43 (d, *J* = 8.9Hz, 2H), 7.03 (d, *J* = 9.0Hz, 2H), 6.94 (m, 2H), 6.80 (m, 2H), 4.80 (m, 2H), 4.36 (m, 1H), 4.28 (m, 1H), 3.92

(m, 1H), 3.81 (m, 2H), 3.48 (m, 1H), 3.36 (m, 4H), 3.23 (m, 4H), 1.86 (m, 1H), 1.72 (m, 1H), 1.39 (d, *J* = 6.7 Hz, 3H), 0.90 (t, *J* = 7.4 Hz, 3H). ^{13}C NMR (126 MHz, $CDCl_3$) δ 152.6, 151.4, 150.5, 146.0, 144.8, 136.0, 134.0, 133.8, 133.1, 131.4, 129.6, 127.2, 125.9, 123.5, 118.4, 116.6, 115.2, 109.9, 107.6, 74.7, 67.6, 67.4, 53.6, 52.6, 50.5, 49.2, 28.4, 19.2, 10.7. DART-HRMS: *m/z* calcd. for $C_{35}H_{39}Cl_2N_8O_4$ $[MH]^+$, 705.2471; Found: 705.2465. IR (solid) *v*max: 2967, 2930, 2878, 1695, 1586, 1552, 1509, 1451, 1378, 1226, 1183, 1130, 1038, 947, 816, 736. Purity: 97.9% (Method A).

4-(4-(4-(4-((2-((1H-1,2,4-triazol-1-yl)methyl)-2-(2,4-dichlorophenyl)-1,3-dioxolan-4-yl)methoxy)phenyl)piperazin-1-yl)phenyl)-2-((R)-sec-butyl)-2,4-dihydro-3H-1,2,4-triazol-3-one (52). ITZ analogue **52** was prepared using the general method described above for analogue **46** utilizing the requisite linker/side chain and dioxolane intermediates (77%). ^{1}H NMR (500 MHz, $CDCl_3$) δ 8.20 (s, 1H), 7.89 (s, 1H), 7.64 – 7.54 (m, 2H), 7.50 – 7.40 (m, 3H), 7.03 (d, *J* = 8.6 Hz, 2H), 6.95 (s, 1H), 6.81 (d, *J* = 8.4 Hz, 2H), 4.84 (d, *J* = 14.7 Hz, 1H), 4.76 (d, *J* = 14.7 Hz, 1H), 4.39 – 4.25 (m, 2H), 3.92 (m, 1H), 3.86 – 3.77 (m, 2H), 3.50 (m, 1H), 3.38 (s, 2H), 3.25 (s, 3H), 1.87 (m, 1H), 1.72 (m, 1H), 1.39 (d, *J* = 6.7 Hz, 3H), 0.91 (t, *J* = 7.4 Hz, 3H). ^{13}C NMR (126 MHz, $CDCl_3$) δ 152.5, 152.0, 151.3, 150.5, 146.0, 136.0, 134.0, 133.8, 133.1, 131.4, 129.5, 127.2, 125.9, 123.5, 118.4, 116.6, 115.2, 107.6, 77.2, 74.7, 67.6, 67.4, 53.6, 52.6, 50.5, 49.2, 28.4, 19.2, 10.7. DART-HRMS: *m/z* calcd. for $C_{35}H_{39}Cl_2N_8O_4$ $[MH]^+$, 705.2471; Found: 705.2468. IR (solid) *v*max: 3067, 2966, 2934, 2878, 2832, 1695, 1585, 1551, 1509, 1450, 1379, 1225, 1180, 1136, 1039, 944, 820, 794. Purity: 95.0% (Method A).

4-(4-(4-(4-((2-((1*H*-1,2,4-triazol-1-yl)methyl)-2-(2,4-dichlorophenyl)-1,3-dioxolan-4-yl)methoxy)phenyl)piperazin-1-yl)phenyl)-1-propyl-1*H*-1,2,4-triazol-5(4*H*)-one (53).

ITZ analogue **53** was prepared using the general method described above for analogue **47** utilizing the requisite linker/side chain and dioxolane intermediates (50 mg, 68%). ^{1}H NMR (500 MHz, $CDCl_3$) δ 8.20 (s, 1H), 7.89 (s, 1H), 7.59 (d, *J* = 21.6 Hz, 2H), 7.48 (s, 1H), 7.41 (s, 2H), 7.04 (s, 2H), 6.93 (s, 2H), 6.81 (s, 2H), 4.80 (d, *J* = 23.3 Hz, 2H), 4.36 (s, 1H), 3.92 (s, 1H), 3.82 (s, 4H), 3.52 (s, 1H), 3.37 (s, 4H), 3.24 (s, 5H), 1.84 (s, 2H), 0.98 (s, 3H). ^{13}C NMR (126 MHz, $CDCl_3$) δ 152.60, 136.48, 134.30, 133.55, 131.85, 130.02, 127.65, 123.98, 117.08, 115.73, 108.05, 75.13, 68.11, 54.05, 51.01, 49.60, 47.62, 22.43, 11.50. DART-HRMS: *m/z* calcd. for $C_{34}H_{36}Cl_2N_8O_4$ $[MH]^+$, 691.2315; Found: 691.2329. IR (solid) *v*max: 3068, 2960, 2925, 2873, 2835, 1696, 1585, 1553, 1510, 1452, 1379, 1225, 1160, 1136, 1045, 944, 823, 794. Purity: 95.2% (Method A).

1-(4-((2-((1*H*-1,2,4-triazol-1-yl)methyl)-2-(2,4-dichlorophenyl)-1,3-dioxolan-4-yl)methoxy)phenyl)-4-(4-nitrophenyl)piperazine (54). To a solution of **44** (100 mg, 0.336 mmol) in DMSO (4 mL) was added Cs_2CO_3 (1.1 g, 3.36 mmol) and **43** (0.29 g, 0.604 mmol). The solution was warmed to 90° C and stirred for 12 h. The mixture was cooled to room temperature and water was added slowly with vigorous stirring (~6 mL). A yellow precipitate formed, which was filtered and recrystallized in EtOH to yield **54** (150 mg, 73%). ^{1}H NMR (500 MHz, $CDCl_3$) δ 8.22 – 8.12 (m, 3H), 7.90 (s, 1H), 7.58 (d, *J* = 8.5 Hz, 1H), 7.48 (d, *J* = 2.1 Hz, 1H), 6.95 – 6.86 (m, 4H), 6.86 – 6.78 (m, 2H), 4.84 (d, *J* = 14.8 Hz, 1H), 4.76 (d, *J* = 14.7 Hz, 1H), 4.36 (m, 1H), 3.92 (m, 1H), 3.85 – 3.75 (m, 3H), 3.61 – 3.55 (m, 4H), 3.48 (m, 1H), 3.26 – 3.20 (m, 4H). ^{13}C NMR (126 MHz, $CDCl_3$) δ 154.79, 152.90, 151.42, 145.67, 144.94, 138.79, 136.14, 134.08, 133.17, 131.49, 129.63, 127.28, 125.99, 118.58, 115.39, 112.90, 107.69, 74.72, 67.71, 67.45, 53.63, 50.33, 47.29. DART-HRMS: *m/z* calcd. for $C_{29}H_{28}Cl_2N_6O_5$ $[MH]^+$, 611.1577;

Found: 611.1601. IR (solid) *v*max: 3116, 2923, 2852, 1589, 1557, 1506, 1456, 1377, 1318, 1226, 1136, 1029, 975, 942, 896, 823, 737, 691. Purity: 95.0% (Method A).

4-(4-(4-((2-((1*H*-1,2,4-triazol-1-yl)methyl)-2-(2,4-dichlorophenyl)-1,3-dioxolan-4-yl)methoxy)phenyl)piperazin-1-yl)aniline (55). 10% palladium on carbon (1.04 mg, 5% mole ratio) was added to a dry round bottom flask. Ethanol (25 mL) was added followed by slow addition of **54** (120 mg, 0.196 mmol). Hydrazine monohydrate (0.06 mL, 1.96 mmol) was added dropwise and the mixture was stirred at reflux for 2 h. Upon cooling to RT, the mixture was filtered through celite. The celite was washed with ethanol (100 mL) and chloroform (250 mL) to ensure complete elution of the aniline. The filtrate was concentrated to afford a yellow solid, which was recrystallized in EtOH to afford **55** (70 mg, 61%). ^{1}H NMR (500 MHz, $CDCl_3$) δ 8.20 (s, 1H), 8.15 (d, *J* = 9.4Hz, 2H), 7.89 (s, 1H), 7.57 (d, *J* = 8.4Hz, 1H), 7.47 (m, 1H), 7.25 (m, 1H), 6.92 (m, 2H), 6.88 (d, *J* = 9.5Hz, 2H), 6.80 (d, *J* = 9.0Hz, 2H), 4.80 (m, 2H), 4.36 (m, 1H), 3.91 (m, 1H), 3.80 (m, 2H), 3.58 (m, 4H), 3.47 (m, 1H), 3.22 (m, 4H). ^{13}C NMR (126 MHz) δ 154.7, 152.8, 151.3, 145.6, 144.9, 138.7, 136.1, 134.0, 133.1, 131.4, 129.6, 127.2, 125.9, 118.5, 115.3, 112.8, 107.6, 74.6, 67.6, 67.4, 53.6, 50.3, 47.2. DART-HRMS: *m/z* calcd. for $C_{29}H_{31}Cl_2N_6O_3$ $[MH]^+$, 581.1835; Found: 581.1818. IR (solid) *v*max: 3084, 2886, 2827, 1558, 1504, 1313, 1224, 113, 1030, 942, 821, 749. Purity: 96.1% (Method A).

General protocol for tosylate/phenol coupling and final analogue purification. To a solution of alkyl-substituted phenol **(28-31)** (40 mg, 0.102 mmol) in DMSO (2.0 mL) was added *des*-triazole-tosylate (**57b**-**57c, 59**-**62**) (46 mg, 0.110 mmol) followed by Cs_2CO_3 (0.82 mmol). The mixture was warmed to 80° C and stirred for 16 h. The mixture was then cooled to RT and water was added slowly (6 mL) with vigorous

stirring, which resulted in formation of a precipitate. The mixture was transferred to a separatory funnel, diluted with EtOAc (60 mL) and washed with water (50 mL). The aqueous layer was washed with EtOAc (1 X 60 mL). The organic layers were combined, dried ($MgSO_4$), filtered, and concentrated. The crude residue was purified by column chromatography (SiO_2, 0 to 24% acetone in hexanes) to afford **47, 63-76** as white to slightly off-white solids in good yields (45-88%). Final analogues were subsequently sonicated in pentanes (10-30 min) to remove a "grease-like" impurity (observed in ^1H NMRs at 0.88, 1.31 ppm) and collected for purity analysis and biological evaluation following filtration on a fine-fritted glass Buchner style filter funnel.

4-(4-(4-(4-((2-((1H-1,2,4-triazol-1-yl)methyl)-2-(2,4-dichlorophenyl)-1,3-dioxolan-4-yl)methoxy)phenyl)piperazin-1-yl)phenyl)-2-(*sec*-butyl)-2,4-dihydro-3H-1,2,4-triazol-3-one (63). ^1H NMR (500 MHz, $CDCl_3$) δ 7.62 (m, 2H), 7.42 (m, 3H), 7.23 (m, 1H), 7.03 (m, 2H), 6.92 (m, 2H), 4.31 (m, 2H), 4.11 (m, 1H), 4.01 (m, 1H), 3.97 (m, 1H), 3.84 (m, 1H), 3.36 (m, 4H), 3.24 (m, 4H), 1.87 (m, 1H), 1.81 (s, 3H), 1.72 (m, 1H), 1.39 (d, *J* = 6.7 Hz, 3H), 0.91 (t, *J* = 7.4 Hz, 3H). ^{13}C NMR (126 MHz, $CDCl_3$) δ 152.7, 152.0, 150.5, 145.8, 139.2, 134.2, 133.8, 132.7, 130.9, 128.5, 126.6, 125.9, 123.5, 118.3, 116.6, 115.2, 109.1, 73.9, 69.3, 66.9, 52.6, 50.6, 49.2, 28.4, 25.6, 19.2, 10.7. DART-HRMS: *m/z* calcd. for $C_{33}H_{38}Cl_2N_5O_4$ $[MH]^+$, 638.2301; Found: 638.2328. IR (solid) *v*max 2961, 2918, 2849, 1694, 1584, 1556, 1509, 1449, 1374, 1329, 1294, 1224, 1186, 1149, 1094, 1035, 1017, 942, 873, 821, 802, 734. Purity: 97.0% (Method B).

4-(4-(4-(4-((2-((1H-1,2,4-triazol-1-yl)methyl)-2-(2,4-dichlorophenyl)-1,3-dioxolan-4-yl)methoxy)phenyl)piperazin-1-yl)phenyl)-2-(*sec*-butyl)-2,4-dihydro-3H-1,2,4-triazol-3-one (64). ^1H NMR (500 MHz, $CDCl_3$) δ 7.63 (d, *J* = 8.5 Hz, 1H), 7.61 (s, 1H),

7.42 (m, 2H), 7.38 (d, *J* = 2.1 Hz, 1H), 7.19 (m, 1H), 7.01 (m, 2H), 6.89 (m, 2H), 6.73 (m, 2H), 4.60 (m, 1H), 4.29 (m, 2H), 3.94 (m, 1H), 3.73 (m, 1H), 3.35 (m, 4H), 3.21 (m, 4H), 1.85 (m, 1H), 1.77 (s, 3H), 1.71 (m, 1H), 1.39 (d, *J* = 6.7 Hz, 3H), 0.90 (t, *J* = 7.4 Hz, 3H). ^{13}C NMR (126 MHz, $CDCl_3$) δ 152.7, 152.0, 150.5, 145.8, 139.2, 134.2, 133.8, 132.7, 130.9, 128.5, 126.6, 125.9, 123.5, 118.3, 116.6, 115.2, 109.1, 75.0, 68.3, 67.3, 52.6, 50.5, 49.2, 28.4, 25.8, 19.2, 10.7. HRMS: *m/z* calcd. for $C_{33}H_{38}Cl_2N_5O_4$ $[MH]^+$, 638.2301; Found: 638.2325. IR (solid) *v*max 3102, 3008, 2961, 2918, 2899, 2849, 1699, 1597, 1538, 1515, 1411, 1355, 1337, 1254, 1236, 1189 1159, 1106, 1064, 1036, 1024, 999, 936, 896, 831, 807, 741. Purity: 95.1% (Method B).

2-((*S*)-*sec*-butyl)-4-(4-(4-(4-(((2*S*,4*S*)-2-(2,4-dichlorophenyl)-2-methyl-1,3-dioxolan-4-yl)methoxy)phenyl)piperazin-1-yl)phenyl)-2,4-dihydro-3H-1,2,4-triazol-3-one (65). ^{1}H NMR (500 MHz, $CDCl_3$) δ 7.61 (m, 3H), 7.42 (m, 2H), 7.40 (m, 1H), 7.23 (m, 1H), 7.02 (m, 2H), 6.94 (m, 2H), 6.88 (m, 2H), 4.31 (m, 2H), 4.11 (m, 1H), 4.00 (m, 1H), 3.96 (m, 1H), 3.36 (m, 4H), 3.23 (m, 4H), 1.85 (m, 1H), 1.81 (s, 3H), 1.72 (m, 1H), 1.39 (d, *J* = 6.7 Hz, 3H), 0.91 (t, *J* = 7.4 Hz, 3H). ^{13}C NMR (126 MHz, $CDCl_3$) δ 152.9, 152.0, 150.5, 145.9, 138.1, 134.5, 133.8, 132.8, 131.1, 128.8, 126.7, 125.9, 123.5, 118.4, 116.6, 115.4, 109.0, 73.9, 69.2, 66.9, 52.6, 50.6, 49.2, 28.4, 25.7, 19.2, 10.7. DART-HRMS: *m/z* calcd. for $C_{33}H_{38}Cl_2N_5O_4$ $[MH]^+$, 638.2301; Found: 638.2282. IR (solid) *v*max 2962, 2875, 2826, 1694, 1555, 1509, 1448, 1374, 1224, 1186, 1149, 1035, 942, 824, 735. Purity: 97.4% (Method A).

2-((*S*)-*sec*-butyl)-4-(4-(4-(4-(((2*R*,4*S*)-2-(2,4-dichlorophenyl)-2-methyl-1,3-dioxolan-4-yl)methoxy)phenyl)piperazin-1-yl)phenyl)-2,4-dihydro-3H-1,2,4-triazol-3-one (66). ^{1}H NMR (500 MHz, $CDCl_3$) δ 7.64 (d, *J* = 8.4 Hz, 2H), 7.61 (s, 1H), 7.42 (d, *J* = 8.5 Hz,

2H), 7.38 (d, *J* = 2.2 Hz, 2H), 7.19 (m, 1H), 7.02 (d, *J* = 8.5 Hz, 2H), 6.90 (d, *J* = 8.5 Hz, 2H), 6.73 (d, *J* = 8.5 Hz, 2H), 4.60 (m, 1H), 4.30 (m, 2H), 3.94 (m, 1H), 3.73 (m, 2H), 3.35 (m, 4H), 3.21 (m, 4H), 1.86 (m, 1H), 1.78 (s, 3H), 1.72 (m, 1H), 1.39 (d, *J* = 6.7 Hz, 3H), 0.91 (t, *J* = 7.4 Hz, 3H). ^{13}C NMR (126 MHz, $CDCl_3$) δ 152.8, 152.0, 150.5, 145.8, 139.3, 134.3, 133.8, 132.7, 130.9, 128.5, 126.6, 125.9, 123.5, 118.4, 116.6, 115.2, 109.1, 75.0, 68.4, 67.3, 52.6, 50.6, 49.2, 28.4, 25.8, 19.2, 10.7. DART-HRMS: *m/z* calcd. for $C_{33}H_{38}Cl_2N_5O_4$ $[MH]^+$, 638.2301; Found: 638.2288. IR (solid) *v*max 2923, 2851, 1714, 1703, 1683, 1613, 1548, 1509, 1452, 1374, 1271, 1226, 1188, 1150, 1094, 1035, 965, 942, 817, 735. Purity: 95.5% (Method A).

2-((*S*)-*sec*-butyl)-4-(4-(4-(4-(((2*R*,4*R*)-2-(2,4-dichlorophenyl)-2-methyl-1,3-dioxolan-4-yl)methoxy)phenyl)piperazin-1-yl)phenyl)-2,4-dihydro-3H-1,2,4-triazol-3-one (67). ^{1}H NMR (500 MHz, $CDCl_3$) δ 7.61 (m, 2H), 7.41 (m, 3H), 7.23 (m, 1H), 7.02 (m, 2H), 6.94 (m, 2H), 6.89 (m, 2H), 4.31 (m, 2H), 4.11 (m, 1H), 4.00 (m, 1H), 3.96 (m, 1H), 3.84 (m, 1H), 3.36 (m, 4H), 3.23 (m, 4H), 1.86 (m, 1H), 1.81 (s, 3H), 1.72 (m, 1H), 1.39 (d, *J* = 6.7 Hz, 3H), 0.91 (t, *J* = 7.4 Hz, 3H). ^{13}C NMR (126 MHz, $CDCl_3$) δ 152.9, 152.0, 150.5, 145.9, 138.1, 134.5, 133.8, 132.8, 131.1, 128.8, 126.7, 125.9, 123.5, 118.4, 116.6, 115.4, 109.0, 73.9, 69.2, 66.9, 52.6, 50.6, 49.2, 28.4, 25.7, 19.2, 10.7. DART-HRMS: *m/z* calcd. for $C_{33}H_{38}Cl_2N_5O_4$ $[MH]^+$, 638.2301; Found: 638.2284. IR (solid) *v*max 2966, 2935, 2874, 2824, 1693, 1584, 1555, 1508, 1464, 1447, 1373, 1293, 1223, 1186, 1149, 1095, 1035, 942, 875, 824, 734. Purity: 97.3% (Method A).

2-((*S*)-*sec*-butyl)-4-(4-(4-(4-(((2*S*,4*R*)-2-(2,4-dichlorophenyl)-2-methyl-1,3-dioxolan-4-yl)methoxy)phenyl)piperazin-1-yl)phenyl)-2,4-dihydro-3H-1,2,4-triazol-3-one (68). ^{1}H NMR (500 MHz, $CDCl_3$) δ 7.64 (d, *J* = 8.5 Hz, 1H), 7.61 (s, 1H), 7.42 (m, 2H), 7.38

(d, *J* = 2.1 Hz, 1H), 7.19 (m, 1H), 7.02 (m, 2H), 6.89 (m, 2H), 6.73 (m, 2H), 4.60 (m, 1H), 4.30 (m, 2H), 3.94 (m, 1H), 3.73 (m, 2H), 3.35 (m, 4H), 3.21 (m, 4H), 1.85 (m, 1H), 1.78 (s, 3H), 1.72 (m, 1H), 1.39 (d, *J* = 6.7 Hz, 3H), 0.91 (t, *J* = 7.4 Hz, 3H). ^{13}C NMR (126 MHz, $CDCl_3$) δ 152.8, 152.0, 150.5, 145.8, 139.3, 134.3, 133.8, 132.7, 130.9, 128.5, 126.6, 125.9, 123.5, 118.4, 118.4, 116.6, 115.2, 109.1, 75.0, 68.4, 67.3, 52.6, 50.6, 49.2, 28.4, 25.8, 19.2, 10.7. DART-HRMS: *m/z* calcd. for $C_{33}H_{38}Cl_2N_5O_4$ $[MH]^+$, 638.2301; Found: 638.2281. IR (solid) *v*max 2919, 2876, 2849, 1693, 1585, 1555, 1509, 1450, 1375, 1329, 1295, 1225, 1188, 1149, 1095, 1034, 934, 872, 819, 734. Purity: 98.4% (Method A).

2-((*R*)-*sec*-butyl)-4-(4-(4-(4-(((2*S*,4*S*)-2-(2,4-dichlorophenyl)-2-methyl-1,3-dioxolan-4-yl)methoxy)phenyl)piperazin-1-yl)phenyl)-2,4-dihydro-3H-1,2,4-triazol-3-one (69). ^{1}H NMR (500 MHz, $CDCl_3$) δ 7.61 (m, 2H), 7.42 (m, 2H), 7.41 (m, 1H), 7.23 (m, 1H), 7.03 (m, 2H), 6.94 (m, 2H), 6.89 (m, 2H), 4.31 (m, 2H), 4.11 (m, 1H), 4.01 (m, 1H), 3.96 (m, 1H), 3.84 (m, 1H), 3.36 (m, 4H), 3.23 (m, 4H), 1.87 (m, 1H), 1.81 (s, 3H), 1.72 (m, 1H), 1.39 (d, *J* = 6.7 Hz, 3H), 0.91 (t, *J* = 7.4 Hz, 3H). ^{13}C NMR (126 MHz, $CDCl_3$) δ 152.9, 152.0, 150.5, 145.9, 138.1, 134.5, 133.8, 132.8, 131.1, 128.8, 126.7, 125.9, 123.5, 118.4, 116.6, 115.4, 109.0, 73.9, 69.2, 66.9, 52.6, 50.6, 49.2, 28.4, 25.7, 19.2, 10.7. DART-HRMS: *m/z* calcd. for $C_{33}H_{38}Cl_2N_5O_4$ $[MH]^+$, 638.2301; Found: 638.2282. IR (solid) *v*max 2967, 2932, 2878, 2827, 1695, 1612, 1586, 1552, 1510, 1460, 1377, 1292, 1253, 1225, 1187, 1147, 1096, 1036, 940, 827, 735. Purity: 95.0% (Method B).

2-((*R*)-*sec*-butyl)-4-(4-(4-(4-(((2*R*,4*S*)-2-(2,4-dichlorophenyl)-2-methyl-1,3-dioxolan-4-yl)methoxy)phenyl)piperazin-1-yl)phenyl)-2,4-dihydro-3H-1,2,4-triazol-3-one (70). ^{1}H NMR (500 MHz, $CDCl_3$) δ 7.64 (d, *J* = 8.5 Hz, 1H), 7.61 (s, 1H), 7.42 (m, 2H), 7.38

(m, 1H), 7.20 (m, 1H), 7.02 (m, 2H), 6.90 (m, 2H), 6.73 (m, 2H), 4.60 (m, 1H), 4.30 (m, 1H), 3.94 (m, 1H), 3.73 (m, 1H), 3.35 (m, 4H), 3.21 (m, 4H), 1.86 (m, 1H), 1.78 (s, 3H), 1.71 (m, 1H), 1.39 (d, *J* = 6.7 Hz, 3H), 0.91 (t, *J* = 7.4 Hz, 3H). ^{13}C NMR (126 MHz, $CDCl_3$) δ 152.9, 152.0, 150.5, 145.9, 138.1, 134.5, 133.8, 132.8, 131.1, 128.7, 126.7, 125.9, 123.5, 118.4, 116.6, 115.4, 109.0, 73.9, 69.2, 66.9, 52.6, 50.6, 49.2, 28.4, 25.7, 19.2, 10.7. DART-HRMS: *m/z* calcd. for $C_{33}H_{38}Cl_2N_5O_4$ $[MH]^+$, 638.2301; Found: 638.2287. IR (solid) *v*max 3060, 2967, 2932, 2830, 1698, 1611, 1586, 1550, 1512, 1461, 1384, 1296, 1252, 1225, 1189, 1149, 1098, 1036, 940, 896, 824, 735. Purity: 95.0% (Method B).

2-((*R*)-*sec*-butyl)-4-(4-(4-(4-(((2*R*,4*R*)-2-(2,4-dichlorophenyl)-2-methyl-1,3-dioxolan-4-yl)methoxy)phenyl)piperazin-1-yl)phenyl)-2,4-dihydro-3H-1,2,4-triazol-3-one (71). ^{1}H NMR (500 MHz, $CDCl_3$) δ 7.61 (m, 2H), 7.43 (m, 2H), 7.41 (m, 1H), 7.23 (m, 1H), 7.03 (m, 2H), 6.94 (m, 2H), 6.89 (m, 2H), 4.31 (m, 2H), 4.11 (m, 1H), 4.01 (m, 1H), 3.96 (m, 1H), 3.84 (m, 1H), 3.36 (m, 4H), 3.23 (m, 4H), 1.86 (m, 1H), 1.81 (s, 3H), 1.72 (m, 1H), 1.39 (d, *J* = 6.7 Hz, 3H), 0.91 (t, *J* = 7.4 Hz, 3H). ^{13}C NMR (126 MHz, $CDCl_3$) δ 153.0, 152.0, 150.5, 145.9, 138.1, 134.5, 133.8, 132.8, 131.1, 128.8, 126.7, 125.9, 123.5, 118.4, 116.6, 115.4, 109.0, 73.9, 69.2, 67.0, 52.6, 50.6, 49.2, 28.4, 25.7, 19.2, 10.7. DART-HRMS: *m/z* calcd. for $C_{33}H_{38}Cl_2N_5O_4$ $[MH]^+$, 638.2301; Found: 638.2285. IR (solid) *v*max 2971, 2937, 2879, 2827, 1697, 1509, 1451, 1376, 1296, 1225, 1194, 1147, 1073, 1035, 942, 819, 734. Purity: 97.5% (Method B).

2-((*R*)-*sec*-butyl)-4-(4-(4-(4-(((2*S*,4*R*)-2-(2,4-dichlorophenyl)-2-methyl-1,3-dioxolan-4-yl)methoxy)phenyl)piperazin-1-yl)phenyl)-2,4-dihydro-3H-1,2,4-triazol-3-one (72). ^{1}H NMR (500 MHz, $CDCl_3$) δ 7.64 (d, *J* = 8.5 Hz, 2H), 7.61 (s, 1H), 7.42 (m, 2H), 7.37

(m, 1H), 7.19 (m,1H), 7.02 (m, 2H), 6.90 (m, 2H), 6.73 (m, 2H), 4.60 (m, 1H), 4.30 (m, 2H), 3.95 (m, 1H), 3.73 (m, 2H), 3.35 (m, 4H), 3.22 (m, 4H), 1.86 (m, 1H), 1.78 (s, 3H), 1.72 (m, 1H), 1.39 (d, *J* = 6.7 Hz, 3H), 0.91 (t, *J* = 7.4 Hz, 3H). ^{13}C NMR (126 MHz, $CDCl_3$) δ 152.8, 152.0, 150.5, 145.9, 139.3, 134.3, 133.8, 132.7, 130.9, 128.5, 126.6, 125.9, 123.5, 118.4, 118.4, 116.6, 115.2, 109.1, 75.0, 68.4, 67.3, 52.6, 50.6, 49.2, 28.4, 25.8, 19.2, 10.7. DART-HRMS: *m/z* calcd. for $C_{33}H_{38}Cl_2N_5O_4$ $[MH]^+$, 638.2301; Found: 638.2284. IR (solid) *v*max 2966, 2932, 2904, 2829, 1695, 1553, 1512, 1460, 1444, 1399, 1382, 1254, 1224, 1187, 1148, 1063, 1036, 939, 827, 735. Purity: 96.4% (Method A).

4-(4-(4-(4-(((2*R*,4*R*)-2-(2,4-dichlorophenyl)-2-methyl-1,3-dioxolan-4-yl)methoxy)phenyl)piperazin-1-yl)phenyl)-2-propyl-2,4-dihydro-3H-1,2,4-triazol-3-one (73). ^{1}H NMR (500 MHz, $CDCl_3$) δ 7.61 (m, 2H), 7.41 (m, 3H), 7.23 (m, 1H), 7.02 (m, 2H), 6.94 (m, 2H), 6.89(m, 2H), 4.32 (m, 1H), 4.11 (m, 1H), 4.01 (m, 1H), 3.96 (m, 1H), 3.82 (m, 3H), 3.36 (m, 4H), 3.23 (m, 4H), 1.84 (m, 2H), 1.81 (s, 3H), 0.98 (t, *J* = 7.4 Hz, 3H). ^{13}C NMR (126 MHz, $CDCl_3$) δ 153.0, 152.1, 150.6, 145.9, 138.1, 134.5, 133.8, 132.8, 131.1, 128.8, 126.7, 125.8, 123.5, 118.4, 116.6, 115.4, 109.0, 73.9, 69.2, 66.9, 50.6, 49.2, 47.2, 25.7, 22.0, 11.1. DART-HRMS: *m/z* calcd. for $C_{32}H_{36}Cl_2N_5O_4$ $[MH]^+$, 624.2144; Found: 624.2143. IR (solid) *v*max 3125, 3059, 2935, 2876, 2829, 1703, 1686, 1614, 1585, 1551, 1510, 1454, 1405, 1375, 1336, 1297, 1225, 1194, 1143, 1094, 1035, 944, 869, 814, 733. Purity: 96.6% (Method B).

4-(4-(4-(4-(((2*S*,4*R*)-2-(2,4-dichlorophenyl)-2-methyl-1,3-dioxolan-4-yl)methoxy)phenyl)piperazin-1-yl)phenyl)-2-propyl-2,4-dihydro-3H-1,2,4-triazol-3-one (74). ^{1}H NMR (500 MHz, $CDCl_3$) δ 7.64 (d, *J* = 8.4 Hz, 1H), 7.60 (s, 1H), 7.41 (m,

2H), 7.38 (d, *J* = 2.1 Hz, 1H), 7.20 (m, 1H), 7.02 (d, *J* = 8.9 Hz, 2H), 6.90 (d, *J* = 8.9 Hz, 2H), 6.73 (d, *J* = 8.9 Hz, 2H), 4.64 (m, 1H), 4.30 (m, 1H), 3.94 (m, 1H), 3.82 (t, *J* = 7.2 Hz, 2H), 3.73 (m, 2H), 3.35 (m, 4H), 3.21 (m, 4H), 1.83 (m, 2H), 1.78 (s, 3H), 0.98 (t, *J* = 7.4 Hz, 3H). ^{13}C NMR (126 MHz, $CDCl_3$) δ 152.8, 152.1, 150.5, 145.8, 139.3, 134.3, 133.8, 132.7, 130.9, 128.5, 126.6, 125.8, 123.5, 118.4, 116.6, 115.2, 109.1, 99.9, 75.0, 68.3, 67.3, 50.6, 49.2, 47.2, 25.8, 22.0, 11.1. HRMS: *m/z* calcd. for $C_{32}H_{36}Cl_2N_5O_4$ $[MH]^+$, 624.2144; Found: 624.2142. IR (solid) *v*max 2966, 2932, 2904, 2830, 1698, 1609, 1585, 1550, 1511, 1461, 1402, 1385, 1336, 1296, 1224, 1189, 1148, 1097, 1036, 940, 875, 824, 735. Purity: 96.5% (Method B).

4-(4-(4-(4-(((2*S*,4*S*)-2-(2,4-dichlorophenyl)-2-methyl-1,3-dioxolan-4-yl)methoxy)phenyl)piperazin-1-yl)phenyl)-2-propyl-2,4-dihydro-3H-1,2,4-triazol-3-one (75). ^{1}H NMR (500 MHz, $CDCl_3$) δ 7.64(d, *J* = 8.4 Hz, 1H), 7.60 (s, 1H), 7.41 (d, *J* = 8.8 Hz, 2H), 7.38 (d, *J* = 2.1 Hz, 1H), 7.02 (m, 2H), 6.90 (d, *J* = 8.5 Hz, 2H), 6.73(m, 2H), 4.60 (m, 1H), 4.30 (m, 1H), 3.94 (m, 1H), 3.81 (t, *J* = 7.2 Hz, 2H), 3.73 (m, 2H), 3.35 (m, 4H), 3.22 (m, 4H), 1.83 (m, 2H), 1.78 (s, 3H), 0.98 (t, *J* = 7.4 Hz, 3H). ^{13}C NMR (126 MHz, $CDCl_3$) δ 153.0, 152.1, 150.6, 145.9, 138.1, 134.5, 133.8, 132.8, 131.1, 128.8, 126.7, 125.8, 123.5, 118.4, 116.6, 115.4, 109.0, 73.9, 69.2, 66.9, 50.6, 49.2, 47.2, 25.7, 22.0, 11.1. DART-HRMS: *m/z* calcd. for $C_{32}H_{36}Cl_2N_5O_4$ $[MH]^+$, 624.2144; Found: 624.2140. IR (solid) *v*max 2919, 2876, 2849, 1693, 1601, 1585, 1555, 1509, 1450, 1403, 1375, 1331, 1295, 1225, 1188, 1149, 1095, 1032, 1017, 943, 871, 814, 734. Purity: 95.4% (Method B).

4-(4-(4-(4-(((2*R*,4*S*)-2-(2,4-dichlorophenyl)-2-methyl-1,3-dioxolan-4-yl)methoxy)phenyl)piperazin-1-yl)phenyl)-2-propyl-2,4-dihydro-3H-1,2,4-triazol-3-

one (76). ^{1}H NMR (500 MHz, $CDCl_3$) δ 7.61(m, 2H), 7.41 (m, 3H), 7.23 (m, 1H), 7.03 (m, 2H), 6.95 (m, 2H), 6.89 (m, 2H), 4.32 (m, 1H), 4.11 (m, 1H), 4.00 (m, 1H), 3.94 (m, 1H), 3.82 (m, 3H), 3.37 (m, 4H), 3.24 (m, 4H), 1.83 (m, 2H), 1.81 (s, 3H), 0.98 (t, *J* = 7.4 Hz, 3H). ^{13}C NMR (126 MHz, $CDCl_3$) δ 153.0, 152.1, 150.5, 145.9, 138.0, 134.5, 133.8, 132.7, 131.1, 128.8, 126.7, 125.9, 123.5, 118.4, 116.6, 115.4, 109.0, 73.9, 69.2, 66.9, 50.6, 49.1, 47.2, 25.7, 22.0, 11.0. DART-HRMS: *m/z* calcd. for $C_{32}H_{36}Cl_2N_5O_4$ $[MH]^+$, 624.2144; Found: 624.2105. IR (solid) *v*max 2918, 2876, 2849, 1693, 1585, 1555, 1509, 1464, 1449, 1374, 1330, 1294, 1224, 1187, 1149, 1095, 1035, 964, 942, 872, 817, 734. Purity: 97.8% (Method B).

4.2 Biological Assay Protocols

Gene expression assay protocol (C3H10T1/2): Cells were seeded (50,000 cells per well; 500 µL total volume per well) in a 24-well tissue culture plate. After 24h of incubation (37°C, 5% CO_2), growth media was removed and replaced with low FBS media. DMSO (vehicle control) and analogues (1% DMSO concentration) were added to the wells. Cells were incubated (37°C, 5% CO_2) for 24h and RNA was isolated and evaluated by qRT-PCR.

Gene expression assay protocol (ASZ-001): Cells were seeded (10,000 cells per well; 100 µL total volume per well) in a 96-well tissue culture plate. After 24h of incubation (37°C, 5% CO_2), growth media was removed and replaced with low FBS media. Cells were incubated for an additional 24h. After this time, DMSO (vehicle control) and analogues (1% DMSO concentration) were added to the wells. Cells were incubated (37°C, 5% CO_2) for 48h and RNA was isolated and evaluated by qRT-PCR.

RT-PCR protocol: Following treatment and incubation periods, both RNA extraction and cDNA synthesis were performed using a TaqMan Cells-to-CT (fast) kit. cDNA synthesis utilized a BioRad MyCycler and was programmed according to the manufacturer's instructions. Quantitative RT-PCR was performed on an ABI 7500 system and made use of the following TaqMan Gene Expression Probes: mouse ActB (Mm00607939_s1) and mouse Gli1 (Mm00494654_m1). Relative gene expression levels were computed via ΔΔCT method using GraphPad Prism. Corresponding IC_{50} values were calculated as mean ± SEM for at least three separate experiments performed in triplicate.

CYP3A4 inhibition protocol: ITZ and *des*-triazole ITZ were evaluated for their ability to inhibit CYP3A4 by Cyprotex. This was accomplished by measuring their ability to inhibit the metabolism of the known CYP3A4 substrate testosterone via LC/MS/MS. Briefly, varying concentrations of either ITZ or *des*-triazole ITZ was mixed with microsomes (0.5 mg/mL) and testosterone (50 μM) in 50 mM potassium phosphate buffer containing 2mM NADPH and 3mM MgCl2 at pH 7.4. Following a10 min incubation at 37°C, the assay was quenched with the addition of MeCN containing an internal standard. The samples were centrifuged and the quantity of testosterone metabolite in the supernatant was determined by LC/MS/MS.

Anti-proliferation protocol: HUVECs were seeded (3,000 cells per well; 100 μL) in a 96-well tissue cultured plate and incubated (37°C, 5% CO_2) overnight. After 24h, cells were drugged with DMSO (control), and drugs at varying concentrations (1% DMSO final concentration). Following 72h incubation, cells were treated with MTS: PMS and incubated (37°C, 5% CO_2) for 3h. Plates were read at 490 nm utilizing a BioTek

Synergy H1 Hybrid plate reader. Protocol follows Promega CellTiter 96 ® Aq_{ueous} Non-Radioactive Cell Proliferation Assay.

Tube formation protocol: Matrigel (BD Biosciences) was diluted 1:1 with DMEM (Matrigel protein concentration no less than 3 mg/mL) and used to coat the wells of a 24-well tissue culture dish (280 µL per well). Plates were incubated (37°C, 5% CO_2) for no more than 1h until the Matrigel solidified. HUVECs were suspended in M199 media with 1% FBS and penicillin/streptomycin, and 50,000 cells were added to each well. Plates were incubated at (37°C, 5% CO_2) for 20-30 min to allow HUVECs to attach to the Matrigel. Cells were treated with control (DMSO), known angiogenic inhibitor suramin (10 µM), or varying doses (10, 1, and 0.1 µM) of drug and incubated for 16h. Phase contrast images were taken from multiple locations in each well (8/well) on an inverted microscope and tube formation parameters were quantified using ImageJ software (NIH).

CHAPTER III: Structure-Activity Relationship Studies of Itraconazole Analogue Generations III and IV

1. Introduction

Based on our SAR results from analogue generations I and II, it was determined that the triazole moiety of ITZ is not necessary for potent Hh pathway inhibition. These SAR studies have resulted in a novel class of Hh pathway antagonists: *des*-triazole ITZ analogues. It was also previously determined that the stereochemistry of the dioxolane is important in terms of Hh pathway inhibition; the most potent stereochemical orientation is the 2*R*,4*R*-*trans*-dioxolane region. Thorough SAR studies have been performed in terms of this dioxolane region and there is a solid understanding of what structural functionalities of the dioxolane region of ITZ are necessary and unnecessary for potent Hh pathway inhibition. It has been established that while the chlorine-substituents are less important, the phenyl moiety is necessary for anti-Hh activity. The dioxolane region as a whole cannot be truncated to a smaller functionality without abolishing activity.[115] Further SAR could be performed on this region in terms of exploring different N-containing substituents in replacement of the triazole group. In addition, exploration could also be made in terms of different heteroatom ring systems to compare to the dioxolane region. Eventually, this may be necessary to improve the overall drug properties, such as solubility and stability, of this modified ITZ scaffold.

SAR data from generations I and II also yielded ample information in terms of the triazolone and side-chain regions of the ITZ scaffold. While the stereochemistry is less important, the methyl group of the *sec*-butyl region is crucial for Hh inhibitory activity. Substitution of a propyl side chain region completely abolishes activity. Interestingly, truncation of the side-chain region to the free triazolone maintains anti-Hh activity. In addition, truncation of the entire triazolone region to smaller moieties such as an aniline

or nitro substituent maintains this activity.[115] With that being said, this triazolone/side-chain functionality of the ITZ scaffold remains an interesting region in terms of Hh inhibitory activity. These regions of ITZ are amendable for further modification and the resulting SAR studies could potentially improve both drug-like properties and biological activity.

2. Design, Synthesis, and Evaluation of Generation III Analogues

2.1 Analogue Design

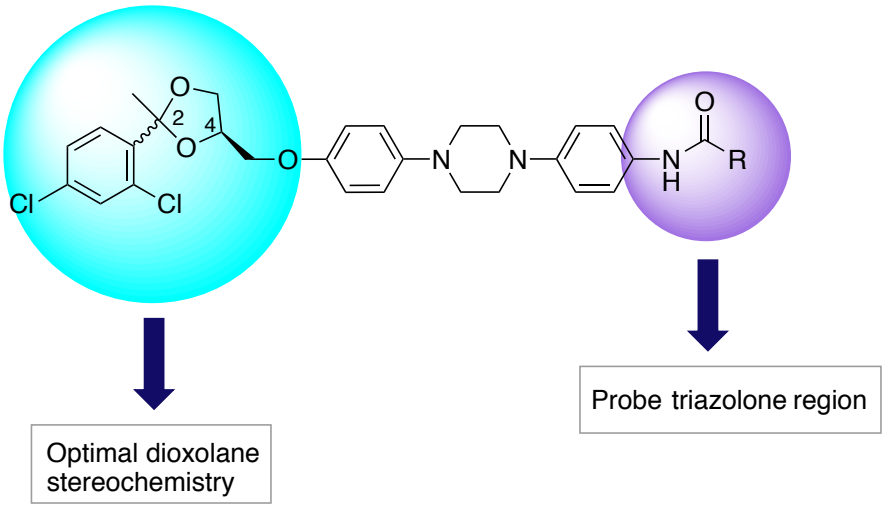

Figure 1. Design of Generation III Analogues

The third generation of ITZ analogues focuses on probing the triazolone/side-chain region of the original ITZ scaffold. In particular, this generation contains the optimal dioxolane stereochemical orientation and substitutes the triazolone/side-chain regions of the molecule with amide functionality (Figure 1). Utilizing amide functionality would aid in exploring the electronics, hydrogen bonding, and sterics of the triazolone/side-chain region of the ITZ scaffold. Amide functionality was chosen due to its chemical stability, solubility, and ease of synthesis. An amide group consists of a carbonyl bond (C=O) and a C—N bond, which both contain dipoles. The dipole of the

carbonyl is stronger than the C—N due to increased π-bonding arrangement and the electronegativity of the oxygen atom; this classifies an amide bond as being a hydrogen-bond acceptor (HBA).[117] The oxygen and nitrogen atoms can both bond with water or protic solvents serving as hydrogen bond acceptors and the N—H bond can serve as a hydrogen-bond donor (Figure 2). Amide bonds are generally stable due to resonance and the synthetic approach towards this functionality is low-cost and time efficient.

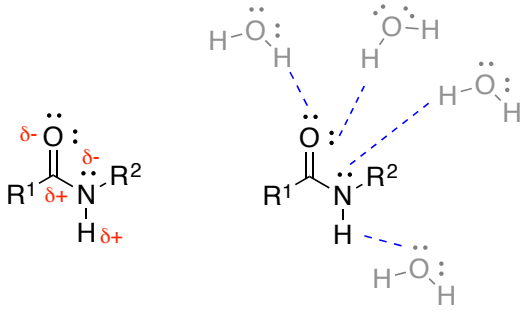

Figure 2. Physiochemical Properties of Amides

Initially, this series of analogues was only going to include the most optimal 2*R*,4*R*-*trans*-dioxolane orientation; however, these initial compounds had very limited activity during our preliminary in vitro evaluation. Because of this, amide analogues were also synthesized containing the 2*S*,4*R*-*cis*-dioxolane region to determine if there was a difference in activity between stereoisomers.

2.2 Synthetic Routes

2.2.1 Synthesis towards Key Aniline Intermediate

The synthetic approach towards the third generation of analogues begins with the coupling of desired dioxolane with the unprotected nitro-linker region (**44**) as described previously. The dioxolane containing nitro (**77** or **87**) can be reduced to the

aniline (**78** or **88**) in the presence of 10% Pd/C and hydrazine monohydrate.[103] This key dioxolane-containing aniline intermediate (**78** or **88**) can then be utilized in amidation reactions with standard amide coupling conditions and various carboxylic acids. This synthetic route was deemed the most optimal due to the ability to produce key intermediate (**78** or **88**) in bulk for rapid amidation with a variety of carboxylic acids (Scheme 1). While there are a few different ways to approach the synthesis of ITZ, and thus ITZ analogues, this synthetic route provides the most efficient production of a diverse set of analogues.

Scheme 1. Synthesis of Aniline Intermediates

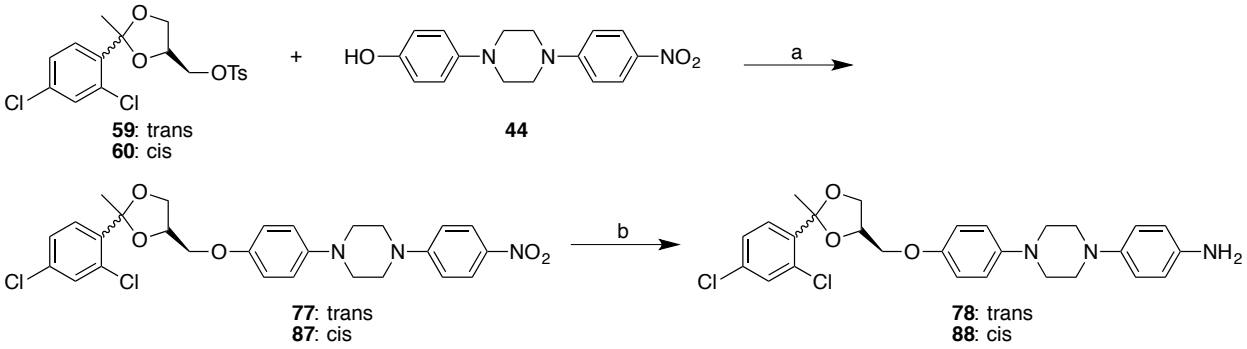

Reagents and conditions: (a) Cs_2CO_3 (10 eq), DMSO, 90ºC, 12 h, 34-85%; (b) EDCI, DMAP, DCM, RT, 12h, < 50%.

2.2.2 Synthesis of Final Amide Analogues

All amide analogues were synthesized utilizing standard amidation reaction conditions: activating agent 1-ethyl-3-(3-dimethylamiopropyl)carboniimide (EDCI), 4-dimethylaminopyridine (DMAP), and various carboxylic acids dissolved in anhydrous DCM and stirred at room temperature for 12h (Scheme 2).[118] This reaction must be anhydrous, as any trace of water will not allow the amidation to proceed. These final amide reactions did not provide an optimal yield < 50%; however, enough analogue was obtained for characterization and preliminary biological evaluation.

Scheme 2. Synthesis towards Amide Analogues

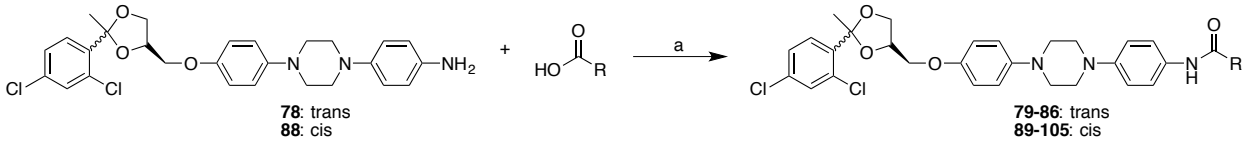

Reagents and conditions: (a) EDCI, DMAP, DCM, RT, 12h, < 50%.

2.2.3 Synthesis towards Phenol-Substituted Amide Analogues

The above amidation method worked well for all amide substitutions except for the phenol-substituted analogues. In the presence of EDCI, DMAP, and free acid, the amidation reaction would not proceed. It was anticipated that the free acid was potentially reacting with itself rather than the aniline. Due to this hypothesis, the free phenol was protected before coupling. Various esters were protected with a methoxy-methyl ether (MOM-) and then saponified to yield MOM-protected carboxylic acids.[119] These acids were then reacted with aniline under the previously described amide conditions to obtain the MOM-protected amide analogue. Ideally, the MOM group could then be cleaved to yield the final desired phenol amide product. However, this reaction did not yield desired product regardless of the reaction conditions (Scheme 3).[119,120] We believe that the MOM- group was removed but that the dioxolane ring was not stable under the acidic and harsh conditions associated with MOM-deprotection reactions.

Scheme 3. MOM- Protected Amidation Route

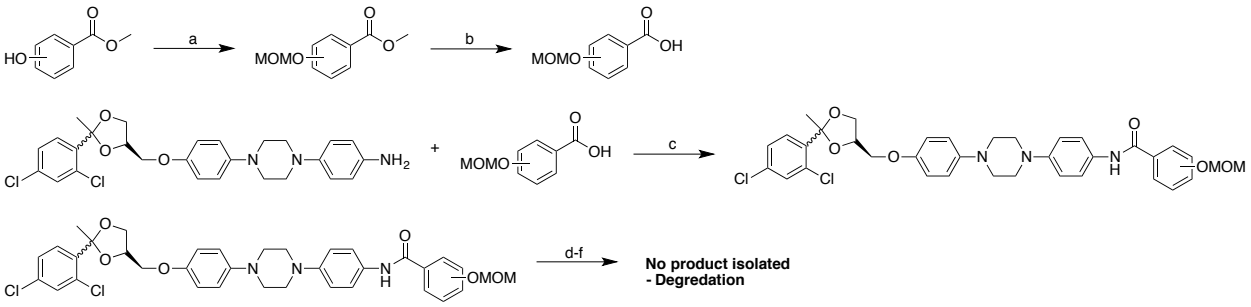

Reagents and conditions: (a) DIPEA, MOM-Cl, 0°C → RT, 12h, 33-84%; (b) 10% NaOH, MeOH, RT, 4h, 48-85%;(c) EDCI, DMAP, DCM, RT, 12h, < 50%;(d) TFA, DCM 40min-1h, RT; (e) 3M HCl (~10 drops), MeOH, RT, 12h; (f) TMSCl (10 eq), NaI (10 eq), ACN: DCM, RT, 20 min

There are a variety of synthetic approaches to form amide bonds.[118,121] It is known that acyl chlorides are generally more reactive than carboxylic acids. We attempted to form MOM- protected and free phenol acyl chlorides and then react them with aniline intermediate (**78** or **88**). Another attempt was made to couple MOM-protected and free phenol esters to the aniline intermediate (**78** or **88**) in the presence of trimethyl aluminum (Scheme 4).[122] Neither of these synthetic routes proved successful despite the use of the more reactive acyl chloride functionality.

Scheme 4. Alternate Amidation Approaches

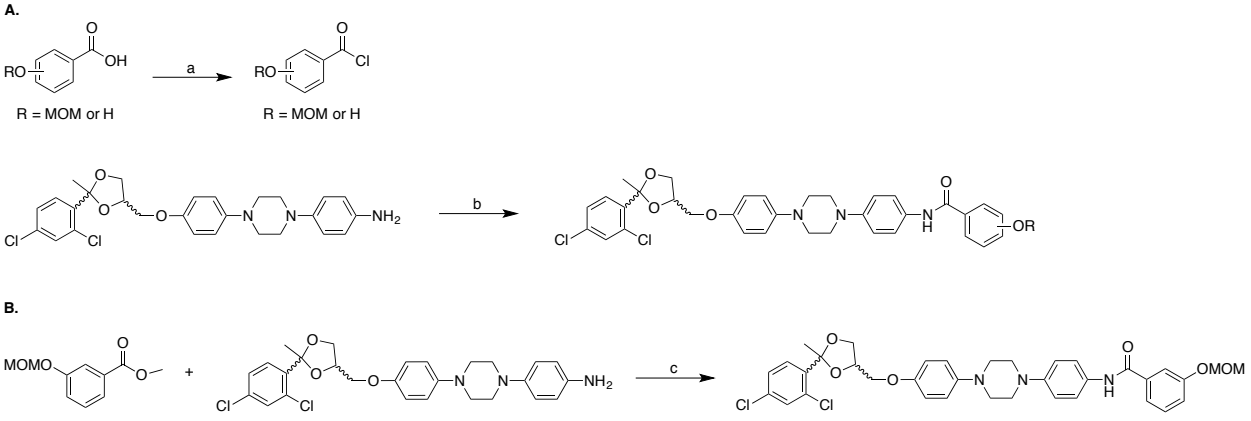

Reagents and conditions: (a) thionyl chloride, DCM, 1 drop of DMF, reflux 4.5 h; (b) Pyr, DMAP, DCM, 4°C, 12h; (c) $AlMe_3$, K_2CO_3, DCM 0°C → RT

As the most successful amidation attempt involved protecting the starting carboxylic acid and only did not yield product due to the deprotection reaction, it was anticipated that a different protecting group could be utilized instead of MOM. Benzyl (Bn) protecting groups were a feasible option as they are easily synthesized and stable. In addition, benzyl groups can be removed under less harsh conditions including Pd/C and H_2. This approach was successful for the phenol-substituted analogues; however, the analogues were obtained in low yields after the final hydrogenation reaction (Scheme 5).[123]

Scheme 5. Benzyl- Protected Amides

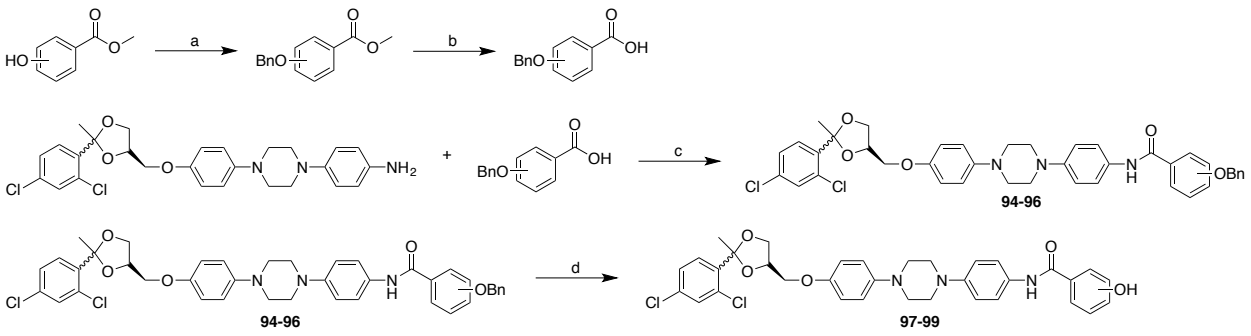

Reagents and conditions: (a) BnBr, K_2CO_3, acetone, RT, 12h, 64-quant.%; (b) LiOH (3 eq), H_2O:THF, 52-66%; (c) EDCI, DMAP, DCM, RT, 12h, < 50%; (d) 10% Pd/C, THF:EtOH, H_2

In an attempt to obtain a higher yield for all of the amidation reactions, a new set of conditions was utilized: N-methylmorpholine (NMM) and 1-[bis(dimethylamino)methylene]-1H-1,2,3-triazolo[4,5,6]pyridinium3-oxidhexafluorophosphate) HATU in DMF for 12h at room temperature (Scheme 6).[124,125] These conditions were chosen as they are not as sensitive to water as are the previously used reagents (EDCI and DMAP). In addition to improving the yield of amide product, these reaction conditions also allowed for direct coupling of free phenol

carboxylic acids to the dioxolane containing aniline intermediate. This is a more efficient approach, as it would eliminate the benzyl-protected intermediate and subsequent additional reactions.

Scheme 6. Synthesis towards Free-Phenol Analogues

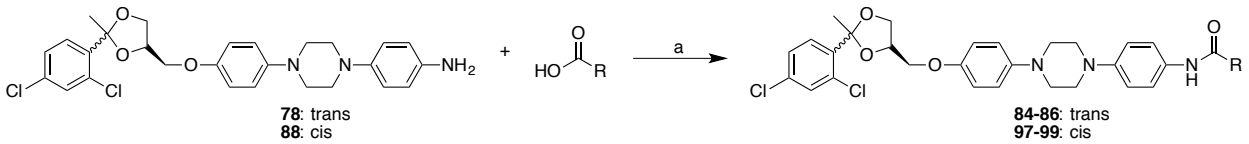

Reagents and conditions: (a) HATU, NMM, DMF, RT, 12h

2.3 Biological Evaluation

Table 1. Generation III Analogues

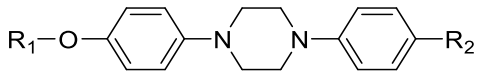

Compound	R_1	R_2	Final Stereochemistry
77	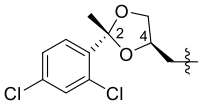		*Trans*-2*R*,4*R*
78	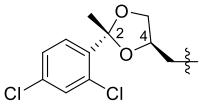		*Trans*-2*R*,4*R*
79	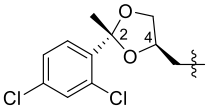	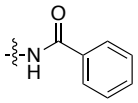	*Trans*-2*R*,4*R*
80	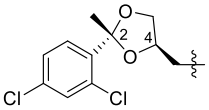	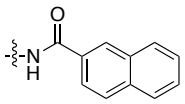	*Trans*-2*R*,4*R*
81	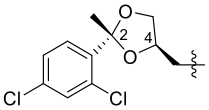	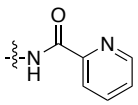	*Trans*-2*R*,4*R*
82	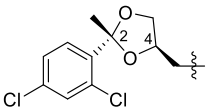	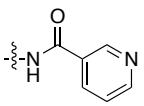	*Trans*-2*R*,4*R*
83	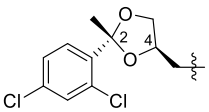	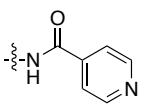	*Trans*-2*R*,4*R*

84	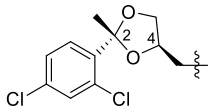	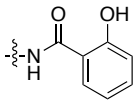	*Trans*-2*R*,4*R*
85	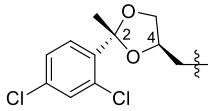	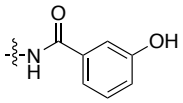	*Trans*-2*R*,4*R*
86	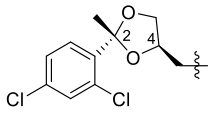	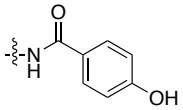	*Trans*-2*R*,4*R*
87	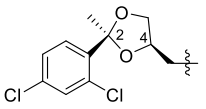		*Cis*-2*S*,4*R*
88	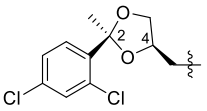		*Cis*-2*S*,4*R*
89	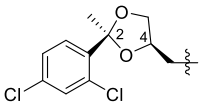	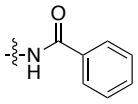	*Cis*-2*S*,4*R*
90	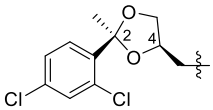	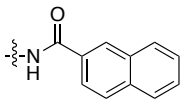	*Cis*-2*S*,4*R*
91	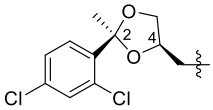	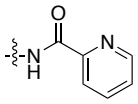	*Cis*-2*S*,4*R*
92	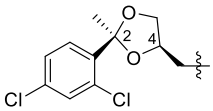	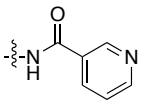	*Cis*-2*S*,4*R*
93	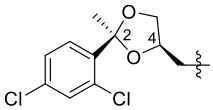	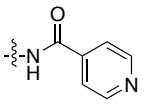	*Cis*-2*S*,4*R*
94	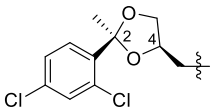	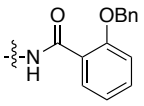	*Cis*-2*S*,4*R*
95	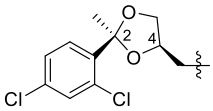	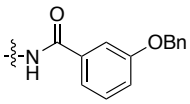	*Cis*-2*S*,4*R*
96	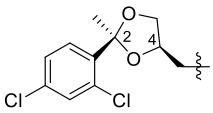	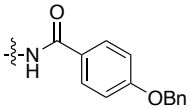	*Cis*-2*S*,4*R*
97	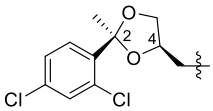	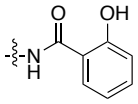	*Cis*-2*S*,4*R*

98	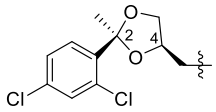	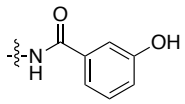	*Cis*-2*S*,4*R*
99	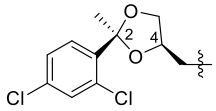	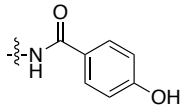	*Cis*-2*S*,4*R*
100	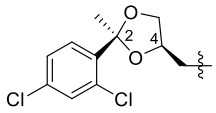	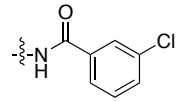	*Cis*-2*S*,4*R*
101	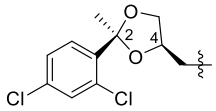	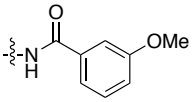	*Cis*-2*S*,4*R*
102	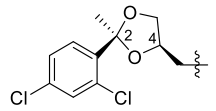	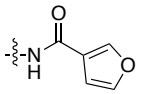	*Cis*-2*S*,4*R*
103	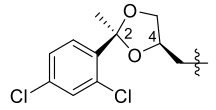	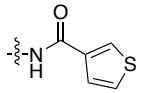	*Cis*-2*S*,4*R*
104	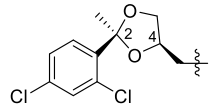	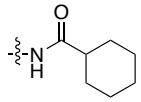	*Cis*-2*S*,4*R*
105	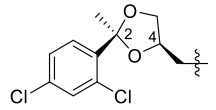	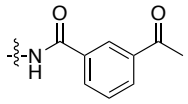	*Cis*-2*S*,4*R*

The third generation of ITZ analogues was evaluated for Hh pathway inhibitory activity by monitoring endogenous Gli1 mRNA levels in ASZ-001 cells (Table 1). Analogues were tested in a dose-dependent manner in 96-well tissue culture plates; this was done for efficiency and in an attempt to test these analogues in a higher-throughput fashion. *Des*-triazole ITZ analogues were not evaluated in the initial mouse embryonic fibroblast (C3H10T1/2) cells due to conflicting results from generation II analogue biological evaluation.[115] It was established from this generation II data that the ASZ cell line represents a more appropriate model for Hh pathway activity in MB.[126] Overall, the evaluation of generation III analogues and their ability to inhibit Hh signaling in the ASZ cell line provided interesting results (Tables 2, 3, and 4).

Table 2. In Vitro Activity of *Trans*-Amide Analogues

Compound	IC_{50} (μM) [a, b]	Compound	IC_{50} (μM) [a, b]
77	0.31 ± 0.04	**82**	4.3 ± 0.2
78	0.92 ± 0.04	**83**	>10
79	>10	**84**	>>10
80	>10	**85**	0.19 ± 0.008
81	>10	**86**	>>10

[a]IC_{50} values represent the Mean ± SEM of at least two separate experiments performed in triplicate. [b]All analogues evaluated following 48 hr incubation.

Generation III analogue synthesis began with the 2*R*,4*R*-*trans*-dioxolane stereochemistry because this was the most potent orientation determined in previous SAR studies. This initial amide series with 2*R*,4*R*-*trans*-dioxolane stereochemistry yielded minimally active compounds with most IC_{50} values >10 μM (Table 2). However, the truncated nitro (**77**) and aniline (**78**) intermediates exhibited moderate potency (IC_{50} = 0.31 ± 0.04 and 0.92 ± 0.04 μM, respectively) indicating that the truncation of both the triazolone region and the triazole group is acceptable. Despite limited Hh inhibitory activity within this first class of amides, the SAR data indicated that the *meta*-position functionality off of the phenyl ring was favorable as **82** was moderately active (IC_{50} = 4.3 ± 0.2 μM) and **85** was potent (IC_{50} = 0.19 ± 0.008 μM) when compared to the *ortho*- and *para*- position analogues (Table 2). The nitrogen atom in the pyridine ring of **82** serves as an H-bond acceptor while the oxygen in the phenol of **85** may serve as both an H-bond donor and an H-bond acceptor supporting the increased potency. These results from this initial amide series indicate that functionality capable of hydrogen bonding at the *meta*-position of the phenyl ring may be advantageous to binding with Smo, the hypothesized target of these *des*-triazole ITZ analogues.

Table 3. In Vitro Activity of *Cis*-Amide Analogues

Compound	IC_{50} (μM) [a, b]	Compound	IC_{50} (μM) [a, b]
87	0.26 ± 0.04	**94**	1.8 ± 0.4
88	0.39 ± 0.09	**95**	2.3 ± 0.05
89	>10	**96**	>10
90	>10	**97**	2.2 ± 0.3
91	3.9 ± 0.3	**98**	0.16 ± 0.03
92	0.19 ± 0.09	**99**	3.0 ± 0.1
93	>10		

[a]IC_{50} values represent the Mean ± SEM of at least two separate experiments performed in triplicate. [b]All analogues evaluated following 48 hr incubation.

Despite the majority of analogues being inactive, this initial series of *trans*-amides provided interesting SAR information in terms of the triazolone/side-chain region of the ITZ scaffold (Table 2). Thus, a second series of amide analogues was synthesized containing the 2*S*,4*R*-*cis*-dioxolane orientation. These *cis*-amide analogues contained the same functionality and substituents as the *trans*-amide analogues in order to better compare the stereoisomers. Evaluation of the *cis*-amide analogues provided confounding data (Table 3). First, all of the *cis*-amide analogues were more potent than the *trans*-amide analogues, specifically amongst the phenol and pyridine containing compounds. Second, following the same trend as the *trans*-amide analogues, substituents at the *meta*-position better inhibited the Hh pathway in comparison to the *ortho*- and *para*- positions. The *meta*-pyridine analogues had a modest difference in potency (**82** = 4.3 ± 0.2 and **96** = 0.19 ± 0.09 μM) while the *meta*-phenol analogues resulted in similar IC_{50} values (**85** = 0.19 ± 0.008 and **98** = 0.16 ±

0.03 μM). It is possible that the *cis*-amide analogues are more permeable than the *trans*-amide analogues, accounting for their increased potency within these preliminary cellular assays (Table 2 and Table 3). The SAR results from the stereochemically-defined amide analogues reiterated the importance of the triazolone/side-chain region and Hh pathway inhibitory activity. This highlights the need to further explore this region of the ITZ scaffold.

Table 4. In Vitro Activity of *Cis*-Amide Analogues: *Meta*-Functionality

Compound	IC_{50} (μM) [a, b]	Compound	IC_{50} (μM) [a, b]
100	>10	**103**	>10
101	5.7 ± 1.9	**104**	>10
102	>10	**105**	0.089 ± 0.01

[a]IC_{50} values represent the Mean ± SEM of at least two separate experiments performed in triplicate. [b]All analogues evaluated following 48 hr incubation.

Taken together, a third series of amide analogues was designed and synthesized to contain optimal *cis*-dioxolane stereochemistry and optimal amide *meta*-substitution. This series of amides was necessary to further probe the sterics, electronics, and hydrogen bonding of the triazolone/side-chain region of the original ITZ scaffold. Analogues were designed according to the availability of carboxylic acids resulting in six diverse derivatives, which included both 6-membered rings and 5-membered rings. SAR studies concluded that the 5-membered ring analogues (**102** and **103**) are not optimal for Hh pathway inhibition (Table 4). Not surprisingly due to the results from the benzene and naphthalene analogues, the cyclohexane derivative (**104**) did not inhibit the Hh pathway. Results further indicated that the most potent analogue, **105**, contained an acetyl- functionality (Table 4). The trend in Hh inhibitory activity can partially be attributed to polarity at the *meta*-position of the phenyl ring. Although,

alcohol or amine functionality is typically more polar than a ketone, other characteristics of this moiety may be contributing to its potent activity (Figure 3).

Ketone >> Alcohol >> Amine >> Methoxy >> Halogen

Figure 3. Relative Potency of *Meta*-Functionality in Amide Analogues

One difference between a ketone and an alcohol is that ketones are considered to be electron-withdrawing groups (EWG) while alcohols are considered to be electron-donating groups (EDG). In addition, a ketone serves as a hydrogen bond acceptor (HBA) while an alcohol can act as a hydrogen bond donor (HBD) or an HBA. The bond length of the carbonyl and position of the oxygen atom may allow for tighter binding to a particular residue in the Smo binding pocket. It is also interesting to note that the Hh pathway inhibitor posaconazole (PSZ), an azole antifungal similar in structure to ITZ, contains a hydroxylated side-chain region. These structural-similarities further support adding polar moieties to the triazolone/side-chain region to improve drug-like properties yet maintain Hh-pathway inhibitory activity (Figure 4).

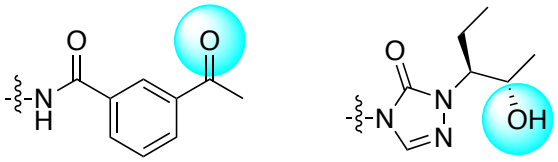

Figure 4. Triazolone/side-chain regions of PSZ vs. **105**

Due to promising in vitro activity, a few select compounds were evaluated in preliminary in vitro pharmacokinetic (PK) assays. These PK data helped determine if any of the changes made to the ITZ scaffold improved their overall drug-like properties (Table 5). Surprisingly, the amide substituents did not aid in increased solubility. The half-life ($T_{1/2}$) did not significantly change between ITZ and analogue **98**. Interestingly,

stereoisomers **82** and **92** had significantly different half-lives suggesting that the stereochemistry plays a role in compound metabolism and clearance ($T_{1/2}$ = 59.9 ± 2.0 and 8.9 ± 0.03 min, respectively). It was previously determined that removal of the triazole group abolishes inhibition of CYP3A4. This also translates over to the generation III *des*-triazole amide analogues. Lastly, as these compounds are being targeted to treat MB, they were screened in a parallel artificial membrane permeability assay (PAMPA) for their ability to passively permeate cell membranes. Unfortunately, while ITZ had moderate PAMPA permeability, none of the *des*-triazole ITZ analogues were able to passively cross this artificial membrane barrier (Table 5).

Table 5. Pharmacokinetic Evaluation of Amide Analogues

Compound	$T_{1/2}$ (HLM, min)	Solubility (μM)	PAMPA	CYP3A4 IC_{50} (μM)
ITZ	27.0 ± 6.2	0.8	Moderate	0.04
82	59.9 ± 2.0	0.0042	Poor	>20
92	8.9 ± 0.03	0.0069	Poor	>30
98	19.9 ± 0.6	0.0016	Poor	11.4

3. Design, Synthesis, and Evaluation of Generation IV Analogues

3.1 Analogue Design

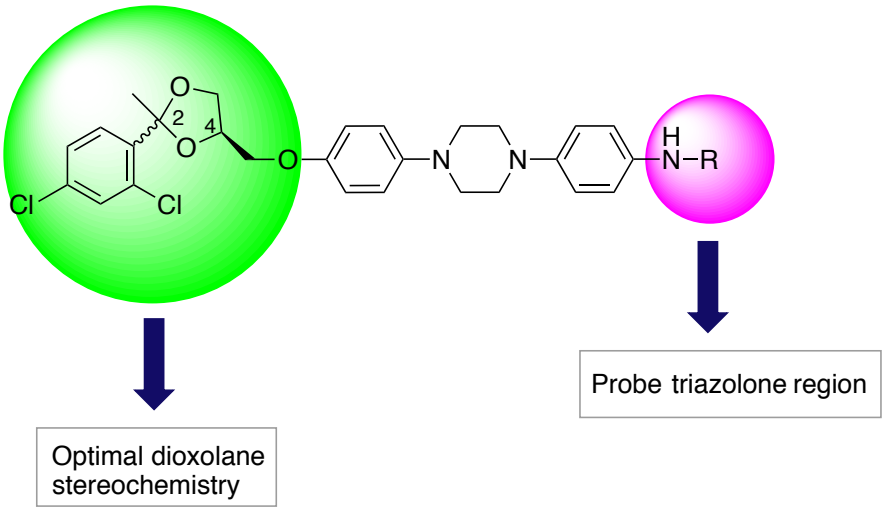

Figure 5. Design of Generation IV Analogues

The fourth generation of ITZ analogues focuses on further probing the triazolone/side-chain region of the original ITZ scaffold. In particular, this generation contains the optimal 4*R*-*cis*/*trans*-dioxolane stereochemistry determined through previous SAR studies. In addition, this series of compounds will substitute the right-most portion of the molecule with various functional moieties: carbamates, hydrazine carboxamides, and triazolones (Figure 5). These functional groups were chosen, as they are the intermediates leading up to the formation of the triazolone ring during the linker region synthesis. Utilizing this diverse set of functionality will further aid in probing the electronics, hydrogen bonding, and sterics of the triazolone/side-chain region of ITZ. This series of "triazolone mimic analogues" will provide a broader subset of SAR data as it explores a variety of functionality that have differing physiochemical properties. The overall goal of this series is to determine a potent ITZ analogue with improved drug-like properties. These moieties may contribute to improved solubility

while decreasing molecule size. This, along with truncation of the triazole region, will greatly improve both drug-like properties and target selectivity of the ITZ scaffold in terms of its Hh-inhibitory activity.

3.2 Synthetic Routes

Originally, the synthetic plan for the triazolone mimic analogues followed the same route as the previously mentioned amide analogues (Figure 6). Stereochemically-defined dioxolane would be coupled to the unprotected-nitro-linker (**44**); this dioxolane containing nitro-linker (**77** or **87**) would then be reduced to the aniline in the presence of Pd/C to yield key intermediate **78** or **88**.[103] However, as previously noted, the dioxolane region is not stable under acidic conditions. A multitude of these triazolone mimic analogue reactions require use of acid in order to form the designated product. As a result, the synthetic approach was adjusted to avoid exposing the dioxolane region to acid; this synthetic plan contains a few extra steps and unfortunately is not as efficient as amide analogue production.

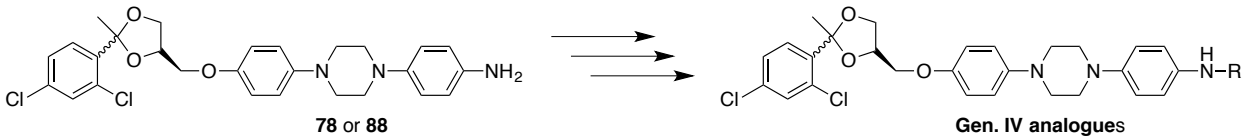

Figure 6. Original Synthetic Approach

As ITZ is FDA-approved, there are several synthetic approaches that have been reported previously. One of which, involves the coupling of dioxolane to the linker region at the beginning. After this initial coupling, the subsequent transformations can be made towards the triazolone region.[103] In order to effectively perform this synthesis, the initial coupling must be done at a large enough scale to undergo all of these transformations and result in ample product. While this is a possible synthetic route for

des-triazole ITZ analogues, it is not necessarily feasible to produce a large amount of stereochemically-defined dioxolane. For this reason, methoxy-protected linker regions (carbamate, hydrazine carboxamide, and triazolone) were deprotected using HBr at reflux (Scheme 7).

Scheme 7. Deprotection of Linker Intermediates

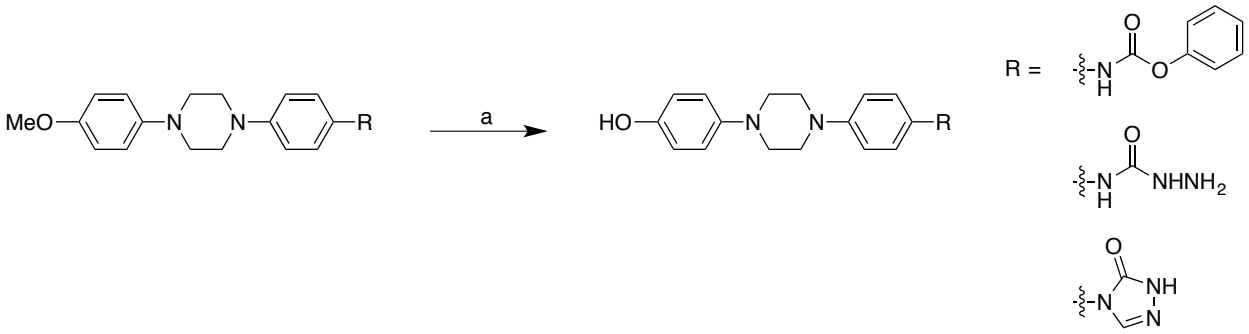

Reagents and conditions: (a) HBr, AcOH, reflux 12h.

The resulting phenols were then utilized in the coupling reaction with stereochemically-defined dioxolane and Cs_2CO_3 in DMSO. This reaction was performed at 90°C for the carbamate analogue and 40°C for the hydrazine carboxamide and triazolone analogues. The temperature was adjusted in an attempt to discourage dual dioxolane addition to both the phenol and hydrazine carboxamide/triazolone moieties. Despite the temperature of the reaction, only the hydrazine carboxamide substituent was successful. The carbamate coupling reaction did not proceed and the triazolone coupling reaction underwent duel-addition of dioxolane to both the phenol and the free triazolone. In an attempt to avoid going through all of the linker region transformations starting from **44**, previously synthesized analogues served as building blocks for the carbamate and triazolone analogues (Scheme 8). The carbamate analogues (**106** or **108**) were synthesized from the aniline intermediate (**78** or **88**) with

the previously utilized conditions of phenyl chloroformate and pyridine. The triazolone analogue (**110**) was ultimately synthesized from the hydrazine carboxamide analogue (**109**) with the previously utilized conditions of formamidine acetate.[115] It is important to note that this reaction also calls for the use of acetic acid (AcOH). AcOH is utilized to aid in the crystallization of the triazolone product during linker synthesis. As this reaction was performed on a < 10 mg scale, precipitation of the desired product was not expected to be the means of purification. As a result, this reagent could successfully be removed without affecting the formation of the triazolone ring.

Scheme 8. Synthesis towards Triazolone Intermediates

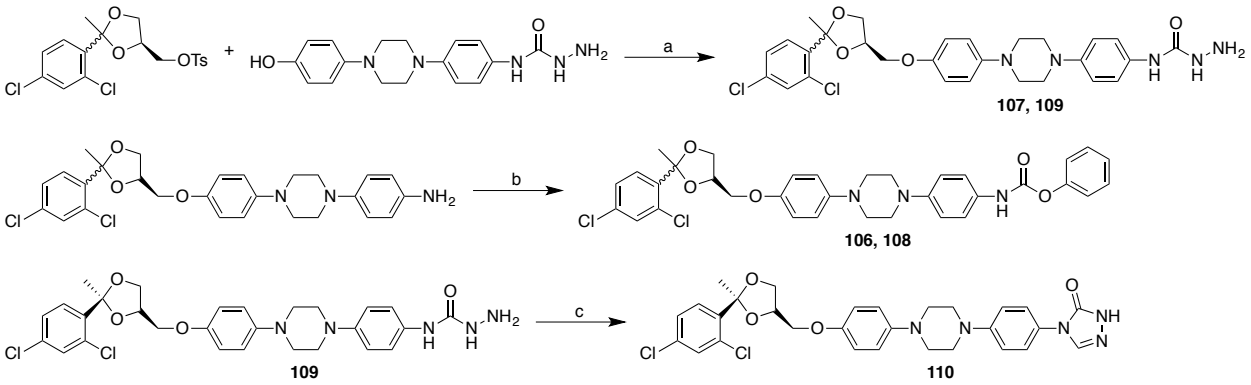

Reagents and conditions: (a) Cs_2CO_3 (10 eq), DMSO, 40ºC, 12 h, 56-94%; (b) Pyr (17 eq), ClCOOPh (1.1 eq), 3 h, 24-40%; (c) formamidine acetate (4.5 eq), reflux, 3 h, 20%

It was also attempted to protect the triazolone region with a Boc-protecting group.[127] However, this proved unsuccessful, as the Boc group could not be added before methoxy- deprotection; Boc-protection in the presence of both phenol and aniline functionality resulted in dual-Boc addition. Selective Boc-deprotection was also attempted and did not yield desired product (Scheme 9).[128]

Scheme 9. Protection of Free Triazolone Intermediate

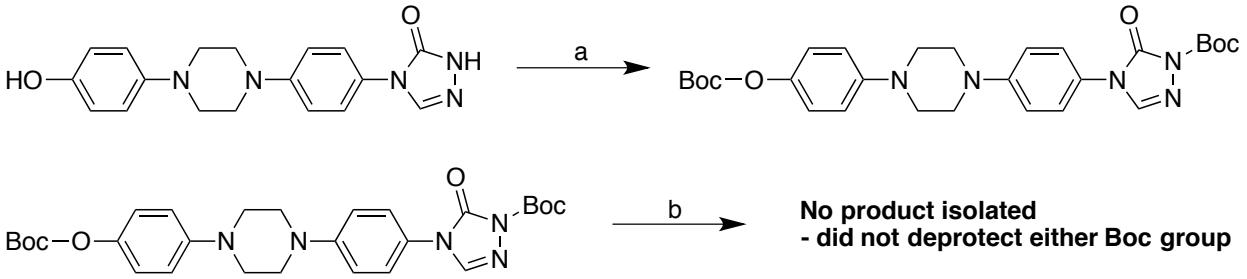

Reagents and conditions: (a) Boc anhydride, DMAP (10% mol), ACN, RT, 12 h; (b) 20% KOH, MeOH, RT, 12h

3.3 Biological Evaluation

Table 6. Generation IV Analogues

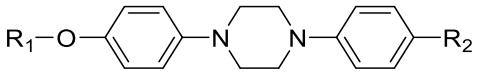

Compound	R_1	R_2	Final Stereochemistry
106	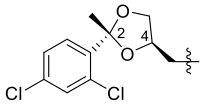	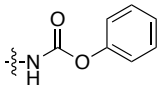	*Trans*-2*R*,4*R*
107	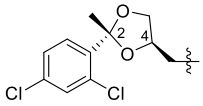	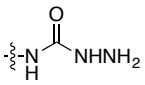	*Trans*-2*R*,4*R*
108	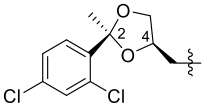	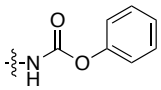	*Cis*-2*S*,4*R*
109	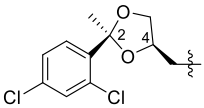	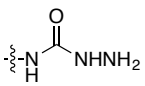	*Cis*-2*S*,4*R*
110	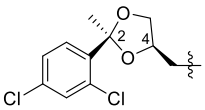	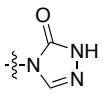	*Cis*-2*S*,4*R*

The fourth generation of *des*-triazole ITZ analogues was evaluated for Hh inhibitory activity by monitoring endogenous Gli1 mRNA levels in ASZ-001 cells (Table 6). It was previously established that this cell line represents an appropriate model for

Hh pathway activity in MB.[115] This fourth generation of analogues was designed to further probe the triazolone/side-chain region of the ITZ scaffold. These analogues offer a wide range of functionality including carbamates, hydrazine carboxamides, and triazolones. While these moieties were mainly chosen as they serve as intermediates leading up to the formation of the triazolone ring, they also may aid in improving the drug-like properties of this scaffold. For instance, carbamate functionality has been widely studied within the field of medicinal chemistry and is a key structural moiety in many FDA-approved compounds and prodrugs. Carbamates offer chemical stability and hydrogen bonding; in addition, they are capable of penetrating cell membranes.[129]

Table 7. In Vitro Evaluation of Generation IV

Compound	IC_{50} (μM) [a, b]	Compound	IC_{50} (μM) [a, b]
106	3.2 ± 0.6	**109**	0.28 ± 0.01
107	0.29 ± 0.08	**110**	0.95 ± 0.08
108	1.0 ± 0.4		

[a]IC_{50} values represent the Mean ± SEM of at least two separate experiments performed in triplicate. [b]All analogues evaluated following 48 hr incubation.

SAR results for generation IV analogues indicate that the most potent carbonyl derivatives are the hydrazine carboxamides (**107** and **109**) (Table 7). This is likely due to the increased polarity and ability to donate and accept hydrogen atoms. Interestingly, the hydrazine carboxamide is an acyclic motif providing evidence that anti-Hh activity can still be achieved without the cyclic functionality seen in the original triazolone region and generation III analogues. The carbamate analogues (**106** and **108**) are the least potent in this series and this may be attributed to the presence of the bulky nonsubstituted hydrophobic ring. Surprisingly, the *des*-triazole ITZ analogue containing

the free triazolone was not as potent as the structurally similar triazole-containing analogue **53** (IC_{50} = 0.12 ± 0.03 μM).[115] This may be due to decreased solubility or ability to penetrate the cell membrane. A similar trend is seen in terms of the stereochemistry of the dioxolane ring: the *cis*-analogues are more potent than the *trans*-analogues. Both dioxolane orientations were synthesized as the *trans*-isomer is formed more readily in the ketalization reaction. The *trans*-dioxolane was utilized during reaction optimization and then the corresponding *cis*-analogue was subjected to these reaction conditions. These SAR data support the design and synthesis of a further subset of analogues containing truncated triazolone regions with acyclic polar moieties. This will ultimately decrease overall size of the *des*-triazole ITZ scaffold as well as increase Hh inhibitory activity.

4. Conclusion

Two subsequent *des*-triazole ITZ analogue generations were designed, synthesized, and evaluated for their ability to inhibit the Hh pathway. The goal of these analogues was to further probe the sterics, electronics, and hydrogen bonding in terms of the triazolone/side-chain region of the ITZ scaffold. *Des*-triazole ITZ analogues contained the optimal 2*S*,4*R*-dioxolane region determined from previous SAR studies. The triazolone/side-chain region was replaced with various functionalities: amide, carbamate, hydrazine carboxamide, or triazolone. SAR generation III analogues determined the 2*S*,4*R*-*cis*-dioxolane amide analogues to be more potent than the 2*R*,4*R*-*trans*-dioxolane amide analogues. In addition, different substituents and positions around the phenyl ring were explored to determine if either of these components contributed to potent Hh pathway inhibition. The most potent *des*-triazole

ITZ analogues contained the 4*R*-*cis*-dioxolane region and *meta*-substitution around the phenyl ring. Generally, anti-Hh activity becomes more potent with increasing *meta*-substituent polarity.

SAR results from generation IV analogues also determined that the 2*S*,4*R*-*cis*-dioxolane containing analogues were the most potent. Within this small subset of compounds, the most potent analogues contained the hydrazine carboxamide moiety in replacement of the triazolone/side-chain region. These results indicate that a small, polar, acyclic motif may be favorable within this region of the ITZ scaffold; this would be an ideal way to further scale down the overall size of these novel Hh pathway inhibitors. Additional SAR studies should be performed to probe the triazolone/side-chain region for potent Hh pathway inhibitory activity while also improving the overall properties of the scaffold.

4.1 Experimental

Previously Characterized Intermediates: Benzyl-protected intermediates were prepared as described previously and are described in the Appendix A.

1-(4-(((2*R*,4*R*)-2-(2,4-dichlorophenyl)-2-methyl-1,3-dioxolan-4-yl)methoxy)phenyl)-4-(4-nitrophenyl)piperazine (77) To a solution of **44** (0.77 g, 2.61 mmol) in DMSO (30 mL) was added Cs_2CO_3 (8.5 g, 26.14 mmol) and **59** (1.2 g, 2.87 mmol). The solution was warmed to 90° C and stirred for 12 h. The mixture was cooled to room temperature and water was added slowly with vigorous stirring (~20 mL). A yellow precipitate formed, which was filtered and recrystallized in EtOH to yield **77** (1.2g, 85%). ^{1}H NMR

(500 MHz, Chloroform-*d*) δ 8.28 – 8.14 (m, 2H), 7.66 (d, 1H), 7.46 (d, 1H), 7.28 (m, 1H), 7.03 – 6.87 (m, 6H), 4.37 (m, 1H), 4.16 (m, 1H), 4.11 – 3.95 (m, 2H), 3.89 (m, 1H), 3.69 – 3.53 (m, 4H), 3.35 – 3.18 (m, 4H), 1.86 (s, 3H). ^{13}C NMR (126 MHz, $CDCl_3$) δ 153.29, 134.59, 131.21, 128.89, 126.79, 125.98, 118.58, 115.56, 112.90, 109.99, 109.12, 77.28, 77.02, 76.77, 73.94, 69.27, 66.99, 50.39, 47.31, 25.73. DART-HRMS: *m/z* calcd. for $C_{27}H_{27}Cl_2N_3O_5$ $[MH]^+$, 544.1406; Found: 544.1388. IR (solid) *v*max: 3060, 2926, 2880, 2828, 1556, 1507, 1485, 1446, 1376, 1222, 1190, 1142, 1047, 995, 942, 821, 737.

4-(4-(4-(((2*R*,4*R*)-2-(2,4-dichlorophenyl)-2-methyl-1,3-dioxolan-4-yl)methoxy)phenyl)piperazin-1-yl)aniline (78) 10% palladium on carbon (24.4 mg, 5% mole ratio) was added to a dry round bottom flask. Ethanol (100 mL) was added followed by slow addition of **77** (250 mg, 0.459 mmol). Hydrazine monohydrate (0.14 mL, 4.59 mmol) was added dropwise and the mixture was stirred at reflux for 2 h. Upon cooling to RT, the mixture was filtered through celite. The celite was washed with ethanol (500 mL) to ensure complete elution of the aniline. The filtrate was concentrated to afford a yellow solid, which was recrystallized in EtOH to afford **78** (100 mg, 42%). ^{1}H NMR (500 MHz, Chloroform-*d*) δ 8.20 (d, 1H), 7.66 (d, 1H), 7.46 (t, 1H), 7.06 – 6.85 (m, 6H), 6.72 (d, 1H), 4.37 (s, 1H), 4.16 (m, 1H), 4.13 – 3.94 (m, 2H), 3.94 – 3.82 (m, 1H), 3.63 (t, 2H), 3.50 (s, 1H), 3.35 – 3.16 (m, 6H), 1.86 (s, 3H). ^{13}C NMR (126 MHz, $CDCl_3$) δ 131.20, 128.91, 126.79, 125.99, 118.85, 118.59, 118.25, 116.23, 115.56, 115.46, 112.90, 77.28, 77.03, 76.78, 73.97, 69.29, 67.04, 51.25, 50.86, 50.39, 47.31, 25.74, 0.02. DART-HRMS: *m/z* calcd. for $C_{27}H_{29}Cl_2N_3O_3$ $[MH]^+$, 514.1664; Found: 514.1648. IR (solid) *v*max: 2919, 2850, 1595, 1560, 1510, 1464, 1450, 1375, 1228, 1196, 1150, 1037, 877, 825, 754.

***N*-(4-(4-(4-(((2*R*,4*R*)-2-(2,4-dichlorophenyl)-2-methyl-1,3-dioxolan-4-yl)methoxy)phenyl)piperazin-1-yl)phenyl)benzamide (79)** Aniline **78** (20 mg, 0.039 mmol), benzoic acid (14.3 mg, 0.117 mmol), EDCI (22.4 mg, 0.117 mmol), and DMAP (14.3 mg, 0.117 mmol) was dissolved in anhydrous DCM (10mL) and stirred under argon for 12h at room temperature. The crude reaction was immediately purified via column chromatography (SiO_2, 0-60% acetone in hexanes) to afford **79** (13.0 mg, 54%). ^{1}H NMR (500 MHz, Chloroform-*d*) δ 7.92 (d, 2H), 7.73 (s, 1H), 7.66 (d, 1H), 7.59 (m, 2H), 7.54 (t, 2H), 7.46 (d, 1H), 7.28 (m, 1H), 7.05 (d, 2H), 7.02 – 6.97 (m, 2H), 6.94 (d, 2H), 4.37 (m, 1H), 4.17 (m, 1H), 4.09 – 3.98 (m, 2H), 3.89 (t, 1H), 3.38 (m, 4H), 3.29 (m, 4H), 1.86 (s, 3H). ^{13}C NMR (126 MHz, $CDCl_3$) δ 165.48, 152.92, 148.50, 146.09, 138.15, 135.17, 134.56, 132.83, 131.69, 131.19, 130.61, 128.91, 128.78, 126.95, 126.79, 121.64, 118.40, 116.95, 115.48, 110.66, 109.09, 77.27, 77.23, 77.02, 76.76, 73.96, 69.29, 67.03, 50.74, 49.88, 29.72, 25.74. DART-HRMS: *m/z* calcd. for $C_{34}H_{33}Cl_2N_3O_4$ $[MH]^+$, 618.1926; Found: 618.1919. IR (solid) *v*max: 3367, 3333, 2958, 2924, 2853, 1693, 1638, 1547, 1511, 1450, 1375, 1248, 1230, 1194, 1157, 1037, 941, 822, 703.

***N*-(4-(4-(4-(((2*R*,4*R*)-2-(2,4-dichlorophenyl)-2-methyl-1,3-dioxolan-4-yl)methoxy)phenyl)piperazin-1-yl)phenyl)-2-naphthamide (80)** Aniline **78** (20 mg, 0.039 mmol), naphtholic acid (20.1 mg, 0.117 mmol), EDCI (22.4 mg, 0.117 mmol), and DMAP (14.3 mg, 0.117 mmol) was dissolved in anhydrous DCM (10mL) and stirred under argon for 12h at room temperature. The crude reaction was immediately purified via column chromatography (SiO_2, 0-60% acetone in hexanes) to afford **80** (6.0 mg, 23%). ^{1}H NMR (500 MHz, Chloroform-*d*) δ 8.39 (d, 1H), 7.97 (d, 1H), 7.93 – 7.85 (m,

1H), 7.75 (d, 1H), 7.66 – 7.48 (m, 7H), 7.41 (d, 1H), 7.24 (m, 1H), 7.03 (d, 2H), 6.96 (d, 2H), 6.90 (d, 2H), 4.33 (m, 1H), 4.12 (m, 1H), 4.05 – 3.93 (m, 2H), 3.85 (m, 1H), 3.38 – 3.30 (m, 5H), 3.26 (m, 5H), 1.82 (s, 3H). ^{13}C NMR (126 MHz, $CDCl_3$) δ 167.31, 152.94, 148.59, 146.09, 138.15, 134.75, 134.56, 133.81, 132.84, 131.20, 130.94, 130.75, 130.17, 128.91, 128.43, 127.33, 126.79, 126.59, 125.38, 125.02, 124.79, 121.41, 118.41, 117.01, 115.92, 115.49, 111.61, 109.09, 106.00, 101.89, 97.74, 77.28, 77.22, 77.02, 76.77, 73.96, 69.29, 67.03, 50.74, 49.92, 29.72, 25.74, 0.02. DART-HRMS: *m/z* calcd. for $C_{38}H_{35}Cl_2N_3O_4$ $[MH]^+$, 668.2083; Found: 668.2075. IR (solid) *v*max: 3294, 3247, 3042, 2985, 2873, 1639, 1586, 1509, 1450, 1373, 1226, 1192, 1146, 1035, 942, 821, 733.

***N*-(4-(4-(4-(((2*R*,4*R*)-2-(2,4-dichlorophenyl)-2-methyl-1,3-dioxolan-4-yl)methoxy)phenyl)piperazin-1-yl)phenyl)picolinamide (81)** Aniline **78** (20 mg, 0.039 mmol), picolinic acid (14.4 mg, 0.117 mmol), EDCI (22.4 mg, 0.117 mmol), and DMAP (14.3 mg, 0.117 mmol) was dissolved in anhydrous DCM (10mL) and stirred under argon for 12h at room temperature. The crude reaction was immediately purified via column chromatography (SiO_2, 0-80% acetone in hexanes) to afford **81** (9.0 mg, 37%). ^{1}H NMR (500 MHz, Chloroform-*d*) δ 9.96 (s, 1H), 8.69 – 8.62 (m, 1H), 8.35 (d, 1H), 7.95 (m, 1H), 7.76 (d, 2H), 7.66 (d, 1H), 7.55 – 7.48 (m, 1H), 7.46 (d, 1H), 7.28 (m, 1H), 7.06 (d, 2H), 7.00 (d, 2H), 6.94 (d, 2H), 4.37 (s, 1H), 4.17 (m, 1H), 4.09 – 3.97 (m, 2H), 3.89 (m, 1H), 3.38 (m, 4H), 3.33 – 3.25 (m, 4H), 1.86 (s, 3H). ^{13}C NMR (126 MHz, $CDCl_3$) δ 161.67, 152.90, 150.10, 148.20, 147.94, 146.11, 138.16, 137.64, 134.56, 132.84, 131.20, 130.66, 128.91, 126.79, 126.26, 122.32, 120.91, 118.38, 116.97, 115.48, 111.61, 109.09, 106.05, 102.12, 77.28, 77.23, 77.03, 76.77, 73.97, 69.30, 67.04, 50.75,

49.91, 25.74. DART-HRMS: *m/z* calcd. for $C_{33}H_{32}Cl_2N_4O_4$ $[MH]^+$, 619.1879; Found: 619.1872. IR (solid) *v*max: 3367, 2923, 2851, 1672, 1585, 1552, 1509, 1454, 1385, 1268, 1227, 1192, 1148, 1020, 940, 912, 814, 747, 620.

***N*-(4-(4-(4-(((2*R*,4*R*)-2-(2,4-dichlorophenyl)-2-methyl-1,3-dioxolan-4-yl)methoxy)phenyl)piperazin-1-yl)phenyl)nicotinamide (82)** Aniline **78** (20 mg, 0.039 mmol), nicotinic acid (14.4 mg, 0.117 mmol), EDCI (22.4 mg, 0.117 mmol), and DMAP (14.3 mg, 0.117 mmol) was dissolved in anhydrous DCM (10mL) and stirred under argon for 12h at room temperature. The crude reaction was immediately purified via column chromatography (SiO_2, 0-80% acetone in hexanes) to afford **82** (6.2 mg, 25%). ^{1}H NMR (500 MHz, Chloroform-*d*) δ 9.14 (s, 1H), 8.83 (s, 1H), 8.26 (d, 1H), 7.72 (s, 1H), 7.66 (d, 1H), 7.59 (d, 2H), 7.49 (d, 1H), 7.46 (d, 1H), 7.28 (m, 1H), 7.05 (d, 2H), 7.00 (d, 2H), 6.96 – 6.90 (m, 2H), 4.37 (m, 1H), 4.17 (m, 1H), 4.10 – 3.94 (m, 2H), 3.89 (m, 1H), 3.44 – 3.33 (m, 4H), 3.33 – 3.20 (m, 4H), 1.86 (s, 3H). ^{13}C NMR (126 MHz, $CDCl_3$) δ 131.20, 128.91, 126.80, 121.87, 118.43, 116.86, 115.49, 111.26, 109.10, 105.77, 101.72, 77.28, 77.23, 77.03, 76.77, 73.96, 69.29, 67.03, 50.73, 49.72, 25.74. DART-HRMS: *m/z* calcd. for $C_{33}H_{32}Cl_2N_4O_4$ $[MH]^+$, 619.1879; Found: 619.1876. IR (solid) *v*max: 3639, 3570, 2920, 2824, 1644, 1509, 1447, 1374, 1227, 1194, 1150, 1037, 941, 828, 733, 534.

***N*-(4-(4-(4-(((2*R*,4*R*)-2-(2,4-dichlorophenyl)-2-methyl-1,3-dioxolan-4-yl)methoxy)phenyl)piperazin-1-yl)phenyl)isonicotinamide (83)** Aniline **78** (20 mg, 0.039 mmol), isonicotinic acid (14.4 mg, 0.117 mmol), EDCI (22.4 mg, 0.117 mmol), and DMAP (14.3 mg, 0.117 mmol) was dissolved in anhydrous DCM (10mL) and stirred under argon for 12h at room temperature. The crude reaction was immediately purified

via column chromatography (SiO_2, 0-80% acetone in hexanes) to afford **83** (12.0 mg, 49%). ^{1}H NMR (500 MHz, Chloroform-*d*) δ 8.85 (d, 2H), 7.75 (d, 3H), 7.66 (d, 1H), 7.60 (d, 2H), 7.05 (d, 2H), 7.00 (d, 2H), 6.94 (d, 2H), 4.17 (m, 1H), 4.09 – 3.95 (m, 2H), 3.44 – 3.33 (m, 4H), 3.33 – 3.24 (m, 4H). ^{13}C NMR (126 MHz, Chloroform-*d*) δ 150.79 , 131.19 , 126.79 , 121.81 , 120.79 , 118.43 , 116.79 , 115.50 , 115.25 , 110.09 , 104.91 , 77.22 , 73.96 , 69.30 , 67.02 , 50.72 , 49.66 , 25.73 . DART-HRMS: *m/z* calcd. for $C_{33}H_{32}Cl_2N_4O_4$ $[MH]^+$, 619.1879; Found: 619.1871. IR (solid) *v*max: 3302, 3290, 2950, 2936, 1662, 1587, 1512, 1458, 1377, 1249, 1225, 1194, 1151, 1035 943, 823, 690.

***N*-(4-(4-(4-(((2*R*,4*R*)-2-(2,4-dichlorophenyl)-2-methyl-1,3-dioxolan-4-yl)methoxy)phenyl)piperazin-1-yl)phenyl)-2-hydroxybenzamide (84)** Salicylic acid (13.4 mg, 0.097 mmol) and HATU (81.3 mg, 0.21 mmol) were added to a round bottom flask. Anhydrous DMF was added (5 mL) followed by NMM (0.1 mL, 0.38 mmol) and this reaction was stirred at room temperature for 30 mins. Aniline **88** (50 mg, 0.097) was added to the reaction mixture and stirred for 12h at room temperature. The reaction was then added to ice cold water and extracted with EtOAc (3 x 20 mL). Organic layers were combined and washed with H_2O (2 x 20 mL) and brine (1 x 20 mL). The organic layers were dried over Na_2SO_4 and evaporated to dryness. Crude material was purified via column chromatography (SiO_2, 0-50% acetone in hexanes) to afford **84** (10.0 mg, 16%). ^{1}H NMR (500 MHz, Chloroform-*d*) δ 7.87 (s, 1H), 7.58 – 7.42 (m, 5H), 7.28 (m, 1H), 7.07 (m, 3H), 7.02 – 6.91 (m, 5H), 4.37 (m, 1H), 4.17 (m, 1H), 4.09 – 3.98 (m, 2H), 3.93 – 3.85 (m, 1H), 3.44 – 3.35 (m, 4H), 3.29 (t, 4H), 1.86 (s, 2H). ^{13}C NMR (126 MHz, Chloroform-*d*) δ 134.52 , 131.20 , 128.91 , 126.79 , 125.25 , 122.85 , 118.97 , 118.43 , 116.79 , 115.49 , 73.96 , 69.29 , 67.03 , 50.72 , 49.65 . DART-HRMS IR

(solid) *v*max: 3310, 2956, 2916, 2848, 1646, 1596, 1511, 1453, 1373, 1250, 1228, 1196, 1152, 1036, 942, 821, 755.

***N*-(4-(4-(4-(((2*R*,4*R*)-2-(2,4-dichlorophenyl)-2-methyl-1,3-dioxolan-4-yl)methoxy)phenyl)piperazin-1-yl)phenyl)-3-hydroxybenzamide (85)** 3-Hydroxybenzoic acid (5.4 mg, 0.038 mmol) and HATU (31.7 mg, 0.083 mmol) were added to a round bottom flask. Anhydrous DMF was added (5 mL) followed by NMM (0.1 mL, 0.15 mmol) and this reaction was stirred at room temperature for 30 mins. Aniline **88** (20 mg, 0.038 mmol) was added to the reaction mixture and stirred for 12h at room temperature. The reaction was then added to ice cold water and extracted with EtOAc (3 x 20 mL). Organic layers were combined and washed with H_2O (2 x 20 mL) and brine (1 x 20 mL). The organic layers were dried over Na_2SO_4 and evaporated to dryness. Crude material was purified via preparative thin layer chromatography (Analtech Uniplate 20x20 cm 2000 micron, 3% acetone in hexanes) to afford **85** (6.0 mg, 24.8%). ^{1}H NMR (500 MHz, Chloroform-*d*) δ 7.74 (d, 4H), 7.63 – 7.48 (m, 6H), 7.48 – 7.37 (m, 6H), 7.17 – 6.84 (m, 8H), 5.21 (s, 1H), 4.37 (s, 1H), 4.16 (m, 1H), 4.12 – 3.95 (m, 2H), 3.37 (d, 4H), 3.29 (t, 4H), 1.88 (m, 2H). ^{13}C NMR (126 MHz, Chloroform-*d*) δ 131.20 , 130.08 , 126.79 , 125.30 , 121.68 , 118.41 , 116.94 , 115.49 , 114.42 , 69.29 , 67.03 , 50.73 , 49.84 , 25.73 . DART-HRMS: *m/z* calcd. for $C_{34}H_{33}Cl_2N_3O_5$ $[MH]^+$, 634.1876; Found: 634.1847. IR (solid) *v*max: 3311, 2967, 2926, 2877, 1736, 1644, 1586, 1513, 1449, 1375, 1230, 1198, 1038, 945, 825, 746.

***N*-(4-(4-(4-(((2*R*,4*R*)-2-(2,4-dichlorophenyl)-2-methyl-1,3-dioxolan-4-yl)methoxy)phenyl)piperazin-1-yl)phenyl)-4-hydroxybenzamide (86)** (13.4 mg, 0.097 mmol) and HATU (81.3 mg, 0.21 mmol) were added to a round bottom flask.

Anhydrous DMF was added (5 mL) followed by NMM (0.1 mL, 0.38 mmol) and this reaction was stirred at room temperature for 30 mins. Aniline **88** (50 mg, 0.097) was added to the reaction mixture and stirred for 12h at room temperature. The reaction was then added to ice cold water and extracted with EtOAc (3 x 20 mL). Organic layers were combined and washed with H_2O (2 x 20 mL) and brine (1 x 20 mL). The organic layers were dried over Na_2SO_4 and evaporated to dryness. Crude material was purified via column chromatography (SiO_2, 0-50% acetone in hexanes) to afford **84** (5.0 mg, 8%).

1-(4-(((2*S*,4*R*)-2-(2,4-dichlorophenyl)-2-methyl-1,3-dioxolan-4-yl)methoxy)phenyl)-4-(4-nitrophenyl)piperazine (87) To a solution of **44** (260 mg, 0.87 mmol) in DMSO (20 mL) was added Cs_2CO_3 (3.1 g, 9.58 mmol) and **60** (400 mg, 0.0958 mmol). The solution was warmed to 90° C and stirred for 12 h. The mixture was cooled to room temperature and water was added slowly with vigorous stirring (~10 mL). A yellow precipitate formed, which was filtered and recrystallized in EtOH to yield **87** (175 mg, 34%) ^{1}H NMR (500 MHz, Chloroform-*d*) δ 8.22 – 8.17 (m, 2H), 7.68 (d, 1H), 7.42 (d, 1H), 7.24 (m, 1H), 6.96 – 6.89 (m, 4H), 6.81 – 6.76 (m, 2H), 4.65 (m, 1H), 4.35 (m, 1H), 3.99 (m, 1H), 3.81 – 3.76 (m, 2H), 3.64 – 3.59 (m, 4H), 3.26 (m, 4H), 1.83 (s, 3H). ^{13}C NMR (126 MHz, $CDCl_3$) δ 154.78, 153.09, 145.50, 139.34, 138.76, 134.35, 132.82, 130.97, 128.55, 126.70, 125.98, 118.53, 115.31, 112.89, 109.18, 77.29, 77.03, 76.78, 75.05, 68.41, 67.33, 50.38, 47.30, 25.90. DART-HRMS: *m/z* calcd. for $C_{27}H_{27}Cl_2N_3O_5$ $[MH]^+$, 544.1406; Found: 544.1409. IR (solid) *v*max: 2922, 2850, 1596, 1555, 1509, 1450, 1375, 1321, 1228, 1195, 1151, 1036, 944, 827, 753.

4-(4-(4-(((2*S*,4*R*)-2-(2,4-dichlorophenyl)-2-methyl-1,3-dioxolan-4-yl)methoxy)phenyl)piperazin-1-yl)aniline (88) 10% palladium on carbon (10 mg, 5% mole ratio) was added to a dry round bottom flask. Ethanol (50 mL) was added followed by slow addition of **87** (100 mg, 0.184 mmol). Hydrazine monohydrate (0.06 mL, 1.84 mmol) was added dropwise and the mixture was stirred at reflux for 2 h. Upon cooling to RT, the mixture was filtered through celite. The celite was washed with ethanol (300 mL) to ensure complete elution of the aniline. The filtrate was concentrated to afford a yellow solid, which was recrystallized in EtOH to afford **88** (89 mg, 94%). ^{1}H NMR (500 MHz, Chloroform-*d*) δ 8.20 (d, 1H), 7.68 (d, 1H), 7.43 (s, 1H), 7.24 (d, 1H), 6.92 (m, 3H), 6.81 – 6.68 (m, 3H), 4.70 – 4.59 (m, 1H), 4.35 (m, 1H), 4.00 (d, 1H), 3.78 (m, 2H), 3.61 (m, 1H), 3.49 (s, 1H), 3.25 (m, 5H). ^{13}C NMR (126 MHz, $CDCl_3$) δ 130.97, 128.59, 126.70, 125.99, 118.85, 118.54, 118.21, 116.24, 115.21, 112.90, 77.28, 77.03, 76.78, 75.07, 68.43, 67.40, 51.24, 50.85, 50.38, 47.30, 25.90. DART-HRMS: *m/z* calcd. for $C_{27}H_{29}Cl_2N_3O_3$ $[MH]^+$, 514.1664; Found: 514.1666. IR (solid) *v*max: 2921, 2823, 1590, 1510, 1450, 1375, 1321, 1227, 1193, 1149, 1037, 944, 824, 753.

***N*-(4-(4-(4-(((2*S*,4*R*)-2-(2,4-dichlorophenyl)-2-methyl-1,3-dioxolan-4-yl)methoxy)phenyl)piperazin-1-yl)phenyl)benzamide (89)** Aniline **88** (20 mg, 0.039 mmol), benzoic acid (14.3 mg, 0.117 mmol), EDCI (22.4 mg, 0.117 mmol), and DMAP (14.3 mg, 0.117 mmol) was dissolved in anhydrous DCM (10mL) and stirred under argon for 12h at room temperature. The crude reaction was immediately purified via column chromatography (SiO_2, 0-60% acetone in hexanes) to afford **89** (5.0 mg, 20.6%). ^{1}H NMR (500 MHz, Chloroform-*d*) δ 7.91 (d, 2H), 7.73 (s, 1H), 7.69 (d, 1H), 7.59 (m, 2H), 7.54 (t, 2H), 7.04 (d, 2H), 6.95 (d, 2H), 6.78 (d, 2H), 4.65 (m, 1H), 4.35 (m,

1H), 4.00 (m, 1H), 3.82 – 3.74 (m, 2H), 3.36 (d, 3H), 3.28 (d, 4H), 1.83 (s, 3H). ^{13}C NMR (126 MHz, $CDCl_3$) δ 131.68, 130.97, 128.78, 128.58, 126.95, 126.70, 121.64, 118.35, 116.95, 115.24, 112.04, 109.16, 106.31, 77.27, 77.22, 77.02, 76.77, 75.07, 68.44, 67.39, 50.73, 49.88, 25.90. DART-HRMS: *m/z* calcd. for $C_{34}H_{33}Cl_2N_3O_4$ $[MH]^+$, 618.1926; Found: 618.1916. IR (solid) *v*max: 3305, 2964, 2824, 1637, 1592, 1511, 1448, 1374, 1226, 1192, 1152, 1034, 943, 818, 728, 703.

***N*-(4-(4-(4-(((2*S*,4*R*)-2-(2,4-dichlorophenyl)-2-methyl-1,3-dioxolan-4-yl)methoxy)phenyl)piperazin-1-yl)phenyl)-2-naphthamide (90)** Aniline **88** (20 mg, 0.039 mmol), naphtholic acid (20.1 mg, 0.117 mmol), EDCI (22.4 mg, 0.117 mmol), and DMAP (14.3 mg, 0.117 mmol) was dissolved in anhydrous DCM (10mL) and stirred under argon for 12h at room temperature. The crude reaction was immediately purified via column chromatography (SiO_2, 0-60% acetone in hexanes) to afford **90** (3.0 mg, 11.5%). ^{1}H NMR (500 MHz, Chloroform-*d*) δ 8.43 (s, 1H), 8.08 – 7.92 (m, 4H), 7.89 (s, 1H), 7.73 – 7.58 (m, 5H), 7.06 (d, 2H), 6.96 (d, 2H), 6.78 (d, 2H), 4.65 (m, 1H), 4.35 (m, 1H), 4.00 (m, 2H), 3.86 – 3.71 (m, 2H), 3.45 – 3.33 (m, 4H), 3.33 – 3.21 (m, 4H), 1.83 (s, 3H). ^{13}C NMR (126 MHz, $CDCl_3$) δ 165.53, 152.75, 148.50, 146.03, 139.34, 134.83, 134.36, 132.80, 132.69, 132.36, 130.97, 130.68, 128.96, 128.73, 128.59, 127.83, 127.41, 126.94, 126.71, 123.57, 121.69, 118.36, 116.96, 115.63, 115.24, 111.68, 109.16, 105.89, 77.27, 77.22, 77.02, 76.77, 75.07, 68.44, 67.40, 50.74, 49.87, 25.91, 1.04. DART-HRMS: *m/z* calcd. for $C_{38}H_{35}Cl_2N_3O_4$ $[MH]^+$, 668.2083; Found: 668.2116. IR (solid) *v*max: 3326, 2920, 2851, 1663, 1596, 1558, 1513, 1450, 1373, 1229, 1195, 1151, 1037, 948, 822, 760.

***N*-(4-(4-(4-(((2*S*,4*R*)-2-(2,4-dichlorophenyl)-2-methyl-1,3-dioxolan-4-yl)methoxy)phenyl)piperazin-1-yl)phenyl)picolinamide (91)** Aniline **88** (20 mg, 0.039 mmol), picolinic acid (14.4 mg, 0.117 mmol), EDCI (22.4 mg, 0.117 mmol), and DMAP (14.3 mg, 0.117 mmol) was dissolved in anhydrous DCM (10mL) and stirred under argon for 12h at room temperature. The crude reaction was immediately purified via column chromatography (SiO_2, 0-80% acetone in hexanes) to afford **91** (5.0 mg, 20.6%). Aniline **78** (20 mg, 0.039 mmol), picolinic acid (14.4 mg, 0.117 mmol), EDCI (22.4 mg, 0.117 mmol), and DMAP (14.3 mg, 0.117 mmol) was dissolved in anhydrous DCM (10mL) and stirred under argon for 12h at room temperature. The crude reaction was immediately purified via column chromatography (SiO_2, 0-80% acetone in hexanes) to afford **81** (9.0 mg, 37%). ^{1}H NMR (500 MHz, Chloroform-*d*) δ 9.96 (s, 1H), 8.71 – 8.60 (m, 1H), 8.34 (m, 1H), 7.95 (m, 1H), 7.76 (m, 2H), 7.69 (d, 1H), 7.57 – 7.48 (m, 1H), 7.25 (m, 1H), 7.06 (d, 2H), 6.96 (d, 2H), 6.78 (d, 2H), 4.65 (m, 1H), 4.35 (m, 1H), 4.00 (m, 1H), 3.83 – 3.74 (m, 2H), 3.37 (s, 5H), 3.28 (s, 4H), 1.83 (s, 3H). ^{13}C NMR (126 MHz, $CDCl_3$) δ 147.93, 137.64, 130.97, 128.58, 126.71, 122.31, 120.91, 118.33, 116.96, 115.25, 111.75, 77.28, 77.02, 76.77, 75.06, 68.44, 67.39, 50.74, 49.90, 25.91. DART-HRMS: *m/z* calcd. for $C_{33}H_{32}Cl_2N_4O_4$ $[MH]^+$, 619.1879; Found: 619.1862. IR (solid) *v*max: 3365, 2955, 2849, 1675, 1586, 1568, 1510, 1453, 1373, 1268, 1229, 1193, 1151, 1097, 1037, 942, 823, 747.

***N*-(4-(4-(4-(((2*S*,4*R*)-2-(2,4-dichlorophenyl)-2-methyl-1,3-dioxolan-4-yl)methoxy)phenyl)piperazin-1-yl)phenyl)nicotinamide (92)** Aniline **88** (20 mg, 0.039 mmol), nicotinic acid (14.4 mg, 0.117 mmol), EDCI (22.4 mg, 0.117 mmol), and DMAP (14.3 mg, 0.117 mmol) was dissolved in anhydrous DCM (10mL) and stirred under

argon for 12h at room temperature. The crude reaction was immediately purified via column chromatography (SiO_2, 0-80% acetone in hexanes) to afford **92** (6.0 mg, 24.7%). ^{1}H NMR (500 MHz, Chloroform-*d*) δ 9.15 (s, 1H), 8.83 (s, 1H), 8.26 (d, 1H), 7.86 (s, 1H), 7.68 (d, 1H), 7.60 (d, 2H), 7.49 (s, 1H), 7.43 (d, 1H), 7.28 – 7.20 (m, 1H), 7.01 (m, 4H), 6.83 – 6.73 (m, 2H), 4.65 (m, 1H), 4.35 (m, 1H), 4.00 (m, 1H), 3.83 – 3.74 (m, 2H), 3.44 – 3.34 (m, 4H), 3.29 (t, 4H), 1.83 (s, 3H). ^{13}C NMR (126 MHz, $CDCl_3$) δ 139.33, 134.36, 132.80, 130.97, 128.58, 126.71, 121.92, 118.54, 116.92, 115.27, 109.17, 77.29, 77.24, 77.03, 76.78, 75.05, 68.43, 67.36, 50.88, 49.67, 25.90. DART-HRMS: *m/z* calcd. for $C_{33}H_{32}Cl_2N_4O_4$ $[MH]^+$, 619.1879; Found: 619.1866. IR (solid) *v*max: 3364, 3315, 2960, 2924, 2853, 1673, 1511, 1456, 1372, 1259, 1227, 1193, 1097, 1035, 826, 807.

***N*-(4-(4-(4-(((2*S*,4*R*)-2-(2,4-dichlorophenyl)-2-methyl-1,3-dioxolan-4-yl)methoxy)phenyl)piperazin-1-yl)phenyl)isonicotinamide (93)** Aniline **88** (20 mg, 0.039 mmol), isonicotinic acid (14.4 mg, 0.117 mmol), EDCI (22.4 mg, 0.117 mmol), and DMAP (14.3 mg, 0.117 mmol) was dissolved in anhydrous DCM (10mL) and stirred under argon for 12h at room temperature. The crude reaction was immediately purified via column chromatography (SiO_2, 0-80% acetone in hexanes) to afford **93** (8.0 mg, 33%). ^{1}H NMR (500 MHz, Chloroform-*d*) δ 8.85 (s, 2H), 7.82 – 7.70 (m, 3H), 7.68 (d, 1H), 7.59 (d, 2H), 7.43 (d, 1H), 7.24 (m, 1H), 7.04 (d, 2H), 7.01 – 6.88 (m, 2H), 6.82 – 6.72 (m, 2H), 4.66 (m, 1H), 4.35 (m, 1H), 4.00 (m, 1H), 3.85 – 3.71 (m, 2H), 3.38 (m, 4H), 3.27 (m, 4H), 1.86 (s, 3H). ^{13}C NMR (126 MHz, $CDCl_3$) δ 152.80, 150.80, 145.98, 139.36, 134.36, 132.81, 130.97, 128.58, 126.70, 121.81, 120.80, 118.38, 116.79, 115.27, 111.58, 109.16, 77.27, 77.22, 77.02, 76.77, 75.07, 68.46, 67.39, 50.71, 49.65,

29.72, 25.90, 1.03. DART-HRMS: *m/z* calcd. for $C_{33}H_{32}Cl_2N_4O_4$ $[MH]^+$, 619.1879; Found: 619.1866. IR (solid) *v*max: 3256, 2963, 2854, 1660, 1587, 1510, 1449, 1376, 1261, 1226, 1193, 1150, 1034, 940, 826, 740.

2-(benzyloxy)-*N*-(4-(4-(4-(((2*S*,4*R*)-2-(2,4-dichlorophenyl)-2-methyl-1,3-dioxolan-4-yl)methoxy)phenyl)piperazin-1-yl)phenyl)benzamide (94) Aniline **88** (100 mg, 0.194 mmol), 2-(benzyloxy)benzoic acid (133 mg, 0.583 mmol), EDCI (111.8 mg, 0.583 mmol), and DMAP (14.3 mg, 0.583 mmol) was dissolved in anhydrous DCM (10mL) and stirred under argon for 12h at room temperature. The crude reaction was immediately purified via column chromatography (SiO_2, 0-30% acetone in hexanes) to afford **94** (20 mg, 14.2%). ^{1}H NMR (500 MHz, Chloroform-*d*) δ 9.91 (s, 1H), 8.39 (m, 1H), 7.69 (d, 1H), 7.62 – 7.49 (m, 6H), 7.43 (d, 1H), 7.29 – 7.15 (m, 5H), 6.97 – 6.91 (m, 2H), 6.91 – 6.85 (m, 2H), 6.82 – 6.73 (m, 2H), 4.65 (m, 1H), 4.35 (m, 1H), 4.00 (m, 1H), 3.82 – 3.74 (m, 2H), 3.31 (m, 4H), 3.25 (m, 4H), 1.83 (s, 3H).^{13}C NMR (126 MHz, $CDCl_3$) δ 156.61, 135.35, 132.99, 132.63, 131.57, 130.97, 129.15, 129.08, 128.59, 126.71, 122.13, 121.96, 120.88, 118.31, 116.81, 115.23, 112.58, 109.15, 77.28, 77.03, 76.77, 75.07, 71.81, 68.44, 67.40, 50.73, 49.99, 25.90.

3-(benzyloxy)-*N*-(4-(4-(4-(((2*R*,4*R*)-2-(2,4-dichlorophenyl)-2-methyl-1,3-dioxolan-4-yl)methoxy)phenyl)piperazin-1-yl)phenyl)benzamide (95) Aniline **88** (100 mg, 0.194 mmol), 3-(benzyloxy)benzoic acid (133 mg, 0.583 mmol), EDCI (111.8 mg, 0.583 mmol), and DMAP (14.3 mg, 0.583 mmol) was dissolved in anhydrous DCM (10mL) and stirred under argon for 12h at room temperature. The crude reaction was immediately purified via column chromatography (SiO_2, 0-30% acetone in hexanes) to afford **95** (60 mg, 43%). ^{1}H NMR (500 MHz, Chloroform-*d*) δ 7.80 (s, 1H), 7.69 (d, 1H), 7.62 – 7.54

(m, 3H), 7.52 – 7.35 (m, 10H), 7.27 – 7.22 (m, 1H), 7.18 (m, 1H), 7.03 (d, 2H), 6.96 (d, 2H), 6.78 (d, 2H), 5.16 (d, 3H), 4.65 (m, 1H), 4.35 (m, 1H), 4.00 (m, 1H), 3.78 (m, 2H), 3.42 – 3.32 (m, 4H), 3.28 (m, 4H), 1.83 (s, 3H). ^{13}C NMR (126 MHz, $CDCl_3$) δ 159.13, 139.34, 136.64, 136.53, 134.36, 132.80, 130.98, 129.82, 128.69, 128.59, 128.17, 127.59, 126.72, 121.62, 119.02, 118.61, 118.41, 116.97, 115.24, 113.50, 109.16, 77.31, 77.05, 76.80, 75.07, 70.25, 68.42, 67.38, 50.74, 49.85, 25.91. DART-HRMS: *m/z* calcd. for $C_{41}H_{39}Cl_2N_3O_5$ $[MH]^+$, 724.2345; Found: 724.2377. IR (solid) *v*max: 3289, 2928, 2878, 2824, 1693, 1639, 1583, 1556, 1509, 1484, 1451, 1225, 1188, 1027, 941, 820, 732, 622, 600

4-(benzyloxy)-*N*-(4-(4-(4-(((2*S*,4*R*)-2-(2,4-dichlorophenyl)-2-methyl-1,3-dioxolan-4-yl)methoxy)phenyl)piperazin-1-yl)phenyl)benzamide (96) Aniline **88** (100 mg, 0.194 mmol), 3-(benzyloxy)benzoic acid (133 mg, 0.583 mmol), EDCI (111.8 mg, 0.583 mmol), and DMAP (14.3 mg, 0.583 mmol) was dissolved in anhydrous DCM (10mL) and stirred under argon for 12h at room temperature. The crude reaction was immediately purified via column chromatography (SiO_2, 0-30% acetone in hexanes) to afford **95** (50 mg, 35%). ^{1}H NMR δ 9.04 (s, 2H), 7.91 – 7.84 (m, 7H), 7.71 – 7.63 (m, 2H), 7.57 (d, *J* = 8.5 Hz, 2H), 7.52 – 7.36 (m, 22H), 7.09 (d, *J* = 8.6 Hz, 6H), 7.05 – 6.96 (m, 5H), 6.95 (d, *J* = 8.7 Hz, 2H), 6.78 (d, *J* = 8.9 Hz, 2H), 5.13 (s, 2H), 4.65 (m, 1H), 4.35 (m, 1H), 3.85 – 3.73 (m, 2H), 3.35 (d, *J* = 5.5 Hz, 5H), 3.28 (d, *J* = 5.3 Hz, 5H), 1.83 (s, 3H). DART-HRMS: *m/z* calcd. for $C_{41}H_{39}Cl_2N_3O_5$ $[MH]^+$, 724.2345; Found: 724.2329.

***N*-(4-(4-(4-(((2*S*,4*R*)-2-(2,4-dichlorophenyl)-2-methyl-1,3-dioxolan-4-yl)methoxy)phenyl)piperazin-1-yl)phenyl)-2-hydroxybenzamide (97)** DART-HRMS: *m/z* calcd. for $C_{34}H_{33}Cl_2N_3O_5$ $[MH]^+$, 634.1876; Found: 634.1843.

N-(4-(4-(4-(((2S,4R)-2-(2,4-dichlorophenyl)-2-methyl-1,3-dioxolan-4-yl)methoxy)phenyl)piperazin-1-yl)phenyl)-3-hydroxybenzamide (98) Protected ester **95** (20 mg, 0.0276 mmol) was dissolved in EtOH: THF (2:1). 10% palladium on carbon (10 mg) was then added. The reaction vessel was sealed with a rubber septum and charged with an atmosphere of hydrogen gas. The reaction was stirred overnight at room temperature. The reaction mixture was filtered over a pad of celite and rinsed with EtOAc and concentrated under reduced pressure. The crude residue was purified via column chromatography (SiO_2, 0-80% acetone in hexanes) to yield **98** (8 mg, 45.5%). ^{1}H NMR (500 MHz, Chloroform-*d*) δ 7.70 (s, 1H), 7.64 (d, 1H), 7.52 (d, 2H), 7.46 (s, 1H), 7.38 (s, 1H), 7.34 (s, 2H), 7.24 – 7.17 (m, 1H), 7.04 – 6.96 (m, 3H), 6.90 (d, 2H), 6.73 (d, 2H), 5.72 (s, 1H), 4.65 – 4.56 (m, 1H), 4.31 (t, 1H), 3.95 (m, 1H), 3.74 (t, 2H), 3.31 (d, 4H), 3.23 (d, 4H), 1.80 (d, 3H). ^{13}C NMR (126 MHz, Chloroform-*d*) δ 130.05 , 128.58 , 126.71 , 121.75 , 118.47 , 118.36 , 116.92 , 115.25 , 114.62 , 111.69 , 106.06 , 102.05 , 77.22 , 75.07 , 67.39 , 50.71 , 49.81 , 25.90 . DART-HRMS: *m/z* calcd. for $C_{34}H_{33}Cl_2N_3O_5$ $[MH]^+$, 634.1876; Found: 634.1884. IR (solid) *v*max: 3279, 2925, 2852, 2824, 1639, 1590, 1446, 1409, 1373, 1228, 1190, 115, 1036, 944, 826, 747.

***N*-(4-(4-(4-(((2*S*,4*R*)-2-(2,4-dichlorophenyl)-2-methyl-1,3-dioxolan-4-yl)methoxy)phenyl)piperazin-1-yl)phenyl)-4-hydroxybenzamide (99)** DART-HRMS: *m/z* calcd. for $C_{34}H_{33}Cl_2N_3O_5$ $[MH]^+$, 634.1876; Found: 634.1843.

3-chloro-*N*-(4-(4-(4-(((2*S*,4*R*)-2-(2,4-dichlorophenyl)-2-methyl-1,3-dioxolan-4-yl)methoxy)phenyl)piperazin-1-yl)phenyl)benzamide (100) Aniline **88** (20 mg, 0.039 mmol), 3-chlorobenzoic acid (18.3 mg, 0.117 mmol), EDCI (22.4 mg, 0.117 mmol), and DMAP (14.3 mg, 0.117 mmol) was dissolved in anhydrous DCM (10mL) and stirred

under argon for 12h at room temperature. The crude reaction was immediately purified via column chromatography (SiO_2, 0-80% acetone in hexanes) to afford **100** (6.0 mg, 23.5%). ^{1}H NMR (500 MHz, Chloroform-*d*) δ 7.90 (t, 1H), 7.78 (d, 1H), 7.68 (d, 2H), 7.60 – 7.54 (m, 3H), 7.47 (t, 1H), 7.43 (d, 1H), 7.24 (m, 1H), 7.04 (d, 2H), 6.98 – 6.92 (m, 2H), 6.81 – 6.75 (m, 2H), 4.65 (m, 1H), 4.35 (m, 1H), 4.00 (m, 1H), 3.82 – 3.73 (m, 2H), 3.41 – 3.32 (m, 4H), 3.27 (m, 4H), 1.83 (s, 3H). ^{13}C NMR (126 MHz, $CDCl_3$) δ 130.97, 130.10, 128.58, 127.34, 126.71, 121.74, 118.36, 116.88, 115.24, 111.47, 109.16, 105.92, 101.77, 77.27, 77.02, 76.76, 75.06, 68.44, 67.39, 50.72, 49.77, 25.90. DART-HRMS: *m/z* calcd. for $C_{34}H_{32}Cl_3N_3O_4$ $[MH]^+$, 648.2032; Found: 648.1998. IR (solid) *v*max: 3311, 3283, 3254, 2961, 2854, 1640, 1588, 1512, 1451, 1375, 1228, 1192, 1152, 1037, 943, 820, 755.

***N*-(4-(4-(4-(((2*S*,4*R*)-2-(2,4-dichlorophenyl)-2-methyl-1,3-dioxolan-4-yl)methoxy)phenyl)piperazin-1-yl)phenyl)-3-methoxybenzamide (101)** Aniline **88** (20 mg, 0.039 mmol), m-anisic acid (17.8 mg, 0.117 mmol), EDCI (22.4 mg, 0.117 mmol), and DMAP (14.3 mg, 0.117 mmol) was dissolved in anhydrous DCM (10mL) and stirred under argon for 12h at room temperature. The crude reaction was immediately purified via column chromatography (SiO_2, 0-60% acetone in hexanes) to afford **101** (4.0 mg, 15.7%). ^{1}H NMR (500 MHz, Chloroform-*d*) δ 7.74 (s, 1H), 7.68 (d, 1H), 7.59 (d, 2H), 7.51 – 7.46 (m, 1H), 7.45 – 7.41 (m, 3H), 7.24 (m, 1H), 7.14 – 7.08 (m, 1H), 7.04 (d, 2H), 6.95 (d, 2H), 6.81 – 6.75 (m, 2H), 4.65 (m, 1H), 4.35 (m, 1H), 4.00 (m, 1H), 3.92 (s, 3H), 3.81 – 3.74 (m, 2H), 3.42 – 3.31 (m, 5H), 3.27 (t, 4H), 1.83 (s, 3H). ^{13}C NMR (126 MHz, Chloroform-*d*) δ 129.75 , 121.58 , 118.35 , 118.35 , 116.93 , 116.93 , 115.24 , 110.72 , 109.81 , 104.93 , 100.60 , 96.72 , 77.21 , 55.52 , 50.72 , 49.86 .

DART-HRMS: *m/z* calcd. for $C_{35}H_{35}Cl_2N_3O_5$ $[MH]^+$, 652.1537; Found: 652.1532. IR (solid) *v*max: 3289, 2922, 2823, 138, 1580, 1510, 1450, 1374, 1288, 1190, 1150, 1033, 943, 817, 746, 686, 524

***N*-(4-(4-(4-(((2*S*,4*R*)-2-(2,4-dichlorophenyl)-2-methyl-1,3-dioxolan-4-yl)methoxy)phenyl)piperazin-1-yl)phenyl)furan-3-carboxamide (102)** Aniline **88** (20 mg, 0.039 mmol), 3-thiophene carboxylic acid (14.9 mg, 0.117 mmol), EDCI (22.4 mg, 0.117 mmol), and DMAP (14.3 mg, 0.117 mmol) was dissolved in anhydrous DCM (10mL) and stirred under argon for 12h at room temperature. The crude reaction was immediately purified via column chromatography (SiO_2, 0-50% acetone in hexanes) to afford **102** (2.0 mg, 8.1%). ^{1}H NMR (500 MHz, Chloroform-*d*) δ 7.53 (s, 3H), 7.02 (d, 2H), 6.98 – 6.90 (m, 2H), 6.83 – 6.71 (m, 3H), 4.35 (m, 1H), 3.78 (m, 2H), 3.43 – 3.30 (m, 4H), 3.30 – 3.17 (m, 4H), 1.83 (s, 3H). DART-HRMS *m/z* calcd. for $C_{32}H_{31}Cl_2N_3O_5$ $[MH]^+$, 608.1719; Found: 608.1701

***N*-(4-(4-(4-(((2*S*,4*R*)-2-(2,4-dichlorophenyl)-2-methyl-1,3-dioxolan-4-yl)methoxy)phenyl)piperazin-1-yl)phenyl)thiophene-3-carboxamide (103)** Aniline **88** (20 mg, 0.039 mmol), 3-furic acid (13.1 mg, 0.117 mmol), EDCI (22.4 mg, 0.117 mmol), and DMAP (14.3 mg, 0.117 mmol) was dissolved in anhydrous DCM (10mL) and stirred under argon for 12h at room temperature. The crude reaction was immediately purified via column chromatography (SiO_2, 0-50% acetone in hexanes) to afford **90** (3.0 mg, 12.6%). ^{1}H NMR (500 MHz, Chloroform-*d*) δ 7.99 (d, 1H), 7.68 (d, 1H), 7.59 – 7.49 (m, 4H), 7.44 (m, 2H), 7.24 (m, 1H), 7.03 (d, 2H), 6.95 (d, 2H), 6.78 (d, 2H), 4.65 (m, 1H), 4.35 (m, 1H), 4.00 (m, 1H), 3.78 (m, 2H), 3.41 – 3.32 (m, 4H), 3.27 (m, 4H). ^{13}C NMR (126 MHz, $CDCl_3$) δ 152.75, 146.02, 139.34, 134.36, 130.97, 128.58, 128.36,

126.83, 126.70, 126.03, 121.67, 119.77, 118.35, 116.93, 115.88, 115.24, 111.51, 109.16, 105.96, 101.84, 97.85, 93.77, 77.27, 77.22, 77.01, 76.76, 75.07, 68.44, 67.39, 50.72, 49.84, 31.95, 30.18, 29.72, 29.38, 25.90, 22.71, 14.13, 1.04. DART-HRMS: *m/z* calcd. for $C_{32}H_{31}Cl_2N_3O_4S$ $[MH]^+$, 624.1491; Found: 624.1473.

N-(4-(4-(4-(((2S,4R)-2-(2,4-dichlorophenyl)-2-methyl-1,3-dioxolan-4-yl)methoxy)phenyl)piperazin-1-yl)phenyl)cyclohexanecarboxamide (104) ^{1}H NMR (500 MHz, Chloroform-*d*) δ 8.19 (s, 1H), 7.56 (d, *J* = 7.5 Hz, 2H), 7.46 – 7.33 (m, 3H), 6.92 (dd, *J* = 18.1, 8.7 Hz, 4H), 6.79 (dd, *J* = 12.5, 8.7 Hz, 2H), 6.72 (d, *J* = 8.5 Hz, 2H), 4.42 – 4.28 (m, 1H), 4.00 (dd, *J* = 9.6, 5.8 Hz, 1H), 3.83 – 3.66 (m, 2H), 3.40 (s, 4H), 3.24 (d, *J* = 6.3 Hz, 8H), 2.28 – 2.18 (m, 2H), 1.93 (d, *J* = 12.9 Hz, 3H), 1.89 – 1.79 (m, 5H), 1.72 (s, 4H), 1.68 (s, 1H), 1.52 (t, *J* = 12.7 Hz, 5H).

3-acetyl-N-(4-(4-(4-(((2S,4R)-2-(2,4-dichlorophenyl)-2-methyl-1,3-dioxolan-4-yl)methoxy)phenyl)piperazin-1-yl)phenyl)benzamide (105) ^{1}H NMR (500 MHz, Chloroform-*d*) δ 8.47 (s, 1H), 8.15 (t, *J* = 8.6 Hz, 2H), 7.92 (s, 1H), 7.71 – 7.52 (m, 5H), 7.45 – 7.32 (m, 2H), 7.29 – 7.22 (m, 1H), 7.04 (d, *J* = 8.7 Hz, 2H), 6.95 (t, *J* = 6.5 Hz, 2H), 6.84 – 6.74 (m, 2H), 4.65 (m, 1H), 4.35 (m, 1H), 4.00 (m, 1H), 3.82 – 3.66 (m, 2H), 3.36 (m, 4H), 3.27 (m, 4H), 2.71 (d, *J* = 6.6 Hz, 3H).

phenyl (4-(4-(4-(((2*R*,4*R*)-2-(2,4-dichlorophenyl)-2-methyl-1,3-dioxolan-4-yl)methoxy)phenyl)piperazin-1-yl)phenyl)carbamate (106) ^{1}H NMR (500 MHz, Chloroform-*d*) δ 7.66 (m, 1H), 7.52 – 7.36 (m, 6H), 7.30 – 7.21 (m, 4H), 7.21 – 7.17 (m, 1H), 7.04 – 6.96 (m, 4H), 6.96 – 6.90 (m, 2H), 6.86 (s, 1H), 4.38 (m, 1H), 4.16 (m, 1H), 4.09 – 4.04 (m, 1H), 4.04 – 3.97 (m, 1H), 3.90 (m, 1H), 3.44 (m, 1H), 3.35 (m, 3H), 3.28 (m, 4H), 1.87 (s, 3H). ^{13}C NMR (126 MHz, Chloroform-*d*) δ 152.92 , 138.15 , 134.56 ,

132.83 , 131.20 , 129.39 , 128.91 , 126.80 , 125.59 , 121.66 , 121.30 , 120.32 , 118.38 , 117.16 , 116.17 , 115.49 , 109.09 , 77.24 , 73.96 , 69.30 , 67.03 , 50.74 , 49.98 , 48.91 , 25.75. IR (solid) *v*max: 3332, 3292, 2926, 2825, 1733, 1706, 1510, 1490, 1450, 1414, 1227, 1179, 1161, 1034, 943, 823, 747, 687.

***N*-(4-(4-(4-(((2*R*,4*R*)-2-(2,4-dichlorophenyl)-2-methyl-1,3-dioxolan-4-yl)methoxy)phenyl)piperazin-1-yl)phenyl)hydrazinecarboxamide (107)** ^{1}H NMR (500 MHz, Chloroform-*d*) δ 7.66 (d, 1H), 7.45 (d, 1H), 7.28 (m, 1H), 7.02 – 6.95 (m, 2H), 6.92 (m, 4H), 6.76 – 6.68 (m, 2H), 4.37 (m, 1H), 4.16 (m, 1H), 4.06 (m, 1H), 4.01 (m, 1H), 3.89 (m, 1H), 3.41 (d, 1H), 3.32 – 3.26 (m, 4H), 3.26 – 3.17 (m, 3H), 1.86 (s, 3H). ^{13}C NMR (126 MHz, Chloroform-*d*) δ 131.19 , 128.91 , 126.79 , 118.85 , 118.25 , 116.23 , 115.46 , 110.18 , 77.23 , 73.97 , 69.30 , 67.04 , 51.25 , 50.86 , 25.74. IR (solid) *v*max: 2916, 2848, 1546, 1510, 1462, 1450, 1375, 1225, 1197, 1037, 945, 824.

phenyl (4-(4-(4-(((2*S*,4*R*)-2-(2,4-dichlorophenyl)-2-methyl-1,3-dioxolan-4-yl)methoxy)phenyl)piperazin-1-yl)phenyl)carbamate (108) ^{1}H NMR (500 MHz, Chloroform-*d*) δ 7.59 – 7.53 (m, 2H), 7.47 – 7.37 (m, 11H), 7.27 – 7.22 (m, 6H), 7.01 (d, *J* = 8.9 Hz, 3H), 6.95 (d, *J* = 9.0 Hz, 2H), 6.88 (d, *J* = 7.9 Hz, 2H), 6.84 – 6.73 (m, 3H), 4.65 (p, *J* = 6.1 Hz, 1H), 4.39 – 4.30 (m, 1H), 4.00 (s, 2H), 3.82 – 3.69 (m, 3H), 3.40 (s, 3H), 3.33 (d, *J* = 5.4 Hz, 4H), 3.27 (dd, *J* = 6.3, 3.7 Hz, 4H). IR (solid) *v*max: 3332, 2958, 2926, 2853, 1757, 1736, 1553, 1510, 1491, 1417, 1229, 1195, 1181, 1162, 1024, 911, 828, 751, 688.

***N*-(4-(4-(4-(((2*S*,4*R*)-2-(2,4-dichlorophenyl)-2-methyl-1,3-dioxolan-4-yl)methoxy)phenyl)piperazin-1-yl)phenyl)hydrazinecarboxamide (109)** ^{1}H NMR (500 MHz, Chloroform-*d*) δ 7.68 (d, 1H), 7.43 (d, 1H), 7.24 (m, 1H), 6.99 – 6.87 (m, 5H),

6.81 – 6.68 (m, 4H), 4.65 (m, 1H), 4.35 (m, 1H), 4.00 (m, 1H), 3.85 – 3.74 (m, 3H), 3.40 (s, 2H), 3.30 – 3.20 (m, 8H), 1.82 (s, 3H). ^{13}C NMR (126 MHz, Chloroform-*d*) δ 128.59 , 126.71 , 119.01 , 118.35 , 116.21 , 115.22 , 110.03 , 105.12 , 76.87 , 75.06 , 68.43 , 67.39, 50.80 , 29.72 , 25.89. IR (solid) *v*max: 2920, 2876, 2851, 1554, 1511, 1464, 1450, 1377, 1225, 1184, 1151, 1035, 944, 826.

4-(4-(4-(4-(((2S,4R)-2-(2,4-dichlorophenyl)-2-methyl-1,3-dioxolan-4-yl)methoxy)phenyl)piperazin-1-yl)phenyl)-1H-1,2,4-triazol-5(4H)-one (110). ^{1}H NMR (500 MHz, Chloroform-*d*) δ 8.55 (d, *J* = 11.6 Hz, 0H), 8.38 (s, 0H), 7.68 (d, *J* = 8.4 Hz, 1H), 7.50 (d, *J* = 16.7 Hz, 1H), 7.43 (s, 1H), 7.23 (d, *J* = 2.1 Hz, 1H), 7.08 (d, *J* = 18.3 Hz, 1H), 7.00 (d, *J* = 15.3 Hz, 2H), 6.93 (s, 2H), 6.78 (s, 2H), 4.65 (s, 1H), 4.36 (s, 1H), 3.98 (s, 1H), 3.81 – 3.75 (m, 2H), 3.40 (s, 1H), 3.26 (q, *J* = 4.6, 3.6 Hz, 5H), 1.83 (s, 3H).

4.2 Biological Assay Protocols

Gene expression assay protocol (ASZ-001): Cells were seeded (10,000 cells per well; 100 µL total volume per well) in a 96-well tissue culture plate. After 24h of incubation (37°C, 5% CO_2), growth media was removed and replaced with low FBS media. Cells were incubated for an additional 24h. After this time, DMSO (vehicle control) and analogues (1% DMSO concentration) were added to the wells. Cells were incubated (37°C, 5% CO_2) for 48h and RNA was isolated and evaluated by qRT-PCR.

RT-PCR protocol: Following treatment and incubation periods, both RNA extraction and cDNA synthesis were performed using a TaqMan Cells-to-CT (fast) kit. cDNA synthesis utilized a BioRad MyCycler and was programmed according to the manufacturer's

instructions. Quantitative RT-PCR was performed on an ABI 7500 system and made use of the following TaqMan Gene Expression Probes: mouse ActB (Mm00607939_s1) and mouse Gli1 (Mm00494654_m1). Relative gene expression levels were computed via ΔΔCT method using GraphPad Prism. Corresponding IC_{50} values were calculated as mean ± SEM for at least three separate experiments performed in triplicate.

CHAPTER IV: Using Nanotechnology for Targeted ITZ Delivery

1. Introduction

Nanoscience refers to research at a scale of 100 nm or less and it represents a broad range of scientific disciplines. Nanomedicine consists of utilizing nanoscience for medical diagnosis, prevention, and treatment of a disease. Applying nanoscience to drug delivery is seen to be extremely promising and represents the bulk usage of nanoscience.[130,131] Often times, clinically approved drugs are not necessarily the most potent but rather have the most optimal physicochemical properties. Nanoparticles mask a drug's limiting properties as the drug of interest is dissolved, entrapped, absorbed, attached and/or encapsulated into or onto the nano-matrix.[132] As a result, utilizing nanotechnology will aid in the approval of compounds with the most potent activity rather than the most optimal drug properties. Nanotechnology offers a wide range of advantages including improved delivery of water insoluble drugs, targeted delivery of drugs in a cell or tissue specific manner, crossing of drugs across tight epithelial/endothelial barriers, delivery of large macromolecule drugs to intracellular sites of action, co-delivery of two or more drugs, visualization of drug delivery with imagining, and real-time read out of in vivo efficacy experiments.[133] To date, there are over two-dozen nanotechnology therapeutic products that are clinically approved and this number is expected to increase as research in the nanomedicine field is rapidly growing.[133]

The most studied nanoparticles, liposomes, were first discovered in the 1960s.[134] Liposomes can be described as molecules that self-assemble into hollow spherical structures into which a wide variety of cargo molecules can be packaged.[135,134] Liposomes bring tremendous promise towards achieving targeted drug-delivery.

Various lipids can be utilized to form liposomes and these lipids affect the overall size and charge of the liposome.[134,136] In addition, there are a variety of different ways to manufacture liposomes, and this process ultimately affects these same properties of the liposomes. The flexibility in making liposomes presents an ideal way to selectively target certain types of diseases such as cancer.[134,136]

2. Liposomes

Liposomes are composed of naturally occurring or synthetically produced phospholipids such as phosphatidyl choline (PC), phosphatidyl ethanolamine (PE), phosphatidyl serine (PS), phosphatidyl inositol (PI), and phosphatidyl glycerol (PG).[135] Phospholipids themselves have rotational freedom, which can lead to leaky liposomes, and the addition of cholesterol helps stabilize this bilayer. The hydroxyl group of cholesterol is positioned towards the aqueous surface and the aliphatic chain is aligned in parallel to the hydrocarbon chains of the bilayer.[134,135] The high solubility of cholesterol within the phospholipid bilayer is attributed to its aliphatic chemical structure. Cholesterol is usually added to the liposome formulation in high concentrations; however, large amounts of cholesterol have been attributed to larger liposome vesicles.[134,135] This is important to consider if a certain size liposome is necessary for targeted drug delivery. Polyethylene glycol (PEG) is the standard polymer that is attached to the drug molecule or added to the liposome formulation to aid with safety and efficacy.[134,135] By covalently linking PEG to liposomes, the active drug is protected from the immune system and therefore increases its blood circulatory time. PEG has also been shown to aid in binding efficiency and general targeted transport in vitro and in vivo.[137]

2.1 Liposome Formation

There are four conventional ways to prepare liposomes: thin-film hydration method, reverse-phase evaporation technique, ethanol-injection method, and detergent dialysis.[132,134] The thin-film hydration method involves dissolving lipids in organic solvent and then evaporating off the solvent resulting in a thin-film. To ensure that solvents are removed completely, the film is put on high vacuum overnight.[132,134] Rehydration with aqueous solvent forms the liposomes: vigorous shaking yields multilamellar vesicles (MLVs) and gentle shaking yields giant unilamellar vesicles. Small unilamellar vesicles can be formed with various size reduction techniques. The reverse-phase evaporation technique involves dissolving lipid in organic solvent and then evaporating off the solvent to create a thin film.[132,134] The film is redissolved in solvent and aqueous buffer is added to create a two-phase system. Slow evaporation of the organic solvent leads to liposome formation. The ethanol-injection method involves dissolving phospholipids in organic solvent (ethanol) and adding to aqueous solvent. Upon addition of the ethanol solution, liposomes are formed.[132,134] The detergent dialysis method uses phospholipids dissolved in detergents to create micelles, which are added to an aqueous phase. Removal of the detergent via dialysis or size-exclusion gel chromatography results in large unilamellar vesicles.[132,134]

All four of these liposome formation methods typically result in larger-sized liposomes.[134] However, small unilamellar vesicles can be formed with various size reduction techniques. As liposome size and size distribution are the most important liposome characteristics, it is often necessary to utilize additional size reduction techniques after the initial liposome formation.[134,132] Size reduction can be achieved via

sonication or extrusion. Probe sonication uses a titanium probe inserted into the liposome preparation. This generates smaller liposomes efficiently and can be used to prepare a desired liposome size.[134] Water sonication can also be used if there is concern of metal contamination or high temperature affecting liposomes/lipid components. Alternatively, the size extrusion method uses a pressurized instrument to force liposomes through a polycarbonate membrane. The number of extrusion cycles depends on the size of the polycarbonate membrane pores.[134]

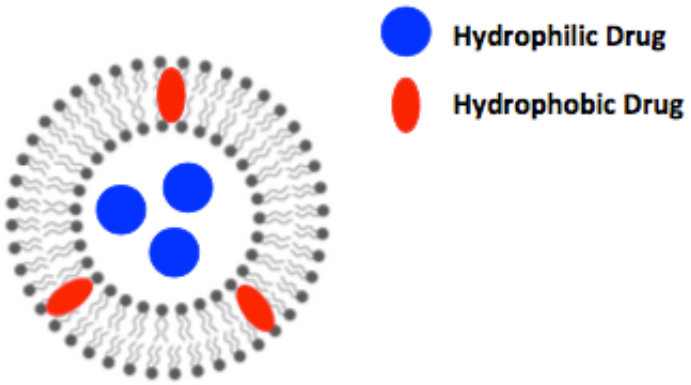

Figure 1. Structure of Liposome

Liposomes are useful drug delivery vehicles as they can carry hydrophilic, lipophilic, and amphiphilic drugs.[134] Hydrophilic drugs reside in the core of the nanoparticle while hydrophobic drugs are incorporated into the lipid bilayer (Figure 1). It is important to understand the physicochemical properties of both the drug and the lipids being used in the formulation. For instance during the thin film hydration method, lipophilic drugs are often highly embedded in the lipid bilayer during the step when liposomes self-assemble.[134] However, hydrophilic drugs often do not get encapsulated as well due to water content being higher outside of the liposome than inside of the liposome. Drug

loading is dependent not only on the physicochemical properties of drug/lipids but it is also dependent on the method of liposome formulation. There are two types of drug loading: passive and active.[134] Passive loading consists of drug loading during the method of preparation without any additional steps. Active loading involves forming the liposome without the drug and adding it into the liposome after. This is done with a series of buffers to actively load a drug into the liposome and keep it within the liposome.[134]

2.2 Liposome Characterization

As previously described, the characteristics of the liposomes depend heavily on the lipid composition and liposome formation method. Liposome characteristics such as size, membrane lamellarity, and charge are crucial for ultimately determining a route of administration (Table 1).[134] Liposome size varies from very small (0.025 μM) to large vesicles (2.5 μM). The liposome size is important for in vivo distribution, biological fate, toxicity, and target specificity.[132] In addition, particle size affects drug release and storage. Smaller particles have a larger surface area-to-volume ratio and result in faster drug release while larger particles encapsulate more drug particles and allow for slower release. In terms of storage, smaller particles have a greater risk of aggregation.[132] It is also important to consider the liposome size dispersion throughout a sample. This is referred to as the polydispersity index (PDI) and samples with uniform size distribution are optimal (PDI = 0.1).[132] Liposomes can be classified by different bilayers, also known as membrane lamellarity, (Table 1) and this affects a wide-range of properties such as drug entrapment capacity, the addition of surface bound ligands, drug release from the system, storage characteristics, and liposome cell interaction and internalization.[134]

Unilamellar liposomes consist of one lipid bilayer while multilamellar liposomes consist of multiple concentric lipid bilayers, similar to an onion.[138] Liposomes can be either negatively or positively charged depending on their composition. The addition of oleic acid generates negatively charged liposomes while the addition of N-[1(2,3-dioleoyloxy)propyl]-N,N,N-trimethylammonium chloride (DOTAP) results in the generation of positively charged liposomes.[134] When liposomes are charged, they exhibit electrostatic repulsion, which is favorable for storage conditions as the liposomes are unable to aggregate. In addition, cell membranes are negatively charged and there is an electrostatic interaction with positively charged (cationic) liposomes. This ultimately increases cell permeability and internalization.[134]

Table 1. Classification of Liposomes[134]

Vesicle	Size (nm)	Composition
Small unilamellar (SUV)	20-100	Conventional liposomes
Large unilamellar (LUV)	> 100	Long-circulating liposomes
Giant unilamellar (GUV)	> 1000	Cationic liposomes
Oligolamellar (OLV)	100-1000	Stimuli-sensitive liposomes
Multilamellar (MLV)	> 500	Immunoliposomes

Liposome size can be determined by a variety of different methods, which include dynamic light scattering (DLS), size exclusion chromatography (SEC), nuclear magnetic resonance (NMR), and microscope technologies including transmission electron microscopy (TEM), cryogenic-TEM, and atomic force microscopy.[134] Dynamic light scattering is the easiest and most popular technique. DLS analyzes Brownian motion of colliding particles resulting from scattering of the incident light; light scattering depends on the refractive index between suspended particles and solvent.[134] Size exclusion chromatography with the use of HPLC provides high-resolution results while

only using a small amount of sample.[134] This can be used alone or in combination with DLS. While this method is efficient in determining and separating size, it also may lead to issues as a result of the liposome chemistry and columns. Microscopy is used to visualize and measure the size of liposomes. The downside to this method is that liposomes must be removed from their native environment and the lipid chemistry may be disturbed.[134]

In addition to affecting cell permeability, liposome charge is also important for stability. The charge of a liposome sample can be calculated via the zeta-potential.[134] The zeta-potential is measured by adding liposomes to a sample cell, which is then illuminated with light. The scattered light measures the zeta potential as the liposomes move due to their electric fields.[134] The number of bilayers in a liposome will influence in vivo fate and applications. There are various chemical based techniques that use labeled reagents or radiolabeled ions that aid in estimating the number of layers or the amounts of lipids on the surface. Other techniques used include cryo-TEM analysis, NMR and small-angle x-ray scattering (SAXS).[134]

2.3 Liposome-Cell Interactions

There are four different in vitro mechanisms of liposome-cell interaction: exchange of lipids or proteins with cell membranes, adsorption or binding of liposomes to cells, internalization of liposomes by endocytosis or phagocytosis, and fusion of bound bilayer with the cell membrane (Figure 2).[139] All four of these interactions are dependent on lipid composition, type of cell, and presence of specific receptors/targeting vectors. Stable absorption consists of the association of intact liposomes with the cell surface, without internalization.[139] This adsorption may be mediated by nonspecific forces

(hydrophobic, electrostatic) or by specific components (surface receptors, antibodies). Endocytosis is the uptake of intact liposomes into endocytotic vesicles.[139] Endocytosis leads to delivery to the lysosome; however, in some cases content may be released into the cytoplasm. Fusion is the merging of the lipid bilayer with the plasma membrane and simultaneous release of liposome contents into the cytoplasm.[139] It is possible that liposome contents release into the medium during this process. Lipid transfer includes the transfer of lipid molecules between liposomes and cells without cell association of aqueous liposome contents.[139]

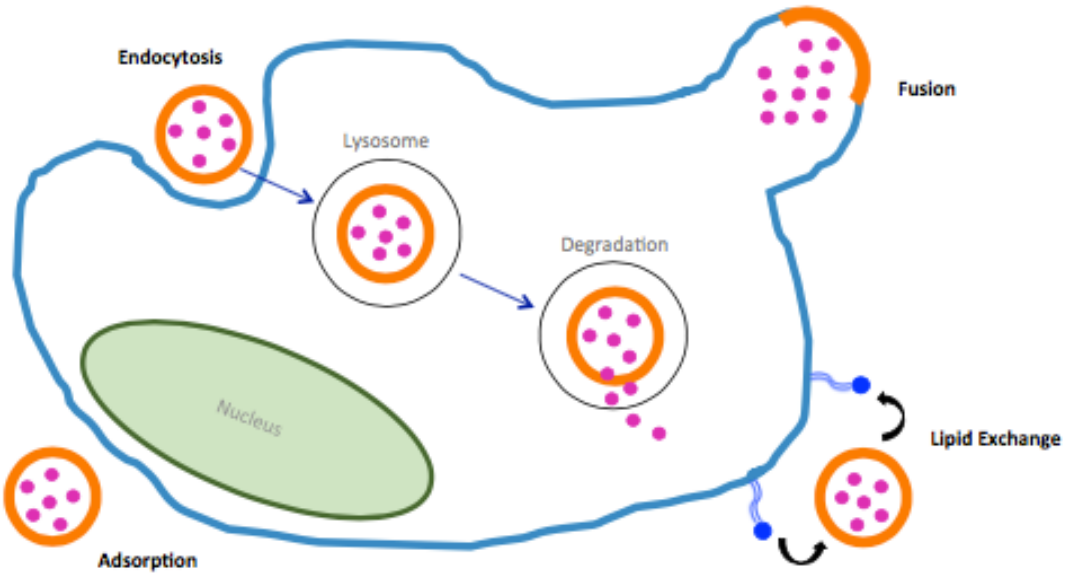

Figure 2. Schematic Liposome-Cell Interactions[139]

3. Coaxial Continuous Liposome Formation

As previously described, there are a variety of methods to form liposomes. After this initial formation, liposomes must often undergo size reduction to attain the optimal size liposome and to improve the uniformity of the particle size distribution. This complete process may take hours or days to obtain the desired size liposome.[132,134]

These methods of formation are not optimal or convenient for large-scale liposome processing. It is necessary to have direct control over the size and distribution of liposomes as the size ultimately affects cellular uptake and biodistribution.[140] As a result, recent advances in technology have been utilized to create novel methods to mass-produce liposomes of a particular size in an efficient and sterile manner.

The most well-known liposomal formulation is the ethanol-injection method. This method offers a plethora of advantages including using less toxic solvents, control over particle size/distribution, avoiding size reduction measures, and most importantly, that it is a naturally continuous process.[140] Continuous processing offers benefits in comparison to batch processing and is thus important to consider in the pharmaceutical industry. Continuous processing is faster, more efficient, and may also be safer than batch processing. In addition, continuous processing has the potential to be automated and this reduces human involvement and error.[140] Both of these factors are important to consider when scaling up a pharmaceutical process.

With this in mind, Dr. Diane Burgess and her lab at the University of Connecticut set out to determine a continuous processing method for the production of monodispersed liposomes.[140] This production method depends heavily on fluid mechanics and physics. There have been a few reports of utilizing the ethanol-injection method for the production of unilamellar liposomes and these processes involve the use of two different fluid mixing techniques: laminar and turbulent.[140] In terms of the ethanol-injection method, laminar flow consists of smooth, steady fluid motion and relies heavily on fluid viscosity and turbulent flow consists of chaotic fluid motion and relies less on the viscosity of the fluid.[141] Reynolds number (R_e) is an important factor in fluid flow and

is described as the ratio of inertial to viscous forces. Reynolds number takes into account the fluid's resistance to change of motion and the amount of friction due to viscosity of fluid.[142] Laminar conditions consist of water slowly mixing with the alcohol phase (low Reynolds number). Turbulent conditions consist of rapid mixing of the alcohol stream with the aqueous stream (high Reynolds number).[142] Taking this into consideration, the liposome formation process was explored by relating these fluid dynamic properties with liposomal physical properties.

The Burgess lab successfully identified a novel continuous processing method for the formation of liposomes that utilizes a coaxial turbulent jet in co-flow. The turbulent jet co-flow apparatus begins with preparation containers that house lipid and aqueous solutions separately (Figure 3).[140] A solution containing lipids and a water-miscible organic solvent is prepared by heating the solution to 50-60°C and sonication. Once the components are dissolved, the lipid solution can be taken up by stainless steel tanks, which are pressurized and can be heated to help maintain lipid solubility.[140] These three tanks converge at a single point and static mixers are used to make sure the lipid solutions from three different tanks are mixed appropriately before introducing the aqueous phase. The aqueous phase enters the apparatus straight from its preparation container. The lipid solution is injected into the aqueous phase at different flow rates (5-40 mL/min or 60-400 mL/min, respectively).[140] It is important to note that a hydrophilic drug would be incorporated into the aqueous solution and a hydrophobic drug would be incorporated into the lipid solution. This apparatus is controlled by a computer program, which was custom designed by the Burgess lab. The entire system is automated and exceptionally user friendly.[140] The user only needs to define the final

lipid concentration and the molar ratios of the lipid formulation. This apparatus is also attached to a Zetasizer® which records the size and polydispersity index (PDI) of a liposome population. This allows the lipid and aqueous phase flow rates to be adjusted in real-time to obtain the optimal size liposomes.[140]

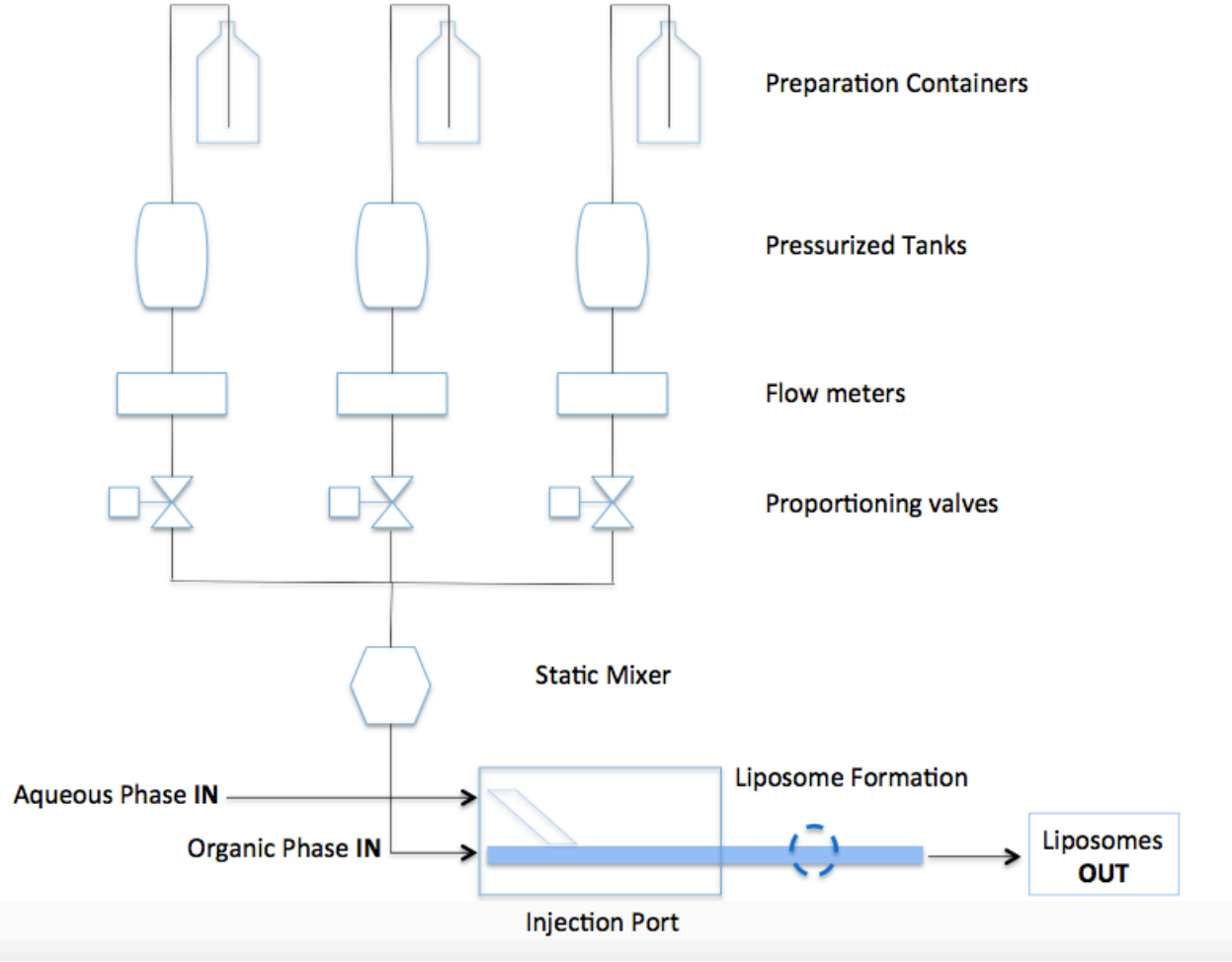

Figure 3. Coaxial Turbulent Jet in Co-Flow Schematic[140]

4. FDA-Approved and Clinical Stage Liposome Formulations

To date, liposomal drug formulations are becoming increasingly popular within the clinic. Liposomes are the first nanoparticles that have been successfully translated into clinically utilized applications. Liposomes have been FDA-approved for a wide

variety of indications including cancer, fungal infections, viral infections, and pain management (Table 2).[143]

Table 2. Clinically Approved Liposomes[143]

Clinical Products (Approval Year)	Administration	Active Agent	Indication
Doxil® (1995)	i.v.	Doxorubicin	Cancer
DaunoXome® (1996)	i.v.	Daunorubicin	Cancer
Depocyt® (1999)	Spinal	Cytarabine/Ara-C	Cancer
Myocet® (2000)	i.v.	Doxorubicin	Cancer
Mepact® (2004)	i.v.	Mifamurtide	Cancer
Marqibo® (2012)	i.v.	Vincristine	Cancer
Onivyde® (2015	i.v.	Irinotecan	Fungal
Abelcet® (1995)	i.v.	Amphotericin B	Fungal
Ambisome® (1997)	i.v.	Amphotericin B	Fungal
Amphotec® (1996)	i.v.	Amphotericin B	Fungal
Visudyne® (2000)	i.v.	Verteporphin	Fungal
DepoDur® (2004)	Epidural	Morphine sulfate	Pain
Exparel® (2011)	i.v.	Bupivacaine	Pain
Epaxal® (1993)	i.m.	Inactivated hepatitis A virus (strain RGSB)	Hepatitis A
Inflexal®V (1997)	i.m.	Inactivated hemaglutinine of Influenza virus strains A/B	Influenza

i.v. (Intravenous); i.m. (Intramuscular)

The first liposome formulation approved in the U.S. in 1995 was Doxil®, which delivered doxorubicin and was approved for the treatment of patients with ovarian cancer and AIDS-related Kaposi's sarcoma.[143] A year later DaunoXome® was approved for the delivery of daunorubicin for the management of advanced HIV-associated Kaposi's sarcoma. Depocyt® was approved in 1999 for the delivery of Cytarabine/Ara-C for the treatment of neoplastic meningitis. In 2000, Myocet® was another approved doxorubicin formulation for combinatory chemotherapeutic treatment alongside cyclophosphamide in metastatic breast cancer.[143] Liposome formulation

containing mifamurtide, Mepact®, was approved in 2004 for the treatment of high-grade resectable non-metastatic osteosarcoma. In 2012, Marqibo® (vincristine) was approved for acute lymphoblastic leukemia.[143] In 2015, Onivyde™, which contains Irinotecan, was approved for the treatment of metastatic pancreas adenocarcinoma in combination with fluorouracil and leocovorin. While the majority of research in terms of liposomes and drug discovery is aimed at cancer, a few liposome formulations are approved for other indications (Figure 4).[143]

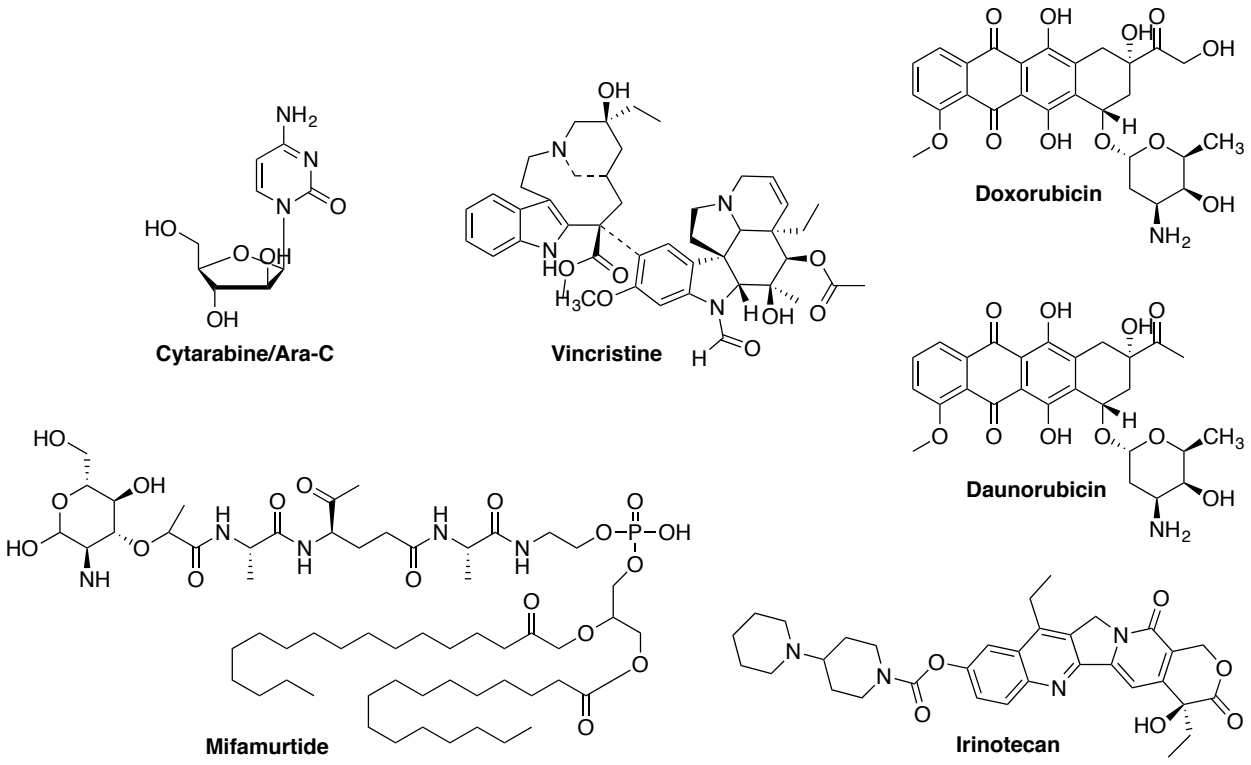

Figure 4. Structures of Liposome-Encapsulated Chemotherapeutic Drugs

During 1995-1997, the FDA approved three different formulations (Abelcet®, Ambisome®, and Amphotec®) containing amphotericin B for various fungal infections.[143] These three liposome formulations treat invasive and life-threating fungal infections, especially if patients have renal impairment or experience unexpected

toxicity to typical amphotericin B treatment. Visudyne® was the first light-activated drug available for eradicating abnormal blood vessels that result from age-related macular degeneration.[143] This liposome contains verteporfin, which absorbs light at 692nm. DepoDur®, a liposome formulation of morphine, is intended for administration before surgery or following clamping of the umbilical cord during caesarean section. Exparel® is an approved formulation containing bupivacaine, designed for extended release of drug up to 72h.[143] In 1993, the first approved liposome vaccine (virosome) was FDA-approved for hepatitis A and this formulation causes fewer adverse local side effects. Inflexal® V is a virosomal influenza vaccine that shows superior immunogenicity above other influenza vaccines and this was FDA-approved in 1997 (Figure 5).[143]

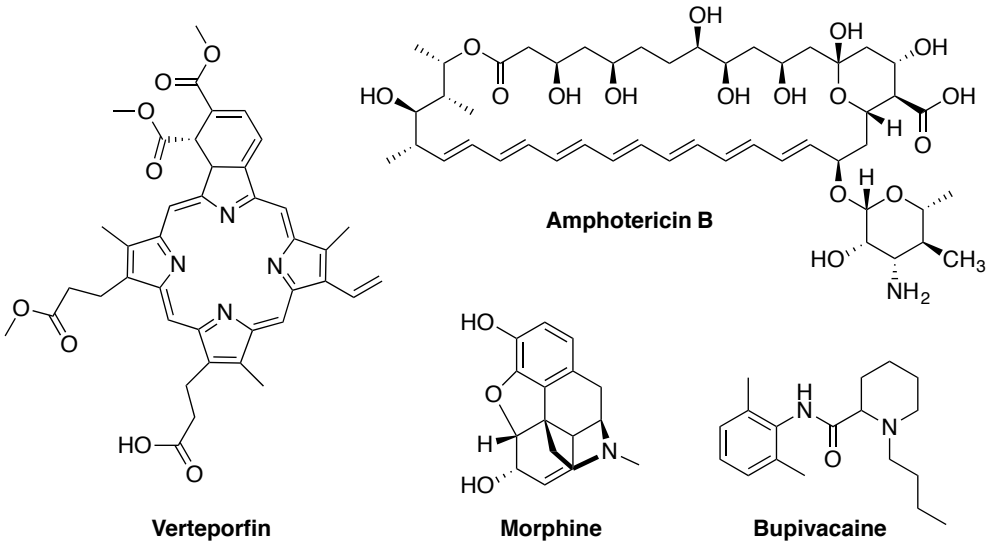

Figure 5. Structures of Liposome-Encapsulated Therapeutic Agents

Due to their success in the clinic to date, there has been extensive research in regards to liposomes and drug discovery. This has led to a multitude of formulations that are currently being studied in clinical trials for the treatment of various diseases (Figure 6).[143] Current liposomes in Phase III clinical trials include Stimuvax®, a vaccine

that has shown positive results in cancer patients. Thermodox is a temperature sensitive liposome formulation that does not release drug until 42°C. Most of the liposome formulations in Phase III clinical trials are tumor or site specific for more targeted therapy. Current treatments in Phase II clinical trials include liposomes that contain both novel and established chemotherapeutic agents.[143] This includes two Paclitaxel liposome formulations that decrease side effects; Endotag-1 contains Paclitaxel and also consists of a cationic lipid formulation that can interact with the negatively charged endothelial cells required for tumor angiogenesis. OSO-211 contains a novel topoisomerase I inhibitor, lurtotecan, which will be a competitor to topotecan. Phase I clinical trials include both liposomal formulations composed of siRNA and sphingosomal encapsulations (INX-0125 and INX-0076).[143] Phospholipids are compounds of fatty acids, a nitrogenous base, phosphoric acid, and either glycerol, inositol, or sphingosine. Sphingosomal liposome formulations consist of sphingosine, which is an amino alcohol that contains a long unsaturated hydrocarbon chain.[144] While sphingosomal encapsulation is a novel form of targeted drug delivery, utilizing sphingoloids has demonstrated increased cell permeability and increased tumor targeting specificity.[143]

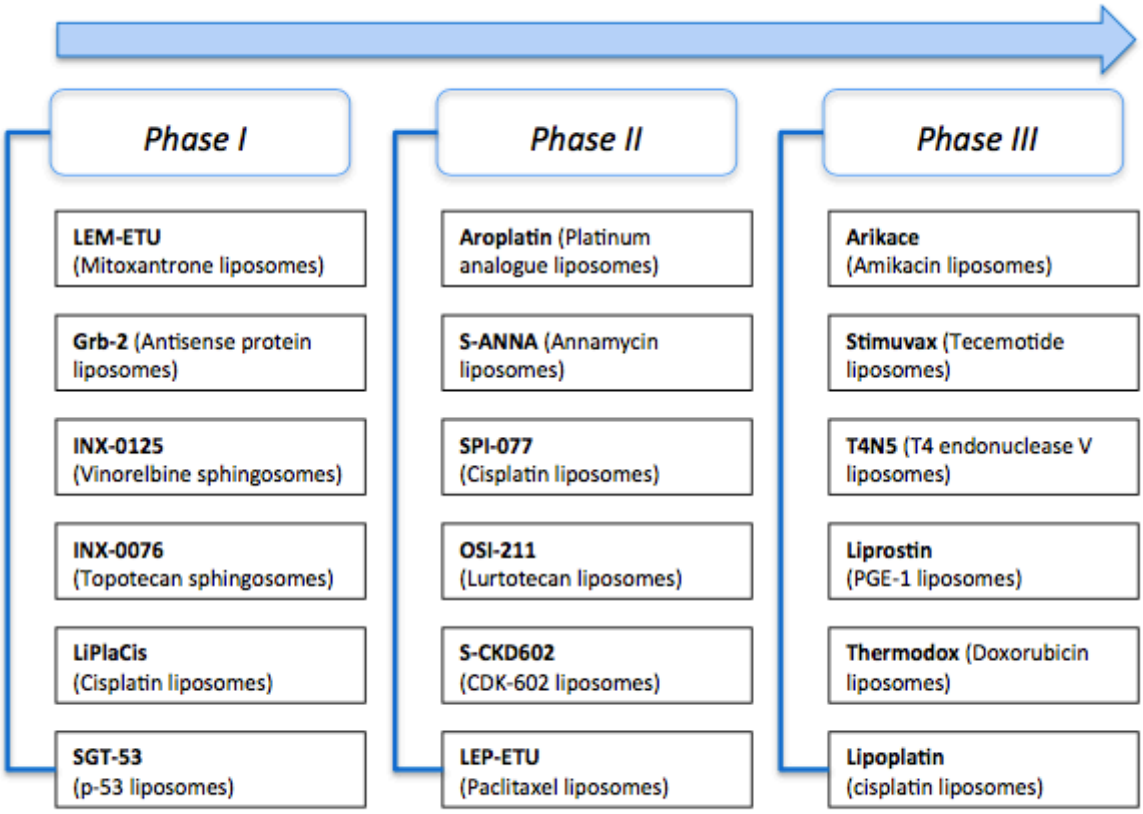

Figure 6. Liposomes in Clinical-Development[143]

5. Liposome-Based Strategies for Effective Drug Delivery

5.1 Brain Cancer

Currently, there are an estimated 700,000 Americans living with a brain tumor. There are more than 140 types of malignant brain tumors and most of these tumors also have their own subtypes.[145] Despite the amount of brain tumors and their devastating prognosis, there are only 4 FDA-approved drugs and one device being used to treat brain tumors. In children, brain tumors are the leading cause of cancer-related death (Figure 7).[146] It is important to highlight that there has never been a drug developed and approved specifically for malignant pediatric brain tumors despite the relatively high diagnosis rate. Brain tumors are still a difficult health challenge due to their fast

development and poor prognosis despite the application of aggressive surgery, radiation, and chemotherapy treatments.[145]

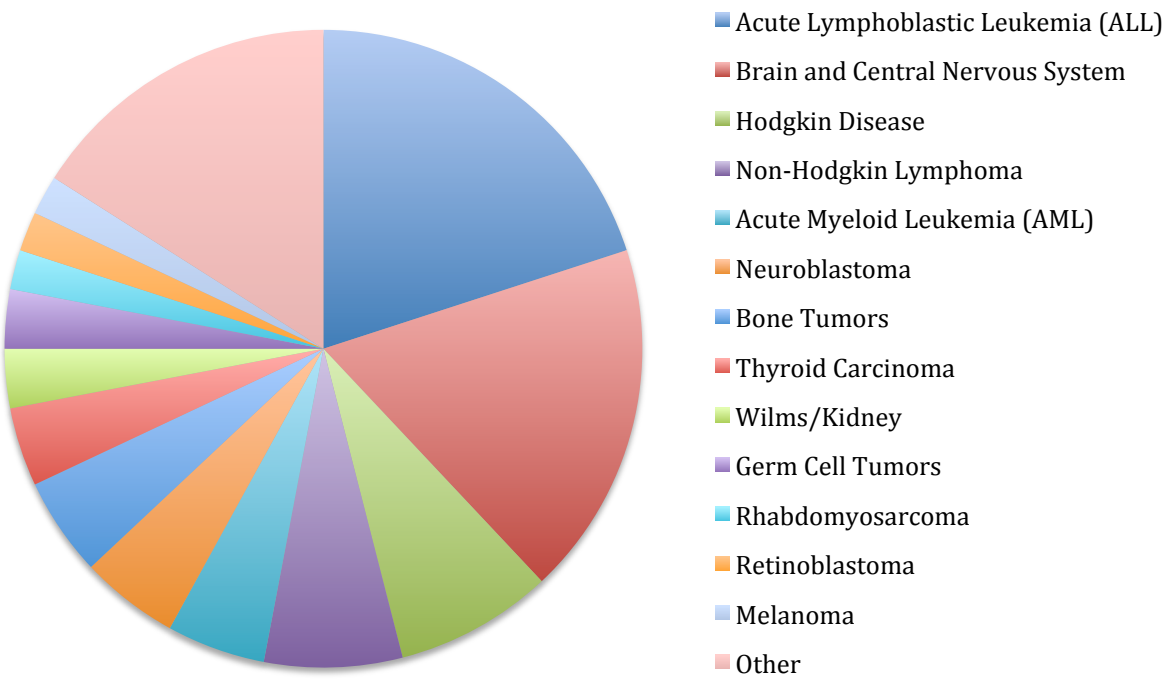

Figure 7. Pediatric Cancer Diagnosis[146]

Malignant brain tumors are difficult to treat with chemical and pharmaceutical compounds due to the presence of the blood brain barrier. The blood-brain barrier (BBB) is an intricate network of vascular endothelial cells, cerebral endothelial cells, glial cells, pericytes, and neurons.[147] The BBB endothelium is uniquely characterized by the presence of tight junctions, which consist of transmembrane proteins including claudin (3,5, and 12), occludin (1,2, and 3), and junctional-adhesion molecules (JAM-A, -B, and –C).[148] The BBB has dual functions as it restricts the transport of potentially toxic and harmful substances from the blood to the brain and it also allows for the selective transport of nutrients to the brain and removal of metabolites from the cerebral spinal fluid that surrounds CNS tissue.[147] The BBB contains efflux transporters that

significantly limit delivery of numerous therapeutics that could otherwise diffuse across the plasma membrane. Two such efflux transporters are P-glycoprotein (P-gp) and breast cancer resistance protein (BCRP) which are classified as ATP-binding cassette (ABC) transporters.[149,150] ABC transporters are ATP-dependent pumps that are ubiquitous membrane bound proteins that can move substances into (influx) and out (efflux) of the cell. These transporters are predominantly found in the liver, BBB, kidney, and placenta.[151] Thus, the BBB remains a constant challenge in the world of drug discovery and development.

Liposomes offer an alternative mode of delivery of drugs to the brain. Often times, drugs that could be advantageous chemotherapeutic agents are not considered due to their physicochemical properties. A nanoparticle vehicle such as a liposome holds promise as a large percentage of small molecules and antibodies are not able to penetrate the BBB. In addition to modifying liposome properties via different lipids and different formation methods, liposomes can also be tagged with proteins that can aid in BBB penetration.[152] For instance, liposomes can be formulated to contain a target ligand that can aid in penetrating the BBB and reaching the brain; these proteins include but are not limited to transferrin receptor (TfR), lipoprotein receptor-related protein (LRP), and nicotinic acetylcholine receptor (nAChRs). Transferrin receptors are widely expressed in endothelial cells of the BBB. While nanotechnology has proved successful with transferrin ligand, it is not optimal to have this drug delivery system competing with natural ligand.[152] A mouse monoclonal antibody (MAb) against rat TfR, OX26, has successfully been used to target liposomes across the BBB and coined "immunoliposome-based drug delivery." LRP has been reported to mediate transport of

various lipid-conjugated nanoparticles across the BBB. The LRP ligand Aprotinin and more specifically, Angioprep, have effectively increased liposome treatment to the brain and have increased survival time of brain tumor-bearing mice.[152] Nicotinic acetylcholine receptors (nAChRs) are ligand-ion channels that are expressed in the brain and brain capillary endothelial cells. Various peptides derived from viruses and toxins have been tagged to nanoparticles and enabled successful brain-targeted drug delivery.[152] In addition to being advantageous for brain cancers, liposomes serve as a promising route of drug delivery for pediatric cancers.

5.2 Pediatric Cancer

In the mid-1970s, the 5-year survival rate for pediatric cancer was 58%. While this number has improved to 80%, this survival rate has remained steady for the past few decades.[153,154] In addition, chemotherapy has become more aggressive and long-term toxicities are becoming more frequent in children that survive through adulthood. Current chemotherapy involves administration of drug with the hope that enough of the active agent permeates tumor cells and does not prove cytotoxic to the rest of the body. Nanotechnology presents an alternative drug delivery system for the treatment of pediatric malignancies.[154] Specifically, liposomes serve as flexible drug delivery vehicles that have the potential to improve targeted delivery while minimizing effective drug dose.[154] In addition to improving drug specificity and minimizing short and long-term side effects, more efficacious drugs could be utilized despite their undesired physicochemical properties. Macromolecules, such as siRNA, hold promise as specific chemotherapeutic agents in pediatric bone and soft tissue sarcomas such as Ewing sarcoma, rhabdomyosarcoma, and synovial sarcoma.[154] These promising

macromolecules could be formulated into liposomes and provide a more promising form of treatment for these children. There are a few liposomal drug formulations in clinical trials to date reiterating the promise of this drug delivery system for the treatment of pediatric malignancies (Table 3).[11]

Table 3. Liposomal Drug Formulations in Clinical Trials for Pediatric Indications

Formulation	Active Agent	Pediatric Indication	Phase
ThermoDox	Doxorubicin	Solid tumors, Ewing sarcoma, soft tissue sarcoma, osteosarcoma, neuroblastoma, Wilms' tumors, hepatic tumors, and germ cell tumors	I
LipoDox	Doxorubicin	Liver cancer and soft tissue sarcoma	I
VSLI	Vincristine	Soft tissue sarcoma, lymphoma, leukemia, Wilms' tumors, and osteosarcoma	II
MM-398	Irinotecan	Recurrent or refractory solid tumors, Ewing sarcoma, rhabdomyosarcoma, neuroblastoma, and osteosarcoma	I

6. Itraconazole Liposome Formulations: Fungal Infections

There have been numerous efforts to aid in improving the physicochemical properties of itraconazole (ITZ). These efforts include utilizing nanotechnology such as nano-amorphous powders and nanocrystalline suspensions.[155,156] Both of these drug formulations have improved the bioavailability of this poorly soluble drug. Due to the success of amphotericin B liposomes for the treatment of fungal infections, there have been attempts at formulating azole antifungals into liposomes. ITZ, specifically, offers treatment to a wide range of fungal infections. However, orally available compounds are not necessarily ideal for immunocomprised patients.[157] There have been significant efforts to formulate ITZ into liposomes to improve solubility and aid in producing an intravenous ITZ formulation (Table 4).[157,158,159] These liposome formulations improved bioavailability, maintained fungal activity, and in one instance resulted in BBB

penetration. Formulating ITZ into liposomes proves promising for the ultimate treatment of MB. However, there are currently no FDA-approved or clinical stage ITZ liposome formulations.[11]

Table 4. Experimental ITZ Liposome Formulations

	Lipids	Solvent	Aqueous Phase	Ref
1	Soy phosphatidyl choline, cholesterol, stearylamine	$CHCl_3$	Phosphate buffer (pH = 7.4)	[160]
2	Lecithin, cholesterol,	$CHCl_3$	Phosphate buffer (pH = 5.8)	[157]
3	Lecithin, cholesterol, cyclodextrin	$CHCl_3$: MeOH	N/A	[161]
4	Soy lecithin, cholesterol, carboxymethyl chitosan	$CHCl_3$	Phosphate buffer (pH = 7.4)	[158]
5	DPPC, cortisone acetate, polyethylene glycol (PEG200)	$CHCl_3$	Phosphate buffer (pH = 7.4)	[159]
6	DPPC	$CHCl_3$	10 mM PBS (pH = 7.4)	[162]
7	Egg PC, MPEG-2000 DSPE, cholesterol	$CHCl_3$	6.67 mM KH_2PO_4 (pH = 6)	[163]

Dipalmitoylphosphotidylcholine (DPPC), potassium dihydrogen phosphate (KH_2PO_4), 1,2-distearoyl-phosphitdylehtanolamine-methyl-polyethylene glycol-2000 (DSPE)

7. Itraconazole Liposome Formulation: Medulloblastoma

There is tremendous promise in utilizing liposomes to attain more targeted treatment regimens for both pediatric and brain cancers. If ITZ or *des*-triazole ITZ analogues are going to be used for the treatment of MB, they must be able to penetrate the BBB and reach the brain. Due to their large size, it is anticipated that ITZ and our *des*-triazole ITZ analogues will have trouble crossing the BBB and liposomes serve as a viable option for achieving this targeted drug delivery. Modifying the characteristics of liposomes, such as size and composition, can aid in the nanoparticles' ability to cross the BBB. Liposomes containing ITZ or *des*-triazole ITZ analogues would be advantageous for the targeted treatment of pediatric SHH subtype MB.

7.1 ITZ Liposome Formulation

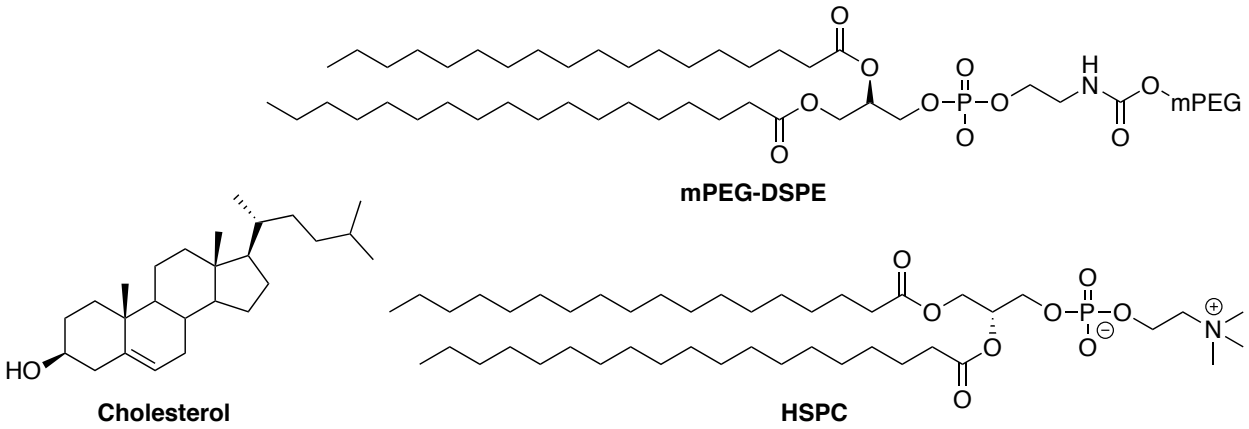

Figure 8. Structures of Lipid Components

Our liposome formulation was based on previous ITZ formulations with a few modifications. The lipids used were hydrogenated soy phosphatidyl choline (HSPC), 1,2-distearoyl-phosphitdylethanolamine-methyl-polyethylene glycol-2000 (mPEG-2000 DSPE), and cholesterol (Figure 5).[163] This liposome formulation consists of PEG, cholesterol, and synthetic lipid (HSPC) while other ITZ liposome formulations contain natural ligand and either PEG or cholesterol. Synthetic lipid is present in all FDA-approved parenteral liposome formulations while natural lipid is utilized in FDA-approved liposome formulations with a variety of administration routes.[164,165] In addition, these liposomes are being formed with the novel coaxial jet in co-flow apparatus established by the Burgess Lab. As the liposomes were being manufactured with the turbulent coaxial jet in co-flow, lipids and ITZ could not be dissolved in a water-immiscible solvent such as chloroform ($CHCl_3$). Because of this, the solubility of ITZ was determined in a variety of water-miscible solvents such as ethanol (EtOH), methanol (MeOH), and isopropanol (IPA). ITZ was most soluble in EtOH (0.6 mg/mL) after heating and sonication. The aqueous solvent utilized was 6.67 mM potassium

dihydrogen phosphate (KH_2PO_4) at pH = 6. The flow rates of both the organic phase and the aqueous phase were adjusted until the optimal size liposomes (ITZ liposomes = 67.72 nm – 75.23 nm; empty liposomes = 65.42 – 72.39 nm) and reasonable poly-dispersion index (PDI) values were attained. It was determined that faster flow rates for both the lipid solution (30 mL/min) and aqueous solution (300 mL/min) resulted in smaller particle size and optimal PDI values (Table 5). Sample #6 had a particle size of 66.82 nm and a PDI of 0.086. It is important to note that the optimal size liposome to achieve BBB penetration is less than 100 nm and an optimal PDI for a sample of liposomes is around 0.1.[166,167] To date, ITZ liposomes have not been formed with the coaxial jet in co-flow apparatus, and as a result, this preliminary batch of liposomes was utilized solely for optimization of the formulation within this instrument (Table 5). After this initial optimization, a second batch of liposomes was formulated and analyzed for encapsulation efficiency and in vitro Hh pathway inhibitory activity.

Table 5. ITZ Liposome Batch 1: Flow Rate Optimization

	Lipid Solution (mL/min)	Aqueous Solution (mL/min)	Particle Size (nm)	PDI
#1	10	90	174.8	0.446
#2	10	100	204.3	0.676
#3	10	300	170.1	0.362
#4	30	300	112.4	0.235
#5	30	300	100.6	0.173
#6	30	300	66.82	0.086

7.2 Separation of Free Drug

Inevitably, free drug will remain in the aqueous environment after liposome formulation because not all of the drug will be encapsulated into the liposomes. Free drug must be removed before determining the encapsulation efficiency. With

hydrophilic drugs, this is often done with filtration. Liposomes can be rinsed on a filter with water; however, this will not work for hydrophobic drugs. Liposomes containing hydrophobic drug could be rinsed with organic solvent, but ITZ is soluble only in harsh solvents (dichloromethane and chloroform) that may disrupt the liposome. Therefore, a centrifugation method was utilized to separate free hydrophobic drug from liposomes.[168] This method relies on the size and density of free drug. As ITZ is large, hydrophobic, dense (d = 1.41 g/cm^3), and poorly water-soluble it was anticipated that free ITZ would form a pellet upon centrifugation. Liposomes remain suspended in the aqueous solution and upon decanting, are separated from free drug. Removal of free drug is necessary for further liposome evaluation including calculating the encapsulation efficiency.

7.3 Encapsulation Efficiency

It is necessary to determine the amount of drug encapsulated into the liposomes. Encapsulation efficiency is described as the concentration of the incorporated material, in this instance ITZ, detected in the formulation over the initial concentration used to make the formulation.[169] Lysing the liposomes and measuring drug content via UV or fluorescence detection can determine the drug concentration. When comparing to a standard curve of drug, the concentration can be determined. The absorbance of various concentrations of ITZ was measured using a UV-vis-spectrophotometer at 254 nm. Plotting absorbance versus concentration created a standard curve of ITZ (Appendix A). After removal of free drug via centrifugation, the liposomes were lysed to release ITZ. ITZ liposomes were lysed with 5% Triton solution and heated for 2 h at 60°C. Upon heating for shorter time periods (20 min), less ITZ was released from the

liposomes. This may be due to the way ITZ is being encapsulated into the lipid bilayer of the liposome or the way it is interacting with the other lipids. Absorbance of these liposome samples was measured and concentrations of drug released were determined by using the slope equation of the standard curve. Drug concentrations ranged from 115.3 μg/mL – 162.2 μg/mL throughout the liposome samples collected (Table 6). If 100% of ITZ (60 mg) were encapsulated into the collected volume (~350 mL) of liposomes, the concentration would be 171 μg/mL. The encapsulation efficiency of ITZ into this liposome formulation was averaged to be 80.2% across the different samples.[170]

$$Encapsulation\ Efficiency\ = \frac{Total\ drug - free\ drug}{Total\ drug} \times 100\%$$

Table 6. ITZ Liposome Batch #2: Encapsulation Efficiency

	ITZ Concentration (μg/mL)	Encapsulation Efficiency (%)		ITZ Concentration (μg/mL)	Encapsulation Efficiency (%)
#1	162.2	94.8	**#5**	124.7	72.9
#2	146.9	85.9	**#6**	147.9	86.5
#3	115.3	67.4	**#7**	124.6	72.8
#4	138.6	81.1			

7.4 In Vitro Biological Evaluation

After determining the encapsulation efficiency and concentration of ITZ in liposomes, they were used in our cellular assays to determine if ITZ liposomes exhibit biological activity comparable to free drug. Empty liposomes were also utilized during in vitro evaluation as a secondary control. Ideally, ITZ liposomes will exhibit potent Hh

pathway inhibitory activity similar to free ITZ. Both ITZ and empty liposomes utilized within in vitro assays were formulated in a second liposome batch with a previously optimized flow rate of 30 mL/min (lipid solution) and 300 mL/min (aqueous solution); these ITZ liposome encapsulation efficiencies are described in Table 6.

ITZ liposomes, empty liposomes, and free ITZ were evaluated in our gene expression assay utilizing ASZ cells. Before testing liposomes in vitro, a drug concentration of encapsulated ITZ needed to be determined and this was calculated from the same ITZ concentration used to determine the encapsulation efficiency (Appendix A). It is important to note that the same ITZ liposome sample was used throughout all in vitro assays. Liposomes were also frequently checked via UV (254 nm) to confirm that they were not leaking drug contents over time. Initial gene expression assays were run in a time dependent manner. Instead of immediately lysing cells after 48h incubation with treatment, cells were lysed at various time points (24h, 48h, 72h, and 96h) to determine if liposomes exhibited anti-Hh activity in a similar manner to free drug. Evaluation of Hh pathway inhibition at various time points was performed as it is unknown how long it would take ITZ liposomes to enter the cell and release drug. Two subsequent time course experiments were performed, each exploring different concentrations of liposomes and free drug. An initial experiment was performed utilizing 0.195 mM, 0.01 mM, and 0.001 mM concentrations of treatment (Figure 9A). This experiment resulted in ~50% Gli1 mRNA expression when cells were treated with 0.195 mM of liposomes at all time points explored. However, lower concentrations of ITZ liposomes (0.01 and 0.001 mM) as well as empty liposomes exhibited 100% Gli1 mRNA expression indicating that the Hh pathway remained active.

While there was a dose-dependent trend with free ITZ, there was no clear dose-dependent trend in terms of the ITZ liposomes. In fact, this early data suggested that low concentrations of ITZ liposomes and empty liposomes might be upregulating the Hh pathway as some Gli1 mRNA expression values exceeded 100%. Because of this, a second gene expression assay was performed utilizing 0.195 mM, 0.075 mM, and 0.01 mM concentrations of treatment (Figure 9B). This assay resulted in more of a dose-dependent trend within the ITZ liposomes at all the observed time points. Interestingly, empty liposomes at 48h and 72h time points resulted in high Gli1 mRNA values further suggesting that empty liposomes may actually upregulating the Hh pathway. It is important to note that in both assays, treatment with empty liposomes resulted in cell death at 96h.

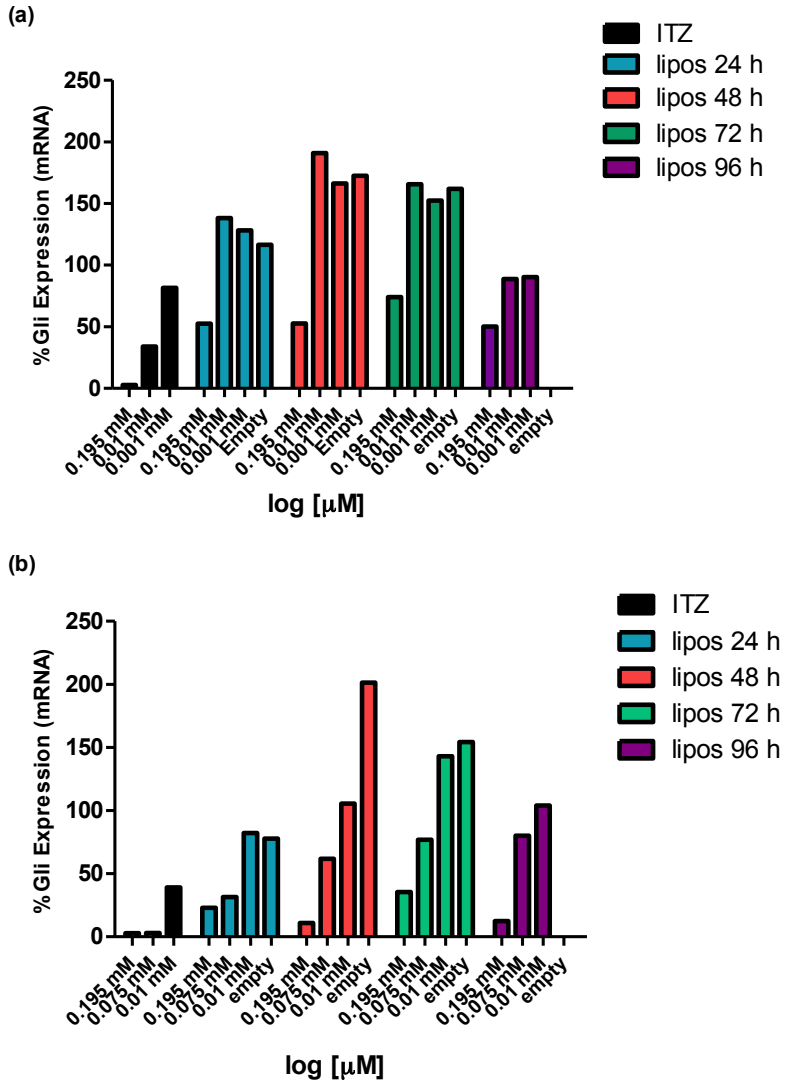

Figure 9. Time Dependent Gli1 mRNA Expression in ASZ Cells
Cells were treated with ITZ liposomes/empty liposomes and incubated for various time periods (24h, 48h, 72h, and 96h). At each time period, cells were lysed and the Gli1 mRNA expression was determined via q-PCR. **(a)** Treatment with 0.195 mM, 0.01 mM, and 0.001 mM of drug/liposome; **(b)** Treatment with 0.195 mM, 0.075 mM, and 0.01 mM of drug/liposome.

Due to these preliminary ASZ results, it was hypothesized that the cholesterol component of the liposome formulation may be upregulating the Hh pathway. Oxysterols, oxidated forms of cholesterol, are known to upregulate the Hh pathway and are a well-characterized method to activate Hh signaling in MEFs. Due to cholesterol

having a similar steroidal structure to oxysterols, we needed to determine if the liposomes themselves were having an effect on the Hh pathway. Empty liposomes, centrifuged and not centrifuged, were treated in our gene expression assay with MEF cells. This cell line does not have aberrant Hh signaling and therefore these cells need to typically be treated with Hh pathway activators (Hh ligand or oxysterols). Cells were only treated with empty liposomes at various volumes and it was determined that they did not activate Hh signaling. Water was set to "100% Gli1 activation" despite the pathway not being activated with Hh ligand or oxysterols. Empty liposomes that were centrifuged and not centrifuged exhibited similar Gli1 expression levels to water, indicating that the liposomes themselves were not activating or deactivating Gli1 mRNA expression in C3H10T1/2 cells (Figure 7).

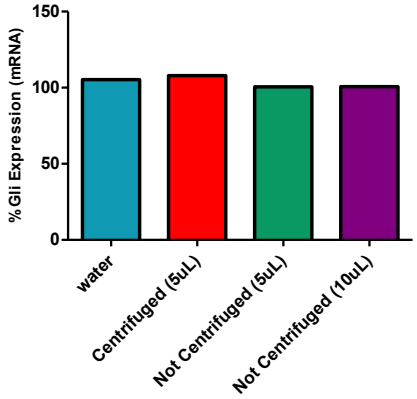

Figure 10. Relative Gli1 mRNA Expression in C3H10T1/2 Cells
Cells were treated with empty liposomes for 24h at different volumes, as a "drug" concentration could not be experimentally determined. Water (no liposomes) was set to 100% and mRNA expressions for empty liposomes were calculated accordingly.

After determining that the liposomes themselves were not upregulating the Hh pathway, ITZ liposomes were tested in a dose dependent manner alongside free ITZ (Figure 8). Two liposome samples were utilized: one that was centrifuged and one that

was not centrifuged. Both liposome samples were tested to confirm removal of free ITZ; however, there should be a difference in activity between liposomes alone and liposomes with free drug. At two different time points (48h and 96h) results indicated that the most potent compound was free ITZ, followed by non-centrifuged liposomes, and then centrifuged liposomes. ITZ potently inhibited the Hh pathway (IC_{50} = 0.11 ± 0.025 μM at 48h) followed by liposome + free drug treatment (IC_{50} = 0.49 ± 0.04 μM at 48h) and liposome treatment alone (IC_{50} = 2.5 ± 0.37 μM at 48h). There is a trend in this data indicating that the liposomes containing free ITZ were more potent than the ITZ liposomes that were subjected to centrifugation (Table 6). This further confirms that free drug was removed with the centrifugation method. It is important to note that at 96h, liposome potency slightly increased (IC_{50} = 1.04 ± 0.17 μM) in comparison to 48h (IC_{50} = 2.5 ± 0.37 μM) indicating that more drug may have been released during this longer incubation period resulting in increased Hh inhibitory activity (Table 6).

(a)

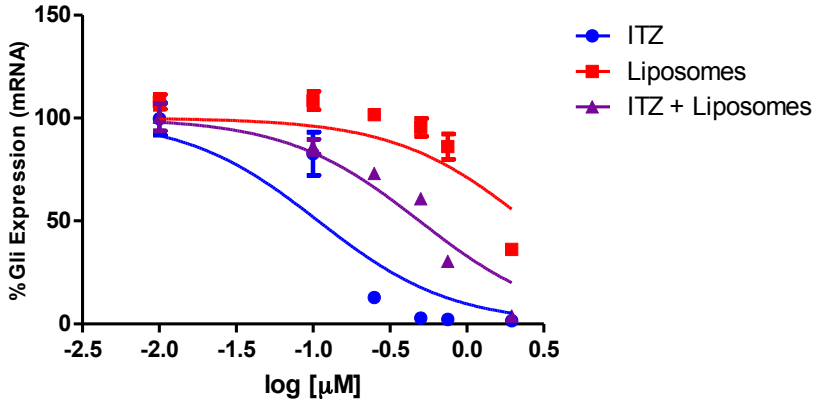

(b)

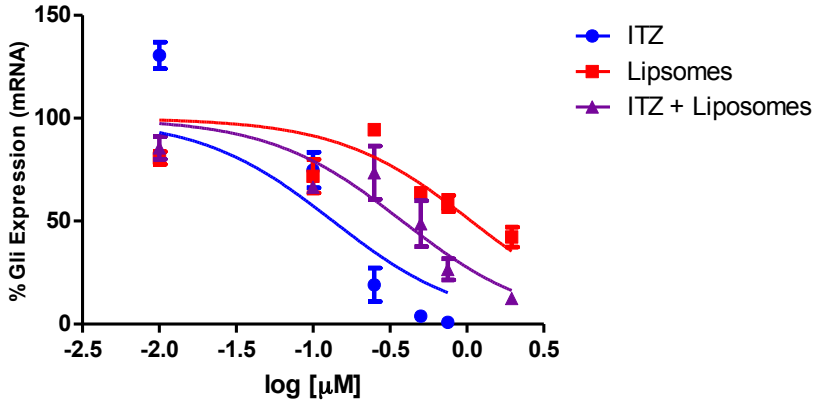

Figure 11. Relative Gli1 mRNA Expression in ASZ Cells
Cells were treated with ITZ liposomes/empty liposomes for 48h and 96h in a dose dependent manner. At each time point, cells were lysed and Gli1 mRNA expression was determined via q-PCR. **(a)** Dose dependent treatment for 48h **(b)** Dose dependent treatment for 96h

Table 7. In Vitro Analysis of Liposomes

Treatment	IC_{50} (μM) 48h [a, b]	IC_{50} (μM) 96h [a, c]
ITZ	0.11 ± 0.025	0.14 ± 0.012
Liposomes	2.5 ± 0.37	1.04 ± 0.17
Liposomes + ITZ	0.49 ± 0.04	0.45 ± 0.26

[a] IC_{50} values represent the Mean ± SEM of at least two separate experiments performed in triplicate. [b] All analogues evaluated following 48 hr incubation. [c] All analogues evaluated following 96 hr incubation.

8. Conclusion

Liposome formulations would be advantageous to brain cancer patients. Specifically, incorporation of ITZ into liposomes may prove beneficial for the treatment of pediatric SHH subtype MB. Itraconazole was successfully formulated into a novel liposome formulation utilizing a coaxial turbulent jet in co-flow. This ITZ liposome formulation was prepared specifically for BBB penetration and optimal liposomal size was obtained (< 100 nm). ITZ liposomes demonstrated moderate Hh pathway inhibitory activity in comparison to free ITZ. While ITZ liposomes would ideally exhibit similar anti-Hh activity as free drug, this proves to be a good starting point for achieving targeted drug delivery of ITZ utilizing nanotechnology. To date, it is unknown how ITZ liposomes are releasing their drug in vitro. Both drug release and cell permeability issues may explain the difference in anti-Hh activity between ITZ liposomes and free ITZ. Further exploration towards ITZ liposome behavior in vitro will determine how this formulation can be optimized to improve overall biological activity.

Thank you to Dr. Diane Burgess and Rajan Jog for their help and guidance with the formulation and preparation of ITZ liposomes.

8.1 Experimental Protocols

Preparation of liposomes: Liposomes were formulated utilizing the coaxial turbulent jet in co-flow instrument developed by Dr. Diane Burgess and her lab. HSPC (900 mg), DSPC mPEG-2000 (300 mg), cholesterol (300 mg), and ITZ (60 mg) were dissolved in EtOH (100 mL) with the help of slight heating (50°C) and sonication. In parallel, four liters of a 6.6 mM KH_2PO_4 solution were prepared and adjusted to pH 6. Lipid solution was added to stainless steel tank within the coaxial turbulent jet apparatus and this solution were incubated at 50°C to ensure lipids and drug remains in solution. The aqueous solution was attached to the apparatus within its preparation container. The lipid concentration and lipid formulation were added into the computer program and the flow rates were set. Liposome size and PDI were measured with Malvern Zetasizer Nano S and liposomes were collected in 50 mL Eppendorf centrifuge tubes. Liposome samples were stored at 4°C.

Free drug separation: Free ITZ was separated from liposomes by centrifugation. Liposomes were centrifuged in a Beckman J2-HC centrifuge at 13,000 rpm for 90 minutes in a 4°C environment. Liposomes were decanted leaving behind a pellet containing free drug.

Determination of encapsulation efficiency: After removal of free drug, the percentage of drug encapsulated into liposomes was determined by monitoring UV absorbance with a plate reader (BioTek Synergy H1 Hybrid Reader). Liposomes were lysed with 5% triton and heat (60°C) for 2 hours. The concentration of ITZ was determined by measuring UV at 254 nm in triplicate and comparing to a standard curve of ITZ.

Gene expression assay protocol (ASZ-001): Cells are seeded (10,000 cells per well; 100 µL total volume per well) in a 96-well tissue culture plate. After 24h of incubation (37°C, 5% CO_2), growth media was removed and replaced with low FBS media. Cells were incubated for an additional 24 h. After this time, DMSO (vehicle control) and liposomes (Aqueous Solution) were added to the wells. Cells were incubated (37°C, 5% CO_2) for 48h and RNA was isolated and evaluated by qRT-PCR.

RT-PCR protocol: Following treatment and incubation periods, both RNA extraction and cDNA synthesis were performed using a TaqMan Cells-to-CT (fast) kit. cDNA synthesis utilized a BioRad MyCycler and was programmed according to the manufacturer's instructions. Quantitative RT-PCR was performed on an ABI 7500 system and made use of the following TaqMan Gene Expression Probes: mouse ActB (Mm00607939_s1) and mouse Gli1 (Mm00494654_m1). Relative gene expression levels were computed via ΔΔCT method using GraphPad Prism. Corresponding IC_{50} values were calculated as mean ± SEM for at least three separate experiments performed in triplicate.

CHAPTER V: Future Directions in the Development of ITZ and *des*-ITZ Analogues for the Treatment of SHH Subtype Medulloblastoma

1. Contributions of ITZ Project

High-throughput screening efforts have recently been utilized to repurpose FDA-approved and clinical stage compounds for novel biological indications. This idea of "repurposing" or "repositioning" drugs has become a way to bypass the long and expensive process of drug development.[1] Itraconazole (ITZ), a clinically efficacious antifungal agent, has recently been determined to inhibit both the hedgehog (Hh) pathway and angiogenesis.[9,10] Dysregulation of both the Hh pathway and angiogenesis contribute to various types of tumors and cancers. In particular, Hh pathway antagonists that are clinically approved often lose activity due to conferred resistance as a result of a point mutation in Smo.[49–51] ITZ is able to potently inhibit the Hh pathway in the presence of wild type Smo and mutant Smo, making it a very desirable candidate especially for those patients who have acquired resistance from other Hh pathway antagonists.[9,78] As a result, ITZ is currently in clinical trials for various cancers resulting from these aberrant activities.[11] While ITZ is FDA-approved, it still contains a few properties that are not considered to be "drug-like." For instance, ITZ has a large molecular weight and is poorly soluble. In addition, ITZ contains a triazole moiety, while important for its antifungal activity, is able to coordinate with CYP3A4 leading to drug-drug interactions and adverse side effects.[171] As cancer patients are often on a multi-drug treatment regimen to treat the cancer and resulting symptoms, it is necessary to try to minimize these drug-drug interactions and adverse side effects.

The structure of ITZ has been minimally explored in terms of its novel anticancer activities. Thus, a series of thorough structure-activity relationship (SAR) studies were undertaken to determine the ITZ functional groups required for potent Hh pathway and

angiogenesis inhibition.[115] Four generations of analogues were designed, synthesized, and evaluated in preliminary cellular assays. Analogue generations I and II focused on exploring all three regions of the ITZ scaffold and its stereochemistry. SAR data concluded that the triazole moiety of ITZ can be removed and potent Hh pathway inhibition is maintained. Removal of the triazole group also abolishes unwanted inhibition of CYP3A4 and its subsequent adverse side effects.[115] It was also determined that the most potent stereoisomer of *des*-triazole ITZ contains the 2*R*,4*R*-dioxolane orientation and the 2'(*R*)-*sec*-butyl side-chain region (Figure 1). In terms of angiogenesis, there was not a clear SAR pattern; however, none of the generation I and II analogues were more potent than ITZ in two separate in vitro assays indicating that all of the functionality of ITZ, including the triazole region, must be crucial for potent angiogenesis inhibition.[115]

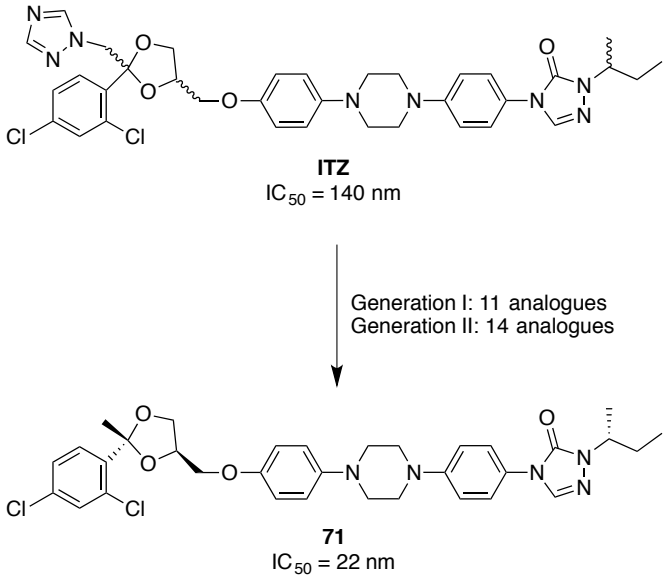

Figure 1. Summary of Generations I and II

SAR results from generations I and II were crucial in the design of subsequent analogues. Generations III and IV contained the optimal *des*-triazole-dioxolane

stereochemistry and focused on probing the triazolone/side-chain region of the original ITZ scaffold. Modulation to this region included a range of functionality such as amides, carbamates, hydrazine carboxamides, and triazolones. SAR data indicated that polar substitution at the *meta*-position of amide functionality was favorable for Hh pathway inhibitory activity (Figure 2). This potency increased in the presence of the 2*S*,4*R*-dioxolane orientation. In terms of other functionalities in this region, the hydrazine carboxamide analogues were moderately potent suggesting that an acyclic moiety can be utilized in replacement of the bulky triazolone ring. SAR results from generations III and IV proved interesting in exploring the triazolone/side-chain region of ITZ and further modifications should be explored in this area to improve the potency and physicochemical properties of these *des*-triazole ITZ analogues.

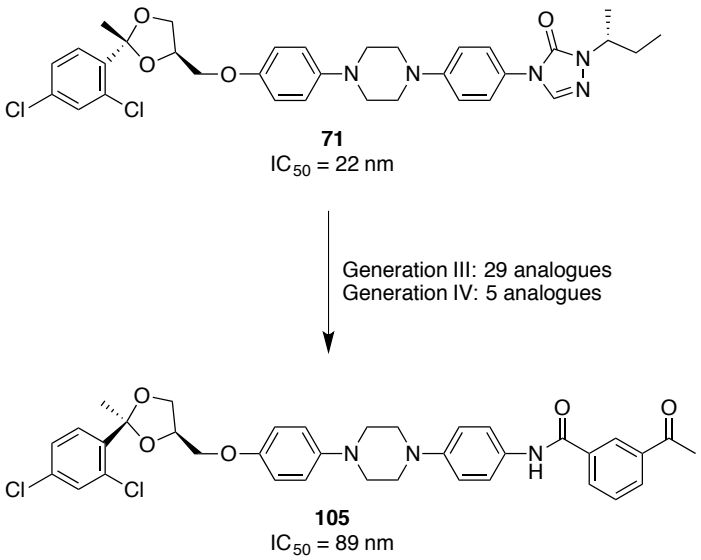

Figure 2. Summary of Generations III and IV

These SAR results from generations I-IV offer interesting information surrounding the ITZ scaffold and its novel anticancer properties. However, preliminary PK studies indicate that the modifications being made to the scaffold are not improving the overall

drug like properties. There are still a few regions and structural features of ITZ that could be further explored in terms of Hh pathway inhibition (Figure 3). For instance, the triazolone/side chain region could be modified to contain different acyclic and cyclic ureas such as modified 5- and 6-membered rings (**113**). The *sec*-butyl side-chain region could also be replaced with modified alkyl chains that contain polar functionality (alcohols, thiols, and amines), similarly to the hydroxylated side-chain region of PSZ (**114**). It is also important to note that previous SAR studies determined that the triazolone region could be truncated to the nitro, aniline, and hydrazine carboxamide functionalities indicating that a cyclic moiety may not be necessary at this position. Acyclic moieties should be synthesized and explored as this is a position to incorporate hydrogen-bonding functionality and this would also reduce the overall size of the molecule (**115**). These additional modifications to the triazolone/side-chain region will offer more information in terms of the electronics, sterics, and hydrogen bonding of this region of the scaffold.

The linker region has generally remained untouched throughout these analogue generations and this may be a way to incorporate polar groups to help aid in the solubility of the scaffold. Such modifications include adding nitrogen atoms to the aromatic rings of the linker region (**116**). In terms of the dioxolane region, it would be worth exploring different polar moieties in replacement of the triazole group. Removal of this triazole substituent abolishes CYP3A4 coordination but also decreases the solubility of the *des*-triazole ITZ analogues. Various polar moieties could be utilized at this position such as amines, alcohols, thiols, amides, and other 5-membered rings such as thiophenes, imidazoles, or pyrroles (**111**). While CF_3 functionality typically adds

lipophilicity, it may be interesting to utilize this moiety to further explore the triazole region in terms of electronegativity. The phenyl ring of the dioxolane region was also determined to be necessary for Hh pathway inhibition. However, the chlorine substitution was not necessary. This functionality of the dioxolane region offers another location for adding polar groups in an attempt to increase solubility. Various heterocycles could substitute the phenyl ring, including pyridine (**112**). As the ITZ scaffold contains a lot of functionality that is amendable for modification, it is important to further explore this structure to both improve the physicochemical properties as well as improve Hh pathway inhibitory activity.

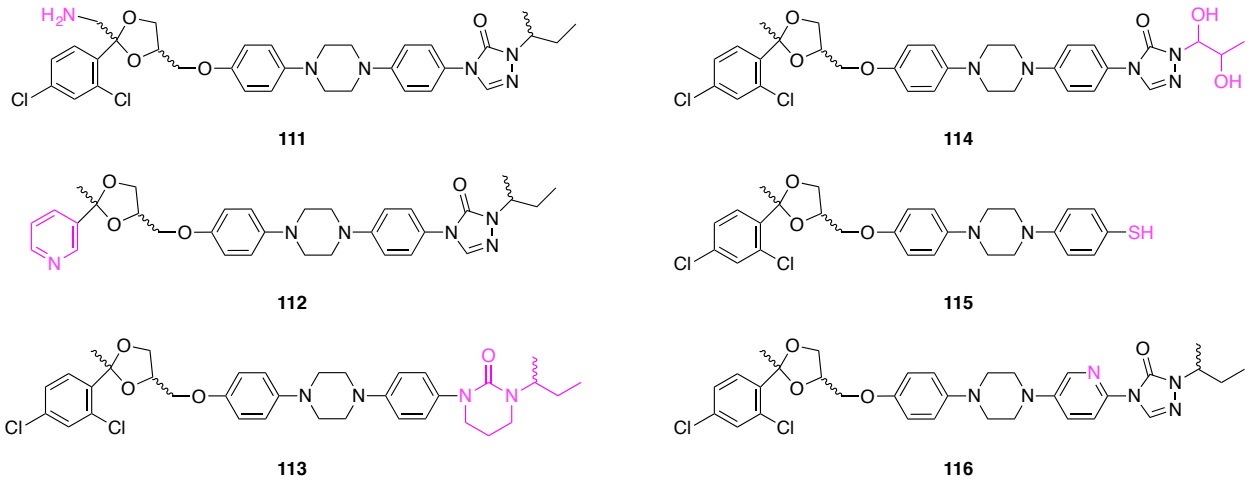

Figure 3. Proposed Future ITZ Analogues

In addition to further SAR studies, it will be necessary to determine the binding mode of ITZ/*des*-triazole ITZ analogues within the Hh pathway. While ITZ has been hypothesized to bind to Smo in a different manner than other Hh pathway antagonists, it has not been experimentally determined. A photo-affinity probe of ITZ has been previously developed and could be utilized to isolate and identify the binding mode of ITZ within the ASZ cell line.[172] Cells could be treated with probe and co-treated with ITZ

to confirm the binding proteins are the same. Treated cells could then be subjected to UV to activate the photolabile diazirine and covalently link the probe to the binding protein. Cells could then be lysed, proteins could be denatured, and denatured lysates could then be subjected to fluorophores via click chemistry and proteins can be resolved on SDS-PAGE. To isolate and identify a protein of interest, biotin can be used, as the fluorophore and biotinylated proteins can be isolated on streptavidin-agarose beads before SDS-PAGE. From this pull down experiment, the band can be cut out and analyzed via mass spectrometry.[172] It is important to note that a *des*-triazole ITZ probe could also be synthesized and subjected to pull down assays. This would confirm if these analogues inhibit the Hh pathway in a similar manner.

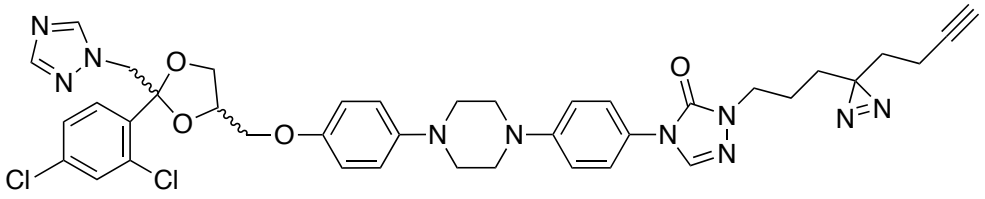

Figure 4. Structure of ITZ Probe

One of the main reasons why ITZ is being explored as an anticancer chemotherapeutic is because of its ability to inhibit the Hh pathway in the presence of both wild type Smo and mutant Smo. It is crucial to determine if *des*-triazole ITZ and our analogues are also able to inhibit the Hh pathway in the presence of these Smo mutants. Two in vitro assays could be utilized to determine the ability of these analogues to remain active in the presence of Smo mutants. Both cell assays would utilize an Hh-dependent mouse embryonic fibroblast (C3H10T1/2). These cells could be transfected with various Smo constructs (Smo mutant constructs were generously gifted to the Hadden lab). For screening a few select ITZ analogues, transfected cells

can be incubated for 24 hours with recombinant sonic hedgehog ligand (rShh) and drug. A gene expression assay measuring endogenous Gli1 mRNA could determine whether the Hh pathway is active or inactive. For a higher-throughput screen of compounds, a Gli-luciferase assay could be utilized. C3H10T1/2 cells could be plated in a 96-well plate (20,000 cells/well). After 24 hours, cells could be transfected with Smo construct, Renilla luciferase control reporter, and Gli-Luc reporter using Gene Juice transfection agent. After 12 hours of incubation, recombinant hedgehog ligand (rShh) or sonic hedgehog (Shh) supplemented media would be added to each well along with drug. Luciferase activities would be determined 48 hours after transfection using DualGlo luciferase reporter assay system.[51,60]

In collaboration with Dr. Robert Wechsler-Reya and the Sanford Burnham Prebys Medical Discovery Institute, the most potent *des*-triazole ITZ analogues can be evaluated for their anti-proliferative and anti-Hh activity in primary Hh dependent murine cells. These cells are isolated from Patched (Ptch) knockout (Math1-Cre-ER; $Ptc^{11/11}$, MERP) mice. Mice with Ptch mutations have been used to mimic human Hh-associated MB.[112–114] These primary cells will more closely represent the disease state of cells in vivo and have been used for the preclinical testing of other Hh pathway inhibitors. Evaluation of these compounds in this primary MB cell line will provide more relevant data in comparison to the preliminary evaluation within our established cell lines (murine embryonic fibroblast C310T1/2 and ASZ). The Sanford Burnham Prebys Medical Discovery Institute will also aid in testing the most potent ITZ analogues in vivo with these same Ptch knockout (MERP) mice.

2. Contributions of ITZ Liposome Project

Thorough SAR studies were undertaken to improve the drug-like properties of ITZ. However, despite our efforts, it is anticipated that ITZ and *des*-triazole ITZ analogues will have issues crossing the BBB and reaching the brain. In addition to medicinal chemistry efforts, nanotechnology can be utilized to encapsulate drugs and improve targeted tissue delivery.[134] Liposomes are the most studied form of nanoparticles and have the potential of improving treatment for patients suffering from pediatric and/or brain cancer.[152,154] ITZ-liposomes have been studied for the treatment of various fungal infections, however, there are currently no ITZ-liposome formulations that are FDA-approved or in clinical trials.[11,157,158–163] In collaboration with Dr. Diane Burgess, a preliminary ITZ liposome formulation for the treatment of MB was developed and studied in vitro. These liposomes were an optimal size for penetrating the BBB (<100 nm) and had good encapsulation efficiency (~80%). While ITZ liposomes were not as potent as free ITZ within our in vitro assays, this formulation still offers promise for the targeted treatment of MB.

More research is still necessary to understand how ITZ liposomes behave in vitro. Further exploration is needed in terms of how ITZ liposomes interact with cells and how they release their drug contents. This information is critical for determining what modifications could be made to the liposome formulation to aid in their cell penetration or to manipulate the speed at which they release their contents. Drug release could be explored with a dialysis assay or by evaluating the media environment of our gene expression assay with the use of mass spectrometry.[173] In addition, liposomes could undergo a BBB model PAMPA assay to determine if this liposome formulation is

actually capable of penetrating the BBB.[174] The Burgess Lab utilizes a PAMPA assay with primary rat brain endothelial cells that would represent a good model of the BBB.[175] Based on these results, it may be necessary to further modify this current ITZ-liposome formulation to improve BBB and/or cellular permeability. Such modifications include adding BBB-targeting proteins to the liposomes or utilizing cationic liposomes as they have been determined to increase BBB permeability and cell permeability, respectively.[134,137]

3. Future Outlook on the Development of ITZ and *Des*-triazole-ITZ Analogues as Anticancer Chemotherapeutic Agents

The treatment of pediatric MB still remains a challenge in modern medicine. Despite the knowledge of MB and its subtypes, a targeted chemotherapeutic treatment has not been clinically developed. Treating MB presents many challenges including the average age of patients (7 years old) and the presence of the BBB. Current treatment involves surgery followed by high-dose chemotherapy and radiation. If the cancer does not spread, survival rates are generally between 70 and 80%. However, this harsh treatment regimen results in long-term side effects in these young patents.[33] It is necessary to develop a more targeted therapeutic for the treatment of pediatric MB.

Due to MB subtypes, it is difficult to develop just one therapeutic and ultimately, each subtype will need to be treated in a different manner. As SHH subtype MB is driven by aberrant Hh pathway activity, a viable strategy to treat this subtype is with Hh pathway inhibitors.[33] FDA-approved Hh pathway inhibitors such as vismodegib often result in decreased activity due to conferred resistance; this was specifically seen in a clinical trial involving vismodegib and an MB patient.[49,50,51] It would be advantageous to identify Hh pathway antagonists that do not lead to resistant forms of Smo.[9,78] One way

to bypass this would be to identify Hh pathway inhibitors that target downstream of Smo. ITZ serves as a promising scaffold due to its ability to inhibit the Hh pathway in the presence of both wild type Smo and mutant forms of Smo. ITZ is already FDA-approved and there is a good understanding of its overall safety and adverse side effects. In addition, this antifungal agent is currently administered to and tolerated by children for the treatment of various fungal infections.[176] Due to these reasons, ITZ serves as a promising starting point for targeted MB therapeutic development with an Hh pathway antagonist. Treatment with an Hh pathway inhibitor such as ITZ may allow for cancer treatment without harsh life-changing side effects seen with current therapy.

The blood brain barrier remains a large roadblock in the development of therapeutics to treat MB. A very small percentage of compounds, regardless of physiochemical properties, are capable of penetrating the BBB.[147] One efficient way to ensure BBB penetration is by using nanoparticles, such as liposomes, to ensure targeted drug delivery. Liposomes can be formulated to contain certain characteristics that are optimal for BBB penetration. In addition, liposomes serve as viable treatment options for patients suffering from brain or pediatric cancer as they have been proven to limit off target toxicities.[137,154] Due to its large size, it is anticipated that ITZ will not be able to cross the BBB and reach the brain. As a result, ITZ has been formulated into a preliminary liposome model that proves promising for Hh pathway inhibitory activity. This liposome formulation should be further explored to increase cell permeability and BBB penetration. An ITZ-liposome formulation may prove advantageous for targeted drug delivery and may aid in the development of ITZ as an anticancer agent. More

specifically, liposome formulations of Hh pathway inhibitors may prove to be a promising chemotherapeutic option for children suffering from SHH subtype MB.

REFERENCES

(1) Nosengo, N. *Nature News* **2016**, *534* (7607), 314.

(2) Strittmatter, S. M. *Nat Med* **2014**, *20* (6), 590–591.

(3) The Drug Repurposing Hub: a next-generation drug library and information resource : Nature Medicine : Nature Research http://www.nature.com/nm/journal/v23/n4/full/nm.4306.html?WT.feed_name=subjects_physical-sciences&foxtrotcallback=true (accessed Oct 9, 2017).

(4) Zheng, W.; Sun, W.; Simeonov, A. *British Journal of Pharmacology* n/a-n/a.

(5) Kouznetsova, J.; Sun, W.; Martínez-Romero, C.; Tawa, G.; Shinn, P.; Chen, C. Z.; Schimmer, A.; Sanderson, P.; McKew, J. C.; Zheng, W.; García-Sastre, A. *Emerg Microbes Infect* **2014**, *3* (12), e84.

(6) Xu, M.; Lee, E. M.; Wen, Z.; Cheng, Y.; Huang, W.-K.; Qian, X.; Tcw, J.; Kouznetsova, J.; Ogden, S. C.; Hammack, C.; Jacob, F.; Nguyen, H. N.; Itkin, M.; Hanna, C.; Shinn, P.; Allen, C.; Michael, S. G.; Simeonov, A.; Huang, W.; Christian, K. M.; Goate, A.; Brennand, K. J.; Huang, R.; Xia, M.; Ming, G.; Zheng, W.; Song, H.; Tang, H. *Nature medicine* **2016**, *22* (10), 1101.

(7) Anighoro, A.; Bajorath, J.; Rastelli, G. *J. Med. Chem.* **2014**, *57* (19), 7874–7887.

(8) Maertens, J. A. *Clin. Microbiol. Infect.* **2004**, *10 Suppl 1*, 1–10.

(9) Kim, J.; Tang, J. Y.; Gong, R.; Kim, J.; Lee, J. J.; Clemons, K. V.; Chong, C. R.; Chang, K. S.; Fereshteh, M.; Reya, T.; Liu, J. O.; Epstein, E. H.; Stevens, D. A.; Beachy, P. A. *Cancer Cell* **2010**, *17* (4), 388–399.

(10) Chong, C. R.; Xu, J.; Lu, J.; Bhat, S.; Sullivan, D. J.; Liu, J. O. *ACS Chem. Biol.* **2007**, *2* (4), 263–270.

(11) Home - ClinicalTrials.gov https://clinicaltrials.gov/ (accessed Oct 10, 2017).

(12) Pantziarka, P.; Sukhatme, V.; Bouche, G.; Meheus, L.; Sukhatme, V. P. *Ecancermedicalscience* **2015**, *9*.

(13) Al-Badr, A. A.; El-Subbagh, H. I. In *Profiles of Drug Substances, Excipients and Related Methodology*; Brittain, H. G., Ed.; Academic Press, 2009; Vol. 34, pp 193–264.

(14) Hadden, M. K.; Banerjee, U. Itraconazole analogues and methods of use thereof. US9650365 B2, May 16, 2017.

(15) Elewski, B.; Tavakkol, A. *Ther Clin Risk Manag* **2005**, *1* (4), 299–306.

(16) Strating, J. R. P. M.; van der Linden, L.; Albulescu, L.; Bigay, J.; Arita, M.; Delang, L.; Leyssen, P.; van der Schaar, H. M.; Lanke, K. H. W.; Thibaut, H. J.; Ulferts, R.; Drin, G.; Schlinck, N.; Wubbolts, R. W.; Sever, N.; Head, S. A.; Liu, J. O.; Beachy, P. A.; De Matteis, M. A.; Shair, M. D.; Olkkonen, V. M.; Neyts, J.; van Kuppeveld, F. J. M. *Cell Rep* **2015**, *10* (4), 600–615.

(17) Allen, D.; Wilson, D.; Drew, R.; Perfect, J. *Expert Review of Anti-infective Therapy* **2015**, *13* (6), 787–798.

(18) Odds, F. C.; Brown, A. J. P.; Gow, N. A. R. *Trends Microbiol.* **2003**, *11* (6), 272–279.

(19) Bell, A. S. In *Comprehensive Medicinal Chemistry II*; Taylor, J. B., Triggle, D. J., Eds.; Elsevier: Oxford, 2007; pp 445–468.

(20) E, F. *Acta Universitatis Agriculturae Sueciae. Agraria (Sweden). no. 57.* **1997**.

(21) Ogu, C. C.; Maxa, J. L. *Proc (Bayl Univ Med Cent)* **2000**, *13* (4), 421–423.

(22) Savjani, K. T.; Gajjar, A. K.; Savjani, J. K. *ISRN Pharm* **2012**, *2012*, 195727.

(23) Pubchem. itraconazole https://pubchem.ncbi.nlm.nih.gov/compound/55283 (accessed Oct 10, 2017).

(24) Domínguez-Gil Hurlé, A.; Sánchez Navarro, A.; García Sánchez, M. J. *Clinical Microbiology and Infection* **2006**, *12* (Supplement 7), 97–106.

(25) Hadden, M. K. *ChemMedChem* **2014**, *9* (1), 27–37.

(26) Banerjee, U.; Hadden, M. K. *Expert Opin Drug Discov* **2014**, *9* (7), 751–771.

(27) Trinh, T. N.; McLaughlin, E. A.; Gordon, C. P.; McCluskey, A. *Med. Chem. Commun.* **2014**, *5* (2), 117–133.

(28) Maschinot, C. A.; Pace, J. R.; Hadden, M. K. *Curr Med Chem* **2015**, *22* (35), 4033–4057.

(29) Ling, G.; Ahmadian, A.; Persson, Å.; Undén, A. B.; Afink, G.; Williams, C.; Uhlén, M.; Toftgård, R.; Lundeberg, J.; Pontén, F. *Oncogene* **2001**, *20* (53), 7770.

(30) Reifenberger, J.; Wolter, M.; Knobbe, C. B.; Köhler, B.; Schönicke, A.; Scharwächter, C.; Kumar, K.; Blaschke, B.; Ruzicka, T.; Reifenberger, G. *British Journal of Dermatology* **2005**, *152* (1), 43–51.

(31) Basal Cell Carcinoma (BCC) - SkinCancer.org https://www.skincancer.org/skin-cancer-information/basal-cell-carcinoma (accessed Jan 7, 2018).

(32) Basal cell carcinoma - Symptoms and causes - Mayo Clinic https://www.mayoclinic.org/diseases-conditions/basal-cell-carcinoma/symptoms-causes/syc-20354187 (accessed Jan 7, 2018).

(33) Medulloblastoma | American Brain Tumor Association http://www.abta.org/brain-tumor-information/types-of-tumors/medulloblastoma.html (accessed Oct 11, 2017).

(34) Medulloblastoma https://www.stjude.org/disease/medulloblastoma.html (accessed Oct 9, 2017).

(35) Gajjar, A. J.; Robinson, G. W. *Nat Rev Clin Oncol* **2014**, *11* (12), 714–722.

(36) Chen, J. K.; Taipale, J.; Cooper, M. K.; Beachy, P. A. *Genes Dev* **2002**, *16* (21), 2743–2748.

(37) Pan, S.; Wu, X.; Jiang, J.; Gao, W.; Wan, Y.; Cheng, D.; Han, D.; Liu, J.; Englund, N. P.; Wang, Y.; Peukert, S.; Miller-Moslin, K.; Yuan, J.; Guo, R.; Matsumoto, M.; Vattay, A.; Jiang, Y.; Tsao, J.; Sun, F.; Pferdekamper, A. C.; Dodd, S.; Tuntland, T.; Maniara, W.; Kelleher, J. F.; Yao, Y.; Warmuth, M.; Williams, J.; Dorsch, M. *ACS Med. Chem. Lett.* **2010**, *1* (3), 130–134.

(38) Munchhof, M. J.; Li, Q.; Shavnya, A.; Borzillo, G. V.; Boyden, T. L.; Jones, C. S.; LaGreca, S. D.; Martinez-Alsina, L.; Patel, N.; Pelletier, K.; Reiter, L. A.; Robbins, M. D.; Tkalcevic, G. T. *ACS Med. Chem. Lett.* **2012**, *3* (2), 106–111.

(39) Yauch, R. L.; Gould, S. E.; Scales, S. J.; Tang, T.; Tian, H.; Ahn, C. P.; Marshall, D.; Fu, L.; Januario, T.; Kallop, D.; Nannini-Pepe, M.; Kotkow, K.; Marsters, J. C.; Rubin, L. L.; de Sauvage, F. J. *Nature* **2008**, *455* (7211), 406–410.

(40) Thayer, S. P.; Pasca di Magliano, M.; Heiser, P. W.; Nielsen, C. M.; Roberts, D. J.; Lauwers, G. Y.; Ping Qi, Y.; Gysin, S.; Fernández-del Castillo, C.; Yajnik, V.; Antoniu, B.; McMahon, M.; Warshaw, A. L.; Hebrok, M. *Nature* **2003**, *425* (6960), 851–856.

(41) Xin, M. *Expert Opin Ther Pat* **2015**, *25* (5), 549–565.

(42) Lin, T. L.; Matsui, W. *Onco Targets Ther* **2012**, *5*, 47–58.

(43) Gupta, S.; Takebe, N.; LoRusso, P. *Ther Adv Med Oncol* **2010**, *2* (4), 237–250.

(44) Robarge, K. D.; Brunton, S. A.; Castanedo, G. M.; Cui, Y.; Dina, M. S.; Goldsmith, R.; Gould, S. E.; Guichert, O.; Gunzner, J. L.; Halladay, J.; Jia, W.; Khojasteh,

C.; Koehler, M. F. T.; Kotkow, K.; La, H.; Lalonde, R. L.; Lau, K.; Lee, L.; Marshall, D.; Marsters, J. C.; Murray, L. J.; Qian, C.; Rubin, L. L.; Salphati, L.; Stanley, M. S.; Stibbard, J. H. A.; Sutherlin, D. P.; Ubhayaker, S.; Wang, S.; Wong, S.; Xie, M. *Bioorg. Med. Chem. Lett.* **2009**, *19* (19), 5576–5581.

(45) Metcalfe, C.; de Sauvage, F. J. *Cancer Res.* **2011**, *71* (15), 5057–5061.

(46) Gendreau, S. B.; Hawkins, D.; Ho, C.-P.; Lewin, A.; Lin, T.; Merchant, A.; Rowley, R. B.; Wang, Q.; Matsui, W.; Fargnoli, J. *Mol Cancer Ther* **2009**, *8* (12 Supplement), B192–B192.

(47) Bender, M. H.; Hipskind, P. A.; Capen, A. R.; Cockman, M.; Credille, K. M.; Gao, H.; Bastian, J. A.; Clay, J. M.; Lobb, K. L.; Sall, D. J.; Thompson, M. L.; Wilson, T.; Wishart, G. N.; Patel, B. K. R. *Cancer Res* **2011**, *71* (8 Supplement), 2819–2819.

(48) Das, S.; Samant, R. S.; Shevde, L. A. *J. Biol. Chem.* **2013**, *288* (17), 11824–11833.

(49) Rudin, C. M.; Hann, C. L.; Laterra, J.; Yauch, R. L.; Callahan, C. A.; Fu, L.; Holcomb, T.; Stinson, J.; Gould, S. E.; Coleman, B.; LoRusso, P. M.; Von Hoff, D. D.; de Sauvage, F. J.; Low, J. A. *N. Engl. J. Med.* **2009**, *361* (12), 1173–1178.

(50) Yauch, R. L.; Dijkgraaf, G. J. P.; Alicke, B.; Januario, T.; Ahn, C. P.; Holcomb, T.; Pujara, K.; Stinson, J.; Callahan, C. A.; Tang, T.; Bazan, J. F.; Kan, Z.; Seshagiri, S.; Hann, C. L.; Gould, S. E.; Low, J. A.; Rudin, C. M.; de Sauvage, F. J. *Science* **2009**, *326* (5952), 572–574.

(51) Dijkgraaf, G. J. P.; Alicke, B.; Weinmann, L.; Januario, T.; West, K.; Modrusan, Z.; Burdick, D.; Goldsmith, R.; Robarge, K.; Sutherlin, D.; Scales, S. J.; Gould, S. E.; Yauch, R. L.; Sauvage, F. J. de. *Cancer Res* **2011**, *71* (2), 435–444.

(52) Pricl, S.; Cortelazzi, B.; Dal Col, V.; Marson, D.; Laurini, E.; Fermeglia, M.; Licitra, L.; Pilotti, S.; Bossi, P.; Perrone, F. *Mol Oncol* **2015**, *9* (2), 389–397.

(53) Sharpe, H. J.; Pau, G.; Dijkgraaf, G. J.; Basset-Seguin, N.; Modrusan, Z.; Januario, T.; Tsui, V.; Durham, A. B.; Dlugosz, A. A.; Haverty, P. M.; Bourgon, R.; Tang, J. Y.; Sarin, K. Y.; Dirix, L.; Fisher, D. C.; Rudin, C. M.; Sofen, H.; Migden, M. R.; Yauch, R. L.; de Sauvage, F. J. *Cancer Cell* **2015**, *27* (3), 327–341.

(54) Atwood, S. X.; Sarin, K. Y.; Whitson, R. J.; Li, J. R.; Kim, G.; Rezaee, M.; Ally, M. S.; Kim, J.; Yao, C.; Chang, A. L. S.; Oro, A. E.; Tang, J. Y. *Cancer Cell* **2015**, *27* (3), 342–353.

(55) Buonamici, S.; Williams, J.; Morrissey, M.; Wang, A.; Guo, R.; Vattay, A.; Hsiao, K.; Yuan, J.; Green, J.; Ospina, B.; Yu, Q.; Ostrom, L.; Fordjour, P.; Anderson, D. L.; Monahan, J. E.; Kelleher, J. F.; Peukert, S.; Pan, S.; Wu, X.; Maira, S.-M.;

García-Echeverría, C.; Briggs, K. J.; Watkins, D. N.; Yao, Y.; Lengauer, C.; Warmuth, M.; Sellers, W. R.; Dorsch, M. *Sci Transl Med* **2010**, *2* (51), 51ra70.

(56) Lee, M. J.; Hatton, B. A.; Villavicencio, E. H.; Khanna, P. C.; Friedman, S. D.; Ditzler, S.; Pullar, B.; Robison, K.; White, K. F.; Tunkey, C.; LeBlanc, M.; Randolph-Habecker, J.; Knoblaugh, S. E.; Hansen, S.; Richards, A.; Wainwright, B. J.; McGovern, K.; Olson, J. M. *Proc Natl Acad Sci U S A* **2012**, *109* (20), 7859–7864.

(57) Wang, Y.; Ding, Q.; Yen, C.-J.; Xia, W.; Izzo, J. G.; Lang, J.-Y.; Li, C.-W.; Hsu, J. L.; Miller, S. A.; Wang, X.; Lee, D.-F.; Hsu, J.-M.; Huo, L.; Labaff, A. M.; Liu, D.; Huang, T.-H.; Lai, C.-C.; Tsai, F.-J.; Chang, W.-C.; Chen, C.-H.; Wu, T.-T.; Buttar, N. S.; Wang, K. K.; Wu, Y.; Wang, H.; Ajani, J.; Hung, M.-C. *Cancer Cell* **2012**, *21* (3), 374–387.

(58) Dlugosz, A.; Agrawal, S.; Kirkpatrick, P. *Nat Rev Drug Discov* **2012**, *11* (6), 437–438.

(59) Peukert, S.; He, F.; Dai, M.; Zhang, R.; Sun, Y.; Miller-Moslin, K.; McEwan, M.; Lagu, B.; Wang, K.; Yusuff, N.; Bourret, A.; Ramamurthy, A.; Maniara, W.; Amaral, A.; Vattay, A.; Wang, A.; Guo, R.; Yuan, J.; Green, J.; Williams, J.; Buonamici, S.; Kelleher, J. F.; Dorsch, M. *ChemMedChem* **2013**, *8* (8), 1261–1265.

(60) Tao, H.; Jin, Q.; Koo, D.-I.; Liao, X.; Englund, N. P.; Wang, Y.; Ramamurthy, A.; Schultz, P. G.; Dorsch, M.; Kelleher, J.; Wu, X. *Chem. Biol.* **2011**, *18* (4), 432–437.

(61) Chenna, V.; Hu, C.; Khan, S. R. *Journal of Environmental Science and Health, Part A* **2014**, *49* (6), 641–647.

(62) Gavalas, N. G.; Liontos, M.; Trachana, S.-P.; Bagratuni, T.; Arapinis, C.; Liacos, C.; Dimopoulos, M. A.; Bamias, A. *Int J Mol Sci* **2013**, *14* (8), 15885–15909.

(63) Manetti, F.; Faure, H.; Roudaut, H.; Gorojankina, T.; Traiffort, E.; Schoenfelder, A.; Mann, A.; Solinas, A.; Taddei, M.; Ruat, M. *Mol Pharmacol* **2010**, *78* (4), 658–665.

(64) Solinas, A.; Faure, H.; Roudaut, H.; Traiffort, E.; Schoenfelder, A.; Mann, A.; Manetti, F.; Taddei, M.; Ruat, M. *J. Med. Chem.* **2012**, *55* (4), 1559–1571.

(65) Hoch, L.; Faure, H.; Roudaut, H.; Schoenfelder, A.; Mann, A.; Girard, N.; Bihannic, L.; Ayrault, O.; Petricci, E.; Taddei, M.; Rognan, D.; Ruat, M. *FASEB J* **2015**, *29* (5), 1817–1829.

(66) Xin, M.; Wen, J.; Tang, F.; Tu, C.; Shen, H.; Zhao, X. *Bioorganic & Medicinal Chemistry Letters* **2013**, *23* (24), 6777–6783.

(67) Xin, M.; Wen, J.; Tang, F.; Tu, C.; Huang, W.; Shen, H.; Zhao, X.; Cheng, L.; Wang, M.; Zhang, L. *Bioorganic & Medicinal Chemistry Letters* **2014**, *24* (3), 983–988.

(68) Xin, M.; Zhang, L.; Tang, F.; Tu, C.; Wen, J.; Zhao, X.; Liu, Z.; Cheng, L.; Shen, H. *Bioorganic & Medicinal Chemistry* **2014**, *22* (4), 1429–1440.

(69) Wu, T.-M.; Wang, D.-C.; Xiang, P.; Zhang, J.-N.; Sang, Y.-X.; Lin, H.-J.; Chen, J.; Xie, G.; Song, H.; Zhao, Y.-L.; Xie, Y.-M. *Bioorganic & Medicinal Chemistry Letters* **2014**, *24* (5), 1426–1431.

(70) Mann, B. S.; Johnson, J. R.; Cohen, M. H.; Justice, R.; Pazdur, R. *Oncologist* **2007**, *12* (10), 1247–1252.

(71) Zhao, J.; Quan, H.; Xie, C.; Lou, L. *Pharmacol Res Perspect* **2014**, *2* (3).

(72) Lu, W.; Geng, D.; Sun, Z.; Yang, Z.; Ma, H.; Zheng, J.; Zhang, X. *Bioorg Med Chem Lett* **2014**, *24* (10), 2300–2304.

(73) Ma, H.; Lu, W.; Sun, Z.; Luo, L.; Geng, D.; Yang, Z.; Li, E.; Zheng, J.; Wang, M.; Zhang, H.; Yang, S.; Zhang, X. *Eur J Med Chem* **2015**, *89*, 721–732.

(74) Betti, M.; Castagnoli, G.; Panico, A.; Sanna Coccone, S.; Wiedenau, P. *Org. Process Res. Dev.* **2012**, *16* (11), 1739–1745.

(75) Nair, S. K.; Planken, S. P. Pyridine- 2- derivatives as smoothened receptor modulators. WO2012052948 A1, April 26, 2012.

(76) Rohner, A.; Spilker, M. E.; Lam, J. L.; Pascual, B.; Bartkowski, D.; Li, Q. J.; Yang, A. H.; Stevens, G.; Xu, M.; Wells, P. A.; Planken, S.; Nair, S.; Sun, S. *Mol Cancer Ther* **2012**, *11* (1), 57–65.

(77) Fan, C.-W.; Chen, B.; Franco, I.; Lu, J.; Shi, H.; Wei, S.; Wang, C.; Wu, X.; Tang, W.; Roth, M. G.; Williams, N. S.; Hirsch, E.; Chen, C.; Lum, L. *Chem Biol* **2014**, *21* (12), 1680–1689.

(78) Kim, J.; Aftab, B. T.; Tang, J. Y.; Kim, D.; Lee, A. H.; Rezaee, M.; Kim, J.; Chen, B.; King, E. M.; Borodovsky, A.; Riggins, G. J.; Epstein, E. H.; Beachy, P. A.; Rudin, C. M. *Cancer Cell* **2013**, *23* (1), 23–34.

(79) Carmeliet, P. *Nat. Med.* **2003**, *9* (6), 653–660.

(80) Carmeliet, P. *Nature* **2005**, *438* (7070), 932–936.

(81) Tahergorabi, Z.; Khazaei, M. *Iran J Basic Med Sci* **2012**, *15* (6), 1110–1126.

(82) Carmeliet, P.; Jain, R. K. *Nature* **2000**, *407* (6801), 249–257.

(83) Nishida, N.; Yano, H.; Nishida, T.; Kamura, T.; Kojiro, M. *Vasc Health Risk Manag* **2006**, *2* (3), 213–219.

(84) Ferrara, N.; Kerbel, R. S. *Nature* **2005**, *438* (7070), 967–974.

(85) Carmeliet, P.; Jain, R. K. *Nature* **2011**, *473* (7347), 298–307.

(86) Weis, S. M.; Cheresh, D. A. *Nat. Med.* **2011**, *17* (11), 1359–1370.

(87) Dimova, I.; Popivanov, G.; Djonov, V. *J BUON* **2014**, *19* (1), 15–21.

(88) Folkman, J. *N. Engl. J. Med.* **1971**, *285* (21), 1182–1186.

(89) Gimbrone, M. A.; Gullino, P. M. *J Natl Cancer Inst* **1976**, *56* (2), 305–318.

(90) Le Tourneau, C.; Raymond, E.; Faivre, S. *Ther Clin Risk Manag* **2007**, *3* (2), 341–348.

(91) Barnett, C. M. *Pharmacotherapy* **2012**, *32* (4), 383–396.

(92) Sloan, B.; Scheinfeld, N. S. *Curr Opin Investig Drugs* **2008**, *9* (12), 1324–1335.

(93) Ferrara, N.; Hillan, K. J.; Gerber, H.-P.; Novotny, W. *Nature Reviews Drug Discovery* **2004**, *3* (5), nrd1381.

(94) Adnane, L.; Trail, P. A.; Taylor, I.; Wilhelm, S. M. *Meth. Enzymol.* **2006**, *407*, 597–612.

(95) Yoo, S. Y.; Kwon, S. M. *Mediators Inflamm.* **2013**, *2013*, 127170.

(96) Nacev, B. A.; Grassi, P.; Dell, A.; Haslam, S. M.; Liu, J. O. *J. Biol. Chem.* **2011**, *286* (51), 44045–44056.

(97) Shi, W.; Nacev, B. A.; Bhat, S.; Liu, J. O. *ACS Med. Chem. Lett.* **2010**, *1* (4), 155–159.

(98) Xu, J.; Dang, Y.; Ren, Y. R.; Liu, J. O. *Proc. Natl. Acad. Sci. U.S.A.* **2010**, *107* (10), 4764–4769.

(99) Del Carratore, R.; Carpi, A.; Beffy, P.; Lubrano, V.; Giorgetti, L.; Maserti, B. E.; Carluccio, M. A.; Simili, M.; Iervasi, G.; Balzan, S. *Biomed. Pharmacother.* **2012**, *66* (4), 312–317.

(100) Trinh, M. N.; Lu, F.; Li, X.; Das, A.; Liang, Q.; De Brabander, J. K.; Brown, M. S.; Goldstein, J. L. *Proc. Natl. Acad. Sci. U.S.A.* **2017**, *114* (1), 89–94.

(101) Head, S. A.; Shi, W. Q.; Yang, E. J.; Nacev, B. A.; Hong, S. Y.; Pasunooti, K. K.; Li, R.-J.; Shim, J. S.; Liu, J. O. *ACS Chem. Biol.* **2017**, *12* (1), 174–182.

(102) Isoherranen, N.; Kunze, K. L.; Allen, K. E.; Nelson, W. L.; Thummel, K. E. *Drug Metab. Dispos.* **2004**, *32* (10), 1121–1131.

(103) Shi, W.; Nacev, B. A.; Aftab, B. T.; Head, S.; Rudin, C. M.; Liu, J. O. *J Med Chem* **2011**, *54* (20), 7363–7374.

(104) Heeres, J.; Backx, L. J. J.; Van Cutsem, J. *J. Med. Chem.* **1984**, *27* (7), 894–900.

(105) Hackettstown, R. R. A. 55 N. R.; NJ. Polarimetry - Optical Rotation Vs Specific Rotation Definition https://rudolphresearch.com/polarimeters-and-polarimetry/ (accessed Jan 8, 2018).

(106) Wu, W.; Li, R.; Malladi, S. S.; Warshakoon, H. J.; Kimbrell, M. R.; Amolins, M. W.; Ukani, R.; Datta, A.; David, S. A. *J. Med. Chem.* **2010**, *53* (8), 3198–3213.

(107) Yamada, K.; Yoshizawa, Y.; Oh, K. *Molecules* **2012**, *17* (4), 4460–4473.

(108) Baji, H.; Kimny, T.; Gasquez, F.; Flammang, M.; Compagnon, P. L.; Delcourt, A.; Mathieu, G.; Viossat, B.; Morgant, G.; Nguyen-Huy, D. *European Journal of Medicinal Chemistry* **1997**, *32* (7), 637–650.

(109) Banerjee, U.; Ghosh, M.; Kyle Hadden, M. *Bioorg. Med. Chem. Lett.* **2012**, *22* (3), 1330–1334.

(110) So, P.-L.; Langston, A. W.; Daniallinia, N.; Hebert, J. L.; Fujimoto, M. A.; Khaimskiy, Y.; Aszterbaum, M.; Epstein, E. H. *Exp. Dermatol.* **2006**, *15* (9), 742–750.

(111) Tang, J. Y.; Xiao, T. Z.; Oda, Y.; Chang, K. S.; Shpall, E.; Wu, A.; So, P.-L.; Hebert, J.; Bikle, D.; Epstein, E. H. *Cancer Prev Res (Phila)* **2011**, *4* (5), 744–751.

(112) Yang, Z.-J.; Ellis, T.; Markant, S. L.; Read, T.-A.; Kessler, J. D.; Bourboulas, M.; Schüller, U.; Machold, R.; Fishell, G.; Rowitch, D. H.; Wainwright, B. J.; Wechsler-Reya, R. J. *Cancer Cell* **2008**, *14* (2), 135–145.

(113) Markant, S. L.; Esparza, L. A.; Sun, J.; Barton, K. L.; McCoig, L. M.; Grant, G. A.; Crawford, J. R.; Levy, M. L.; Northcott, P. A.; Shih, D.; Remke, M.; Taylor, M. D.; Wechsler-Reya, R. J. *Cancer Res.* **2013**, *73* (20), 6310–6322.

(114) Brun, S. N.; Markant, S. L.; Esparza, L. A.; Garcia, G.; Terry, D.; Huang, J.-M.; Pavlyukov, M. S.; Li, X.-N.; Grant, G. A.; Crawford, J. R.; Levy, M. L.; Conway, E. M.; Smith, L. H.; Nakano, I.; Berezov, A.; Greene, M. I.; Wang, Q.; Wechsler-Reya, R. J. *Oncogene* **2015**, *34* (29), 3770–3779.

(115) Pace, J. R.; DeBerardinis, A. M.; Sail, V.; Tacheva-Grigorova, S. K.; Chan, K. A.; Tran, R.; Raccuia, D. S.; Wechsler-Reya, R. J.; Hadden, M. K. *J. Med. Chem.* **2016**, *59* (8), 3635–3649.

(116) DeCicco-Skinner, K. L.; Henry, G. H.; Cataisson, C.; Tabib, T.; Gwilliam, J. C.; Watson, N. J.; Bullwinkle, E. M.; Falkenburg, L.; O'Neill, R. C.; Morin, A.; Wiest, J. S. *J Vis Exp* **2014**, No. 91.

(117) Johansson, A.; Kollman, P.; Rothenberg, S.; McKelvey, J. *J. Am. Chem. Soc.* **1974**, *96* (12), 3794–3800.

(118) Montalbetti, C. A. G. N.; Falque, V. *Tetrahedron* **2005**, *61* (46), 10827–10852.

(119) Banerjee, U.; DeBerardinis, A. M.; Hadden, M. K. *Bioorganic & Medicinal Chemistry* **2015**, *23* (3), 548–555.

(120) Shen, G.; Wang, M.; Welch, T. R.; Blagg, B. S. J. *J. Org. Chem.* **2006**, *71* (20), 7618–7631.

(121) Al-Warhi, T. I.; Al-Hazimi, H. M. A.; El-Faham, A. *Journal of Saudi Chemical Society* **2012**, *16* (2), 97–116.

(122) DeBerardinis, A. M.; Raccuia, D. S.; Thompson, E. N.; Maschinot, C. A.; Kyle Hadden, M. *European Journal of Medicinal Chemistry* **2015**, *93* (Supplement C), 156–171.

(123) DeBerardinis, A. M.; Madden, D. J.; Banerjee, U.; Sail, V.; Raccuia, D. S.; De Carlo, D.; Lemieux, S. M.; Meares, A.; Hadden, M. K. *J. Med. Chem.* **2014**, *57* (9), 3724–3736.

(124) Venkatraman, S.; Bogen, S. L.; Arasappan, A.; Bennett, F.; Chen, K.; Jao, E.; Liu, Y.-T.; Lovey, R.; Hendrata, S.; Huang, Y.; Pan, W.; Parekh, T.; Pinto, P.; Popov, V.; Pike, R.; Ruan, S.; Santhanam, B.; Vibulbhan, B.; Wu, W.; Yang, W.; Kong, J.; Liang, X.; Wong, J.; Liu, R.; Butkiewicz, N.; Chase, R.; Hart, A.; Agrawal, S.; Ingravallo, P.; Pichardo, J.; Kong, R.; Baroudy, B.; Malcolm, B.; Guo, Z.; Prongay, A.; Madison, V.; Broske, L.; Cui, X.; Cheng, K.-C.; Hsieh, Y.; Brisson, J.-M.; Prelusky, D.; Korfmacher, W.; White, R.; Bogdanowich-Knipp, S.;

Pavlovsky, A.; Bradley, P.; Saksena, A. K.; Ganguly, A.; Piwinski, J.; Girijavallabhan, V.; Njoroge, F. G. *J. Med. Chem.* **2006**, *49* (20), 6074–6086.

(125) Venkatraman, S.; Velazquez, F.; Wu, W.; Blackman, M.; Madison, V.; Njoroge, F. G. *Bioorganic & Medicinal Chemistry Letters* **2010**, *20* (7), 2151–2155.

(126) Pace, J. Repurposing the Clinically Efficacious Antifungal Agent Itraconazole as an Anticancer Chemotherapeutic http://pubs.acs.org/doi/pdf/10.1021/acs.jmedchem.5b01718 (accessed Oct 6, 2017).

(127) Darnbrough, S.; Mervic, M.; Condon, S. M.; Burns, C. J. *Synthetic Communications* **2001**, *31* (21), 3273–3280.

(128) Nakamura, K.; Nakajima, T.; Kayahara, H.; Nomura, E.; Taniguchi, H. *Tetrahedron Letters* **2004**, *45* (3), 495–499.

(129) Ghosh, A. K.; Brindisi, M. *J Med Chem* **2015**, *58* (7), 2895–2940.

(130) Park, K. *J Control Release* **2007**, *120* (1–2), 1–3.

(131) Shi, J.; Votruba, A. R.; Farokhzad, O. C.; Langer, R. *Nano Lett* **2010**, *10* (9), 3223–3230.

(132) Singh, R.; Lillard, J. W. *Exp Mol Pathol* **2009**, *86* (3), 215–223.

(133) Farokhzad, O. C.; Langer, R. *ACS Nano* **2009**, *3* (1), 16–20.

(134) Pattni, B. S.; Chupin, V. V.; Torchilin, V. P. *Chem. Rev.* **2015**, *115* (19), 10938–10966.

(135) Daraee, H.; Etemadi, A.; Kouhi, M.; Alimirzalu, S.; Akbarzadeh, A. *Artificial Cells, Nanomedicine, and Biotechnology* **2016**, *44* (1), 381–391.

(136) Akbarzadeh, A.; Rezaei-Sadabady, R.; Davaran, S.; Joo, S. W.; Zarghami, N.; Hanifehpour, Y.; Samiei, M.; Kouhi, M.; Nejati-Koshki, K. *Nanoscale Research Letters* **2013**, *8* (1), 102.

(137) Schnyder, A.; Huwyler, J. *NeuroRx* **2005**, *2* (1), 99–107.

(138) Arai, N.; Yasuoka, K.; Zeng, X. C. *ACS Nano* **2016**, *10* (8), 8026–8037.

(139) Pagano, R. E.; Weinstein, J. N. *Annu. Rev. Biophys. Bioeng.* **1978**, *7*, 435–468.

(140) Costa, A. P.; Xu, X.; Khan, M. A.; Burgess, D. J. *Pharm. Res.* **2016**, *33* (2), 404–416.

(141) turbulent flow | physics https://www.britannica.com/science/turbulent-flow (accessed Nov 11, 2017).

(142) Reynolds number | Definition & History https://www.britannica.com/science/Reynolds-number (accessed Nov 10, 2017).

(143) Bulbake, U.; Doppalapudi, S.; Kommineni, N.; Khan, W. *Pharmaceutics* **2017**, *9* (2).

(144) Berg, J. M.; Tymoczko, J. L.; Stryer, L. **2002**.

(145) Quick Brain Tumor Facts http://braintumor.org/brain-tumor-information/brain-tumor-facts/ (accessed Nov 2, 2017).

(146) Duncan, G. 5-Year Survival Rate | CureSearch https://curesearch.org/5-Year-Survival-Rate (accessed Nov 2, 2017).

(147) Pardridge, W. M. *Mol. Interv.* **2003**, *3* (2), 90–105, 51.

(148) Oberoi, R. K.; Parrish, K. E.; Sio, T. T.; Mittapalli, R. K.; Elmquist, W. F.; Sarkaria, J. N. *Neuro Oncol* **2016**, *18* (1), 27–36.

(149) Staud, F.; Pavek, P. *Int. J. Biochem. Cell Biol.* **2005**, *37* (4), 720–725.

(150) Lin, J. H.; Yamazaki, M. *Clin Pharmacokinet* **2003**, *42* (1), 59–98.

(151) Vasiliou, V.; Vasiliou, K.; Nebert, D. W. *Hum. Genomics* **2009**, *3* (3), 281–290.

(152) Wei, X.; Chen, X.; Ying, M.; Lu, W. *Acta Pharm Sin B* **2014**, *4* (3), 193–201.

(153) Key Statistics for Childhood Cancers https://www.cancer.org/cancer/cancer-in-children/key-statistics.html (accessed Nov 2, 2017).

(154) Federman, N.; Denny, C. T. *Pediatr. Res.* **2010**, *67* (5), 514–519.

(155) Kumar, S.; Jog, R.; Shen, J.; Zolnik, B.; Sadrieh, N.; Burgess, D. J. *J Pharm Sci* **2015**, *104* (9), 3018–3028.

(156) Kumar, S.; Shen, J.; Burgess, D. J. *Journal of Controlled Release* **2014**, *192* (Supplement C), 95–102.

(157) Tang, J.; Wei, H.; Liu, H.; Ji, H.; Dong, D.; Zhu, D.; Wu, L. *Drug Delivery* **2010**, *17* (4), 223–230.

(158) Wang, J.; Huang, G. *Drug Deliv* **2011**, *18* (8), 631–638.

(159) Le Conte, P.; Joly, V.; Saint-Julien, L.; Gillardin, J. M.; Carbon, C.; Yeni, P. *Am. Rev. Respir. Dis.* **1992**, *145* (2 Pt 1), 424–429.

(160) Leal, A. F. G.; Leite, M. C.; Medeiros, C. S. Q.; Cavalcanti, I. M. F.; Wanderley, A. G.; Magalhães, N. S. S.; Neves, R. P. *Mycopathologia* **2015**, *179* (3–4), 225–229.

(161) Lankalapalli, S.; Tenneti, V. S. V. K.; Adama, R. *Der Pharmacia Lettre* **2017**, *7* (8), 1–17.

(162) Conte, P. L.; Faintreny, A.; Potel, G.; Legallou, F.; Bugnon, D.; Baron, D. *Current Therapeutic Research* **1994**, *55* (8), 938–943.

(163) Ćurić, A.; Reul, R.; Möschwitzer, J.; Fricker, G. *International Journal of Pharmaceutics* **2013**, *448* (1), 189–197.

(164) van Hoogevest, P.; Wendel, A. *Eur J Lipid Sci Technol* **2014**, *116* (9), 1088–1107.

(165) Li, J.; Wang, X.; Zhang, T.; Wang, C.; Huang, Z.; Luo, X.; Deng, Y. *Asian Journal of Pharmaceutical Sciences* **2015**, *10* (2), 81–98.

(166) Saraiva, C.; Praça, C.; Ferreira, R.; Santos, T.; Ferreira, L.; Bernardino, L. *Journal of Controlled Release* **2016**, *235* (Supplement C), 34–47.

(167) Soema, P. C.; Willems, G.-J.; Jiskoot, W.; Amorij, J.-P.; Kersten, G. F. *European Journal of Pharmaceutics and Biopharmaceutics* **2015**, *94* (Supplement C), 427–435.

(168) Torchilin, V.; Weissig, V. *Liposomes: A Practical Approach*; OUP Oxford, 2003.

(169) Piacentini, E. In *Encyclopedia of Membranes*; Drioli, E., Giorno, L., Eds.; Springer Berlin Heidelberg, 2016; pp 706–707.

(170) Panwar, P.; Pandey, B.; Lakhera, P. C.; Singh, K. P. *Int J Nanomedicine* **2010**, *5*, 101–108.

(171) Peng, C.-C.; Shi, W.; Lutz, J. D.; Kunze, K. L.; Liu, J. O.; Nelson, W. L.; Isoherranen, N. *Drug Metab. Dispos.* **2012**, *40* (3), 426–435.

(172) Head, S. A.; Shi, W.; Zhao, L.; Gorshkov, K.; Pasunooti, K.; Chen, Y.; Deng, Z.; Li, R.; Shim, J. S.; Tan, W.; Hartung, T.; Zhang, J.; Zhao, Y.; Colombini, M.; Liu, J. O. *PNAS* **2015**, *112* (52), E7276–E7285.

(173) Xu, X.; Khan, M. A.; Burgess, D. J. *International Journal of Pharmaceutics* **2012**, *426* (1), 211–218.

(174) Di, L.; Kerns, E. H.; Fan, K.; McConnell, O. J.; Carter, G. T. *Eur J Med Chem* **2003**, *38* (3), 223–232.

(175) Takata, F.; Dohgu, S.; Yamauchi, A.; Matsumoto, J.; Machida, T.; Fujishita, K.; Shibata, K.; Shinozaki, Y.; Sato, K.; Kataoka, Y.; Koizumi, S. *PLOS ONE* **2013**, *8* (1), e55166.

(176) Gupta, A. K.; Cooper, E. A.; Ginter, G. *Dermatol Clin* **2003**, *21* (3), 521–535.

APPENDIX A: Select ^{1}H and ^{13}C NMR Spectral Data

SYNTHETIC PROCEDURES

Linker Region Intermediates

1-(4-methoxyphenyl)-4-(4-nitrophenyl)piperazine (13). 1-(4-methoxyphenyl)piperazine (**11**) (8.0 g, 41.6 mmol) and 1-chloro-4-nitrobenzene (**12**) (6.3 g, 40.0 mmol) were dissolved in anhydrous DMSO (80 mL). K_2CO_3 (6.0 g, 43.5 mmol) was added and the mixture refluxed at 160°C for 12 h. The reaction was cooled to RT and a red solid precipitated. The red solid was filtered and washed with $CHCl_3$. The filtrate was concentrated to afford **13**, which was immediately utilized as the crude solid.

4-(4-(4-methoxyphenyl)piperazin-1-yl)aniline (14). 10% palladium on carbon (0.88 g, 5% mole ratio) was added to a dry 3-neck round bottom flask. Ethanol (200 mL) was added followed by slow addition of **13** (5.2 g, 16.59 mmol). Hydrazine monohydrate (5.2 mL, 165.9 mmol) was added dropwise and the mixture was stirred at reflux for 3.5 h. Upon cooling to RT, the mixture was filtered through celite. The celite was washed with ethanol (250 mL) and chloroform (1000 mL) to ensure complete elution of the aniline. The filtrate was concentrated to afford **14**, which was immediately utilized as the crude solid.

Phenyl (4-(4-(4-methoxyphenyl)piperazin-1-yl)phenyl)carbamate (15). A solution of aniline (**14**) (2.7 g, 9.51 mmol) and pyridine (12.8 mL, 158.8 mmol) in $CHCl_3$ (100 mL) was cooled to 0°C. Phenyl chloroformate (1.25 mL, 9.9 mmol) was added dropwise and the mixture stirred at RT for 3 h. Water and petroleum ether (50 mL: 50 mL) were added at which point an off-white precipitate formed. The solid was washed with H_2O and

isopropyl alcohol to provide the crude carbamate **15**, which was immediately utilized without further purification.

N-(4-(4-(4-methoxyphenyl)piperazin-1-yl)phenyl)hydrazinecarboxamide (16). A solution of hydrazine hydrate (1.33 mL, 42.8 mmol) and **15** (3.2 g, 7.9 mmol) in 1.4-dioxane (70 mL) was stirred at reflux for 3 h. The mixture was poured into H_2O (250 mL), and the resulting off-white solid was filtered and washed with H_2O and isopropyl alcohol to give carboxamide **16**, which was immediately utilized without further purification.

4-(4-(4-(4-methoxyphenyl)piperazin-1-yl)phenyl)-2,4-dihydro-3H-1,2,4-triazol-3-one (17). A solution of formamidine acetate (2.86 g, 27.5 mmol), **16** (2.1 g, 6.15 mmol), and acetic acid (4 mL) in anhydrous DMF (30 mL) was stirred at 130°C for 3 h. The mixture was cooled to room temperature and diluted with H_2O (100 mL) at which point a light brown precipitate formed. The solid was filtered and washed with $CHCl_3$ to provide triazolone **17**, which was immediately utilized without further purification.

4-(4-(4-nitrophenyl)piperazin-1-yl)phenol (44). N-(4-hydroxyphenyl)-piperazine (5.3 g, 29.7 mmol), 1-chloro-4-nitrobenzene (6.57 g, 41.7 mmol), and DIPEA (7.74 mL, 44.4 mmol) were dissolved in 50 mL anhydrous NMP and heated to 125°C for 12 h. The reaction was cooled to 80°C and isopropanol (250 mL) was added portion wise over 30 mins. The reaction mixture was cooled to room temperature and precipitate started to form. The reaction was further cooled to -20°C and stirred for 30 mins. The precipitate was vacuum filtered and washed with cold isopropanol to give the product, a brown powder, in quantitative yield. Characterization matched that previously reported.[1]

Side Chain Intermediates

(*R*)-*sec*-butyl 4-bromobenzenesulfonate (20). (*R*)-2-butanol (**18**) (3.0 g, 40.5 mmol), Et_3N (12.0 mL, 13.5 mmol), and DMAP (5.0 g, 40.5 mmol) in DCM. Cool the reaction to 0°C and slowly add a solution of 4-bromobenzene-1-sulfonylchloride (22.7 g, 89.1 mmol) in DCM. The mixture was stirred at 0°C for 4h. Dilute the reaction with H_2O and extract with DCM. Combine the organic layers, dry over sodium sulfate, filter, and concentrate. The crude residue was purified by column chromatography (SiO_2, 0-2% EtOAc in hexanes) to afford the product (37.9%, 4.5 g). ^1H NMR (500 MHz, $CDCl_3$) δ 7.68 (m, 2H), 7.57 (m, 2H), 4.47 (m, 1H), 1.45 (m, 2H), 1.15 – 1.09 (m, 3H), 0.65 (m, 3H). ^{13}C NMR (126 MHz, $CDCl_3$) δ 137.12, 132.83, 129.53, 128.95, 83.03, 31.99, 29.88, 23.05, 20.76, 14.51, 9.71. DART-HRMS: *m/z* calcd. for $C_{10}H_{13}BrO_3S$ $[MH]^+$, 294.9827; Found: 294.9822. IR (solid) *v*max: 2954, 2930, 2869, 1588, 1463, 1376, 1364, 1313, 1224, 1188, 1093, 1070, 1034, 942, 903, 821, 752. $[\alpha]_D^{20}$ = -16.0 (c = 1.984, MeOH).

(*S*)-*sec*-butyl 4-bromobenzenesulfonate (21). (*S*)-(+)-2-butanol (**19**) (3.0 g, 40.5 mmol), Et_3N (12.0 mL, 13.5 mmol), and DMAP (5.0 g, 40.5 mmol) in DCM. Cool the reaction to 0°C and slowly add a solution of 4-bromobenzene-1-sulfonylchloride (22.7 g, 89.1 mmol) in DCM. The mixture was stirred at 0°C for 4h. Dilute the reaction with H_2O and extract with DCM. Combine the organic layers, dry over sodium sulfate, filter, and concentrate. The crude residue was purified by column chromatography (SiO_2, 0-2% EtOAc in hexanes) to afford the product (53.9%, 6.4 g). ^1H NMR (500 MHz, $CDCl_3$) δ 7.84 – 7.72 (m, 2H), 7.65 (m, 2H), 4.57 (m, 1H), 1.56 (m, 2H), 1.32 – 1.19 (m, 3H), 0.77 (m, 3H). ^{13}C NMR (126 MHz, $CDCl_3$) δ 136.56, 132.31, 129.00, 128.40, 82.50, 60.22, 31.43, 29.33, 20.21, 14.07, 9.16. DART-HRMS: *m/z* calcd. for $C_{10}H_{13}BrO_3S$ $[MH]^+$,

294.9827; Found: 294.9856. IR (solid) *v*max: 3090, 2975, 2937, 2880, 1576, 1501, 1471, 1389, 1361, 1226, 1185, 1112, 1090, 1068, 994, 895, 819, 751, 608. $[\alpha]_D^{20}$ = +11.5 (c = 4.466, MeOH).

Linker/Triazolone/Side Chain Intermediates.

General Protocol for alkylation of triazolone (propyl- or *sec*-butyl-substitutions) (24-27). To a suspension of triazolone **17** (1.0 g, 2.8 mmol) in anhydrous NMP (30 mL) was added Cs_2CO_3 (2.74 g, 8.4 mmol), and an alkylating agent (**20-23**) (8.4 - 14 mmol). The mixture was stirred at RT for 2 h, then warmed to 60º C for 12 h and finally to 110º C for 4h. The mixture was then cooled to RT, diluted with water (125 mL), and extracted with EtOAc (3 X 150 mL). The organic layers were combined, dried ($MgSO_4$), filtered, and concentrated. The crude residue was purified by column chromatography (SiO_2, 0 to 20% EtOAc in Hex) to afford **24-27** as off-white solids (45-88%). Compounds were further purified as needed via recrystallization (EtOH) to remove a "grease-like" impurity (observed in ^{1}H NMRs at 0.88, 1.31 ppm).

(*S*)-2-(*sec*-butyl)-4-(4-(4-(4-methoxyphenyl)piperazin-1-yl)phenyl)-2,4-dihydro-3*H*-1,2,4-triazol-3-one (24). ^{1}H NMR (500 MHz, $CDCl_3$) δ 7.61 (s, 1H), 7.46 – 7.40 (m, 2H), 7.03 (d, *J* = 9.0 Hz, 2H), 6.96 (d, *J* = 9.0 Hz, 2H), 6.90 – 6.84 (m, 2H), 4.35 – 4.24 (m, 1H), 3.78 (s, 3H), 3.37 (m, 4H), 3.23 (m, 4H), 1.86 (m, 1H), 1.78 – 1.66 (m, 1H), 1.39 (d, *J* = 6.7 Hz, 3H), 0.91 (t, *J* = 7.4 Hz, 3H). ^{13}C NMR (126 MHz, $CDCl_3$) δ 154.24, 152.07, 150.60, 145.53, 133.91, 125.96, 123.55, 118.63, 116.66, 114.57, 55.61, 52.72, 50.83, 49.31, 28.47, 19.25, 10.80. DART-HRMS: *m/z* calcd. for $C_{23}H_{29}N_5O_2$ $[MH]^+$, 408.2400; Found: 408.2368. IR (solid) *v*max: 3120, 3053, 2967, 2935, 2877, 2821, 2765, 1686,

1549, 1507, 1446, 1388, 1240, 1222, 1154, 1117, 1030, 943, 823, 805, 720. $[\alpha]_D^{20}$ = + 12.6 (c = 0.996, DMSO).

(*R*)-2-(*sec*-butyl)-4-(4-(4-(4-methoxyphenyl)piperazin-1-yl)phenyl)-2,4-dihydro-3*H*-1,2,4-triazol-3-one (25). ^{1}H NMR (500 MHz, $CHCl_3$) δ 7.61 (s, 1H), 7.47 – 7.40 (m, 2H), 7.06 – 6.99 (m, 2H), 6.96 (m, 3H), 6.90 – 6.84 (m, 2H), 4.30 (m, 1H), 3.78 (d, *J* = 1.3 Hz, 2H), 3.40 – 3.28 (m, 4H), 3.24 (m, 4H), 1.94 – 1.76 (m, 1H), 1.78 – 1.67 (m, 1H), 1.39 (d, *J* = 6.7 Hz, 2H), 0.91 (t, *J* = 7.4 Hz, 2H). ^{13}C NMR (126 MHz, $CDCl_3$) δ 154.21, 152.06, 150.58, 145.50, 133.94, 125.94, 123.54, 118.62, 116.65, 114.55, 55.60, 52.70, 50.81, 49.29, 28.47, 19.29, 10.83. DART-HRMS: *m/z* calcd. for $C_{23}H_{29}N_5O_2$ $[MH]^+$, 408.2400; Found: 408.2430. IR (solid) *v*max: 3120, 3052, 2967, 2821, 1686, 1549, 1507, 1444, 1386, 1240, 1221, 1030, 943, 824, 805, 719, 530. $[\alpha]_D^{20}$ = -12.2 (c = 0.873, DMSO).

2-(*sec*-butyl)-4-(4-(4-(4-methoxyphenyl)piperazin-1-yl)phenyl)-2,4-dihydro-3H-1,2,4-triazol-3-one (26). ^{1}H NMR (500 MHz, $CDCl_3$) δ 7.67 (d, *J* = 0.6 Hz, 1H), 7.51 – 7.43 (m, 2H), 7.11 – 7.04 (m, 2H), 7.04 – 6.97 (m, 2H), 6.96 – 6.88 (m, 2H), 4.34 (m, 1H), 3.83 (s, 3H), 3.44 – 3.38 (m, 4H), 3.31 – 3.25 (m, 4H), 1.91 (m, 1H), 1.83 – 1.70 (m, 1H), 1.44 (d, *J* = 6.8 Hz, 3H), 0.95 (t, *J* = 7.4 Hz, 3H). ^{13}C NMR (126 MHz, $CDCl_3$) δ 154.22, 152.07, 150.60, 133.98, 125.92, 123.59, 118.66, 116.69, 114.54, 55.61, 52.69, 50.85, 49.29, 32.36, 28.49, 19.33, 10.85. DART-HRMS: *m/z* calcd. for $C_{23}H_{29}N_5O_2$ $[MH]^+$, 408.2400; Found: 408.2388. IR (solid) *v*max: 3120, 3053, 2970, 2877, 2818, 2763, 1686, 1548, 1508, 1444, 1399, 1241, 1223, 1030, 943, 823, 805.

4-(4-(4-(4-methoxyphenyl)piperazin-1-yl)phenyl)-2-propyl-2,4-dihydro-3H-1,2,4-triazol-3-one (27): ^{1}H NMR (500 MHz, $CDCl_3$) δ 7.65 (s, 1H), 7.50 – 7.43 (m, 2H), 7.04

– 6.97 (m, 2H), 6.96 – 6.88 (m, 2H), 3.86 (m, 2H), 3.83 (s, 3H), 3.44 – 3.38 (m, 4H), 3.31 – 3.25 (m, 4H), 1.89 (m, 2H), 1.03 (t, *J* = 7.4 Hz, 3H). ^{13}C NMR (126 MHz, $CDCl_3$) δ 154.22, 152.22, 150.66, 145.51, 133.93, 125.87, 123.60, 118.64, 116.67, 114.55, 55.61, 50.83, 49.28, 47.23, 22.06, 11.13. DART-HRMS: *m/z* calcd. for $C_{22}H_{27}N_5O_2$ $[MH]^+$, 394.2243; Found: 394.2265. IR (solid) *v*max: 3122, 3053, 2956, 2873, 2830, 1686, 1555, 1511, 1451, 1409, 1390, 1250, 1225, 1032, 942, 813, 733.

General Protocol for phenol synthesis (demethylation protocol) (28-31). Hydrogen bromide (48% aqueous solution, 10 mL) was added to a solution of methoxy-alkyl substituted triazolone **24-27** (500 mg, 1.2 mmol) in toluene (6 mL) was refluxed for 6-12 h. The reaction was cooled to RT and water (10 mL) was added. The precipitate that formed was collected by filtration and washed with copious amounts of water. ^{1}H NMR analysis indicated pure phenol in good yields (55-80%). The filtrate was neutralized with saturated $NaHCO_3$ and washed with EtOAc (2 X 150 mL). The organic layers were dried ($MgSO_4$), filtered, and concentrated to afford remaining phenol (**28-31**) in moderate purity that required chromatography.

(*S*)-2-(*sec*-butyl)-4-(4-(4-(4-hydroxyphenyl)piperazin-1-yl)phenyl)-2,4-dihydro-3*H*-1,2,4-triazol-3-one (28). ^{1}H NMR (500 MHz, DMSO) δ 8.38 (s, 1H), 7.58 (m, 2H), 7.53 (s, 1H), 7.19 (m, 2H), 6.91 (d, *J* = 8.4 Hz, 2H), 4.13 (m, 1H), 3.67 (s, 8H), 1.71 (m, 2H), 1.31 (d, *J* = 6.7 Hz, 3H), 0.81 (t, *J* = 6.6 Hz, 3H). ^{13}C NMR (126 MHz, DMSO) δ 161.5, 151.2, 148.5, 134.9, 126.4, 122.9, 122.0, 116.2, 116.1, 53.8, 51.7, 46.4, 27.8, 19.2, 10.5. DART-HRMS: *m/z* calcd. for $C_{22}H_{28}N_5O_2$ $[MH]^+$, 394.2243; Found: 394.2216. IR (solid) *v*max 3331, 2958, 2875, 2832, 2807, 1688, 1509, 1448, 1385, 1222, 1181, 1152, 965, 824, 741, 729. $[\alpha]_D^{20}$ = +13.0 (c = 0.994, DMSO).

(*R*)-2-(*sec*-butyl)-4-(4-(4-(4-hydroxyphenyl)piperazin-1-yl)phenyl)-2,4-dihydro-3*H*-1,2,4-triazol-3-one (29). ^{1}H NMR (500 MHz, DMSO) δ 8.38 (s, 1H), 7.58 (d, *J* = 8.9 Hz, 2H), 7.48 (s, 1H), 7.19 (d, *J* = 8.9 Hz, 2H), 6.89 (m, 2H), 4.14 (m, 1H), 3.62 (s, 8H), 1.70 (m, 2H), 1.31 (d, *J* = 6.7 Hz, 3H), 0.82 (t, *J* = 7.4 Hz, 3H). ^{13}C NMR (126 MHz, DMSO) δ 157.2, 151.4, 148.6, 135.1, 126.4, 123.1, 122.1, 122.0, 116.4, 116.3, 53.9, 51.9, 46.6, 28.0, 19.3, 10.7. DART-HRMS: *m/z* calcd. for $C_{22}H_{28}N_5O_2$ $[MH]^+$, 394.2243; Found: 394.2212. IR (solid) *v*max: 3241, 3055, 2965, 2928, 2855, 1670, 1509, 1451, 1378, 1234, 1185, 1110, 967, 921, 832, 807, 746. $[\alpha]_D^{20}$ = -13.7 (c = 1.254, DMSO).

2-(sec-butyl)-4-(4-(4-(4-hydroxyphenyl)piperazin-1-yl)phenyl)-2,4-dihydro-3H-1,2,4-triazol-3-one (30). ^{1}H NMR (500 MHz, $CDCl_3$) δ 7.61 (d, *J* = 0.6 Hz, 1H), 7.41 – 7.35 (m, 2H), 7.00 – 6.94 (m, 2H), 6.86 – 6.80 (m, 2H), 6.72 – 6.67 (m, 2H), 4.31 (m, 1H), 3.37 – 3.31 (m, 4H), 3.23 – 3.17 (m, 4H), 1.87 (m, 1H), 1.73 (m, 1H), 1.40 (d, *J* = 6.7 Hz, 3H), 0.91 (t, *J* = 7.4 Hz, 3H). ^{13}C NMR (126 MHz, $CDCl_3$) δ 152.72, 151.21, 151.13, 134.68, 125.80, 124.64, 119.18, 116.91, 116.38, 53.32, 51.44, 49.53, 28.85, 19.64, 11.18. DART-HRMS: *m/z* calcd. for $C_{22}H_{27}N_5O_2$ $[MH]^+$, 394.2243; Found: 394.2221. IR (solid) *v*max: 3333, 3058, 2959, 2876, 2833, 2809, 1690, 1509, 1449, 1385, 1224, 1182, 1153, 965, 825, 739.

4-(4-(4-(4-hydroxyphenyl)piperazin-1-yl)phenyl)-2-propyl-2,4-dihydro-3H-1,2,4-triazol-3-one (31): ^{1}H NMR (500 MHz, $CDCl_3$) δ 7.61 (s, 1H), 7.44 – 7.36 (m, 2H), 7.05 – 6.98 (m, 2H), 6.90 (d, *J* = 8.4 Hz, 2H), 6.80 – 6.73 (m, 2H), 3.82 (m, 2H), 3.37 (t, *J* = 5.0 Hz, 4H), 3.22 (m, 4H), 1.82 (m, 2H), 0.99 (t, *J* = 7.4 Hz, 3H). ^{13}C NMR (126 MHz, $CDCl_3$) δ 152.40, 150.78, 150.50, 134.14, 125.58, 124.03, 118.86, 116.60, 115.99, 51.03, 49.16, 47.33, 22.05, 11.12. DART-HRMS: *m/z* calcd. for $C_{21}H_{25}N_5O_2$ $[MH]^+$,

380.2087; Found: 380.2099. IR (solid) *v*max: 3344, 2969, 2934, 2893, 1466, 1378, 1365, 1185, 1160, 1127, 1104, 950, 815.

Dioxolane Region Intermediates.

1-(2,4-dichlorophenyl)-2-(1H-1,2,4-triazol-1-yl)ethan-1-one (38). A solution of 2-chloro-2',4'-dichlorophenylacetone (**34**) (10.0 g, 45.0 mmol), 1*H*-1,2,4-triazole (**35**) (6.2 g, 89.0 mmol), $NaHCO_3$ (6.1 g, 72.0 mmol), and toluene (100 mL) were heated to reflux (110-120°C) overnight. The reaction vessel was then placed in the -20°C freezer for ~6 h. The solid was filtered, dissolved in H_2O, and extracted with ethyl acetate (~50 mL x 3). The organic layer was collected, washed with brine, and dried over sodium sulfate. The solvent was evaporated and the remaining solid was washed with EtOAc/hexanes (1:1, 100 mL) resulting in a yellow solid (7.4 g, 64.2%). Characterization matched that previously reported.[2]

(2,2-dimethyl-1,3-dioxolan-4-yl)methyl 4-methylbenzenesulfonate (39a). DL-1,2-isopropylideneglycerol (**39**) (25 g, 89 mmol) was added to 300 mL of DCM with molecular sieves. Pyridine (30.5 g, 378 mmol) was then added to the mixture. The solution was cooled to 0°C and TsCl (54 g, 283.5 mmol) was added portion wise over 30 mins. The reaction stirred overnight at room temperature. The solution was washed with pH 2.0 H_2O (6M HCl) and brine. The organic layer was collected and concentrated. The crude product was purified via column chromatography (SiO_2, 0 - 25% EtOAc in hexanes) yielding a white solid in quantitative yield. Characterization matched that previously reported.[3]

2,3-dihydroxypropyl 4-methylbenzenesulfonate (40). Tosylated dioxolane **39a** (9.3 g) was dissolved in 300 mL of MeOH and 30 mL of 0.5N HCl was added to the solution.

The reaction was stirred and heated to reflux for 5h. The reaction was cooled to room temperature and neutralized to pH 7 with dropwise addition of saturated $NaHCO_3$. The solution was extracted (~150 mL x 1) with ethyl acetate and then washed with brine. The organic layers were collected, dried over sodium sulfate, filtered, and concentrated (7.7 g, 89.0%). Characterization matched that previously reported.[4]

(2-((1*H*-1, 2,4-triazol-1-yl) methyl)-2-(2,4-dichlorophenyl)-1,3-dioxolan-4-yl) methyl 4-methylbenzenesulfonate (43). Ketone **38** (2.0 g, 7.8 mmol) and **40** (1.98 g, 8.03 mmol) were added to a dry round bottom flask. Anhydrous toluene (15 mL) was added to the reaction. The reaction was cooled to 0°C and TfOH (2.8 mL, 31.9 mmol) was added dropwise with a glass syringe. The reaction was stirred at room temperature for 60 h. The mixture was diluted with 50 mL of ethyl acetate and slowly dropped into a solution of K_2CO_3 (5 g) in water (40 mL). The organic layer was separated with ethyl acetate (50 mL x 3). The organic layers were combined, dried over sodium sulfate, filtered, and concentrated to ~70 mL EtOAc. A solution of TsOH monohydrate (2.0 g) in EtOAc (13 mL) was slowly added at room temperature. The product precipitated as the salt (3.6 g, 70.3%). Characterization matched that previously reported.[5]

(*S*)-2,3-dihydroxypropyl 4-methylbenzenesulfonate. (*S*)-(+)-1,2-isopropylideneglycerol was tosylated following the above procedure for **39a** and was then subjected to the acid-mediated hydrolysis procedure for **40**. Characterization matched that previously reported.

(*R*)-2,3-dihydroxypropyl 4-methylbenzenesulfonate. (*R*)-(-)-1,2-isopropylideneglycerol was tosylated following the above procedure for **39a** and was

then subjected to the acid-mediated hydrolysis procedure for **40**. Characterization matched that previously reported.

Amide Region Intermediates

General Preparation of Benzyl Protected Esters. To a solution of ester phenol (500 mg, 3.2 mmol) in acetone (5 mL) was added potassium carbonate (anhydrous, 6 eq, 19.2 mmol) followed by benzyl bromide (2.5 eq, 8.2 mmol). The reaction was stirred for 12h at room temperature. The mixture was filtered over a celite pad, washed with EtOAc (30 mL), and concentrated under reduced pressure. The crude residue was purified via column chromatography (SiO_2, 5% EtOAc in hexanes) to afford benzyl protected esters.

General Preparation of Benzyl Protected Acids. To a solution of ester (500 mg, 2.1 mmol) in H_2O: THF (3 mL: 9 mL) lithium hydroxide (monohydrate, 3 eq, 6.3 mmol) was added to the reaction. The reaction mixture was refluxed for 12h at which time it was neutralized and then acidified with 1M HCl. The aqueous mixture was extracted with EtOAc (3 x 50 mL). The combined organic layers were dried, filtered, and concentrated under reduced pressure. The crude residue was purified by column chromatography (SiO_2, 30 – 50 % EtOAc in hexanes) to afford benzyl protected esters.

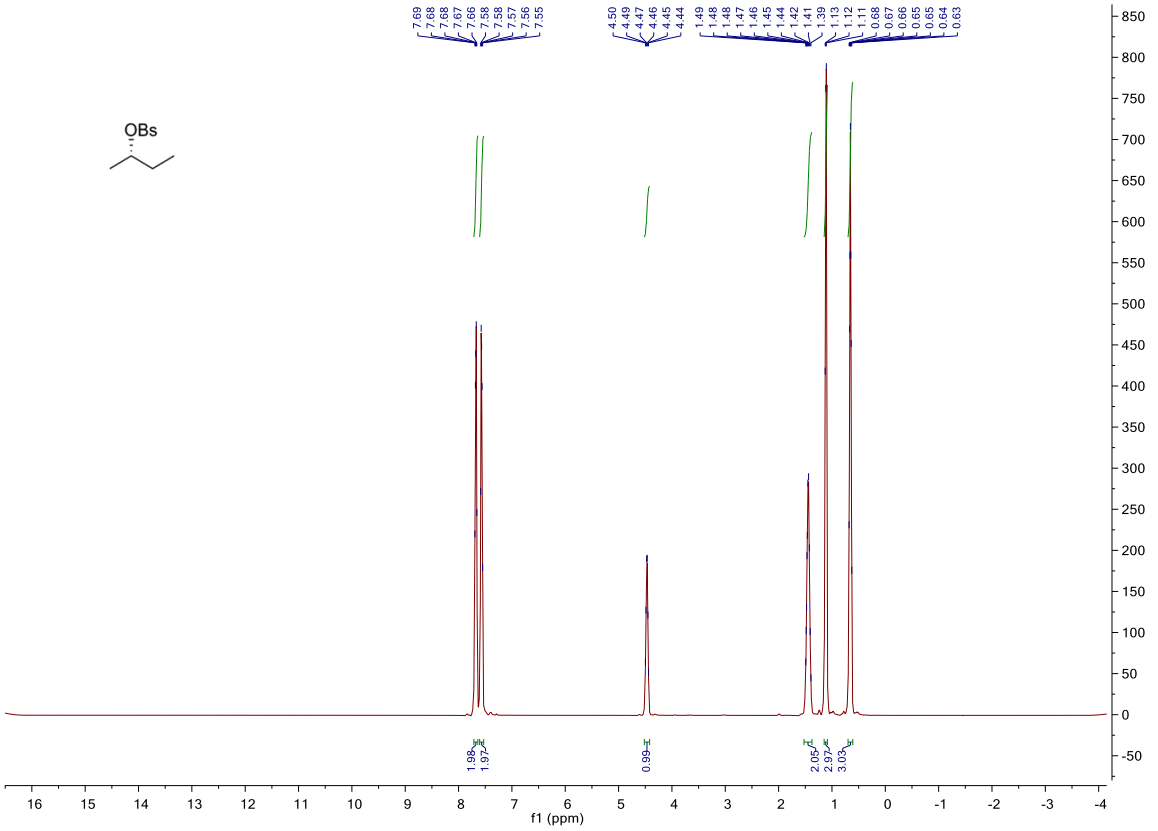
OBs
7.69
7.68
7.68
7.67
7.67
7.66
7.58
7.58
7.57
7.57
7.56
7.56
7.55
4.50
4.49
4.49
4.47
4.47
4.46
4.45
4.44
4.44
1.49
1.48
1.48
1.47
1.46
1.45
1.44
1.42
1.41
1.39
1.13
1.12
1.11
0.68
0.67
0.66
0.65
0.65
0.64
0.63
1.98
1.97
0.99
2.05
2.97
3.03
f1 (ppm)

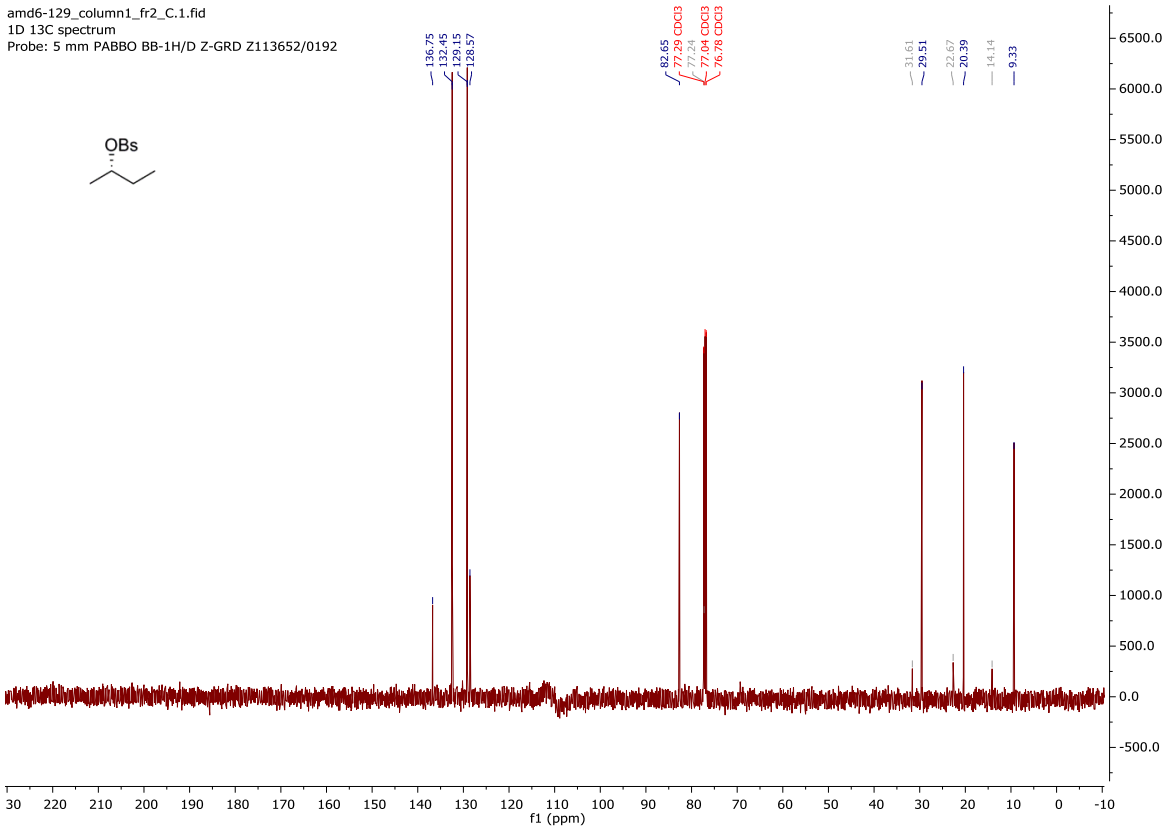
amd6-129_column1_fr2_C.1.fid
1D 13C spectrum
Probe: 5 mm PABBO BB-1H/D Z-GRD Z113652/0192
OBs
136.75
132.45
129.15
128.57
82.65
77.29 CDCl3
77.24
77.04 CDCl3
76.78 CDCl3
31.61
29.51
22.67
20.39
14.14
9.33
f1 (ppm)

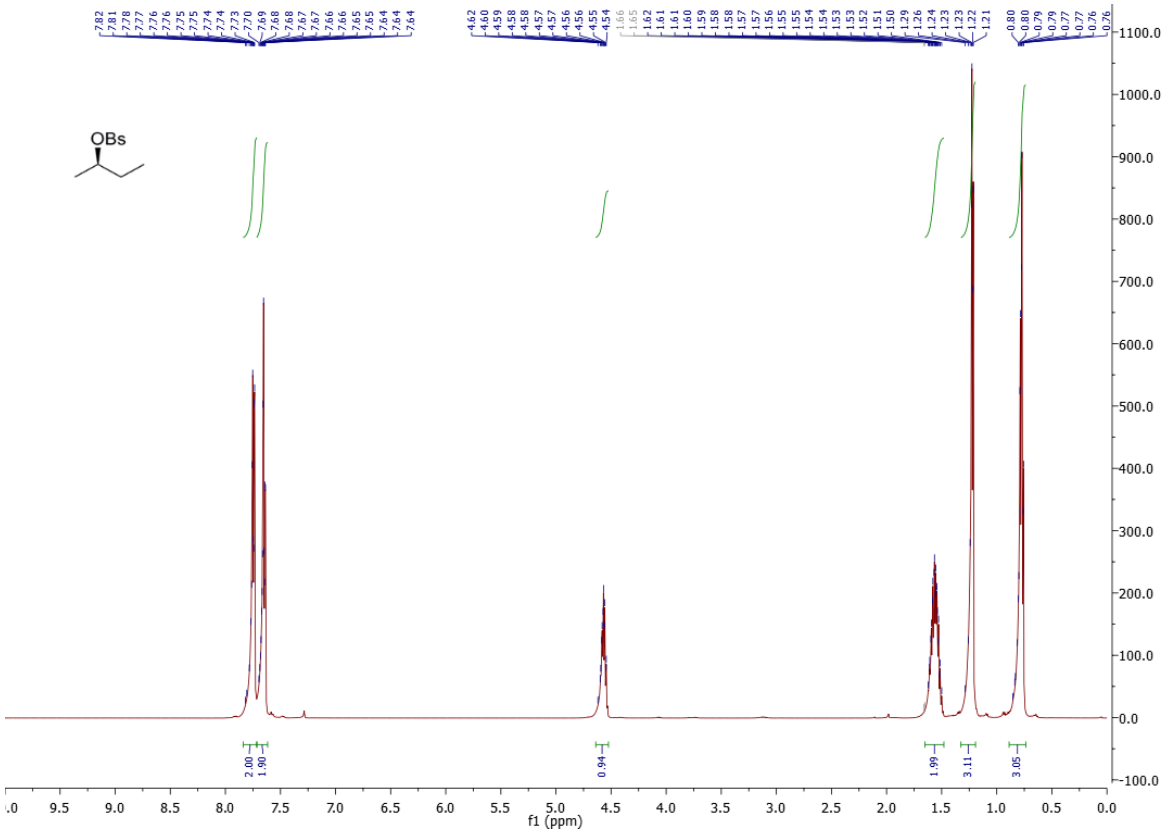
OBs
f1 (ppm)

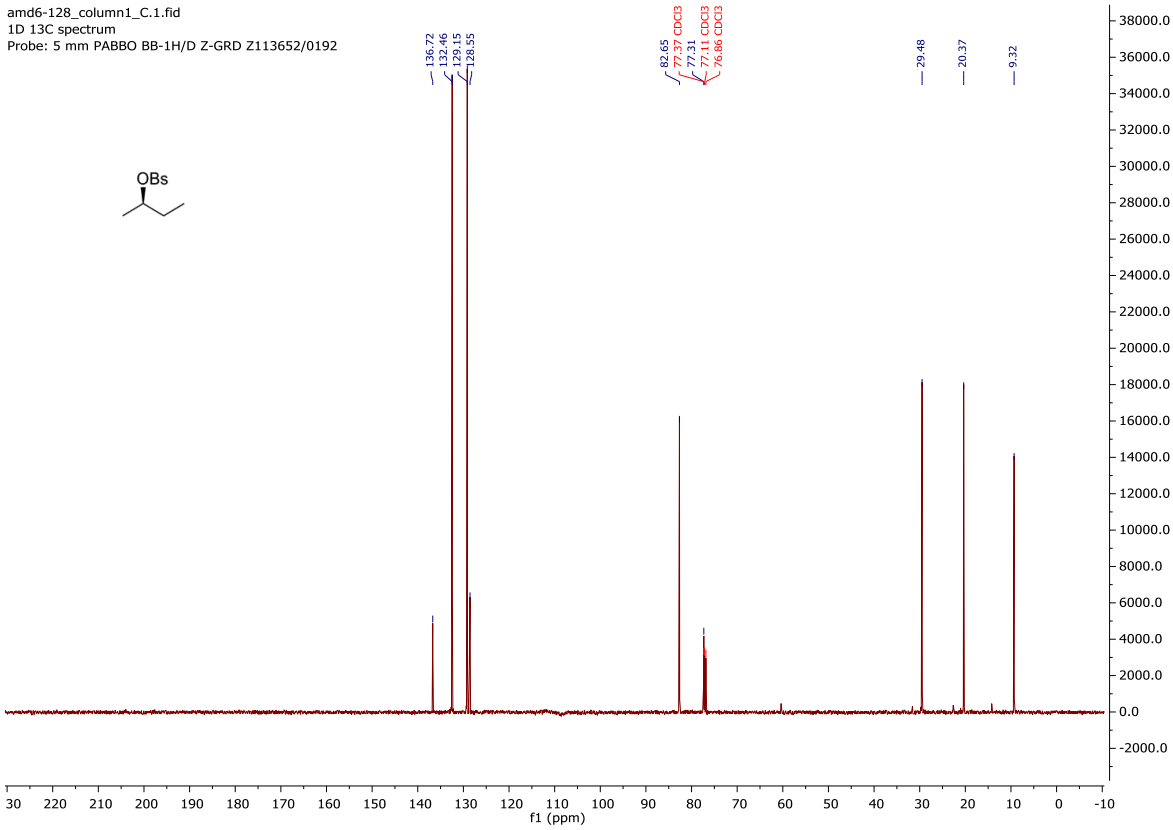
amd6-128_column1_C.1.fid
1D 13C spectrum
Probe: 5 mm PABBO BB-1H/D Z-GRD Z113652/0192
OBs
f1 (ppm)

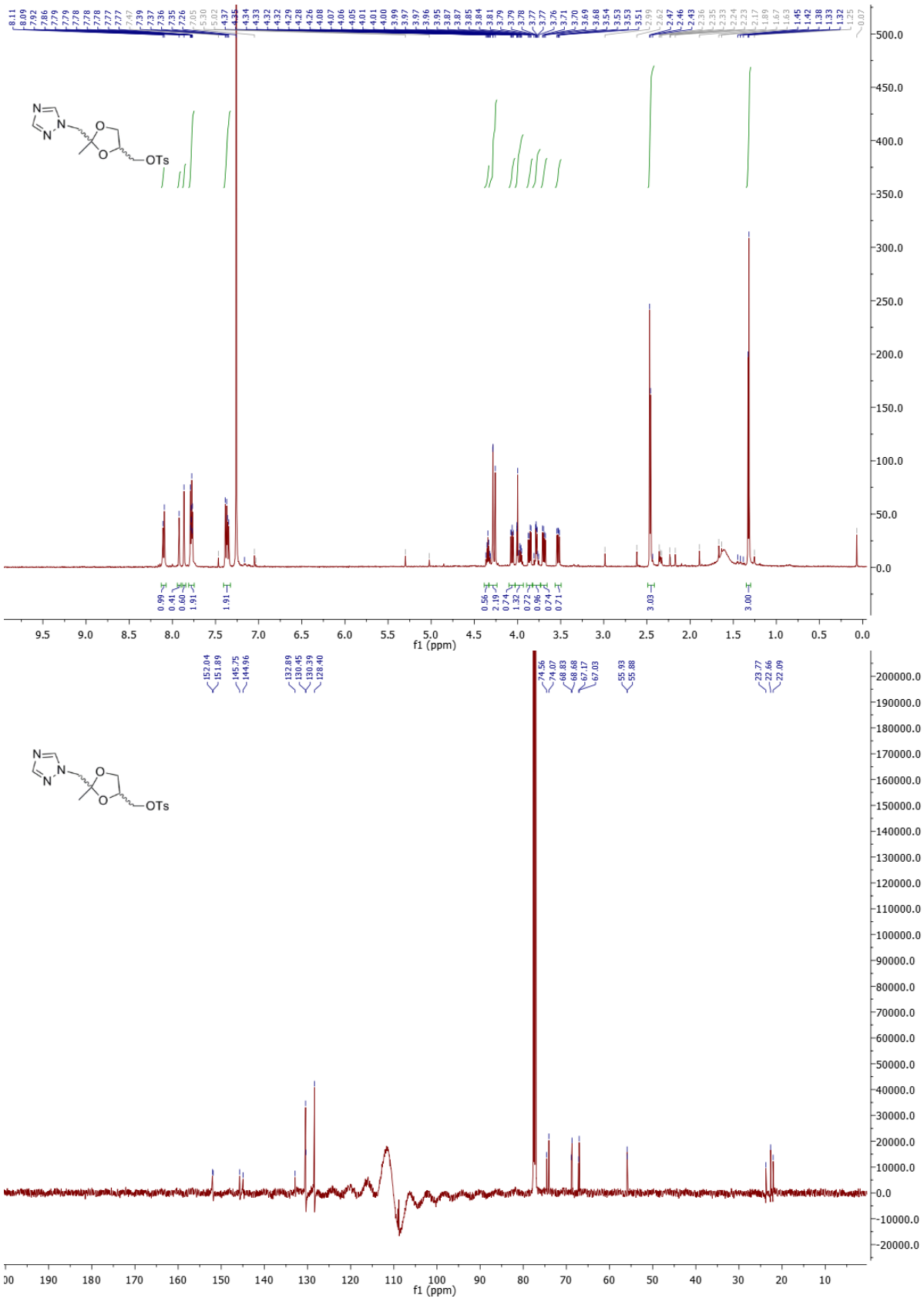
OTs
f1 (ppm)
OTs
f1 (ppm)

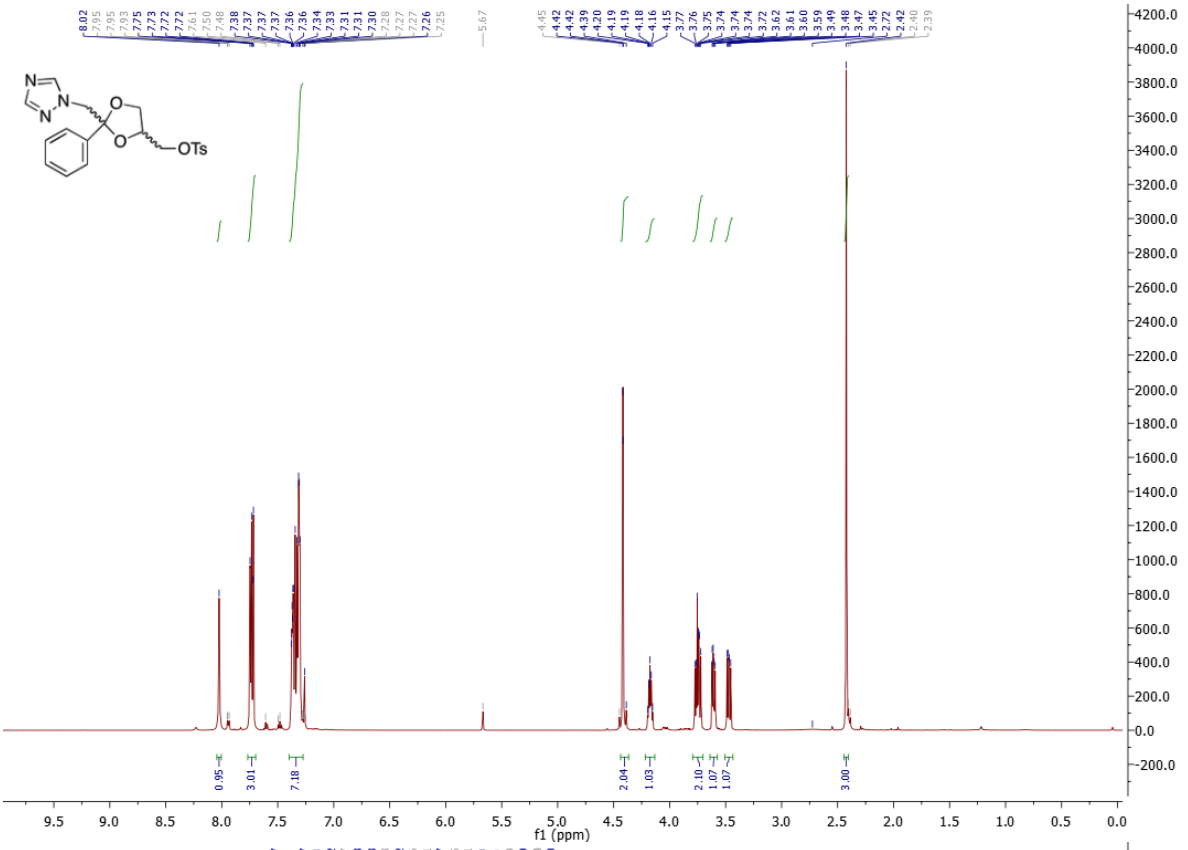
OTs
f1 (ppm)

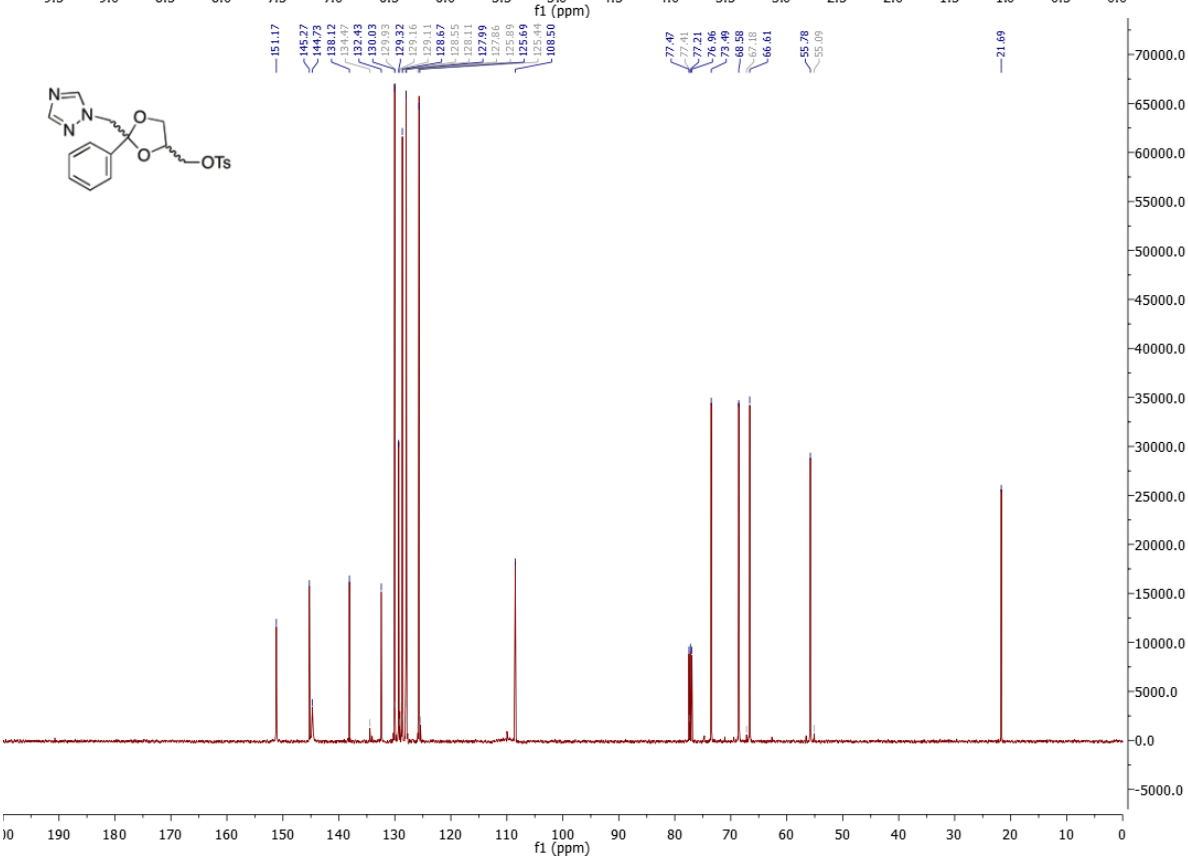
OTs
f1 (ppm)

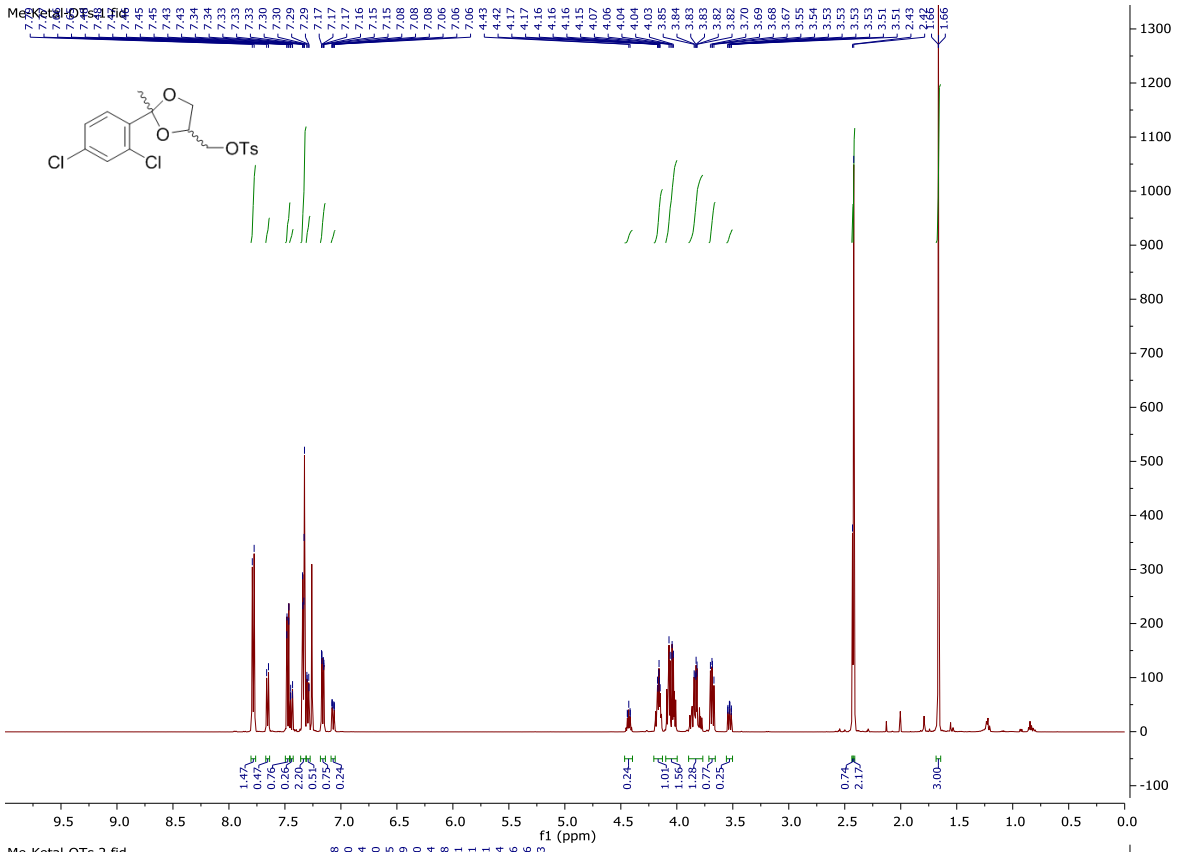
Me-Ketal-OTs.1.fid
Cl
Cl
O
O
OTs
f1 (ppm)

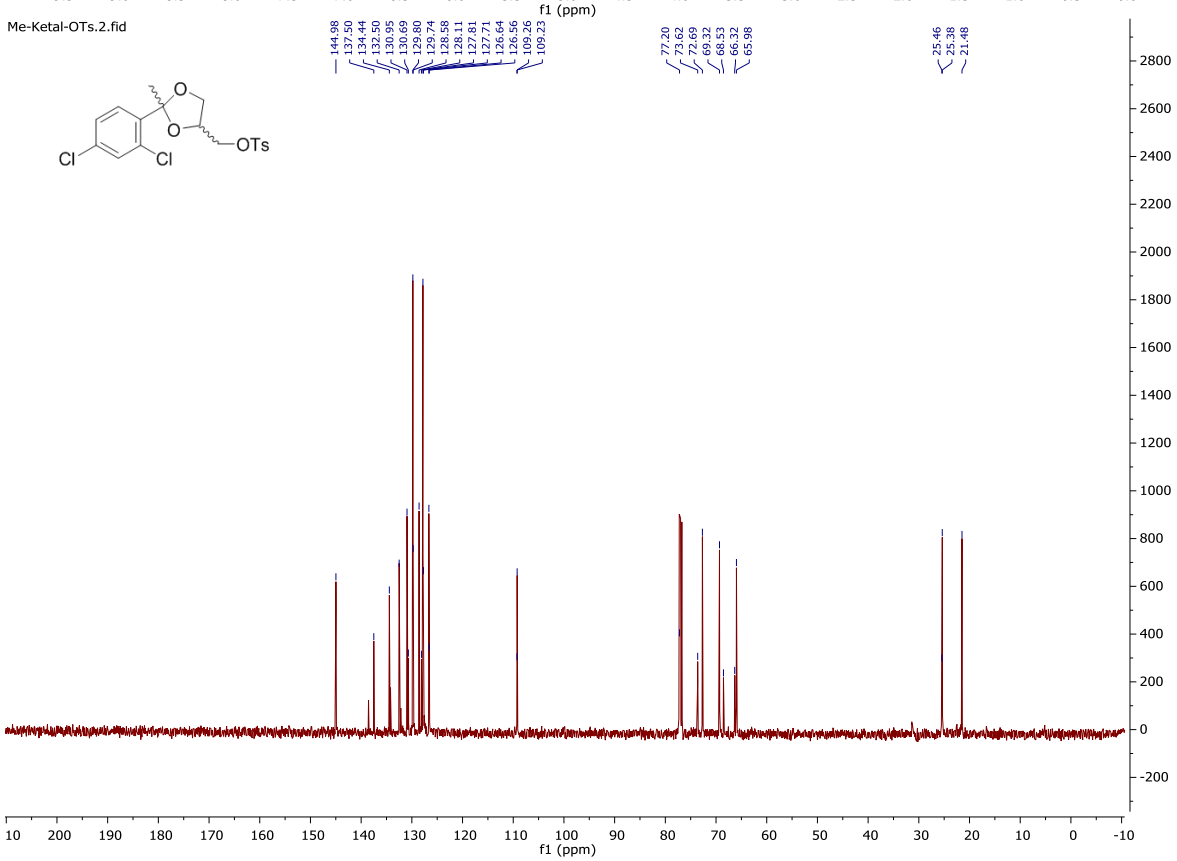
Me-Ketal-OTs.2.fid
Cl
Cl
O
O
OTs
f1 (ppm)

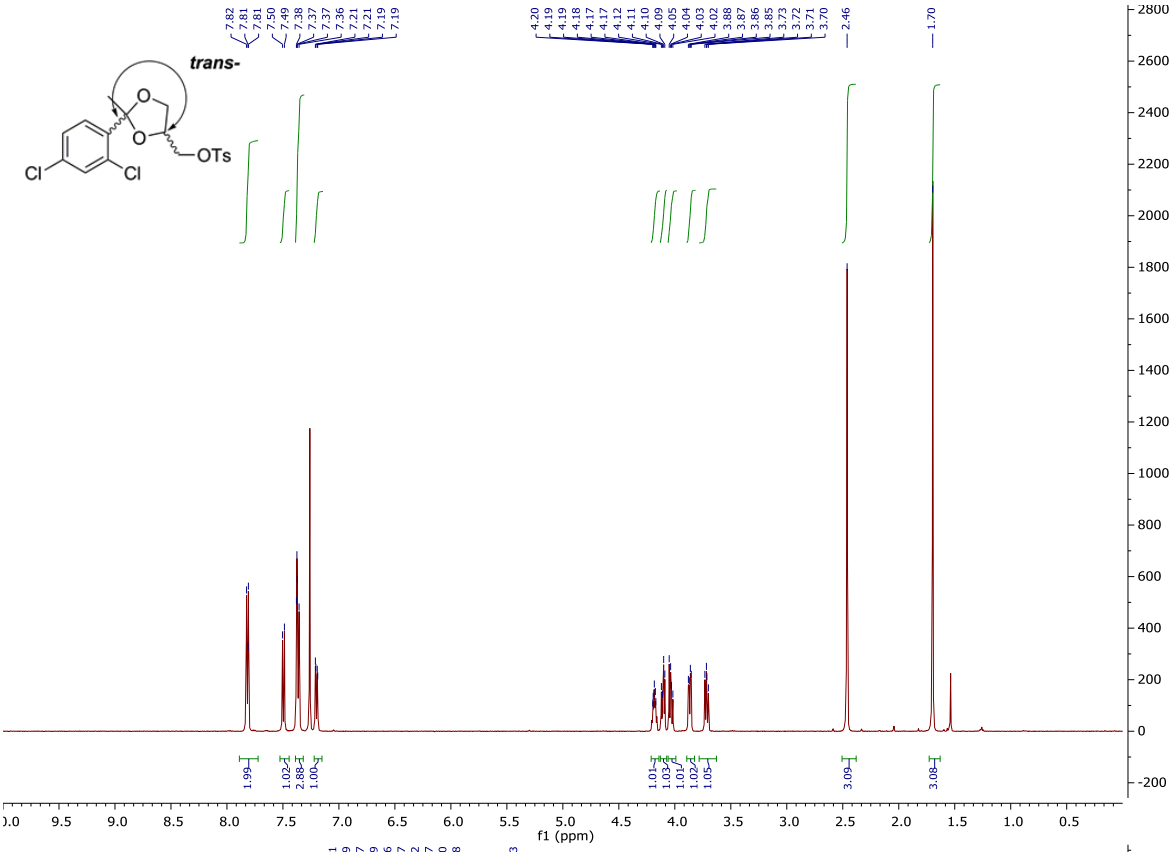
trans-
O
O
OTs
Cl
Cl
7.82
7.81
7.81
7.50
7.49
7.38
7.37
7.37
7.36
7.21
7.21
7.19
7.19
4.20
4.19
4.19
4.18
4.17
4.17
4.12
4.11
4.10
4.09
4.05
4.04
4.03
4.02
3.88
3.87
3.86
3.85
3.73
3.72
3.71
3.70
2.46
1.70
1.99
1.02
2.88
1.00
1.01
1.03
1.01
1.02
1.05
3.09
3.08
f1 (ppm)

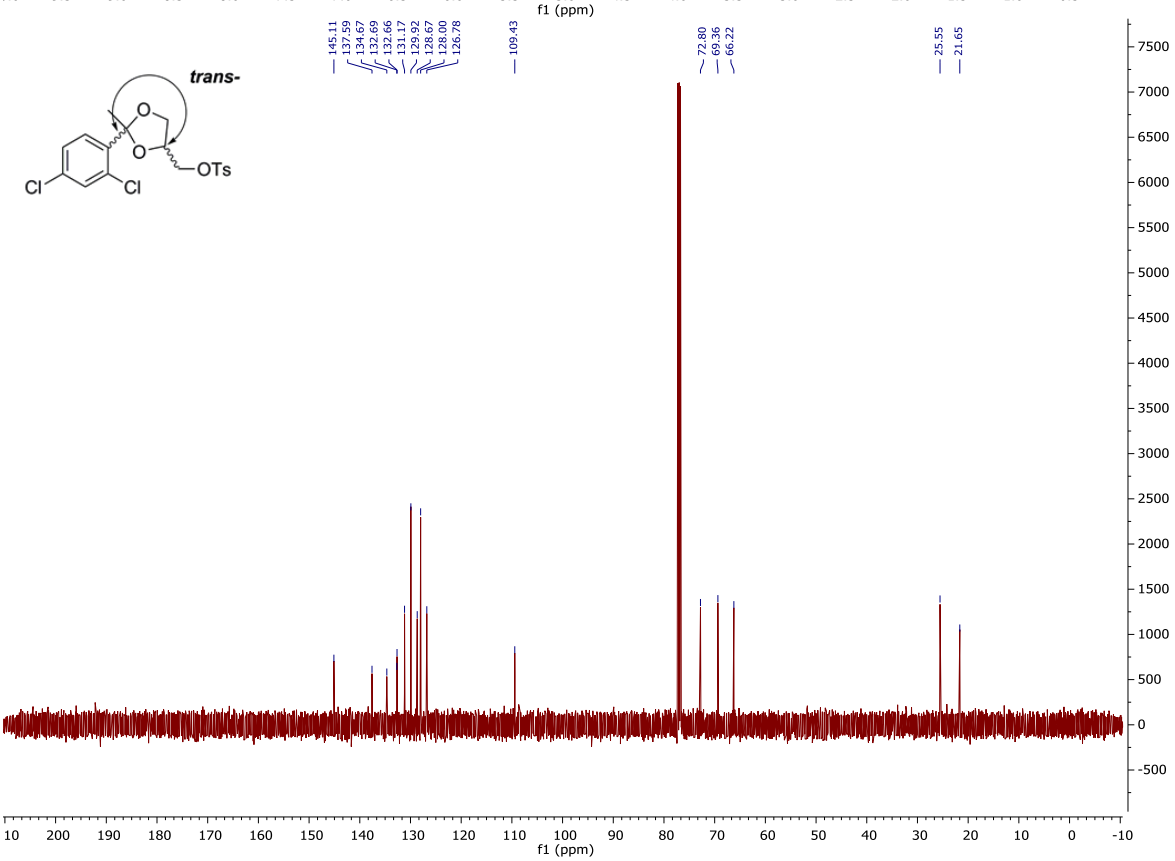
trans-
O
O
OTs
Cl
Cl
145.11
137.59
134.67
132.69
132.66
131.17
129.92
128.67
128.00
126.78
109.43
72.80
69.36
66.22
25.55
21.65
f1 (ppm)

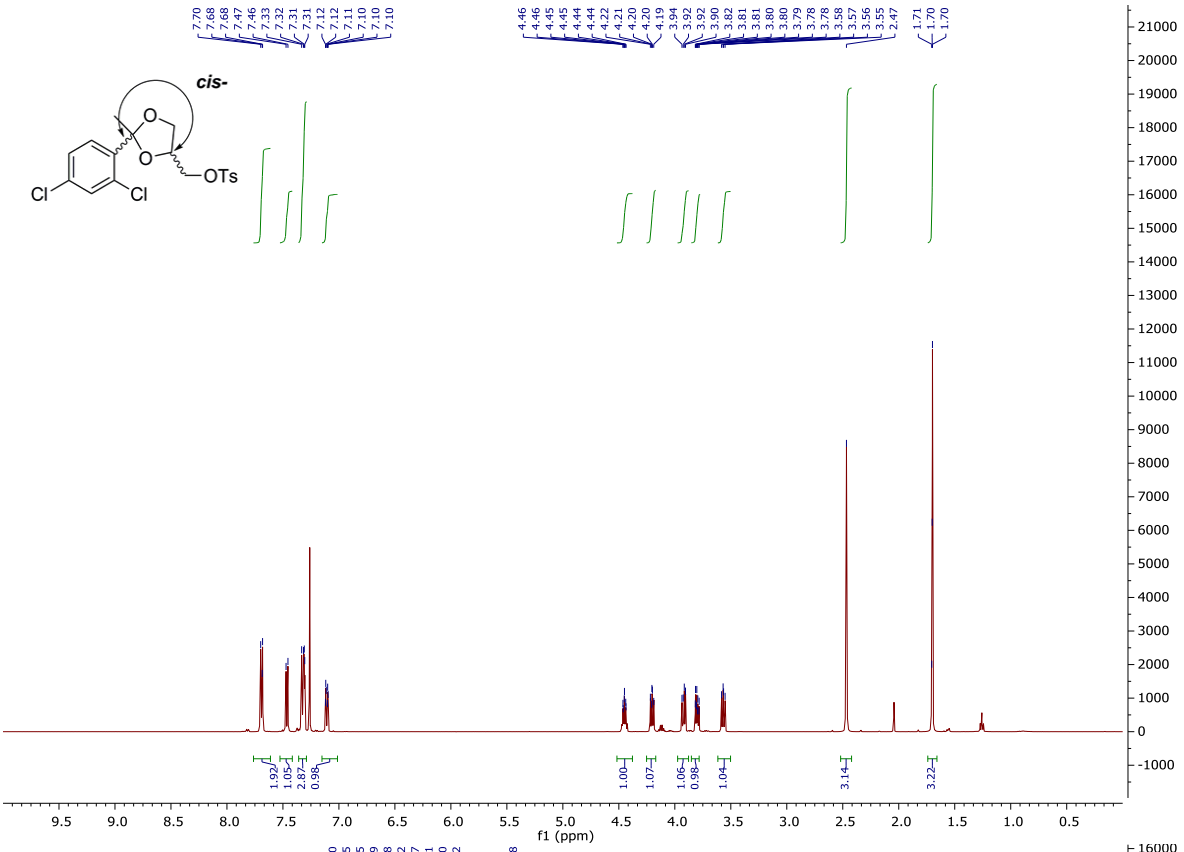
cis-
Cl
Cl
OTs
f1 (ppm)

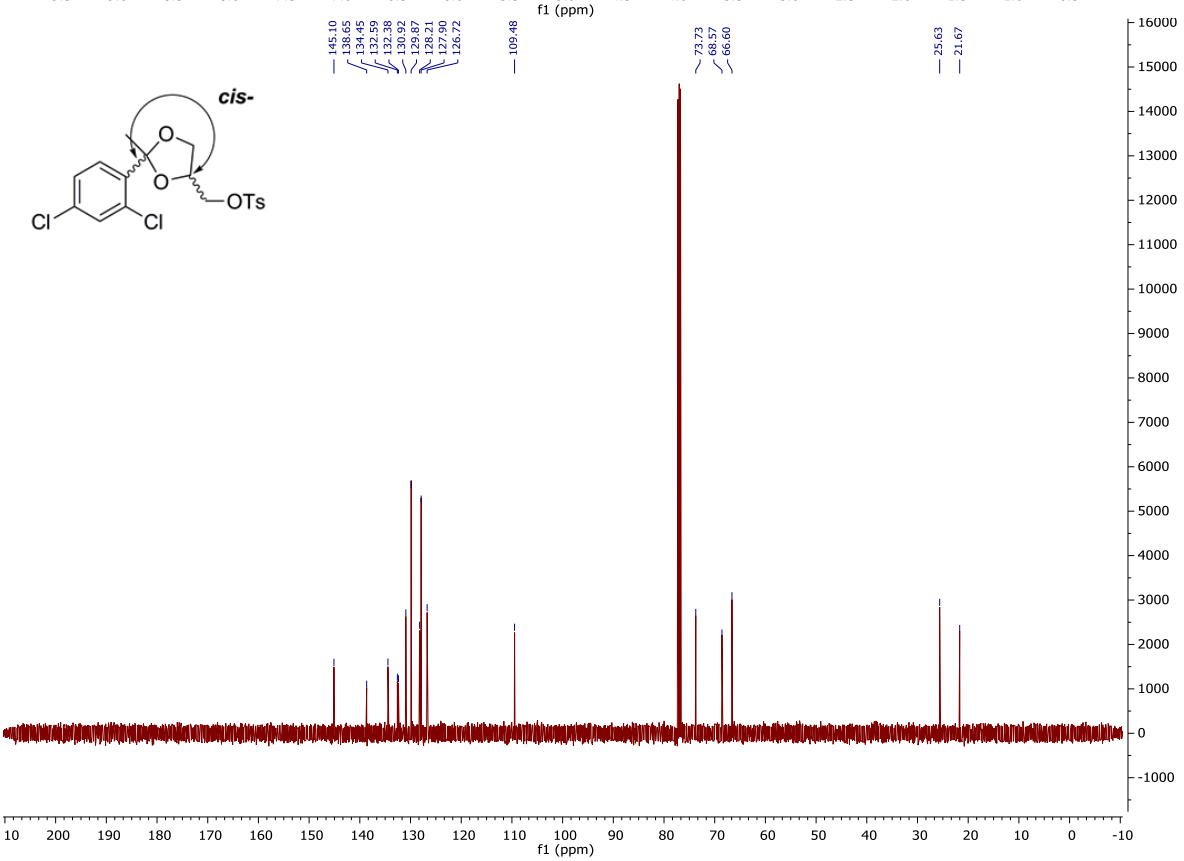
cis-
Cl
Cl
OTs
f1 (ppm)

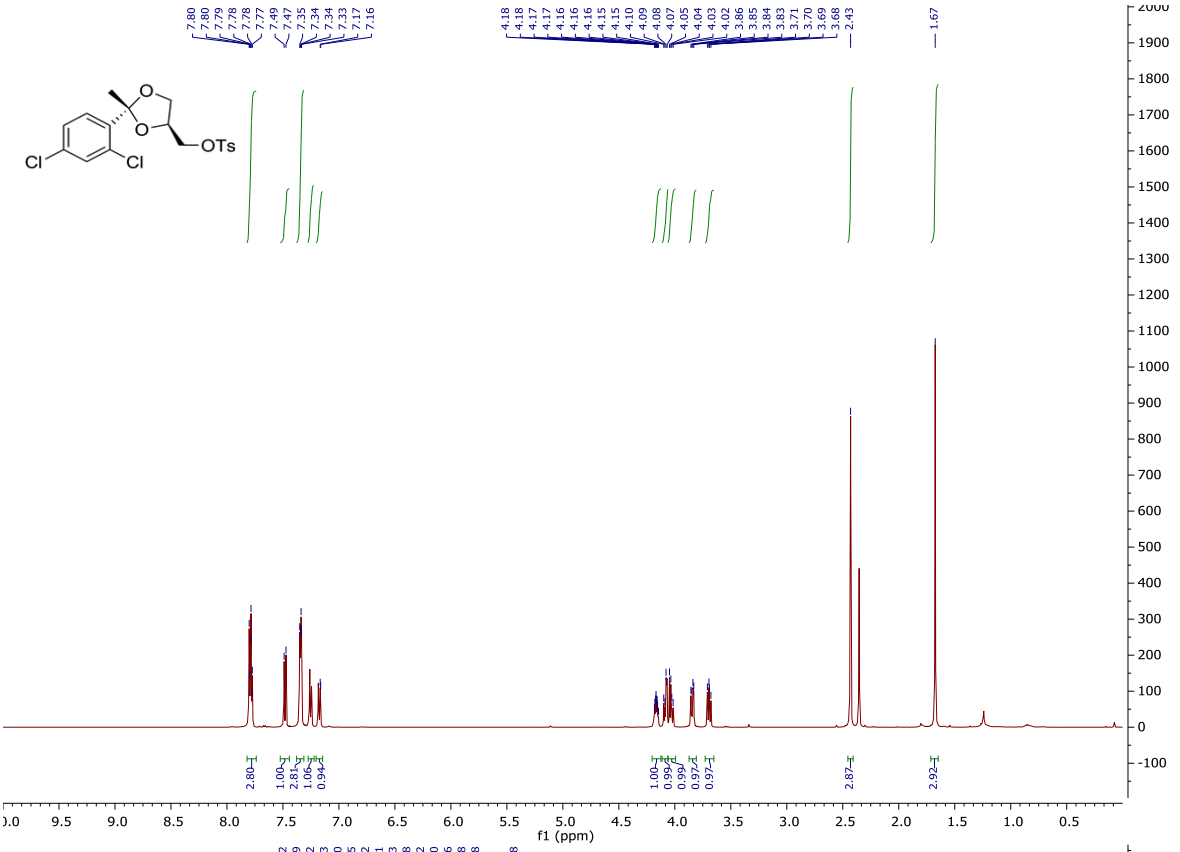
7.80
7.80
7.79
7.78
7.78
7.77
7.49
7.47
7.35
7.34
7.34
7.33
7.17
7.16
4.18
4.18
4.17
4.17
4.16
4.16
4.16
4.15
4.15
4.10
4.09
4.08
4.07
4.05
4.04
4.03
4.02
3.86
3.85
3.84
3.83
3.71
3.70
3.69
3.68
2.43
1.67
OTs
Cl
Cl
2.80
1.00
2.81
1.06
0.94
1.00
0.99
0.99
0.97
0.97
2.87
2.92
f1 (ppm)

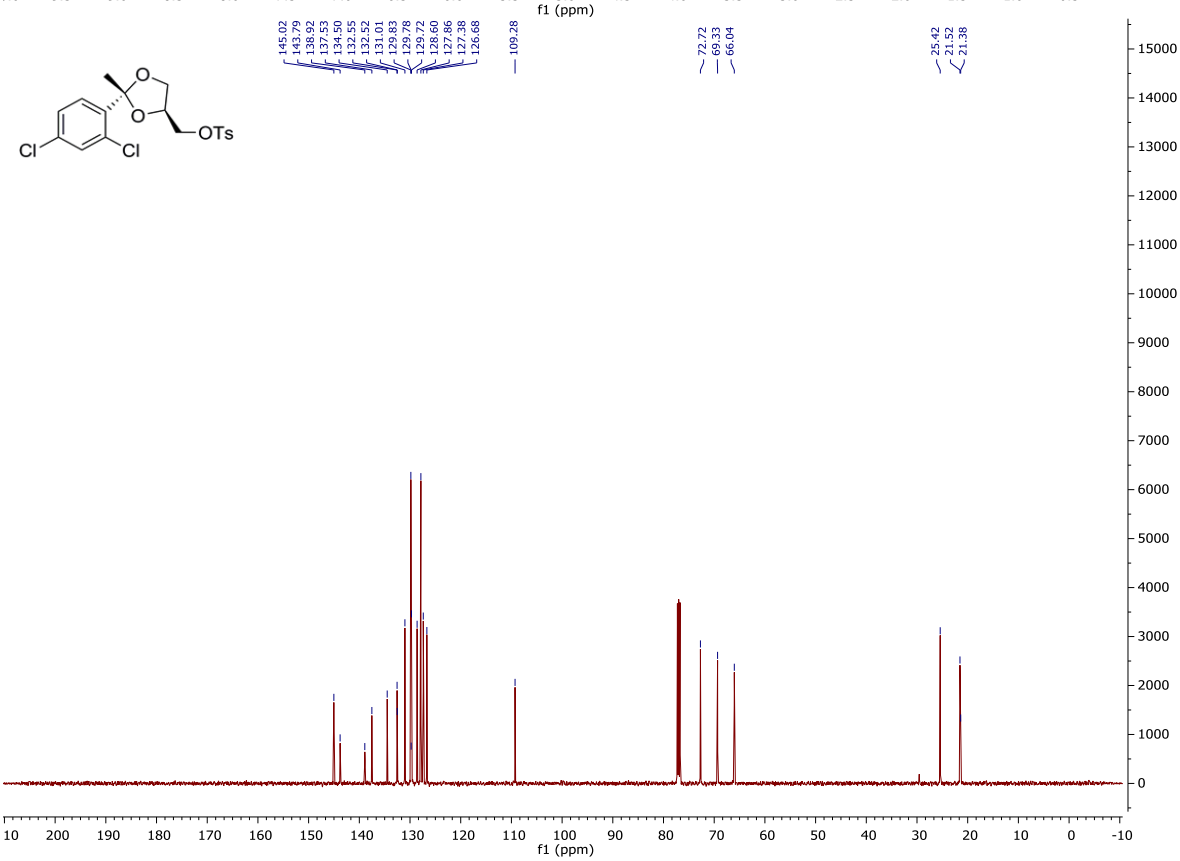
145.02
143.79
138.92
137.53
134.50
132.55
132.52
131.01
129.83
129.78
129.72
128.60
127.86
127.38
126.68
109.28
72.72
69.33
66.04
25.42
21.52
21.38
OTs
Cl
Cl
f1 (ppm)

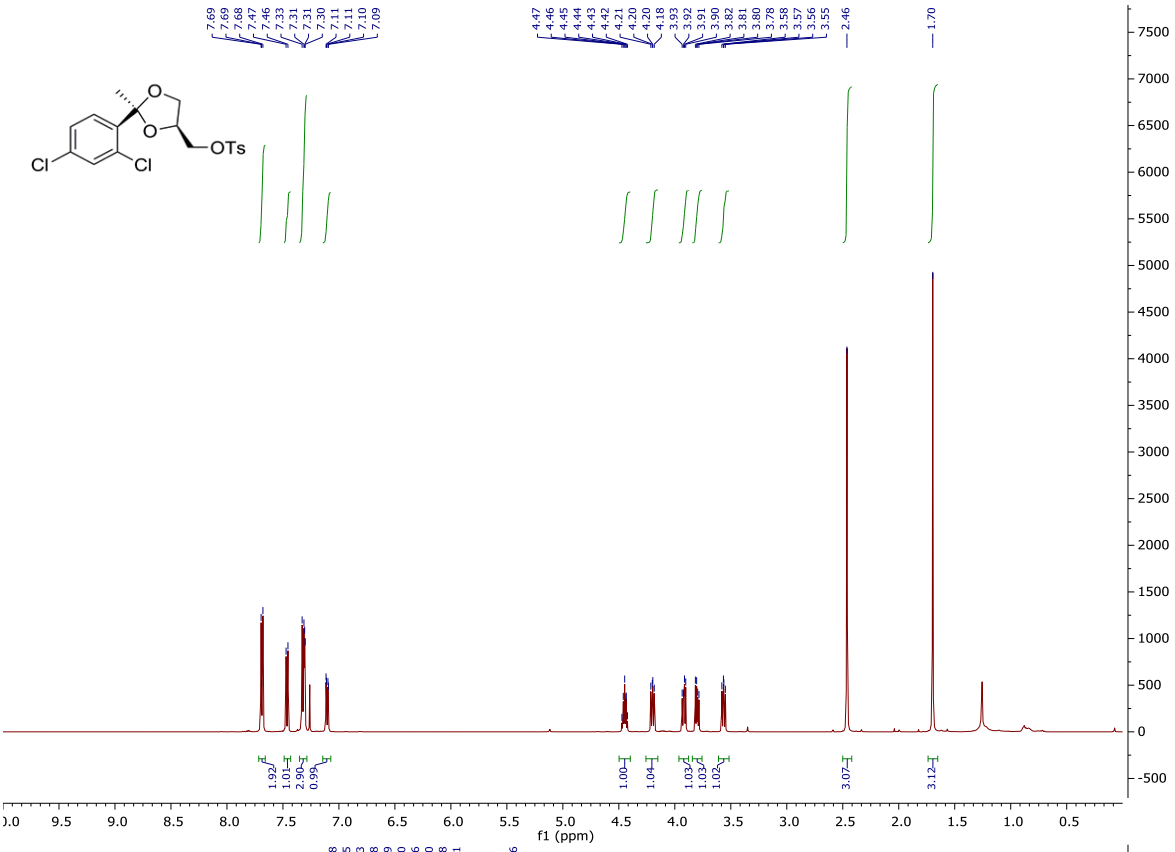
7.69
7.69
7.68
7.47
7.46
7.33
7.31
7.31
7.30
7.11
7.11
7.10
7.09
4.47
4.46
4.45
4.44
4.43
4.42
4.21
4.20
4.20
4.18
3.93
3.92
3.91
3.90
3.82
3.81
3.80
3.78
3.58
3.57
3.56
3.55
2.46
1.70
Cl
Cl
OTs
1.92
1.01
2.90
0.99
1.00
1.04
1.03
1.03
1.02
3.07
3.12
f1 (ppm)

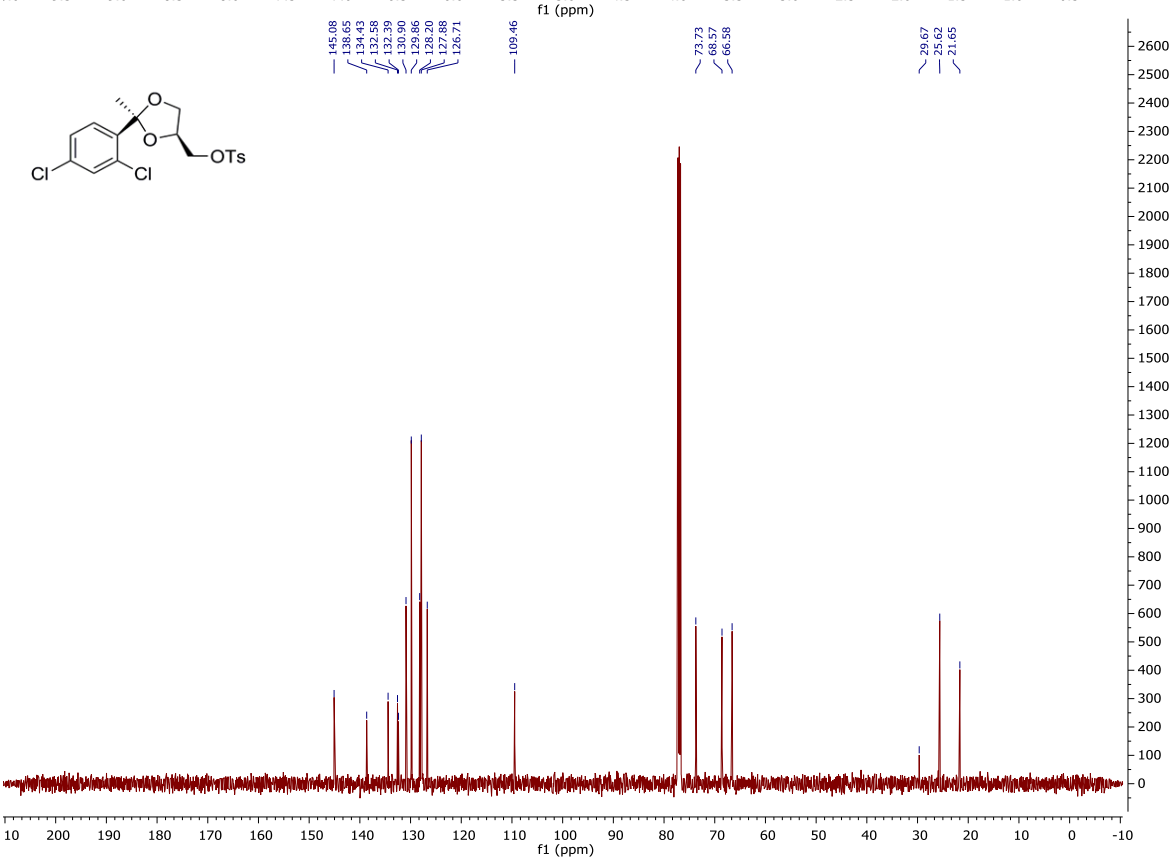
145.08
138.65
134.43
132.58
132.39
130.90
129.86
128.20
127.88
126.71
109.46
73.73
68.57
66.58
29.67
25.62
21.65
Cl
Cl
OTs
f1 (ppm)

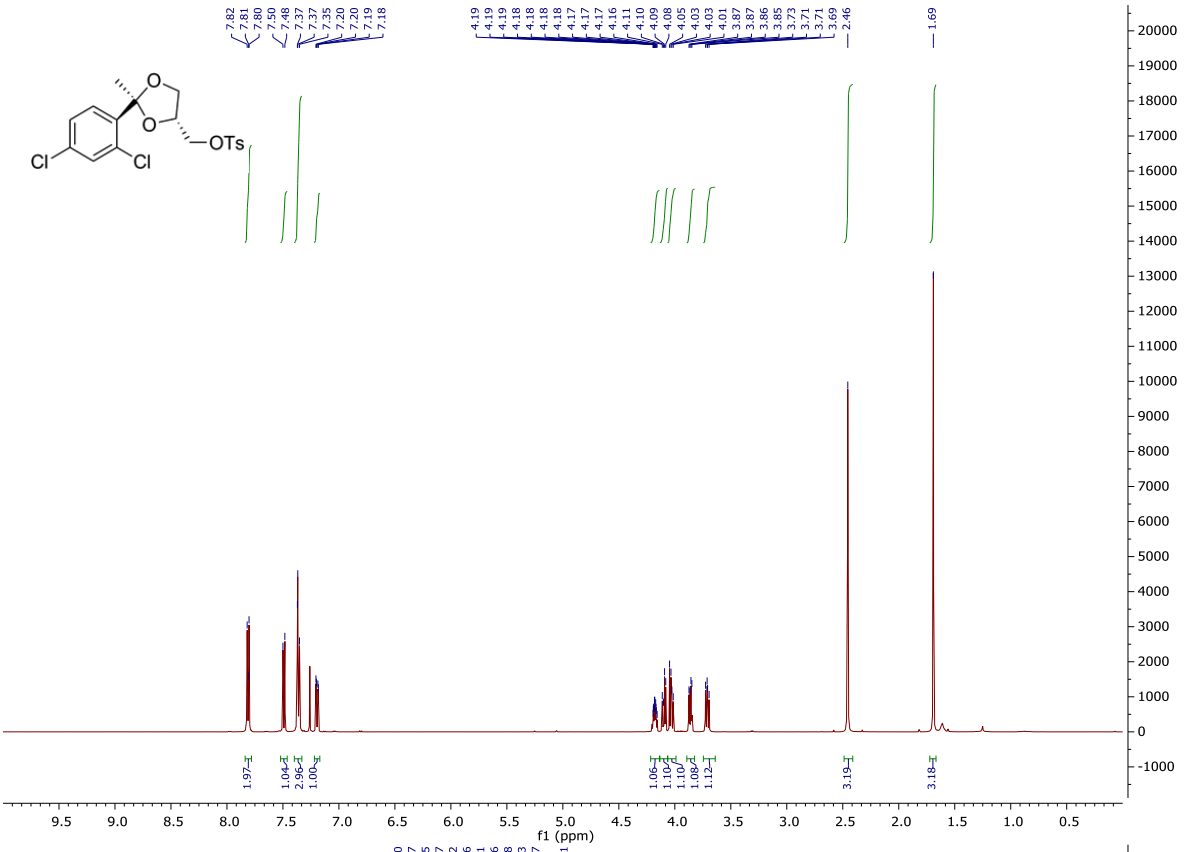
7.82
7.81
7.80
7.50
7.48
7.37
7.37
7.35
7.20
7.19
7.18
4.19
4.19
4.19
4.18
4.18
4.18
4.18
4.17
4.17
4.17
4.16
4.11
4.10
4.09
4.08
4.05
4.03
4.03
4.01
3.87
3.87
3.86
3.85
3.73
3.71
3.71
3.69
2.46
1.69
OTs
Cl
Cl
1.97
1.04
2.96
1.00
1.06
1.10
1.10
1.08
1.12
3.19
3.18
f1 (ppm)

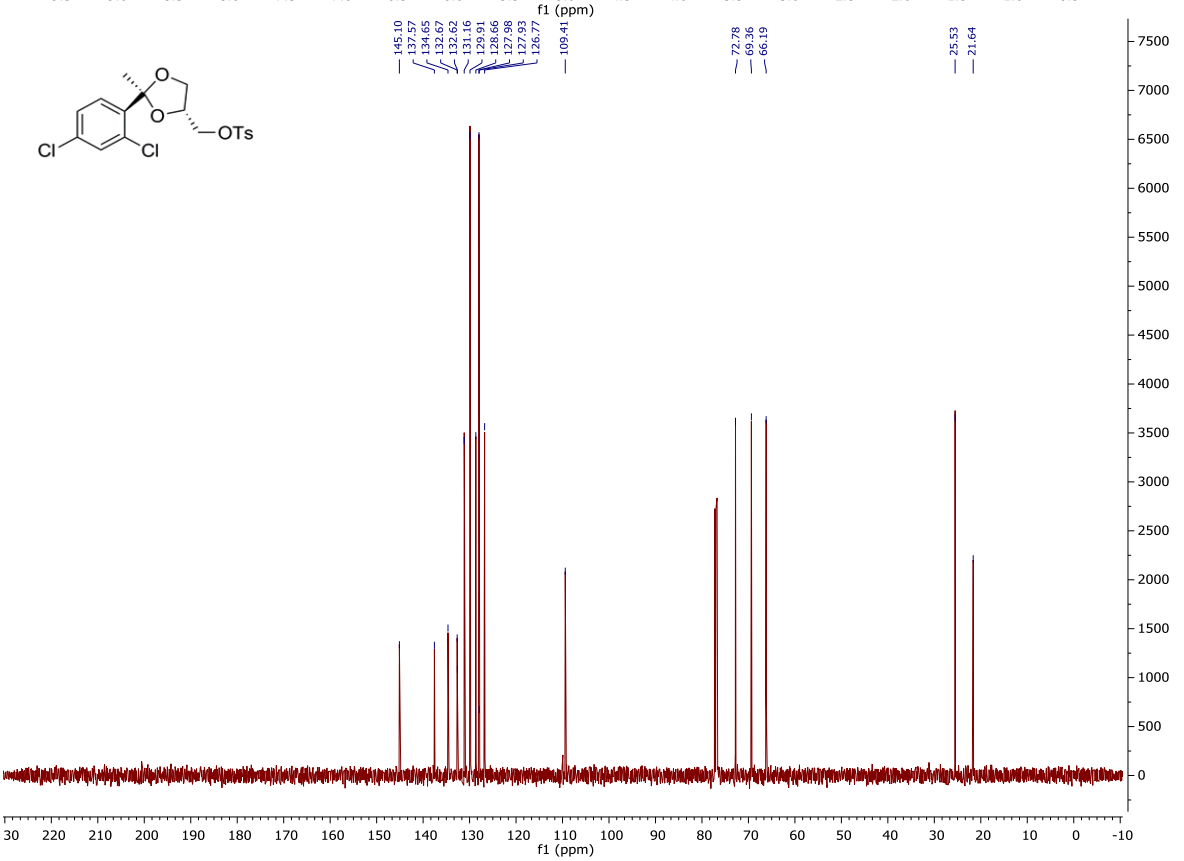
145.10
137.57
134.65
132.67
132.62
131.16
129.91
128.66
127.98
127.93
126.77
109.41
72.78
69.36
66.19
25.53
21.64
OTs
Cl
Cl
f1 (ppm)

HSQC:

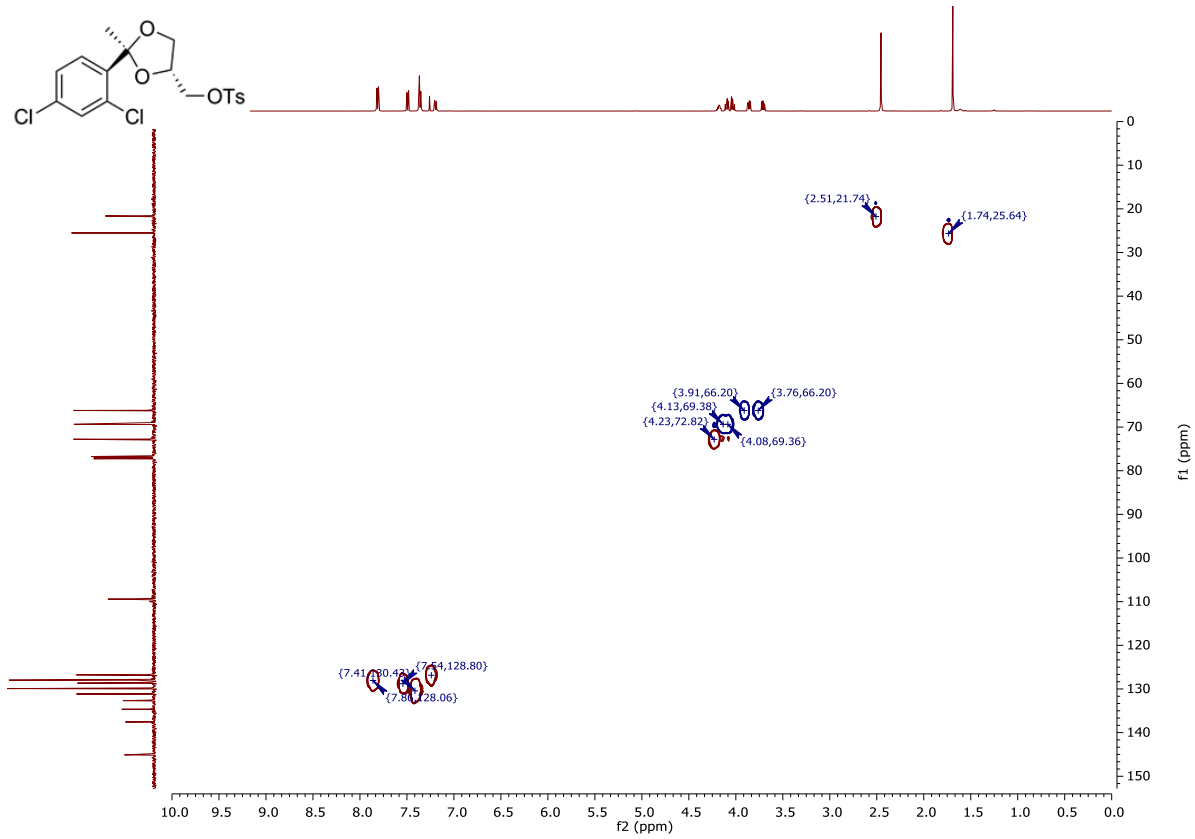
O
O
OTs
Cl
Cl
{2.51,21.74}
{1.74,25.64}
{3.91,66.20}
{3.76,66.20}
{4.13,69.38}
{4.23,72.82}
{4.08,69.36}
{7.54,128.80}
f1 (ppm)
f2 (ppm)

HSQC zoomed (3.2 to 4.8ppm): (1) H_{C4} (methine at C4 of dioxolane) direct correlation via HSQC experiment: 4.23→72.82ppm. (2) Remaining 1H nuclei in the expanded region below are methylene, correlating to the diastereomeric pairs at C5 of dioxolane and α-carbon to tosyl group (not specified: 3.76→66.20ppm; 3.91→66.20ppm; 4.08→69.37ppm; 4.13→69.37ppm).

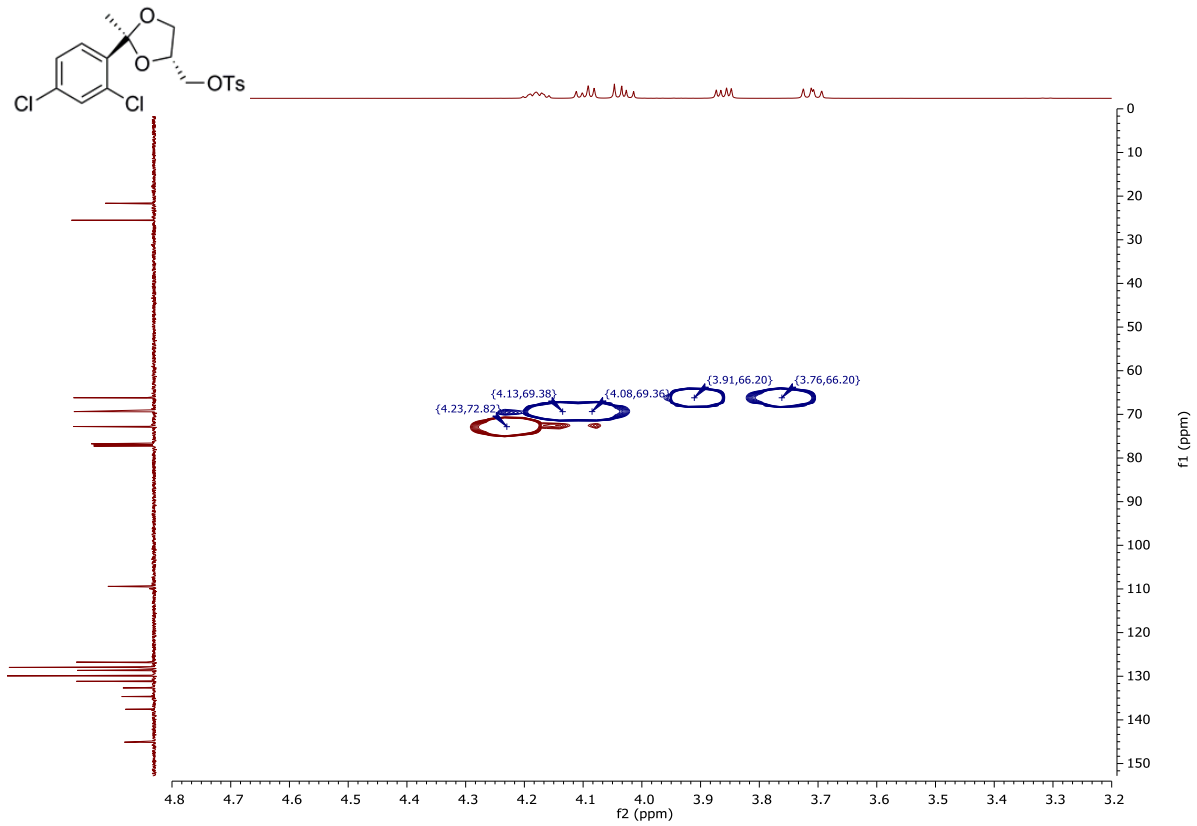

NOESY:

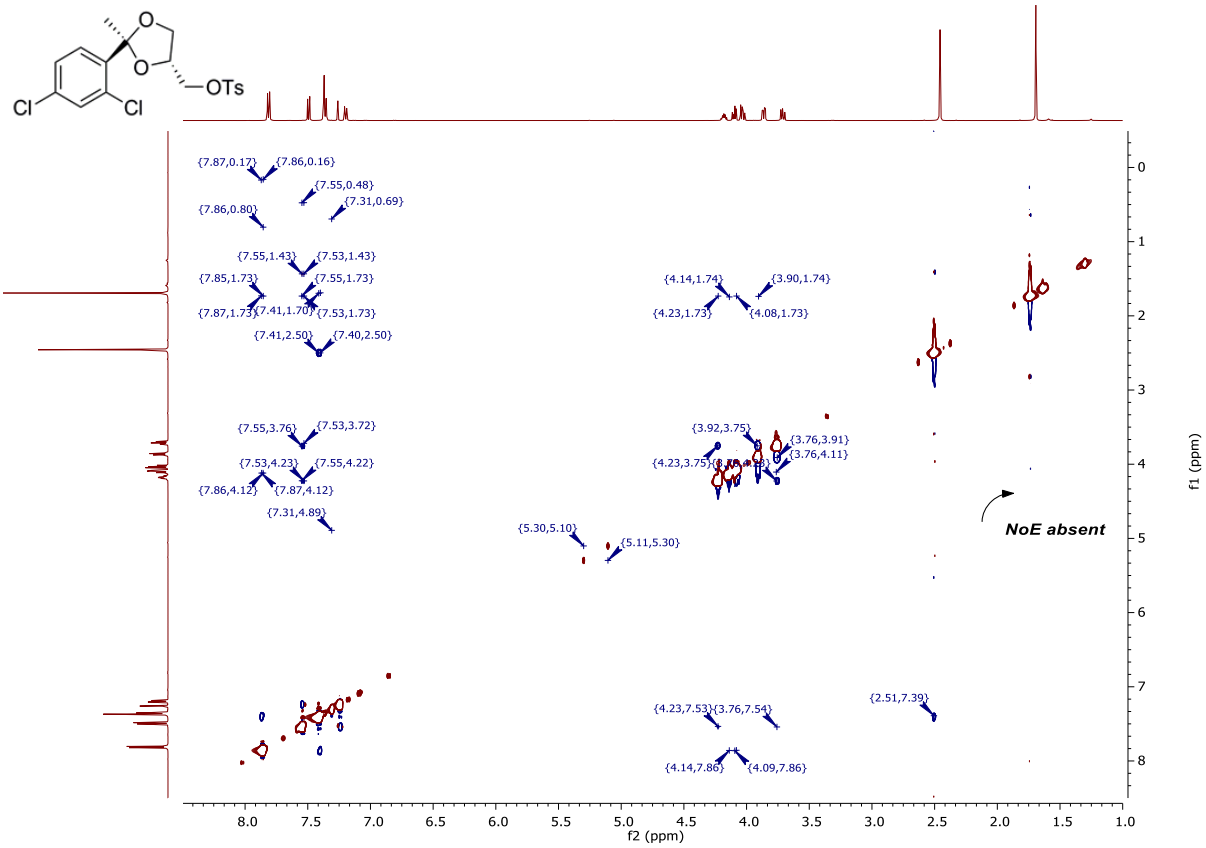
OTs
Cl
Cl
{7.87,0.17}
{7.86,0.16}
{7.55,0.48}
{7.31,0.69}
{7.86,0.80}
{7.55,1.43}
{7.53,1.43}
{7.85,1.73}
{7.55,1.73}
{7.87,1.73}
{7.41,1.70}
{7.53,1.73}
{7.41,2.50}
{7.40,2.50}
{4.14,1.74}
{3.90,1.74}
{4.23,1.73}
{4.08,1.73}
{7.55,3.76}
{7.53,3.72}
{7.53,4.23}
{7.55,4.22}
{7.86,4.12}
{7.87,4.12}
{7.31,4.89}
{3.92,3.75}
{3.76,3.91}
{3.76,4.11}
{5.30,5.10}
{5.11,5.30}
NoE absent
{2.51,7.39}
{4.23,7.53}
{3.76,7.54}
{4.14,7.86}
{4.09,7.86}
f2 (ppm)
f1 (ppm)

NOESY zoomed (3.2 to 4.8ppm): (1) H_{C4} (methine at C4 of dioxolane) very weak to no NoE signal with methyl at C2 of dioxolane (2,4-correlation) in experiment: 4.23→1.73ppm.

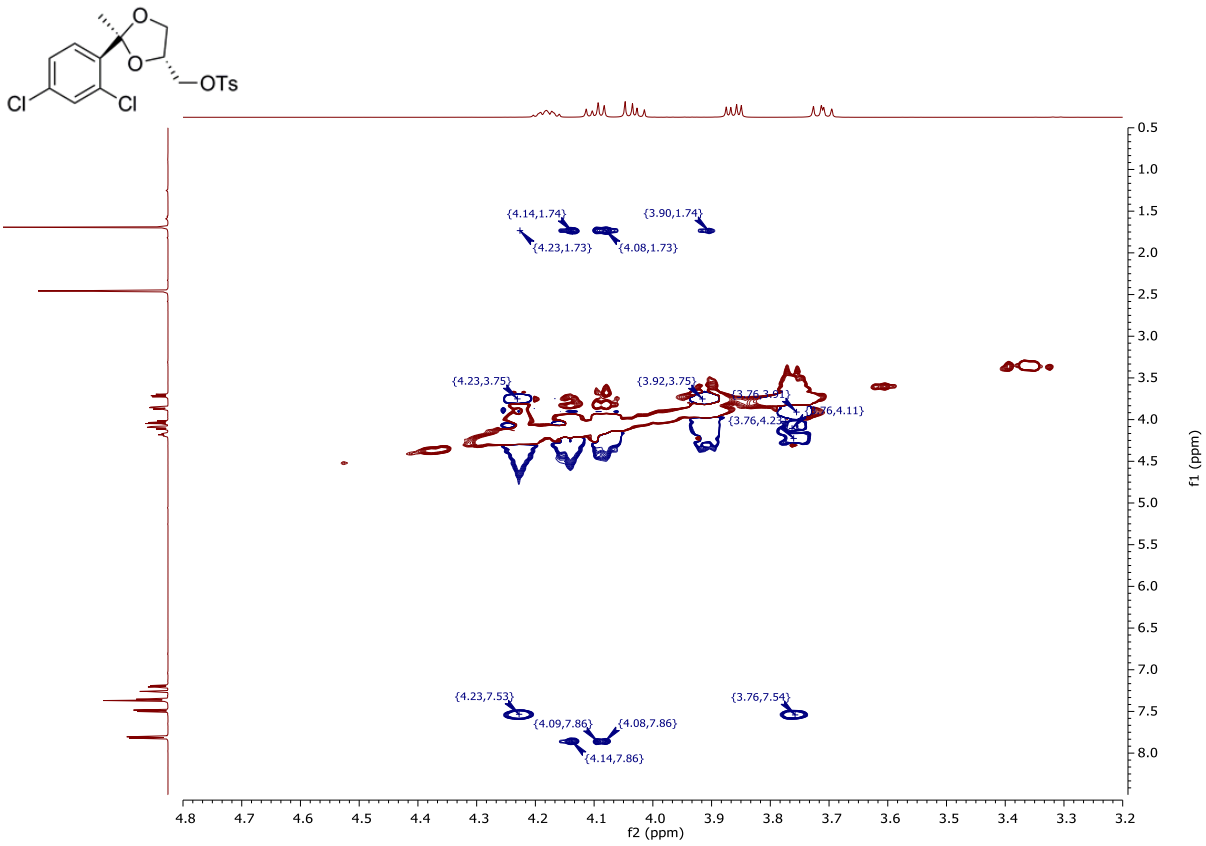

X-RAY:

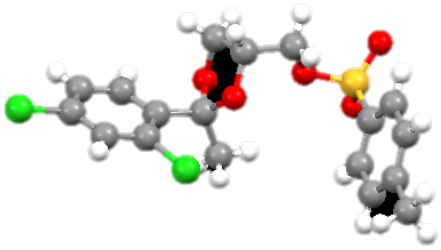

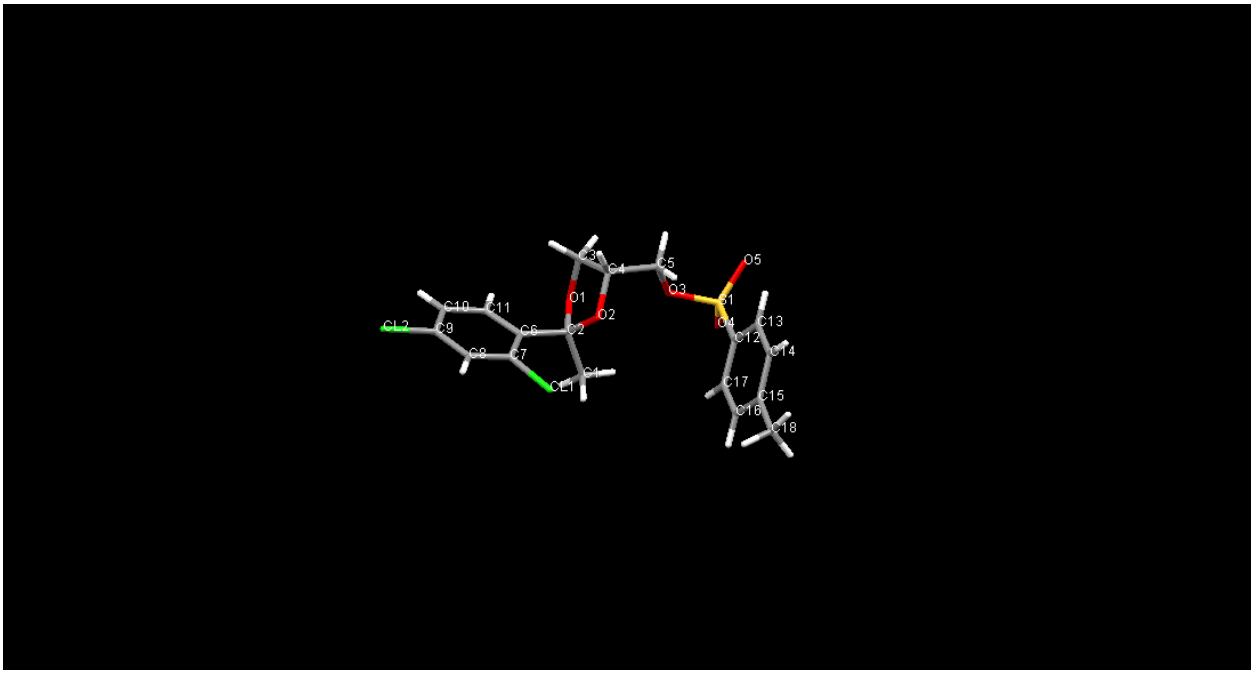
C3
C4
C5
O5
O1
O3
S1
O2
C10
C11
O4
C13
CL2
C9
C6
C12
C14
C8
C7
C1
C17
CL1
C15
C16
C18

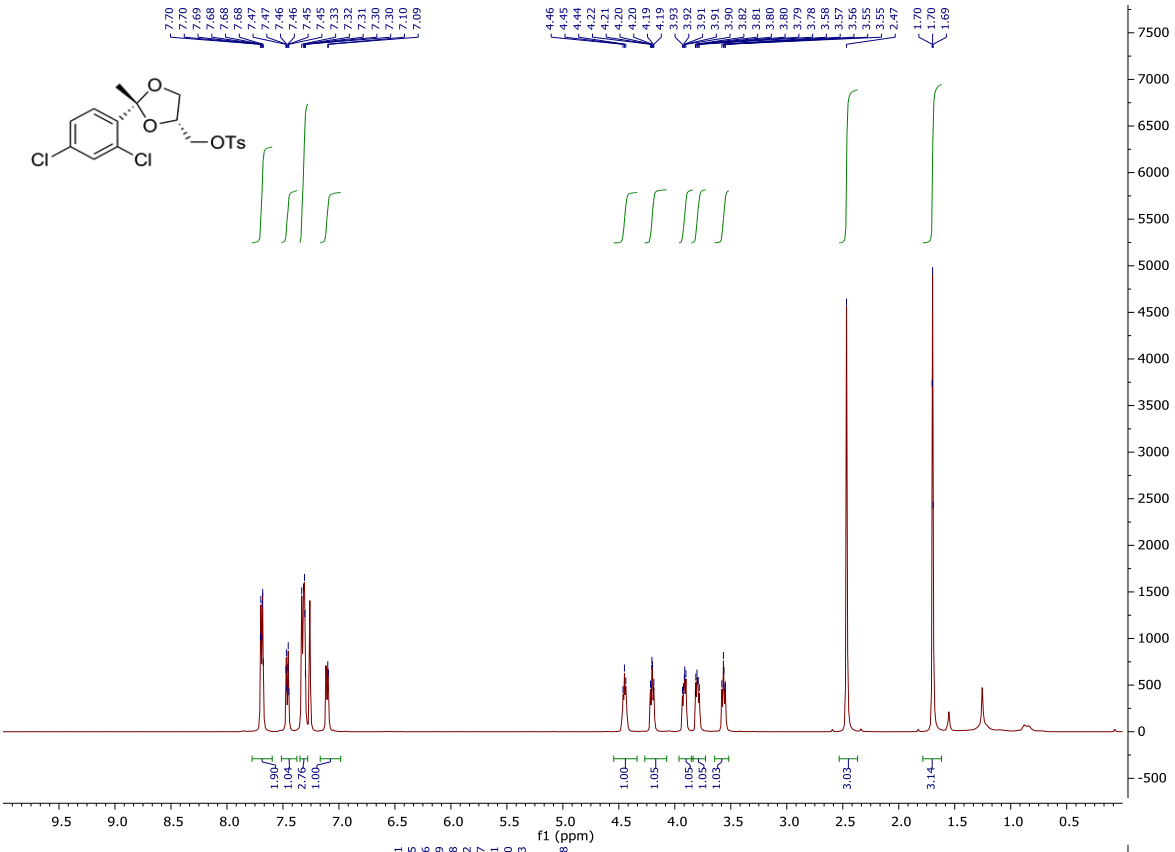
7.70
7.70
7.69
7.68
7.68
7.68
7.47
7.47
7.46
7.46
7.45
7.45
7.33
7.32
7.31
7.30
7.30
7.10
7.09
4.46
4.45
4.44
4.22
4.21
4.20
4.20
4.19
4.19
3.93
3.92
3.91
3.91
3.90
3.82
3.81
3.80
3.80
3.79
3.78
3.58
3.57
3.56
3.55
3.55
2.47
1.70
1.70
1.69
OTs
Cl
Cl
1.90
1.04
2.76
1.00
1.00
1.05
1.05
1.05
1.03
3.03
3.14
f1 (ppm)

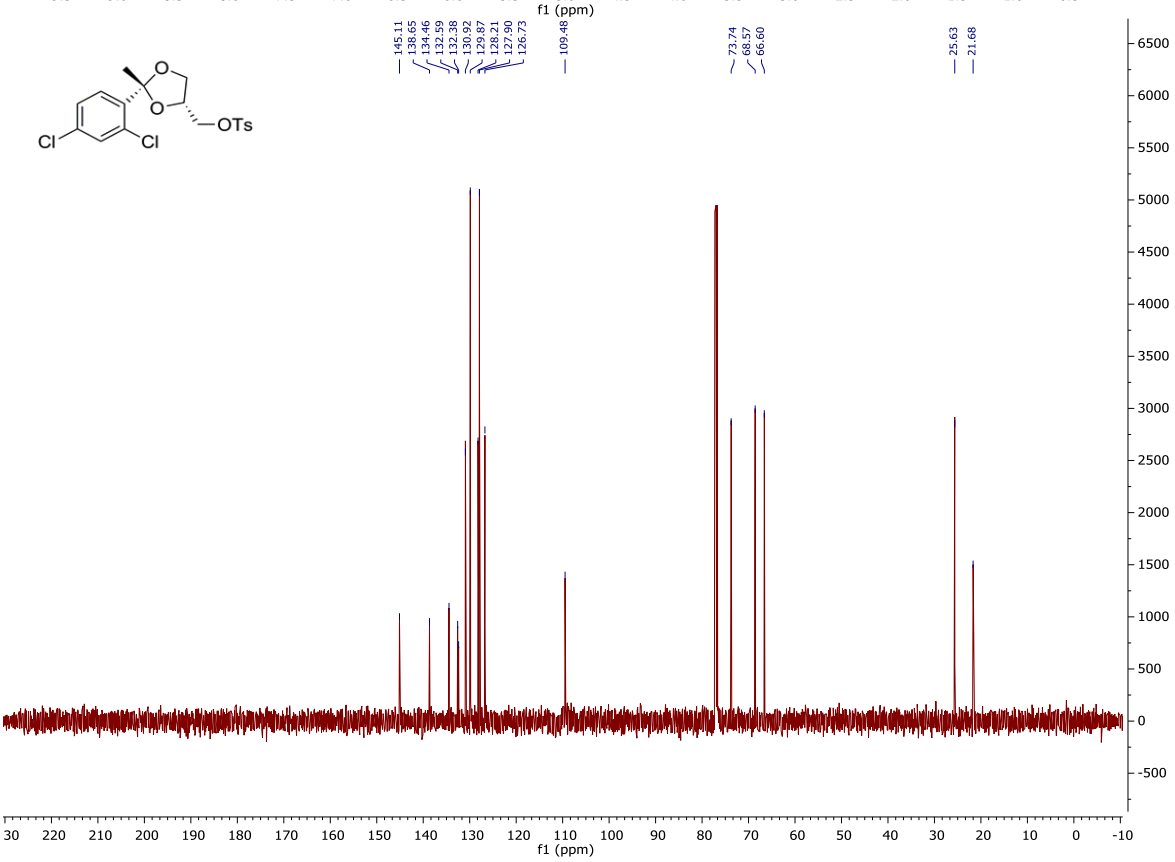
145.11
138.65
134.46
132.59
132.38
130.92
129.87
128.21
127.90
126.73
109.48
73.74
68.57
66.60
25.63
21.68
OTs
Cl
Cl
f1 (ppm)

HSQC:

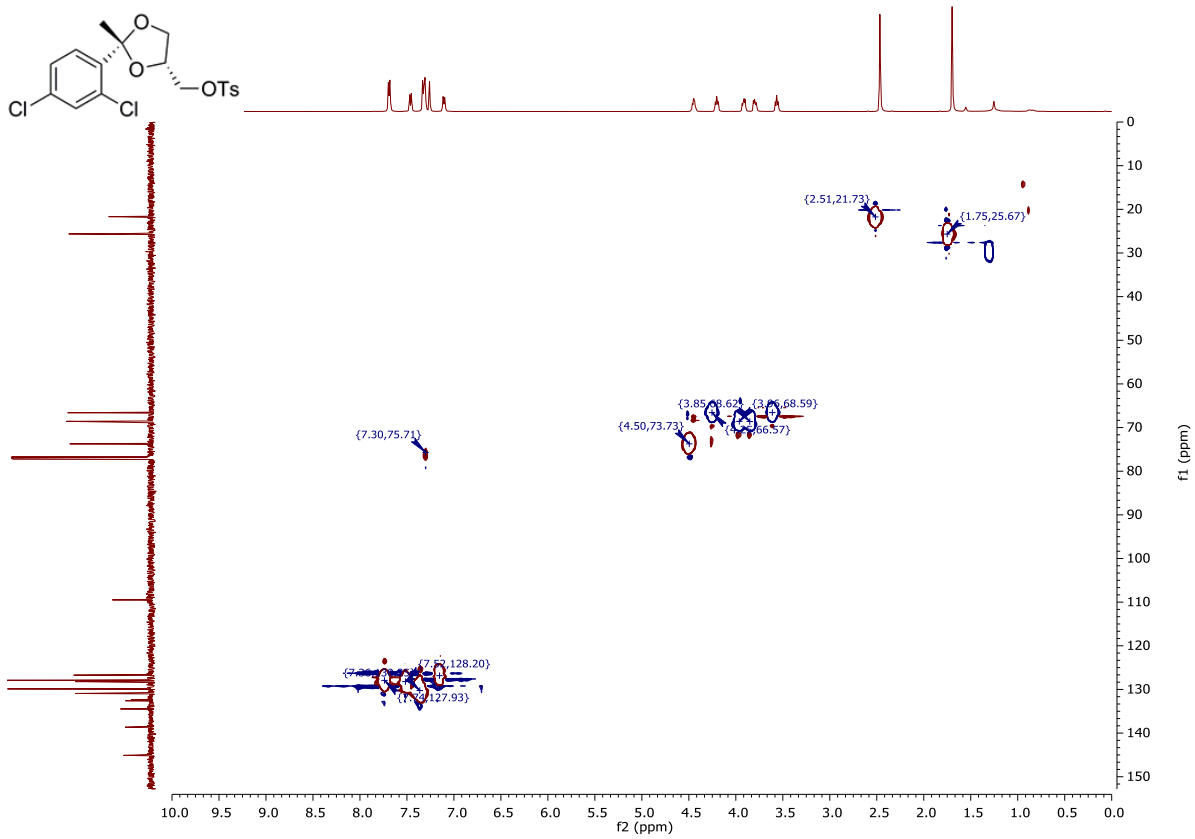

HSQC zoomed (3.2 to 4.8ppm). (1) H_{C4} (methine at C4 of dioxolane) direct correlation via HSQC experiment: 4.50→73.73ppm. (2) Remaining 1H nuclei in the expanded region below are methylene, correlating to the diastereomeric pairs at C5 of dioxolane and α-carbon to tosyl group (not specified: 3.61→66.56ppm; 3.85→68.62ppm; 3.96→68.59ppm; 4.25→66.57ppm).

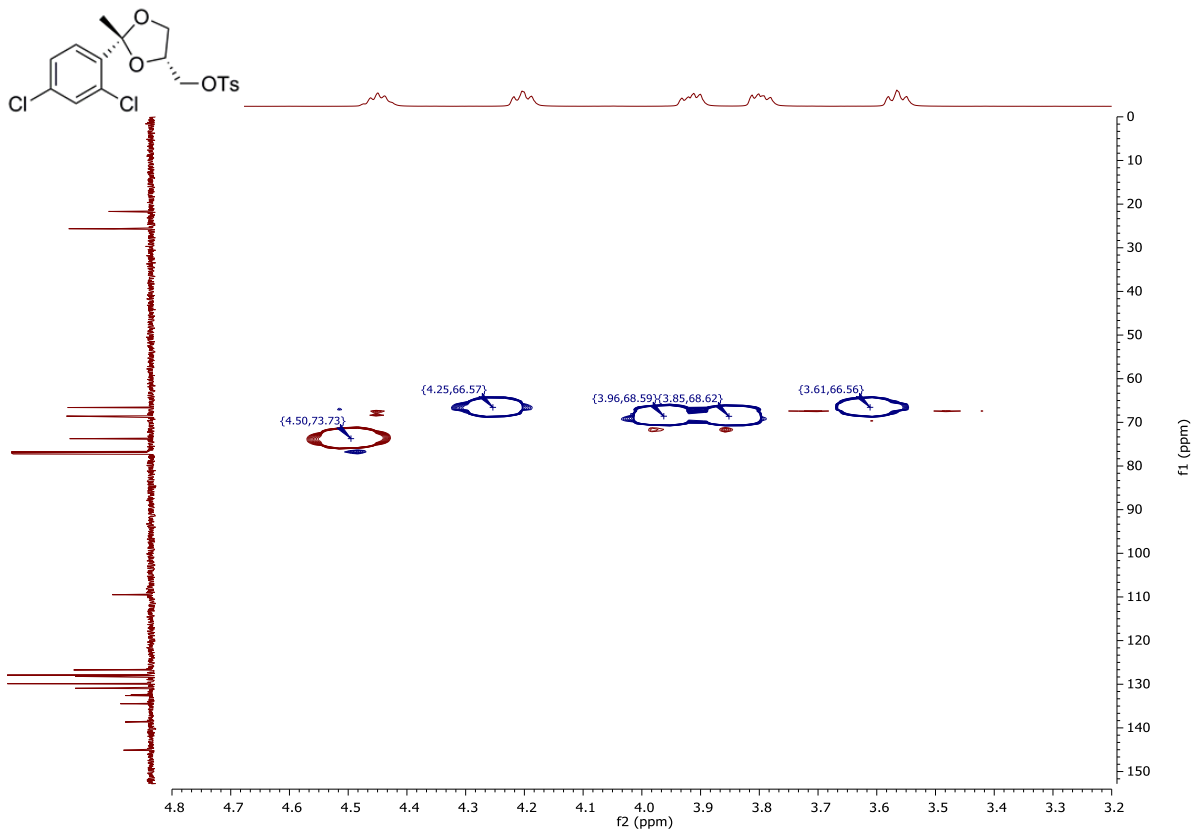

NOESY:

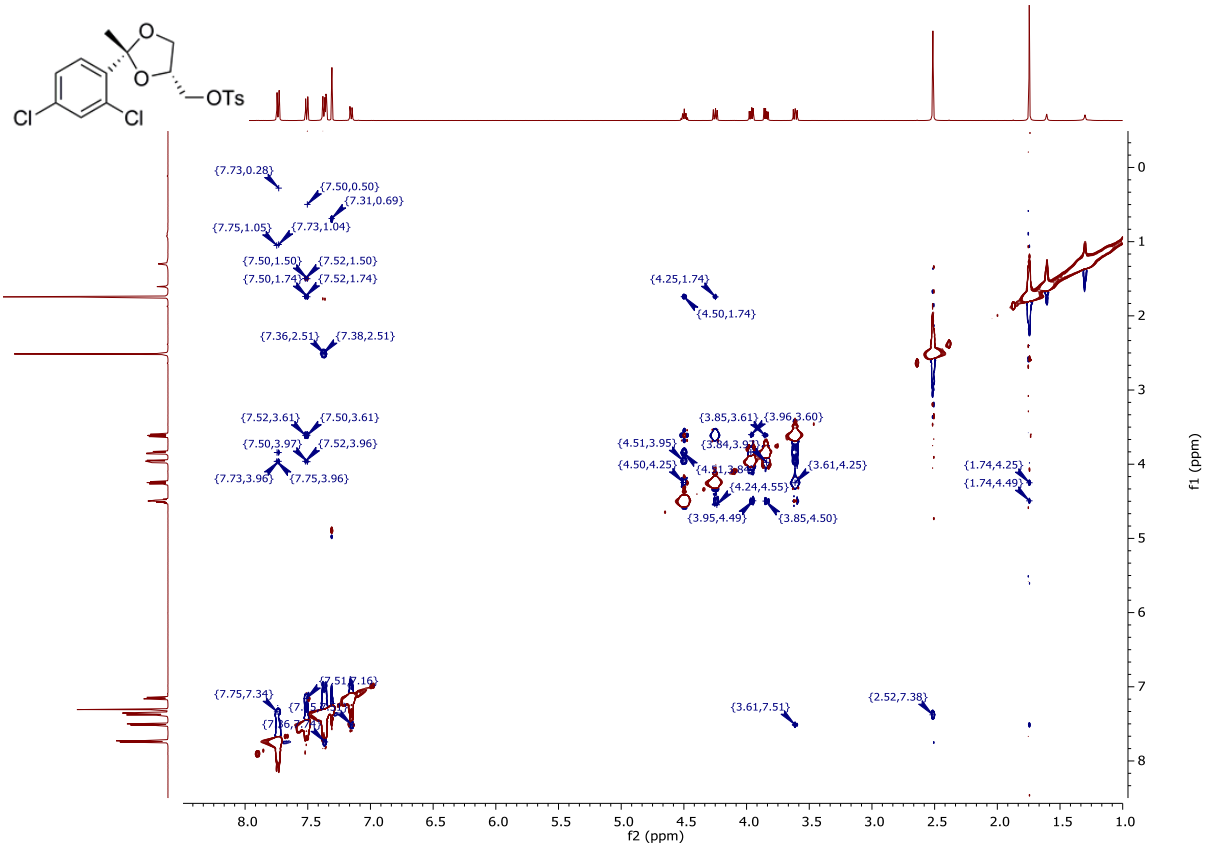
OTs
Cl
Cl
{7.73,0.28}
{7.50,0.50}
{7.31,0.69}
{7.75,1.05}
{7.73,1.04}
{7.50,1.50}
{7.52,1.50}
{7.50,1.74}
{7.52,1.74}
{7.36,2.51}
{7.38,2.51}
{7.52,3.61}
{7.50,3.61}
{7.50,3.97}
{7.52,3.96}
{7.73,3.96}
{7.75,3.96}
{4.25,1.74}
{4.50,1.74}
{3.85,3.61}
{3.96,3.60}
{4.51,3.95}
{4.50,4.25}
{3.61,4.25}
{4.24,4.55}
{3.95,4.49}
{3.85,4.50}
{1.74,4.25}
{1.74,4.49}
{7.75,7.34}
{3.61,7.51}
{2.52,7.38}
f2 (ppm)
f1 (ppm)

NOESY zoomed (3.2 to 4.8ppm): (1) H_{C4} (methine at C4 of dioxolane) moderate NoE signal with methyl at C2 of dioxolane (2,4-correlation) in experiment: 4.50→1.74ppm.

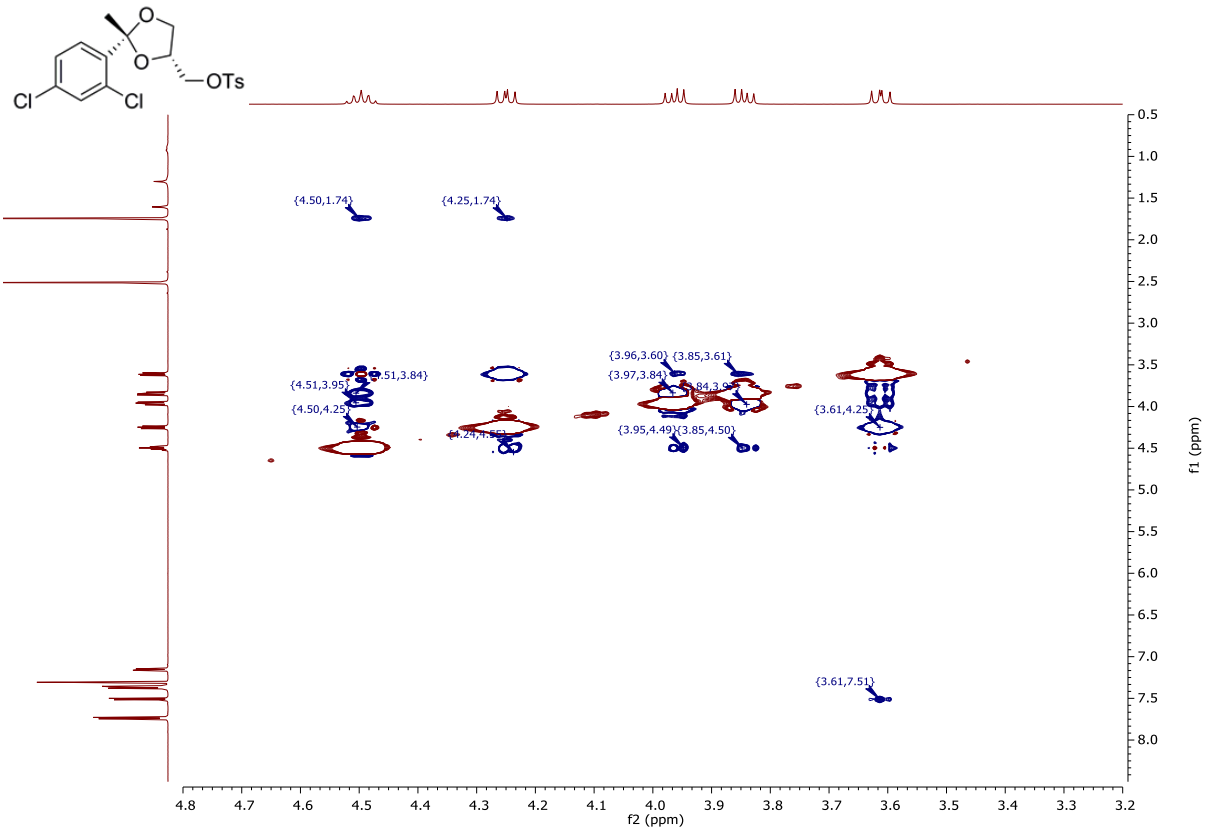

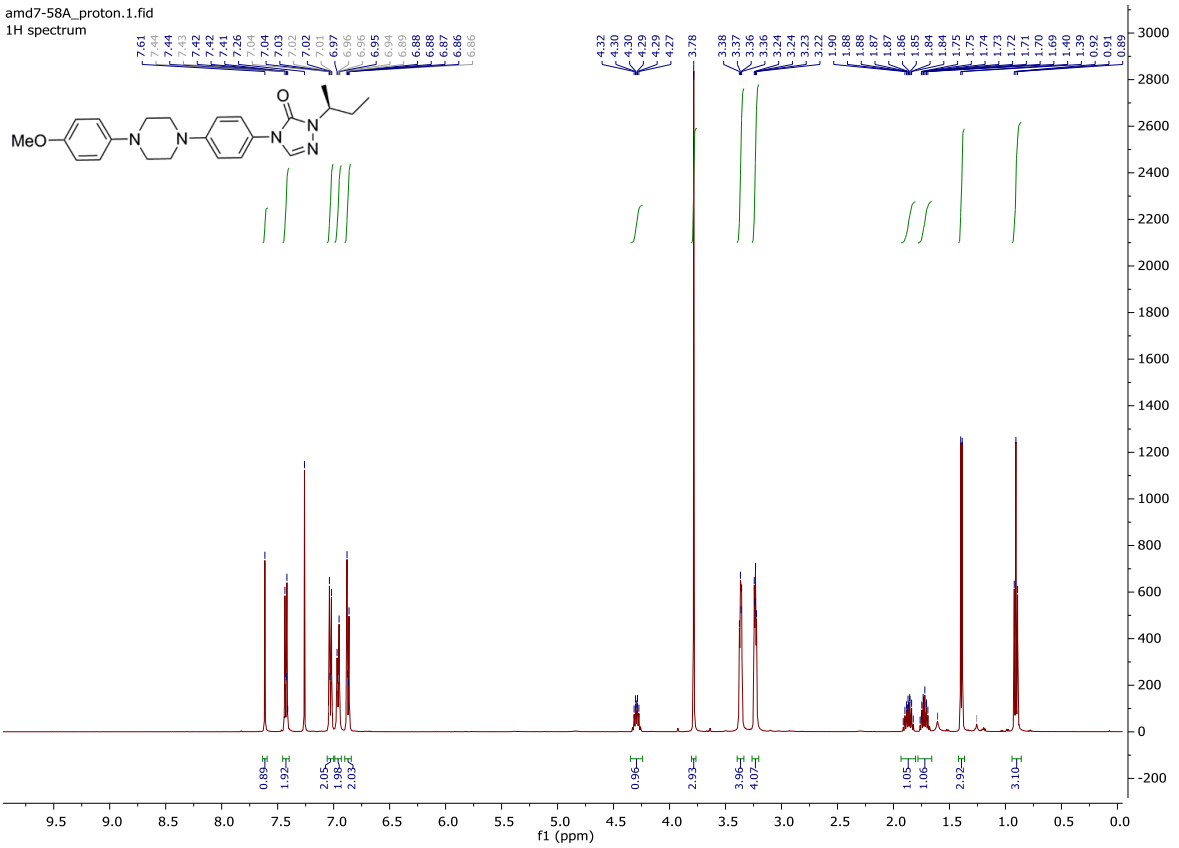
amd7-58A_proton.1.fid
1H spectrum
MeO
f1 (ppm)

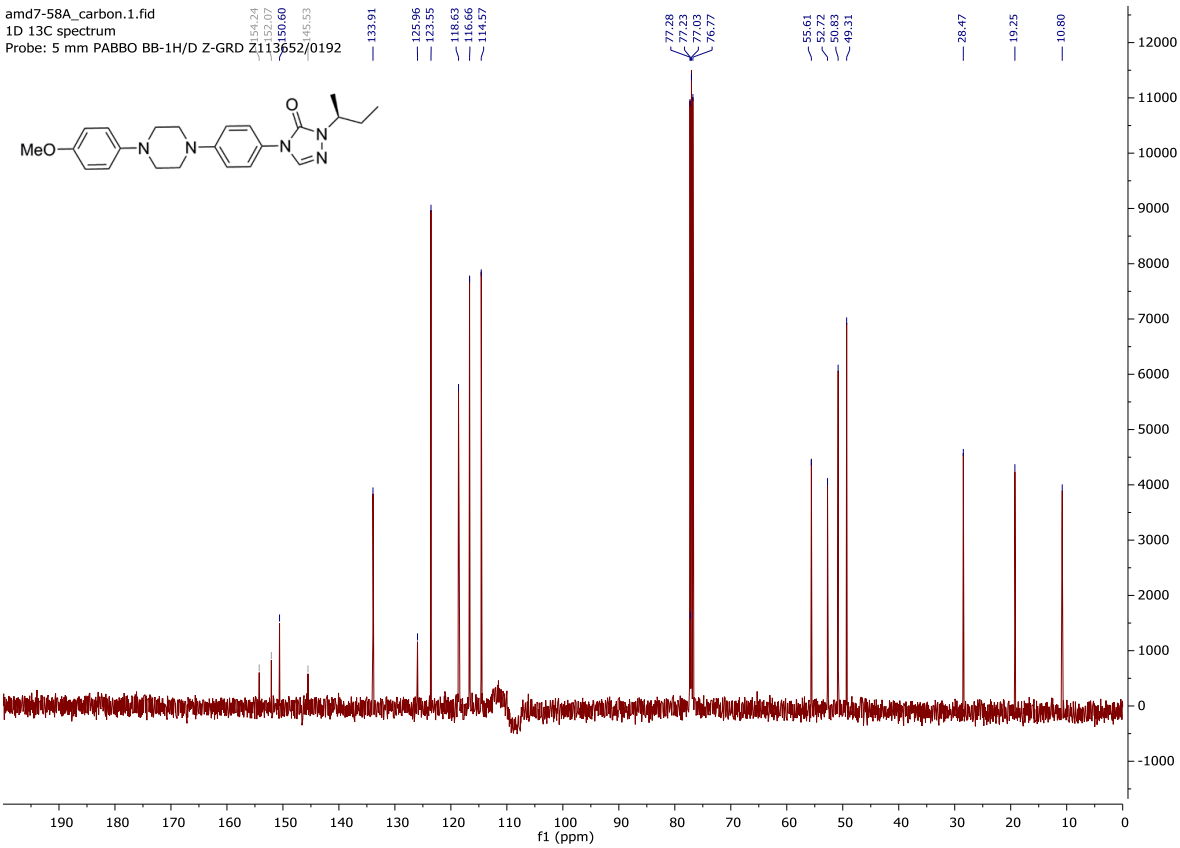
amd7-58A_carbon.1.fid
1D 13C spectrum
Probe: 5 mm PABBO BB-1H/D Z-GRD Z113652/0192
MeO
f1 (ppm)

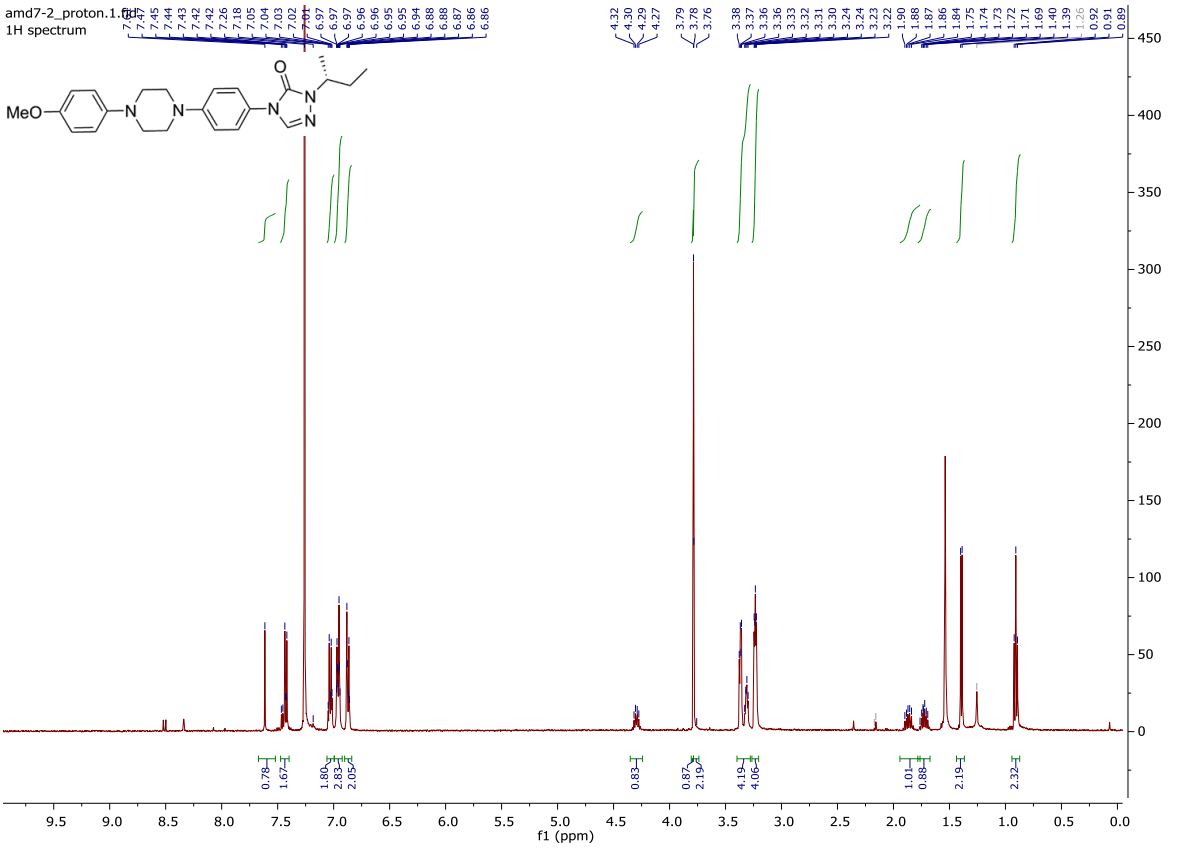
amd7-2_proton.1.fid
1H spectrum
MeO
f1 (ppm)

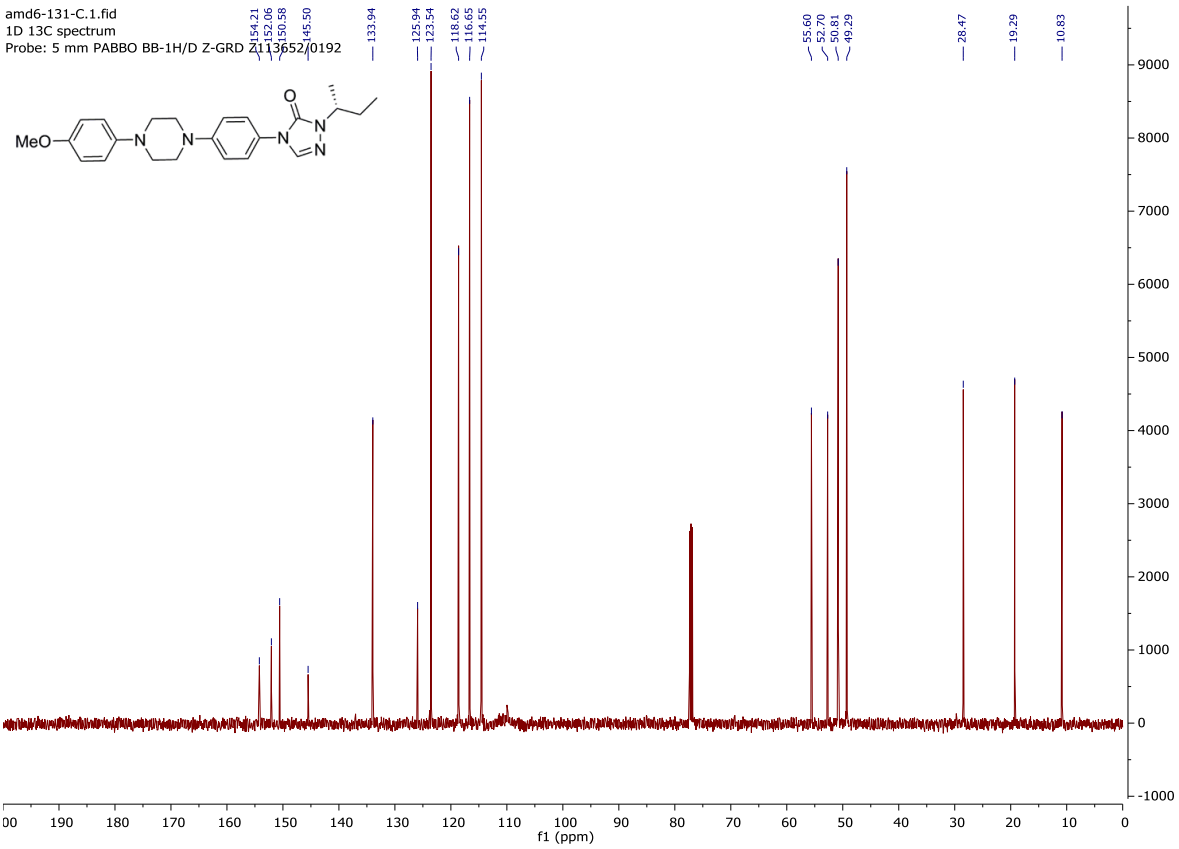
amd6-131-C.1.fid
1D 13C spectrum
Probe: 5 mm PABBO BB-1H/D Z-GRD Z113652/0192
MeO
f1 (ppm)

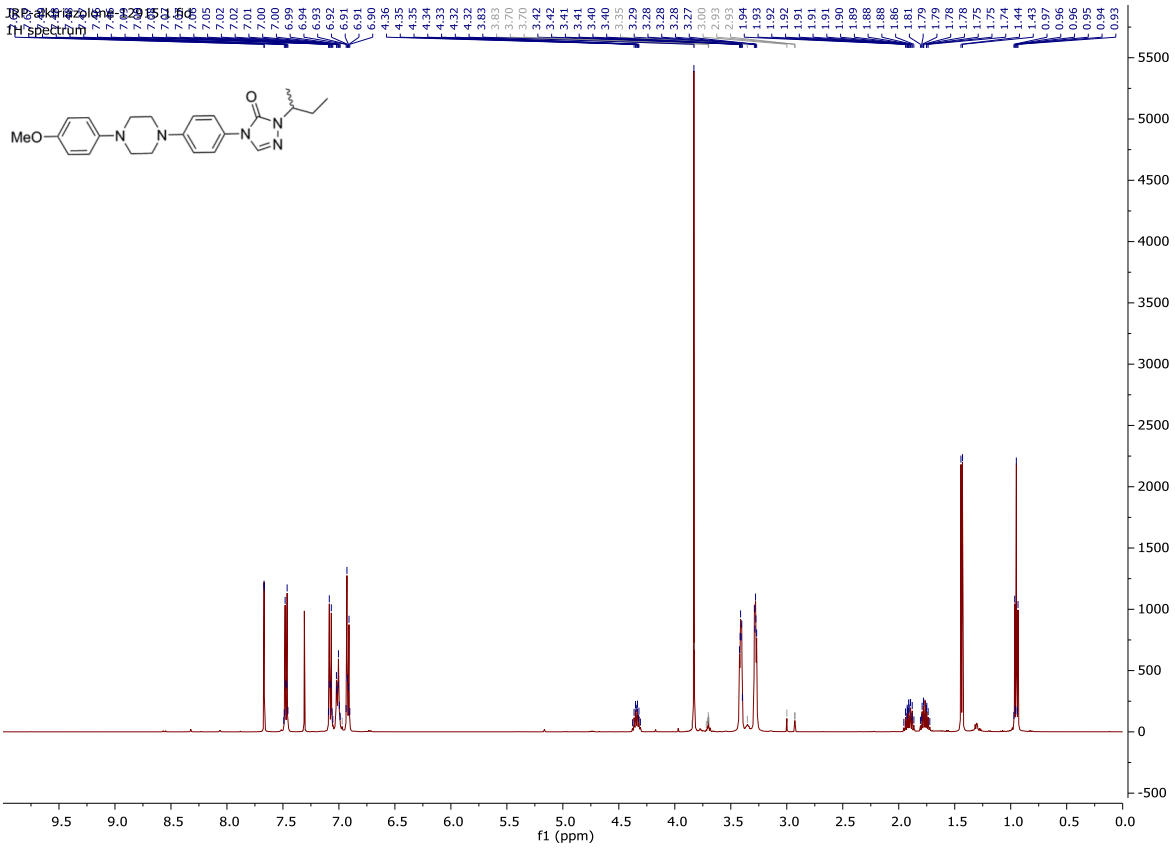
1H spectrum
MeO
f1 (ppm)

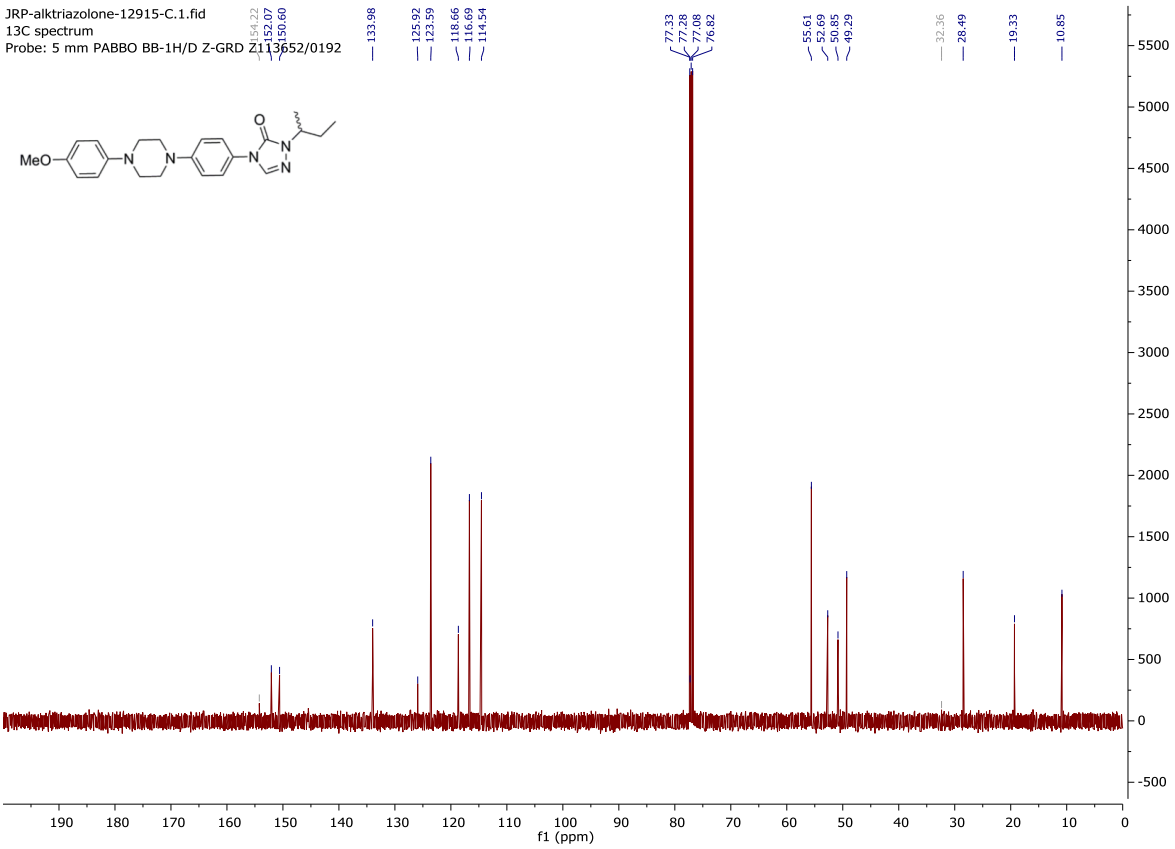
JRP-alktriazolone-12915-C.1.fid
13C spectrum
Probe: 5 mm PABBO BB-1H/D Z-GRD Z113652/0192
MeO
f1 (ppm)

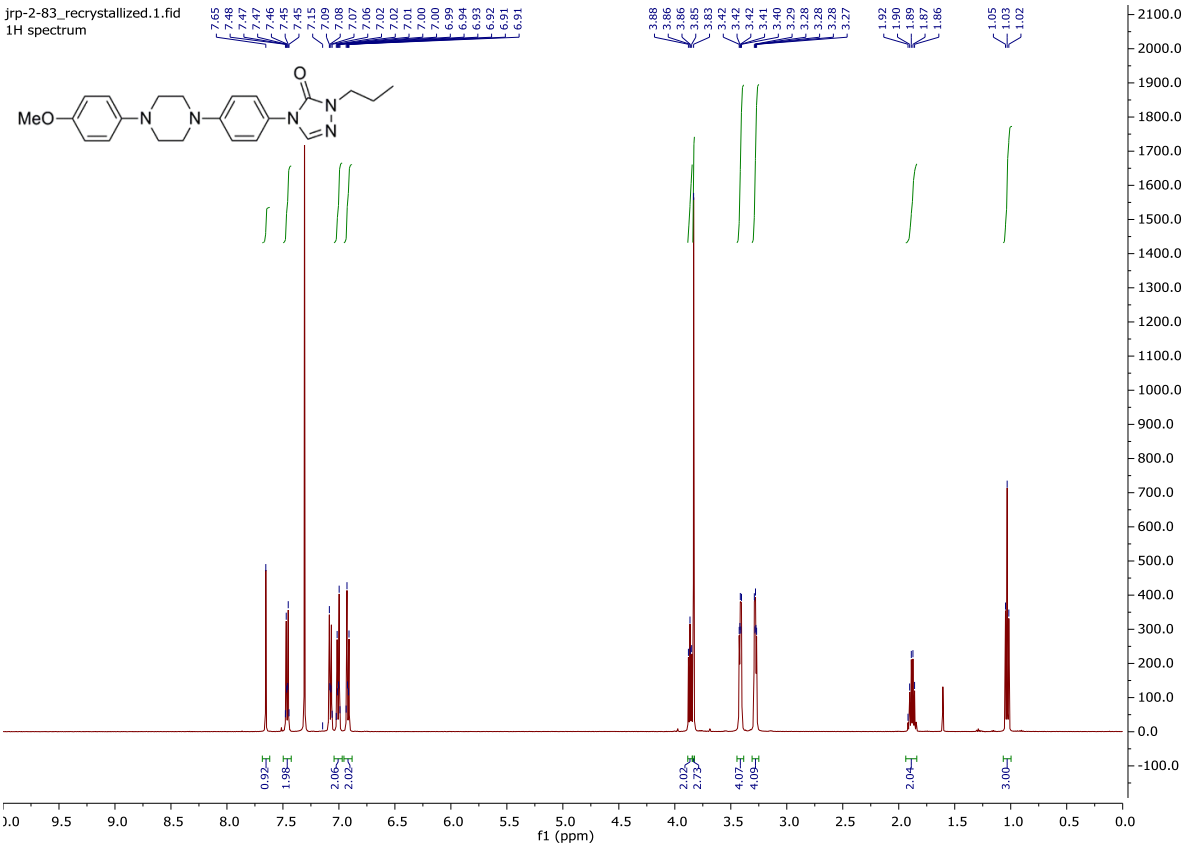
jrp-2-83_recrystallized.1.fid
1H spectrum
MeO
f1 (ppm)

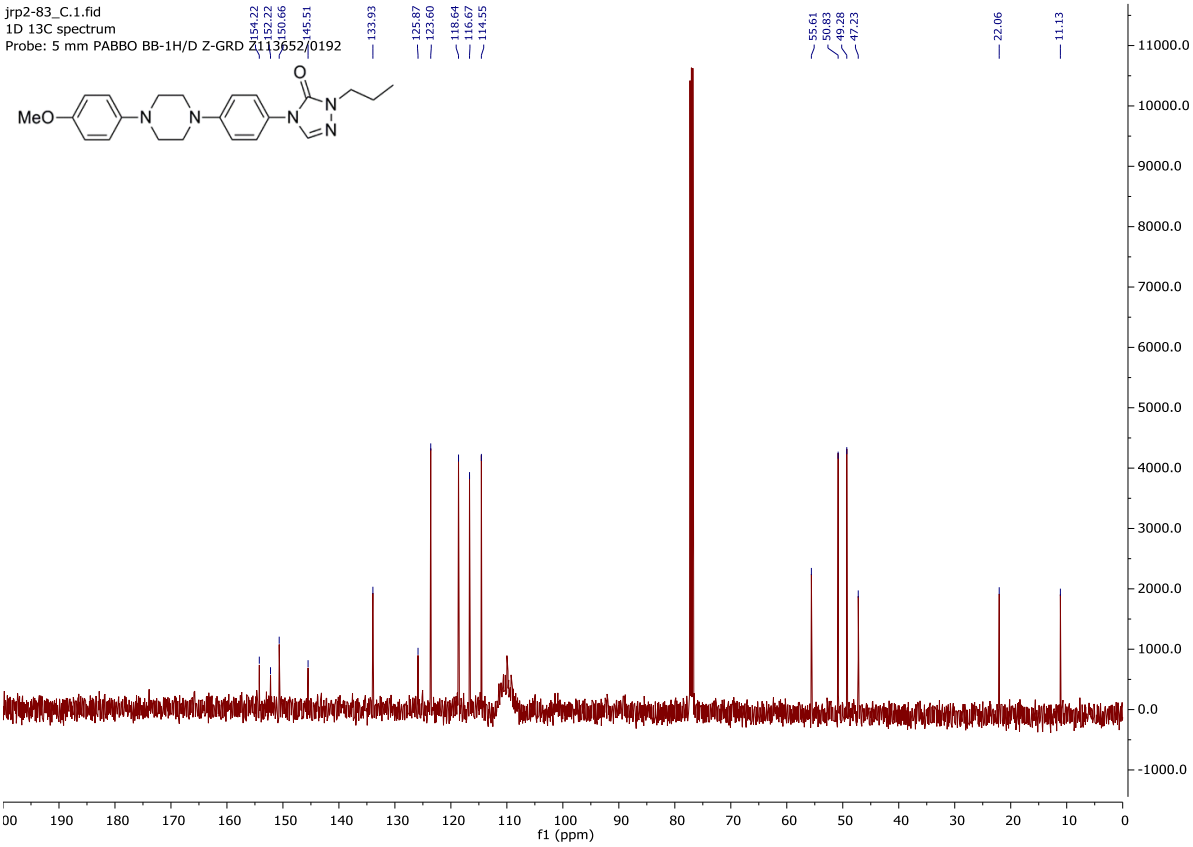
jrp2-83_C.1.fid
1D 13C spectrum
Probe: 5 mm PABBO BB-1H/D Z-GRD Z113652/0192
MeO
f1 (ppm)

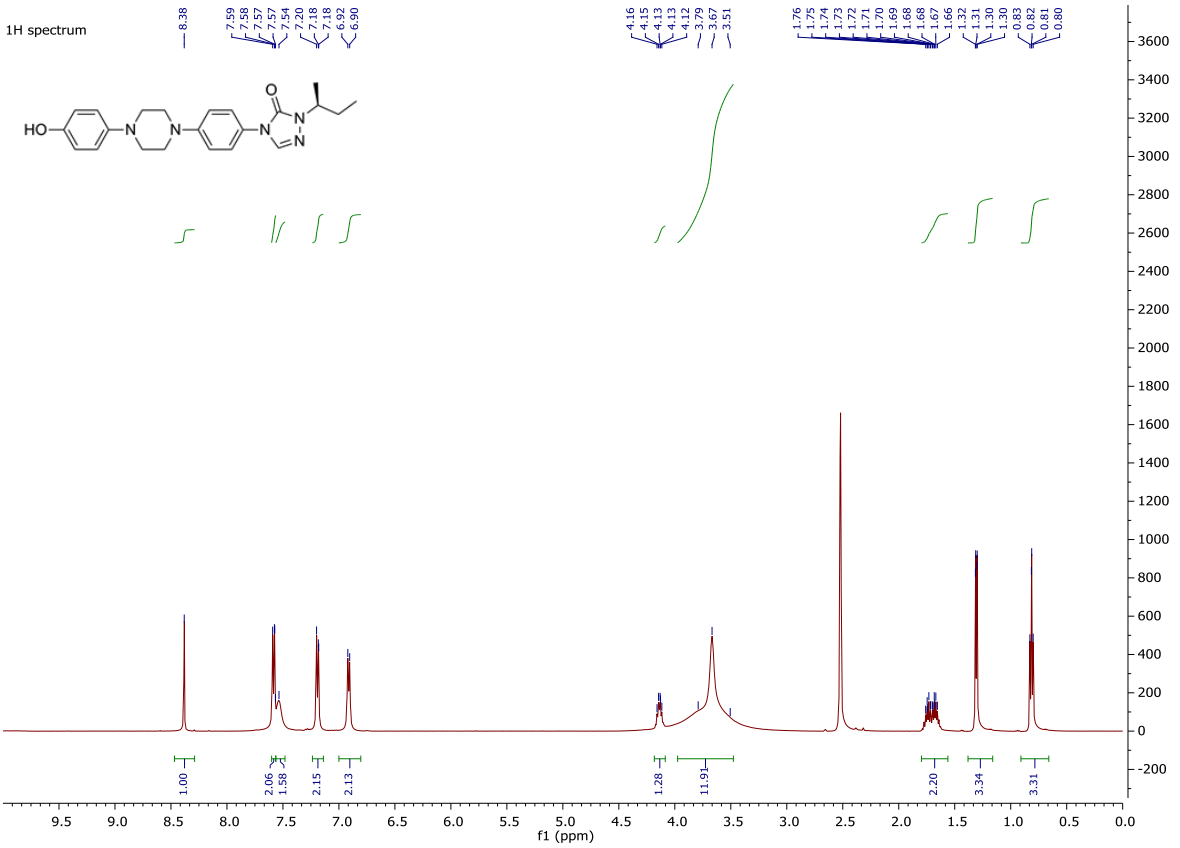
1H spectrum
8.38
7.59
7.58
7.57
7.57
7.54
7.20
7.18
7.18
6.92
6.90
4.16
4.15
4.13
4.13
4.12
3.79
3.67
3.51
1.76
1.75
1.74
1.73
1.72
1.71
1.70
1.69
1.68
1.68
1.67
1.66
1.32
1.31
1.30
1.30
0.83
0.82
0.81
0.80
HO
O
N
N
N
N
1.00
2.06
1.58
2.15
2.13
1.28
11.91
2.20
3.34
3.31
f1 (ppm)

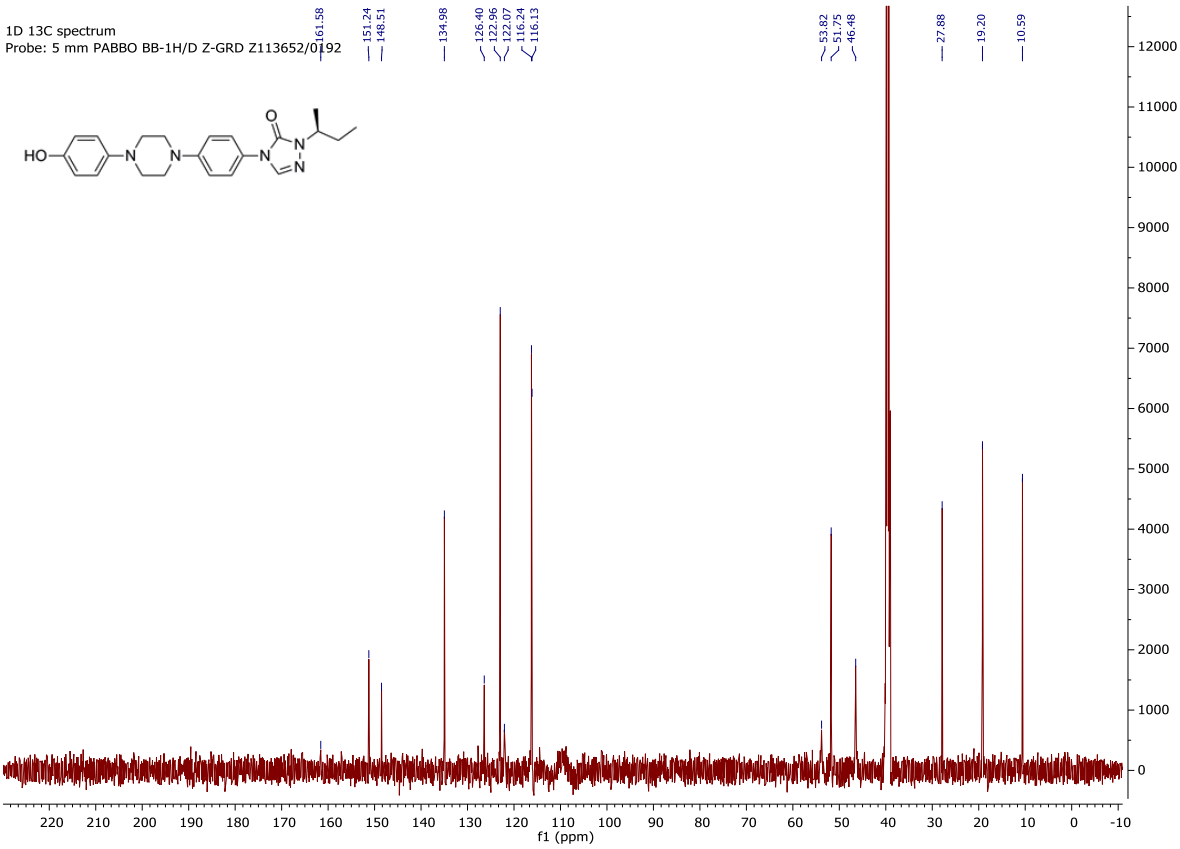
1D 13C spectrum
Probe: 5 mm PABBO BB-1H/D Z-GRD Z113652/0192
161.58
151.24
148.51
134.98
126.40
122.96
122.07
116.24
116.13
53.82
51.75
46.48
27.88
19.20
10.59
HO
O
N
N
N
N
f1 (ppm)

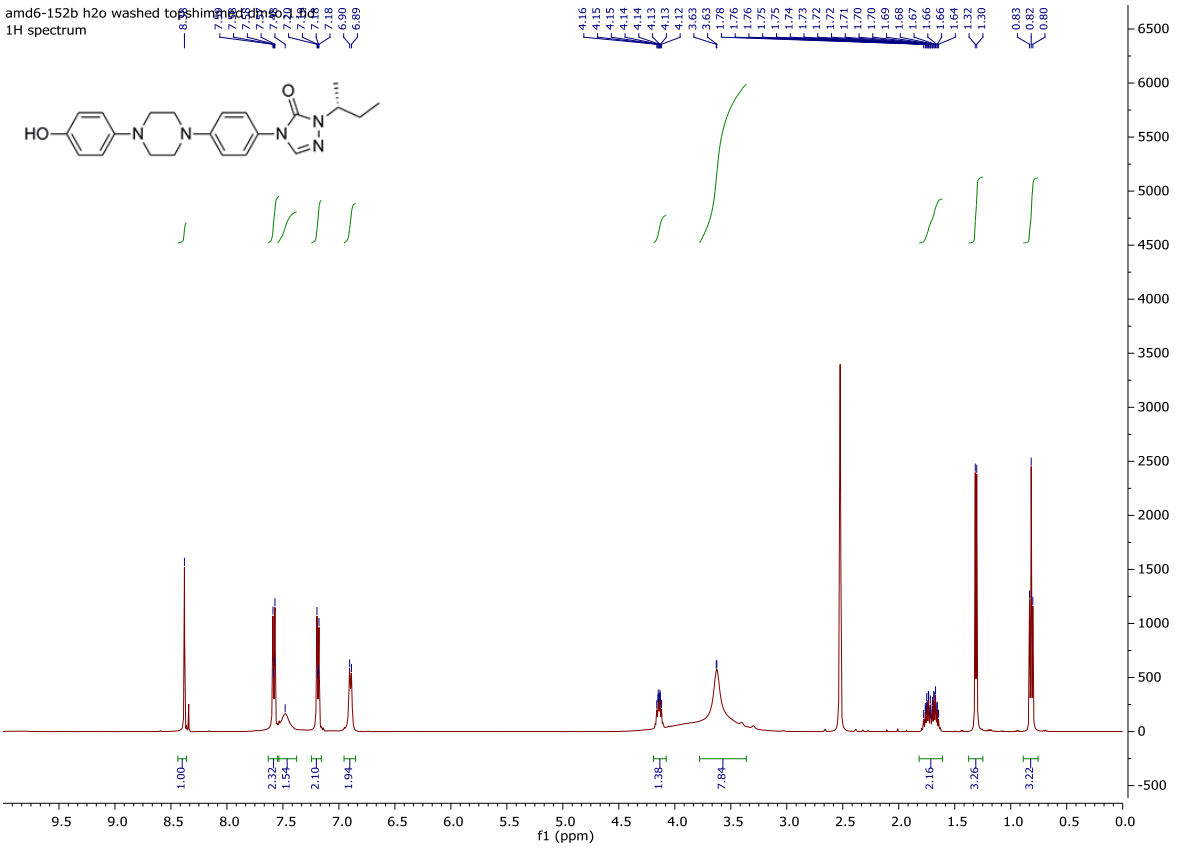
1H spectrum
f1 (ppm)

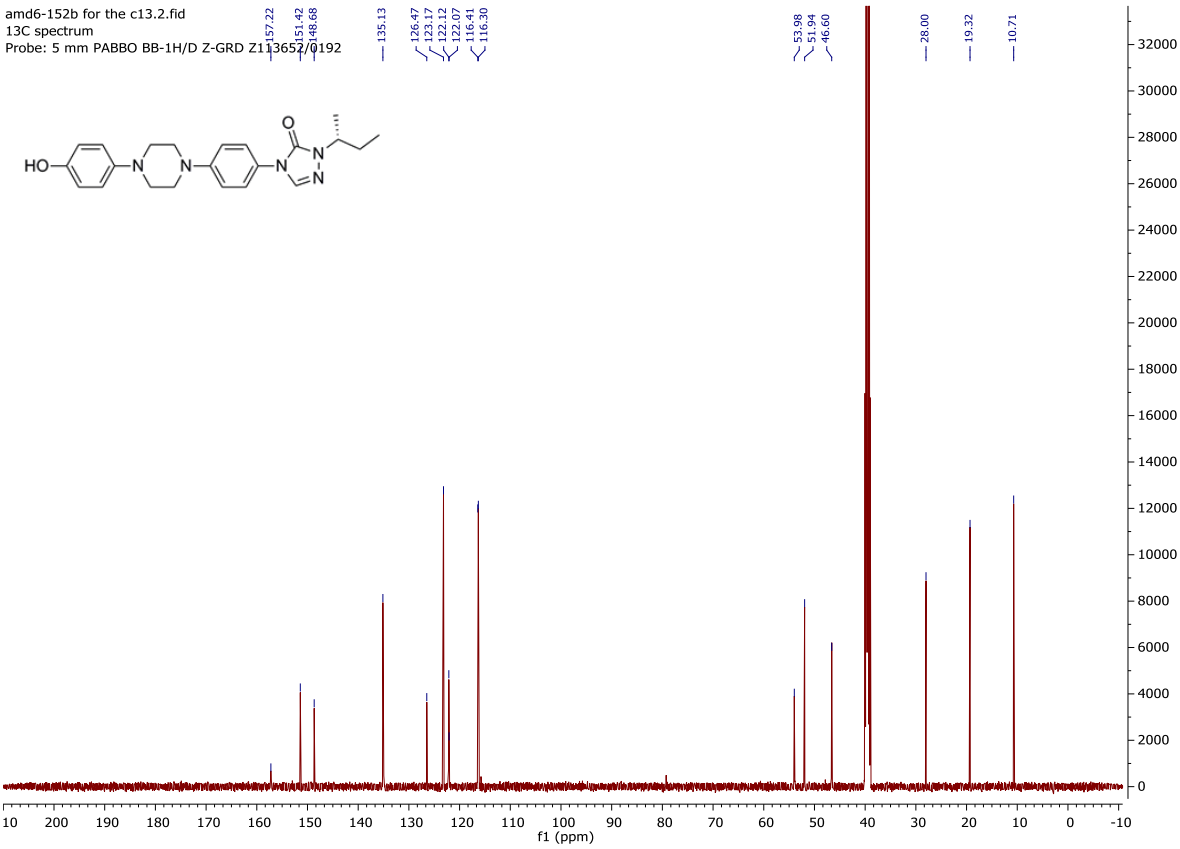
13C spectrum
Probe: 5 mm PABBO BB-1H/D Z-GRD Z113652/0192
f1 (ppm)

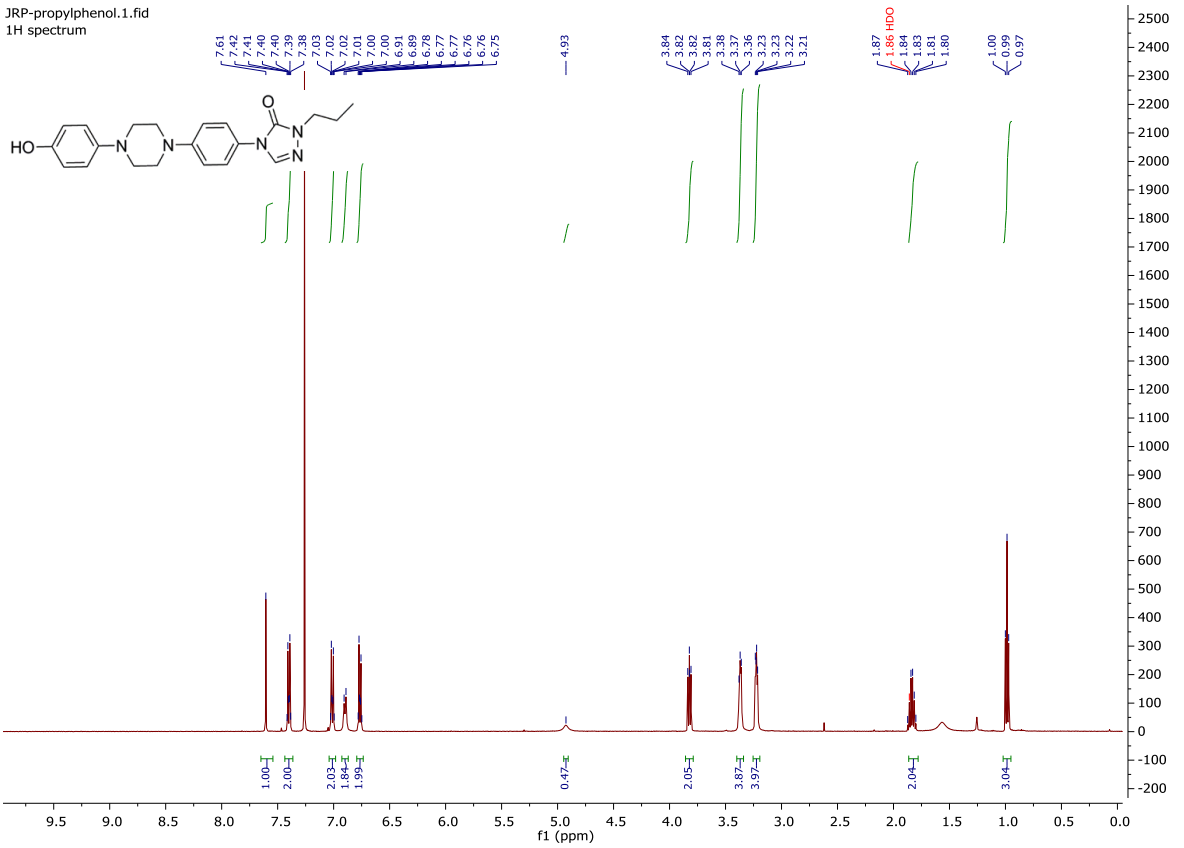
JRP-propylphenol.1.fid
1H spectrum
HO
O
N
N
N
N
7.61
7.42
7.41
7.40
7.40
7.39
7.38
7.03
7.02
7.02
7.01
7.00
7.00
6.91
6.89
6.78
6.77
6.76
6.76
6.75
4.93
3.84
3.82
3.82
3.81
3.38
3.37
3.36
3.23
3.23
3.22
3.21
1.87
1.86 HDO
1.84
1.83
1.81
1.80
1.00
0.99
0.97
1.00
2.00
2.03
1.84
1.99
0.47
2.05
3.87
3.97
2.04
3.04
f1 (ppm)

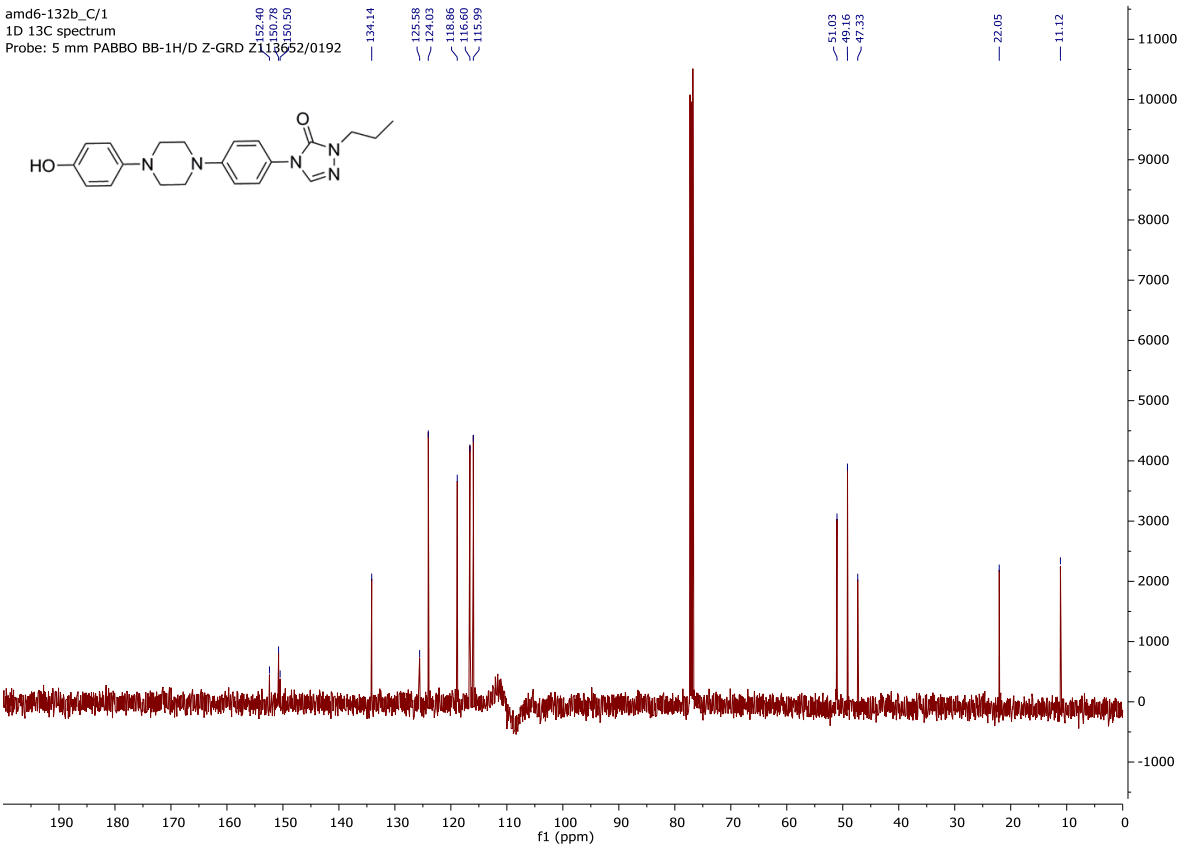
amd6-132b_C/1
1D 13C spectrum
Probe: 5 mm PABBO BB-1H/D Z-GRD Z113652/0192
HO
O
N
N
N
N
152.40
150.78
150.50
134.14
125.58
124.03
118.86
116.60
115.99
51.03
49.16
47.33
22.05
11.12
f1 (ppm)

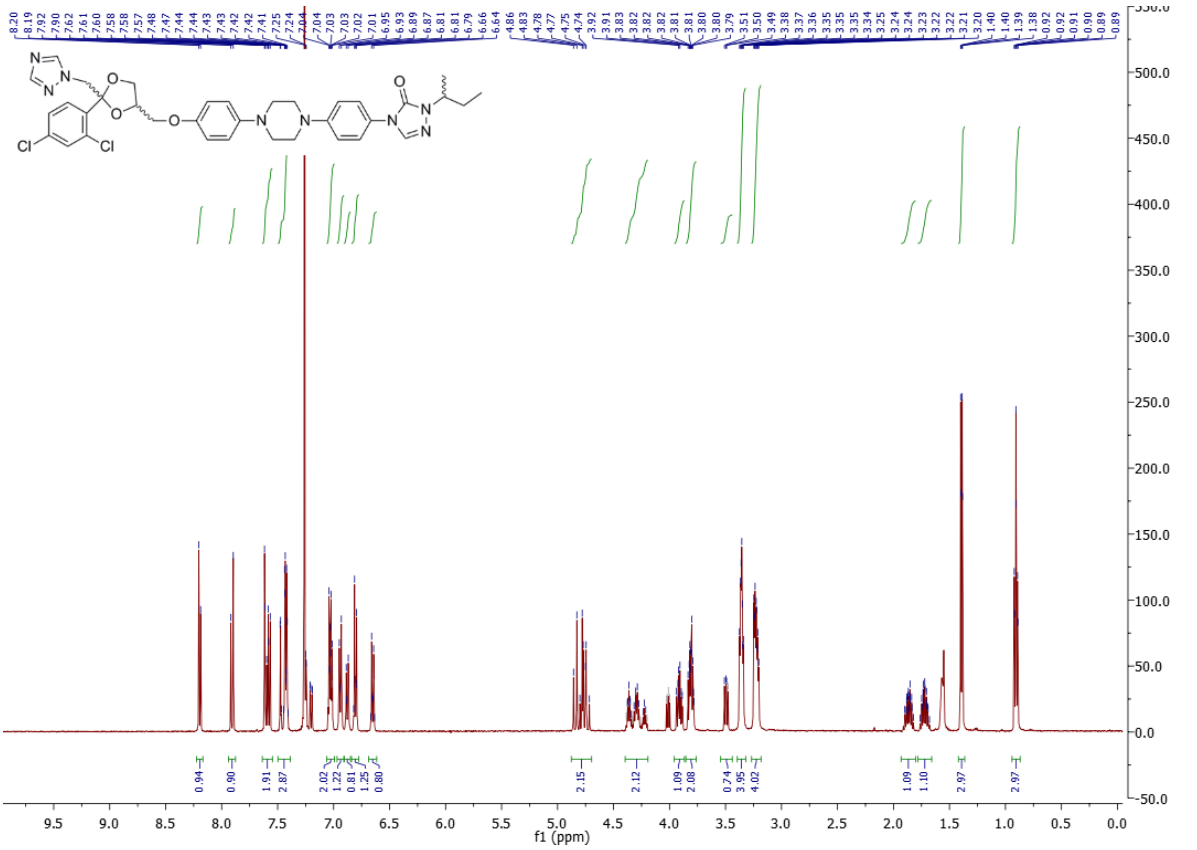
f1 (ppm)

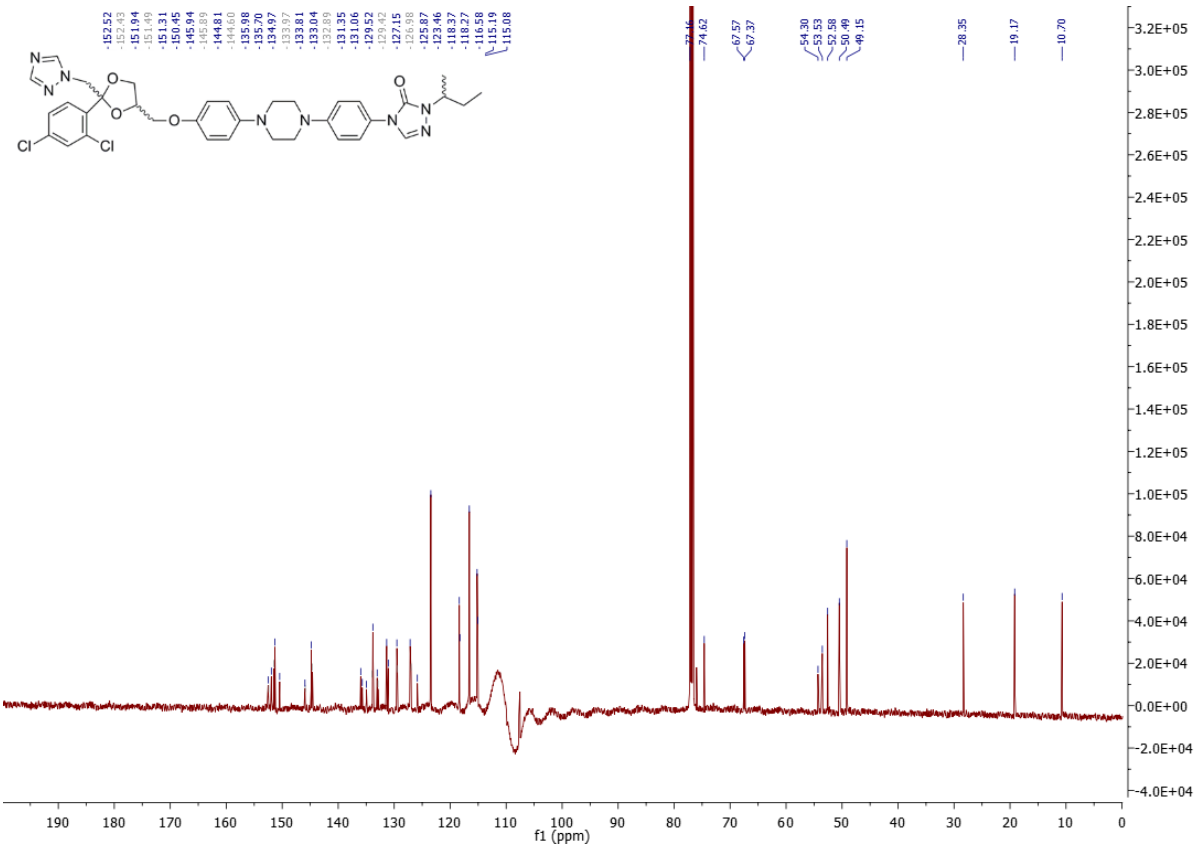
f1 (ppm)

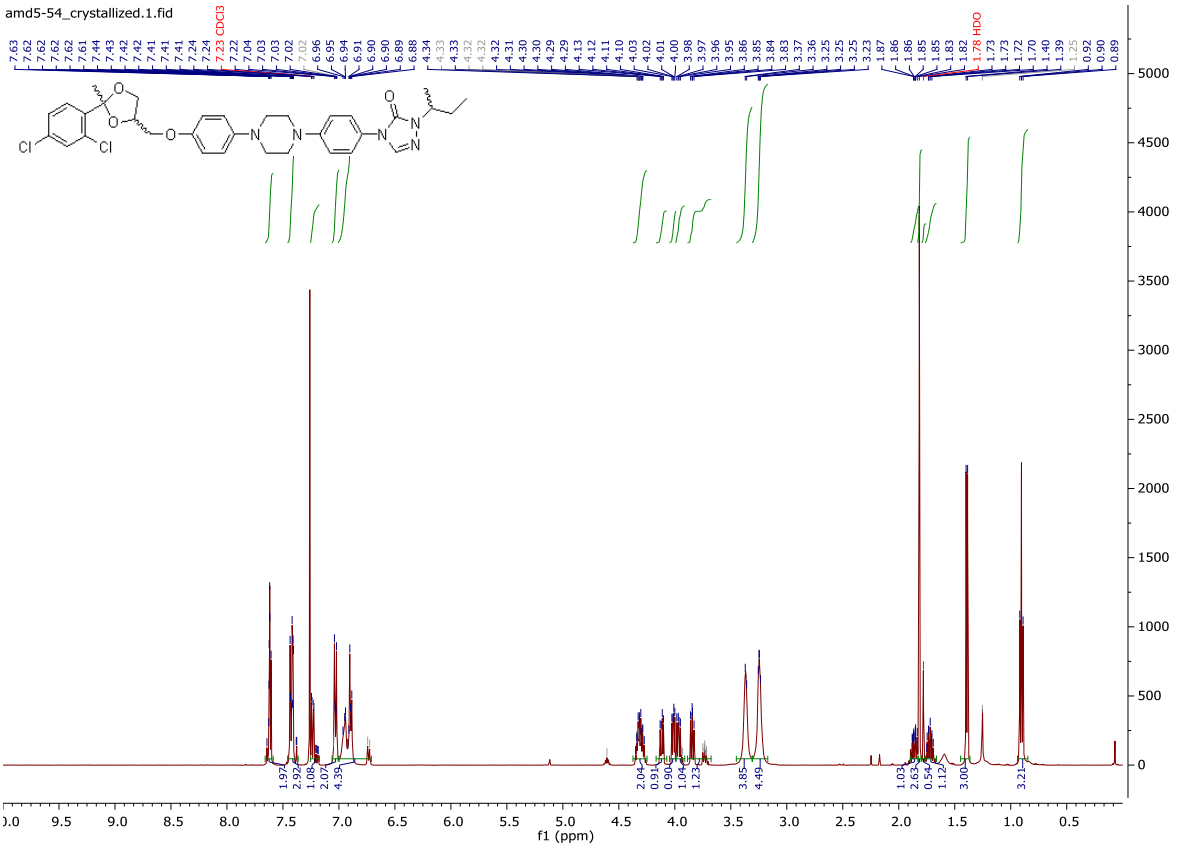
amd5-54_crystallized.1.fid
f1 (ppm)

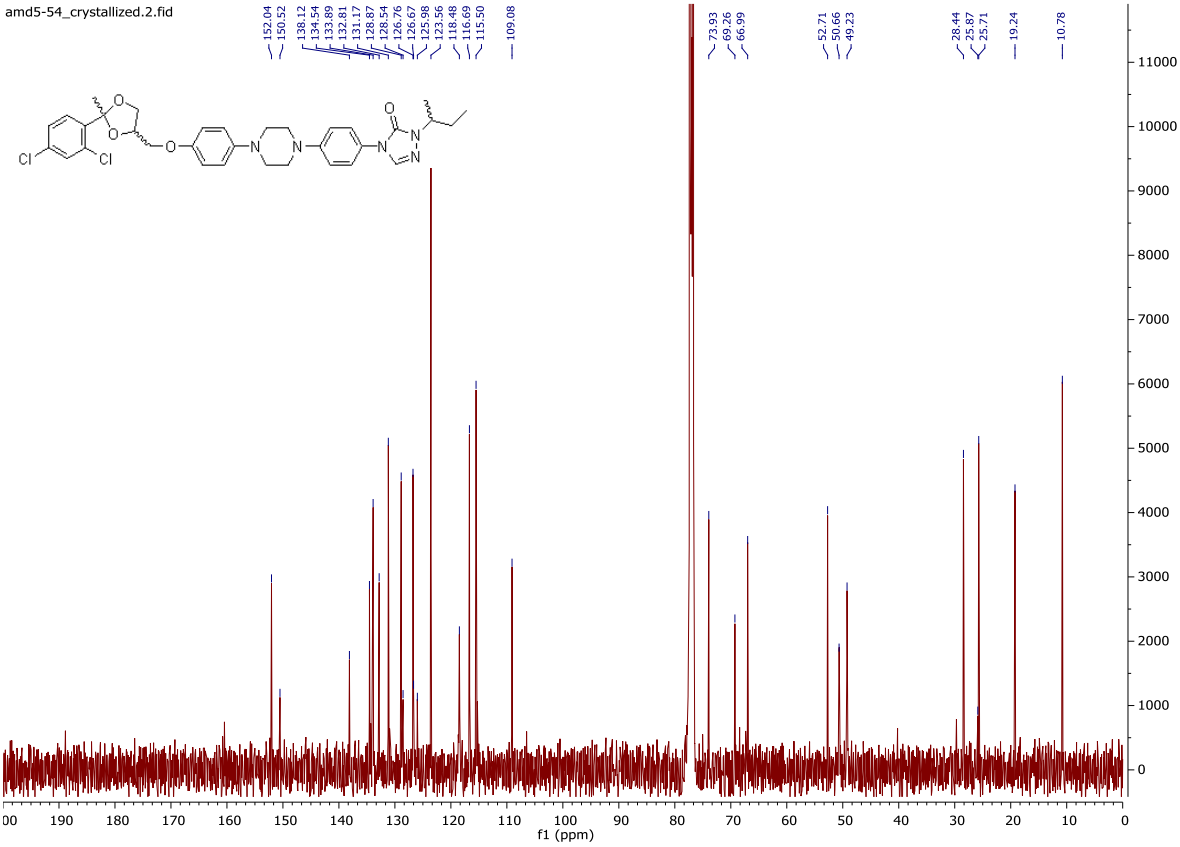
amd5-54_crystallized.2.fid
f1 (ppm)

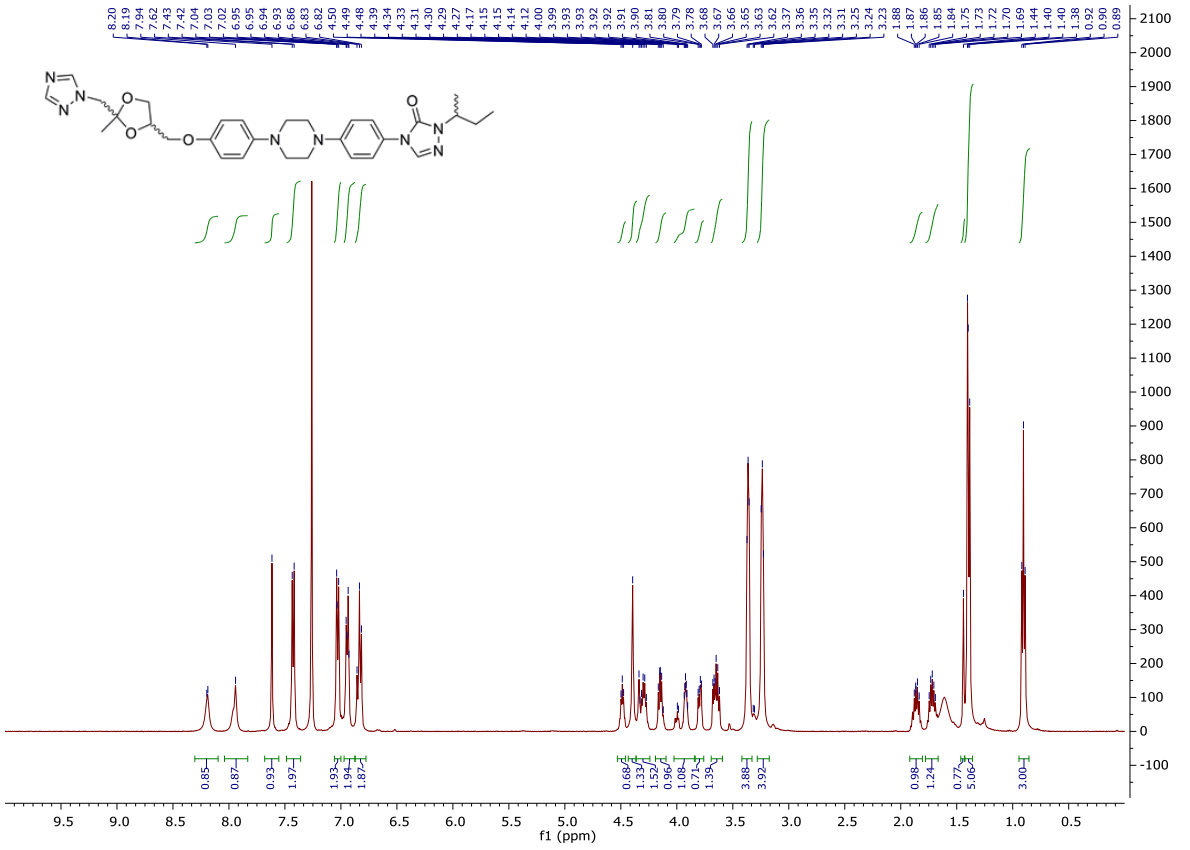
f1 (ppm)

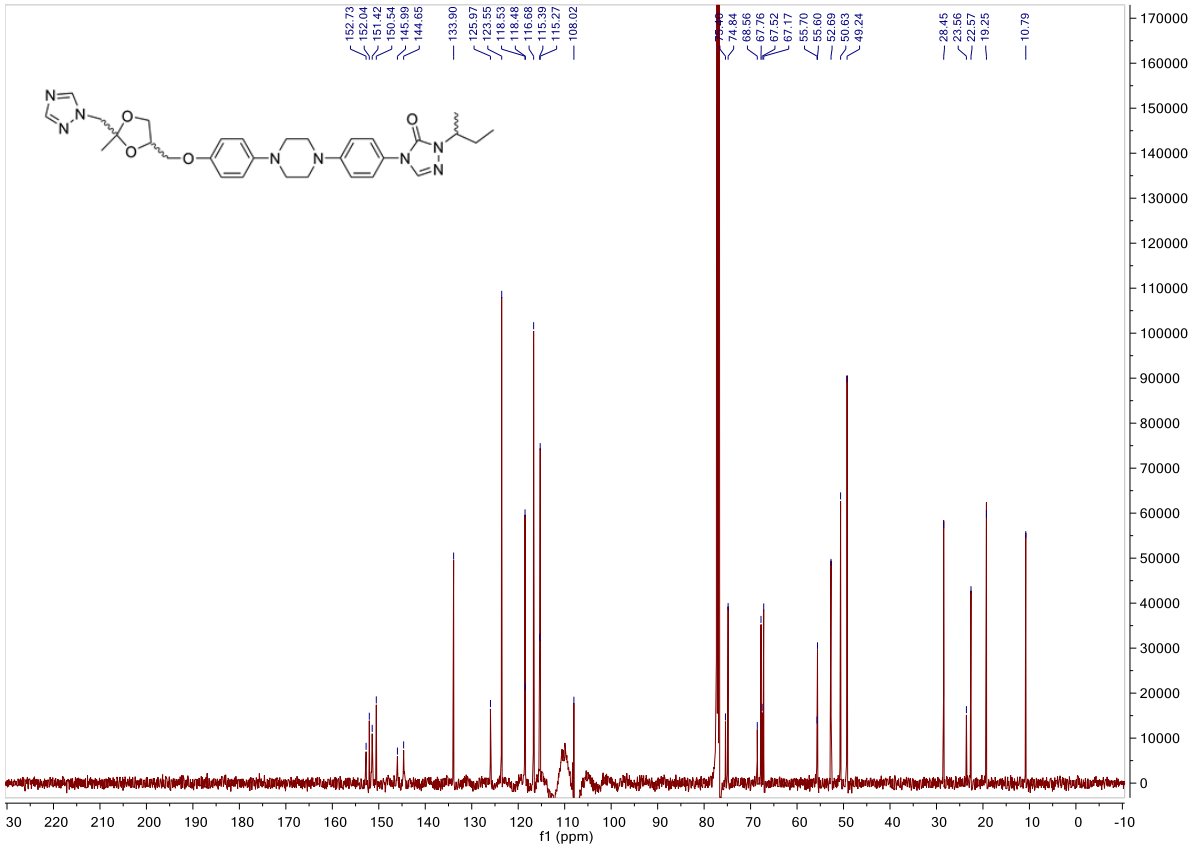
f1 (ppm)

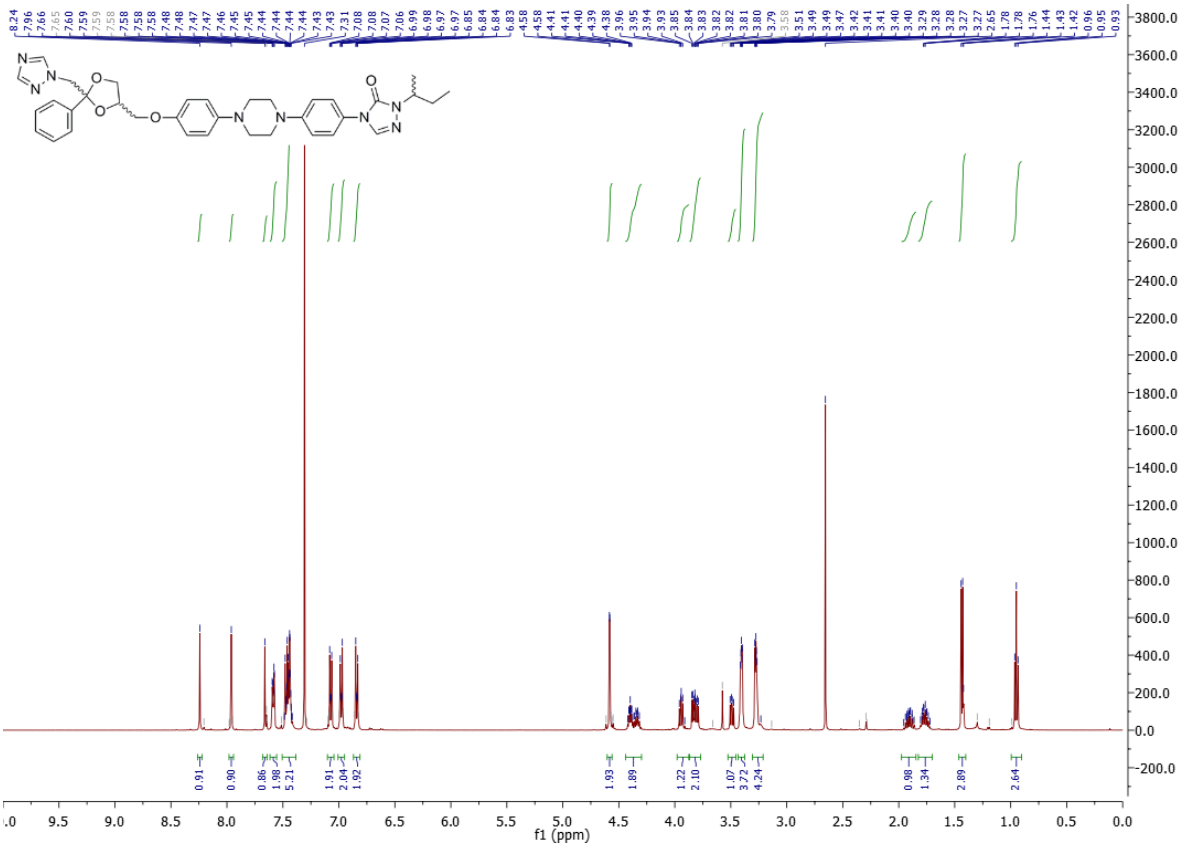
f1 (ppm)

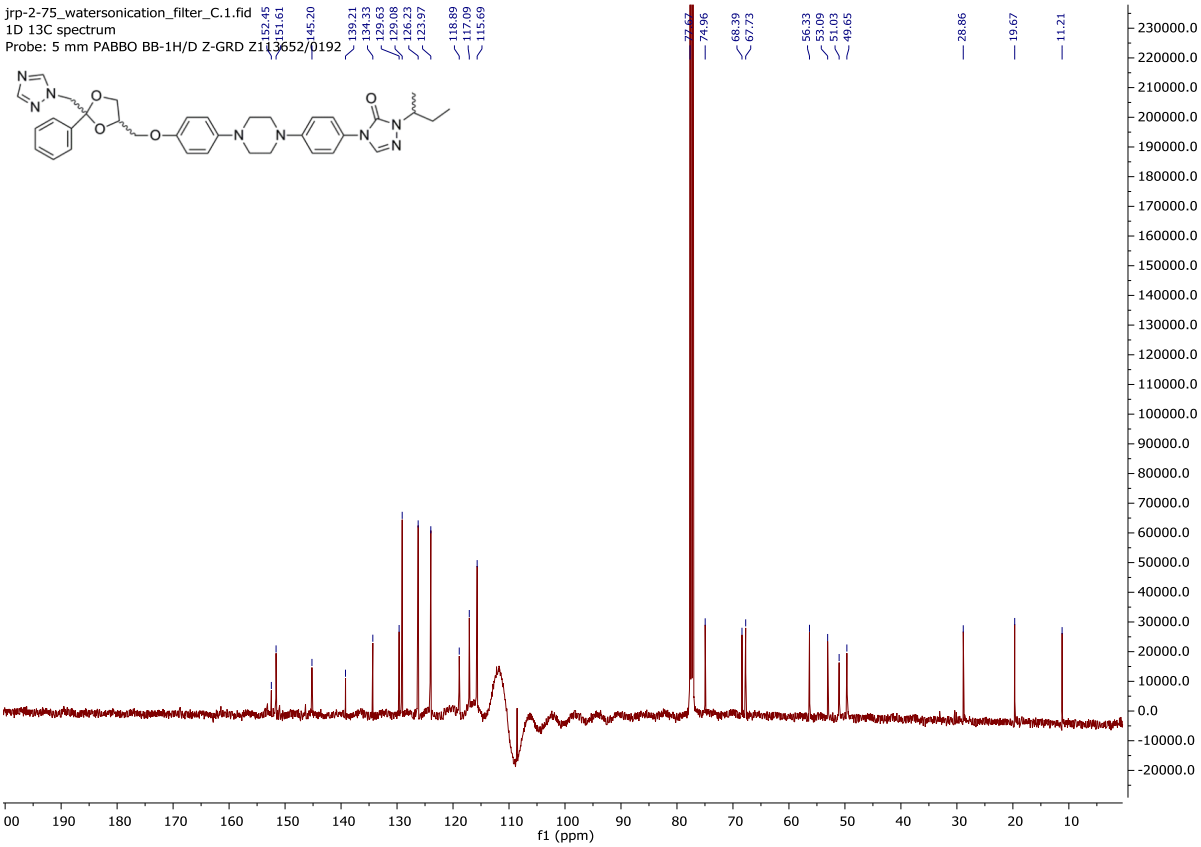
jrp-2-75_watersonication_filter_C.1.fid
1D 13C spectrum
Probe: 5 mm PABBO BB-1H/D Z-GRD Z113652/0192
f1 (ppm)

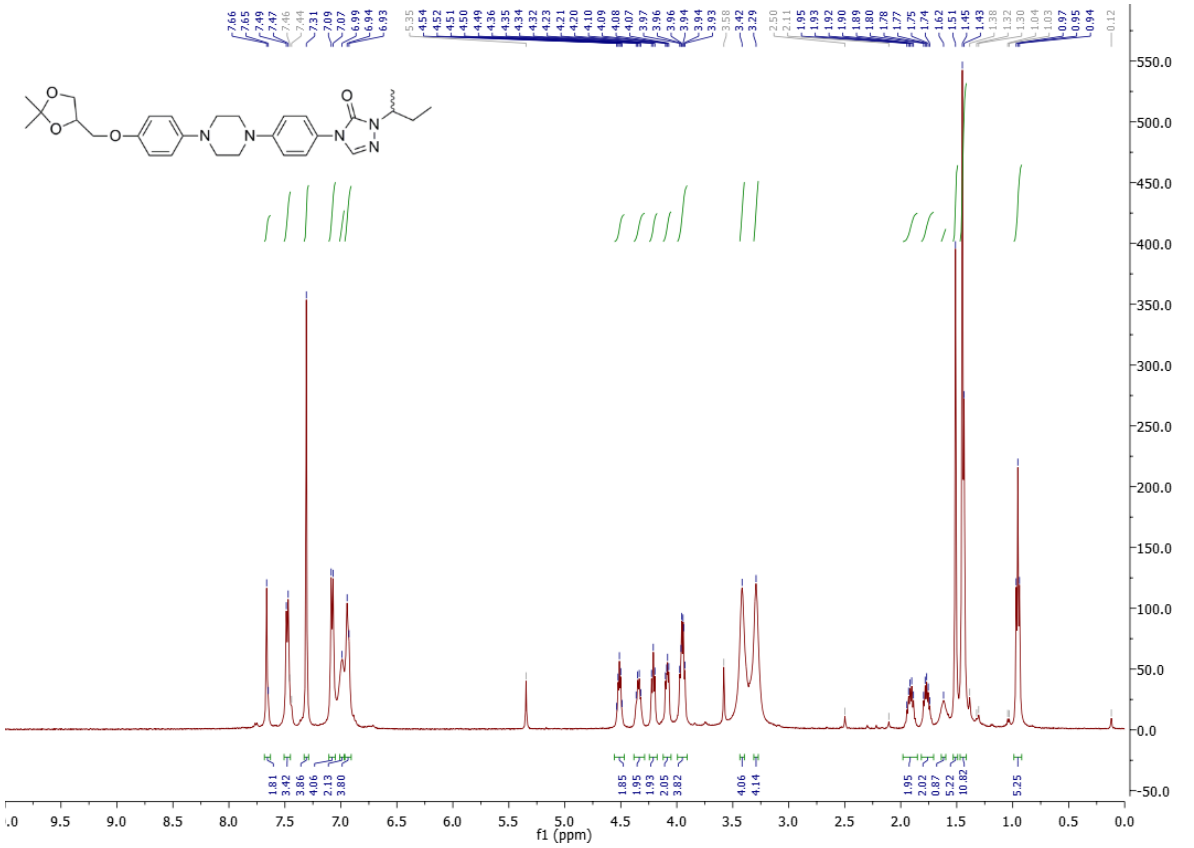
f1 (ppm)

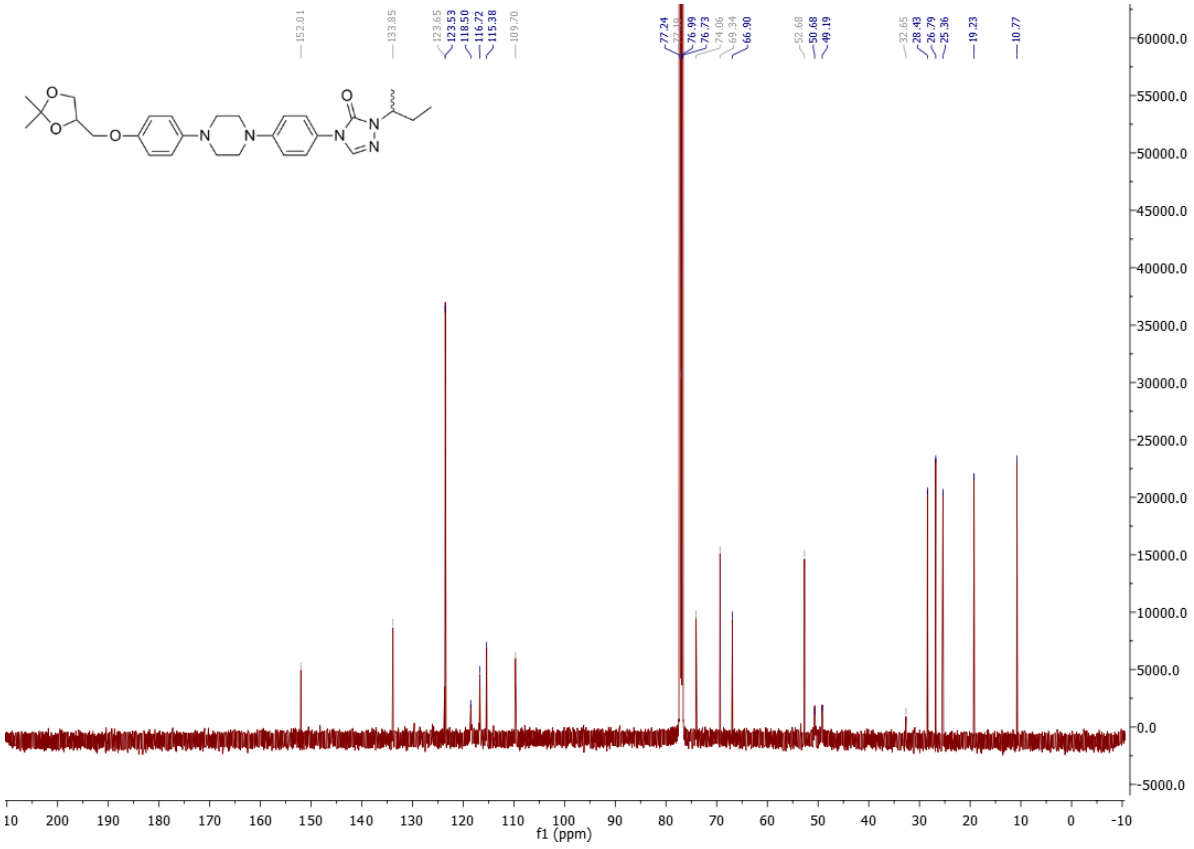
f1 (ppm)

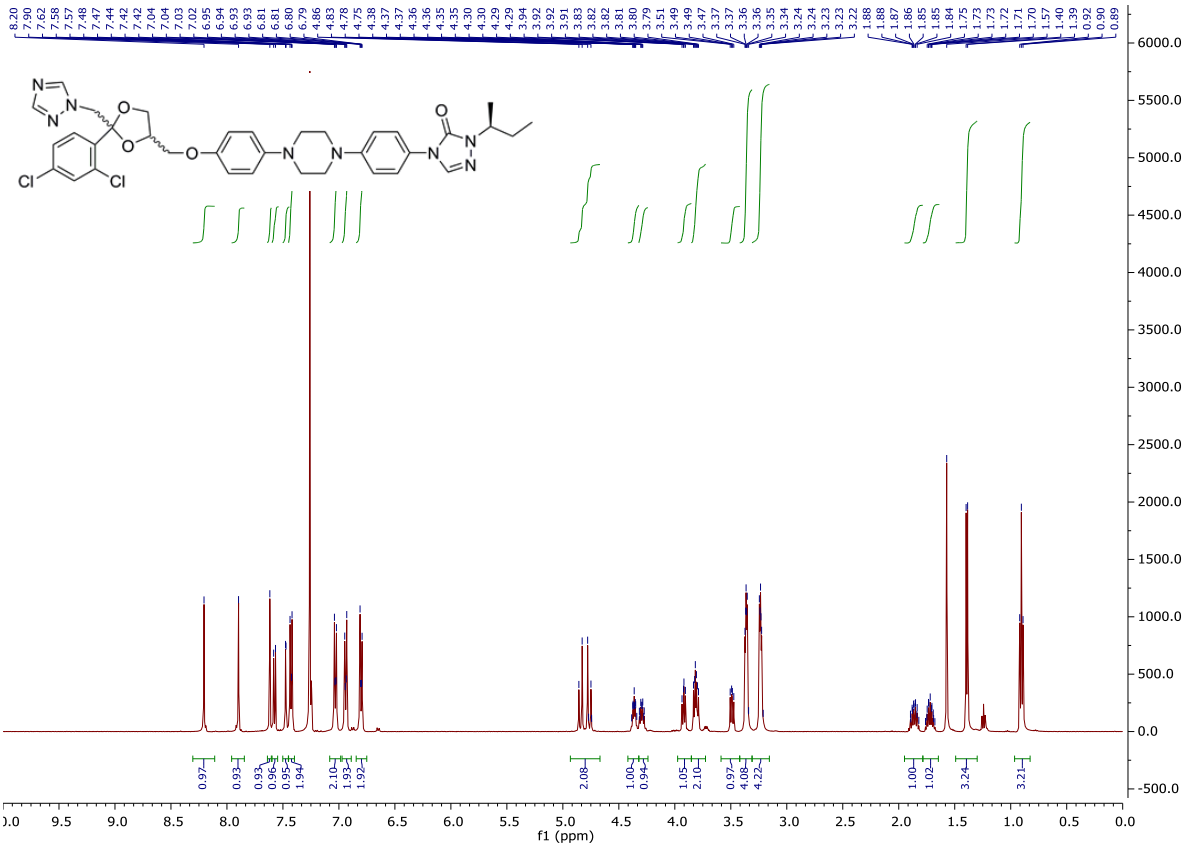
f1 (ppm)

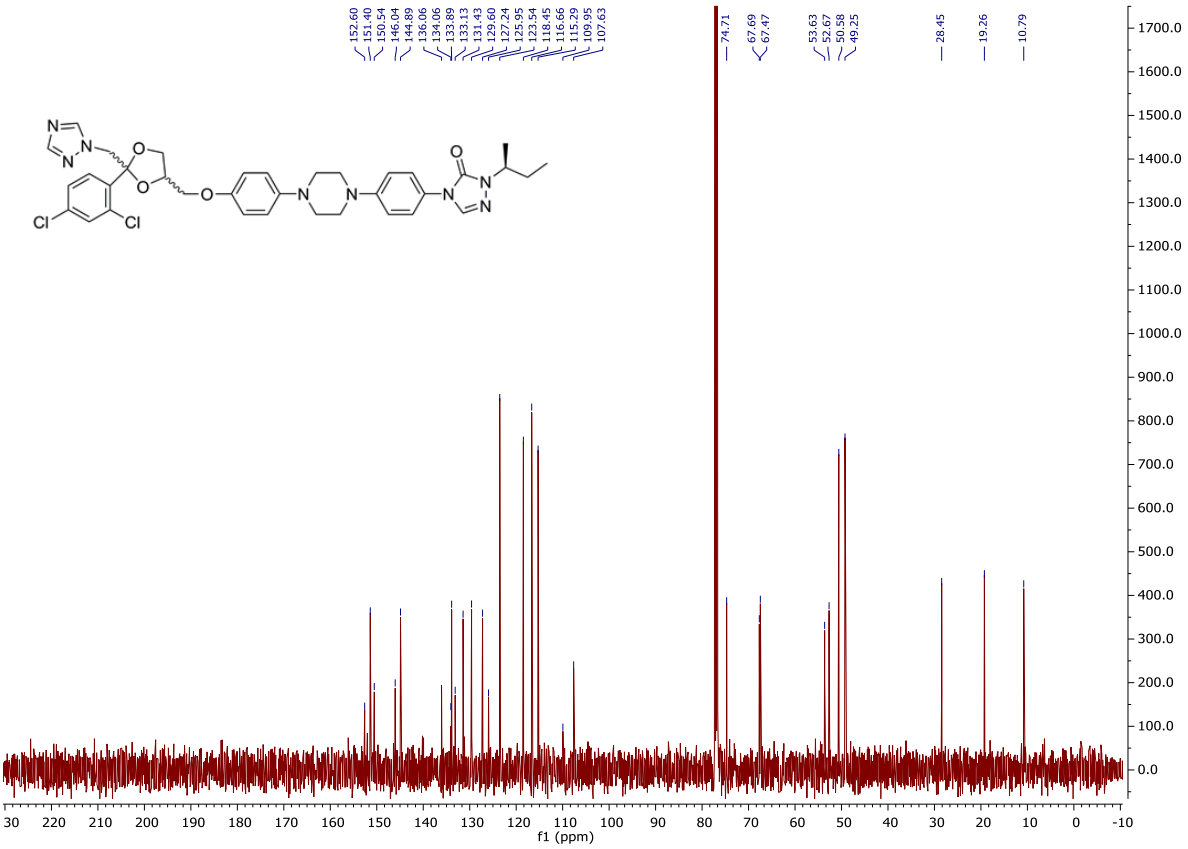
f1 (ppm)

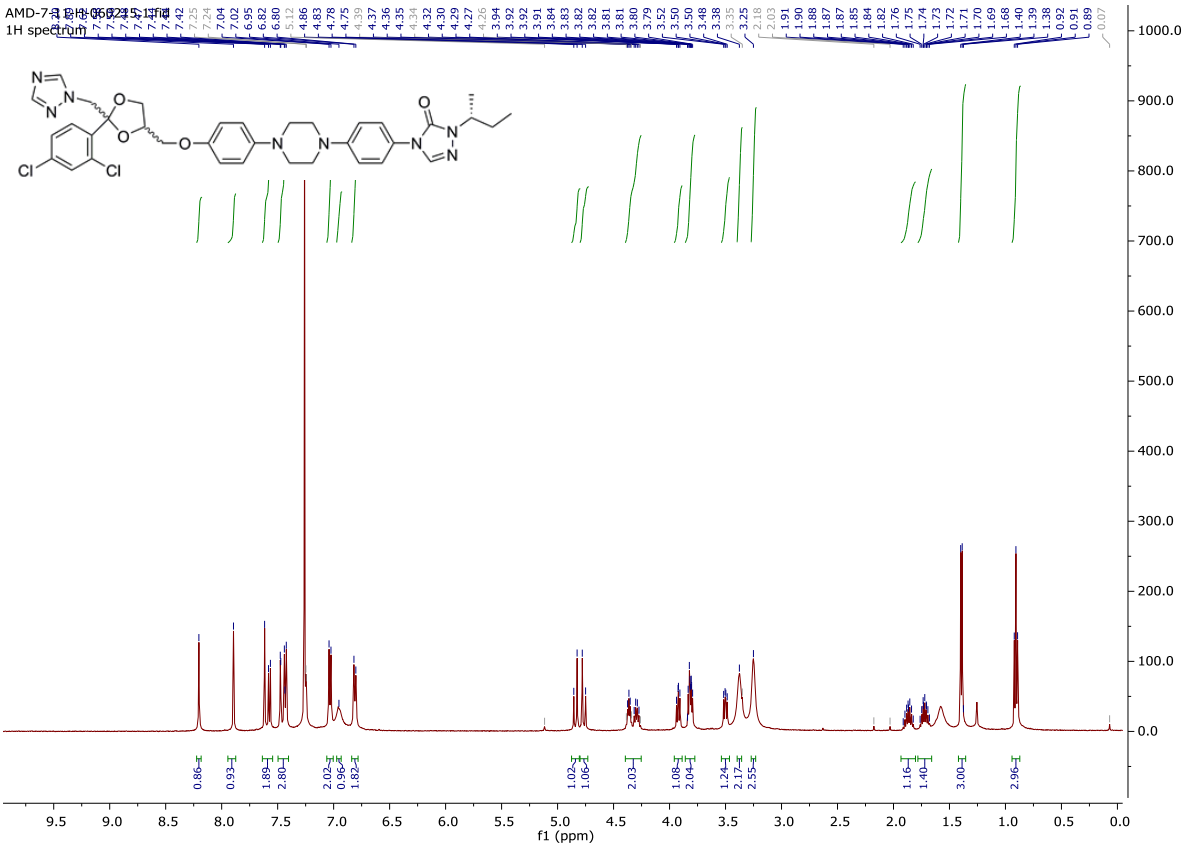
1H spectrum
f1 (ppm)

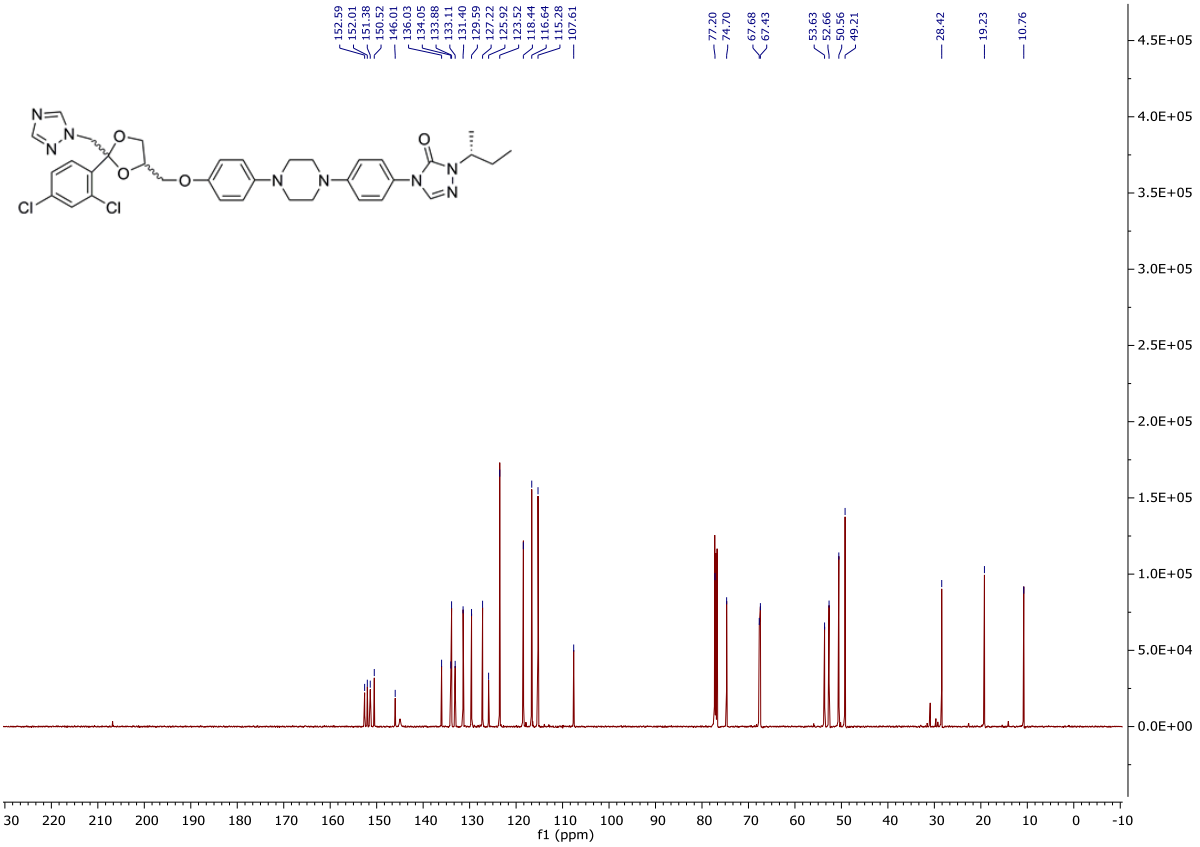
f1 (ppm)

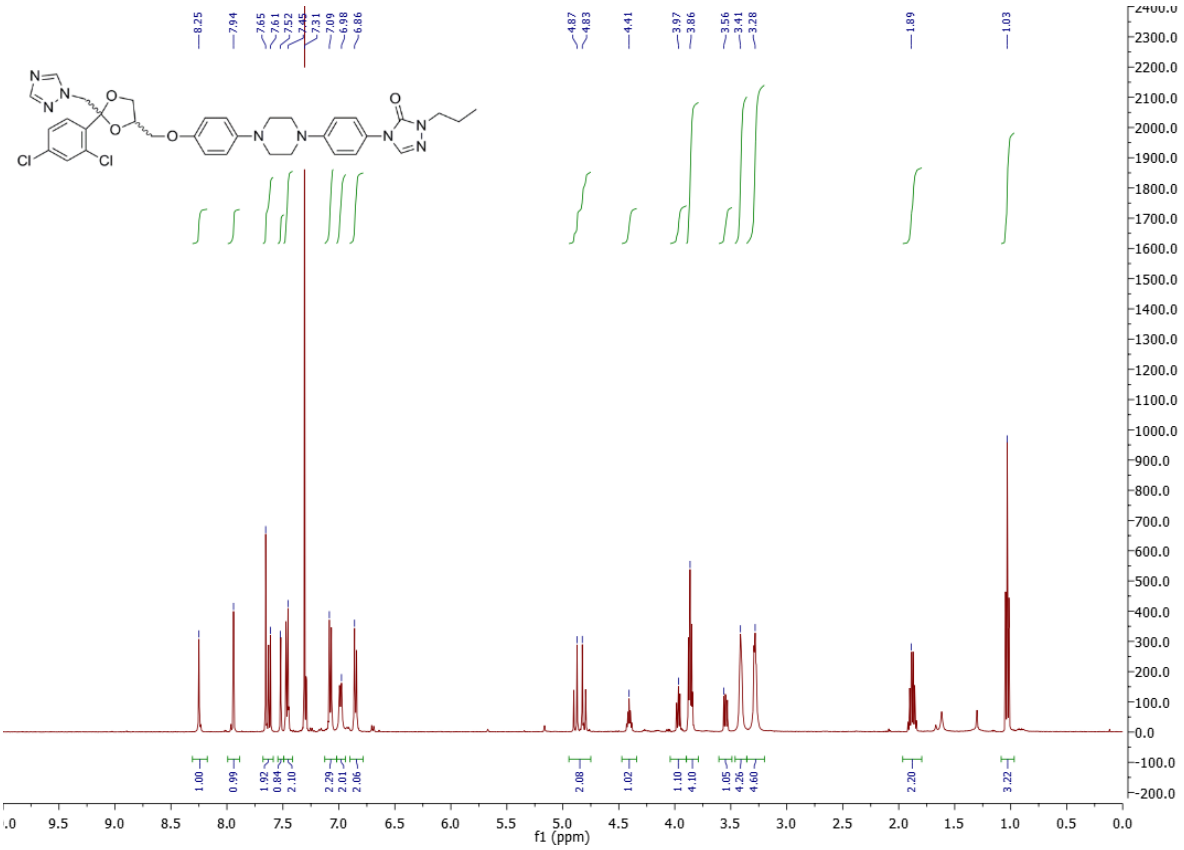
8.25
7.94
7.65
7.61
7.52
7.45
7.31
7.09
6.98
6.86
4.87
4.83
4.41
3.97
3.86
3.56
3.41
3.28
1.89
1.03
1.00
0.99
1.92
0.84
2.10
2.29
2.01
2.06
2.08
1.02
1.10
4.10
1.05
4.26
4.60
2.20
3.22
f1 (ppm)

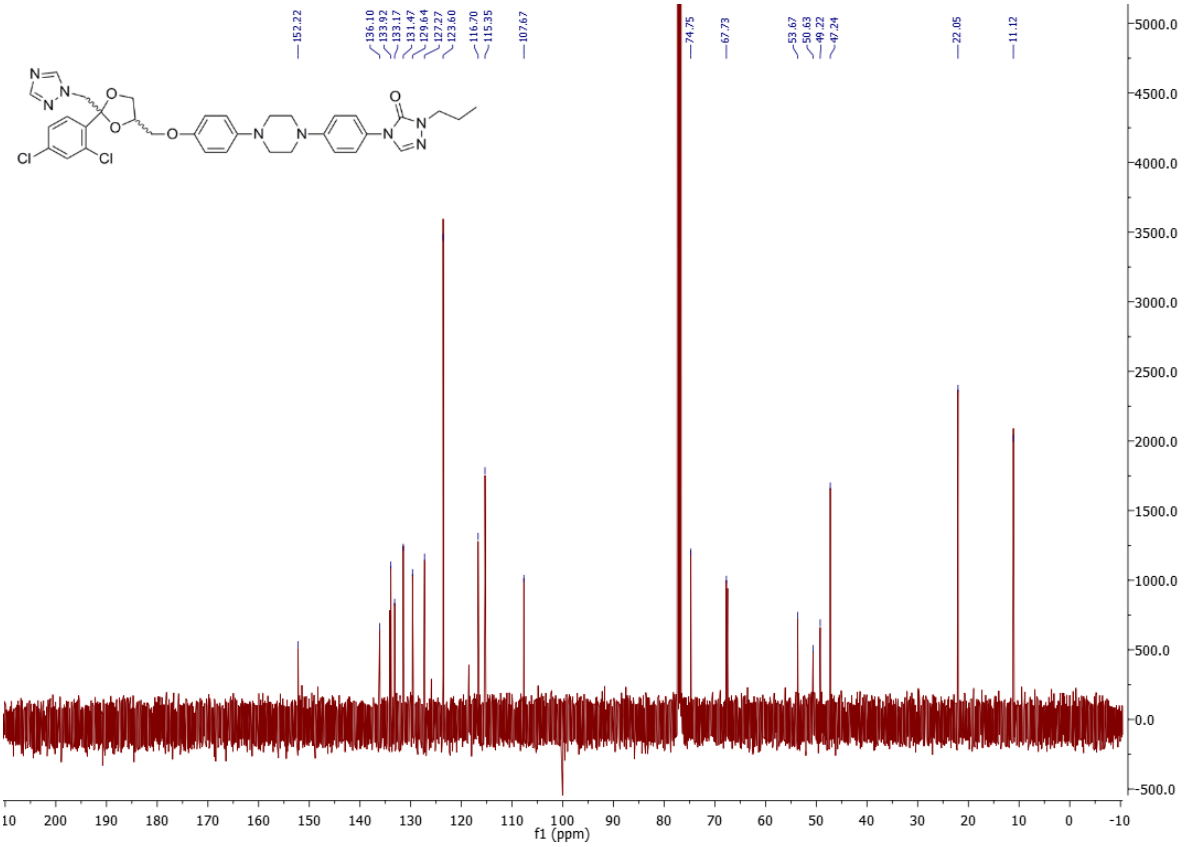
152.22
136.10
133.92
133.17
131.47
129.64
127.27
123.60
116.70
115.35
107.67
74.75
67.73
53.67
50.63
49.22
47.24
22.05
11.12
f1 (ppm)

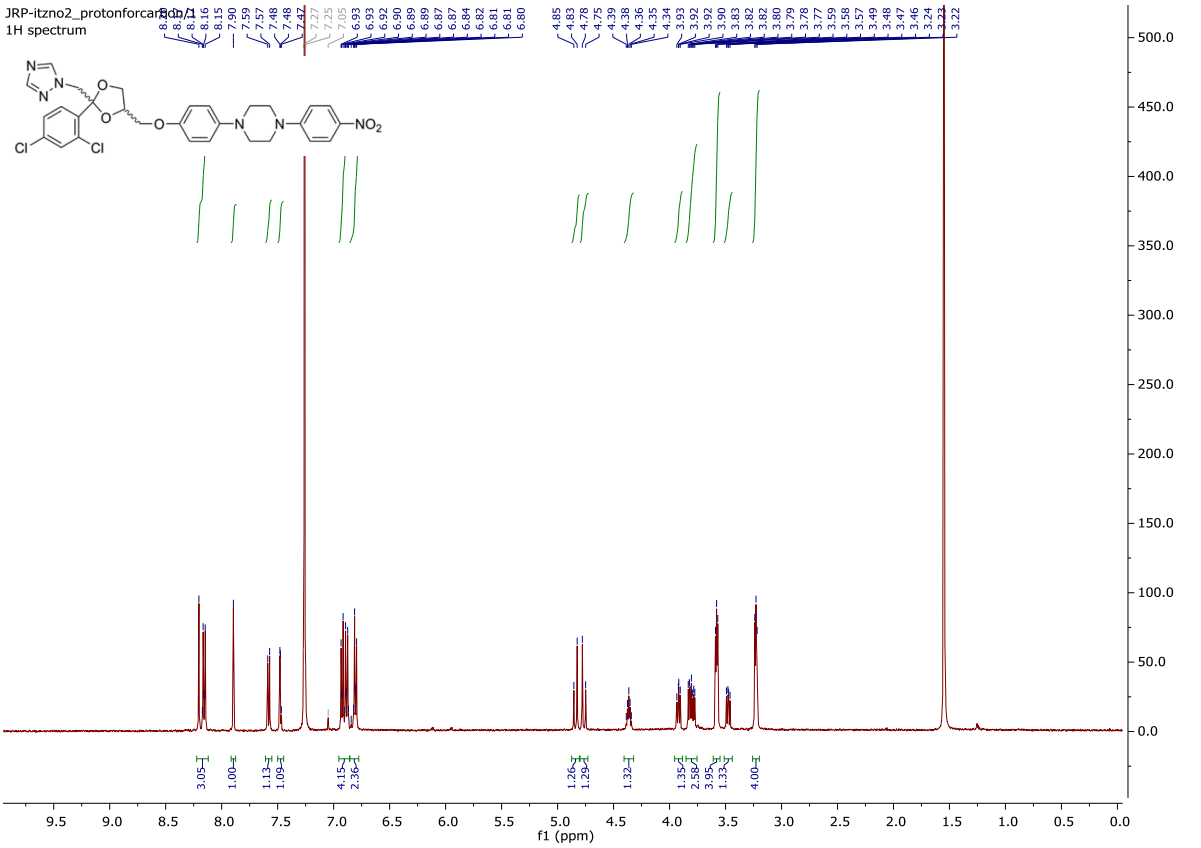
JRP-itzno2_protonforcarbon/1
1H spectrum
f1 (ppm)

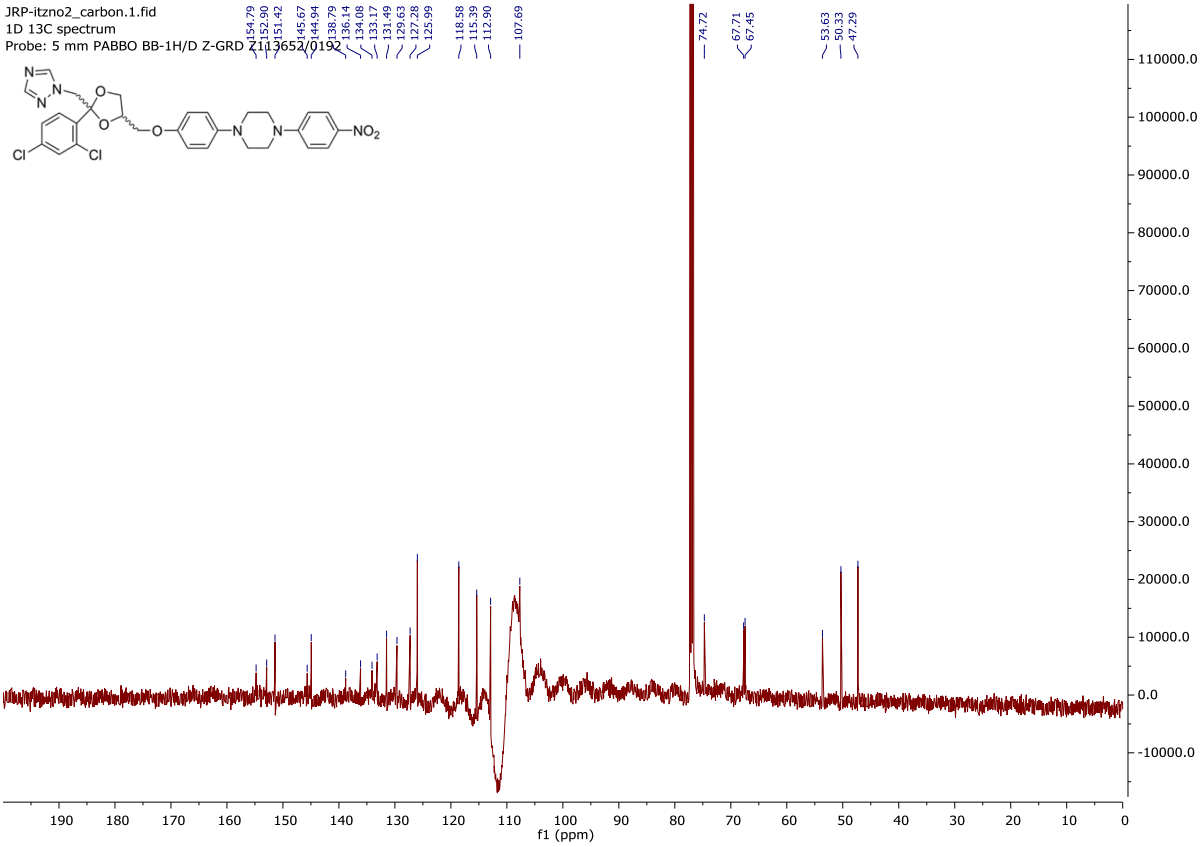
JRP-itzno2_carbon.1.fid
1D 13C spectrum
Probe: 5 mm PABBO BB-1H/D Z-GRD Z113652/0192
f1 (ppm)

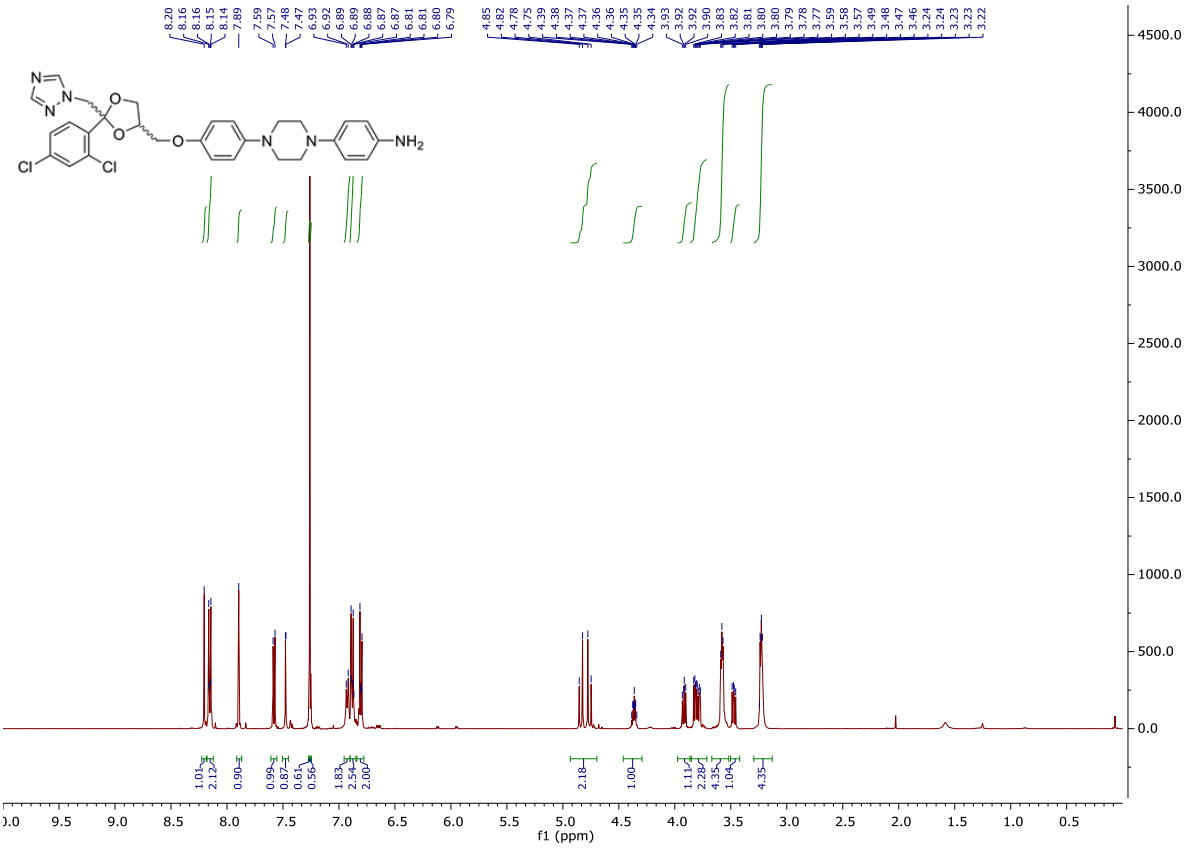
f1 (ppm)

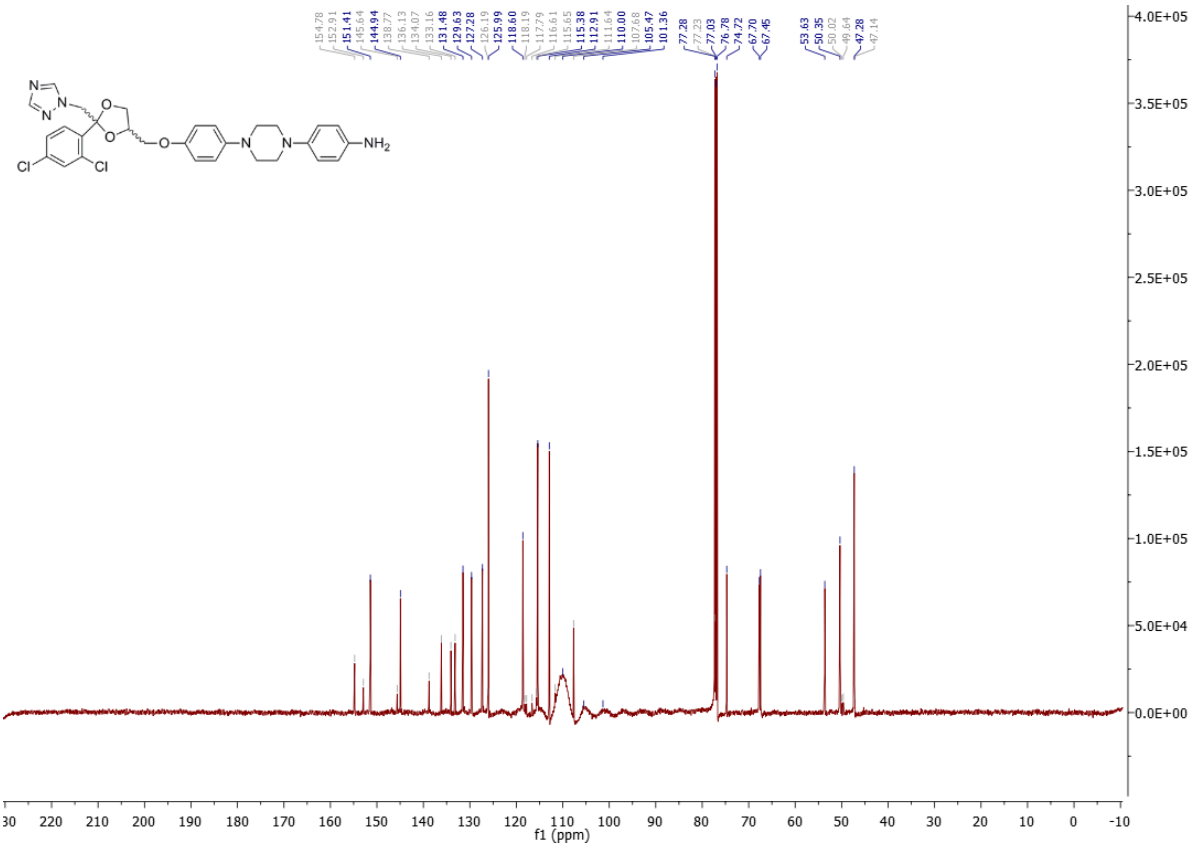
f1 (ppm)

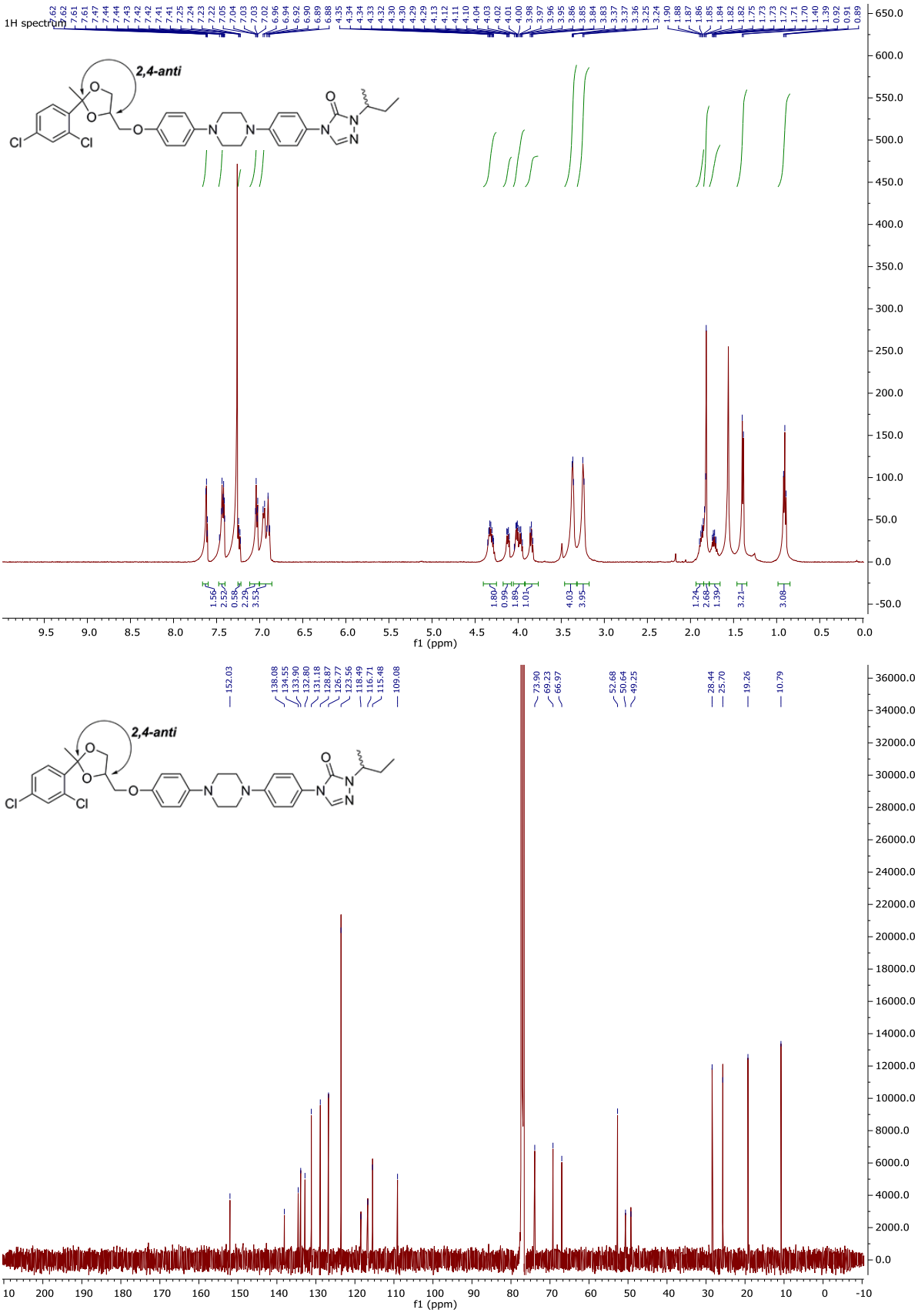
1H spectrum
2,4-anti
f1 (ppm)
2,4-anti
f1 (ppm)

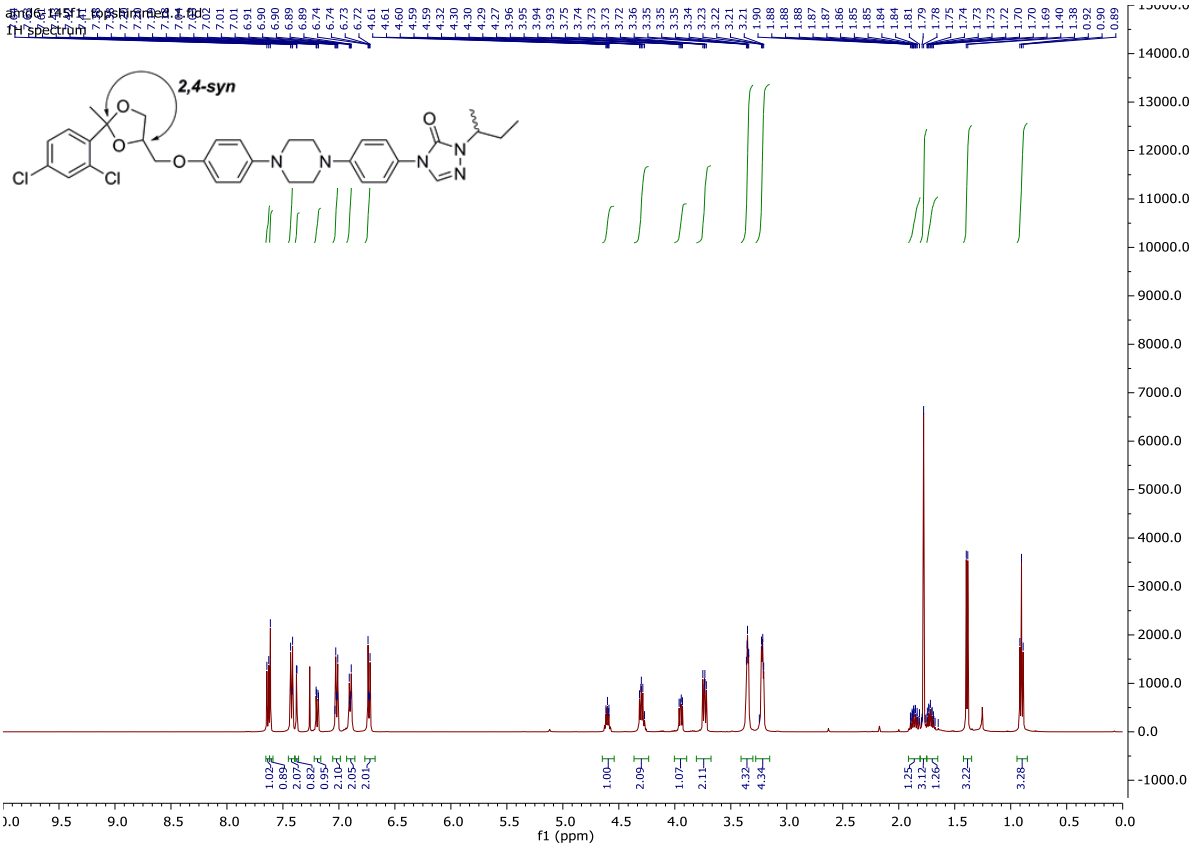
2,4-syn
Cl
Cl
O
N
f1 (ppm)

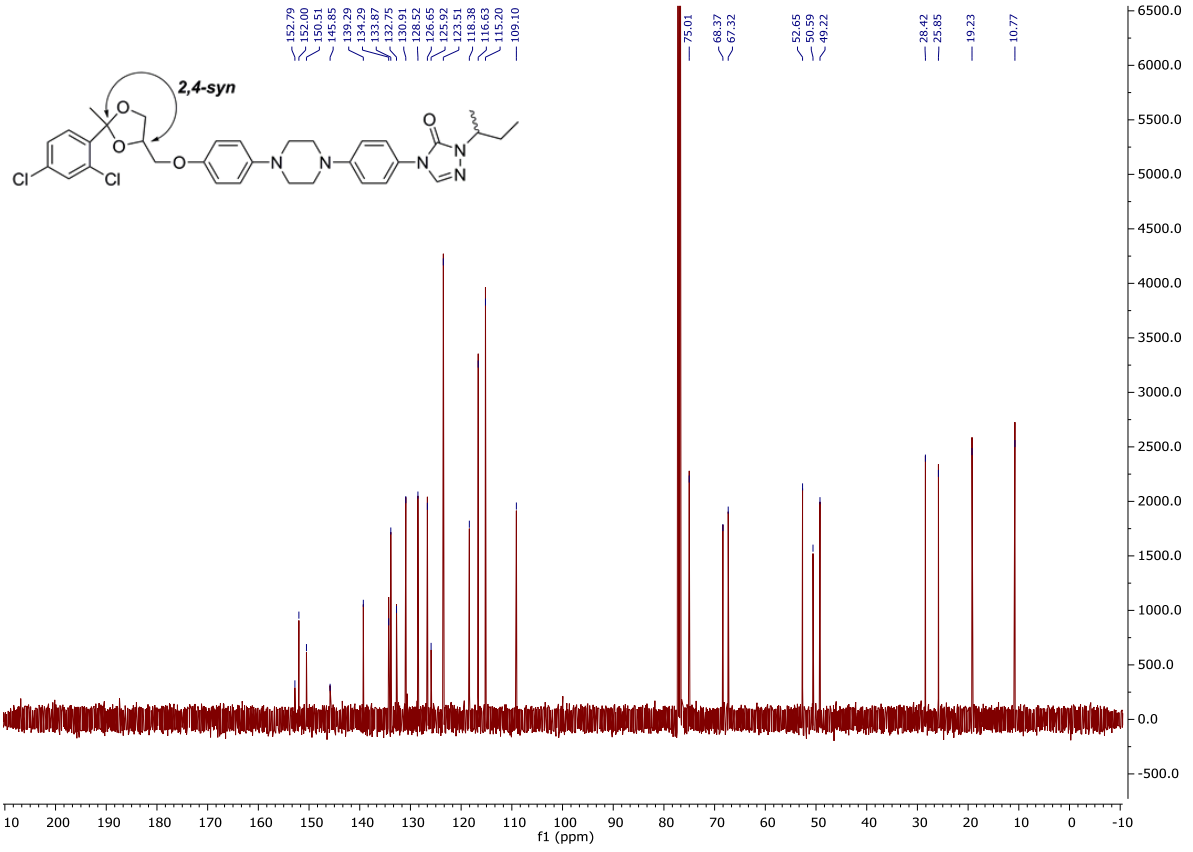
2,4-syn
Cl
Cl
O
N
f1 (ppm)

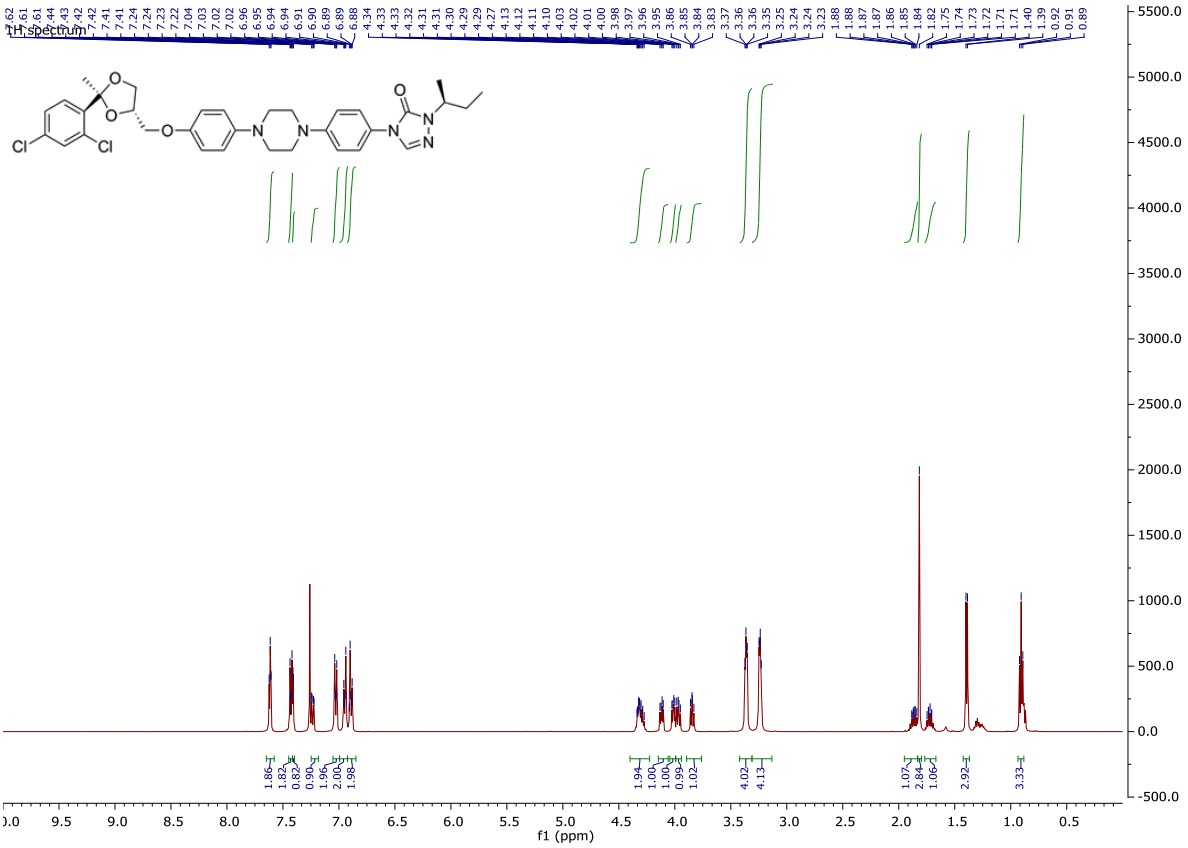
1H spectrum
f1 (ppm)

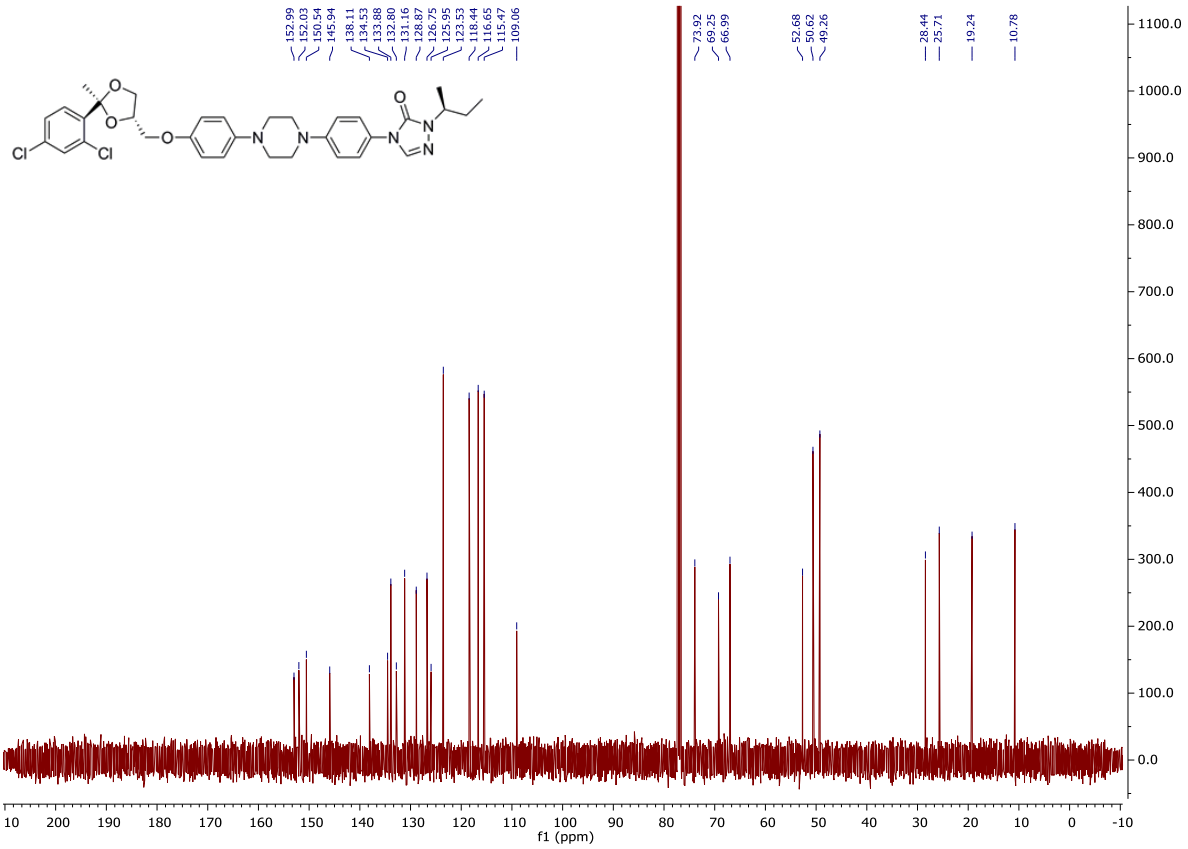
f1 (ppm)

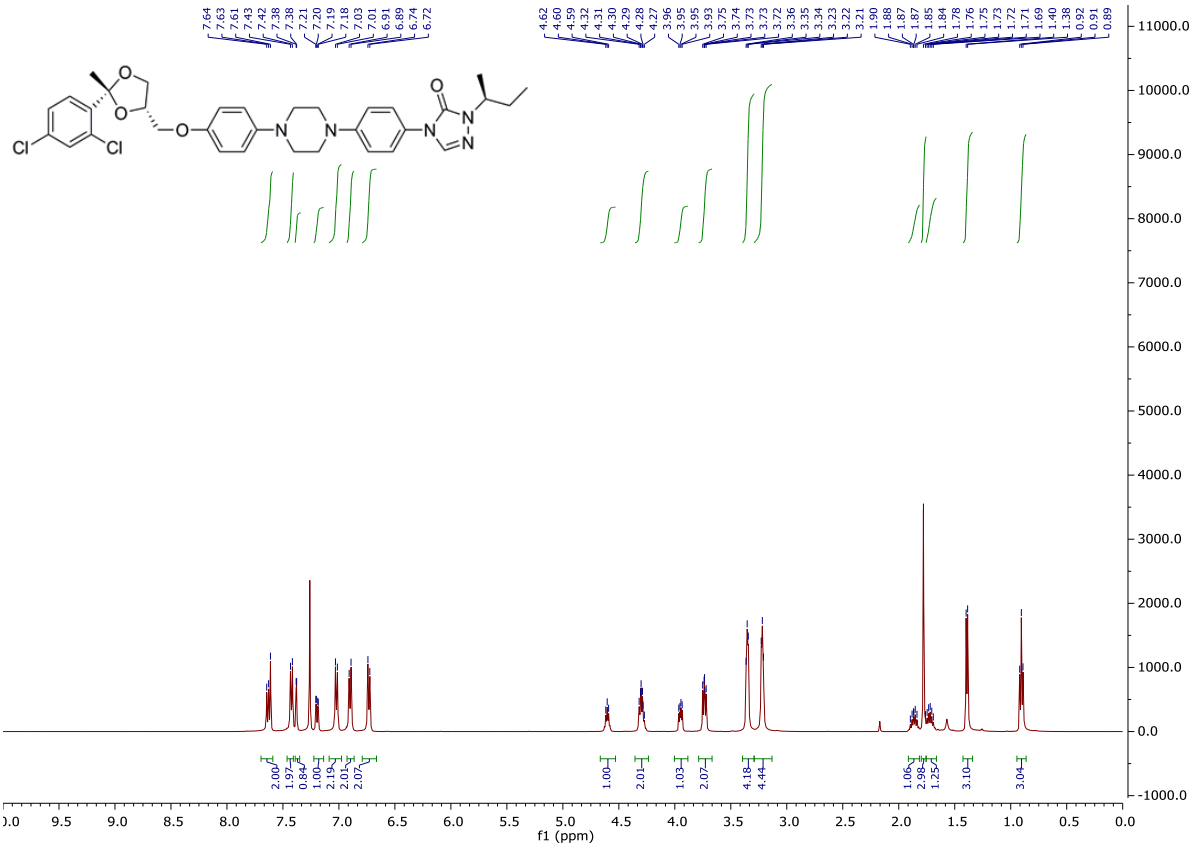
7.64
7.63
7.61
7.43
7.42
7.38
7.38
7.21
7.20
7.19
7.18
7.03
7.01
6.91
6.89
6.74
6.72
4.62
4.60
4.59
4.32
4.31
4.30
4.29
4.28
4.27
3.96
3.95
3.95
3.93
3.75
3.74
3.73
3.73
3.72
3.36
3.35
3.34
3.23
3.22
3.21
1.90
1.88
1.87
1.87
1.85
1.84
1.78
1.76
1.75
1.73
1.72
1.71
1.69
1.40
1.38
0.92
0.91
0.89
2.00
1.97
0.84
1.00
2.19
2.01
2.07
1.00
2.01
1.03
2.07
4.18
4.44
1.06
2.98
1.25
3.10
3.04
f1 (ppm)

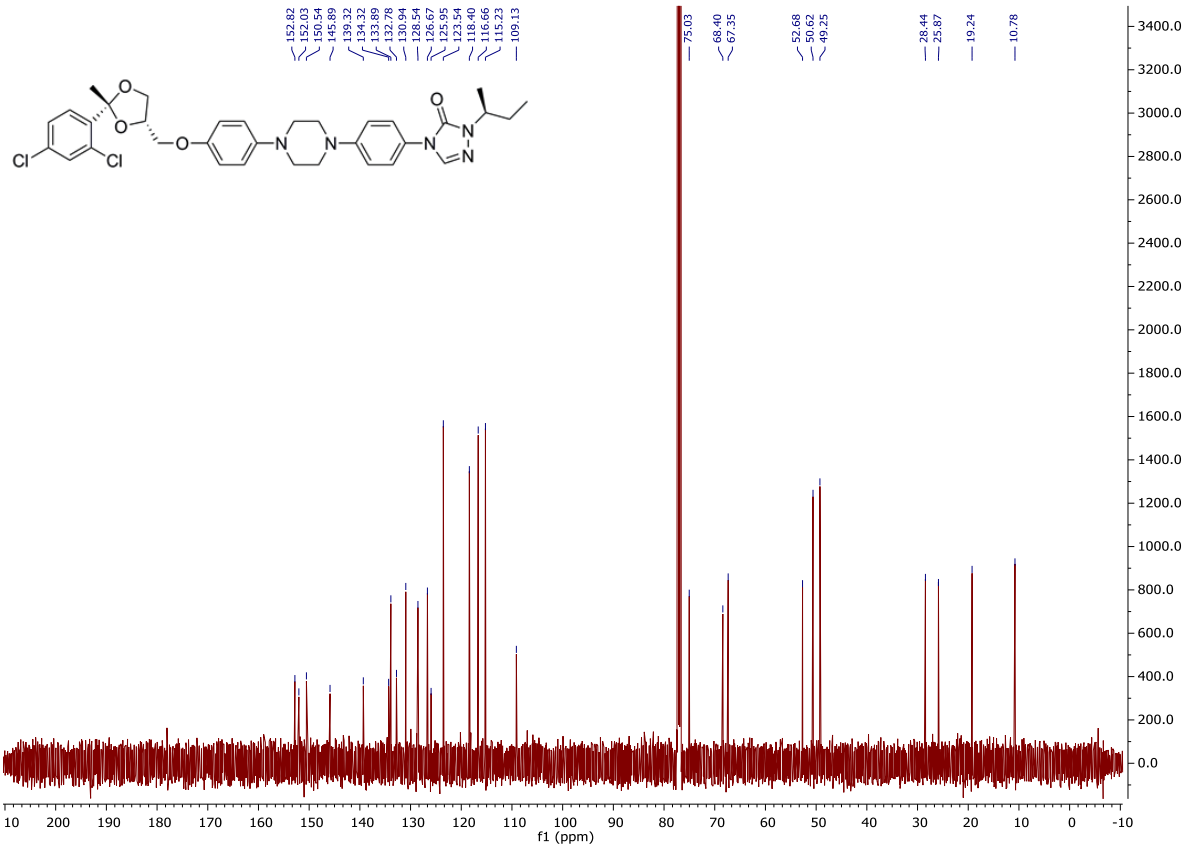
152.82
152.03
150.54
145.89
139.32
134.32
133.89
132.78
130.94
128.54
126.67
125.95
123.54
118.40
116.66
115.23
109.13
75.03
68.40
67.35
52.68
50.62
49.25
28.44
25.87
19.24
10.78
f1 (ppm)

X-Ray:

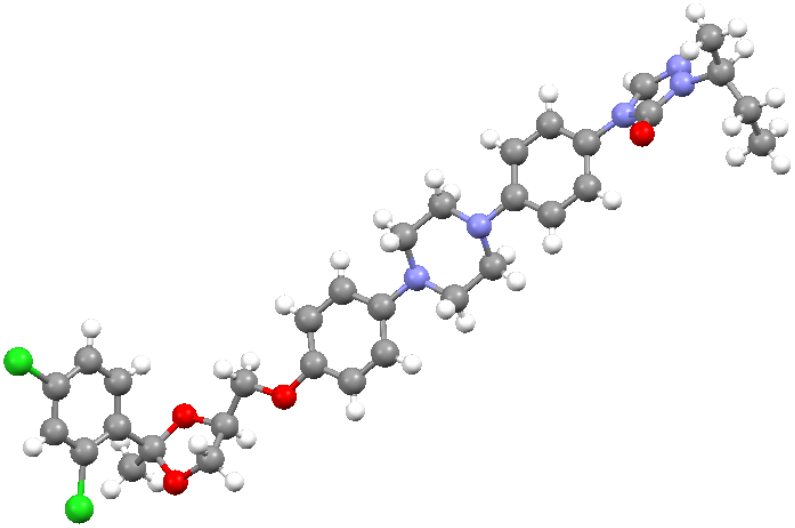

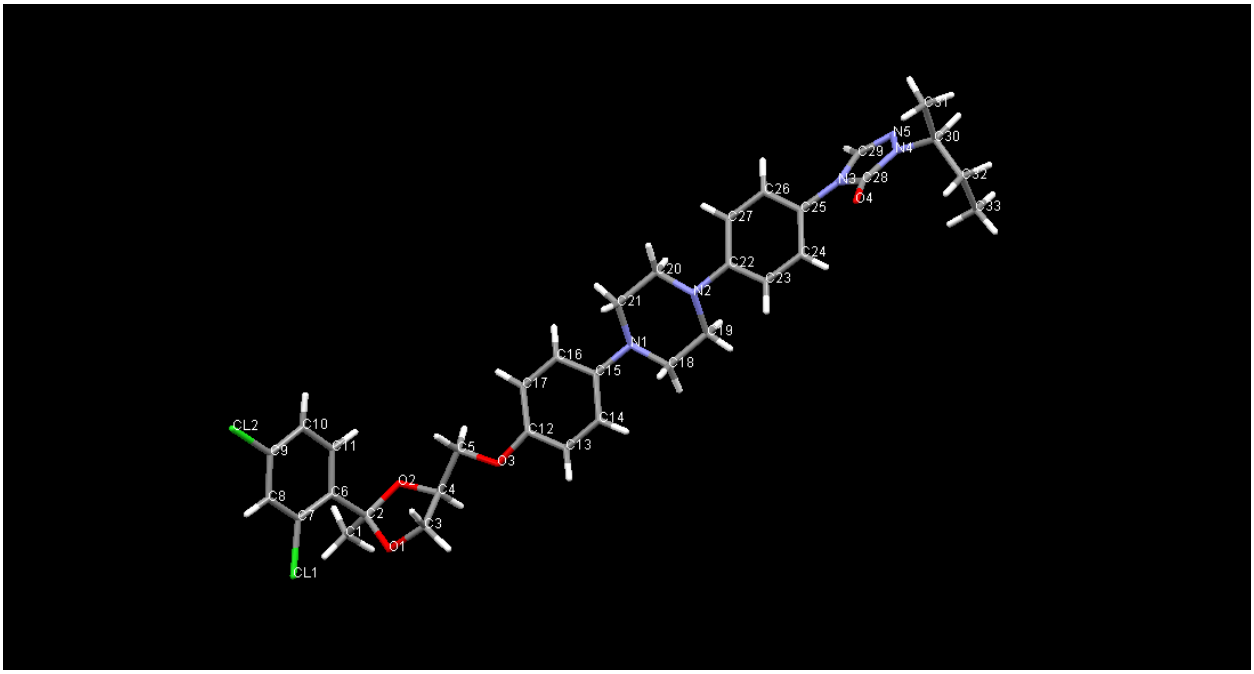
CL2
C10
C9
C11
C8
C6
C7
C1
C2
O1
O2
C4
C3
CL1
C5
O3
C12
C13
C14
C16
C17
C15
N1
C18
C19
C21
C20
N2
C22
C23
C24
C26
C27
C25
O4
C28
N3
N4
C29
N5
C30
C31
C32
C33

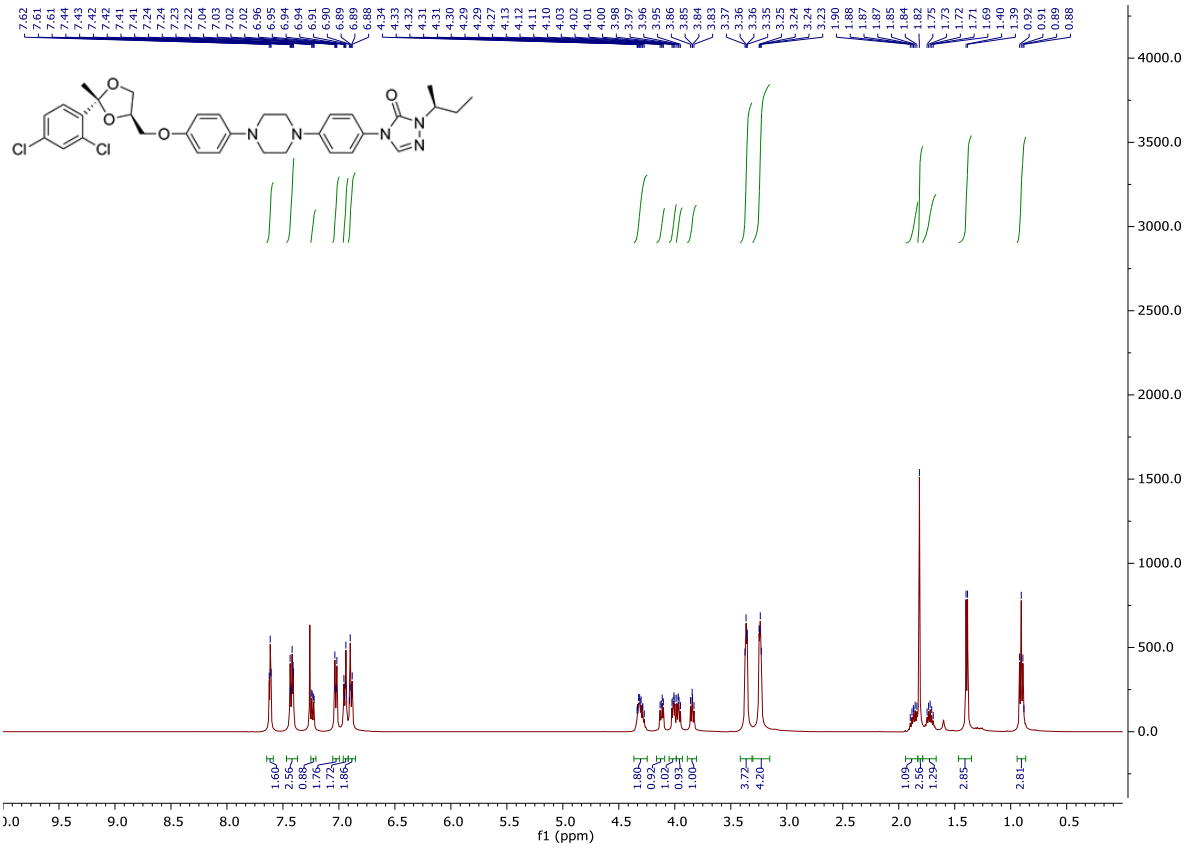
7.62 7.61 7.61 7.61 7.44 7.43 7.42 7.42 7.42 7.41 7.41 7.41 7.24 7.24 7.23 7.22 7.04 7.03 7.02 7.02 6.96 6.95 6.94 6.94 6.91 6.90 6.89 6.89 6.88 4.34 4.33 4.32 4.31 4.31 4.30 4.29 4.29 4.27 4.13 4.12 4.11 4.10 4.03 4.02 4.01 4.00 3.98 3.97 3.96 3.95 3.86 3.85 3.84 3.83 3.37 3.36 3.36 3.35 3.25 3.24 3.24 3.23 1.90 1.88 1.87 1.87 1.85 1.84 1.82 1.75 1.73 1.72 1.71 1.69 1.40 1.39 0.92 0.91 0.89 0.88
Cl
Cl
O
N
N
N
N
O
4000.0
3500.0
3000.0
2500.0
2000.0
1500.0
1000.0
500.0
0.0
1.60 2.56 0.88 1.76 1.72 1.86 1.80 0.92 1.03 1.03 1.00 3.72 4.20 1.09 2.56 1.29 2.85 2.81
9.5 9.0 8.5 8.0 7.5 7.0 6.5 6.0 5.5 5.0 4.5 4.0 3.5 3.0 2.5 2.0 1.5 1.0 0.5
f1 (ppm)

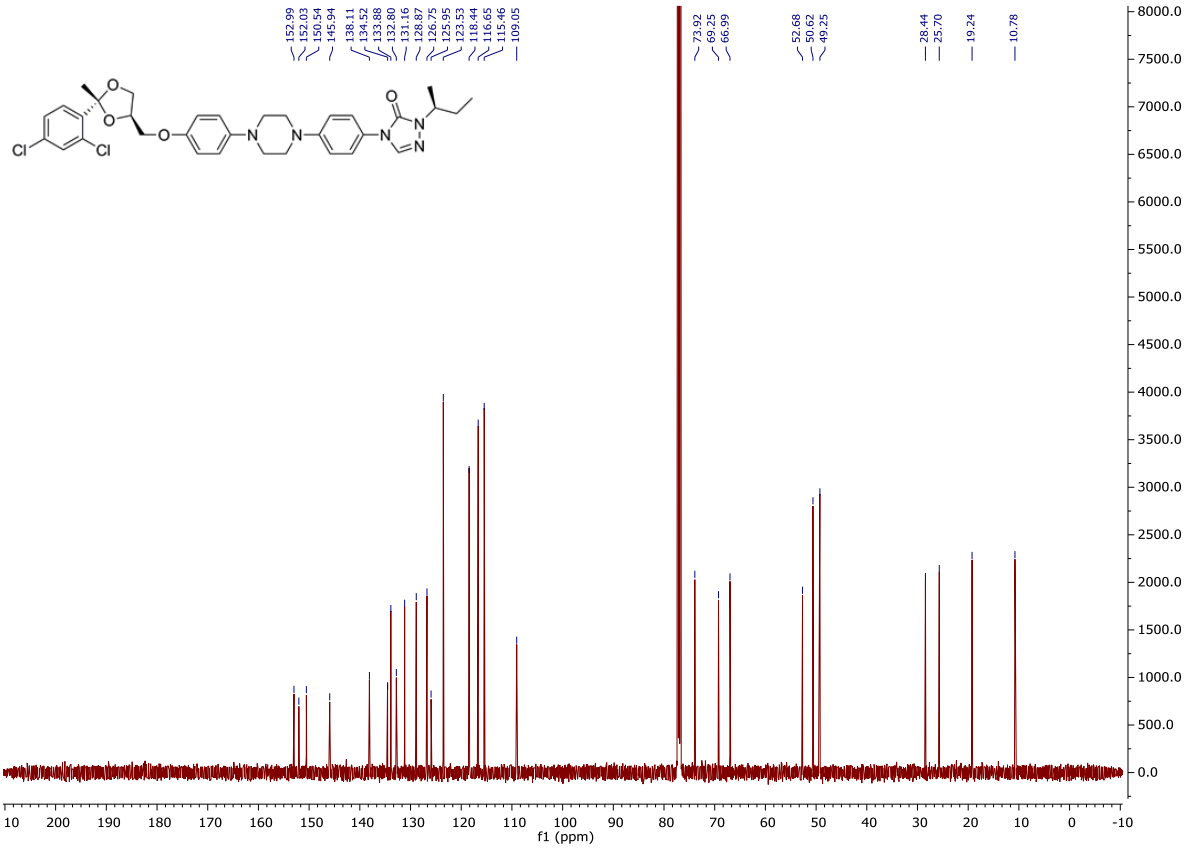
152.99 152.03 150.54 145.94 138.11 134.52 133.88 132.80 131.16 128.87 126.75 125.95 123.53 118.44 116.65 115.46 109.05
73.92 69.25 66.99
52.68 50.62 49.25
28.44 25.70
19.24
10.78
Cl
Cl
O
N
N
N
N
O
8000.0
7500.0
7000.0
6500.0
6000.0
5500.0
5000.0
4500.0
4000.0
3500.0
3000.0
2500.0
2000.0
1500.0
1000.0
500.0
0.0
210 200 190 180 170 160 150 140 130 120 110 100 90 80 70 60 50 40 30 20 10 0 -10
f1 (ppm)

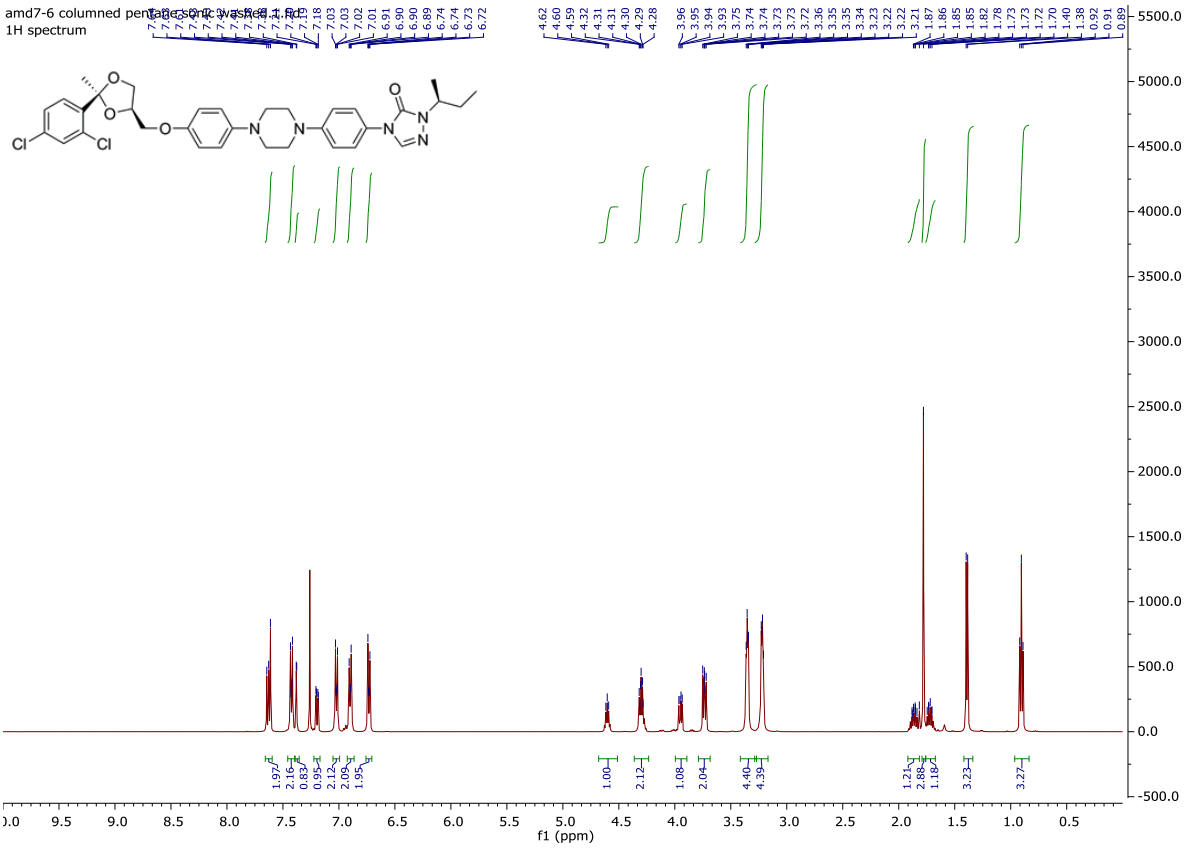
1H spectrum
f1 (ppm)

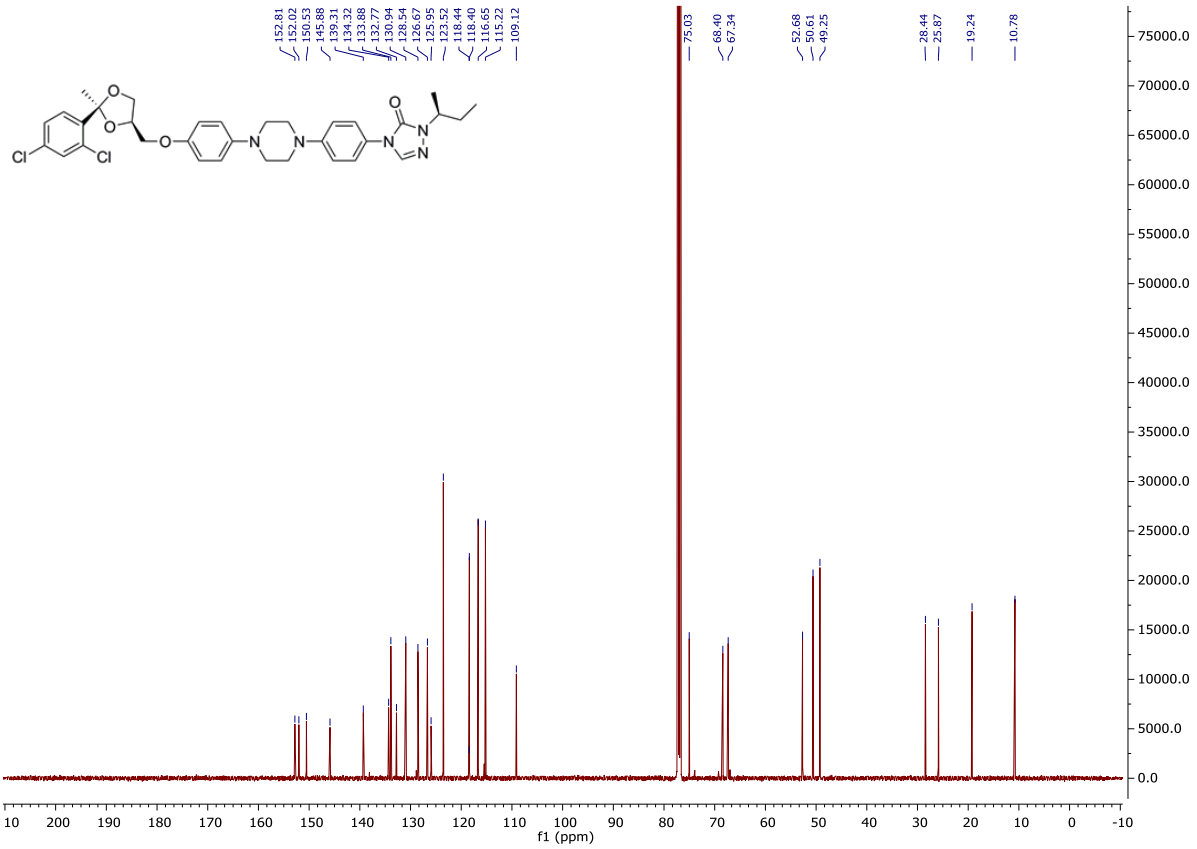
f1 (ppm)

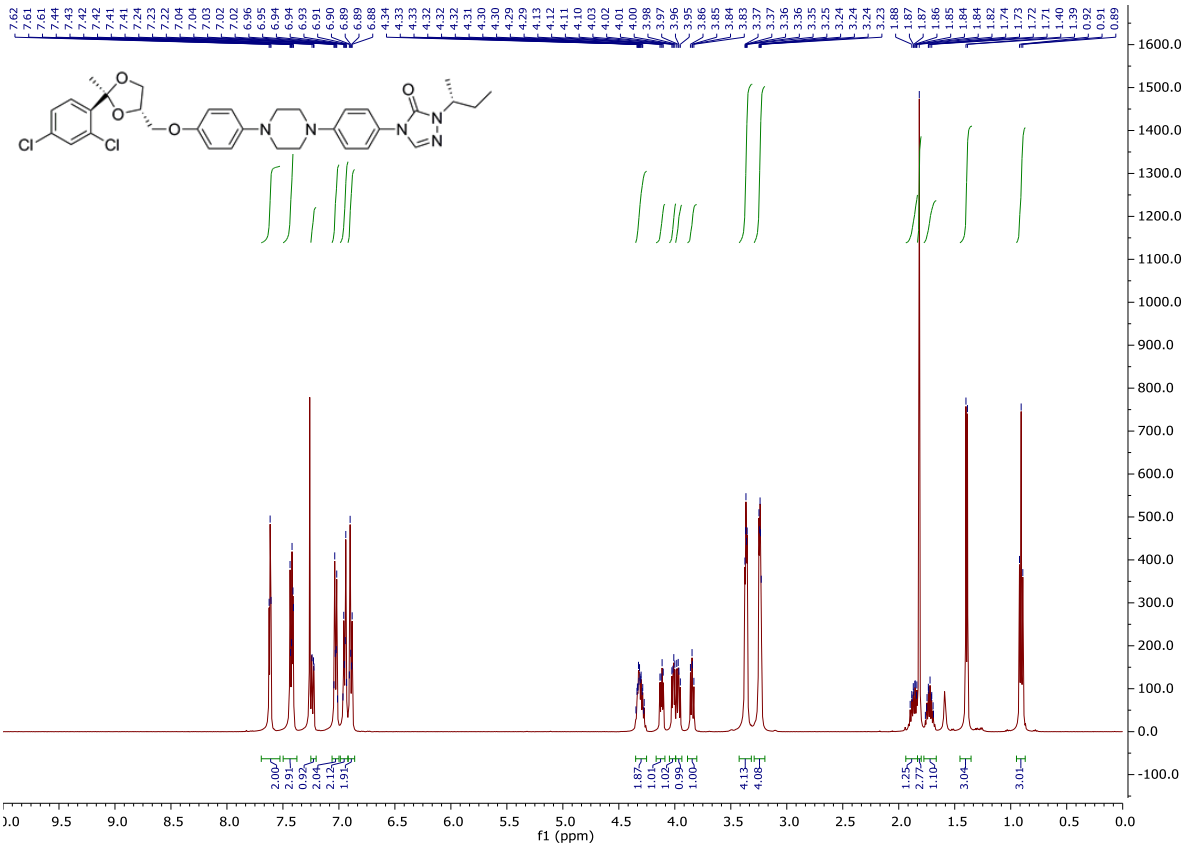
f1 (ppm)

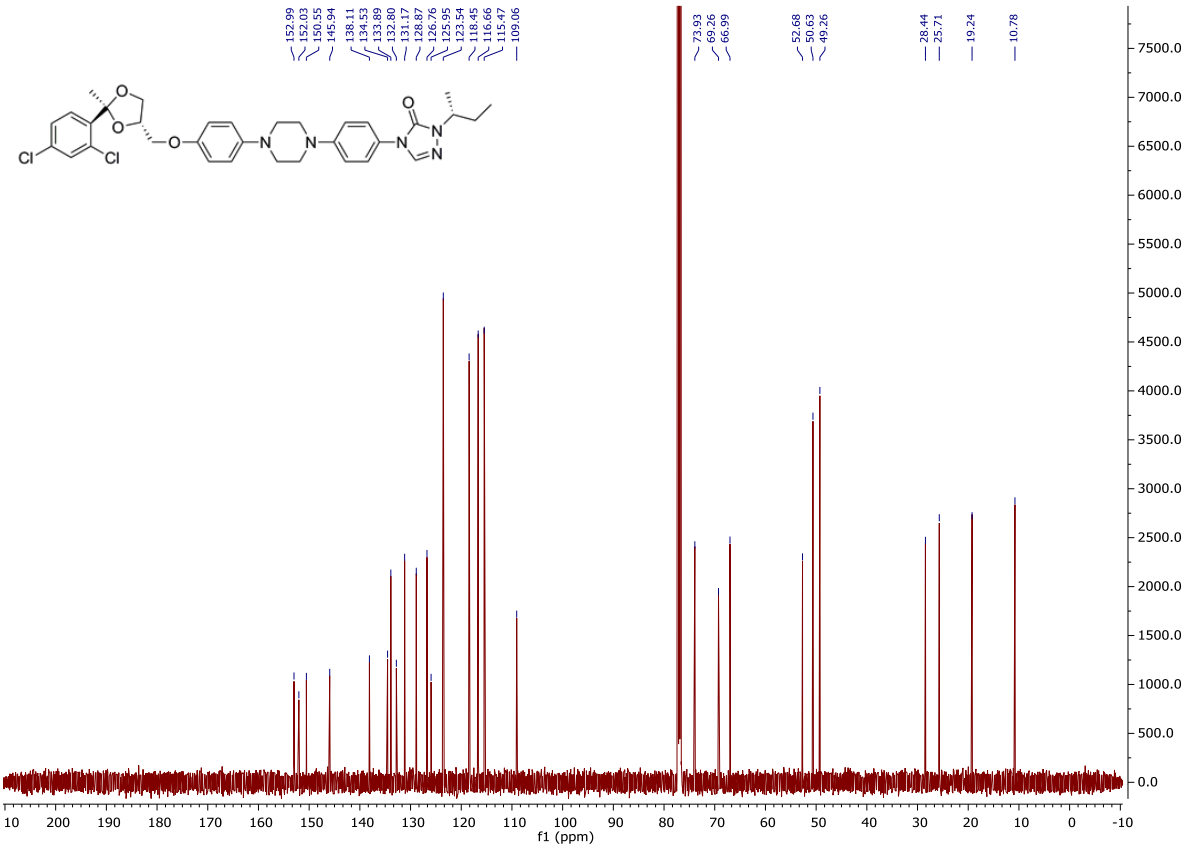
f1 (ppm)

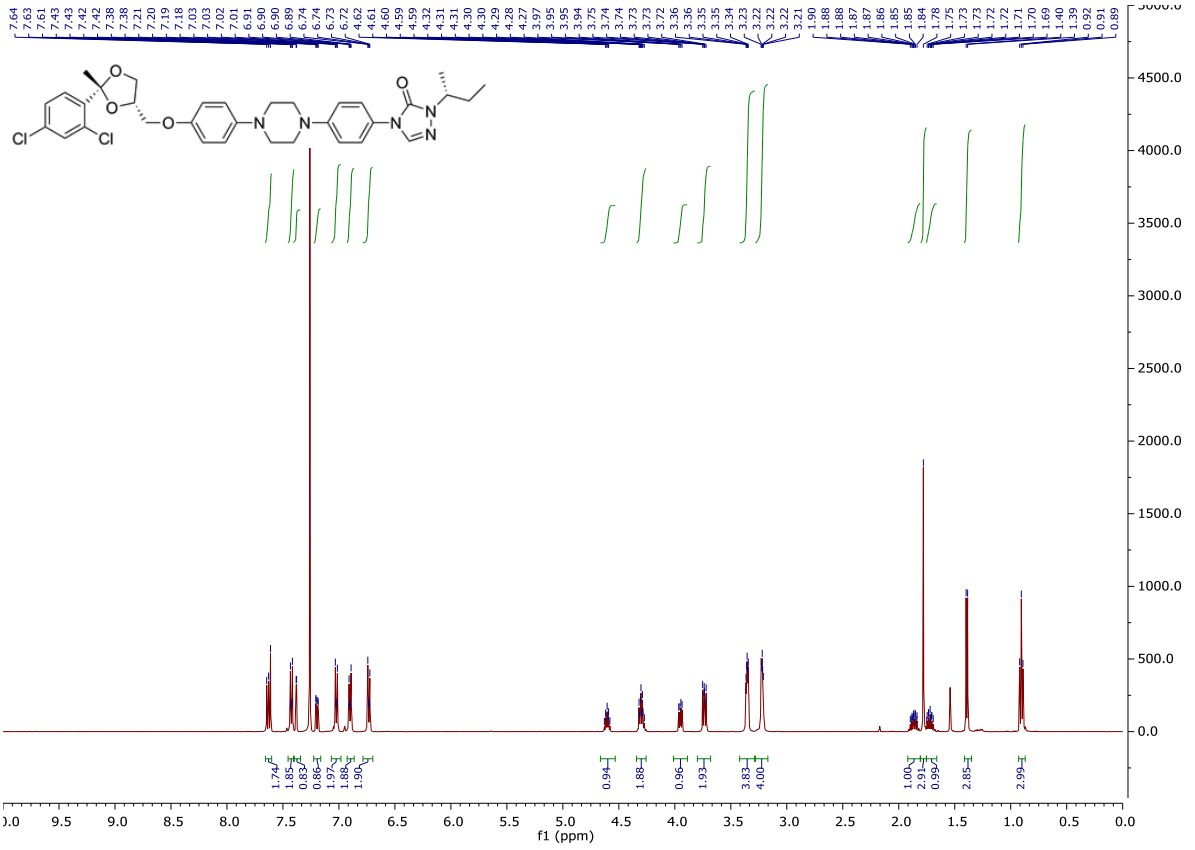
f1 (ppm)

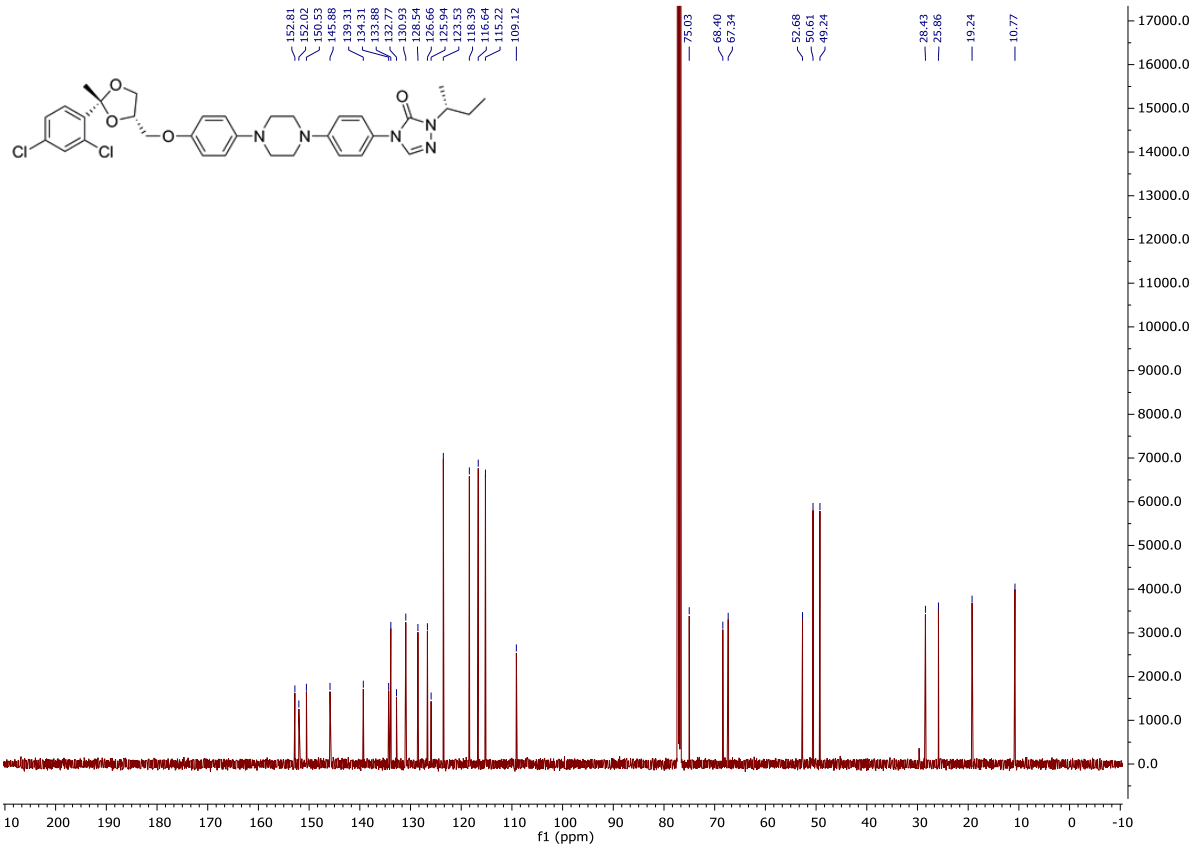
f1 (ppm)

X-RAY:

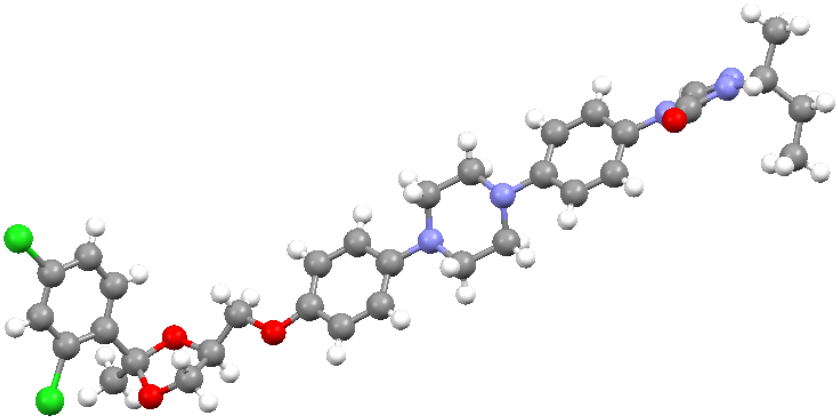

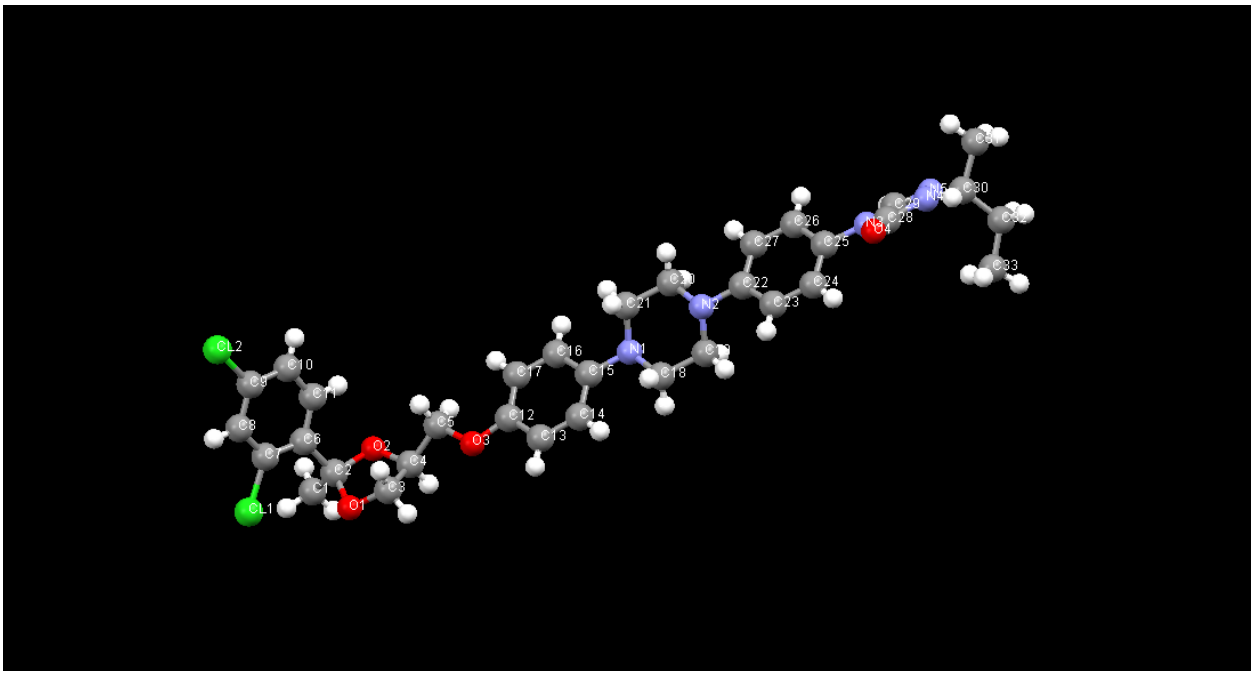
CL2
C10
C9
C11
C8
C6
C7
C2
C4
C1
C3
CL1
O1
O2
O3
C5
C12
C13
C14
C16
C17
C15
N1
C18
C19
C21
N2
C22
C23
C24
C26
C27
C25
N3
O4
C28
C29
N4
C30
C31
C32
C33

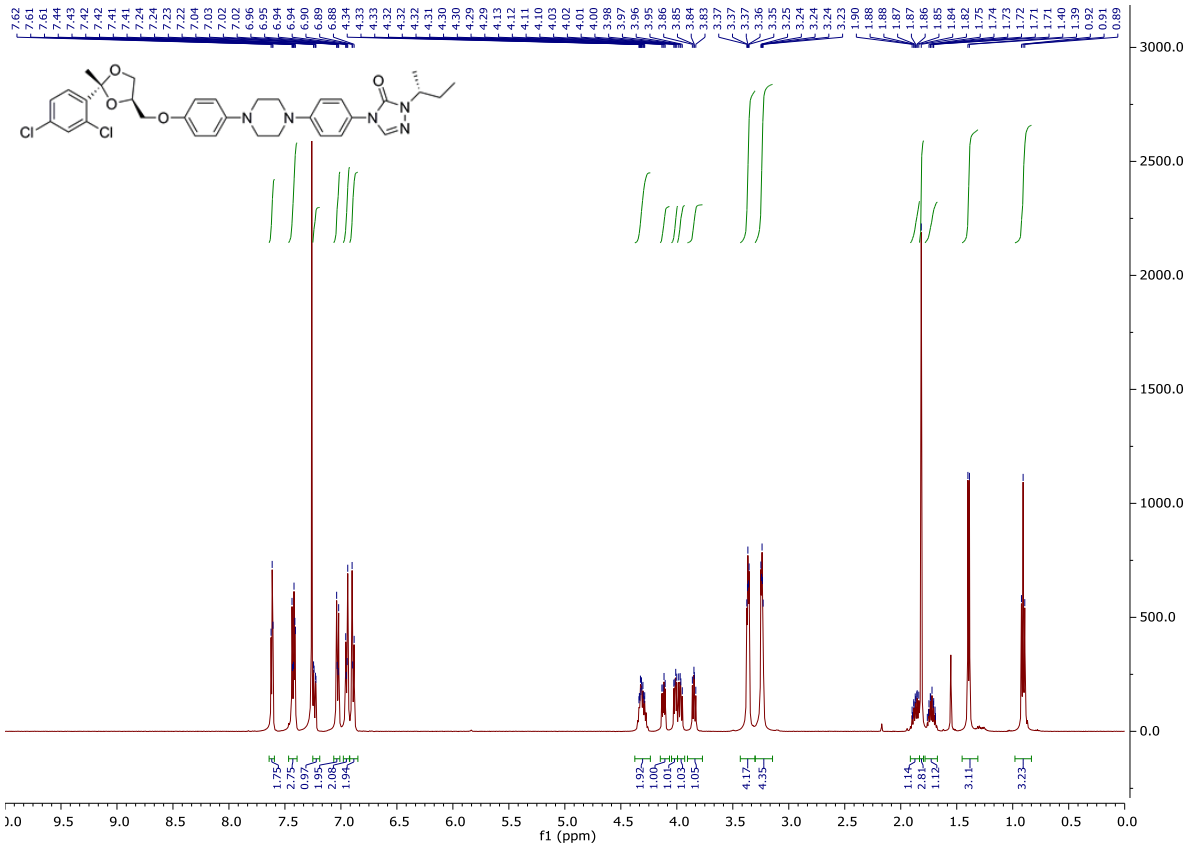
f1 (ppm)

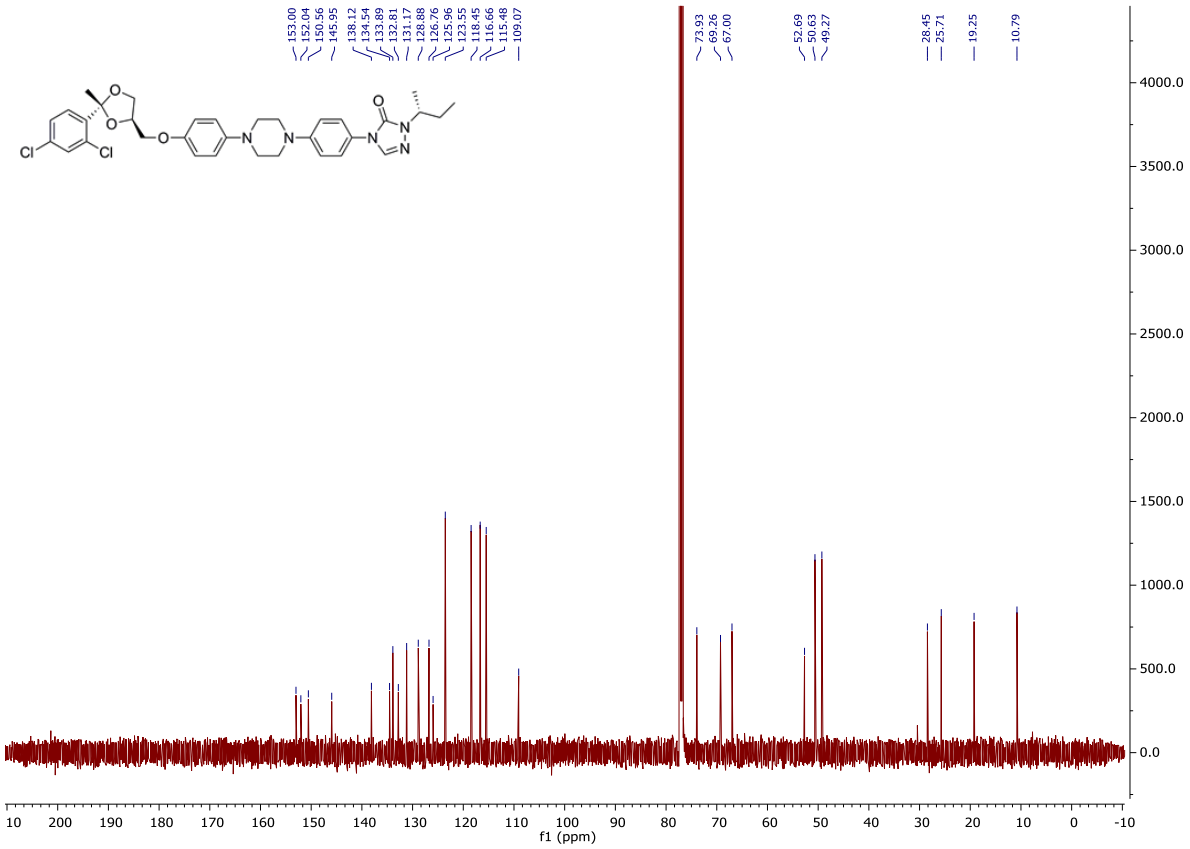
f1 (ppm)

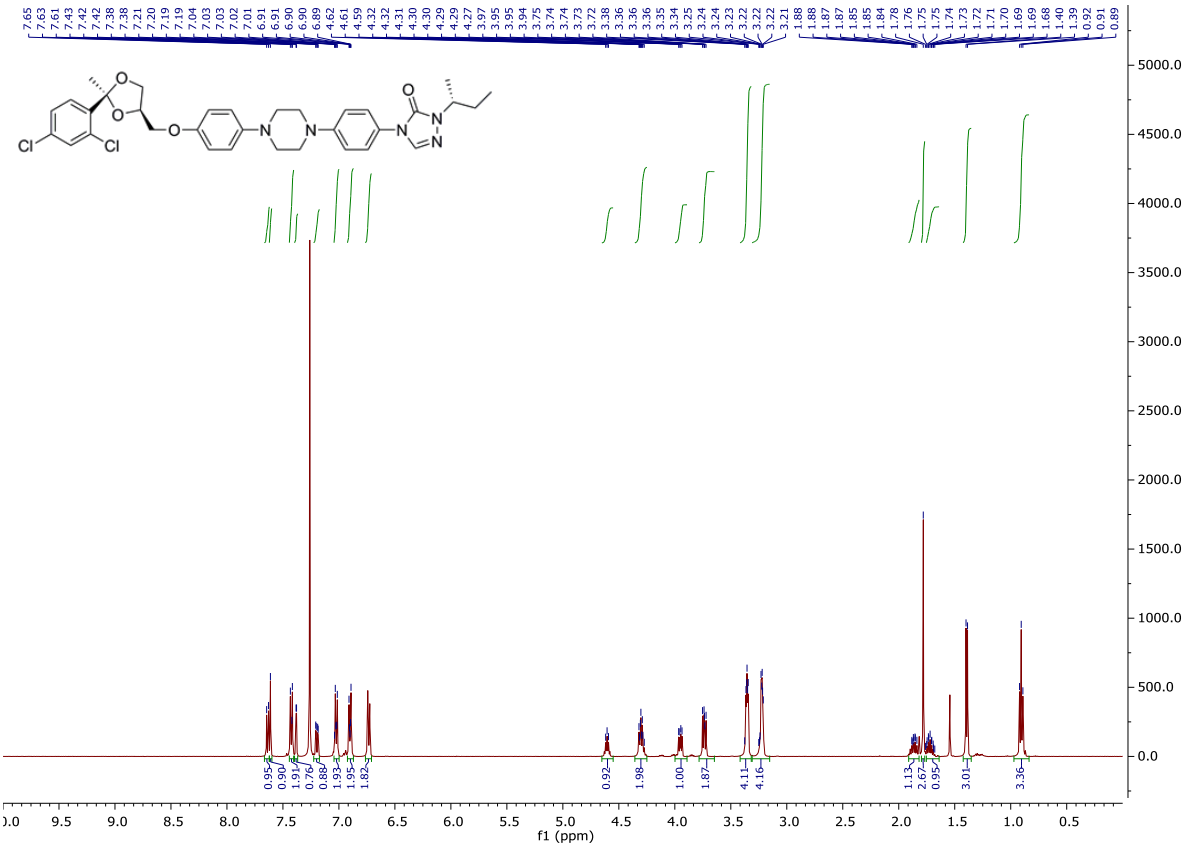
f1 (ppm)

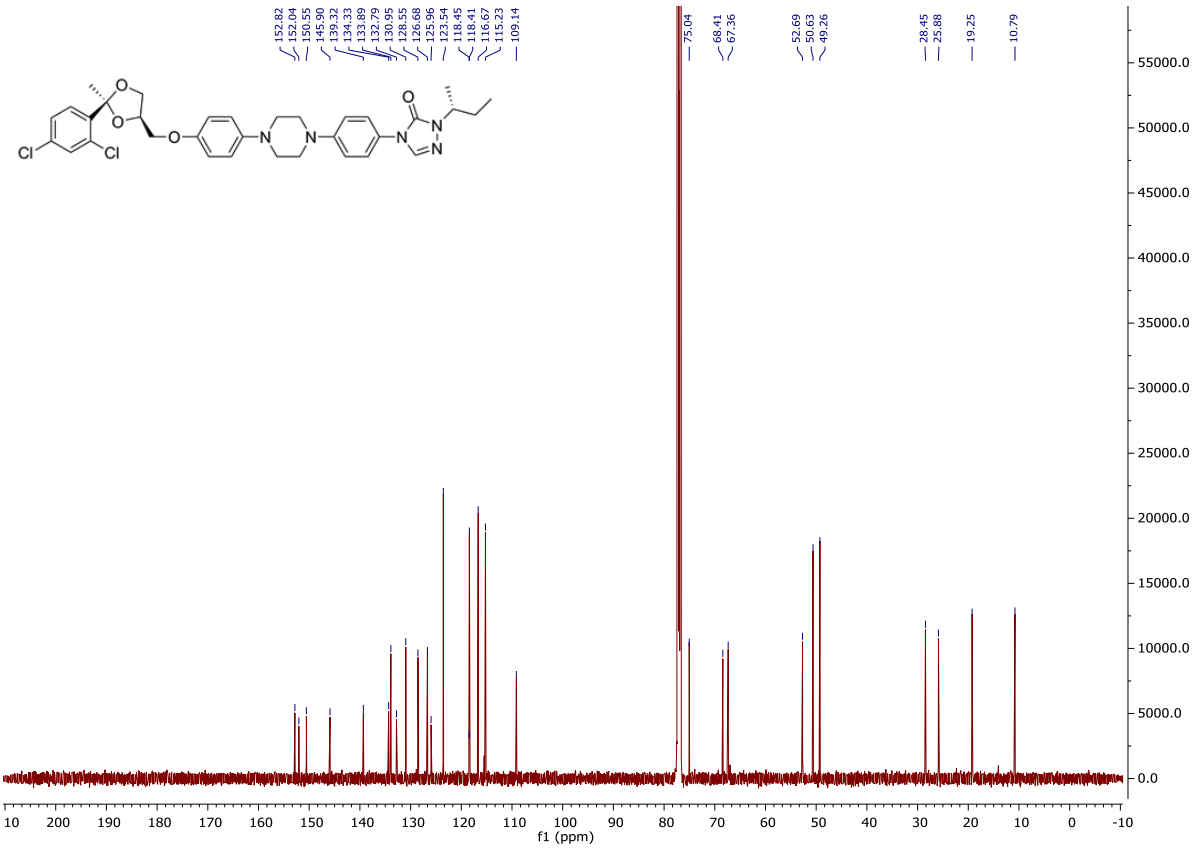
f1 (ppm)

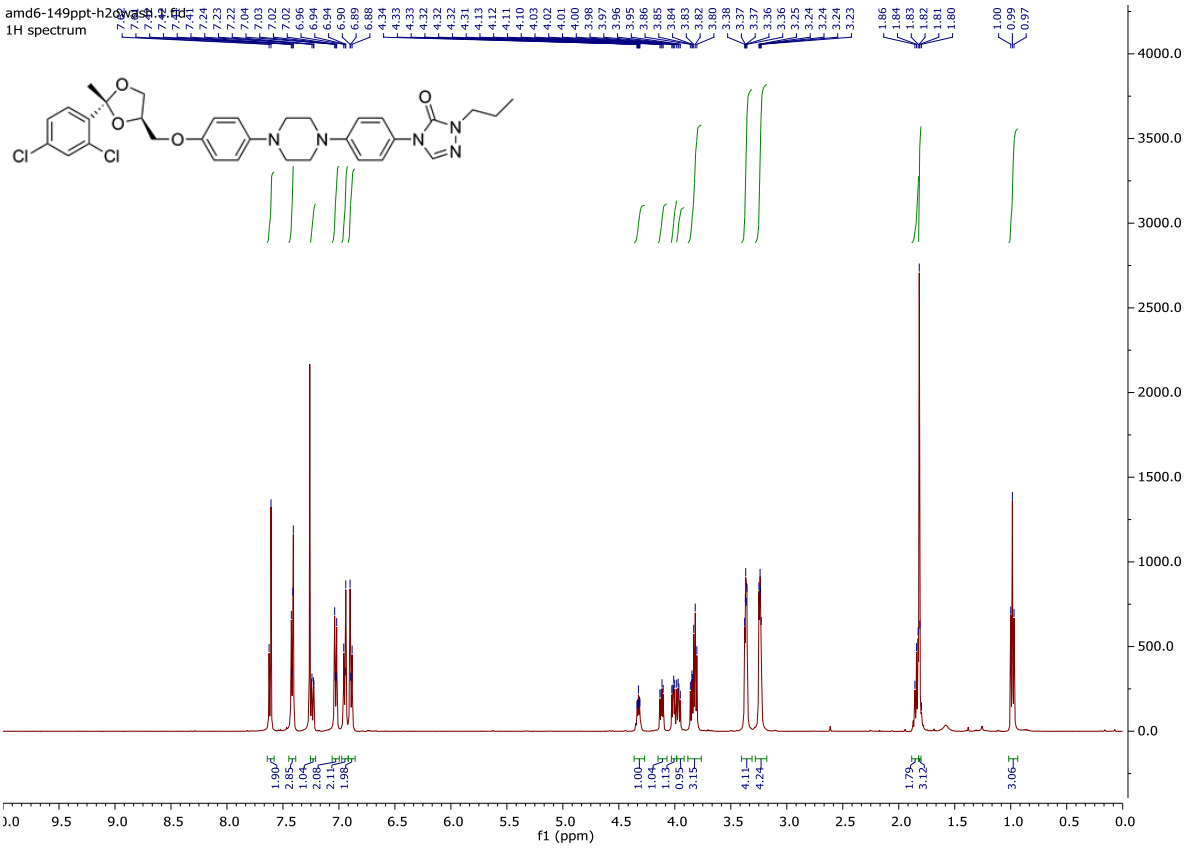
amd6-149ppt-h2cwash.1.fid
1H spectrum
f1 (ppm)

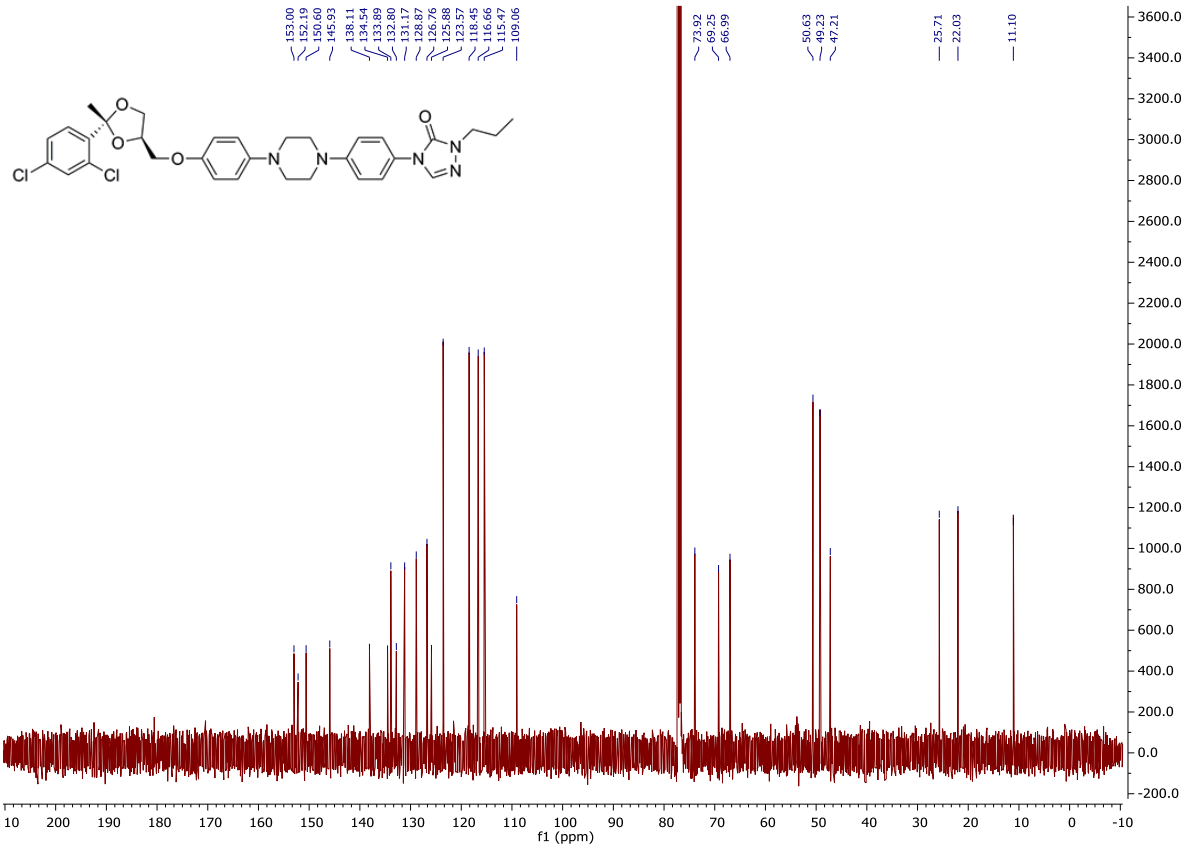
f1 (ppm)

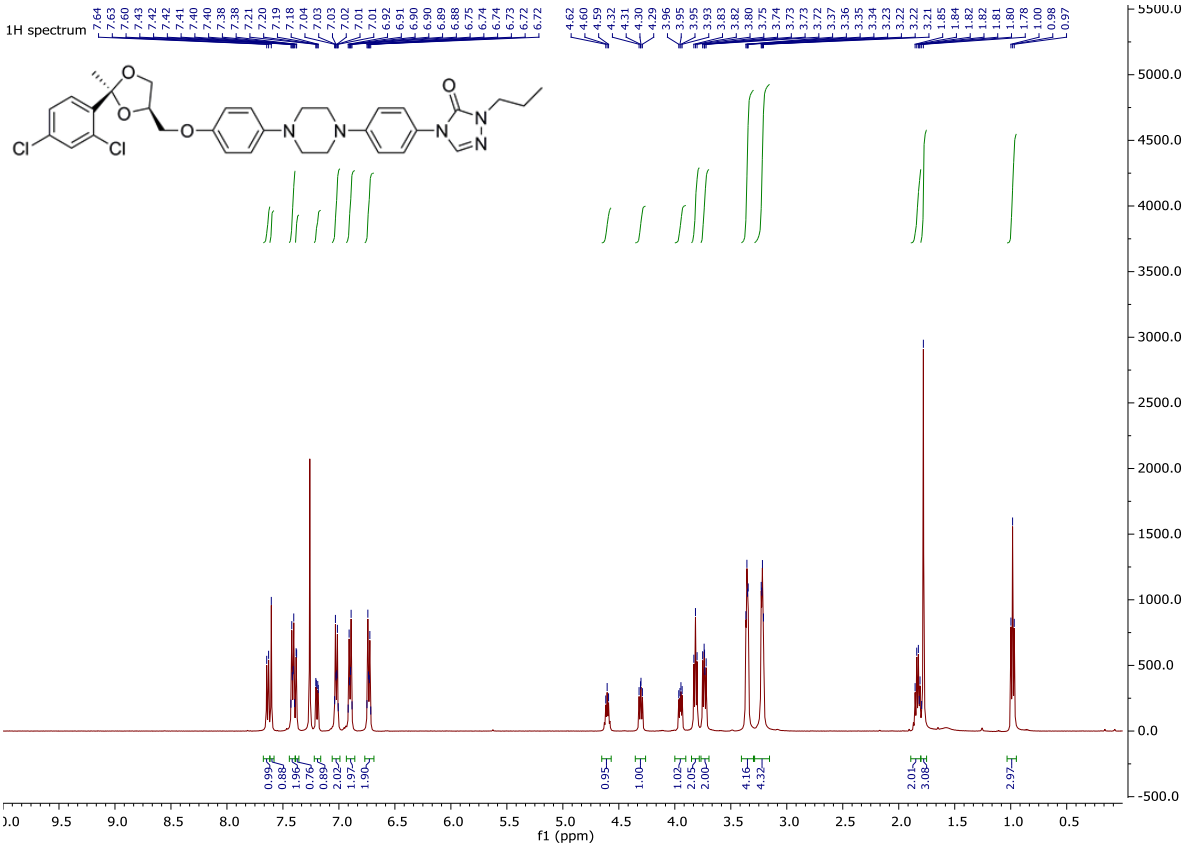
1H spectrum
f1 (ppm)

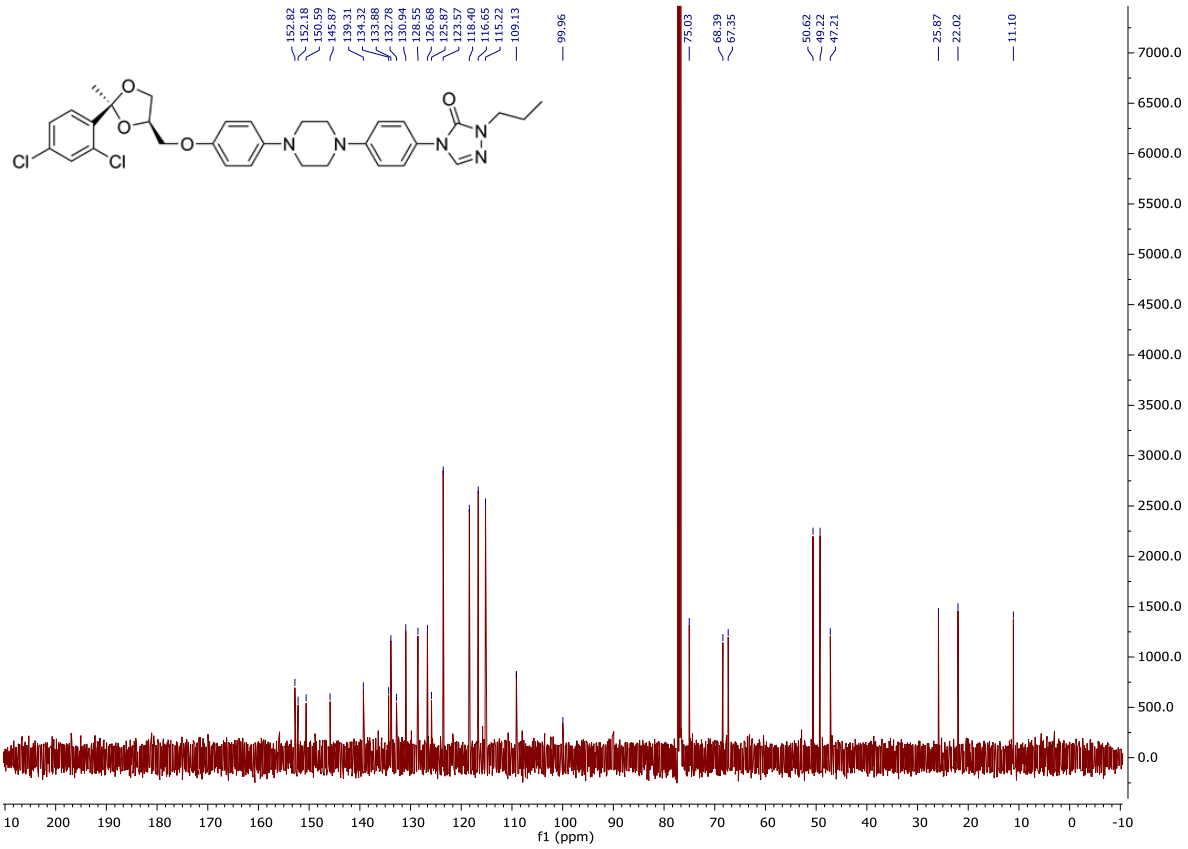
f1 (ppm)

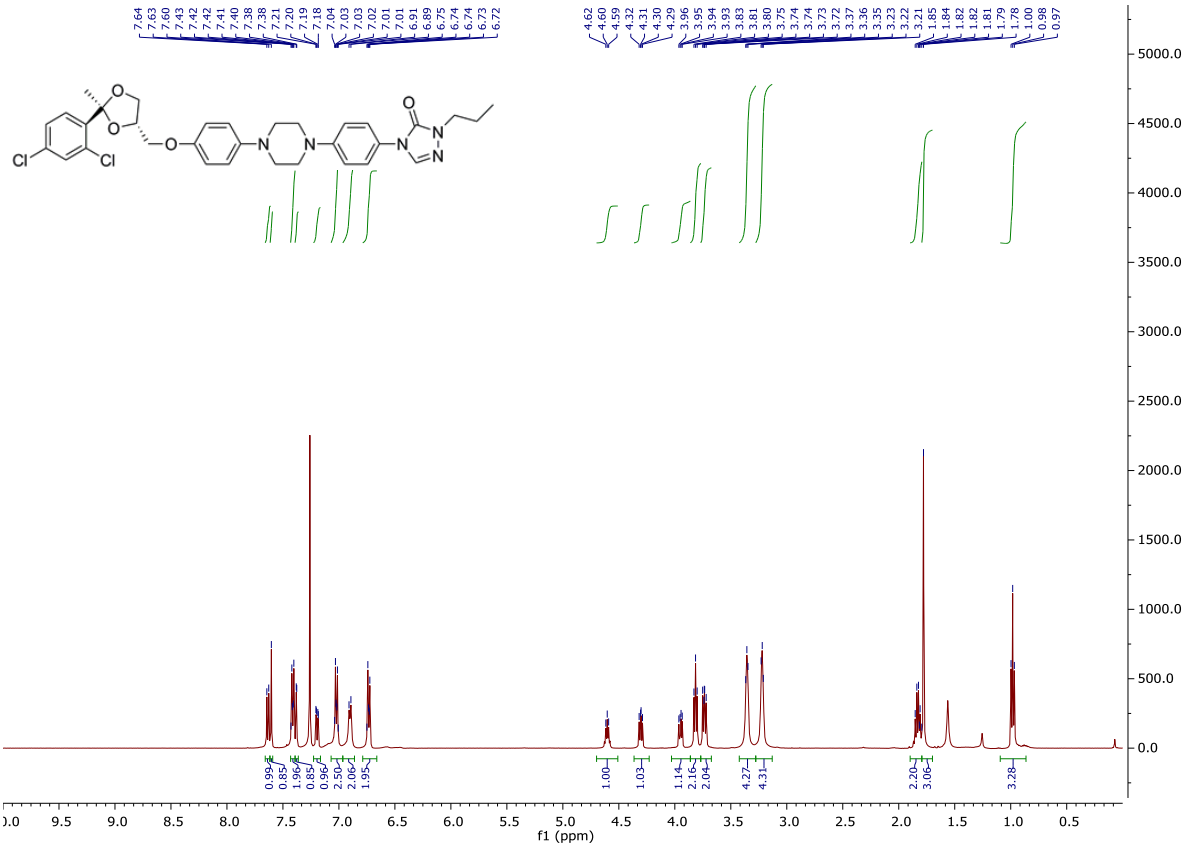
7.64 7.63 7.60 7.43 7.42 7.42 7.41 7.40 7.38 7.38 7.21 7.20 7.19 7.18 7.04 7.03 7.03 7.02 7.01 7.01 6.91 6.89 6.75 6.74 6.74 6.73 6.72
4.62 4.60 4.59 4.32 4.31 4.30 4.29 3.96 3.95 3.94 3.93 3.83 3.81 3.80 3.75 3.74 3.74 3.73 3.72 3.37 3.36 3.35 3.23 3.22 3.21 1.85 1.84 1.82 1.82 1.81 1.79 1.78 1.00 0.98 0.97
Cl
Cl
O
N
N
N
N
O
0.99 0.85 1.96 0.85 0.96 2.50 2.06 1.95 1.00 1.03 1.14 2.16 2.04 4.27 4.31 2.20 3.06 3.28
f1 (ppm)

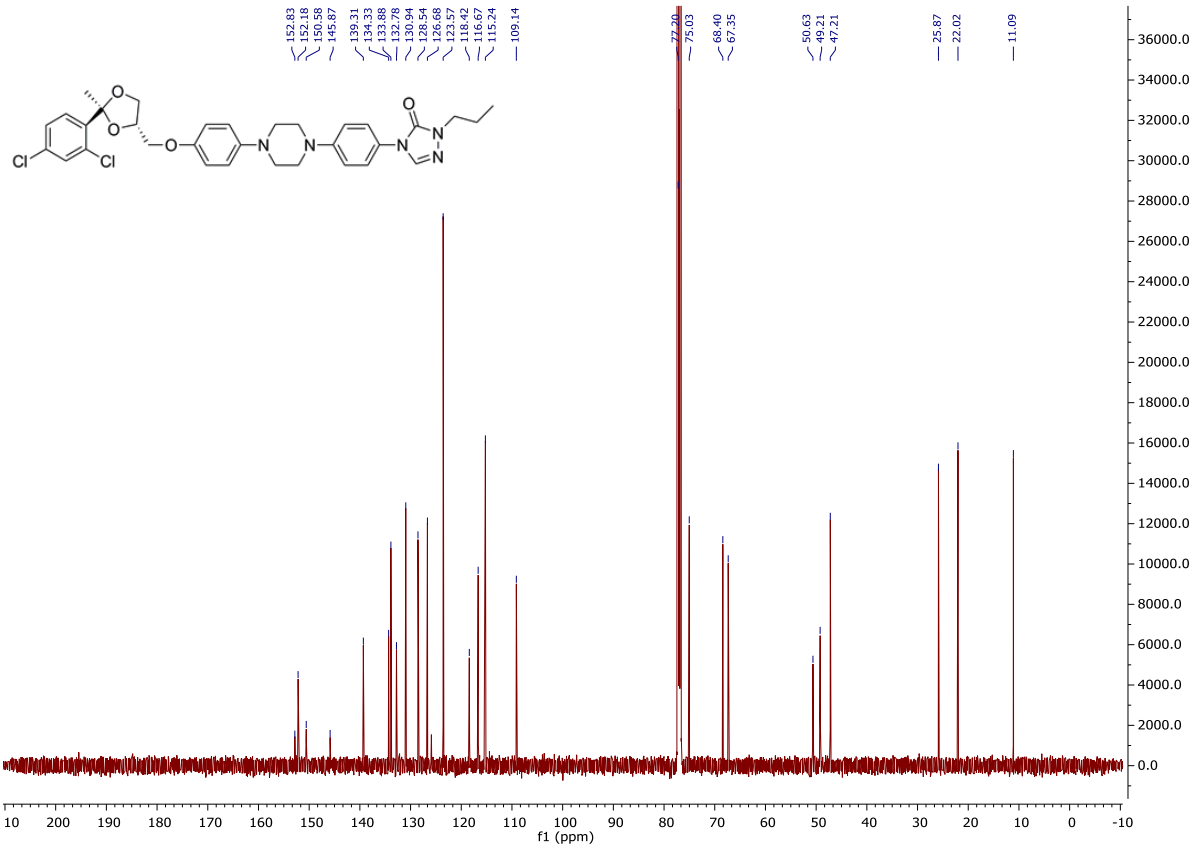
152.83 152.18 150.58 145.87 139.31 134.33 133.88 132.78 130.94 128.54 126.68 123.57 118.42 116.67 115.24 109.14
77.20 75.03 68.40 67.35 50.63 49.21 47.21 25.87 22.02 11.09
Cl
Cl
O
N
N
N
N
O
f1 (ppm)

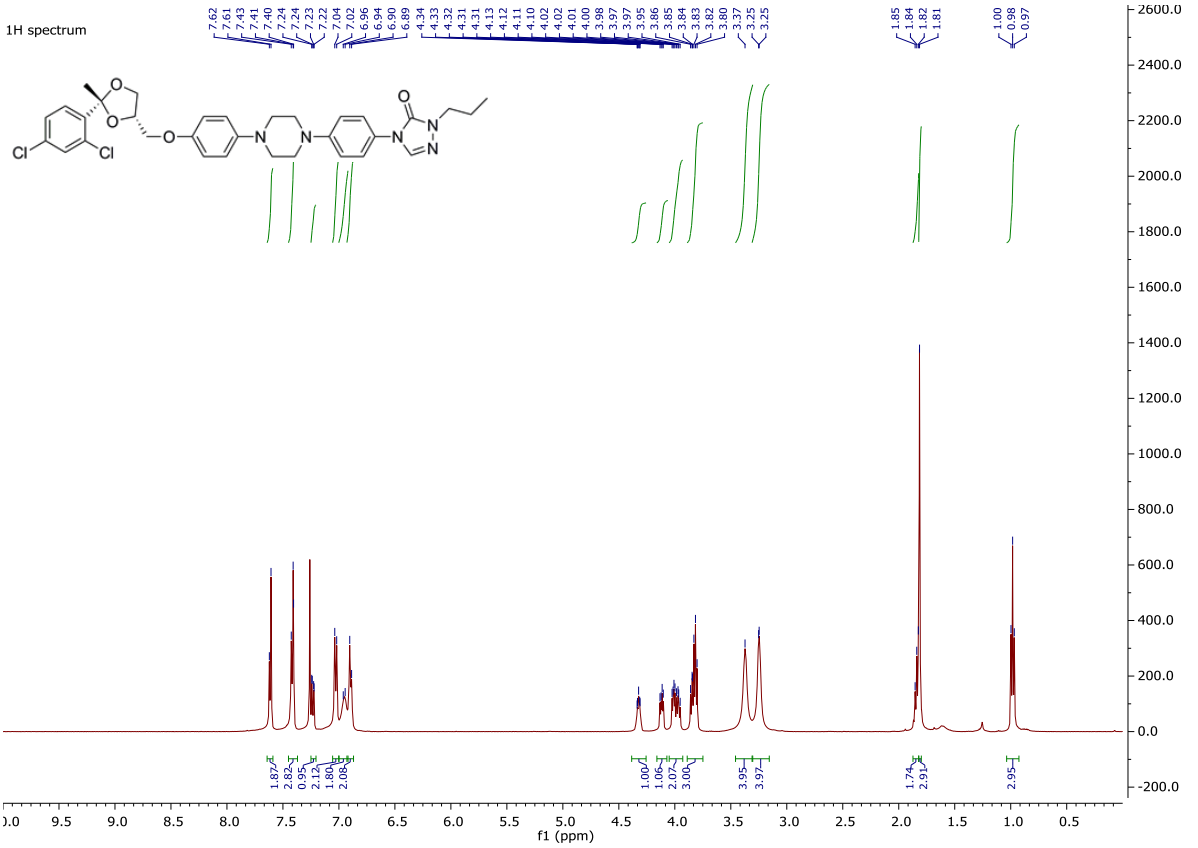
1H spectrum
f1 (ppm)

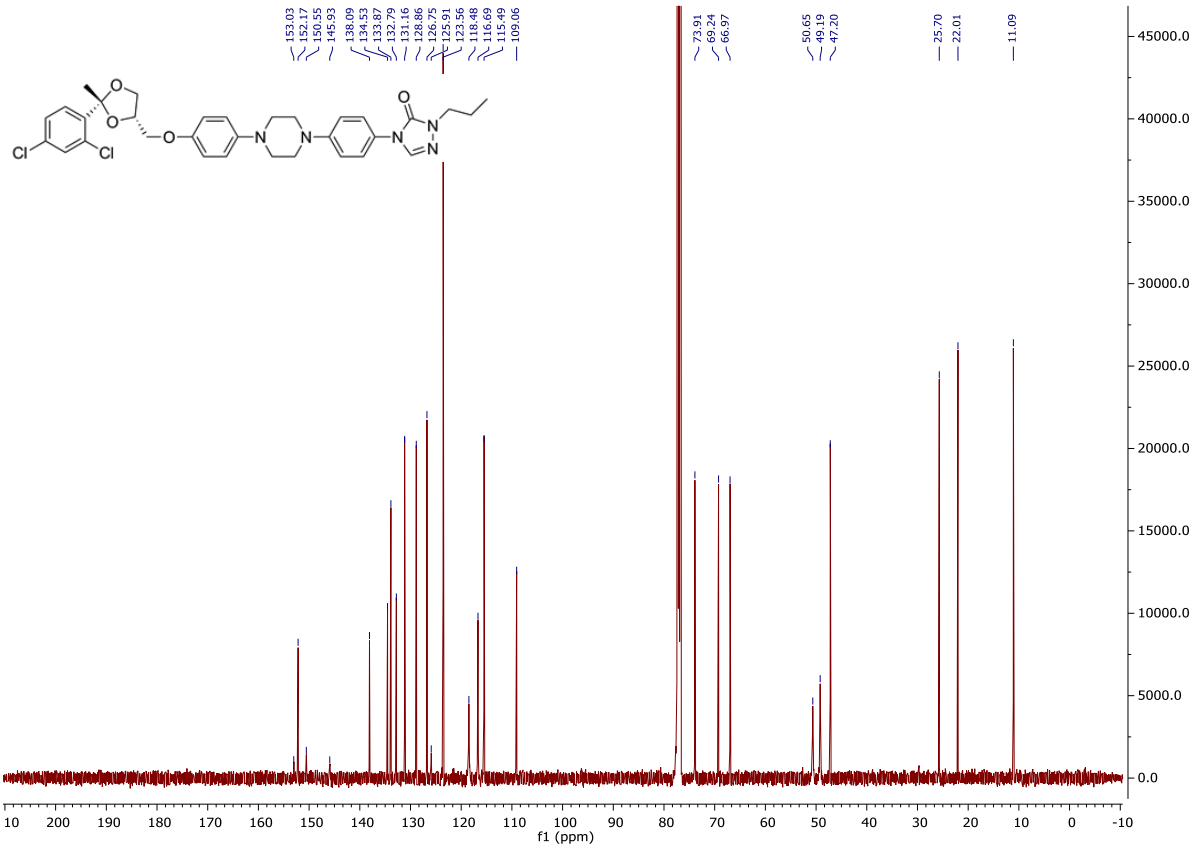
f1 (ppm)

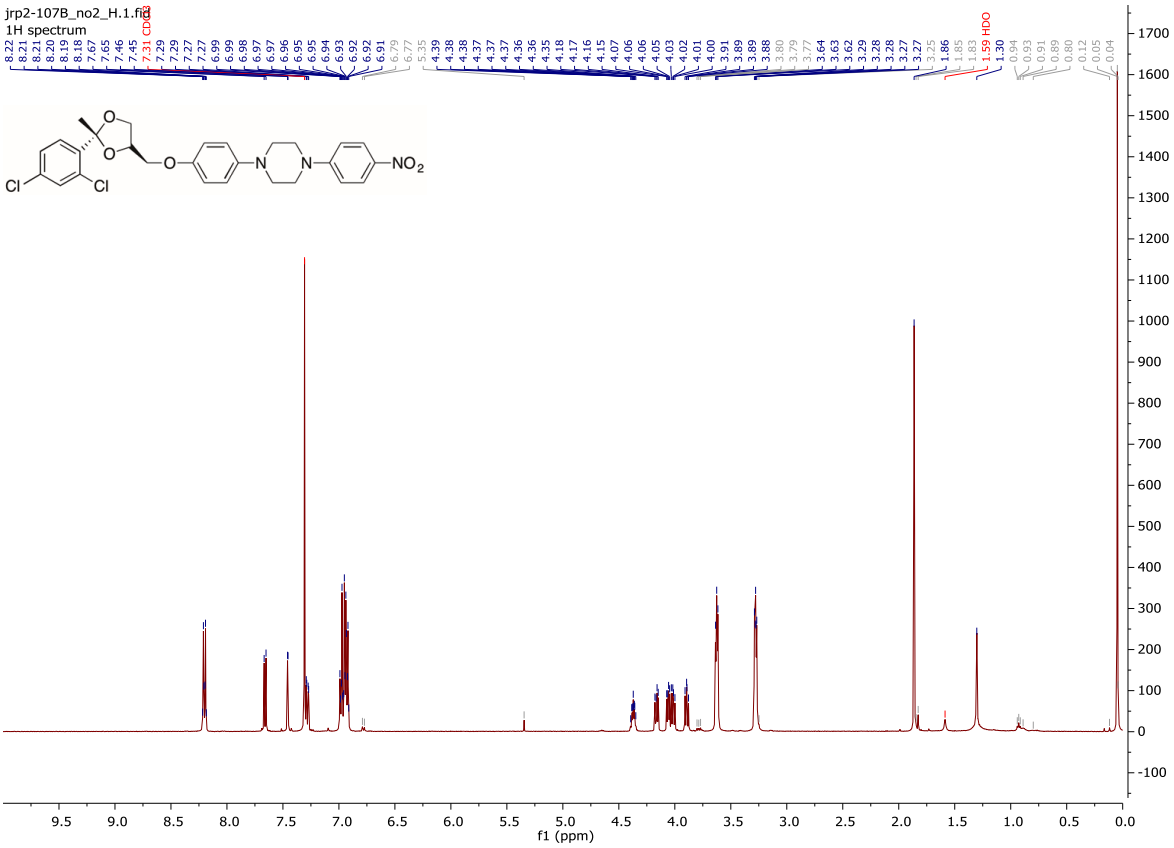
jrp2-107B_no2_H.1.fid
1H spectrum
f1 (ppm)

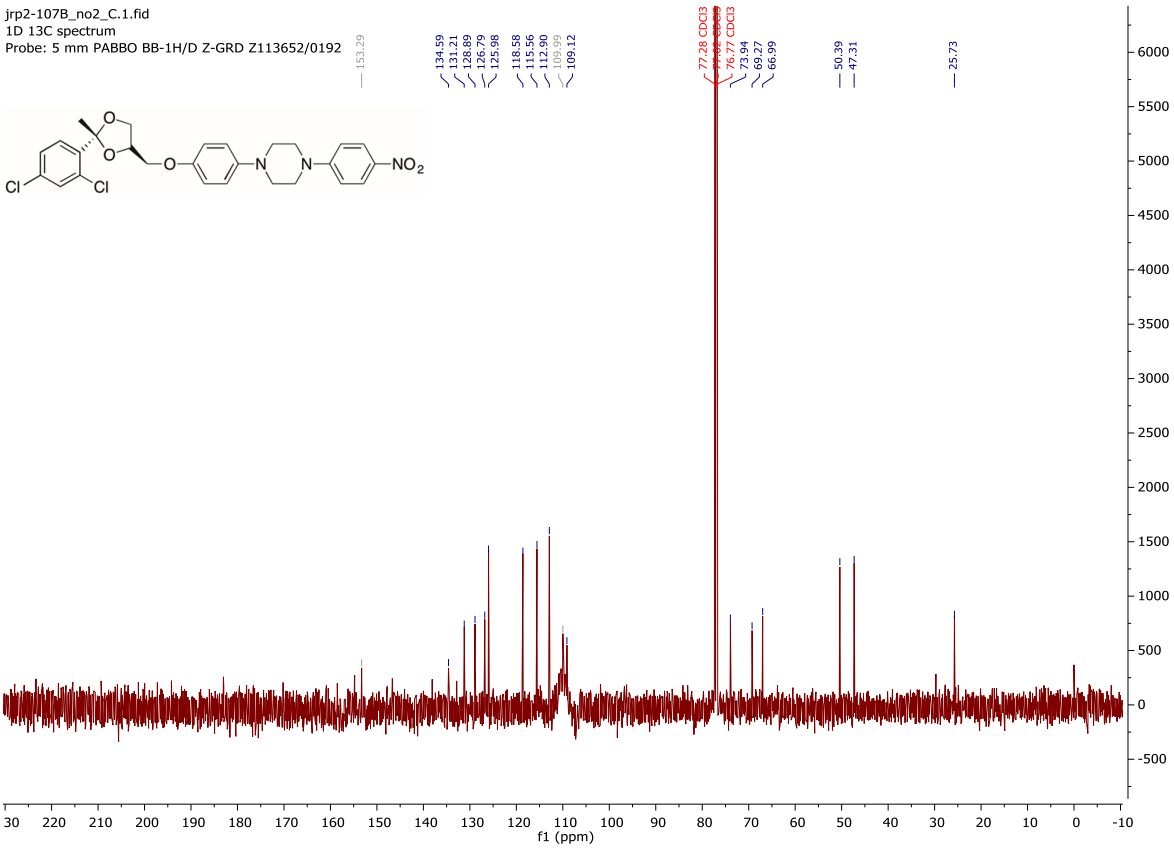
jrp2-107B_no2_C.1.fid
1D 13C spectrum
Probe: 5 mm PABBO BB-1H/D Z-GRD Z113652/0192
f1 (ppm)

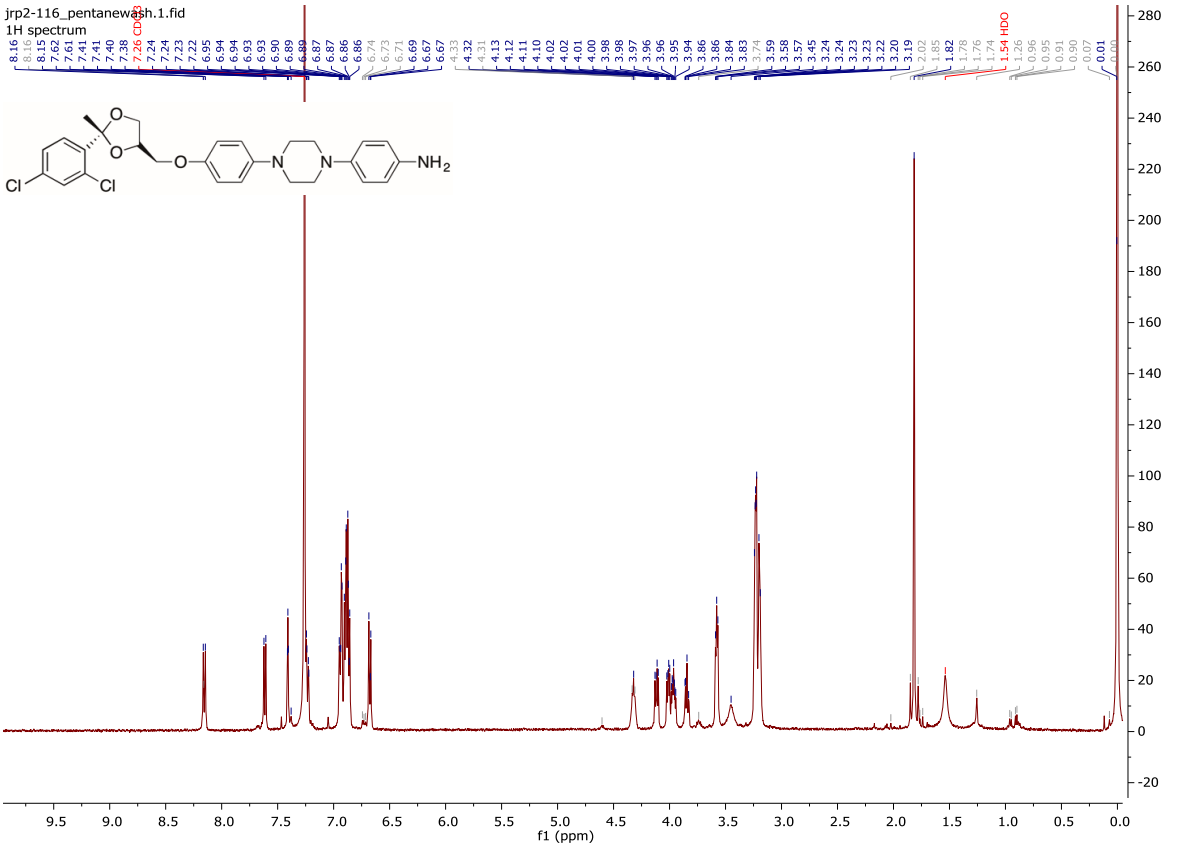
jrp2-116_pentanewash.1.fid
1H spectrum
f1 (ppm)

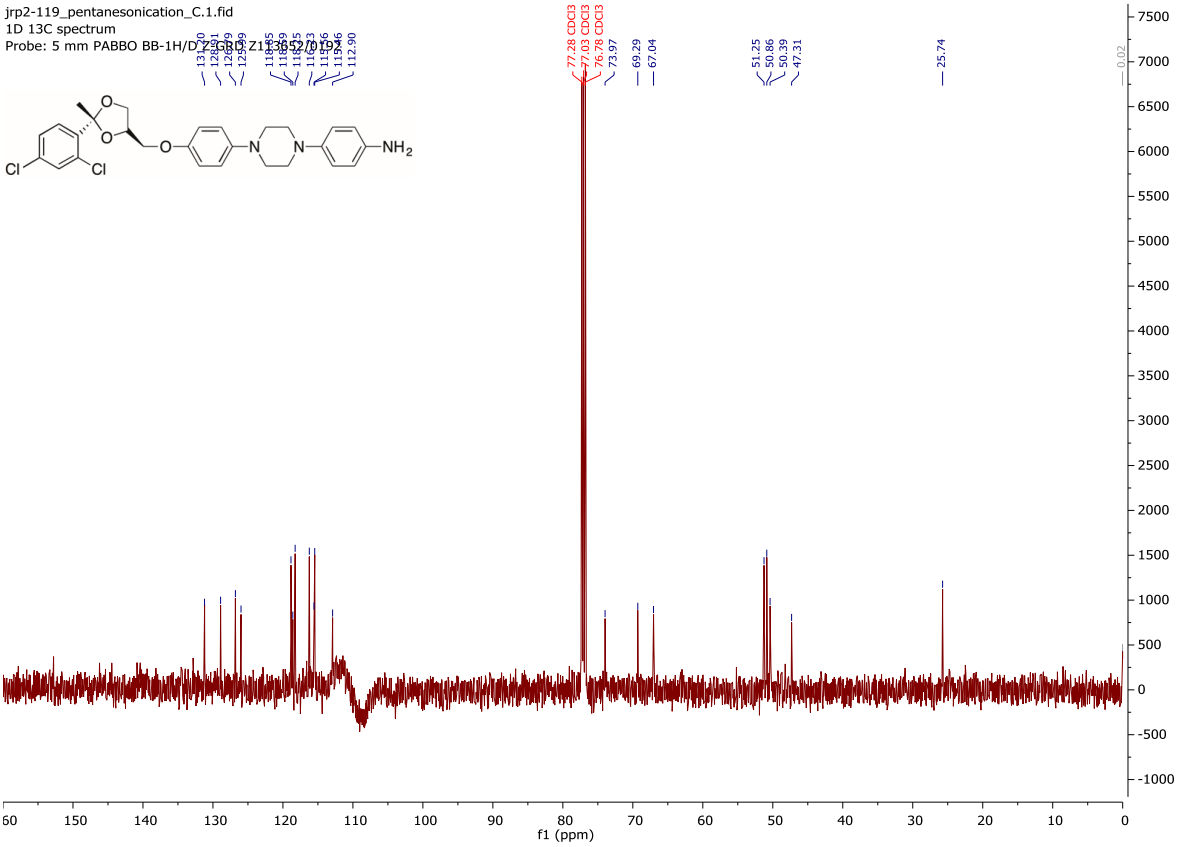
jrp2-119_pentanesonication_C.1.fid
1D 13C spectrum
Probe: 5 mm PABBO BB-1H/D
f1 (ppm)

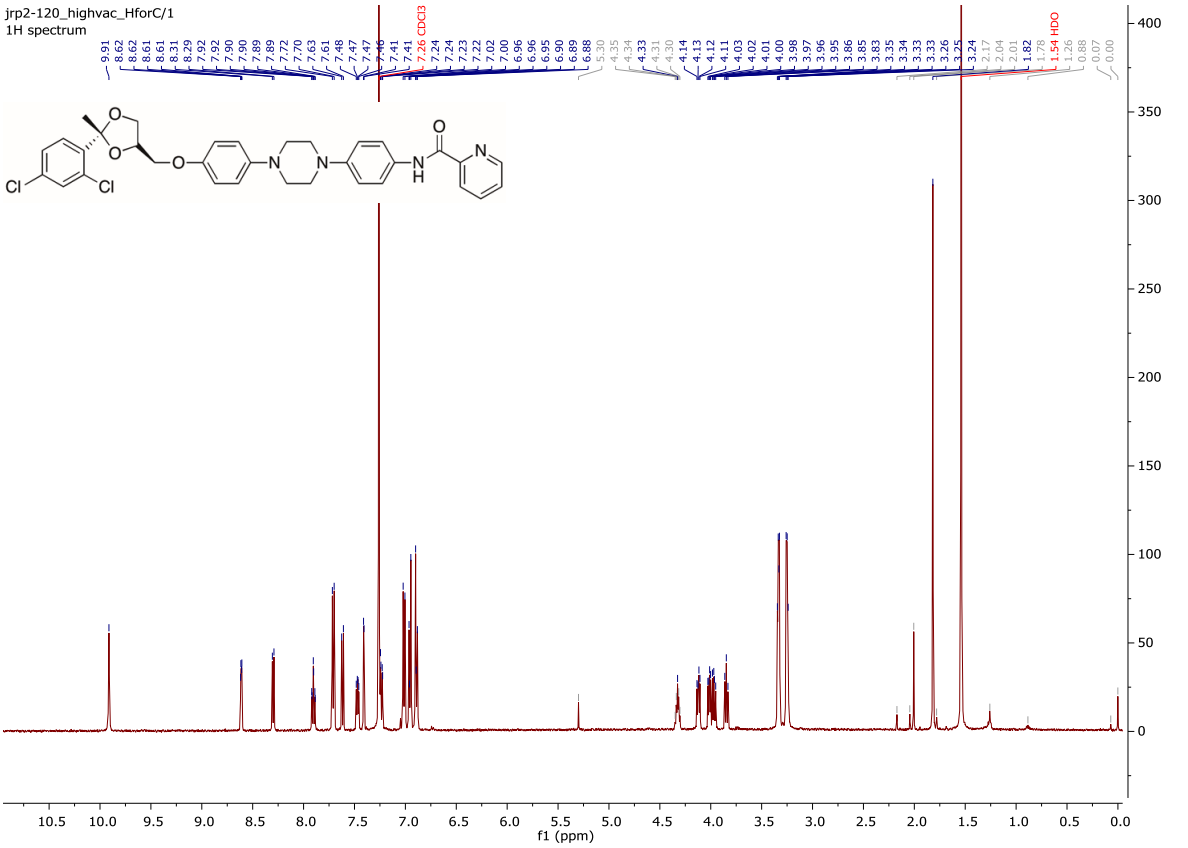
jrp2-120_highvac_HforC/1
1H spectrum
f1 (ppm)

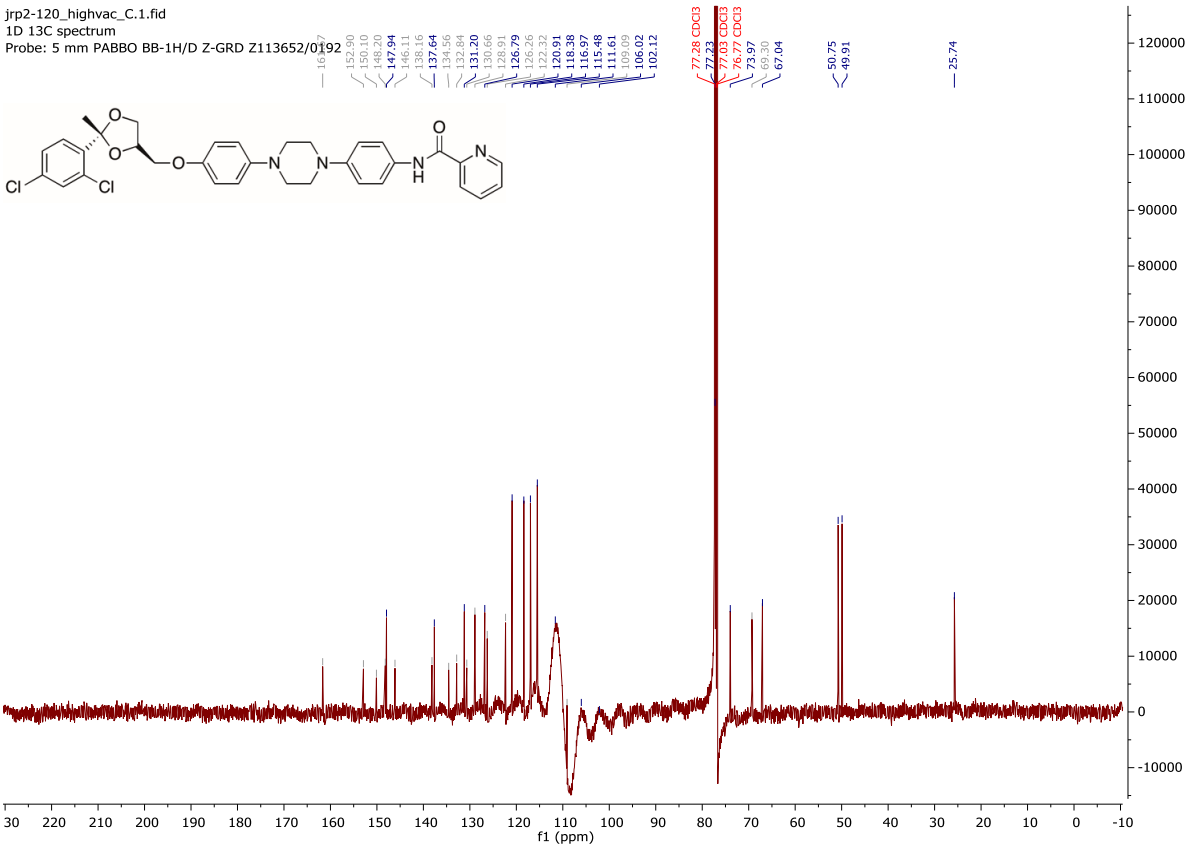
jrp2-120_highvac_C.1.fid
1D 13C spectrum
Probe: 5 mm PABBO BB-1H/D Z-GRD Z113652/0192
f1 (ppm)

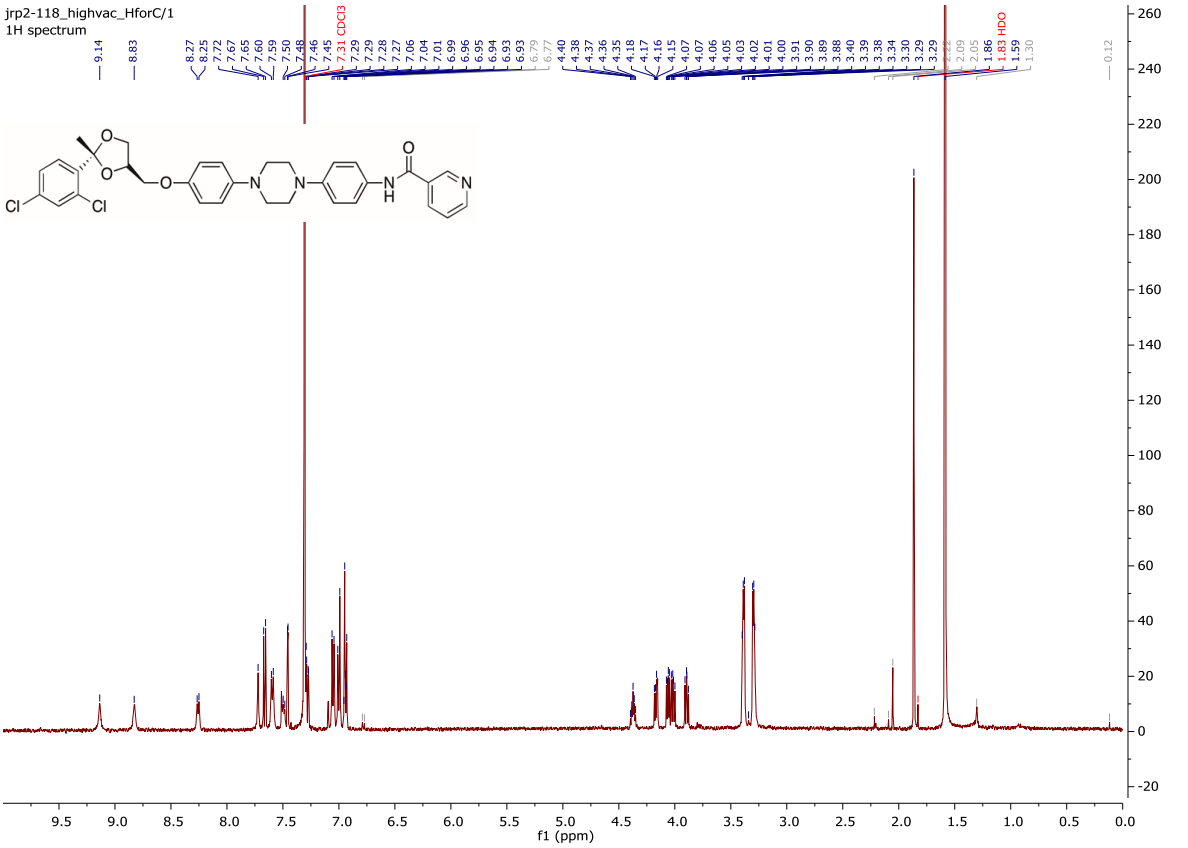
jrp2-118_highvac_HforC/1
1H spectrum
f1 (ppm)

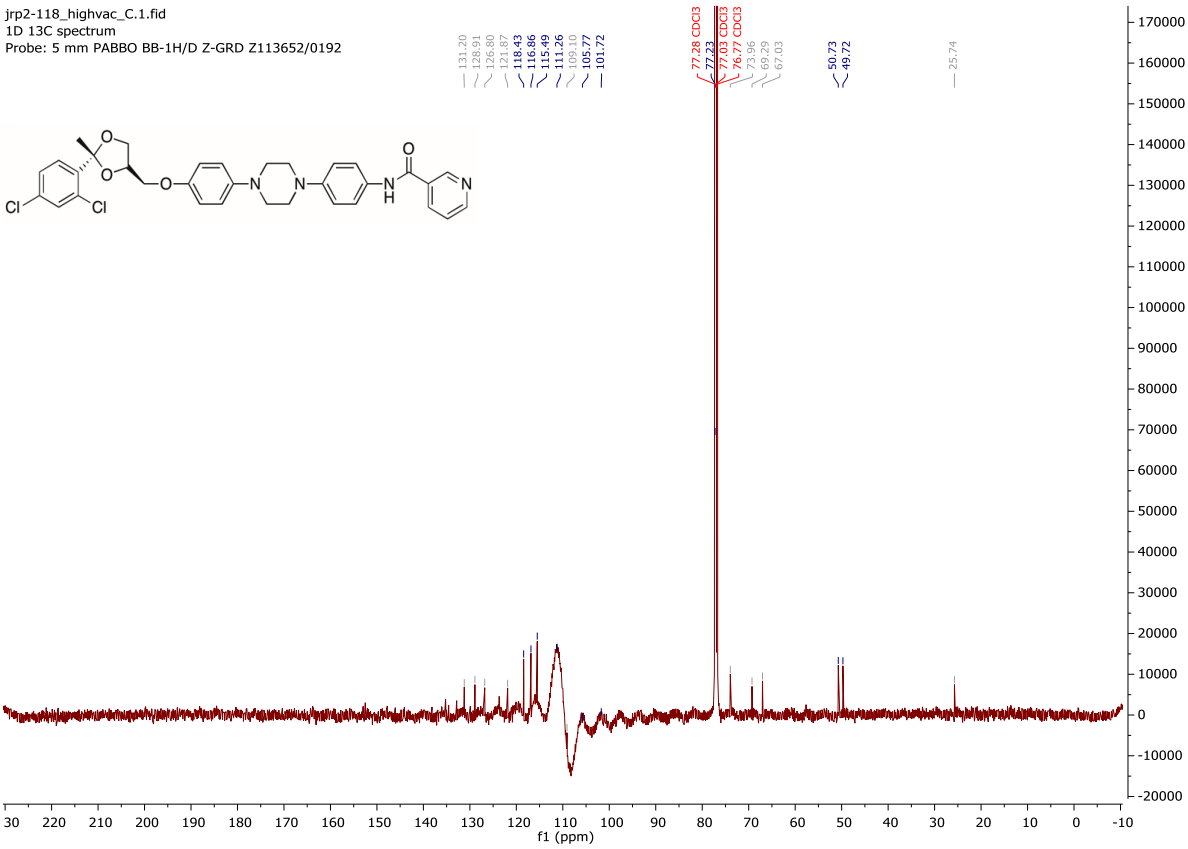
jrp2-118_highvac_C.1.fid
1D 13C spectrum
Probe: 5 mm PABBO BB-1H/D Z-GRD Z113652/0192
f1 (ppm)

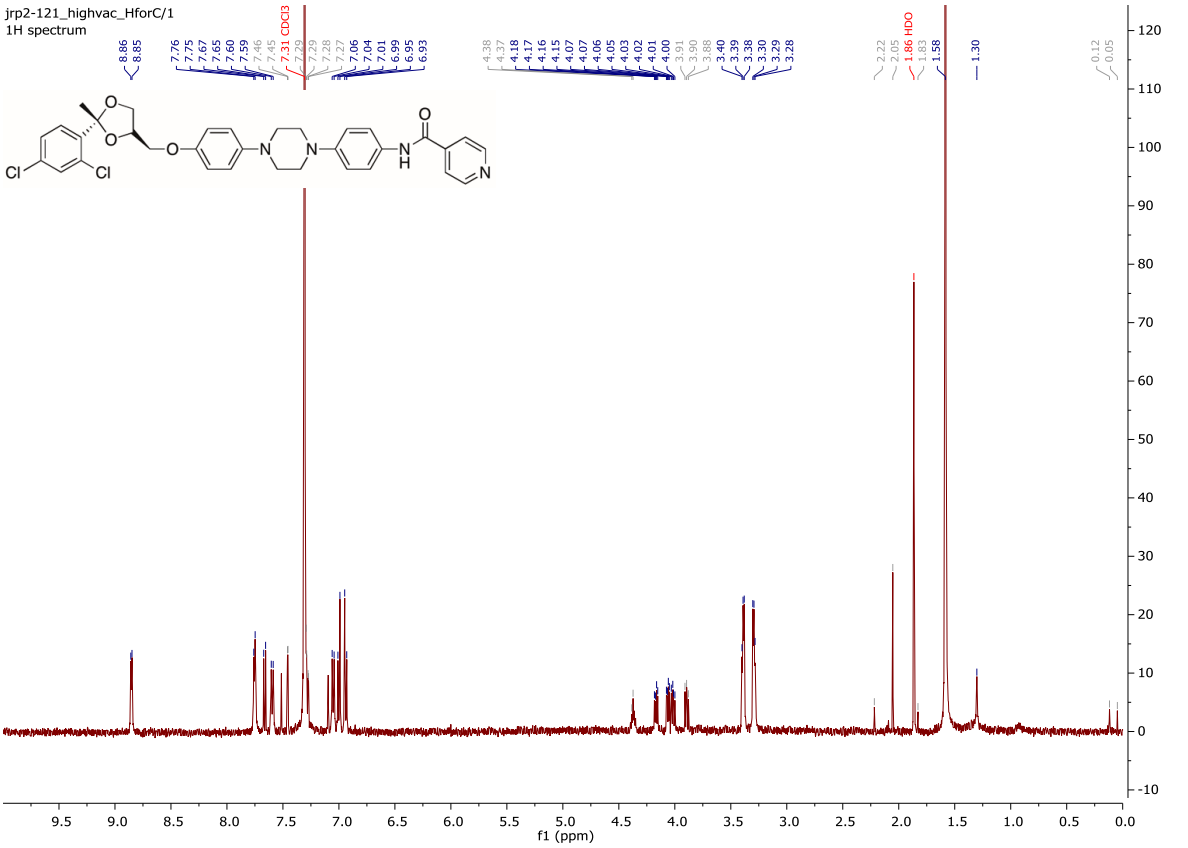
jrp2-121_highvac_HforC/1
1H spectrum
f1 (ppm)

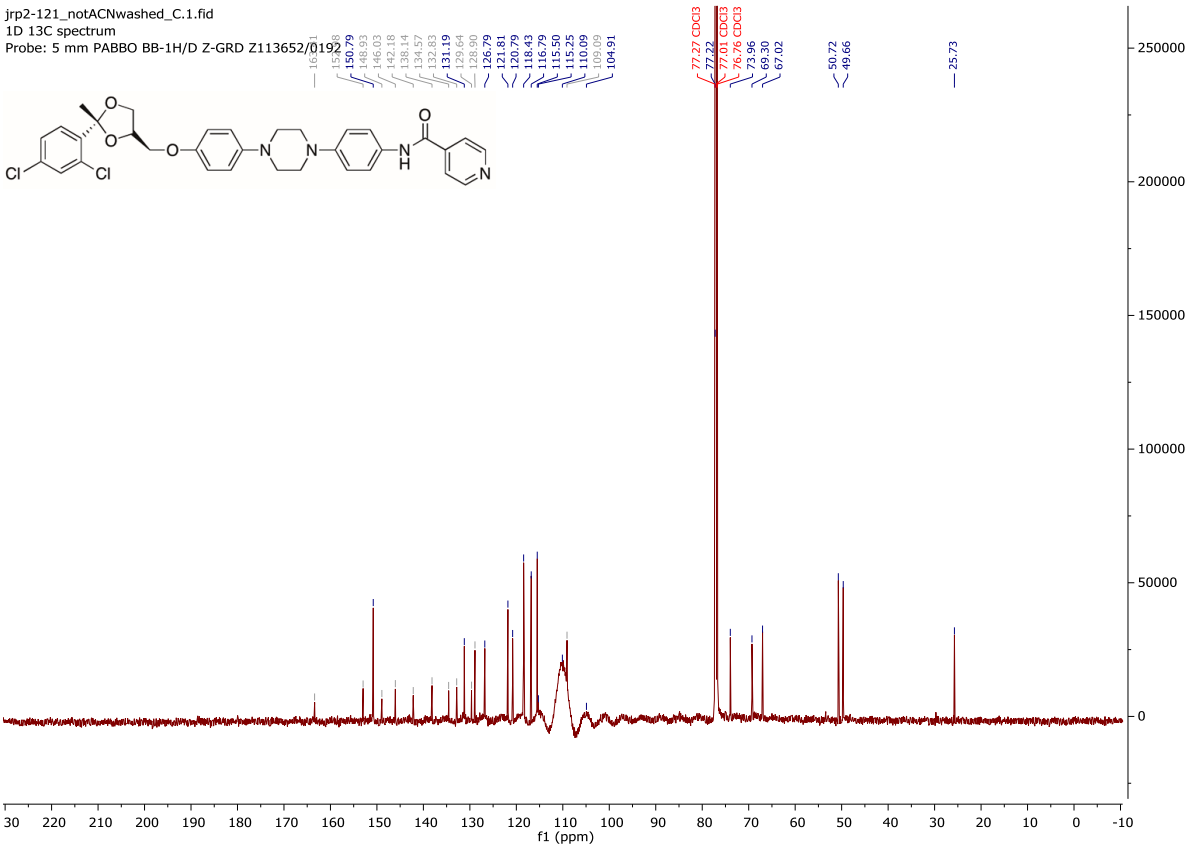
jrp2-121_notACNwashed_C.1.fid
1D 13C spectrum
Probe: 5 mm PABBO BB-1H/D Z-GRD Z113652/0192
f1 (ppm)

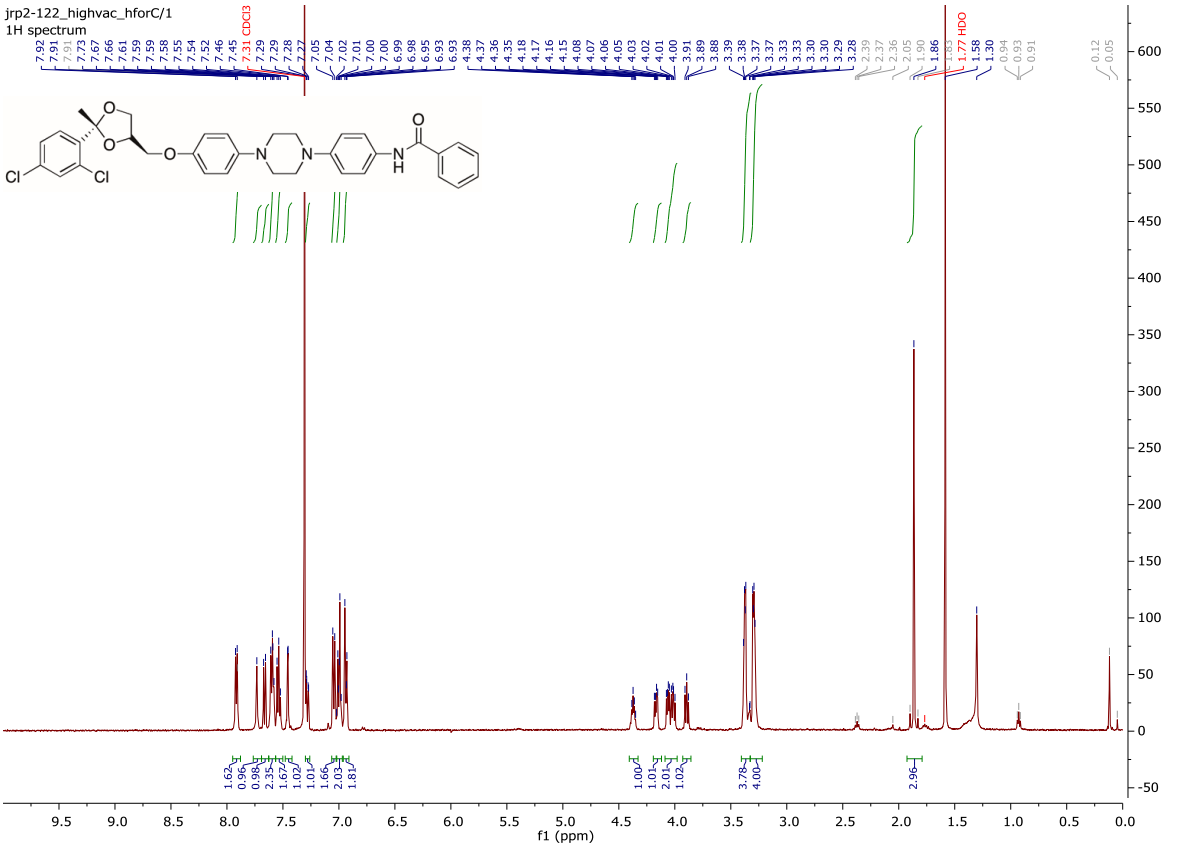
jrp2-122_highvac_hforC/1
1H spectrum
f1 (ppm)

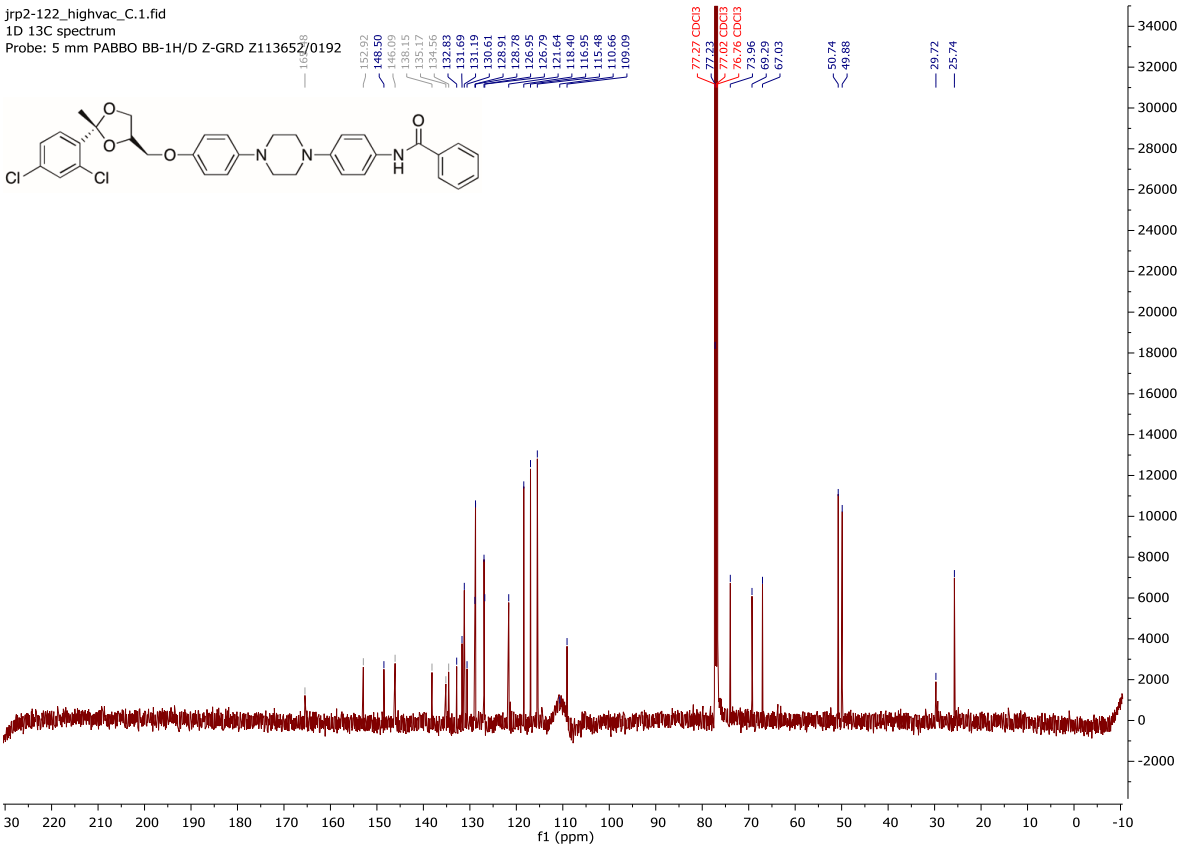
jrp2-122_highvac_C.1.fid
1D 13C spectrum
Probe: 5 mm PABBO BB-1H/D Z-GRD Z113652/0192
f1 (ppm)

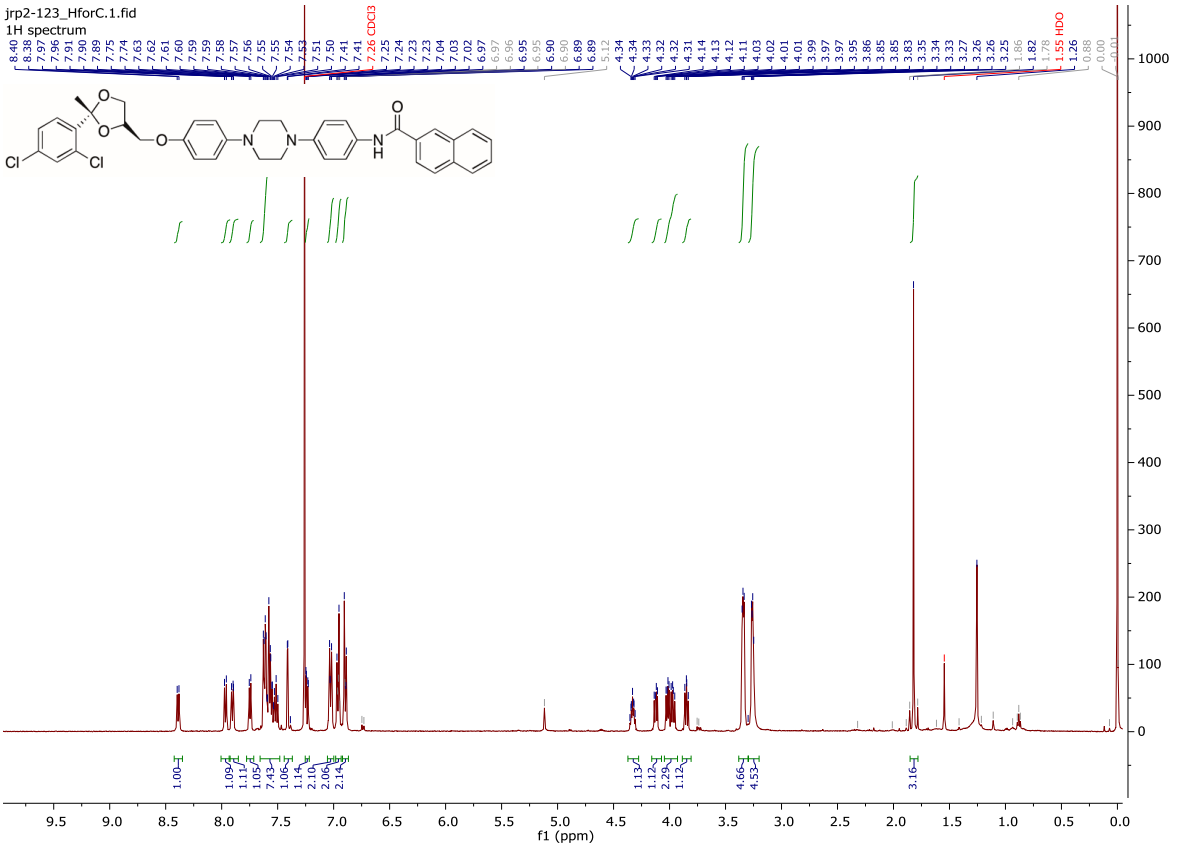
jrp2-123_HforC.1.fid
1H spectrum
f1 (ppm)

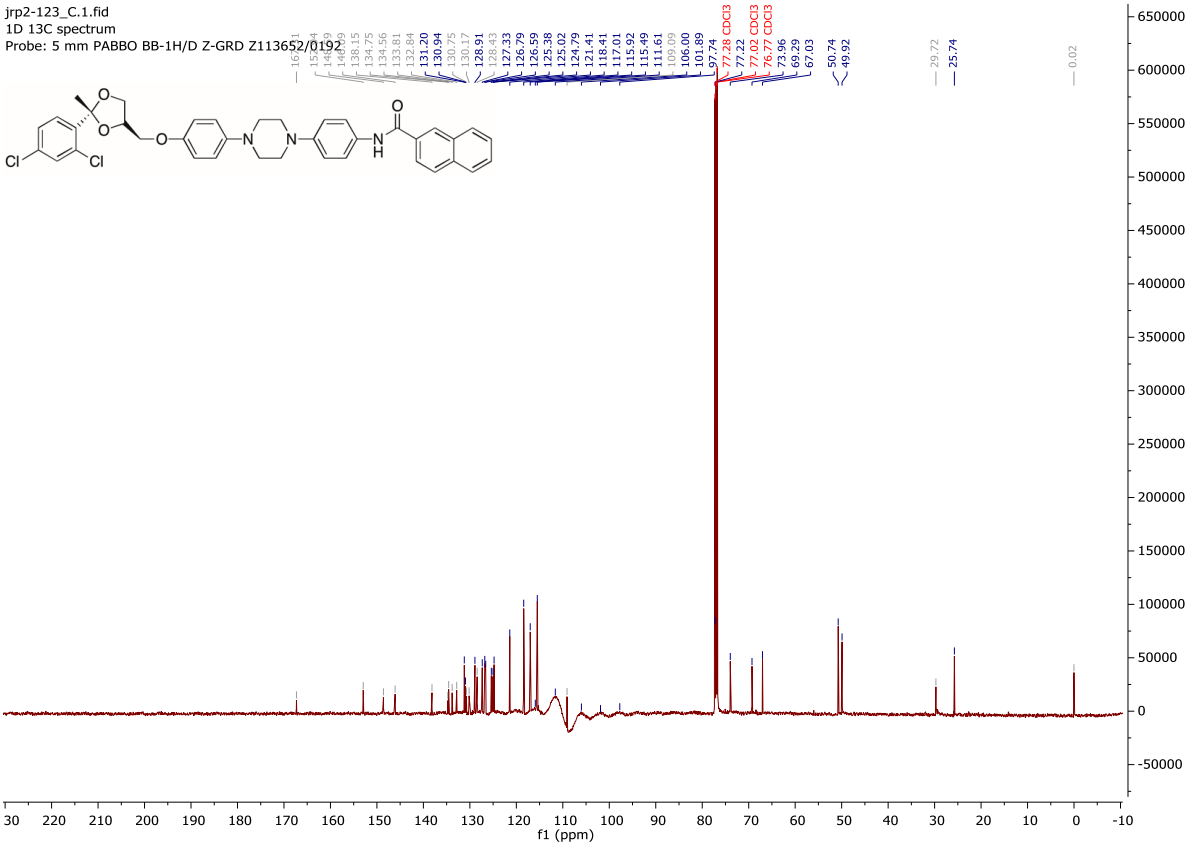
jrp2-123_C.1.fid
1D 13C spectrum
Probe: 5 mm PABBO BB-1H/D Z-GRD Z113652/0192
f1 (ppm)

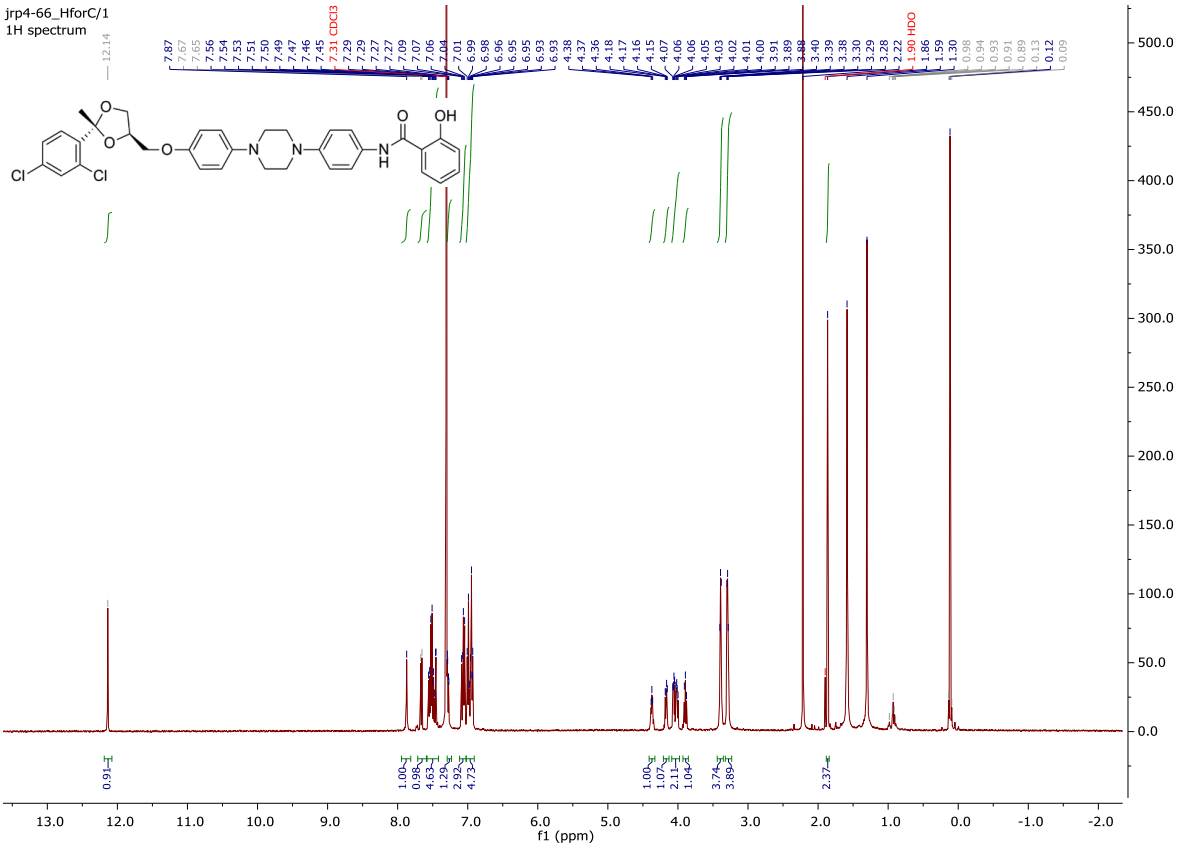
jrp4-66_HforC/1
1H spectrum
f1 (ppm)

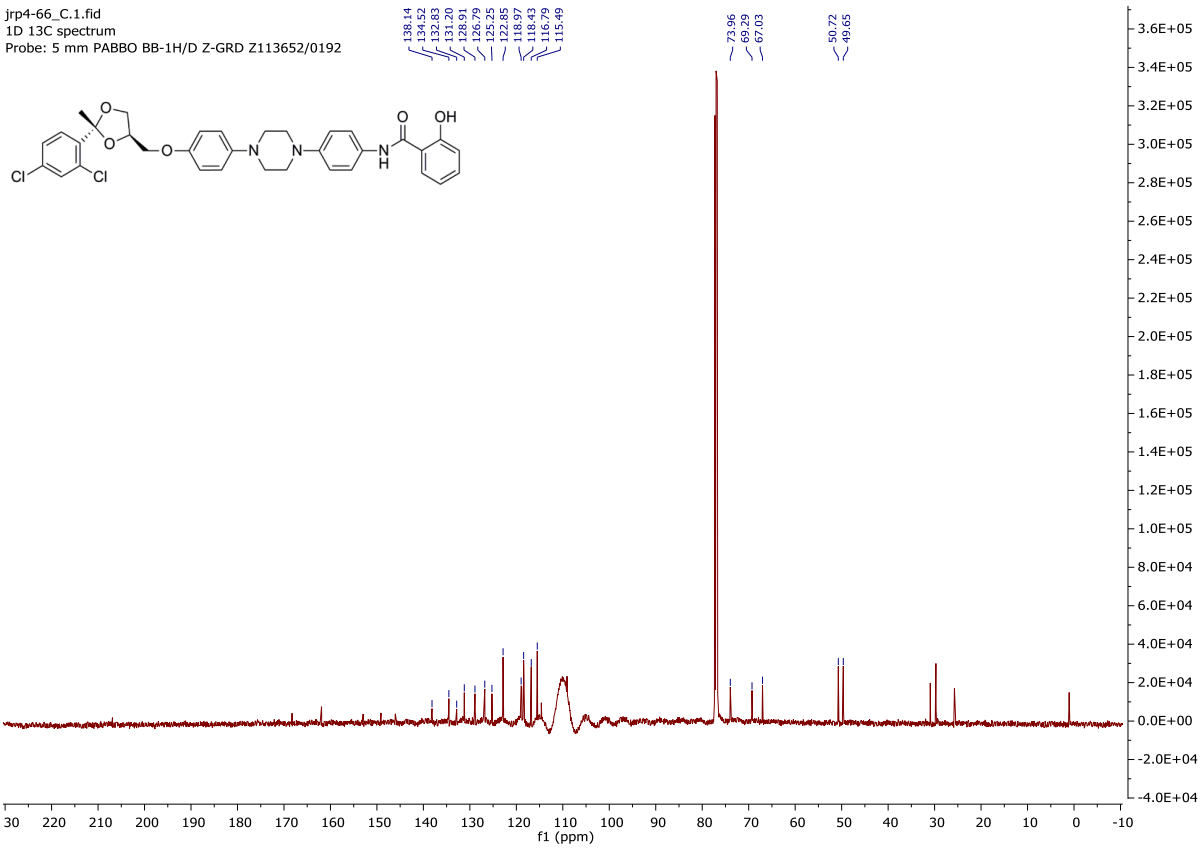
jrp4-66_C.1.fid
1D 13C spectrum
Probe: 5 mm PABBO BB-1H/D Z-GRD Z113652/0192
f1 (ppm)

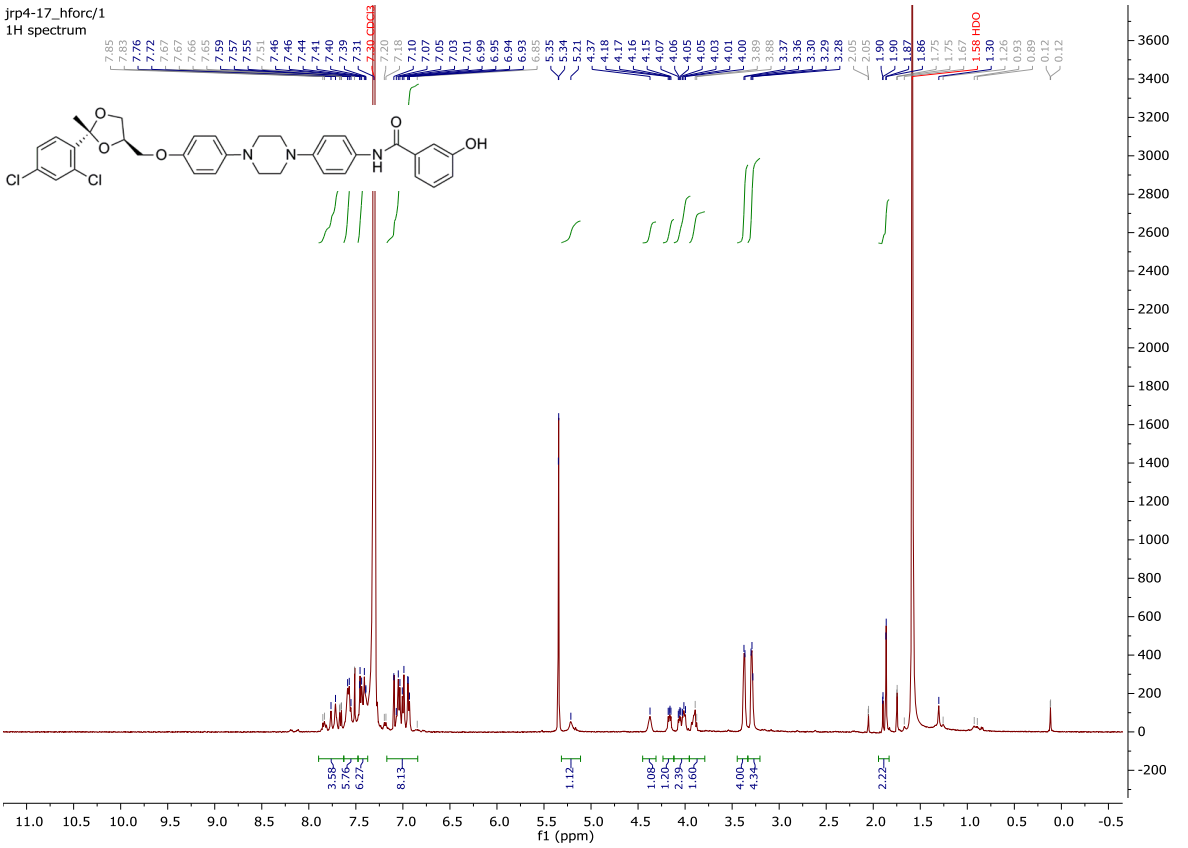
jrp4-17_hforc/1
1H spectrum
f1 (ppm)

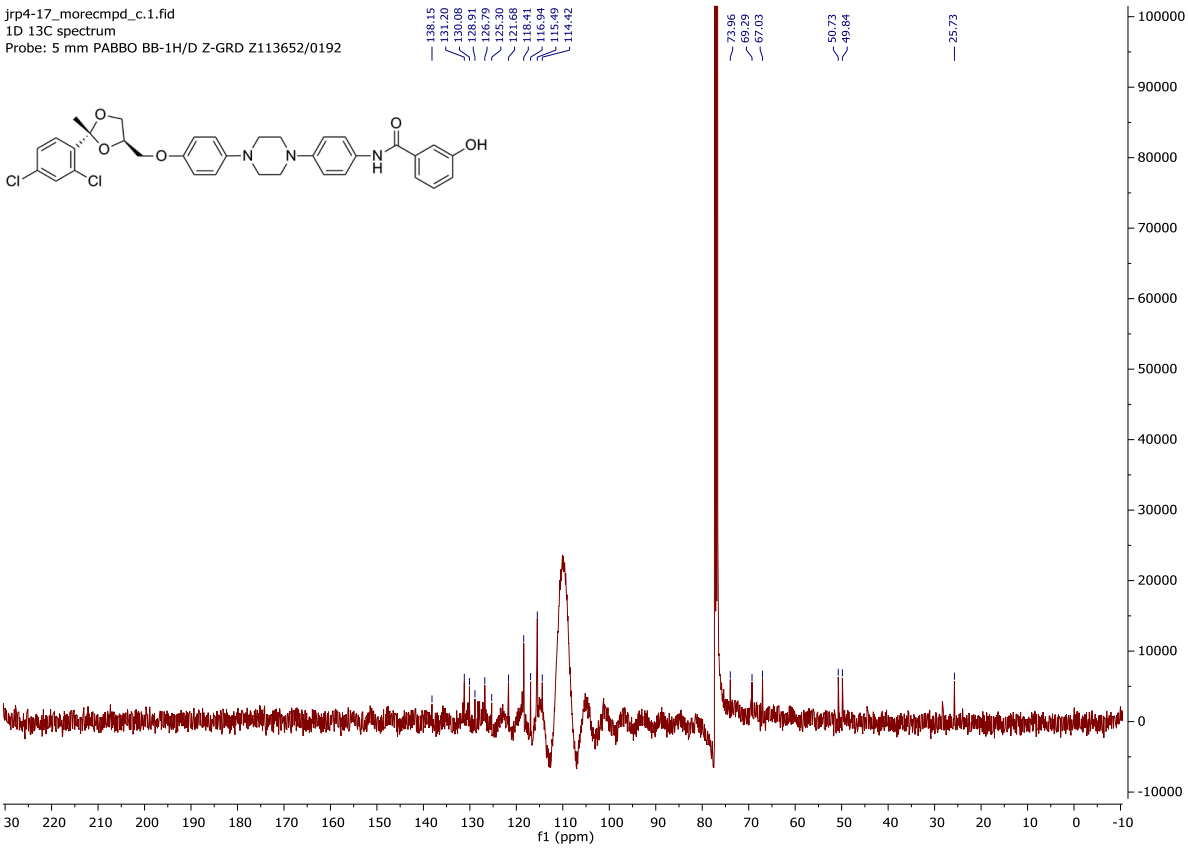
jrp4-17_morecmpd_c.1.fid
1D 13C spectrum
Probe: 5 mm PABBO BB-1H/D Z-GRD Z113652/0192
f1 (ppm)

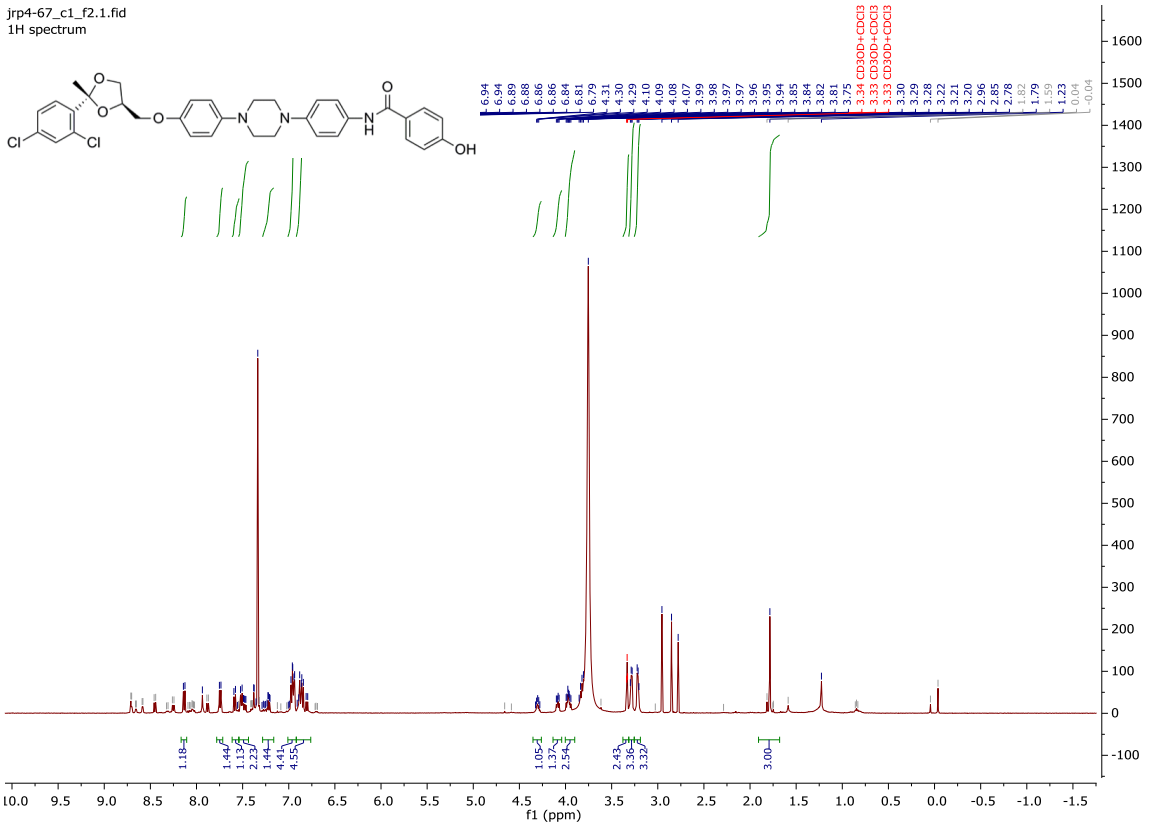
jrp4-67_c1_f2.1.fid
1H spectrum
Cl
Cl
O
O
O
N
N
N
H
O
OH
f1 (ppm)

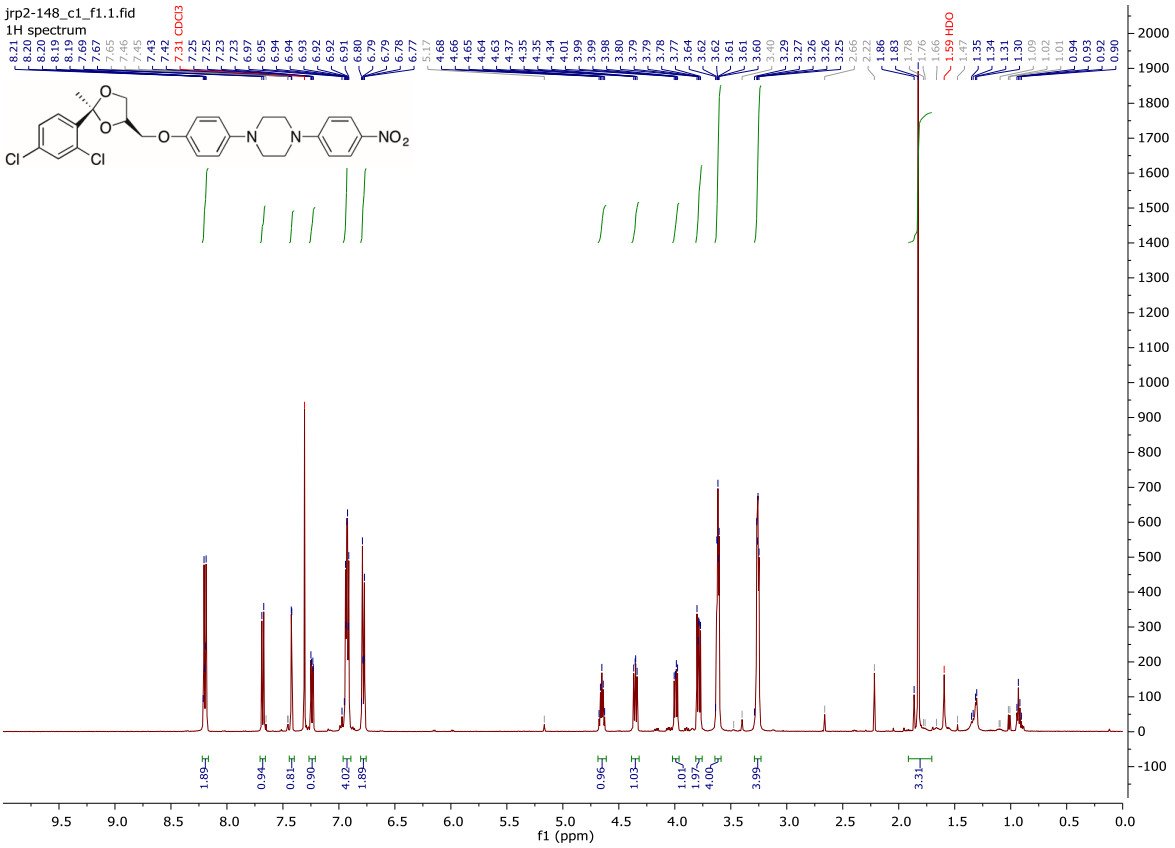
jrp2-148_c1_f1.1.fid
1H spectrum
f1 (ppm)

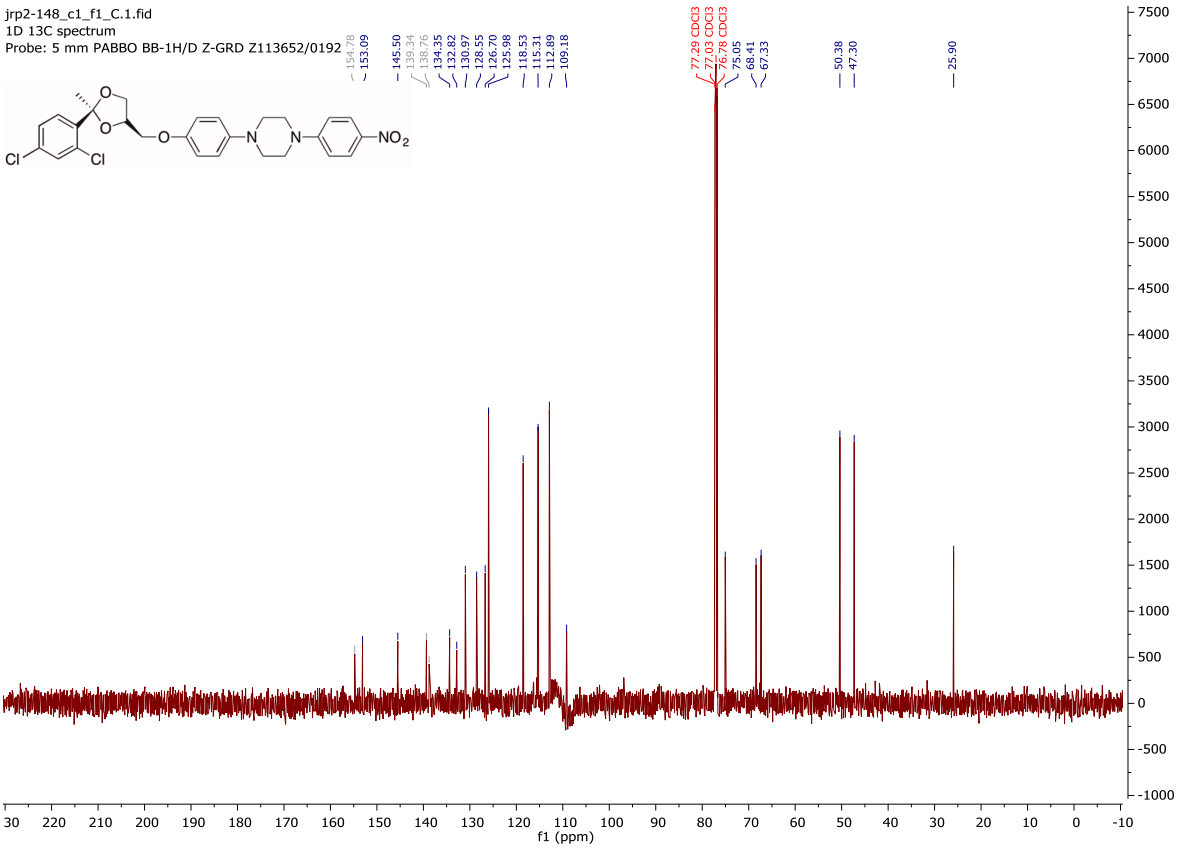
jrp2-148_c1_f1_C.1.fid
1D 13C spectrum
Probe: 5 mm PABBO BB-1H/D Z-GRD Z113652/0192
f1 (ppm)

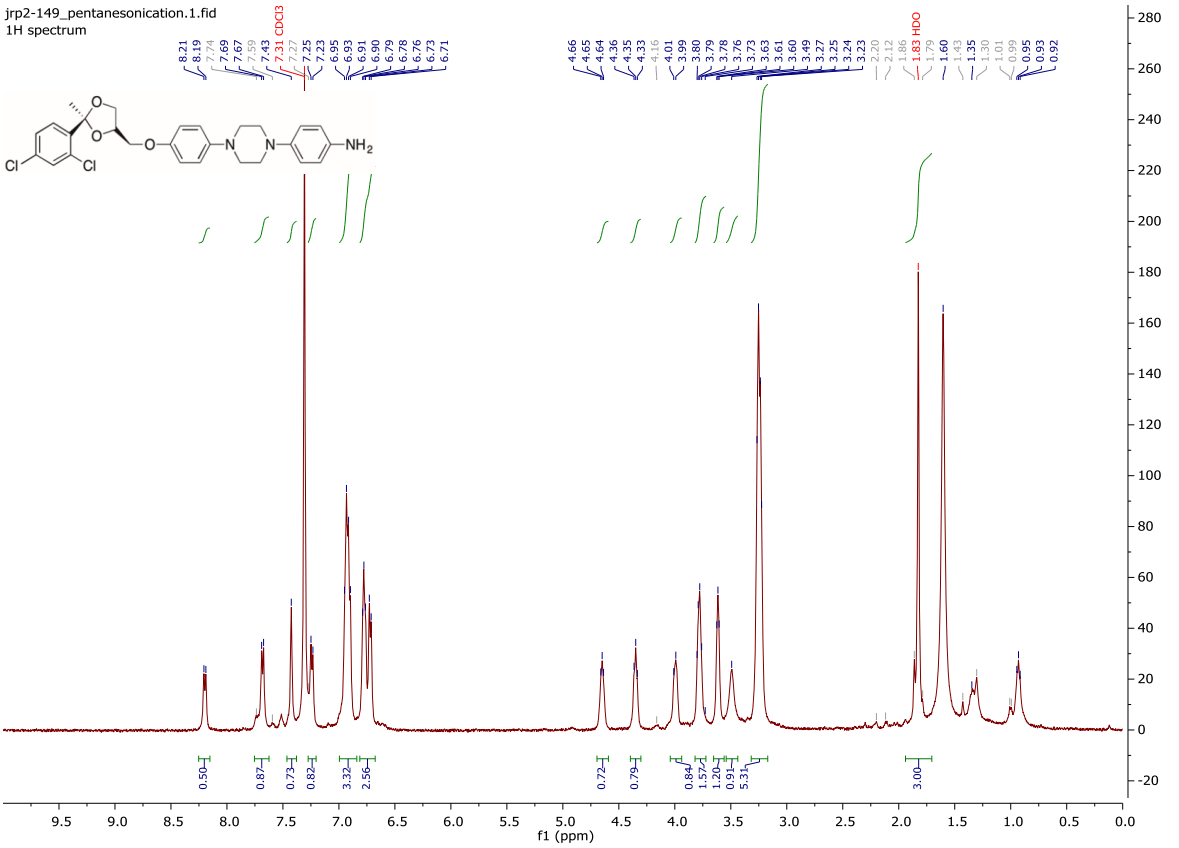
jrp2-149_pentanesonication.1.fid
1H spectrum
f1 (ppm)

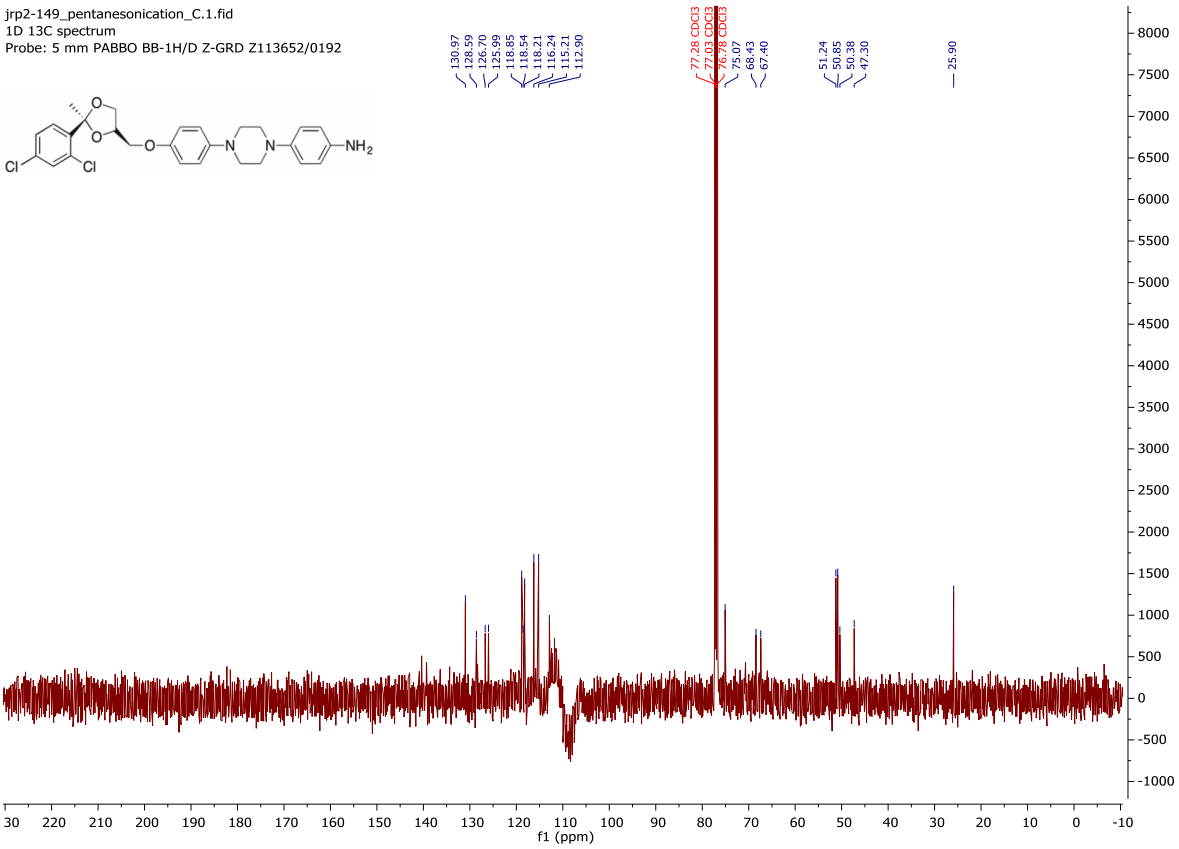
jrp2-149_pentanesonication_C.1.fid
1D 13C spectrum
Probe: 5 mm PABBO BB-1H/D Z-GRD Z113652/0192
f1 (ppm)

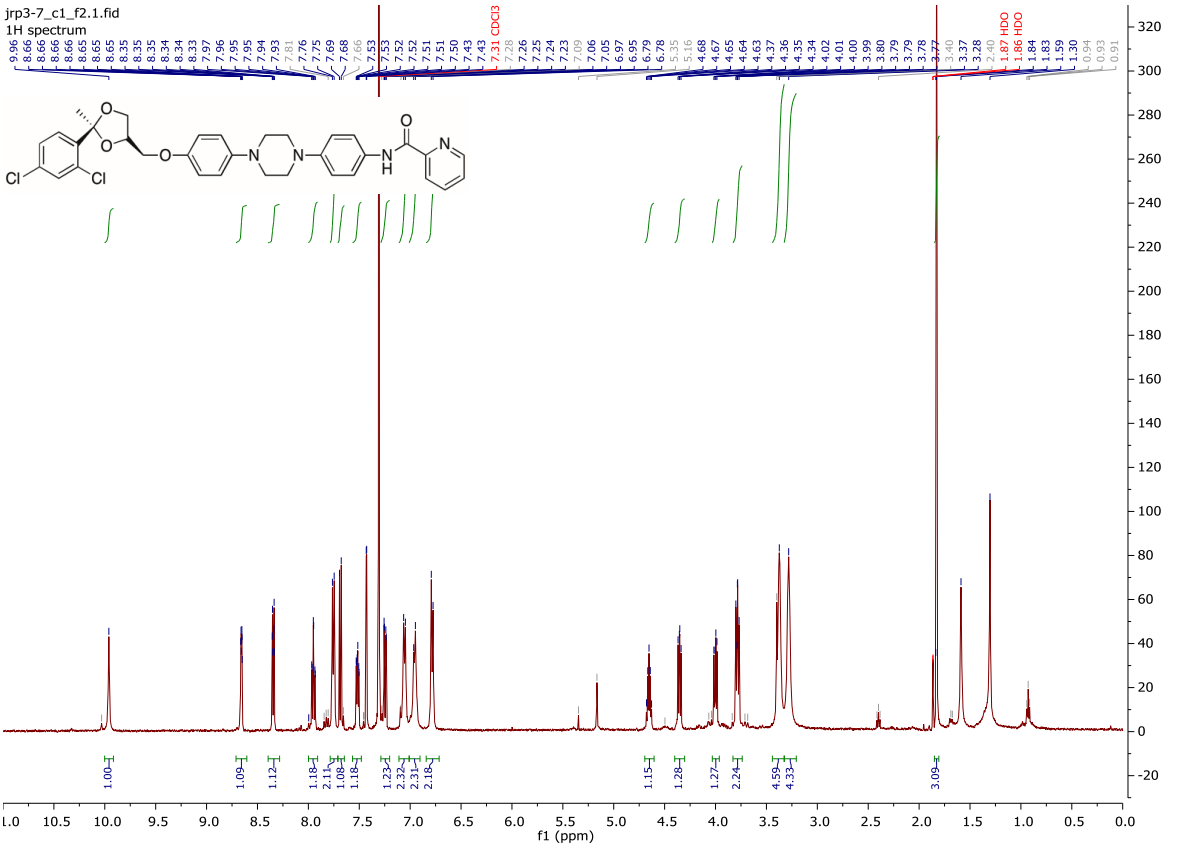
jrp3-7_c1_f2.1.fid
1H spectrum
f1 (ppm)

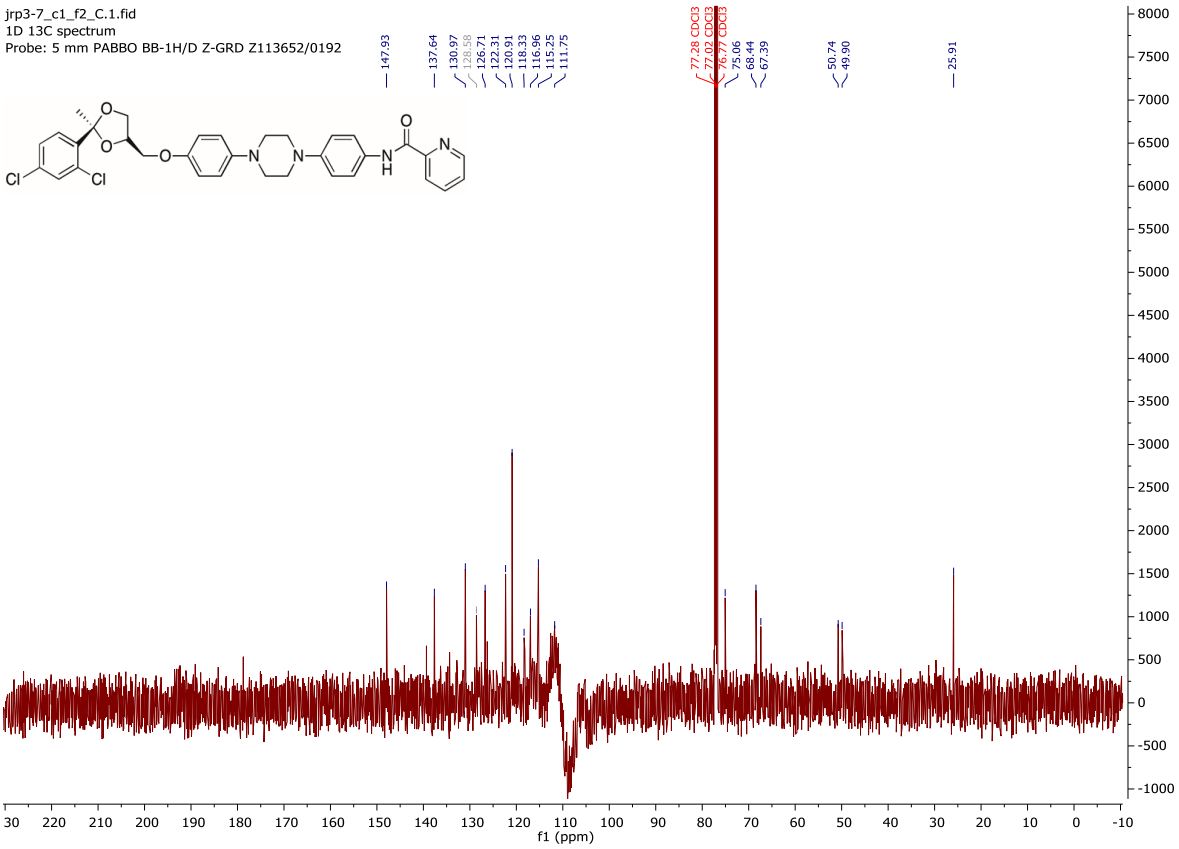
jrp3-7_c1_f2_C.1.fid
1D 13C spectrum
Probe: 5 mm PABBO BB-1H/D Z-GRD Z113652/0192
f1 (ppm)

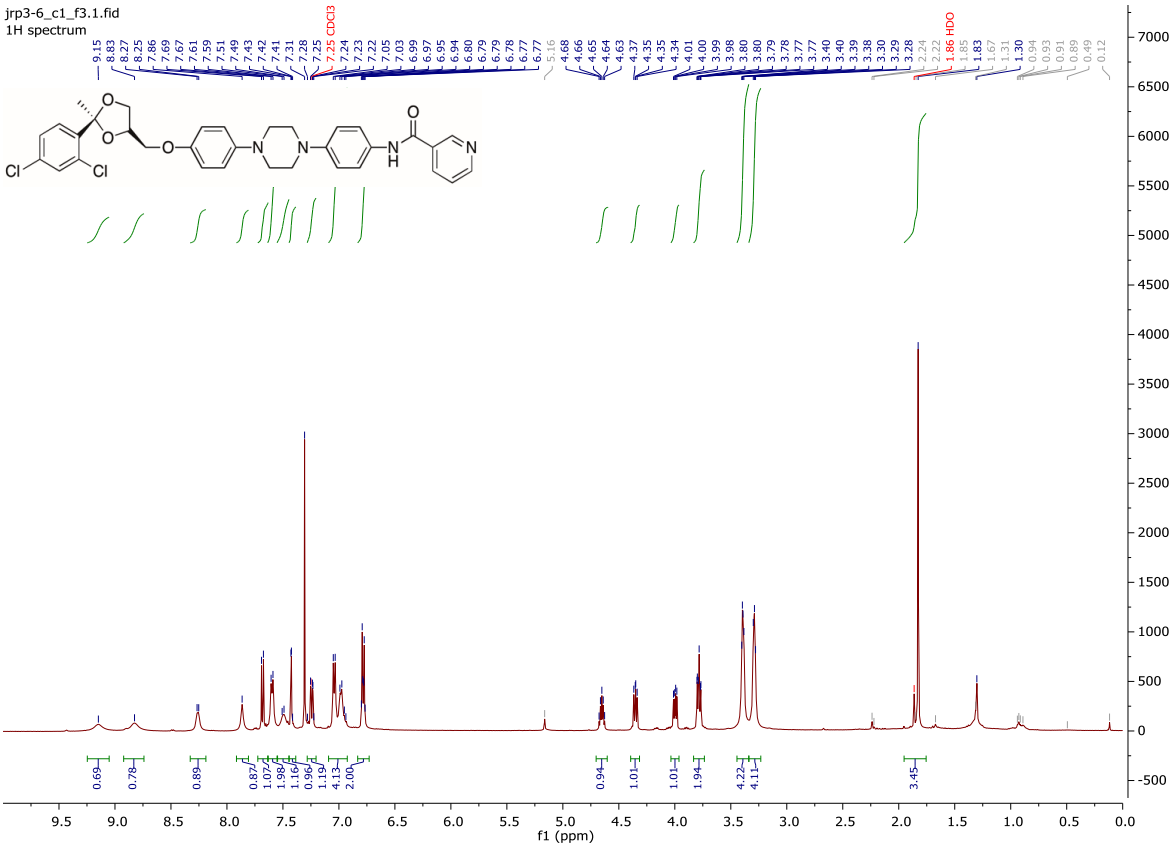
jrp3-6_c1_f3.1.fid
1H spectrum
f1 (ppm)

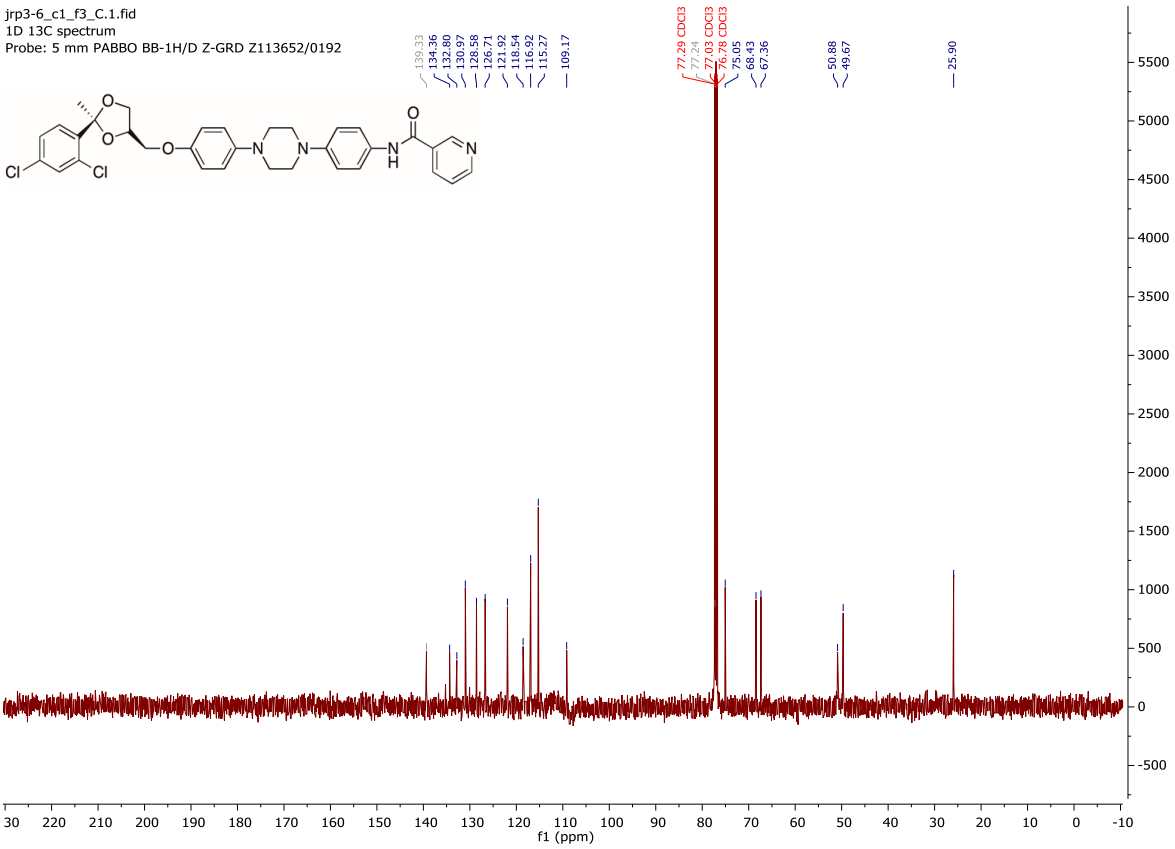
jrp3-6_c1_f3_C.1.fid
1D 13C spectrum
Probe: 5 mm PABBO BB-1H/D Z-GRD Z113652/0192
f1 (ppm)

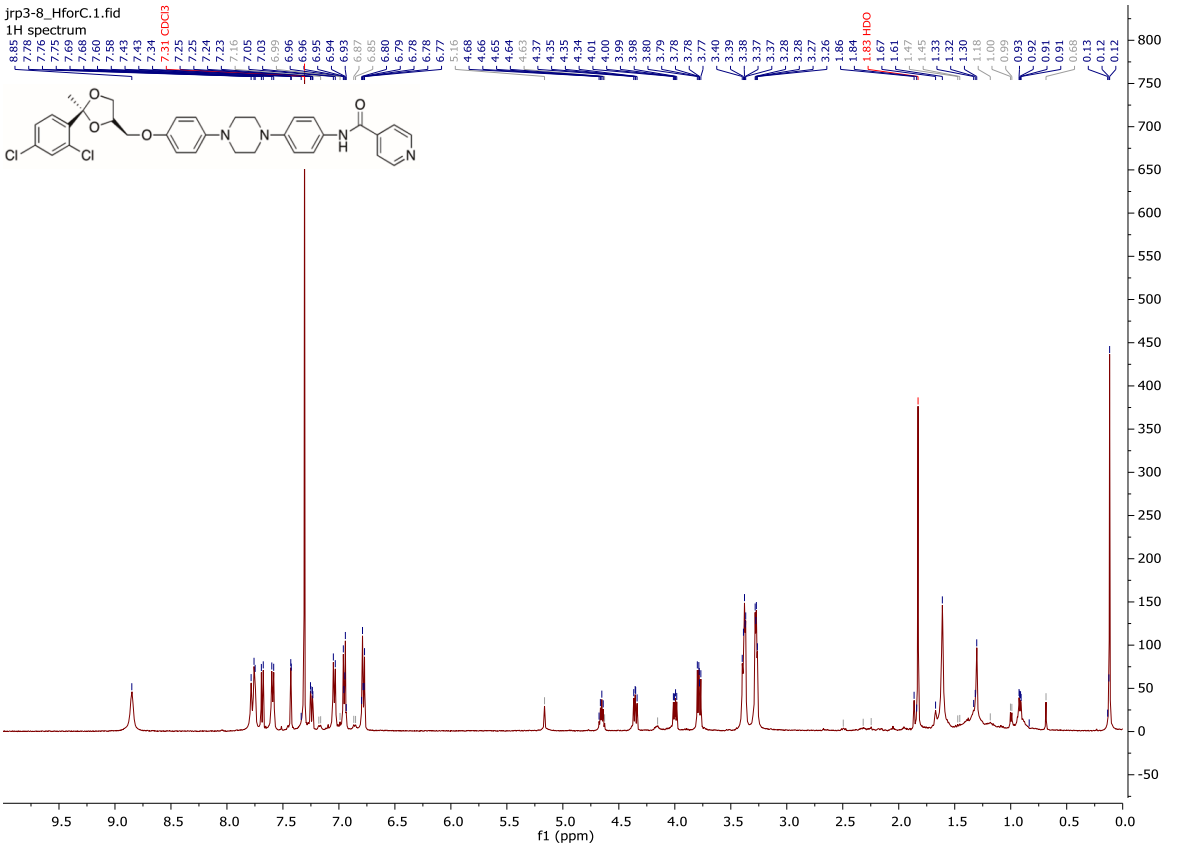
jrp3-8_HforC.1.fid
1H spectrum
f1 (ppm)

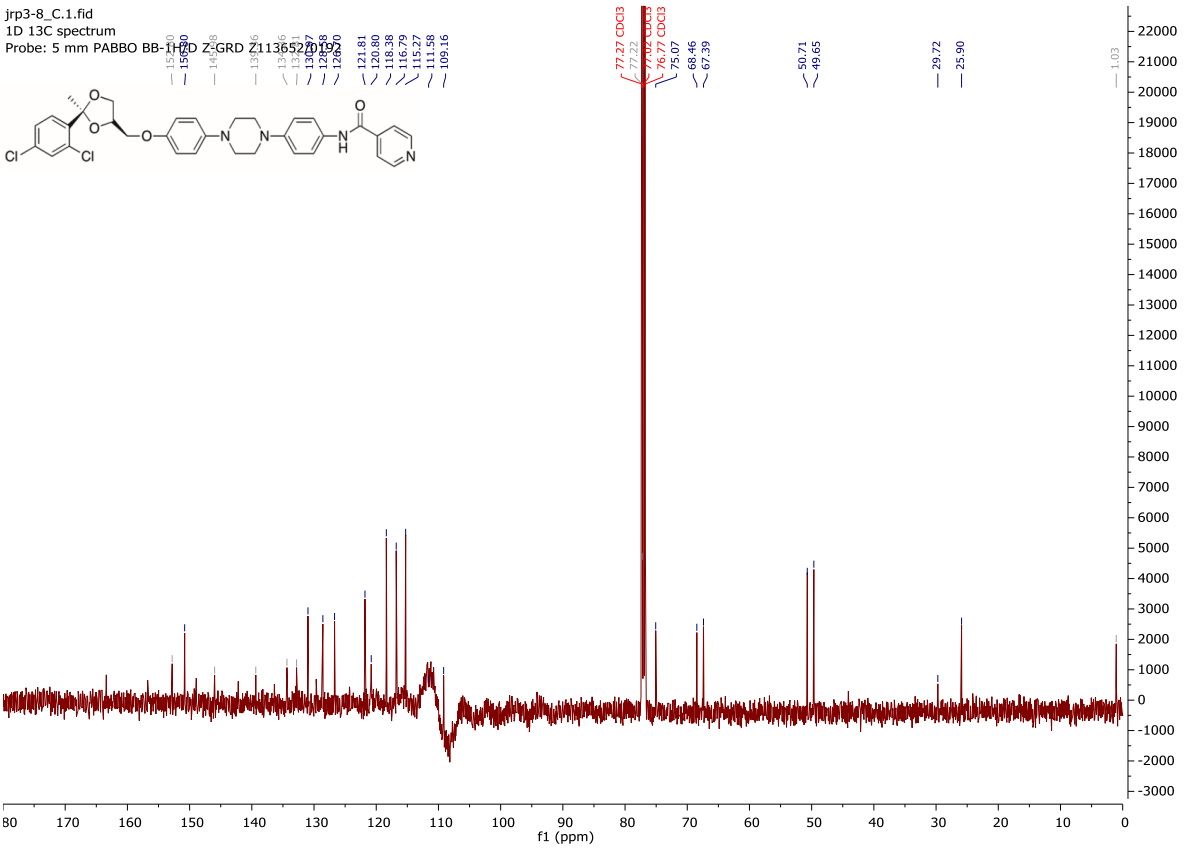
jrp3-8_C.1.fid
1D 13C spectrum
Probe: 5 mm PABBO BB-1H/D Z-GRD Z113652/0159
f1 (ppm)

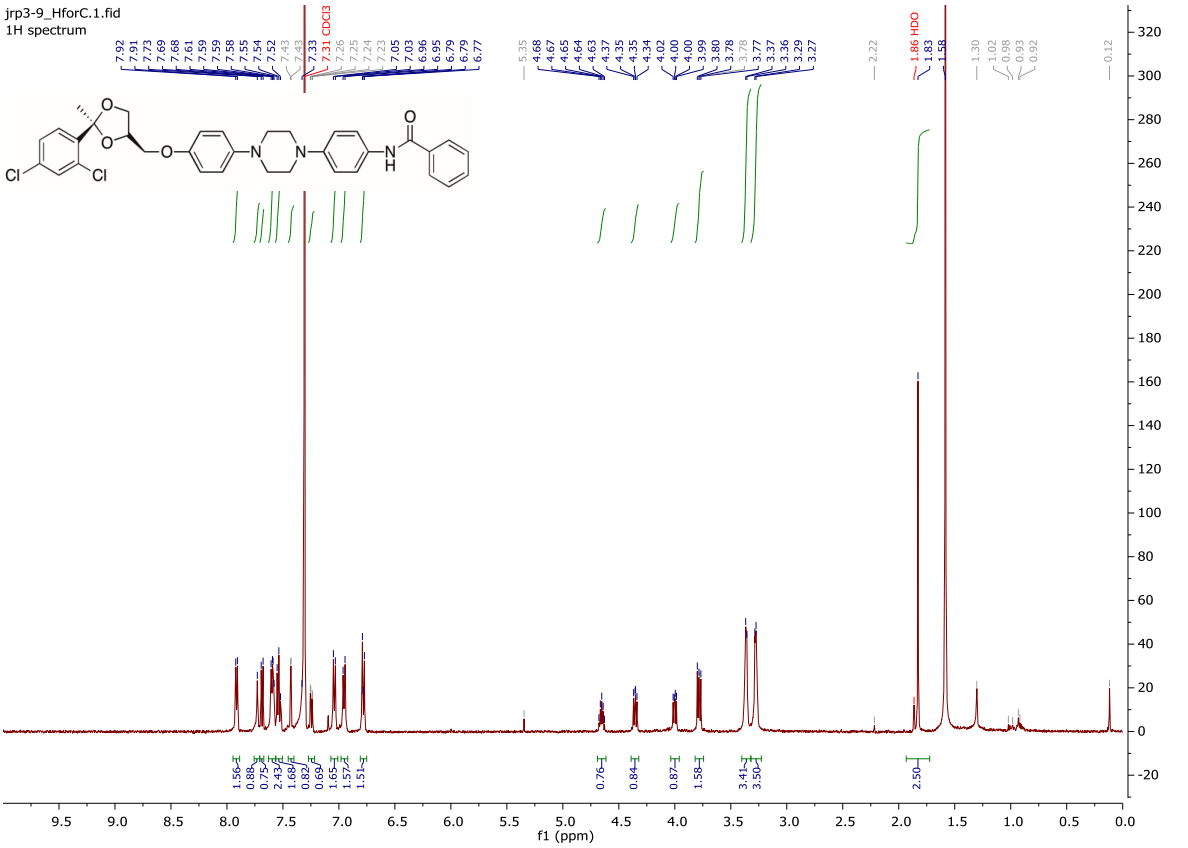
jrp3-9_HforC.1.fid
1H spectrum
f1 (ppm)

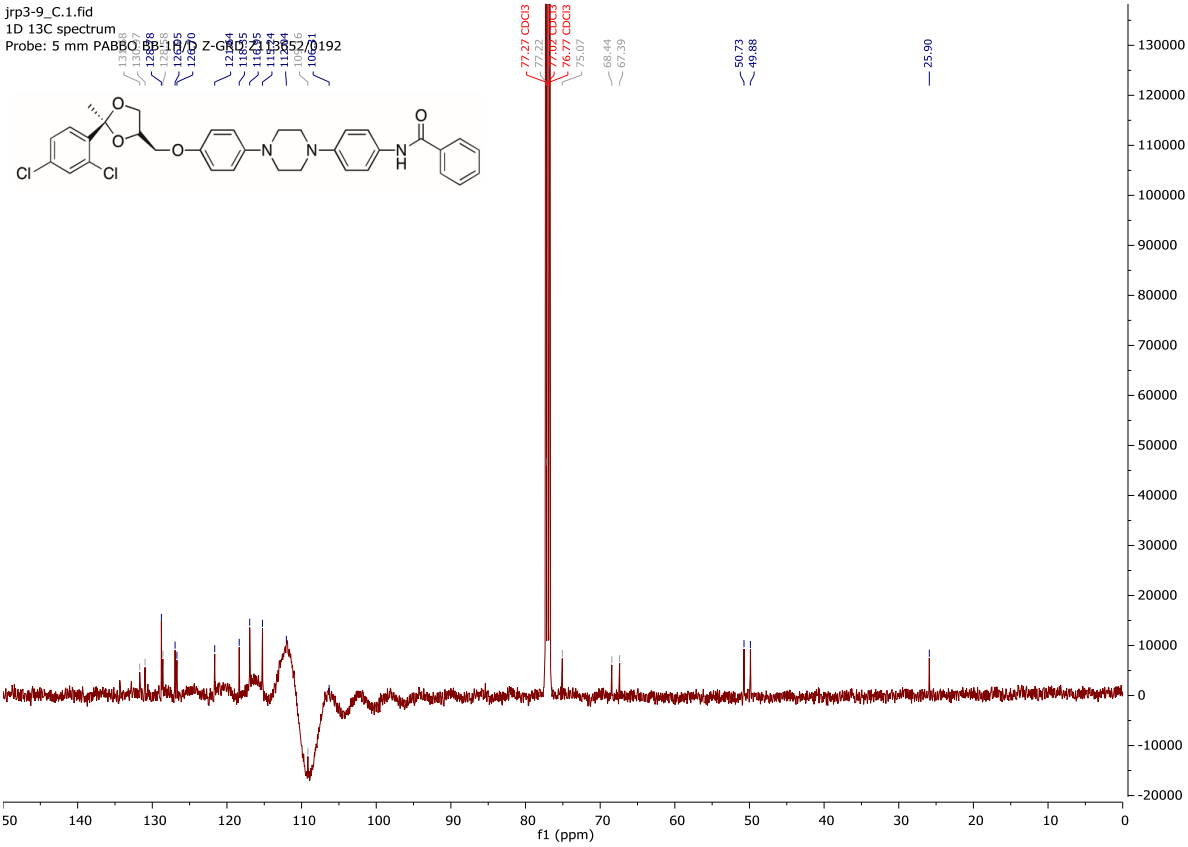
jrp3-9_C.1.fid
1D 13C spectrum
Probe: 5 mm PABBO BB-1H/D Z-GRD Z113852/0192
f1 (ppm)

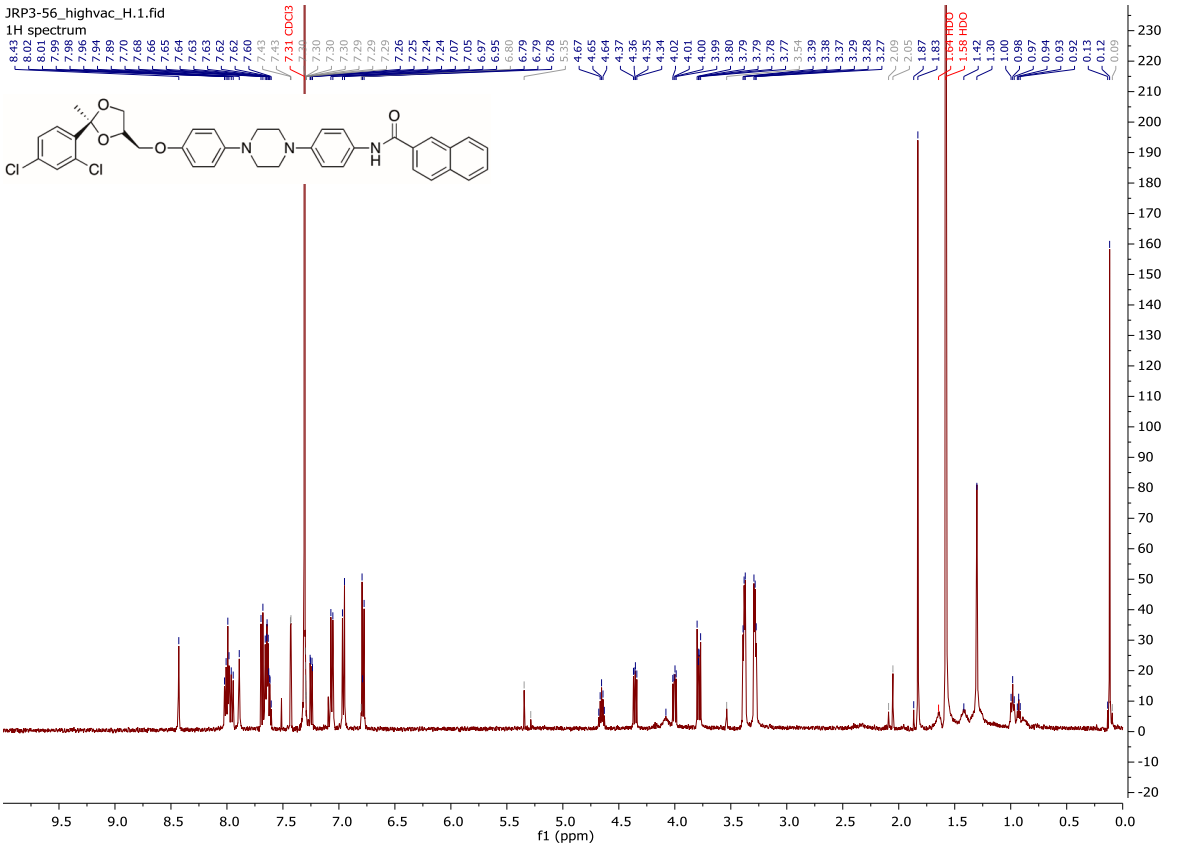
JRP3-56_highvac_H.1.fid
1H spectrum
f1 (ppm)

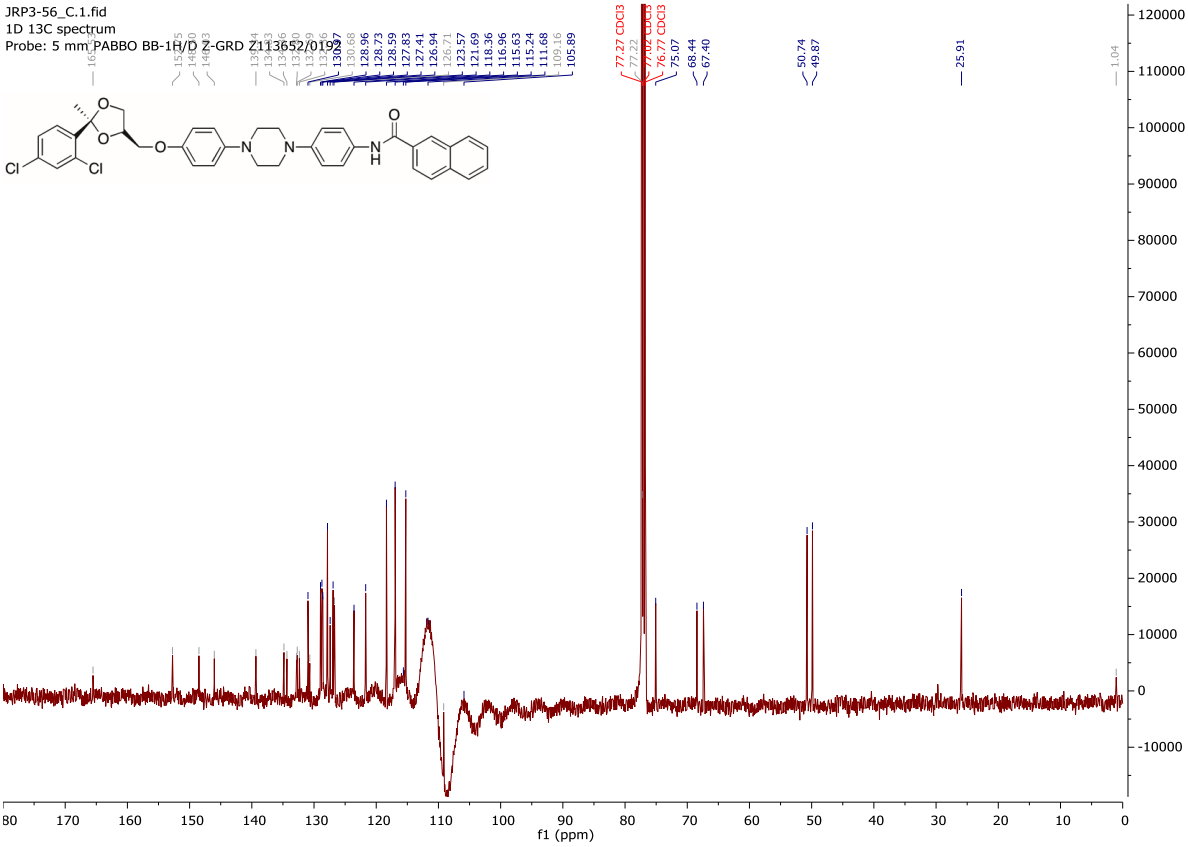
JRP3-56_C.1.fid
1D 13C spectrum
Probe: 5 mm PABBO BB-1H/D Z-GRD Z113652/0197
f1 (ppm)

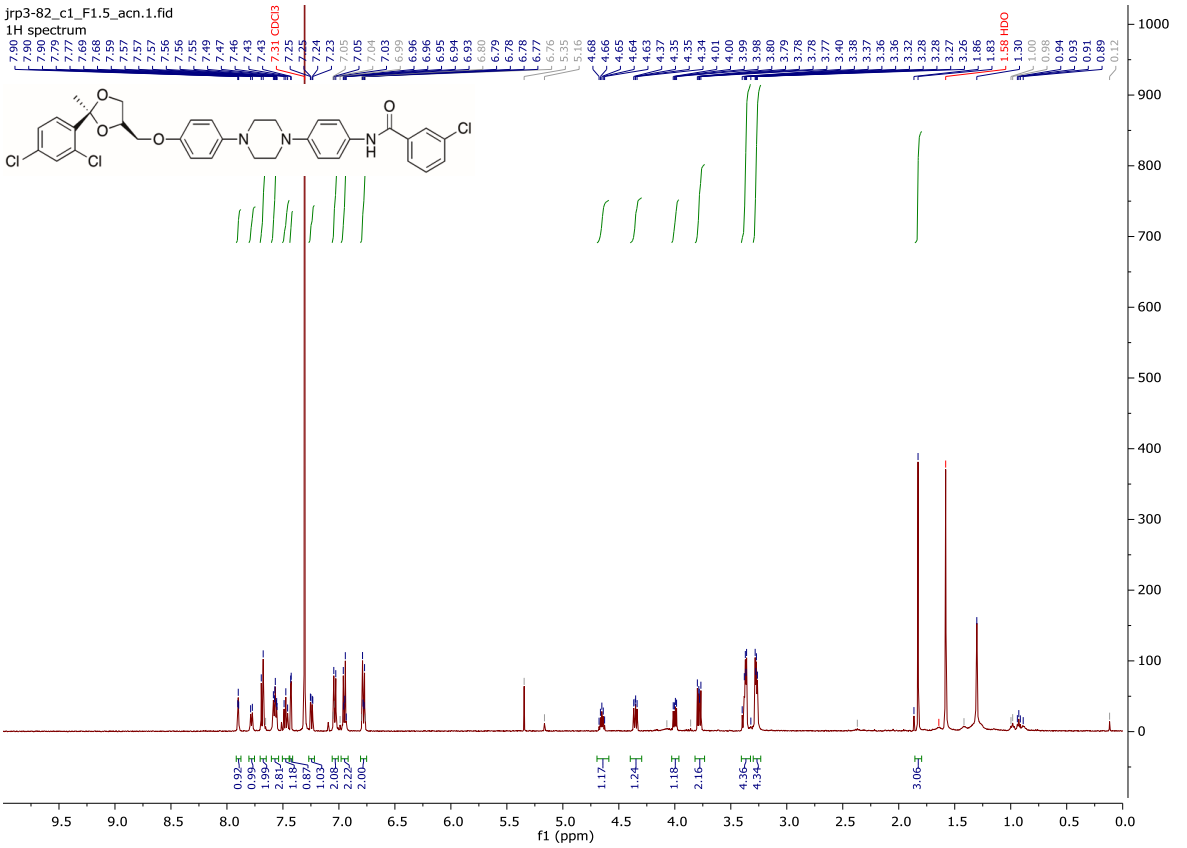
jrp3-82_c1_F1.5_acn.1.fid
1H spectrum
f1 (ppm)

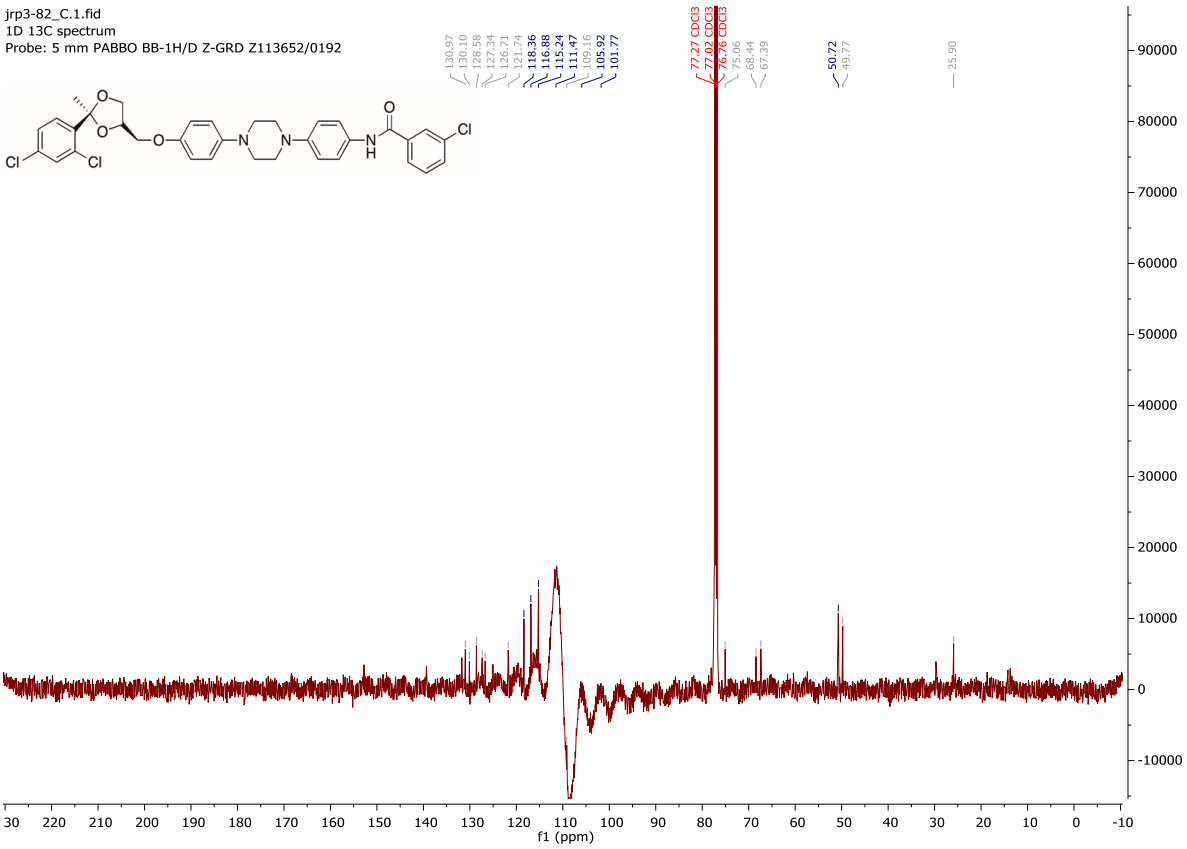
jrp3-82_C.1.fid
1D 13C spectrum
Probe: 5 mm PABBO BB-1H/D Z-GRD Z113652/0192
f1 (ppm)

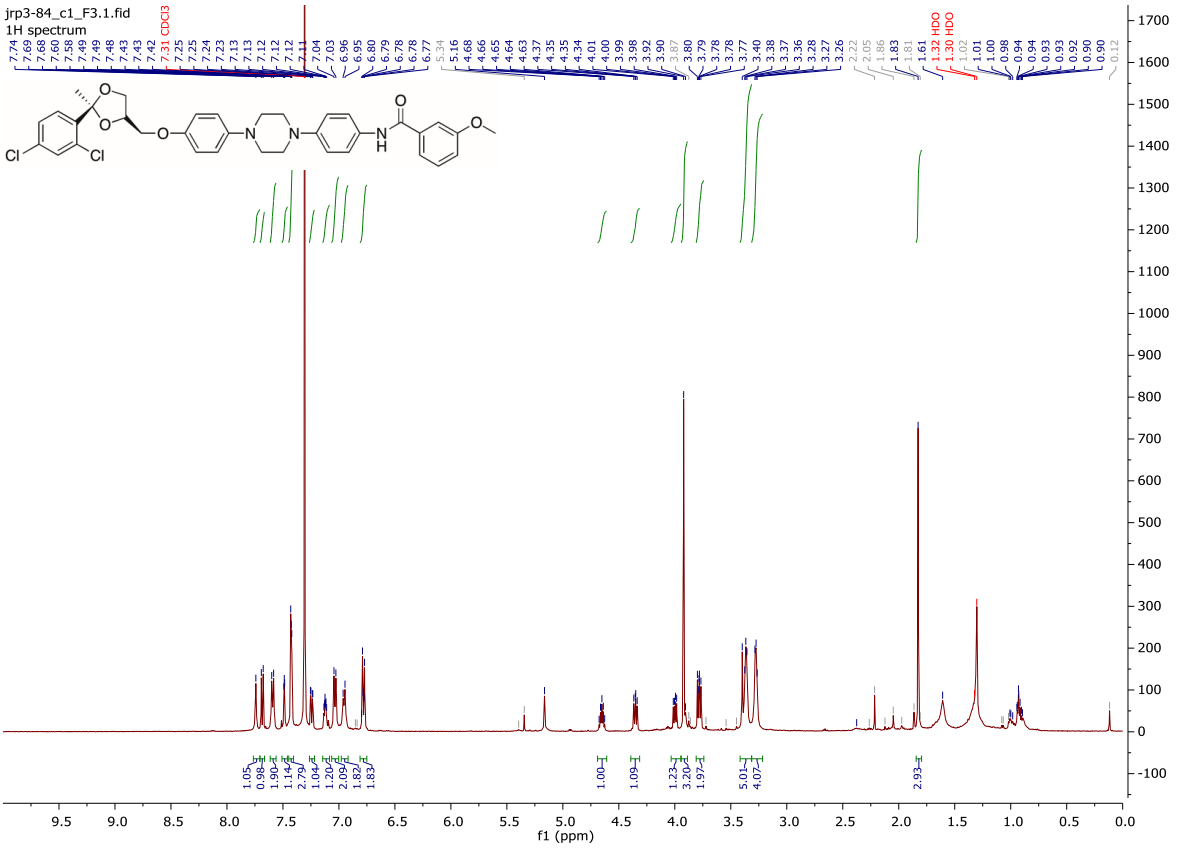
jrp3-84_c1_F3.1.fid
1H spectrum
f1 (ppm)

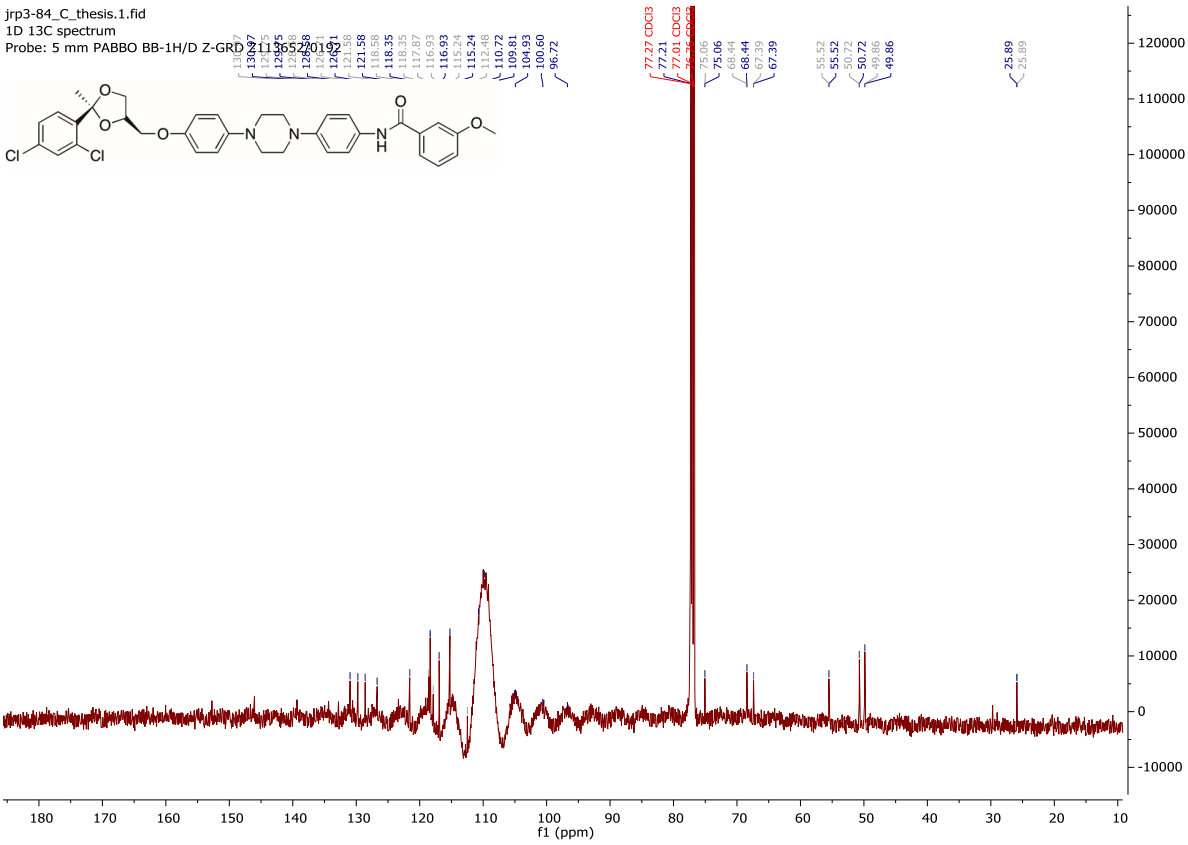
jrp3-84_C_thesis.1.fid
1D 13C spectrum
Probe: 5 mm PABBO BB-1H/D Z-GRD
f1 (ppm)

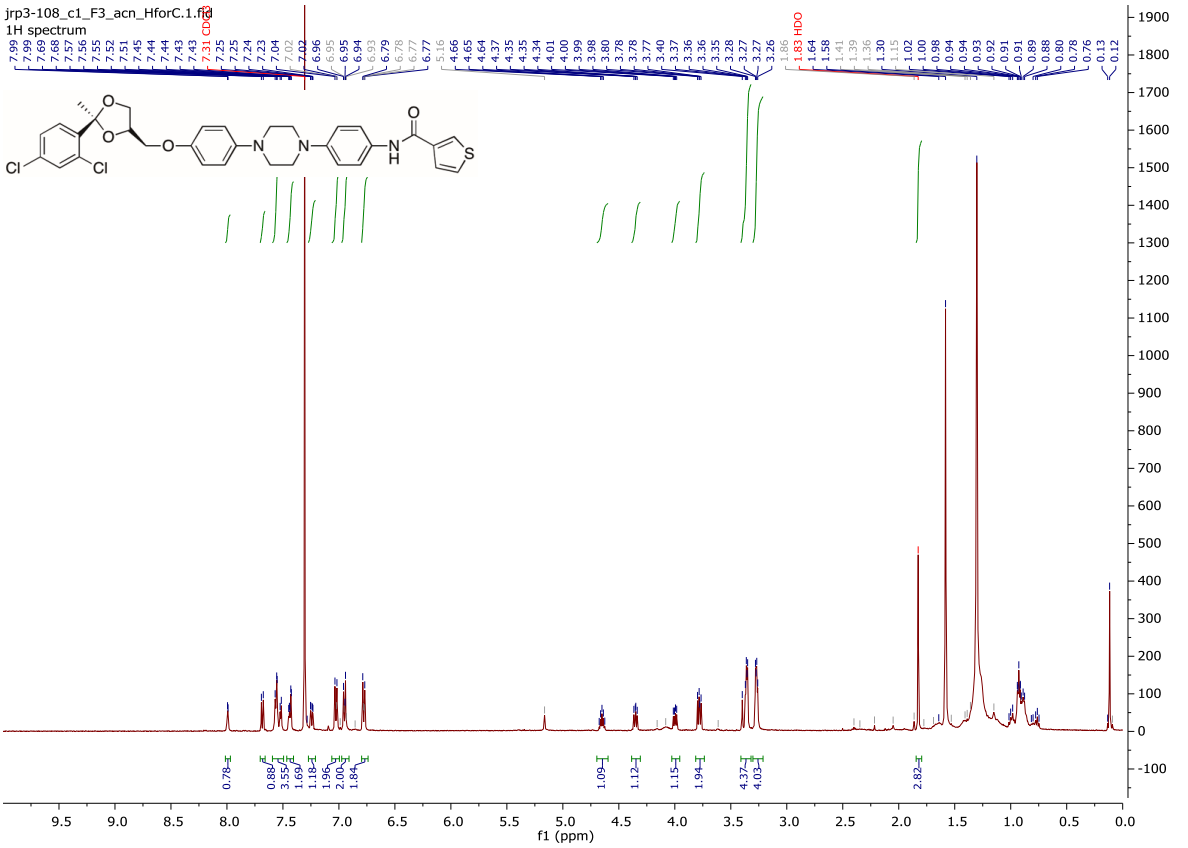
jrp3-108_c1_F3_acn_HforC.1.fid
1H spectrum
f1 (ppm)

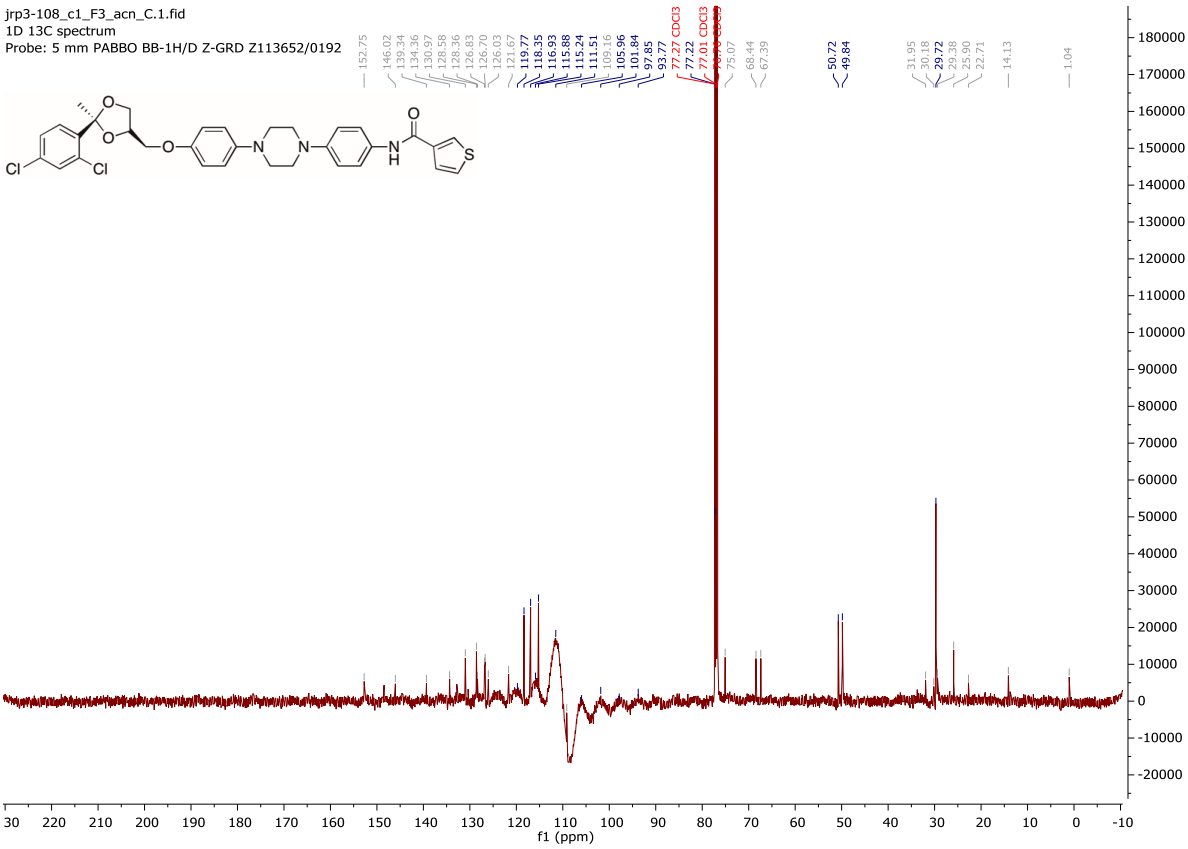
jrp3-108_c1_F3_acn_C.1.fid
1D 13C spectrum
Probe: 5 mm PABBO BB-1H/D Z-GRD Z113652/0192
f1 (ppm)

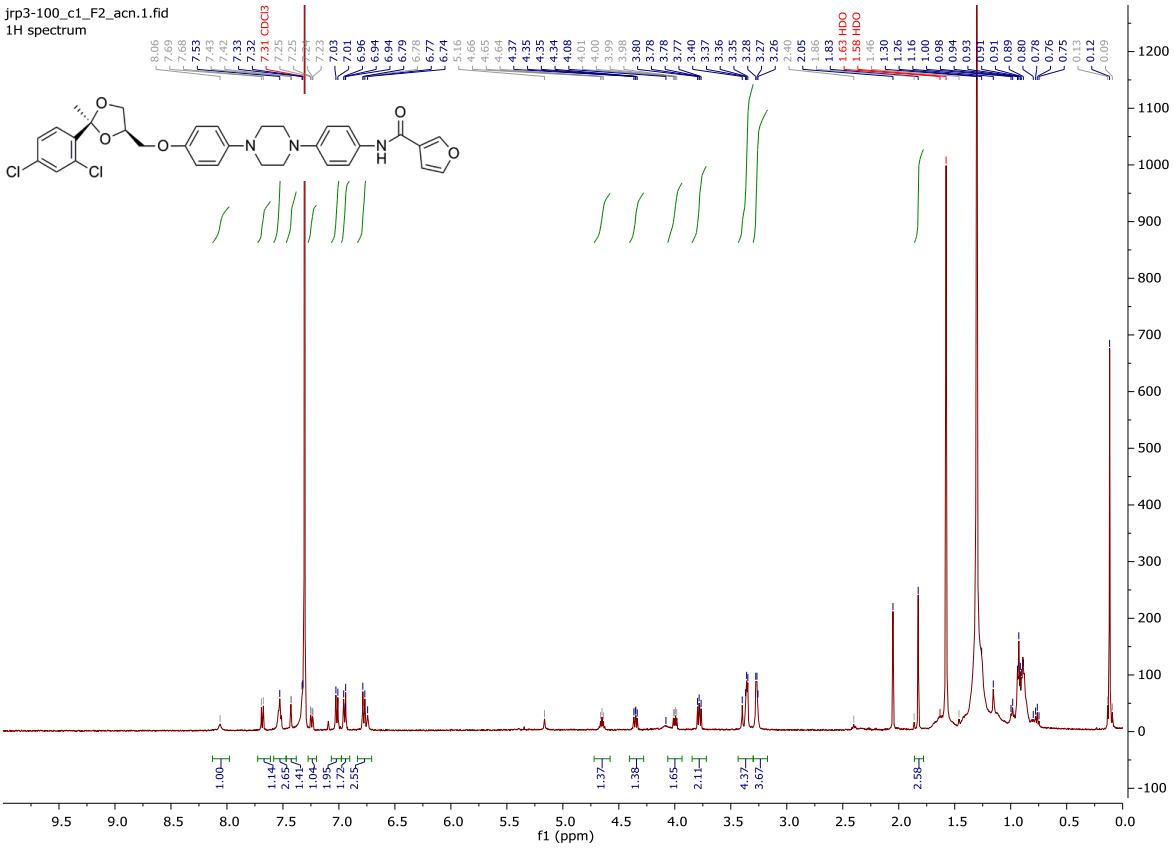
jrp3-100_c1_F2_acn.1.fid
1H spectrum
CDCl3
HDO
HDO
f1 (ppm)

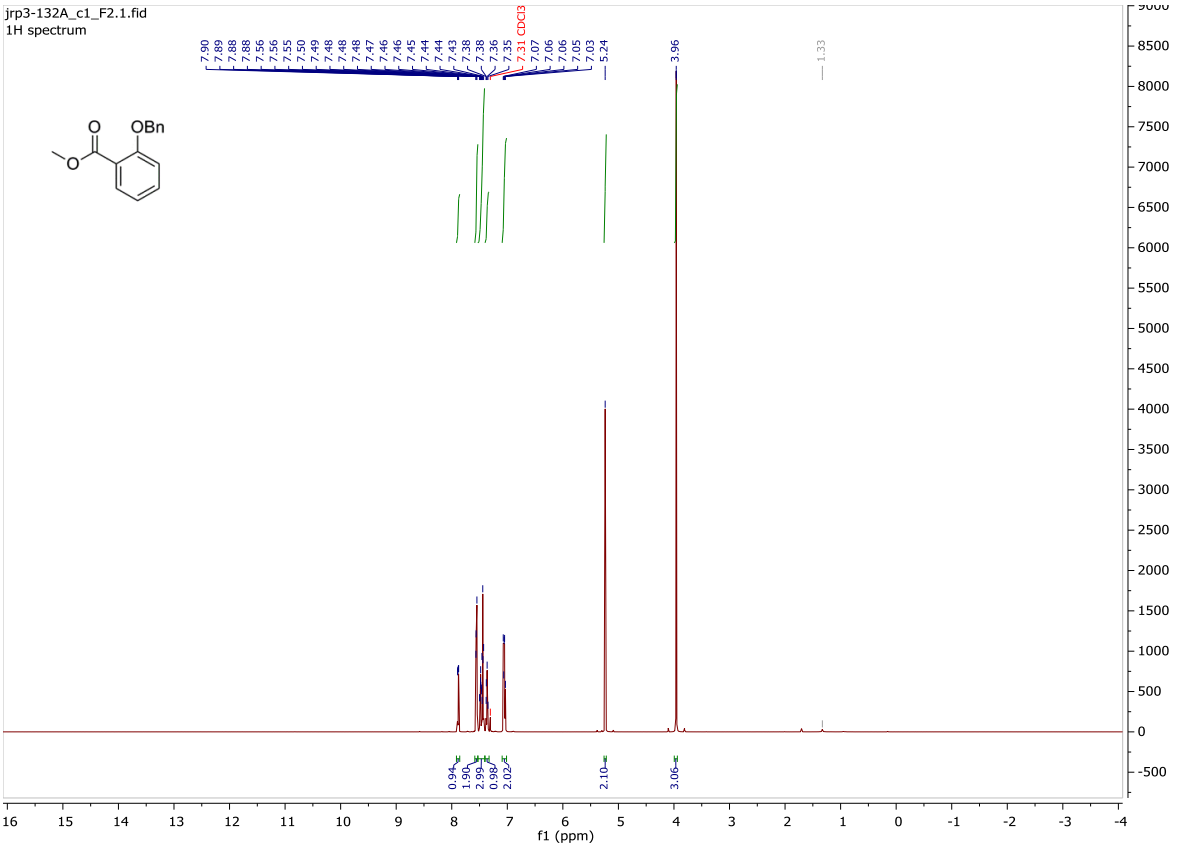
jrp3-132A_c1_F2.1.fid
1H spectrum
O
OBn
f1 (ppm)

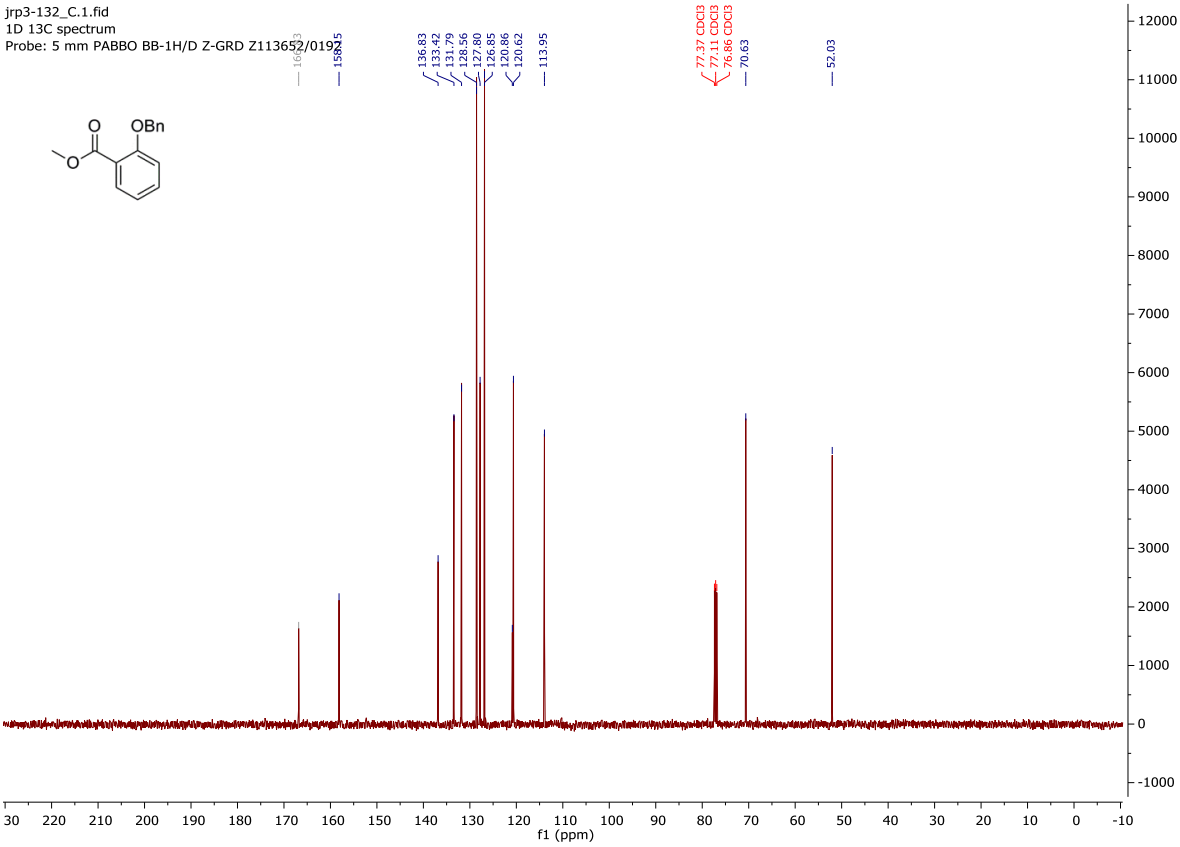
jrp3-132_C.1.fid
1D 13C spectrum
Probe: 5 mm PABBO BB-1H/D Z-GRD Z113652/0191
O
OBn
f1 (ppm)

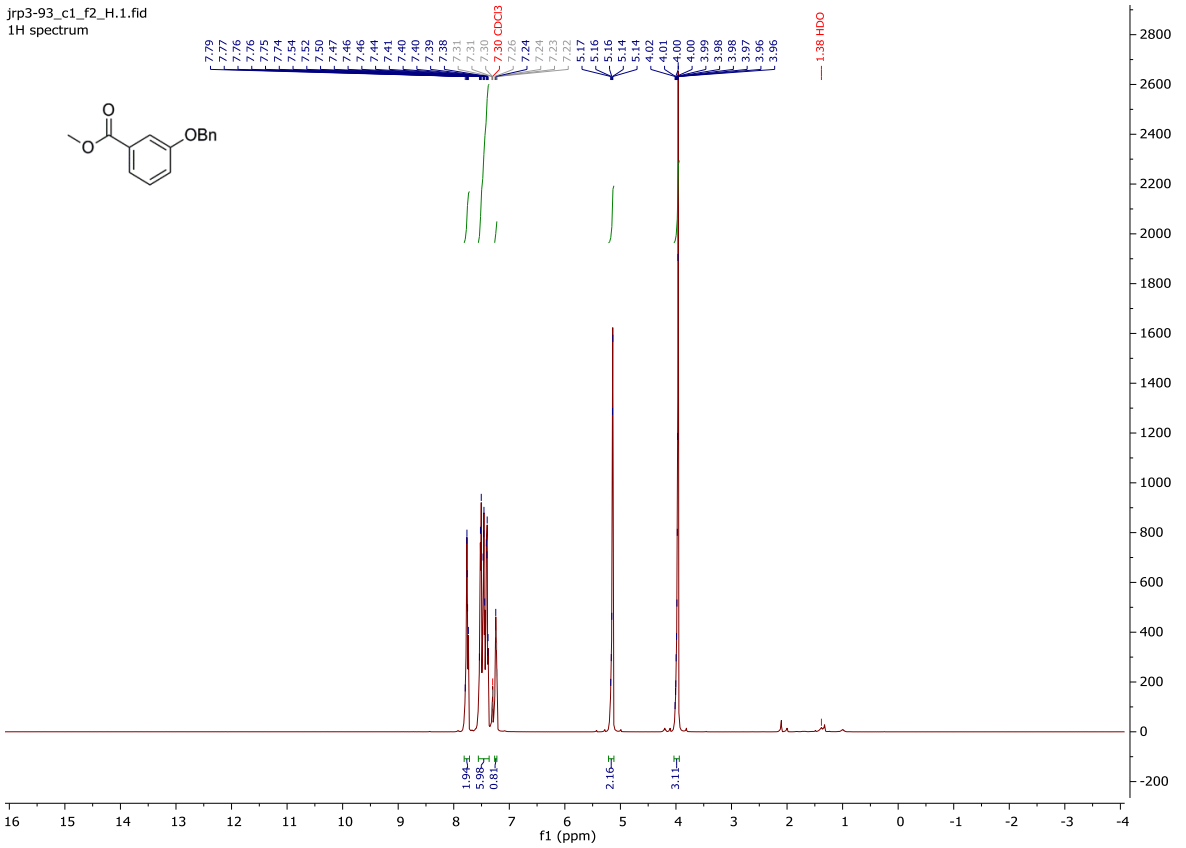
jrp3-93_c1_f2_H.1.fid
1H spectrum
OBn
7.79 7.77 7.76 7.76 7.75 7.74 7.54 7.52 7.50 7.47 7.46 7.46 7.44 7.41 7.40 7.40 7.39 7.38 7.31 7.31 7.30 7.30 CDCl3 7.26 7.24 7.24 7.23 7.22 5.17 5.16 5.16 5.14 5.14 4.02 4.01 4.00 4.00 3.99 3.98 3.98 3.97 3.96 3.96
1.38 HDO
1.94 5.98 0.81 2.16 3.11
f1 (ppm)

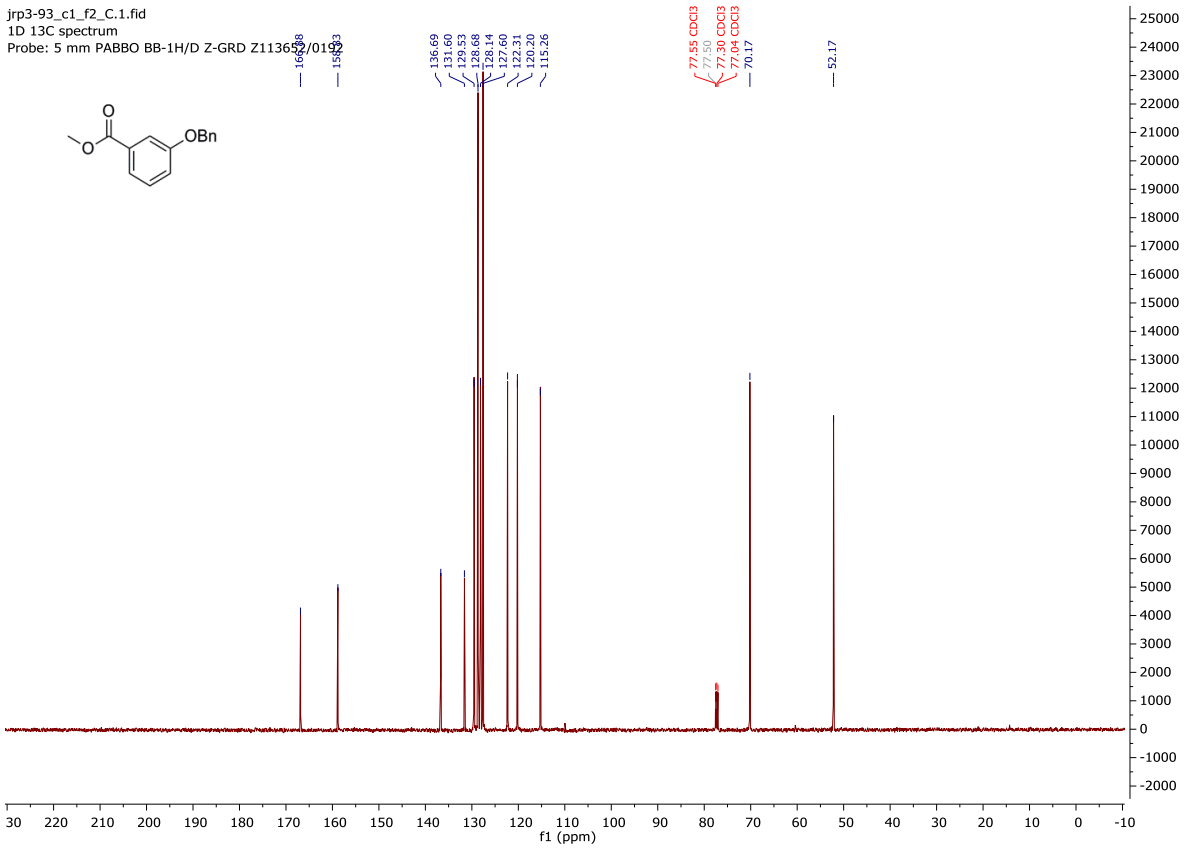
jrp3-93_c1_f2_C.1.fid
1D 13C spectrum
Probe: 5 mm PABBO BB-1H/D Z-GRD Z113682/0193
OBn
136.69 131.60 129.53 128.68 128.14 127.60 122.31 120.20 115.26
77.55 CDCl3 77.30 CDCl3 77.04 CDCl3
70.17
52.17
f1 (ppm)

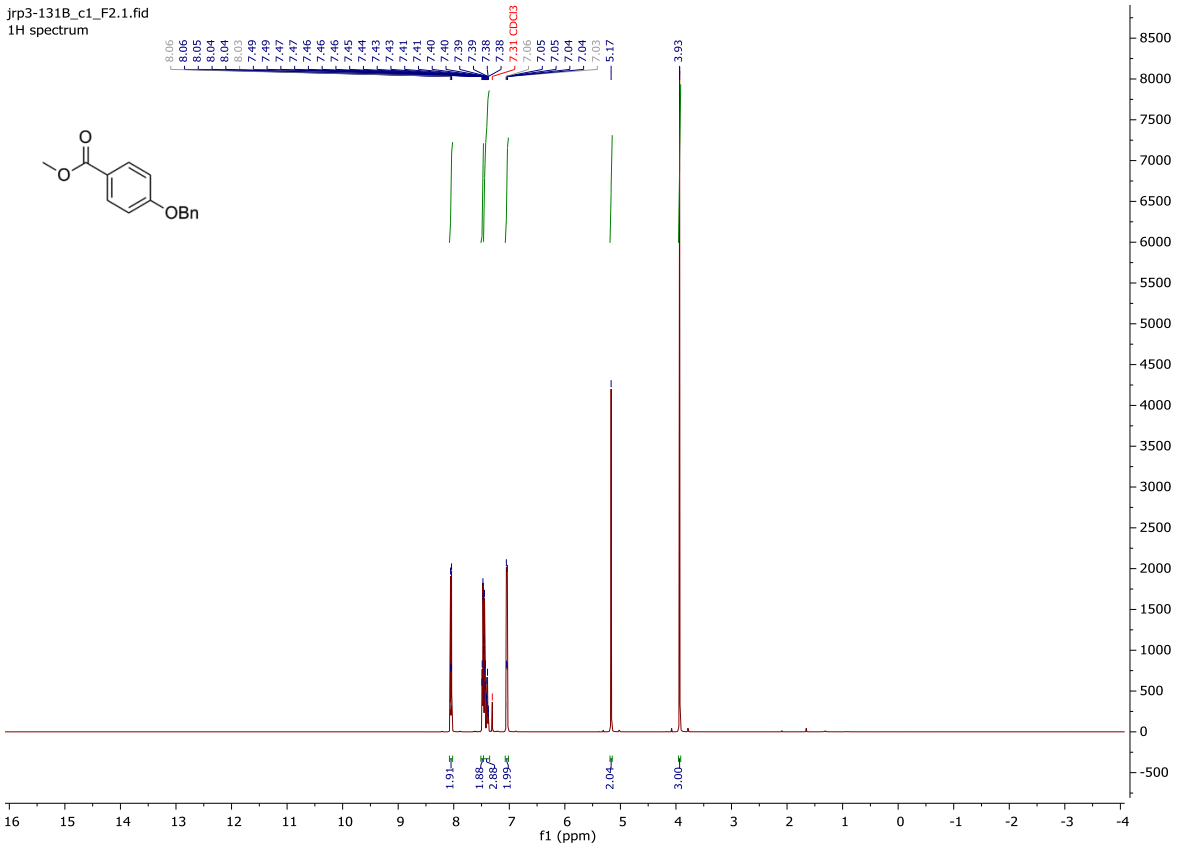
jrp3-131B_c1_F2.1.fid
1H spectrum
8.06
8.06
8.05
8.04
8.04
8.03
7.49
7.49
7.47
7.47
7.46
7.46
7.46
7.45
7.44
7.43
7.43
7.41
7.41
7.40
7.40
7.39
7.39
7.38
7.38
7.31 CDCl3
7.06
7.05
7.05
7.04
7.04
7.03
5.17
3.93
O
O
OBn
1.91
1.88
2.88
1.99
2.04
3.00
f1 (ppm)

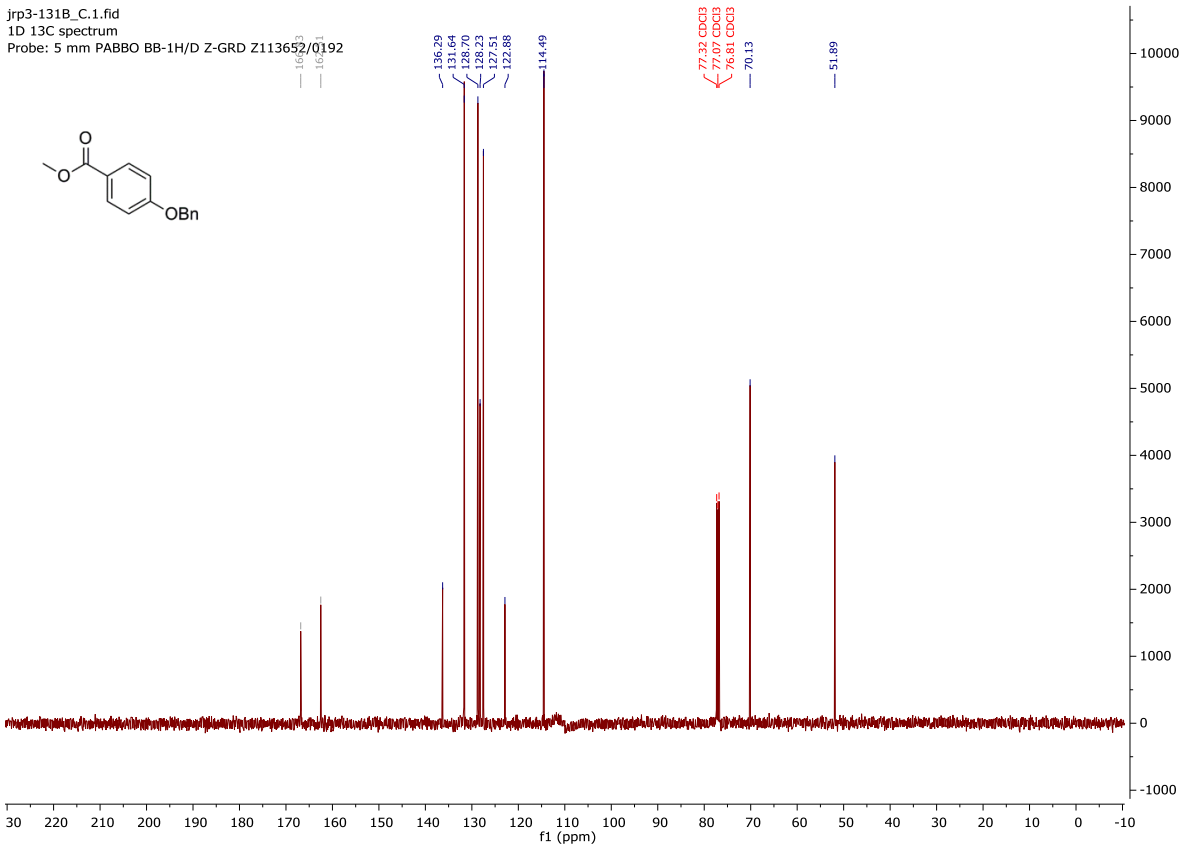
jrp3-131B_C.1.fid
1D 13C spectrum
Probe: 5 mm PABBO BB-1H/D Z-GRD Z113652/0192
136.29
131.64
128.70
128.23
127.51
122.88
114.49
77.32 CDCl3
77.07 CDCl3
76.81 CDCl3
70.13
51.89
O
O
OBn
f1 (ppm)

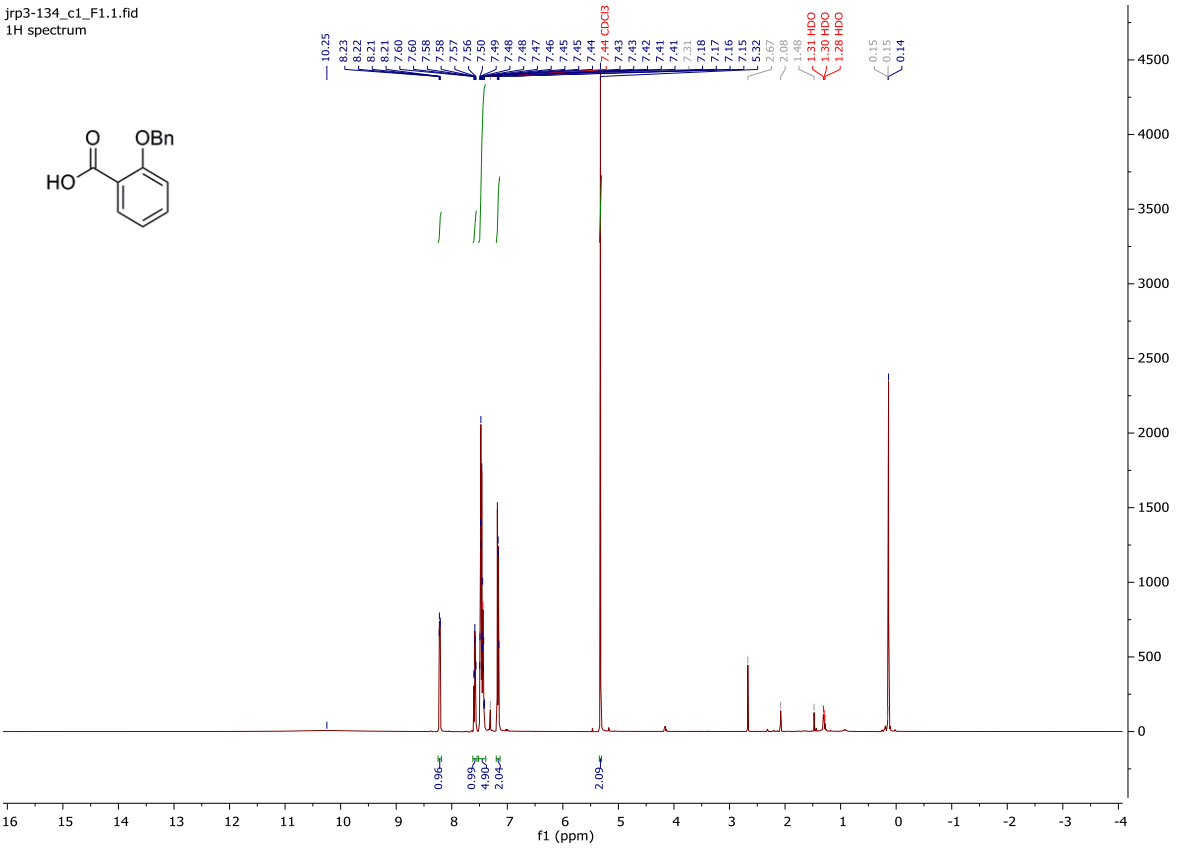
jrp3-134_c1_F1.1.fid
1H spectrum
O
OBn
HO
f1 (ppm)

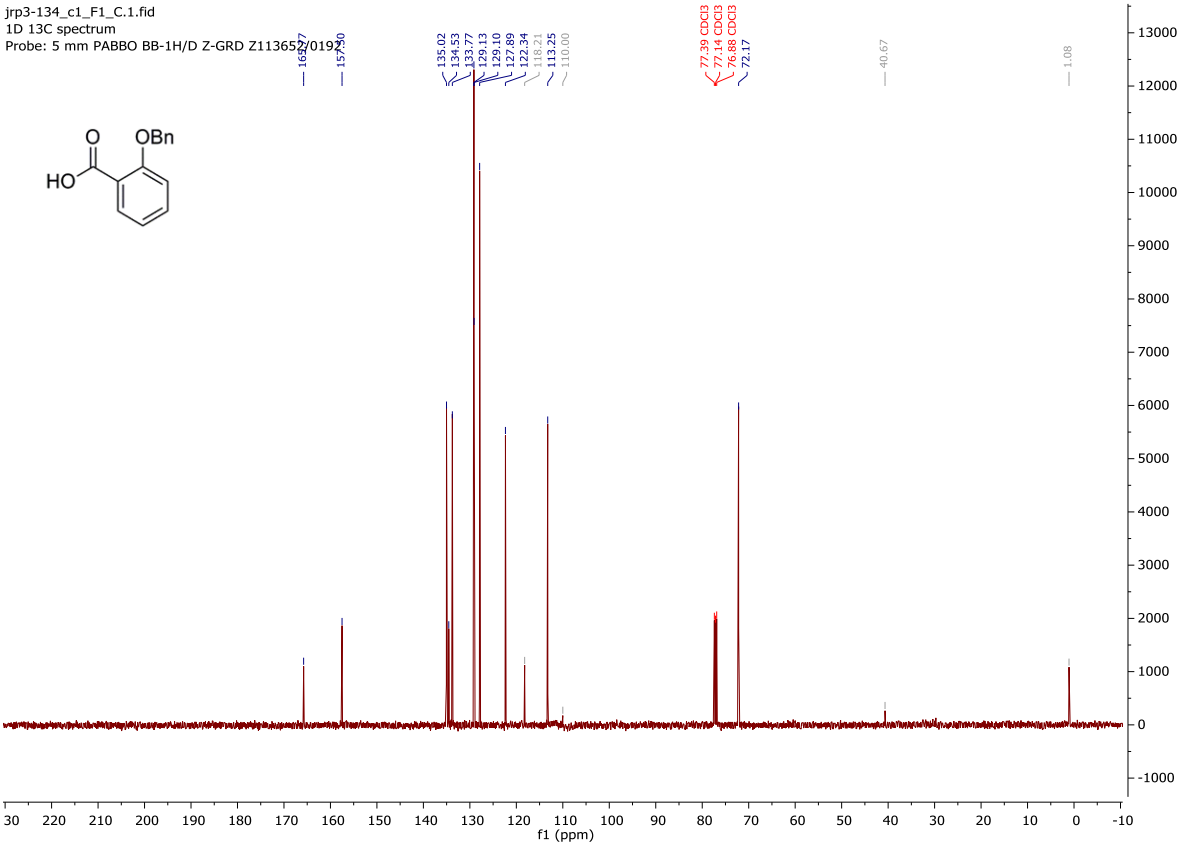
jrp3-134_c1_F1_C.1.fid
1D 13C spectrum
Probe: 5 mm PABBO BB-1H/D Z-GRD Z113652/0197
O
OBn
HO
f1 (ppm)

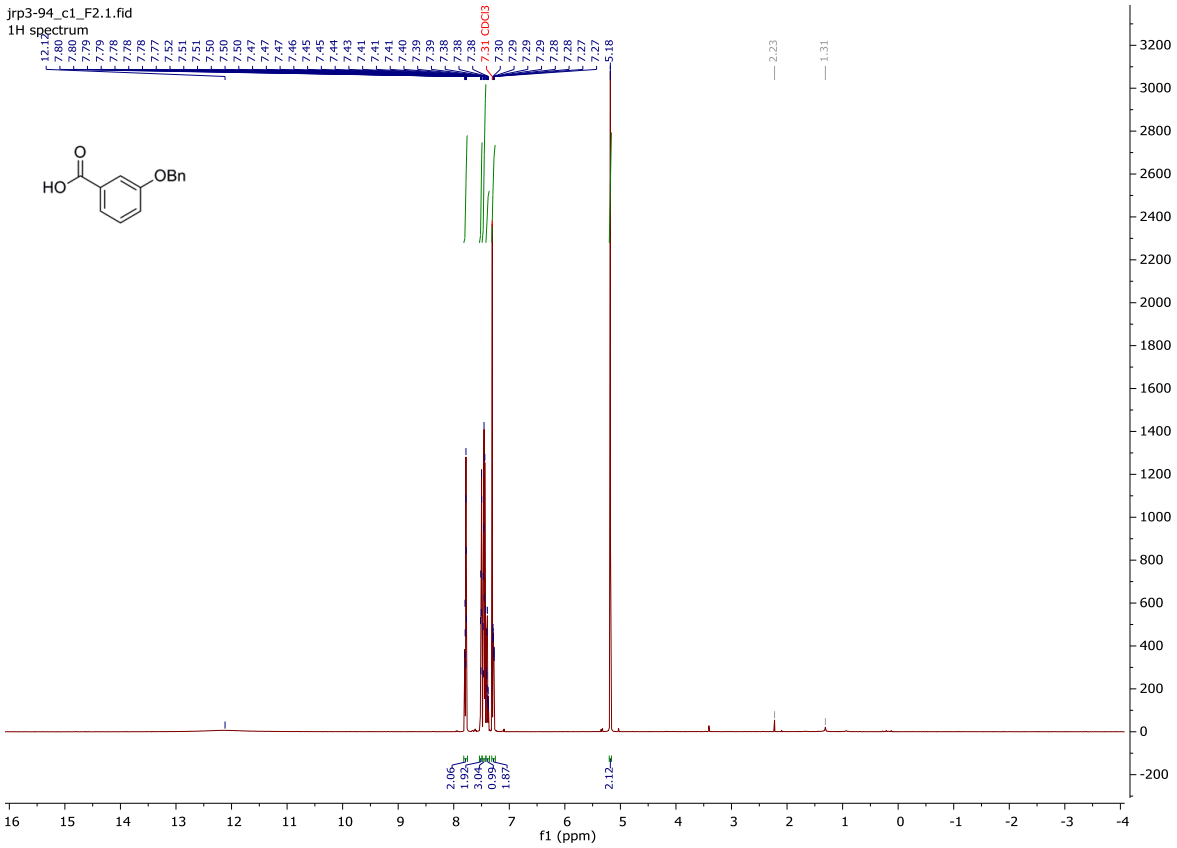
jrp3-94_c1_F2.1.fid
1H spectrum
CDCl3
HO
OBn
f1 (ppm)

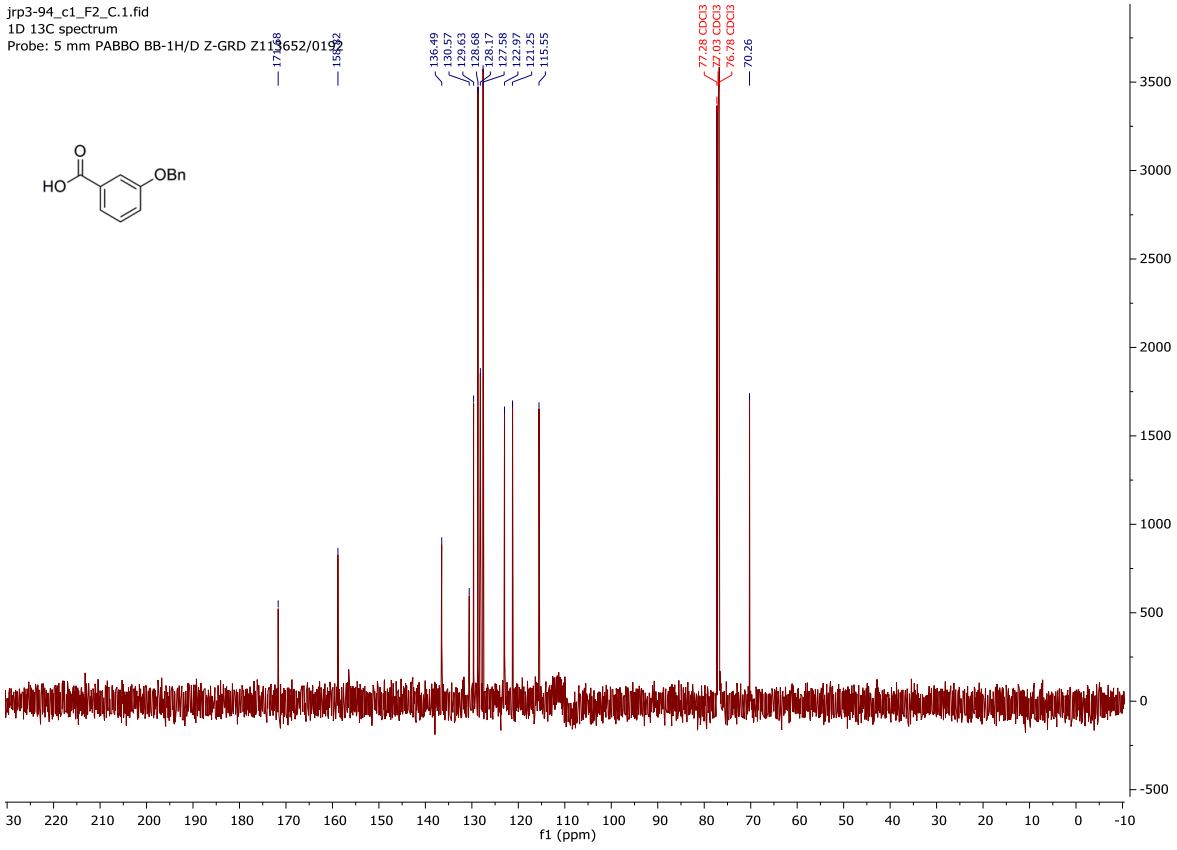
jrp3-94_c1_F2_C.1.fid
1D 13C spectrum
Probe: 5 mm PABBO BB-1H/D Z-GRD Z113652/0193
77.28 CDCl3
77.03 CDCl3
76.78 CDCl3
HO
OBn
f1 (ppm)

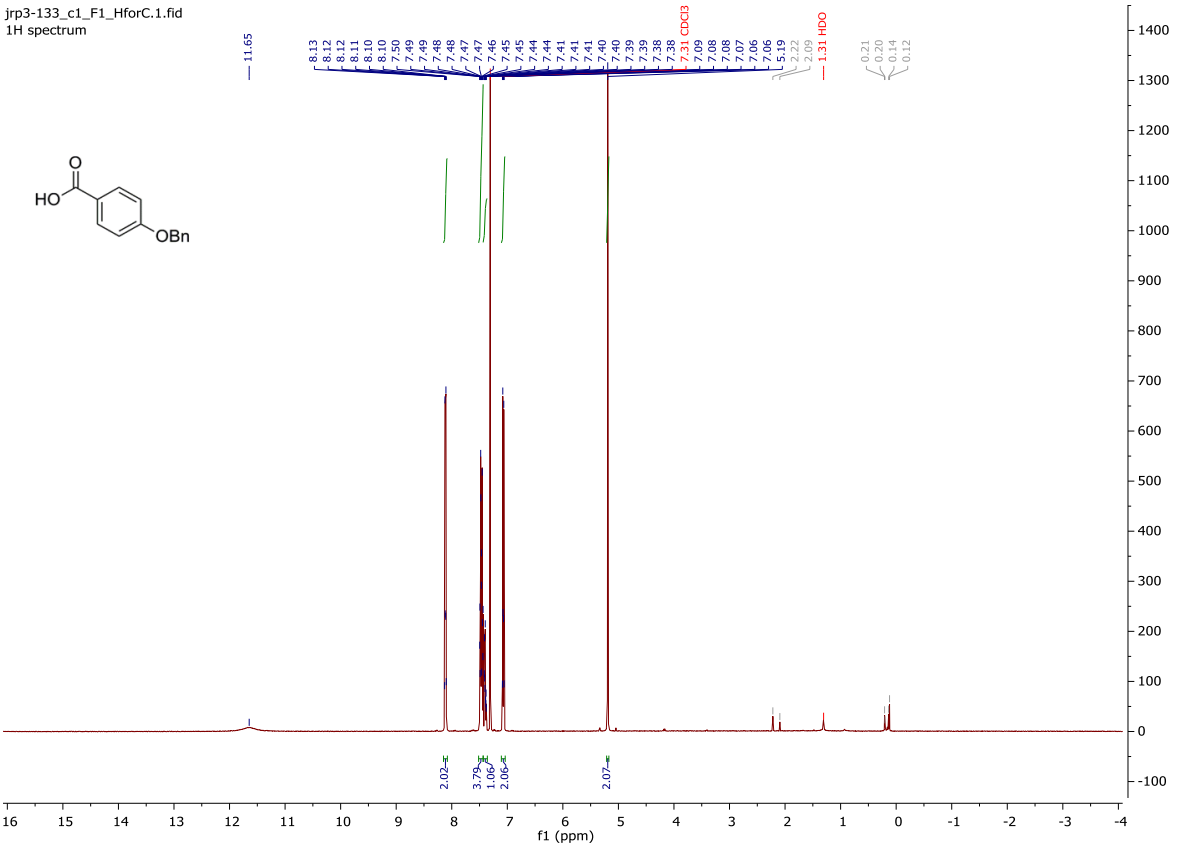
jrp3-133_c1_F1_HforC.1.fid
1H spectrum
11.65
8.13
8.12
8.12
8.11
8.10
8.10
7.50
7.49
7.49
7.48
7.48
7.47
7.47
7.46
7.45
7.45
7.44
7.44
7.41
7.41
7.41
7.40
7.40
7.39
7.39
7.38
7.38
7.31 CDCl3
7.09
7.08
7.08
7.07
7.06
7.06
5.19
2.22
2.09
1.31 HDO
0.21
0.20
0.14
0.12
HO
O
OBn
2.02
3.79
1.06
2.06
2.07
f1 (ppm)

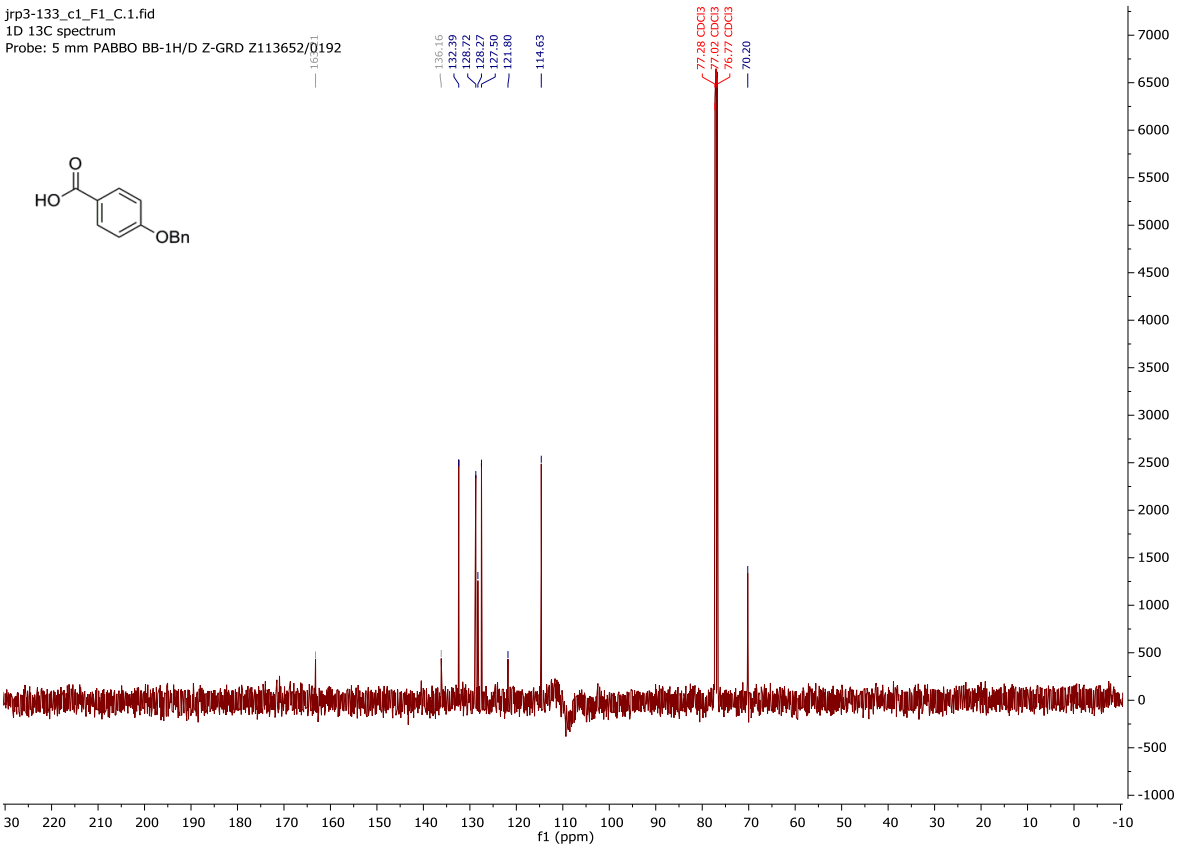
jrp3-133_c1_F1_C.1.fid
1D 13C spectrum
Probe: 5 mm PABBO BB-1H/D Z-GRD Z113652/0192
136.16
132.39
128.72
128.27
127.50
121.80
114.63
77.28 CDCl3
77.02 CDCl3
76.77 CDCl3
70.20
HO
O
OBn
f1 (ppm)

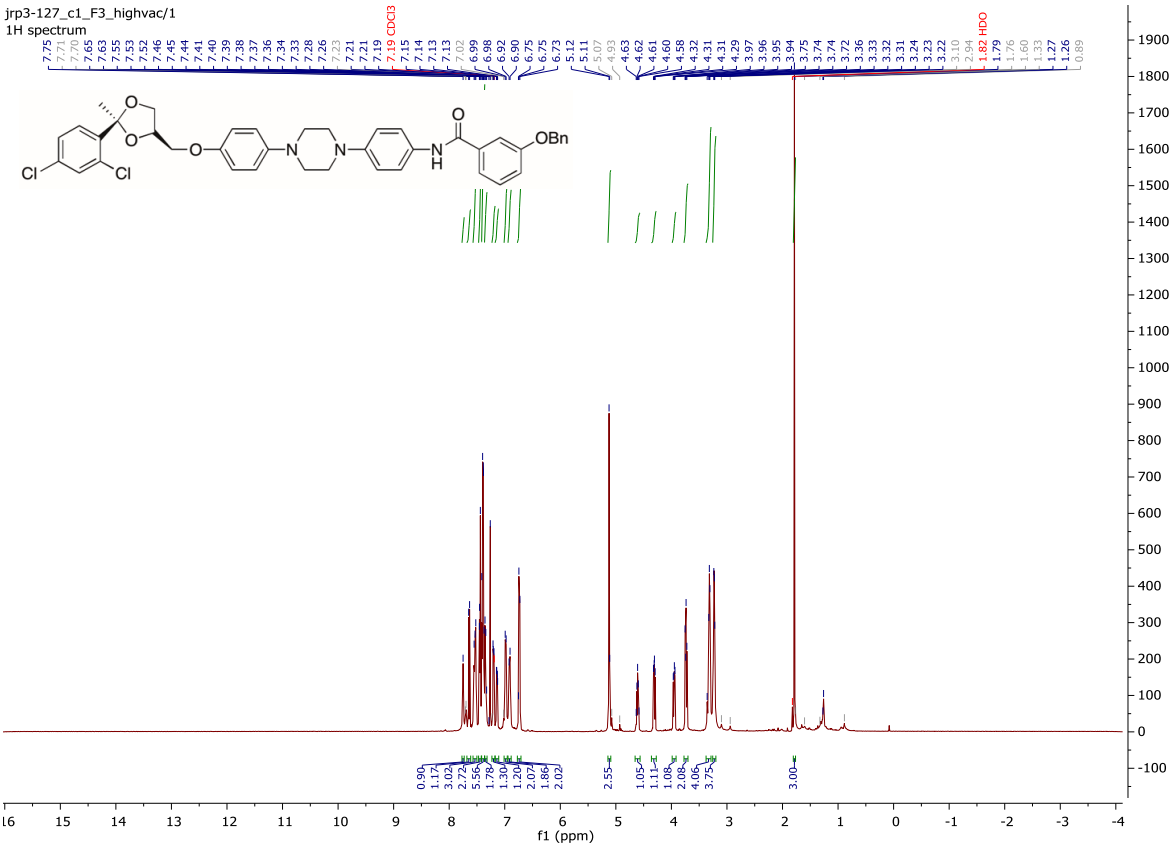
jrp3-127_c1_F3_highvac/1
1H spectrum
f1 (ppm)

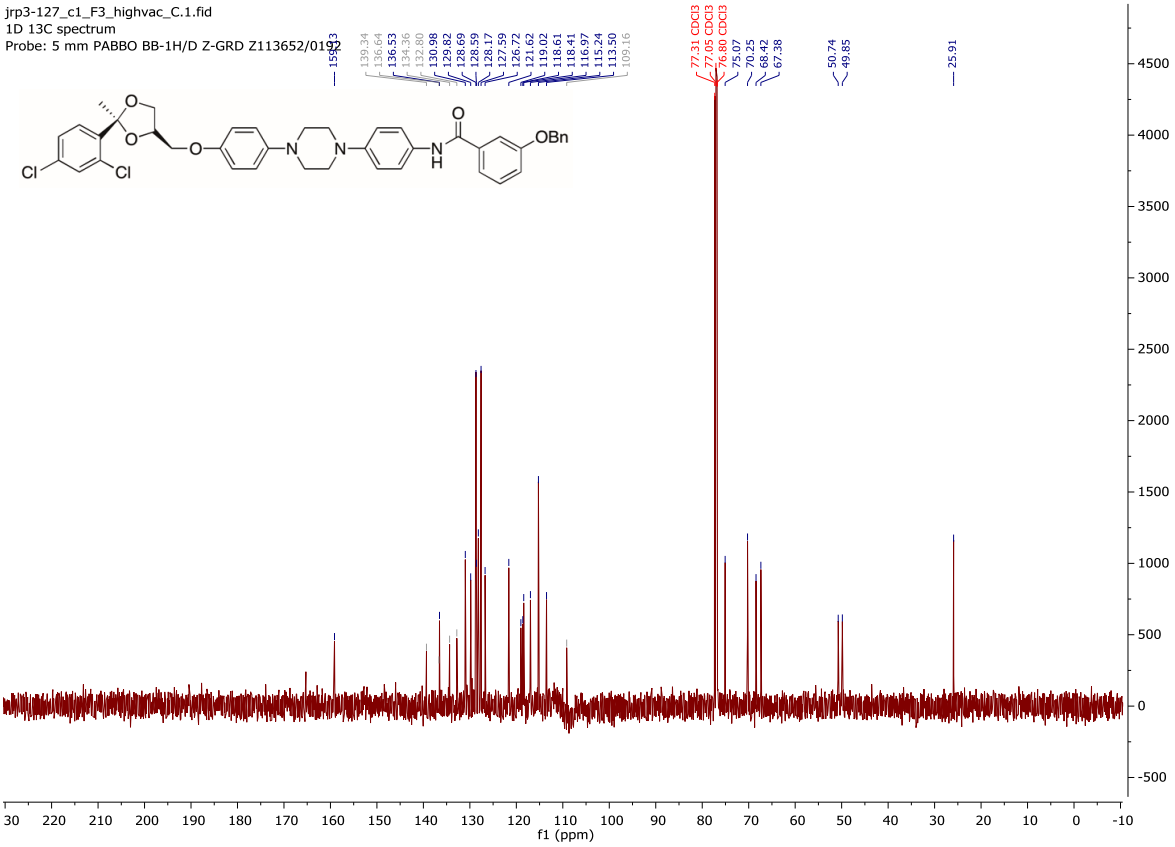
jrp3-127_c1_F3_highvac_C.1.fid
1D 13C spectrum
Probe: 5 mm PABBO BB-1H/D Z-GRD Z113652/0193
f1 (ppm)

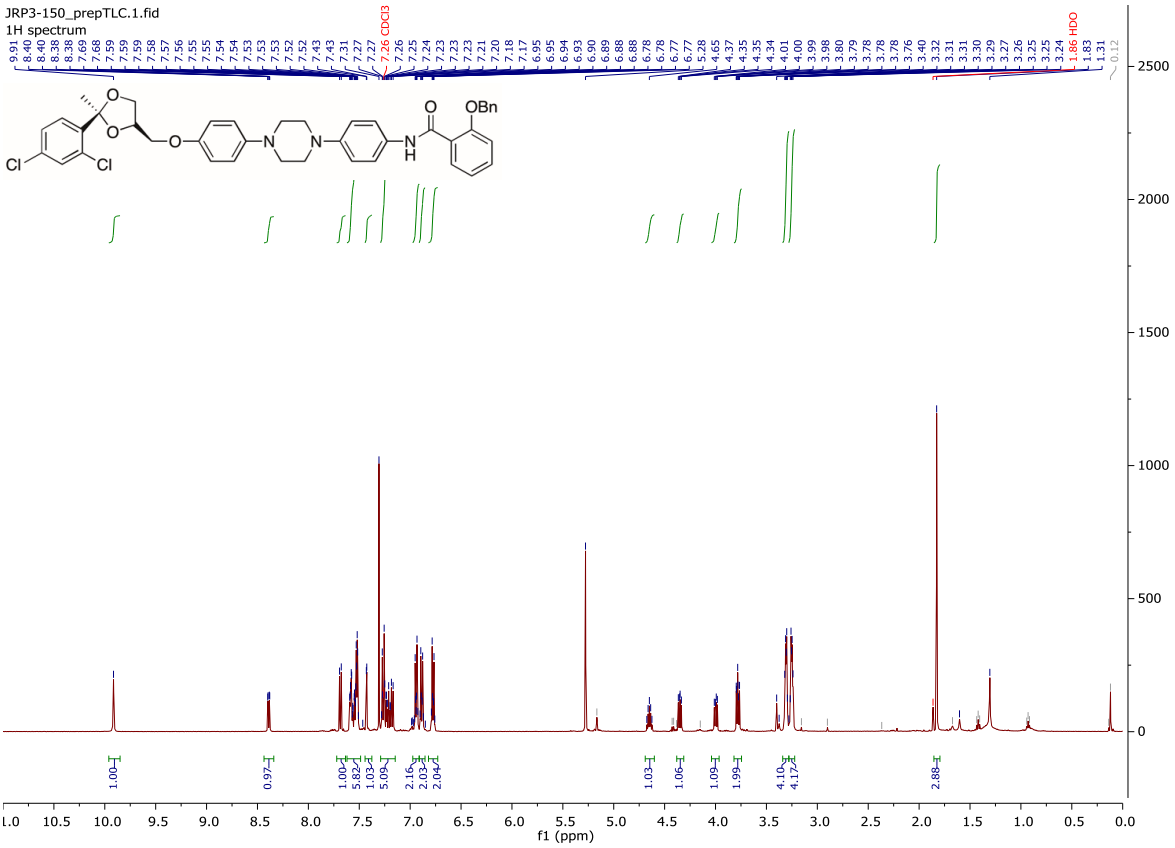
JRP3-150_prepTLC.1.fid
1H spectrum
f1 (ppm)

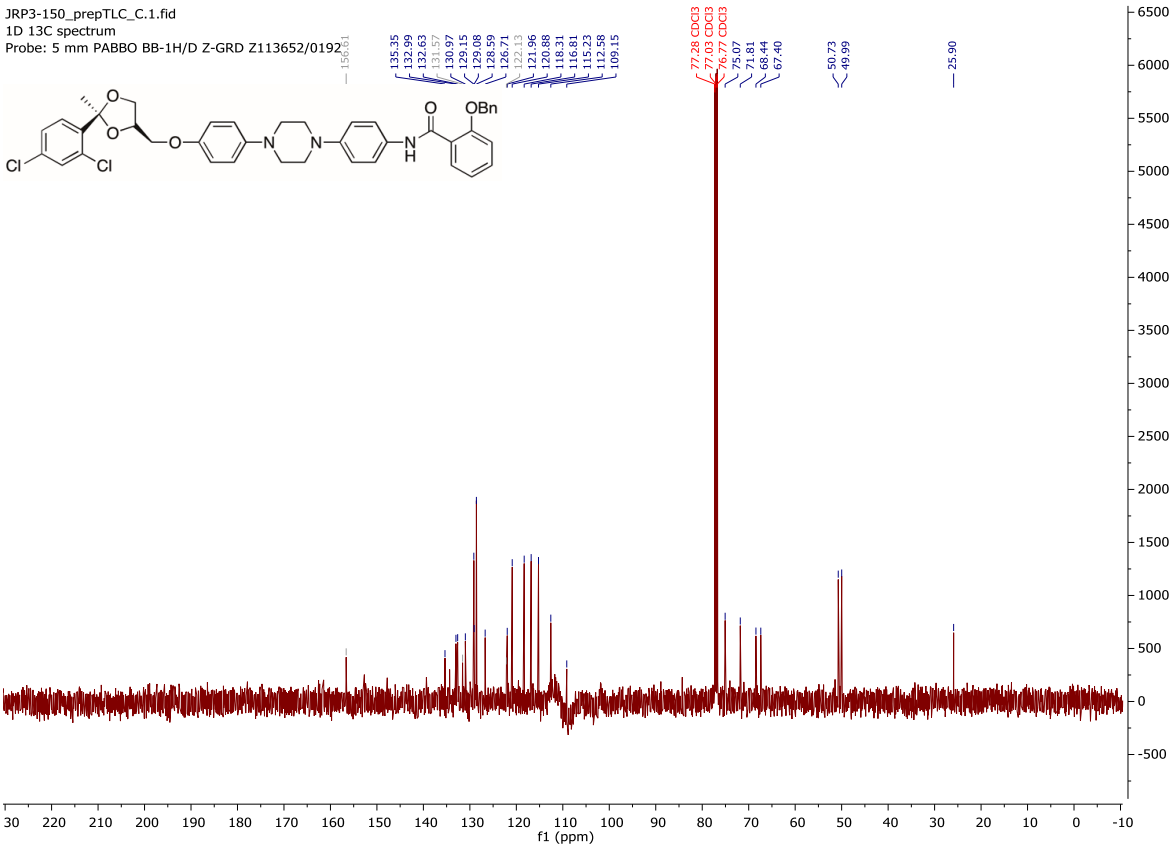
JRP3-150_prepTLC_C.1.fid
1D 13C spectrum
Probe: 5 mm PABBO BB-1H/D Z-GRD Z113652/0192
f1 (ppm)

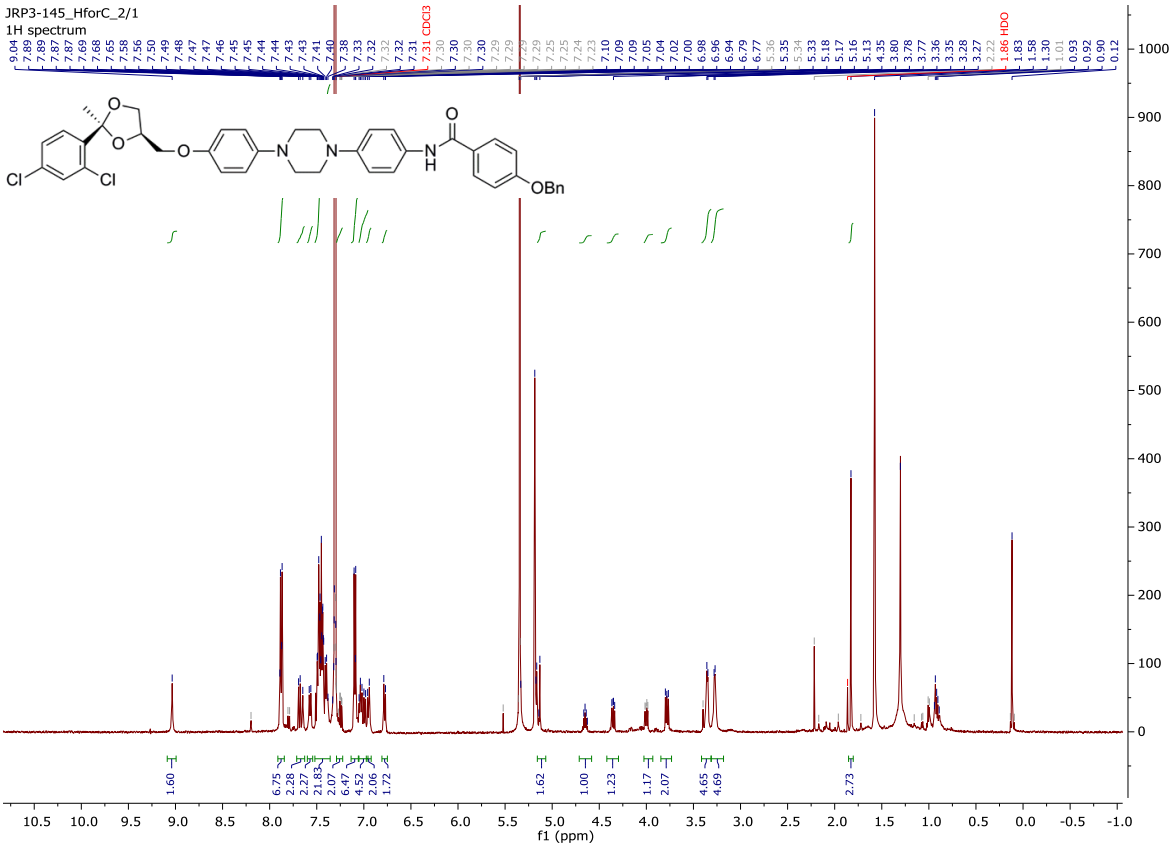
JRP3-145_HforC_2/1
1H spectrum
CDCl3
HDO
Cl
Cl
O
O
O
N
N
H
O
OBn
1.60
6.75
2.28
2.27
21.83
2.07
6.47
4.52
2.06
1.72
1.62
1.00
1.23
1.17
2.07
4.65
4.69
2.73
f1 (ppm)

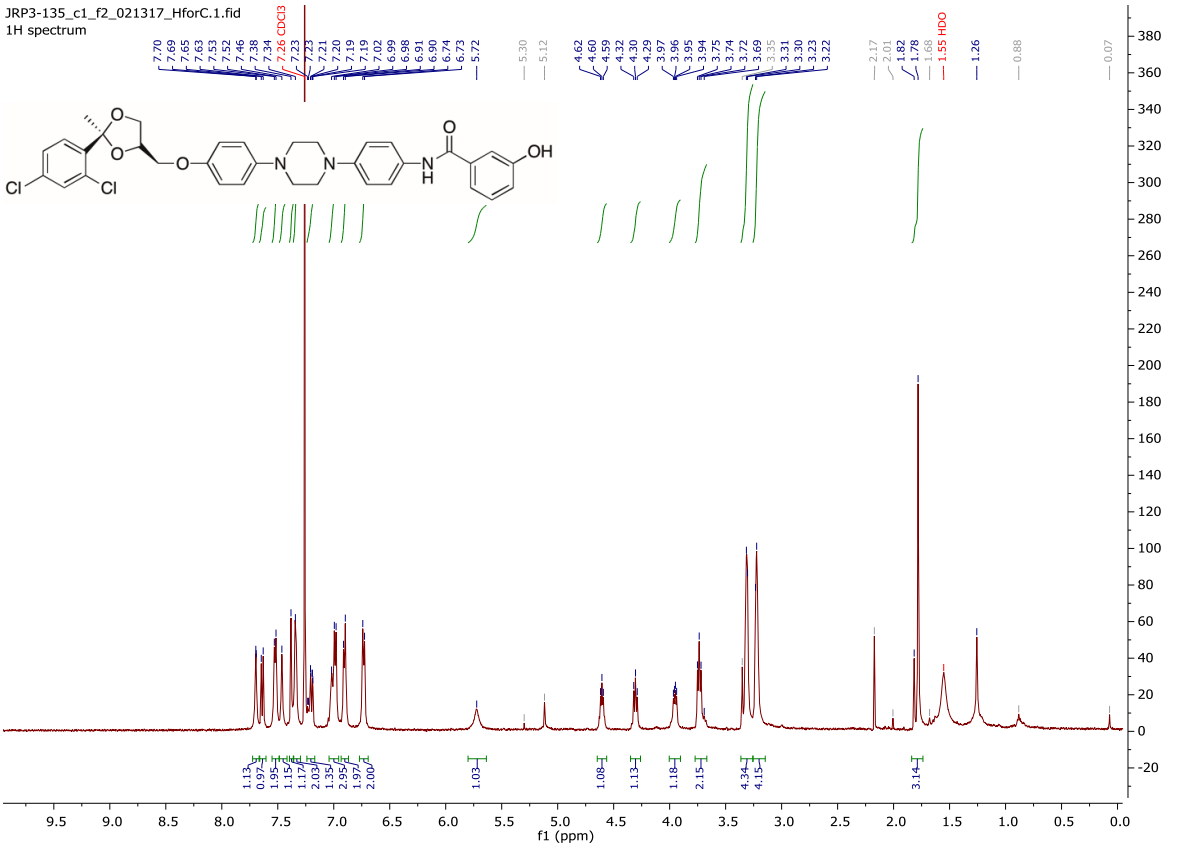
JRP3-135_c1_f2_021317_HforC.1.fid
1H spectrum
f1 (ppm)

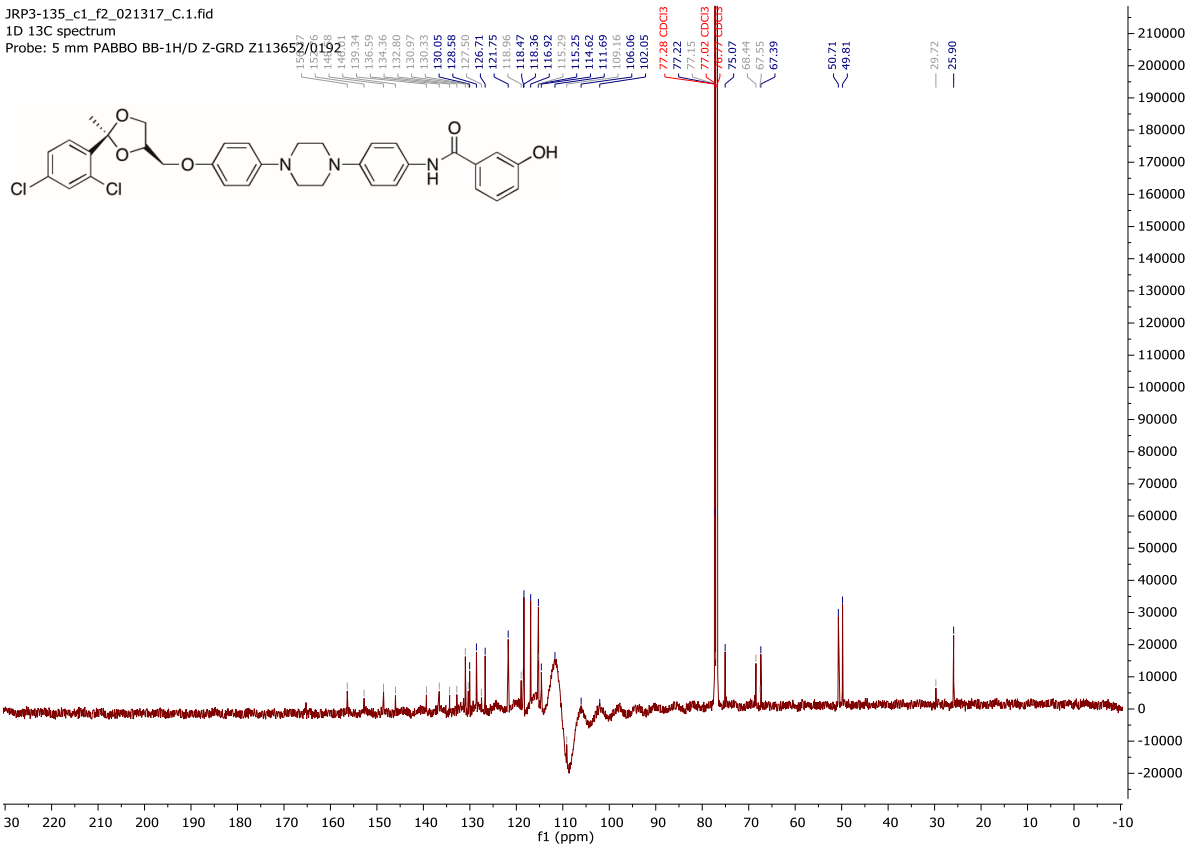
JRP3-135_c1_f2_021317_C.1.fid
1D 13C spectrum
Probe: 5 mm PABBO BB-1H/D Z-GRD Z113652/0192
f1 (ppm)

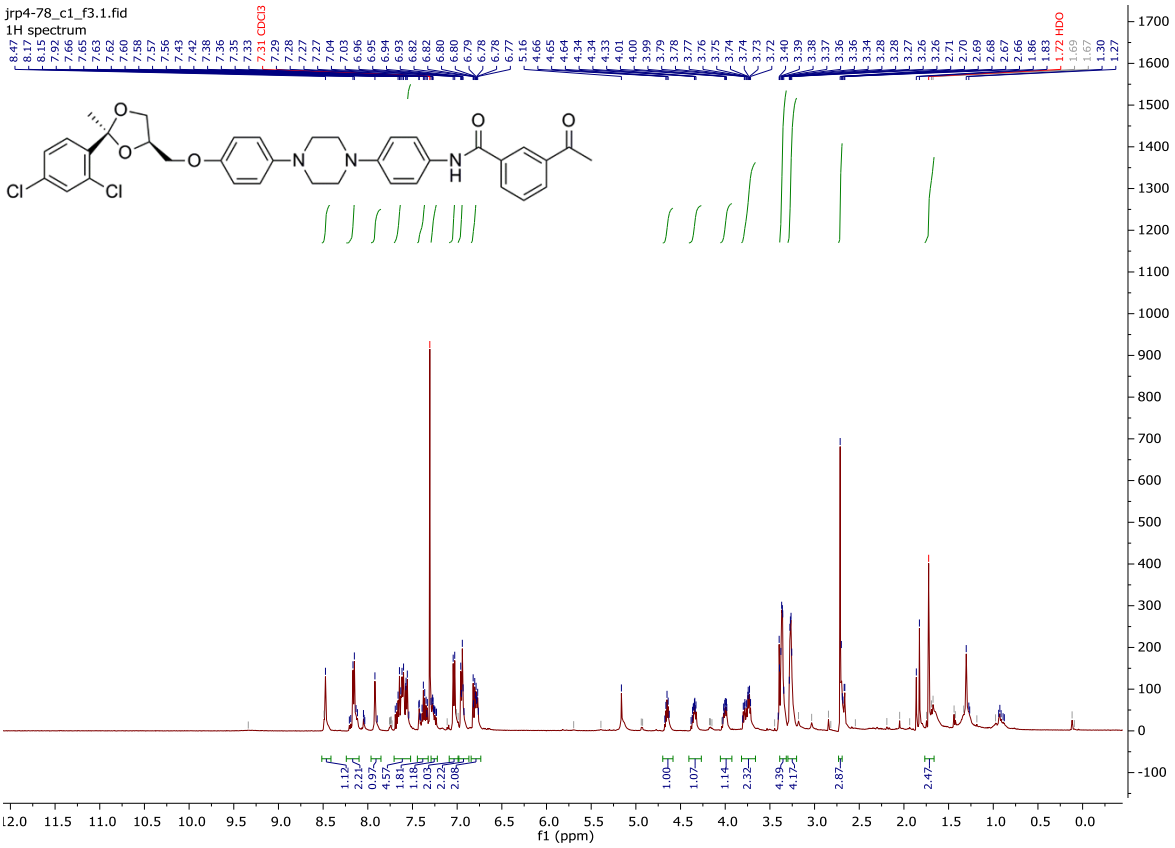
jrp4-78_c1_f3.1.fid
1H spectrum
f1 (ppm)

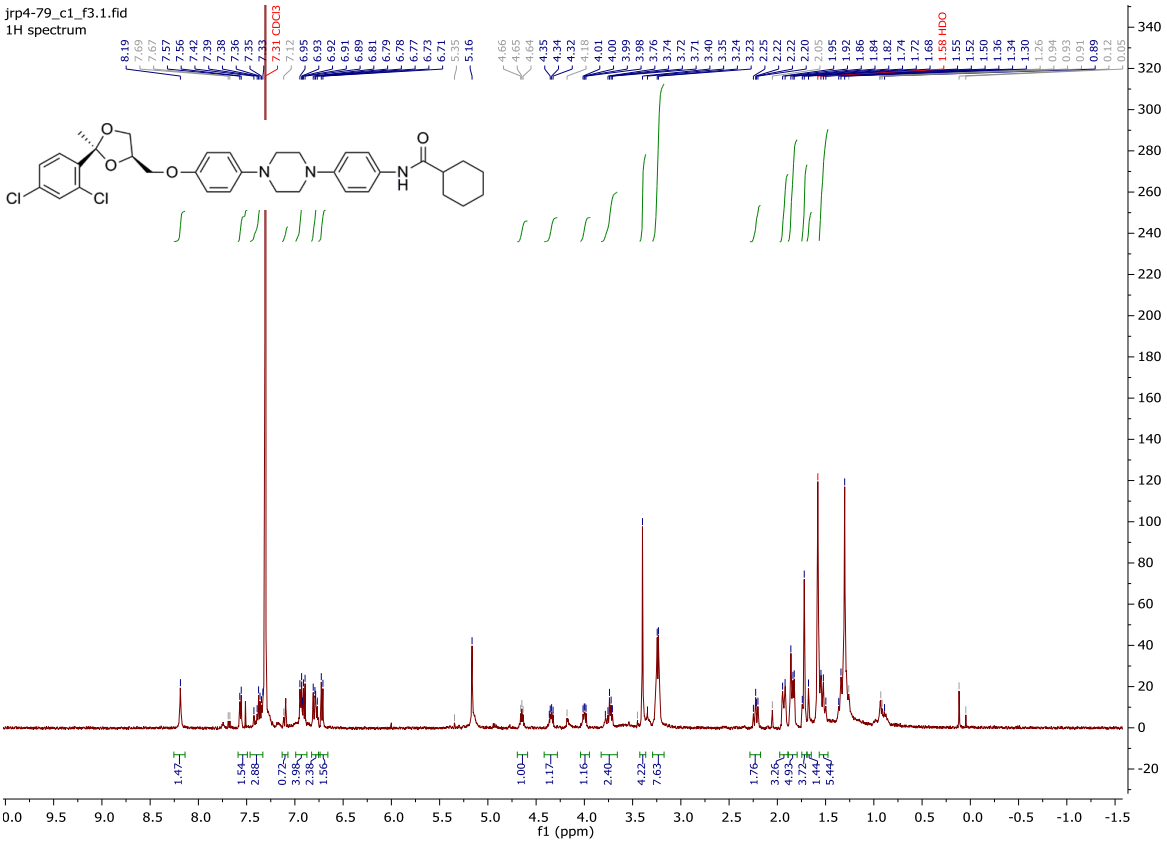
jrp4-79_c1_f3.1.fid
1H spectrum
f1 (ppm)

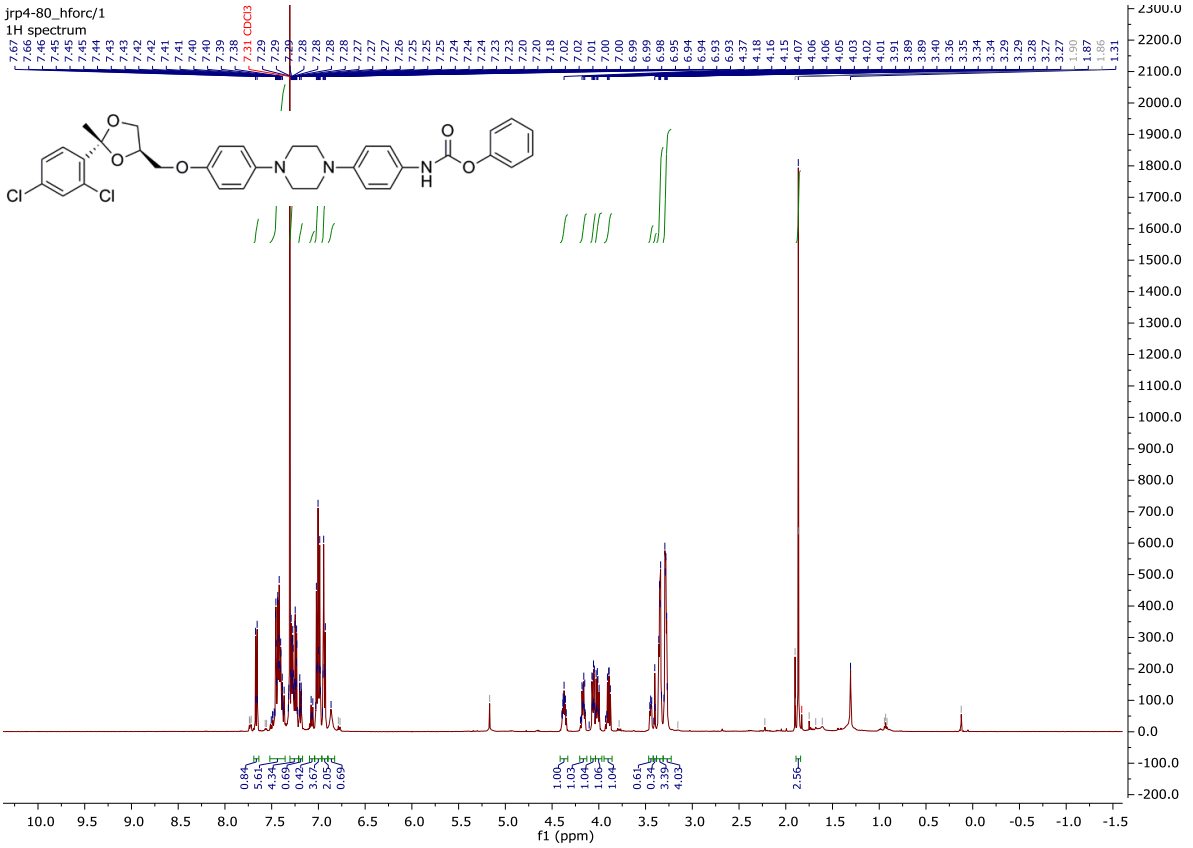
jrp4-80_hforc/1
1H spectrum
f1 (ppm)

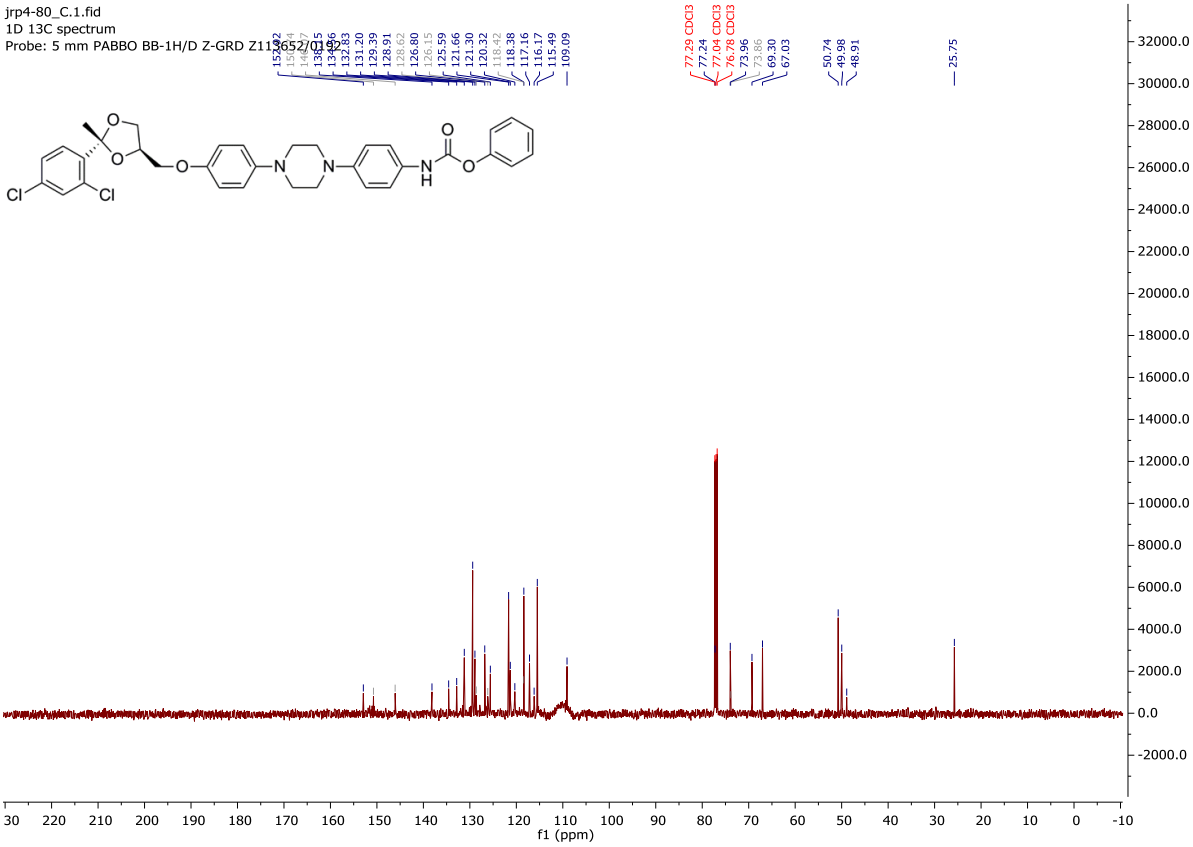
jrp4-80_C.1.fid
1D 13C spectrum
Probe: 5 mm PABBO BB-1H/D Z-GRD Z113652/0419
f1 (ppm)

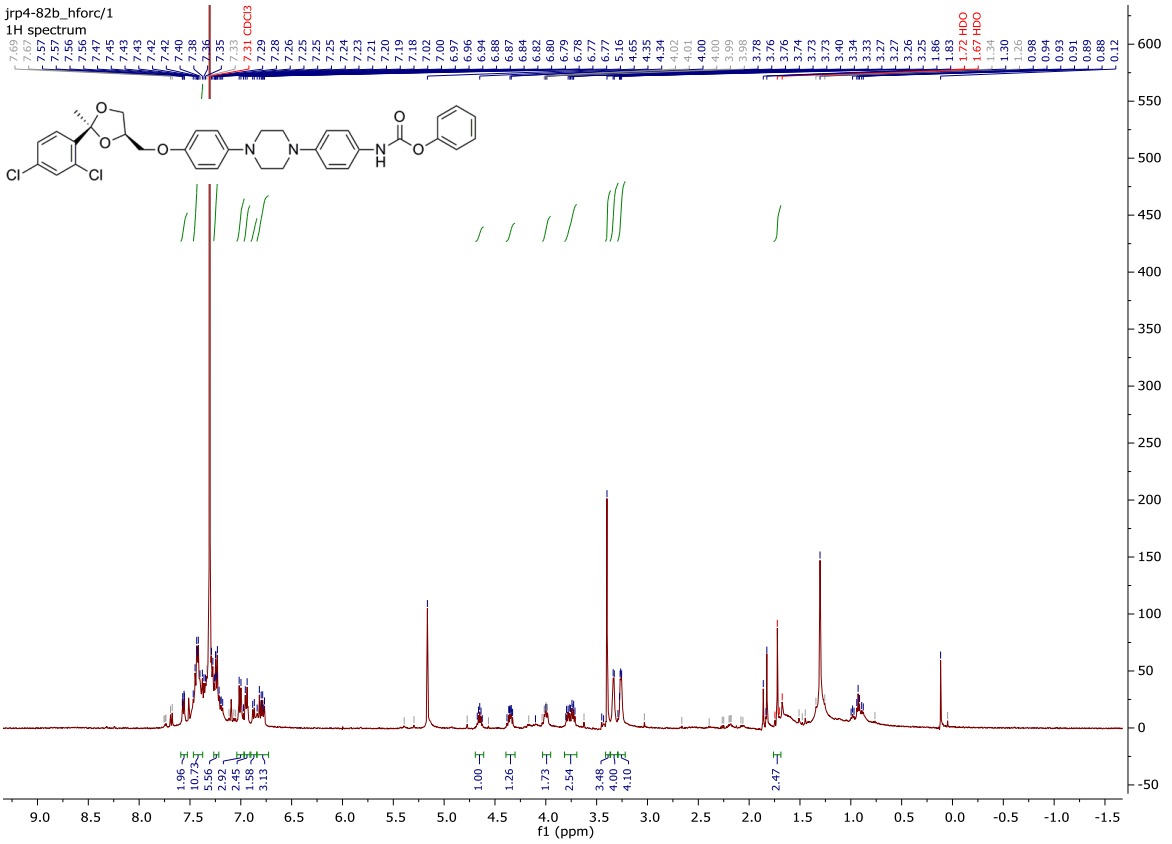
jrp4-82b_hforc/1
1H spectrum
CDCl3
1.72 HDO
1.67 HDO
f1 (ppm)

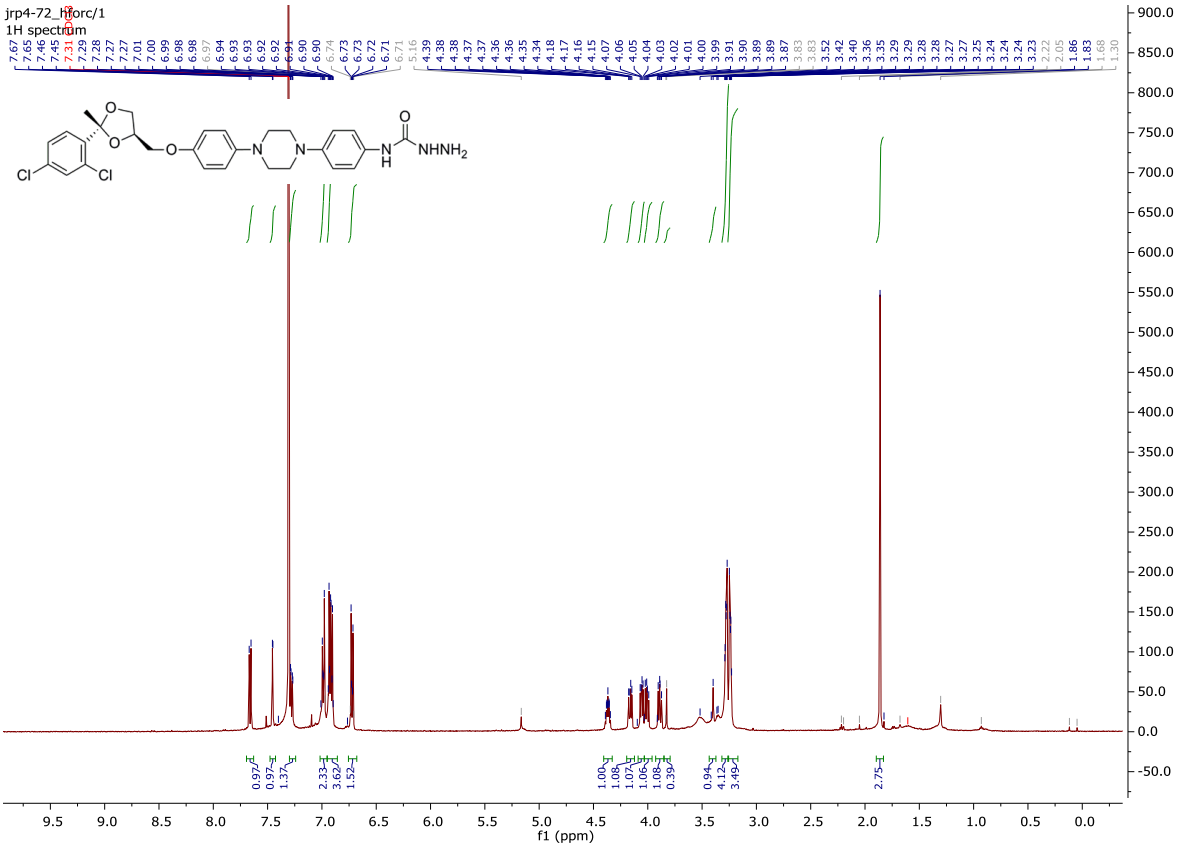
jrp4-72_hforc/1
1H spectrum
f1 (ppm)

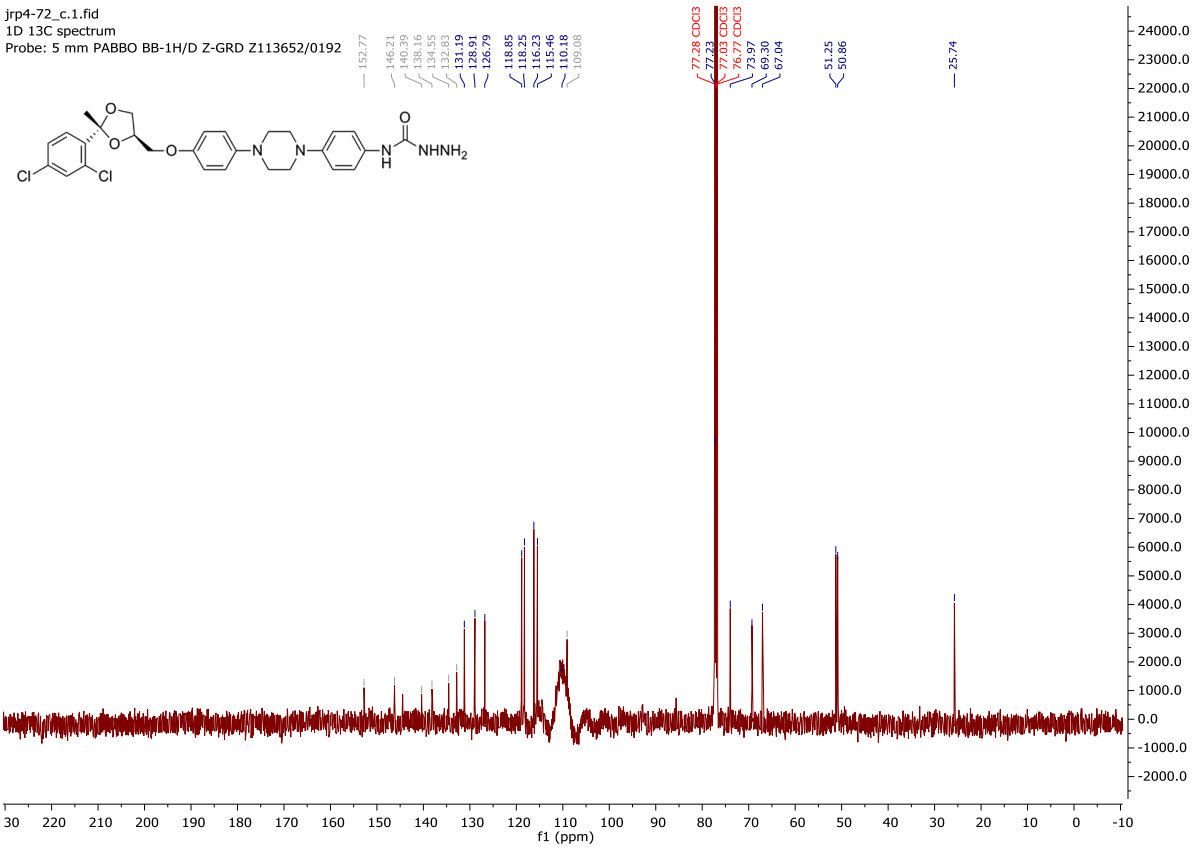
jrp4-72_c.1.fid
1D 13C spectrum
Probe: 5 mm PABBO BB-1H/D Z-GRD Z113652/0192
f1 (ppm)

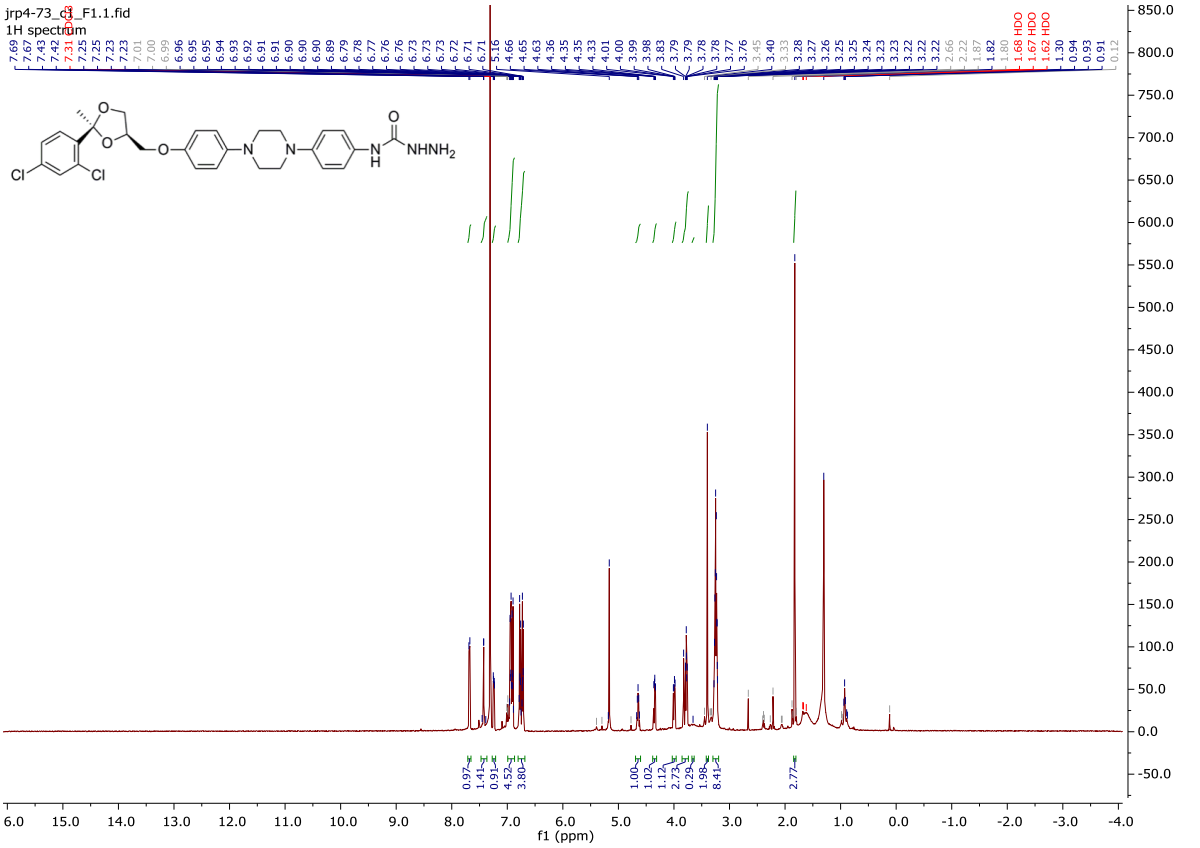
jrp4-73_c1_F1.1.fid
1H spectrum
f1 (ppm)

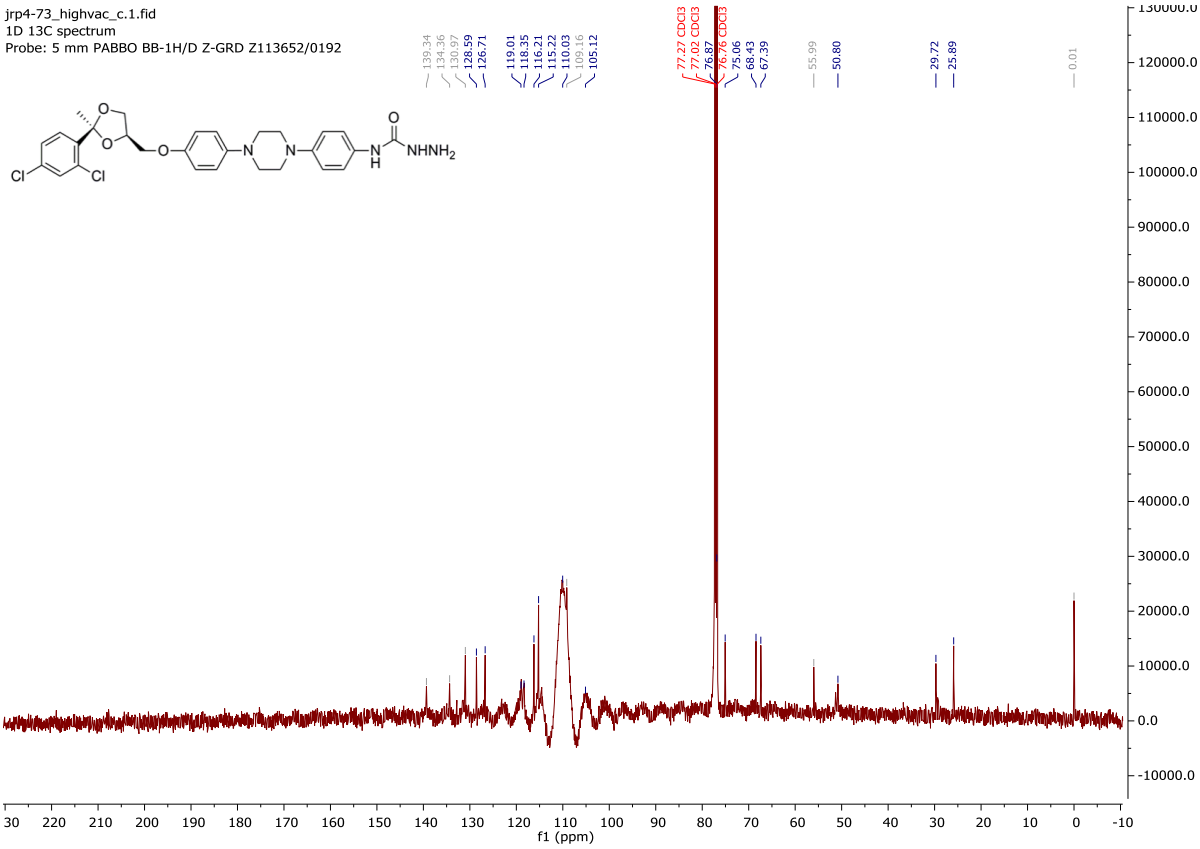
jrp4-73_highvac_c.1.fid
1D 13C spectrum
Probe: 5 mm PABBO BB-1H/D Z-GRD Z113652/0192
f1 (ppm)

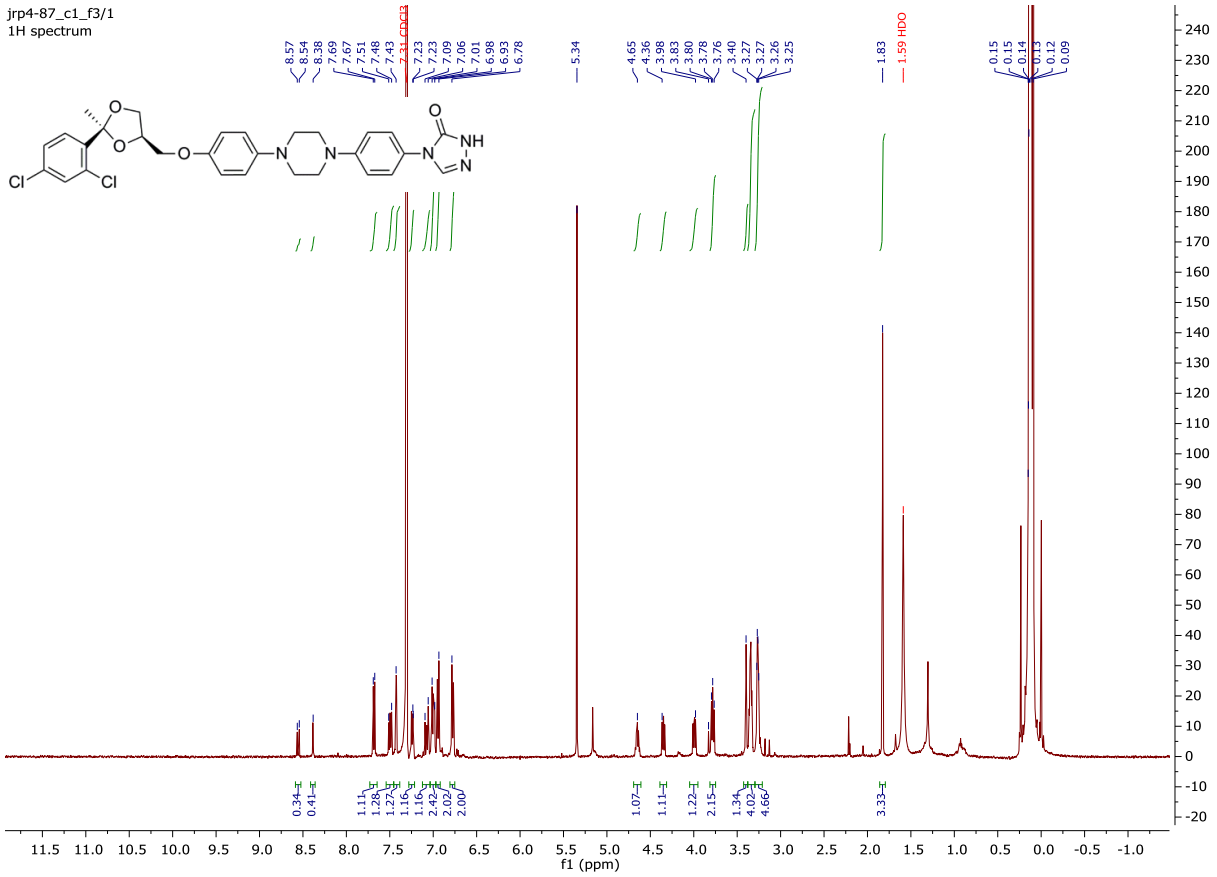
jrp4-87_c1_f3/1
1H spectrum
f1 (ppm)

APPENDIX B: Selected ITZ Liposome Data

Encapsulation Efficiency

ITZ Standard Curve + Raw Data (254 nm)

µg/mL	250	200	150	100	50	25	20	10	5
1	0.944	0.922	0.71	0.51	0.318	0.203	0.174	0.157	0.118
2	0.986	1.067	0.79	0.515	0.327	0.199	0.186	0.14	0.116
3	0.989	1.047	0.83	0.567	0.324	0.215	0.193	0.143	0.12

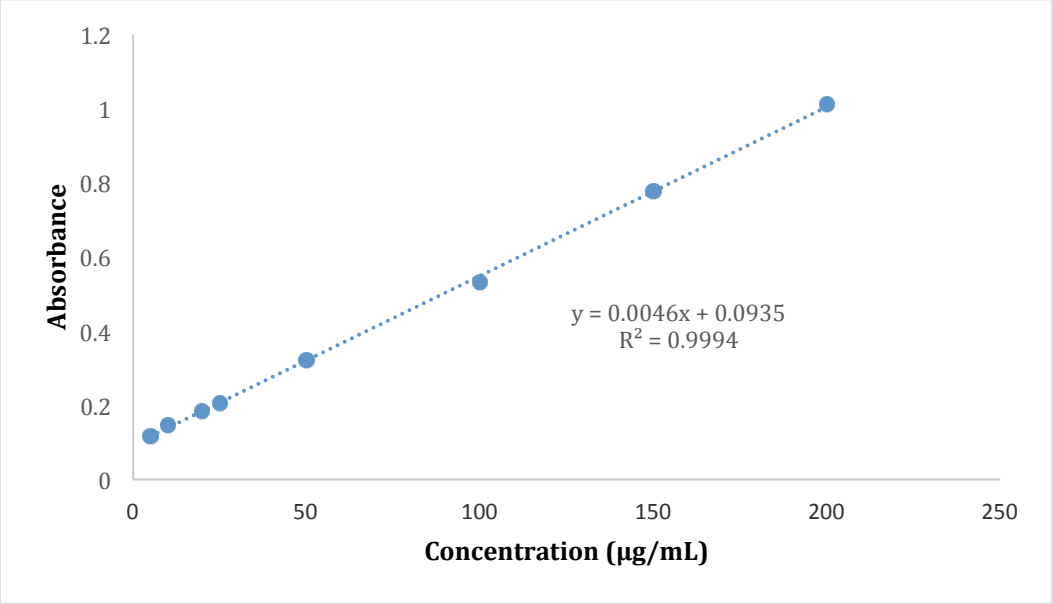

ITZ Liposomes Raw Data

- Each liposome sample was centrifuged @ 13,000 rpm for 90 min to remove free drug
- Each liposome sample (1 mL) was treated with 5% triton X-100 (1 mL), vortexed for 30 seconds, and heated at 60°C for 2-2.5 h
- After heating, liposome samples were vortexed again for 30 seconds
- Aliquot into UV-appropriate 384 well plate in triplicate
- Read absorbance at 254 nm

Sample	1	2	3	Average	Normalized	y = mx + b	Final
A	1.912	1.778	1.693	1.79433333	0.46666667	81.12318841	162.2463768
B	1.776	1.772	1.729	1.759	0.43133333	73.44202899	146.884058
C	1.922	1.412	1.725	1.68633333	0.35866667	57.64492754	115.2898551
D	1.762	1.739	1.719	1.74	0.41233333	69.3115942	138.6231884
E	1.656	1.73	1.738	1.708	0.38033333	62.35507246	124.7101449
F	1.781	1.715	1.788	1.76133333	0.43366667	73.94927536	147.8985507
G	1.648	1.743	1.732	1.70766667	0.38	62.2826087	124.5652174

Controls Raw Data

Control	1	2	3	Average
EtOH	0.103	0.121	0.114	0.11266667
5% Triton	2.614	2.646	2.629	2.62966667
1:1	1.257	1.291	1.435	1.32766667

Intact Liposomes

Sample	1	2	3
Intact empty-liposomes	0.136	0.142	0.139
Intact ITZ-liposomes	0.311	0.403	0.364

Trial 2: Concentration Confirmation for Drug Solution

Sample	1	2	3	Average	Normalized	y = mx+b	Final
A	1.748	2.006	1.867	1.873	0.41	68.8	137.6
B	1.872	1.912	1.807	1.863	0.4	66.6	133.3

1:1 EtOH: 5% Triton Control → 1.46

Concentration Calculation

$$\frac{\text{Trial 1} + \text{Trial 2} + \text{Trial 3}}{\text{Total \# of Trials}} = \text{Average Absorbance}$$

$$\frac{1.912 + 1.778 + 1.693}{3} = 1.794$$

$$\text{Average Absorbance} - \text{Control} = \text{Noramlized Absorbance}$$

$$1.794 - 1.327 = 0.466$$

$$y = 0.0046x + 0.0935$$

$$0.466 = 0.0046x + 0.0935$$

$$0.466 - 0.0935 = 0.0046x$$

$$0.372 = 0.0046x$$

$$\frac{0.372}{0.0046} = 80.07 = x$$

$$x = \frac{1 \text{ mL liposomes}}{2 \text{ mL total volume}}$$

$$2x = \text{Concentration of Drug}$$

$$2\ (80.07) = 161.95\ \mu g/mL$$

Encapsulation Efficiency

Original concentration

$$\frac{60 \text{ mg}}{100} = 0.6 \text{ mg/mL}$$

Collected 7 tubes of ~50 mL of liposomes (350 mL total)

New concentration

$$\frac{60 \text{ mg}}{350 \text{ mL}} = 0.171 \text{ mg/mL}$$

Free Drug

$$\text{Total Concentration}\,\frac{\mu g}{mL} - \text{Experimental Concentration} = \quad \text{Free Drug}$$

$$171\,\frac{\mu g}{mL} - \frac{161 \mu g}{mL} = 8.8\,\frac{\mu g}{mL}$$

Encapsulation Efficiency

$$\frac{\text{Total Drug} - \text{Free Drug}}{\text{Total Drug}}\ \text{x}\ 100\% = \text{Encapsulation Efficiency (EE)}$$

$$\frac{171\,\frac{\mu g}{mL} - 8.8\,\frac{\mu g}{mL}}{171\,\frac{\mu g}{mL}} = \frac{161\,\frac{\mu g}{mL}}{171\,\frac{\mu g}{mL}} = 0.941\ \text{x}\ 100\% = 94.2\ \%\ \text{EE}$$

Drug Solution Concentrations

$$\frac{137.6\ \mu g}{mL}\ \text{x}\ \frac{1\ g}{1{,}000{,}000\ \mu g} = \frac{0.0001376\ g}{mL}$$

$$\frac{0.0001376\ g}{mL}\ \text{x}\ \frac{1{,}000\ mL}{1\ L} = \frac{0.1376\ g}{L}$$

$$\frac{0.1376\ g}{1\ L}\ \text{x}\ \frac{1\ mol}{705.6\ g} = \frac{0.000195\ mol}{L} = 0.195\ mM$$